

Pharmacological and biomolecular profile of purinergic receptors in vascular endothelium: implications for mechanosensation.

Sonia Paz López



A thesis submitted for the degree of Doctor of Philosophy

University of East Anglia

School of Biological Sciences

December 2023

©This copy of this thesis has been supplied on condition that anyone who consults it is understood to recognise that its copyright rests with the author and that use of any information derived therefrom must be in accordance with current UK Copyright Law.

In addition, any quotation or extract must include full attribution.

Declaration

I verify that the work presented in this thesis is my own original work and has not been previously submitted for a degree at this or any other university. Where work by other authors has been included, their work has been fully cited and referenced.

In line with the regulations for submission for a degree of Doctor of Philosophy at the University of East Anglia, this thesis has a word count of approximately 95762 words, which includes all footnotes and bibliography, excluding the appendixes, which consist of approximately 13823 words.

Abstract

The endothelium is the monolayer of cells lining the blood vessels in direct contact with blood flow, detecting mechanical, metabolic, and immunological signals in their surroundings through specific receptors. Endothelial cell's function determines vascular tone, blood vessel formation, and immunological response. Calcium signalling, a universal messenger in cellular activities, is one of the main processes governing vascular endothelial function. The purinergic receptors are a fundamental component of the endothelial calcium toolkit, influencing vasodilation, angiogenesis, and inflammatory responses.

P2 receptors respond to extracellular nucleotides, elevating cytosolic calcium concentration through P2X and P2Y receptors. Various P2 receptors have a role in endothelial calcium homeostasis, with P2Y2 and P2X4 being the most studied receptors in this cell type. However, there is also controversy about which is the primary mediator of ATP-evoked responses in endothelial cells. Despite the P2 receptor's crucial roles in a diverse range of endothelial functions, a comprehensive biomolecular and pharmacological characterization of the P2 receptor's contribution to calcium signalling still needs to be performed. This study aims to characterise the transcriptional and functional expression profile of purinergic signalling in endothelial cells, using human microvascular endothelial cells (HMEC-1) as the primary model. Methodologies included transcriptional profiling via RNA sequencing, pharmacological assays using intracellular calcium mobilisation, and protein expression analysis through western blotting. These methods were applied to investigate the roles of P2 receptors in endothelial ATP, VEGF, and Piezo1-evoked calcium responses.

Here we show that the P2Y2 receptors are the primary mediator of the ATP-evoked calcium responses in HMEC-1, and P2Y11 is involved in the VEGF-evoked calcium responses, suggesting a novel mechanism that might comprise adenylyl cyclase activity and Orai1 activation, distinct from the traditional view of P2 receptors' function. In contrast, the role of P2X4 remains ambiguous, with our findings questioning its functional presence in HMEC-1, as the receptor was absent at the protein level. In addition, the second part of this study faced challenges in dynamically characterising Piezo1 responses due to technical limitations.

By elucidating the roles of these receptors, this research contributes to a more comprehensive understanding of endothelial physiology and pathology, providing new routes for therapeutic intervention in cardiovascular diseases. This study improves our understanding of the endothelial calcium toolkit, revealing new facets of purinergic receptors in endothelial cells. However, additional research is needed to understand the key players in the novel proposed mechanisms involving P2Y11's contribution to the VEGF-dependent responses. Moreover, further research should focus on fully comprehending the P2 receptor's specific roles under dynamic conditions and in different endothelial cell types.

Access Condition and Agreement

Each deposit in UEA Digital Repository is protected by copyright and other intellectual property rights, and duplication or sale of all or part of any of the Data Collections is not permitted, except that material may be duplicated by you for your research use or for educational purposes in electronic or print form. You must obtain permission from the copyright holder, usually the author, for any other use. Exceptions only apply where a deposit may be explicitly provided under a stated licence, such as a Creative Commons licence or Open Government licence.

Electronic or print copies may not be offered, whether for sale or otherwise to anyone, unless explicitly stated under a Creative Commons or Open Government license. Unauthorised reproduction, editing or reformatting for resale purposes is explicitly prohibited (except where approved by the copyright holder themselves) and UEA reserves the right to take immediate 'take down' action on behalf of the copyright and/or rights holder if this Access condition of the UEA Digital Repository is breached. Any material in this database has been supplied on the understanding that it is copyright material and that no quotation from the material may be published without proper acknowledgement.

Table of Contents

| | |
|--|----|
| DECLARATION..... | 2 |
| ABSTRACT..... | 3 |
| LIST OF FIGURES AND TABLES | 8 |
| ABBREVIATIONS..... | 13 |
| ACKNOWLEDGEMENTS..... | 16 |
| CHAPTER 1. INTRODUCTION..... | 18 |
| 1.1 THE ENDOTHELIUM..... | 18 |
| 1.2 CALCIUM SIGNALLING IN THE ENDOTHELIUM..... | 22 |
| 1.3 CALCIUM SIGNALLING TOOLKIT IN THE ENDOTHELIUM..... | 27 |
| 1.3.1. <i>Purinergic signalling and its role in the endothelium.</i> | 27 |
| 1.3.1.1 P1 receptors..... | 28 |
| 1.3.1.2 P2 receptors..... | 30 |
| 1.3.1.2.1 P2Y receptors..... | 30 |
| 1.3.1.2.2 P2X receptors..... | 32 |
| 1.3.2. <i>Piezo1 and its role in the endothelium.</i> | 34 |
| 1.3.3. <i>VEGF and its role in the endothelium.</i> | 35 |
| 1.3.4. <i>TRPs and its role in the endothelium.</i> | 37 |
| 1.4 SHEAR STRESS..... | 38 |
| 1.5 AIMS AND OBJECTIVES..... | 40 |
| CHAPTER 2. MATERIALS AND METHODS..... | 41 |
| 2.1 DRUGS AND REAGENTS..... | 41 |
| 2.2 CELL CULTURE | 42 |
| 2.2.1. <i>Human microvascular endothelial cells (HMEC-1)</i> | 42 |
| 2.2.1.1 General maintenance..... | 42 |
| 2.2.1.2 Cell passage..... | 43 |
| 2.2.1.3 Cryopreservation and thawing..... | 43 |
| 2.2.2. <i>Human umbilical vein endothelial cells (HUVECs)</i> | 43 |
| 2.2.2.1 General maintenance..... | 43 |
| 2.2.2.2 Cell passage..... | 44 |
| 2.2.2.3 Cryopreservation and thawing..... | 44 |
| 2.2.3. <i>Human 1321N1 astrocytoma cells</i> | 44 |
| 2.2.3.1 General maintenance..... | 45 |
| 2.3 CALCIUM MOBILISATION ASSAYS..... | 45 |
| 2.3.1. <i>Calcium mobilisation assays buffers</i> | 46 |
| 2.3.2. <i>Flex Station III assays</i> | 46 |
| 2.3.3. <i>Data analysis for Flex Station III assays</i> | 47 |
| 2.4 CALCIUM IMAGING | 49 |
| 2.4.1 <i>Glycotech parallel flow chamber</i> | 49 |
| 2.4.2 <i>Ibidi μ-slides</i> | 50 |
| 2.4.3 <i>Data analysis for calcium imaging</i> | 52 |
| 2.5 POLYMERASE CHAIN REACTION (PCR) | 55 |
| 2.5.1 <i>RNA extraction</i> | 55 |
| 2.5.2 <i>Complementary DNA (cDNA) synthesis</i> | 55 |
| 2.5.3 <i>Non-quantitative reverse transcription PCR (RT-PCR)</i> | 56 |
| 2.6 RNA SEQUENCING..... | 60 |
| 2.7 WESTERN BLOTTING..... | 62 |
| 2.7.1 <i>Protein extraction and quantification</i> | 62 |

| | |
|--|-----------|
| 2.7.2 SDS-PAGE and membrane transference..... | 62 |
| 2.7.3 Membrane blocking and protein imaging..... | 63 |
| 2.7.4. Data analysis for western blot imaging | 64 |
| 2.8 NITRITE (NO ₂ -) MEASUREMENT | 65 |
| CHAPTER 3. INVESTIGATING THE CONTRIBUTION OF THE PURINERGIC RECEPTORS IN ENDOTHELIAL CELLS' CALCIUM HOMEOSTASIS..... | 68 |
| 3.1 INTRODUCTION | 68 |
| 3.2 AIMS | 69 |
| 3.3 RESULTS..... | 69 |
| 3.3.1. <i>Membrane receptors RNA sequencing profile of human microvascular endothelial cells (HMEC-1)</i> 69 | |
| 3.3.2. <i>Characterisation of the purinergic receptors signalling in human microvascular endothelial cells (HMEC-1).</i> | 72 |
| 3.3.2.1 Nucleotide-evoked calcium responses of human microvascular endothelial cells (HMEC-1)..... | 72 |
| 3.3.2.2 ATP-evoked calcium responses of human microvascular endothelial cells (HMEC-1) are mediated by phospholipase C (PLC) activation, leading to the subsequent release of calcium from intracellular stores. | 77 |
| 3.3.2.3 The broad-spectrum P2 antagonists affected the ATP-evoked calcium responses of human microvascular endothelial cells (HMEC-1)..... | 81 |
| 3.3.2.4 P2X4 antagonists inconsistently affected the ATP-evoked calcium responses of human microvascular endothelial cells (HMEC-1)..... | 88 |
| 3.3.2.5 P2X4 positive allosteric modulator, ivermectin, had an unexpected impact on the ATP-evoked calcium responses of human microvascular endothelial cells (HMEC-1). | 101 |
| 3.3.2.6 P2Y2 selective antagonist significantly affected the ATP and UTP-evoked calcium responses of human microvascular endothelial cells (HMEC-1)..... | 104 |
| 3.3.2.7 P2Y11 selective antagonist did not affect the ATP-evoked calcium responses of human microvascular endothelial cells (HMEC-1)..... | 110 |
| 3.3.2.8 A2B selective antagonist did not affect the ATP-evoked calcium responses of human microvascular endothelial cells (HMEC-1)..... | 110 |
| 3.3.3. <i>Characterisation of the vascular endothelial growth factor calcium signalling in human microvascular endothelial cells (HMEC-1).</i> | 113 |
| 3.3.3.1 VEGF ₁₆₅ -evoked calcium responses of human microvascular endothelial cells (HMEC-1)..... | 113 |
| 3.3.3.2 VEGF ₁₆₅ -evoked calcium responses are mediated by phospholipase C (PLC) activation in human microvascular endothelial cells (HMEC-1)..... | 118 |
| 3.3.3.3 The broad-spectrum P2 antagonists affected the VEGF ₁₆₅ -evoked calcium responses of human microvascular endothelial cells (HMEC-1)..... | 122 |
| 3.3.3.4 P2X4 antagonists inconsistently affected the VEGF ₁₆₅ -evoked calcium responses of human microvascular endothelial cells (HMEC-1). | 127 |
| 3.3.3.5 P2Y2 selective antagonist did not affect the VEGF ₁₆₅ -evoked calcium responses of human microvascular endothelial cells (HMEC-1)..... | 130 |
| 3.3.3.6 P2Y11 selective antagonist significantly inhibited the VEGF ₁₆₅ -evoked calcium responses of human microvascular endothelial cells (HMEC-1)..... | 135 |
| 3.3.3.7 VEGF ₁₆₅ -evoked calcium responses P2Y11-dependent are mediated by the adenylyl cyclase pathway in human microvascular endothelial cells (HMEC-1). | 138 |
| 3.3.3.8 A2B selective antagonist significantly affected the VEGF ₁₆₅ -evoked calcium responses of human microvascular endothelial cells (HMEC-1)..... | 144 |
| 3.3.4. <i>P2 purinergic receptors protein profile of human microvascular endothelial cells (HMEC-1).</i> | 146 |
| 3.3.4.1 P2X4 protein expression was not detected in human microvascular endothelial cells (HMEC-1). | 146 |
| 3.3.4.2 P2Y2 protein expression was ambiguously detected in human microvascular endothelial cells (HMEC-1). | 148 |
| 3.3.4.3 P2Y11 protein expression was detected in human microvascular endothelial cells (HMEC-1)..... | 153 |
| 3.3.5. <i>Purinergic receptor mRNA expression profile of human umbilical vein endothelial cells (HUVECs).</i> | 158 |
| 3.3.6. <i>Characterisation of the vascular endothelial growth factor calcium signalling in human umbilical vein endothelial cells (HUVECs).</i> | 163 |
| 3.3.6.1 VEGF ₁₆₅ -evoked calcium responses in human umbilical vein endothelial cells (HUVECs)..... | 163 |
| 3.3.6.2 The broad-spectrum P2 antagonist, PPADS, affected the VEGF ₁₆₅ -evoked calcium responses of human umbilical vein endothelial cells (HUVECs). | 165 |
| 3.3.6.3 P2Y11 selective antagonist did not affect the VEGF ₁₆₅ -evoked calcium responses of human umbilical vein endothelial cells (HUVECs). | 165 |
| 3.3.6.4 VEGF ₁₆₅ kinetics profile differed between human umbilical vein endothelial cells (HUVECs) and human microvascular endothelial cells (HMEC-1), and this response is characteristic of endothelial cells. | 168 |

| | |
|---|------------|
| 3.3.7. <i>Characterisation of the ATP calcium signalling in human umbilical vein endothelial cells (HUVECs).</i> | 171 |
| 3.3.7.1 ATP-evoked calcium responses in human umbilical vein endothelial cells (HUVECs) | 171 |
| 3.3.7.2 ATP kinetics profile differed between human umbilical vein endothelial cells (HUVECs) and human microvascular endothelial cells (HMEC-1) | 175 |
| 3.4 DISCUSSION | 178 |
| 3.4.1. <i>Human dermal microvascular endothelial cells (HMEC-1) express various purinergic receptors at the transcriptional level.</i> | 178 |
| 3.4.2. <i>Purinergic receptors contribute to the endothelial calcium homeostasis in HMEC-1.</i> | 178 |
| 3.4.2.1 The broad-spectrum P2 antagonists impair ATP calcium influx in HMEC-1. | 180 |
| 3.4.2.2 P2X4 is unlikely to play a role in the ATP-evoked calcium responses in HMEC-1. | 181 |
| 3.4.2.3 P2Y2 mediates ATP-dependent responses in HMEC-1. | 182 |
| 3.4.2.4 P2Y11 and A2B receptors do not mediate ATP responses in HMEC-1. | 183 |
| 3.4.3. <i>Human dermal microvascular endothelial cells (HMEC-1) express various vascular endothelial growth factors receptors and ligands at the transcriptional level.</i> | 183 |
| 3.4.4. <i>VEGF receptors contribute to the endothelial calcium homeostasis in HMEC-1.</i> | 184 |
| 3.4.4.1 The broad-spectrum P2 antagonists impair VEGF ₁₆₅ calcium influx in HMEC-1. | 186 |
| 3.4.4.2 P2X4 selective antagonists inconsistently impair VEGF ₁₆₅ calcium influx in HMEC-1. | 187 |
| 3.4.4.3 P2Y2 selective antagonist did not impair the VEGF ₁₆₅ calcium influx in HMEC-1. | 187 |
| 3.4.4.4 P2Y11 selective antagonist impaired the VEGF ₁₆₅ calcium influx in an adenylyl cyclase-dependent manner in HMEC-1. | 188 |
| 3.4.4.5 A2B selective antagonist impaired the VEGF ₁₆₅ calcium influx in HMEC-1. | 197 |
| 3.4.5. <i>Human dermal microvascular endothelial cells (HMEC-1) express different purinergic receptor patterns at the protein level.</i> | 197 |
| 3.4.5.1 P2X4 is not expressed in HMEC-1 at the protein level. | 197 |
| 3.4.5.2 P2Y2 protein detection is ambiguous in HMEC-1 cells. | 199 |
| 3.4.5.3 P2Y11 is expressed in HMEC-1 at the protein level. | 201 |
| 3.4.6. <i>Human umbilical vein endothelial cells (HUVEC) express various purinergic receptors at the transcriptional level.</i> | 203 |
| 3.4.7. <i>VEGF receptors contribute to endothelial calcium homeostasis in HUVECs, and their trace kinetics differ from those observed in HMEC-1 cells.</i> | 204 |
| 3.4.7.1 P2Y11 selective antagonist did not impair the VEGF ₁₆₅ calcium influx in HUVECs. | 204 |
| 3.4.8. <i>Purinergic receptors contribute to the endothelial calcium homeostasis in HMEC-1, and their trace kinetics differ from those observed in HMEC-1 cells.</i> | 205 |
| 3.4.8.1 The SERCA inhibitor thapsigargin impaired the ATP calcium influx in HUVECs, while BX430 could not inhibit the studied responses. | 205 |
| CHAPTER 4. EXPLORING THE CONTRIBUTION OF PURINERGIC RECEPTORS IN MECHANOSENSITIVE EVOKED CALCIUM RESPONSES. | 207 |
| 4.1 INTRODUCTION | 207 |
| 4.2 AIMS | 207 |
| 4.3 RESULTS | 208 |
| 4.3.1. <i>Characterisation of Piezo1 signalling in human microvascular endothelial cells (HMEC-1) and human umbilical vein cells (HUVEC).</i> | 208 |
| 4.3.1.1 Yoda1 evoked calcium responses in human microvascular endothelial cells (HMEC-1), and this response was inhibited in the presence of GsMTx4. | 208 |
| 4.3.1.2 Yoda1 evoked calcium responses in human umbilical vein endothelial cells (HUVEC), and this response was inhibited in the presence of Dooku1. | 212 |
| 4.3.1.3 Yoda1 kinetics profile differed between human umbilical vein endothelial cells (HUVECs) and human microvascular endothelial cells (HMEC-1). | 216 |
| 4.3.2. <i>Characterisation of broad-spectrum P2 antagonist effects in Yoda1-induced responses in human microvascular endothelial cells (HMEC-1) and human umbilical vein cells (HUVEC).</i> | 218 |
| 4.3.2.1 The broad-spectrum P2 antagonists did not affect the Yoda1-evoked calcium responses of human microvascular endothelial cells (HMEC-1). | 218 |
| 4.3.2.2 The broad-spectrum P2 antagonists affected the Yoda1-evoked calcium responses of human umbilical vein endothelial cells (HUVEC). | 221 |
| 4.3.3. <i>Insights into the suitability of two different parallel flow chambers for mechanical stimulation of cells in vitro.</i> | 232 |
| 4.3.3.1 The Glycotech parallel flow chamber was discarded as an option to stimulate cells in vitro mechanically. | 234 |

| | |
|---|------------|
| 4.3.3.2 The Ibidi μ -slide was an inconsistent but potentially valuable tool to stimulate cells in vitro mechanically. | 238 |
| 4.3.4. <i>Investigation of the benefit of the Griess reagent for quantifying nitric oxide in endothelial cells in vitro.</i> | 244 |
| 4.4 DISCUSSION | 249 |
| 4.4.1. <i>Piezo1 is transcriptionally and functionally expressed in human dermal microvascular endothelial cells (HMEC-1) and human umbilical vein cells (HUVEC).</i> | 249 |
| 4.4.2. <i>The broad-spectrum P2 antagonist impacted the Yoda1 calcium influx differently in HMEC-1 and HUVEC cells.</i> | 251 |
| 4.4.3. <i>The parallel flow system for mechanically stimulating endothelial cells in vitro still needs time to investigate the P2 contribution in the shear stress-dependent responses.</i> | 255 |
| 4.4.4. <i>The Griess reagent was not valuable for measuring nitric oxide release in HMEC-1 cells in the tested conditions.</i> | 258 |
| CHAPTER 5. GENERAL DISCUSSION. | 261 |
| 5.1 KEY FINDINGS AND CONCLUDING REMARKS..... | 261 |
| 5.2 FUTURE DIRECTIONS. | 265 |
| APPENDIX. | 267 |
| APPENDIX I. VEGF RECEPTORS AND LIGANDS EXPRESSION FROM THE HUMAN PROTEIN ATLAS. | 267 |
| APPENDIX II. J. LI ET AL., 2011 VEGF ₁₆₅ TRACE KINETICS IN HUVECS..... | 269 |
| REFERENCES. | 270 |

List of Figures and Tables

CHAPTER 1.

| | |
|--|----|
| FIGURE 1. THE STRUCTURE OF A VESSEL WALL AND THE ENDOTHELIUM. | 21 |
| FIGURE 2. ACTIVATION OF THE PURINERGIC AND CALCIUM SIGNALLING..... | 25 |
| FIGURE 3. P1, P2X, AND P2Y RECEPTORS' INTRACELLULAR SIGNALLING PATHWAYS AND AGONISTS. | 29 |
| TABLE 1. P2Y RECEPTOR AGONIST AND COUPLING G PROTEIN SUBUNITS – HUMAN POTENCIES. | 31 |
| TABLE 2. P2X RECEPTOR AGONIST AND DESENSITIZATION PROFILE – HUMAN POTENCIES..... | 33 |
| FIGURE 4. VEGF FAMILY: RECEPTORS AND LIGANDS..... | 36 |
| TABLE 3. FUNCTIONS OF HUMAN ENDOTHELIAL TRP CHANNEL SUMMARY..... | 38 |
| FIGURE 5. DIFFERENT IN VITRO APPROACHES TO THE ENDOTHELIAL FUNCTION AND FLOW TYPES. | 39 |

CHAPTER 2.

| | |
|--|----|
| TABLE 1. LIST OF EXOGENOUS NUCLEOTIDES AND OTHER SELECTIVE AGONISTS. | 41 |
| TABLE 2. LIST OF NON-SELECTIVE PURINERGIC RECEPTOR ANTAGONISTS..... | 41 |
| TABLE 3. LIST OF SELECTIVE PURINERGIC AND ADENOSINE RECEPTORS ANTAGONISTS OR MODULATORS. | 41 |
| TABLE 4. LIST OF OTHER DRUGS AND INHIBITORS. | 42 |
| TABLE 5. CELL LINES AND CULTURE MEDIA SPECIFICATIONS SUMMARY. | 45 |
| FIGURE 1. CHEMICAL AND FLUORESCENCE PROFILE OF FURA 2-AM. | 48 |
| FIGURE 2. REPRESENTATIVE TIME-RESOLVED INTRACELLULAR CALCIUM RESPONSE. | 48 |
| TABLE 6. SHEAR STRESS VALUES FOR μ -SLIDE I ^{0.4} LUER FOR VISCOSITY η = 1.075 CENTIPOISE. | 51 |
| FIGURE 3. PARALLEL FLOW CHAMBERS SPECIFICATIONS..... | 54 |
| TABLE 7. PRIMER SEQUENCES FOR P1 RECEPTORS AND HOUSEKEEPING GENE (B-ACTIN). | 57 |
| TABLE 8. PRIMER SEQUENCES FOR P2X RECEPTORS..... | 58 |
| TABLE 9. PRIMER SEQUENCES FOR P2Y RECEPTORS..... | 59 |
| FIGURE 4. FOUR HUMAN MICROVASCULAR ENDOTHELIAL CELL (HMEC-1) SAMPLES WITH DIFFERENT LEVELS OF RNA DEGRADATION WERE ANALYSED USING THE 4150 TAPESTATION FROM AGILENT TECHNOLOGIES..... | 61 |
| TABLE 10. STACKING AND RESOLVING GEL COMPOSITION. | 63 |
| TABLE 11. BLOCKING SOLUTIONS CONFIGURATION..... | 64 |
| TABLE 12. LIST OF ANTIBODIES USED FOR WESTERN BLOTTING. | 64 |
| FIGURE 5. NITRITE MEASUREMENT SPECIFICATIONS..... | 67 |

CHAPTER 3. RESULTS.

| | |
|---|----|
| FIGURE 1. NORMALISED GENE EXPRESSION FOR THE EXPECTED NUMBER OF FPKM LEVELS IN VARIOUS RECEPTOR FAMILIES IN HUMAN MICROVASCULAR ENDOTHELIAL CELLS (HMEC-1). | 71 |
| FIGURE 2. ATP ELICITS INTRACELLULAR CALCIUM RESPONSES IN HUMAN MICROVASCULAR ENDOTHELIAL CELLS (HMEC- 1)..... | 73 |
| FIGURE 3. EXTRACELLULAR CALCIUM REMOVAL IMPACTED THE ATP-EVOKED RESPONSE IN HUMAN MICROVASCULAR ENDOTHELIAL CELLS (HMEC-1). | 74 |
| FIGURE 4. ATP, UTP, ADP AND UDP ELICIT INTRACELLULAR CALCIUM RESPONSES IN HUMAN MICROVASCULAR ENDOTHELIAL CELLS (HMEC-1). | 75 |
| TABLE 1. SUMMARY OF NUCLEOTIDES-EVOKED RESPONSES IN HUMAN MICROVASCULAR ENDOTHELIAL CELLS (HMEC-1). | 76 |
| TABLE 2. EFFECTS OF BROAD-SPECTRUM ANTAGONISTS ON THE ATP-EVOKED RESPONSES IN HUMAN MICROVASCULAR ENDOTHELIAL CELLS (HMEC-1). | 76 |
| FIGURE 5. EFFECTS OF THE PHOSPHOLIPASE C (PLC) INHIBITOR U73122 ON THE ATP-EVOKED RESPONSE IN HUMAN MICROVASCULAR ENDOTHELIAL CELLS (HMEC-1). | 78 |
| FIGURE 6. EFFECTS OF THE SARCOENDOPLASMIC RETICULUM CALCIUM TRANSPORT ATPASE (SERCA) INHIBITOR THAPSIGARGIN ON THE ATP-EVOKED RESPONSE IN HUMAN MICROVASCULAR ENDOTHELIAL CELLS (HMEC-1). .. | 79 |

| | |
|---|-----|
| FIGURE 7. TOLERANCE OF THE ATP-EVOKED RESPONSE IN HUMAN MICROVASCULAR ENDOTHELIAL CELLS (HMEC-1) TO 0.1% AND 0.2% DIMETHYL SULFOXIDE (DMSO). | 80 |
| FIGURE 8. INHIBITORY EFFECTS OF APYRASE ON THE ATP-EVOKED RESPONSE IN HUMAN MICROVASCULAR ENDOTHELIAL CELLS (HMEC-1). | 82 |
| FIGURE 9. INHIBITORY EFFECTS OF BROAD-SPECTRUM P2 RECEPTORS ANTAGONIST PPADS ON THE ATP-EVOKED RESPONSE IN HUMAN MICROVASCULAR ENDOTHELIAL CELLS (HMEC-1). | 84 |
| FIGURE 10. INHIBITION CONCENTRATION-RESPONSE CURVES FOR PPADS ON THE ATP-EVOKED RESPONSE IN HUMAN MICROVASCULAR ENDOTHELIAL CELLS (HMEC-1). | 85 |
| FIGURE 11. UNEXPECTED EFFECTS OF BROAD-SPECTRUM P2 RECEPTORS ANTAGONIST SURAMIN ON THE ATP-EVOKED RESPONSE IN HUMAN MICROVASCULAR ENDOTHELIAL CELLS (HMEC-1). | 87 |
| FIGURE 12. LACK OF INHIBITORY EFFECTS OF BAY-1797 P2X4 RECEPTOR ANTAGONIST ON THE ATP-EVOKED RESPONSE IN HUMAN MICROVASCULAR ENDOTHELIAL CELLS (HMEC-1). | 90 |
| TABLE 3. EFFECTS OF SELECTIVE ANTAGONISTS ON THE ATP-EVOKED PEAK RESPONSES IN HUMAN MICROVASCULAR ENDOTHELIAL CELLS (HMEC-1). | 91 |
| TABLE 4. EFFECTS OF SELECTIVE ANTAGONISTS ON THE ATP-EVOKED AUC RESPONSES IN HUMAN MICROVASCULAR ENDOTHELIAL CELLS (HMEC-1). | 92 |
| FIGURE 13. LACK OF INHIBITORY EFFECTS OF 5-BDBD P2X4 RECEPTOR ANTAGONIST ON THE ATP-EVOKED RESPONSE IN HUMAN MICROVASCULAR ENDOTHELIAL CELLS (HMEC-1). | 94 |
| FIGURE 14. LACK OF INHIBITORY EFFECTS OF BX430 P2X4 RECEPTOR ANTAGONIST ON THE ATP-EVOKED RESPONSE IN HUMAN MICROVASCULAR ENDOTHELIAL CELLS (HMEC-1). | 95 |
| FIGURE 15. INHIBITORY EFFECTS ON ATP-EVOKED Ca ²⁺ RESPONSES AFTER TREATMENT WITH BX430 SELECTIVE HUMAN P2X4 RECEPTOR ANTAGONIST IN 1321N1 HUMAN P2X4 STABLE ASTROCYTOMA CELLS. | 97 |
| FIGURE 16. ATP DID NOT CAUSE AN ENDOGENOUS CALCIUM RESPONSE IN 1321N1 PARENTAL ASTROCYTOMA CELLS. | 98 |
| FIGURE 17. INHIBITORY EFFECTS OF PSB12062 P2X4 RECEPTOR ANTAGONIST ON THE ATP-EVOKED RESPONSE IN HUMAN MICROVASCULAR ENDOTHELIAL CELLS (HMEC-1). | 100 |
| FIGURE 18. UNEXPECTED EFFECTS OF IVERMECTIN IN HUMAN MICROVASCULAR ENDOTHELIAL CELLS (HMEC-1). | 102 |
| FIGURE 19. INHIBITORY EFFECTS OF AR-C 118925XX P2Y2 RECEPTOR ANTAGONIST ON THE ATP-EVOKED RESPONSE IN HUMAN MICROVASCULAR ENDOTHELIAL CELLS (HMEC-1). | 106 |
| FIGURE 20. INHIBITION CONCENTRATION-RESPONSE CURVES FOR AR-C 118925XX (P2Y2 RECEPTOR ANTAGONIST) ON THE ATP-EVOKED RESPONSE IN HUMAN MICROVASCULAR ENDOTHELIAL CELLS (HMEC-1). | 107 |
| FIGURE 21. TOLERANCE OF THE UTP-EVOKED RESPONSE IN HUMAN MICROVASCULAR ENDOTHELIAL CELLS (HMEC-1) TO 0.1% DIMETHYL SULFOXIDE (DMSO). | 108 |
| FIGURE 22. INHIBITORY EFFECTS OF AR-C 118925XX P2Y2 RECEPTOR ANTAGONIST ON THE UTP-EVOKED RESPONSE IN HUMAN MICROVASCULAR ENDOTHELIAL CELLS (HMEC-1). | 109 |
| FIGURE 23. LACK OF INHIBITORY EFFECTS OF NF157 P2Y11 RECEPTOR ANTAGONIST ON THE ATP-EVOKED RESPONSE IN HUMAN MICROVASCULAR ENDOTHELIAL CELLS (HMEC-1). | 111 |
| FIGURE 24. INHIBITORY EFFECTS OF MRS 1754 A2A RECEPTOR ANTAGONIST ON THE ATP-EVOKED RESPONSE IN HUMAN MICROVASCULAR ENDOTHELIAL CELLS (HMEC-1). | 112 |
| FIGURE 25. VEGF ₁₆₅ ELICITS INTRACELLULAR CALCIUM RESPONSES IN HUMAN MICROVASCULAR ENDOTHELIAL CELLS (HMEC-1). | 115 |
| FIGURE 26. EXTRACELLULAR CALCIUM REMOVAL IMPACTED THE VEGF ₁₆₅ -EVOKED RESPONSE IN HUMAN MICROVASCULAR ENDOTHELIAL CELLS (HMEC-1). | 116 |
| FIGURE 27. VEGF ₁₆₇ DID NOT ELICIT INTRACELLULAR CALCIUM RESPONSE IN HUMAN MICROVASCULAR ENDOTHELIAL CELLS (HMEC-1). | 117 |
| FIGURE 28. EFFECTS OF THE PHOSPHOLIPASE C (PLC) INHIBITOR U73122 ON THE VEGF ₁₆₅ -EVOKED RESPONSE IN HUMAN MICROVASCULAR ENDOTHELIAL CELLS (HMEC-1). | 119 |
| FIGURE 29. EFFECTS OF THE SARCOENDOPLASMIC RETICULUM CALCIUM TRANSPORT ATPASE (SERCA) INHIBITOR, THAPSIGARGIN, ON THE VEGF ₁₆₅ -EVOKED RESPONSE IN HUMAN MICROVASCULAR ENDOTHELIAL CELLS (HMEC-1). | 120 |

| | |
|--|-----|
| FIGURE 30. TOLERANCE OF THE VEGF ₁₆₅ -EVOKED RESPONSE IN HUMAN MICROVASCULAR ENDOTHELIAL CELLS (HMEC-1) TO 0.1% DIMETHYL SULFOXIDE (DMSO)..... | 121 |
| FIGURE 31. INHIBITORY EFFECTS OF APYRASE ON THE VEGF ₁₆₅ -EVOKED RESPONSE IN HUMAN MICROVASCULAR ENDOTHELIAL CELLS (HMEC-1)..... | 123 |
| FIGURE 32. INHIBITORY EFFECTS OF BROAD-SPECTRUM P2 RECEPTORS ANTAGONIST PPADS ON THE VEGF ₁₆₅ -EVOKED RESPONSE IN HUMAN MICROVASCULAR ENDOTHELIAL CELLS (HMEC-1)..... | 125 |
| FIGURE 33. PPADS INHIBITION DOSE-RESPONSE CURVES FOR VEGF ₁₆₅ IN HUMAN MICROVASCULAR ENDOTHELIAL CELLS (HMEC-1)..... | 126 |
| FIGURE 34. LACK OF INHIBITORY EFFECTS OF BAY-1797 P2X4 RECEPTOR ANTAGONIST ON THE VEGF ₁₆₅ -EVOKED RESPONSE IN HUMAN MICROVASCULAR ENDOTHELIAL CELLS (HMEC-1)..... | 128 |
| FIGURE 35. INHIBITORY EFFECTS OF PSB12062 P2X4 RECEPTOR ANTAGONIST ON THE VEGF ₁₆₅ -EVOKED RESPONSE IN HUMAN MICROVASCULAR ENDOTHELIAL CELLS (HMEC-1)..... | 129 |
| FIGURE 36. LACK OF INHIBITORY EFFECTS OF AR-C 118925XX P2Y2 RECEPTOR ANTAGONIST ON THE VEGF ₁₆₅ -EVOKED RESPONSE IN HUMAN MICROVASCULAR ENDOTHELIAL CELLS (HMEC-1)..... | 131 |
| TABLE 5. EFFECTS OF BROAD-SPECTRUM ANTAGONISTS ON THE VEGF ₁₆₅ -EVOKED RESPONSES IN HUMAN MICROVASCULAR ENDOTHELIAL CELLS (HMEC-1)..... | 132 |
| TABLE 6. EFFECTS OF SELECTIVE ANTAGONISTS ON THE VEGF ₁₆₅ -EVOKED PEAK RESPONSES IN HUMAN MICROVASCULAR ENDOTHELIAL CELLS (HMEC-1)..... | 133 |
| TABLE 7. EFFECTS OF SELECTIVE ANTAGONISTS ON THE VEGF ₁₆₅ -EVOKED AUC RESPONSES IN HUMAN MICROVASCULAR ENDOTHELIAL CELLS (HMEC-1)..... | 134 |
| FIGURE 37. INHIBITORY EFFECTS OF NF157 P2Y11 RECEPTOR ANTAGONIST ON THE VEGF ₁₆₅ -EVOKED RESPONSE IN HUMAN MICROVASCULAR ENDOTHELIAL CELLS (HMEC-1)..... | 136 |
| FIGURE 38. VEGF ₁₆₅ INHIBITION DOSE-RESPONSE CURVES FOR NF157 IN HUMAN MICROVASCULAR ENDOTHELIAL CELLS (HMEC-1)..... | 137 |
| FIGURE 39. UNEXPECTED EFFECTS OF SQ 22536 ADENYLYL CYCLASE INHIBITOR ON THE VEGF ₁₆₅ -EVOKED RESPONSE IN HUMAN MICROVASCULAR ENDOTHELIAL CELLS (HMEC-1)..... | 140 |
| FIGURE 40. EFFECTS OF THE COMBINATION OF NF157 P2Y11 ANTAGONIST AND SQ 22536 ADENYLYL CYCLASE INHIBITOR ON THE VEGF ₁₆₅ -EVOKED RESPONSE IN HUMAN MICROVASCULAR ENDOTHELIAL CELLS (HMEC-1)..... | 142 |
| FIGURE 41. VEGF ₁₆₅ POTENCY FOLD CHANGE COMPARISON BETWEEN THE EFFECTS OF NF157 P2Y11 ANTAGONIST AND THE CO-APPLICATION WITH SQ 22536 ADENYLYL CYCLASE INHIBITOR IN HUMAN MICROVASCULAR ENDOTHELIAL CELLS (HMEC-1)..... | 143 |
| FIGURE 42. INHIBITORY EFFECTS OF MRS 1754 A2A RECEPTOR ANTAGONIST ON THE VEGF ₁₆₅ -EVOKED RESPONSE IN HUMAN MICROVASCULAR ENDOTHELIAL CELLS (HMEC-1)..... | 145 |
| FIGURE 43. P2X4 IS NOT EXPRESSED IN HUMAN MICROVASCULAR ENDOTHELIAL CELLS (HMEC-1) AT THE PROTEIN LEVEL (60 KDA)..... | 147 |
| FIGURE 44. AMBIGUOUS P2Y2 PROTEIN EXPRESSION LEVELS COMPARISON OF WHOLE-CELL EXTRACTS OF HUMAN MICROVASCULAR ENDOTHELIAL CELLS (HMEC-1) AND HUMAN P2X4 1321N1 PARENTAL ASTROCYTOMA CELLS USING MILK-BASED BLOCKING SOLUTION AND ANTI-P2Y2 ANTIBODY FROM <i>ALOMONE (APR-015)</i> (50 KDA)..... | 150 |
| FIGURE 45. DETERMINATION OF THE BLOCKING SOLUTION TO USE FOR P2Y2 PROTEIN EXPRESSION LEVELS COMPARISON OF WHOLE-CELL EXTRACTS OF HUMAN MICROVASCULAR ENDOTHELIAL CELLS (HMEC-1) AND HUMAN P2X4 1321N1 PARENTAL ASTROCYTOMA CELLS USING ANTI-P2Y2 ANTIBODY FROM <i>ABCAM (AB168535)</i> (42 KDA)..... | 151 |
| FIGURE 46. AMBIGUOUS P2Y11 PROTEIN EXPRESSION LEVELS COMPARISON OF WHOLE-CELL EXTRACTS OF HMEC-1 AND 1321N1 PARENTAL ASTROCYTOMA CELLS USING MILK-BASED BLOCKING SOLUTION AND ANTI-P2Y11 ANTIBODY FROM <i>ALOMONE (APR-015)</i> (50 KDA)..... | 152 |
| FIGURE 47. DETERMINATION OF WHICH BLOCKING SOLUTION TO USE FOR P2Y11 PROTEIN EXPRESSION LEVELS COMPARISON OF WHOLE-CELL EXTRACTS OF HMEC-1 AND 1321N1 PARENTAL ASTROCYTOMA CELLS WITH ANTI-P2Y11 ANTIBODY FROM <i>ABCAM (AB180739)</i> (43 KDA)..... | 155 |
| FIGURE 48. P2Y11 IS EXPRESSED IN HUMAN MICROVASCULAR ENDOTHELIAL CELLS (HMEC-1) AT THE PROTEIN LEVEL (43 KDA)..... | 157 |

| | |
|--|-----|
| TABLE 8. NON QUANTITATIVE RT-PCR EXPRESSION PROFILE OF PURINERGIC RECEPTORS IN HUMAN BRAIN AND UMBILICAL VEIN ENDOTHELIAL CELLS (HUVEC)..... | 159 |
| FIGURE 49. NON-QUANTITATIVE RT-PCR EXPRESSION PROFILE OF ADENOSINE AND P2X RECEPTORS IN HUMAN BRAIN AND HUVEC CELLS..... | 160 |
| FIGURE 50. NON-QUANTITATIVE RT-PCR EXPRESSION PROFILE OF P2Y RECEPTORS IN HUMAN BRAIN AND UMBILICAL VEIN ENDOTHELIAL CELLS (HUVEC)..... | 162 |
| FIGURE 51. VEGF ₁₆₅ ELICITS INTRACELLULAR CALCIUM RESPONSES IN HUMAN UMBILICAL VEIN ENDOTHELIAL CELLS (HUVEC)..... | 164 |
| FIGURE 52. PRELIMINARY INHIBITORY EFFECTS OF BROAD-SPECTRUM P2 RECEPTORS ANTAGONIST PPADS ON THE VEGF ₁₆₅ -EVOKED RESPONSE IN HUMAN UMBILICAL VEIN ENDOTHELIAL CELLS (HUVEC)..... | 166 |
| FIGURE 53. LACK OF INHIBITORY EFFECTS OF NF157 P2Y ₁₁ RECEPTOR ANTAGONIST ON THE VEGF ₁₆₅ -EVOKED RESPONSE IN HUMAN UMBILICAL VEIN ENDOTHELIAL CELLS (HUVEC)..... | 167 |
| FIGURE 54. VEGF ₁₆₅ 'S KINETICS PROFILE VARIED BETWEEN HUMAN UMBILICAL VEIN ENDOTHELIAL CELLS (HUVECS) AND HUMAN MICROVASCULAR ENDOTHELIAL CELLS (HMEC-1)..... | 169 |
| FIGURE 55. VEGF ₁₆₅ DID NOT ELICIT INTRACELLULAR CALCIUM RESPONSE IN 1321N1 HUMAN P2X ₄ STABLE ASTROCYTOMA CELLS..... | 170 |
| FIGURE 56. ATP ELICITS INTRACELLULAR CALCIUM RESPONSES IN HUMAN UMBILICAL VEIN ENDOTHELIAL CELLS (HUVEC)..... | 172 |
| FIGURE 57. EFFECTS OF THE SARCOENDOPLASMIC RETICULUM CALCIUM TRANSPORT ATPASE (SERCA) INHIBITOR THAPSIGARGIN ON THE ATP-EVOKED RESPONSE IN HUMAN UMBILICAL VEIN ENDOTHELIAL CELLS (HUVEC)..... | 173 |
| FIGURE 58. LACK OF INHIBITORY EFFECTS OF BX430 P2X ₄ RECEPTOR ANTAGONIST ON THE ATP-EVOKED RESPONSE IN HUMAN UMBILICAL VEIN ENDOTHELIAL CELLS (HUVEC)..... | 174 |
| FIGURE 59. ATP'S KINETICS PROFILE VARIED BETWEEN HUMAN UMBILICAL VEIN ENDOTHELIAL CELLS (HUVECS) AND HUMAN MICROVASCULAR ENDOTHELIAL CELLS (HMEC-1)..... | 176 |
| FIGURE 60. COMPARISON OF PURINERGIC RECEPTOR EXPRESSION PROFILE BETWEEN HUMAN UMBILICAL VEIN ENDOTHELIAL CELLS (HUVEC) AND HUMAN MICROVASCULAR ENDOTHELIAL CELLS (HMEC-1)..... | 177 |

CHAPTER 3. DISCUSSION.

| | |
|--|-----|
| FIGURE 1. NORMALISED GENE EXPRESSION FOR THE EXPECTED NUMBER OF FPKM LEVELS FOR THE DIFFERENT ADENYLYL CYCLASE ISOFORMS IN HUMAN MICROVASCULAR ENDOTHELIAL CELLS (HMEC-1)..... | 190 |
| TABLE 1. PROPOSED MECHANISM INVOLVING ADENYLYL CYCLASE 3 (AC3) ISOFORM..... | 195 |
| TABLE 2. PROPOSED MECHANISM INVOLVING ADENYLYL CYCLASE 6 (AC6) ISOFORM..... | 196 |

CHAPTER 4. RESULTS.

| | |
|--|-----|
| FIGURE 1. YODA1 ELICITED INTRACELLULAR CALCIUM RESPONSES IN HUMAN MICROVASCULAR ENDOTHELIAL CELLS (HMEC-1)..... | 210 |
| FIGURE 2. GSMTX4, THE SPIDER VENOM PEPTIDE, INHIBITED YODA1-INDUCED Ca ²⁺ RESPONSE IN HUMAN MICROVASCULAR ENDOTHELIAL CELLS (HMEC-1)..... | 211 |
| FIGURE 3. YODA1 ELICITED INTRACELLULAR CALCIUM RESPONSES IN HUMAN UMBILICAL VEIN ENDOTHELIAL CELLS (HUVEC)..... | 213 |
| FIGURE 4. REMOVING EXTRACELLULAR CALCIUM DIMINISHED THE YODA1-EVOKED RESPONSE IN HUMAN UMBILICAL VEIN ENDOTHELIAL CELLS (HUVEC)..... | 214 |
| FIGURE 5. INHIBITION CONCENTRATION-RESPONSE CURVES IN THE PRESENCE OF DOOKU1 ON THE YODA1-EVOKED RESPONSE IN HUMAN UMBILICAL VEIN ENDOTHELIAL CELLS (HUVEC)..... | 215 |
| FIGURE 6. YODA1'S KINETICS PROFILE VARIED BETWEEN HUMAN UMBILICAL VEIN ENDOTHELIAL CELLS (HUVECS) AND HUMAN MICROVASCULAR ENDOTHELIAL CELLS (HMEC-1)..... | 217 |
| FIGURE 7. MINIMAL AND ISOLATED EFFECTS OF THE ATP AND ADP SCAVENGER APYRASE ON THE YODA1-EVOKED RESPONSE IN HUMAN MICROVASCULAR ENDOTHELIAL CELLS (HMEC-1)..... | 219 |

| | |
|--|-----|
| FIGURE 8. LACK OF INHIBITORY EFFECTS OF BROAD-SPECTRUM P2 RECEPTORS ANTAGONIST PPADS ON THE YODA1-EVOKED RESPONSE IN HUMAN MICROVASCULAR ENDOTHELIAL CELLS (HMEC-1). | 220 |
| FIGURE 9. INHIBITORY EFFECTS OF THE ATP AND ADP SCAVENGER APYRASE ON THE ATP-EVOKED RESPONSE IN HUMAN UMBILICAL VEIN ENDOTHELIAL CELLS (HUVEC). | 223 |
| FIGURE 10. INHIBITORY EFFECTS OF BROAD-SPECTRUM P2 RECEPTORS ANTAGONIST PPADS ON THE ATP-EVOKED RESPONSE IN HUMAN UMBILICAL VEIN ENDOTHELIAL CELLS (HUVEC). | 225 |
| TABLE 1. EFFECTS OF BROAD-SPECTRUM ANTAGONISTS ON THE ATP-EVOKED RESPONSES IN HUMAN UMBILICAL ENDOTHELIAL CELLS (HUVEC). | 226 |
| TABLE 2. EFFECTS OF BROAD-SPECTRUM ANTAGONISTS ON THE YODA1-EVOKED RESPONSES IN HUMAN UMBILICAL ENDOTHELIAL CELLS (HUVEC). | 226 |
| FIGURE 11. INHIBITORY EFFECTS OF THE ATP AND ADP SCAVENGER APYRASE ON THE YODA1-EVOKED RESPONSE IN HUMAN UMBILICAL VEIN ENDOTHELIAL CELLS (HUVEC). | 229 |
| FIGURE 12. INHIBITORY EFFECTS OF BROAD-SPECTRUM P2 RECEPTORS ANTAGONIST PPADS ON THE YODA1-EVOKED RESPONSE IN HUMAN UMBILICAL VEIN ENDOTHELIAL CELLS (HUVEC). | 231 |
| FIGURE 13. ATP EVOKED DETECTABLE INTRACELLULAR CALCIUM RESPONSES USING THE CALCIUM IMAGING SETUP. | 233 |
| FIGURE 14. SHEAR STRESS STIMULATION ASSAYS USING THE GLYCOTECH PARALLEL FLOW CHAMBER. | 235 |
| FIGURE 15. REPRESENTATIVE TECHNICAL ISSUES WHEN PERFORMING SHEAR STRESS ASSAYS USING THE GLYCOTECH PARALLEL FLOW CHAMBER. | 237 |
| FIGURE 16. SHEAR STRESS STIMULATION ASSAYS USING THE IBIDI μ -SLIDE. | 240 |
| FIGURE 17. SHEAR STRESS STIMULATION ASSAYS IN 3 HOURS-SEEDED HUMAN UMBILICAL VEIN ENDOTHELIAL (HUVEC) CELLS USING THE IBIDI μ -SLIDE. | 241 |
| FIGURE 18. SHEAR STRESS STIMULATION ASSAYS IN 24 HOURS-SEEDED HUMAN UMBILICAL VEIN ENDOTHELIAL (HUVEC) CELLS USING THE IBIDI μ -SLIDE. | 242 |
| FIGURE 19. SHEAR STRESS STIMULATION ASSAYS IN 24 HOURS-SEEDED HUMAN MICROVASCULAR ENDOTHELIAL (HMEC-1) CELLS USING THE IBIDI μ -SLIDE. | 243 |
| FIGURE 20. INVESTIGATION OF CALCIUM-INDUCED RESPONSES FROM RELEVANT AGONISTS IN THE STUDY OF NITRIC OXIDE RELEASE IN HUMAN MICROVASCULAR ENDOTHELIAL CELLS (HMEC-1). | 246 |
| FIGURE 21. ACCUMULATED NITRITE (NO ₂ -) MEASUREMENT UPON DIFFERENT AGONIST STIMULATION IN HUMAN MICROVASCULAR ENDOTHELIAL CELLS (HMEC-1). | 247 |

CHAPTER 4. DISCUSSION.

| | |
|--|-----|
| TABLE 1. COMPOSITION OF GROWTH MEDIA SUPPLEMENT FOR LONZA AND PROMO CELL. | 250 |
| FIGURE 1. PROPOSED PIEZO1 ACTIVATION MECHANISM AND DOWNSTREAM EVENTS UPON SHEAR STRESS STIMULATION. | 252 |
| TABLE 2. PUBLISHED PHYSIOLOGICAL VALUES OF SHEAR STRESS IN DIFFERENT VASCULAR BEDS AND HUVEC CELLS. | 256 |

Abbreviations

| | |
|-----------------------------|--|
| 5-BDBD | 5-(3-bromophenyl)-1,3-dihydro-2H-benzofuro[3,2-e]-1,4-diazepin-2-one |
| AC | Adenylyl Cyclase |
| Ach | Acetylcholine |
| ADP | Adenosine 5'-diphosphate |
| ASIC | Acid-sensing ion channel |
| ATCC | American Type Culture Collection |
| ATP | Adenosine 5'-Triphosphate |
| ATP- γ -S | Adenosine-5'-O-(3-thio-triphosphate) |
| AUC | Area Under the Curve |
| BAY-1797 | N-[4-(3-chlorophenoxy)-3-sulfamoylphenyl]-2-phenylacetamide |
| BSA | Bovine serum albumin |
| BSS | Balanced Salt Solution |
| Ca ²⁺ | Calcium ions |
| CaCl ₂ | Calcium chloride |
| cAMP | Cyclic Adenosine Monophosphate |
| Carbachol | Carbamylcholine |
| Cav-1 | Caveolin-1 |
| cDNA | Complementary deoxyribonucleic acid |
| CO ₂ | Carbon dioxide |
| CRAC | Calcium Release-Activated Calcium channel |
| DAG | Diacylglycerol |
| DMEM | Dulbecco's Modified Eagle Medium |
| dNTP | Deoxynucleotide Triphosphates |
| DTT | Dithiothreitol |
| DSMO | Dimethyl Sulfoxide |
| EAh926 | A human endothelial cell line |
| EBM-2 | Endothelial Basal Medium-2 |
| ECACC | European Collection of Authenticated Cell Cultures |
| EC ₅₀ | Half maximal effective concentration |
| EGF | Epidermal Growth Factor |
| EGM-2 | Endothelial Growth Medium-2 |
| EGTA | Ethylene Glycol Tetraacetic Acid |
| eNOS | Endothelial Nitric Oxide Synthase |
| ER | Endoplasmic Reticulum |
| ERK | Extracellular Signal-Regulated Kinases |
| FBS | Foetal Bovine Serum |
| FIV | Flow-induced vasodilation |
| FURA | Fura-2, a calcium indicator dye |
| G α _{12/13} | G protein subunit alpha 12/13 |
| G α _i | G protein subunit alpha i |
| G α _q | G protein subunit alpha q |
| G α _s | G protein subunit alpha s |
| GPCR | G-protein coupled receptor |
| GsMTx4 | A peptide that inhibits mechanosensitive ion channels |

| | |
|-------------------|---|
| HCl | Hydrochloric Acid |
| HELA | A human cell line derived from cervical cancer cells |
| HEPES | 4-(2-hydroxyethyl)-1-piperazineethanesulfonic acid |
| HMEC-1 | Human Microvascular Endothelial Cells-1 |
| HRP | Horseradish Peroxidase |
| HUVEC | Human Umbilical Vein Endothelial Cells |
| IC ₅₀ | Half maximal inhibitory concentration |
| IL | Interleukin |
| IP3 | Inositol 1,4,5-trisphosphate |
| ICAM-1 | Intercellular Adhesion Molecule 1 |
| iNOS | Inducible Nitric Oxide Synthase |
| IVM | Ivermectin |
| KDa | Kilodaltons |
| LB | Loading Buffer |
| MAPK | Mitogen-Activated Protein Kinase pathway |
| Mg ²⁺ | Magnesium ions |
| MgCl ₂ | Magnesium chloride |
| mRNA | Messenger Ribonucleic Acid |
| MW | Molecular Weight |
| Na ⁺ | Sodium ions |
| NaCl | Sodium chloride |
| NaOH | Sodium hydroxide |
| NFAT | Nuclear Factor of Activated T-cells |
| NO | Nitric Oxide |
| NOS | Nitric Oxide Synthase |
| NRP | Neuropilin |
| ORAI | Calcium release-activated calcium channel |
| P1 | Adenosine receptors |
| P2X | Purinergic Receptor P2X, Ligand-Gated Ion Channel |
| P2Y | Purinergic Receptor P2Y, G-Protein Coupled |
| Pen/Strep | Penicillin/streptomycin antibiotic solution |
| PI3K | Phosphoinositide 3-Kinase |
| PIGF | Placental Growth Factor |
| PIP2 | Phosphatidylinositol 4,5-bisphosphate |
| PKA | Protein Kinase A |
| PKC | Protein Kinase C |
| PLC | Phospholipase C |
| PPADS | Pyridoxal-phosphate-6-azophenyl-2',4'-disulfonic acid |
| PSB-12062 | N-(p-methylphenylsulfonyl) phenoxazine |
| PVDF | Polyvinylidene difluoride |
| RNA | Ribonucleic Acid |
| ROCE | Receptor operated calcium entry |
| ROI | Regions Of Interest |
| RT-PCR | Reverse Transcription Polymerase Chain Reaction |
| SBS | Saline bath solution |
| SEM | Standard error of the mean |
| SERCA | Sarco/Endoplasmic Reticulum Ca ²⁺ -ATPase |

| | |
|---------------|------------------------------------|
| SFM | Serum-Free Medium |
| SOCE | Store-Operated Calcium Entry |
| STIM | Stromal Interaction Molecule |
| siRNA | Small Interfering Ribonucleic Acid |
| SocAMP | Store-operated cAMP signalling |
| TEMED | Tetramethylethylenediamine |
| Tg | Thapsigargin |
| TNF | Tumour Necrosis Factor |
| Tris | Tris(hydroxymethyl)aminomethane |
| TRP | Transient Receptor Potential |
| UDP | Uridine Diphosphate |
| UTP | Uridine Triphosphate |
| VCAM-1 | Vascular Cell Adhesion Molecule 1 |
| VEGF | Vascular Endothelial Growth Factor |
| VRACS | Volume-Regulated Anion Channels |
| vWF | Von Willebrand Factor |

Acknowledgements

I cannot believe this is the ending of my Ph.D. thesis, which is not just mine but a shared effort by those who did not stop supporting me even though I was a permanent drama queen for four years. I am filled with immense gratitude and a deep appreciation for all who contributed to this effort.

First and foremost, I extend my sincerest thanks to my supervisors, Prof. Samuel Fountain and Dr. Stephen Robinson, whose expertise, understanding, and patience added considerably to my graduate experience. Sam, your support and guidance have been the pillars of my research journey. I also want to thank Dr. David Monk for never refusing to help me and extracting the perfect RNA (RIN 10!) with me. Dave, that would not be achievable without your aid. Furthermore, I want to acknowledge the BBSRC Doctoral Training Partnership for funding my research project.

I am profoundly grateful to have shared this experience with my fellows at Fountain Lab, with special thanks to Dr. Anni, Dr. Jess, Dr. Estela, Mich, Kay, and Dan. Your unquestionable support, gossiping moments, the odd tequila shots (with honey), and innumerable scientific dramas made my PhD path extraordinary. If it were not for you, I would not be here, writing my acknowledgments. A special word of thanks goes to my colleagues and friends on the BMRC 02 floor, whose camaraderie and scientific conversations have enriched my academic and personal life—special thanks to Kasia, Perry, Molly-Kay, Dagne, Kelly, Louis, and Roberta. It's not floor 02, but I am immensely grateful also to have Alejandro, Sergio, Margeoux, Marina, Gaia, Martina, and all my Norwich Spanish crew (Maria Chudi, Carlos, Hector, and Jose).

My heartfelt appreciation goes to my family, especially my parents and brother, for their unwavering love. To be honest, there is only one relevant data point in this thesis, and it is that you, Jose, are still here to read it. It also goes to you, Gonzalo, my best friend, love, and partner in crime. I could not imagine a better person to walk this path with me. Thanks for always believing in me and joining me on this travel, one of the many we will do (Should I mention Trello training?). *Graciès Rita, t'estimo molt.*

Finally, to my Spanish friends and my chosen family, thank you for your constant encouragement and for being there through the highs and lows of this journey. However, with the reader's pardon, this paragraph should be continued in Spanish/Galician. Síntome agradecida por haber encontrado familia en cada lugar no que vivín. De Boiro, Jacobo, Tamara, Sara e Lara, gracias por ser os de sempre e para sempre, o voso apoio é incondicional e sen vós non sería a casi doutora que son hoxe. De Madrid, Ana, Rebe, Cobo y Borja, sois los amigos que cualquiera desearía, no solo en su doctorado, sino en su vida. Gracias por estar con la calidad que lo hacéis. Familia Muñiz Duque, gracias por acompañarme en todas mis aventuras de Willy Fog y ser parte de mi familia. De Barcelona, Juli, Marina, Nat, Pol, Vicky, Iván, Inés, Mercè y no acabaría de nombrar. Infinitas gracias por todo lo compartido y aprendido, la científica que soy es gracias a haber compartido parte de mi experiencia con vosotros, junto con algún que otro perreito hasta el suelo. Os quiero. De Norwich, para mis *Spanish speakers*, Anna y Estela, habéis sido refugio y familia, junto con las otras bebés, *the best life bubble* que podría imaginar.

Facendo e desfacendo vai a meniña aprendendo.
- Galician proverb ("The girl learns by doing and undoing").

Chapter 1. Introduction.

1.1 The endothelium.

The vascular system is the first organ to develop during embryogenesis, and it consists of blood and lymphatic vessels that facilitate blood and lymph flow throughout the body (Risau et al., 1995). There are three types of blood vessels: arteries, veins, and capillaries. Arteries and veins convey large volumes of blood between organ systems. These larger blood vessels branch into progressively smaller vessels to regulate local blood pressure and volumetric flow within the tissues and cells of each organ system. Capillaries, the smallest and most densely distributed vessels, are specialized in directly exchanging fluids with cells deep within tissues. While large and small vessels have specialized functions, they coordinate to maintain homeostasis throughout the body (Barrs et al., 2020). Although they performed discrete physiological functions, the majority of vasculature is divided into three histological layers: the intima (the inner), the tunica media (the middle), and the tunica externa (the outer layer) (**Figure 1-a**). The intima comprises endothelial cells, the first point of contact between blood and vasculature cells, which detect mechanical, metabolic, and immunological signals in their surroundings through specific receptors (Cabou et al., 2022; Reinhart-King et al., 2008). These interactions between blood flow and endothelial cells trigger biochemical and mechanical responses in the endothelium, which are crucial for controlling vascular tone, blood pressure, immune cell recruitment during inflammation, angiogenic sprouting and vascular permeability (Cabou et al., 2022; Félétou, 2011; Polk et al., 2022). Depending on whether the interactions occur in a healthy or diseased state, they can either protect or alter the vessel wall. Factors such as high LDL-cholesterol, elevated triglyceride levels, diabetes, obesity, arterial hypertension, inflammation, and a sedentary lifestyle contribute to endothelial dysfunction, potentially leading to cardiovascular disease development (Cabou et al., 2022). A functional endothelium is typically silent with a non-adhesive surface for the passing blood flow. However, once a disruption of homeostasis occurs, the production of antithrombotic mediators decreases, leading to an activation of the endothelium. This activation is necessary for many processes, such as leukocyte adhesion during wound healing, but a continuous activation of endothelial cells can result in atherosclerosis. In addition to the prothrombotic disease states, endothelial dysfunction has also been linked with proinflammatory diseases. Then, vascular homeostasis and improvement of diverse cardiovascular pathologies depend on endothelium activity (Davies, 2009; Reinhart-King et al., 2008).

The vascular intima is formed by endothelial cells connected to an 80-nm-thick basal lamina and has a body surface area of 3000-6000 m² with approximately 1 to 6 x 10¹³ endothelial cells (Félétou, 2011; Krüger-Genge et al., 2019). This basal lamina is a crucial part of blood vessels, acting as the framework for arteries, veins, and capillaries. Inside this framework, endothelial cells form a lining, while smooth muscle cells or pericytes (capillaries, venules) cover the outside (Félétou, 2011). Pericytes are fibroblast-like cells with long extensions of their cytoplasm that surround endothelial cells in small vessels (Herndon et al., 2017). Endothelial cells can produce almost all the basal lamina proteins and generate enzymes essential for remodelling. This remodelling is significant for the flexibility of blood vessels and angiogenesis (Félétou, 2011). Endothelial characteristics are consistent between arteries and veins, showing

continuous cells and a thick monolayer, while in capillaries, the organ looks thin and fenestrated, allowing an easy exchange of metabolites and gases (Sandoo et al., 2010). Endothelial cells exhibit different shapes throughout the vascular system but typically have a thin and slightly elongated form. Their dimensions are approximately 50–70 micrometres in length, 10–30 micrometres in width, and 0.1–10 micrometres in thickness. Within the blood vessel wall, these cells are polarized and align along the vessel's axis, which helps minimize the shear stress forces the flowing blood applies. They have an apical membrane in direct contact with blood and circulating cells and a basolateral surface in contact with the basal lamina (Félétou, 2011; Krüger-Genge et al., 2019). The glycocalyx shields the apical surface of endothelial cells, consisting of an anionic grid of glycosaminoglycans, glycoproteins, and glycolipids anchored to the cell membrane. This hair-like resemblance layer plays a role in regulating access to the cell membrane by acting as a semi-permeable barrier, and it allows selective transport of large molecules, fluids, and cells, contributing to mechanotransduction and vascular signalling processes (Banerjee et al., 2021; Fu et al., 2022). The morphological characteristics suggest that endothelial cells serve as a specialized site for exchange and transfer. Nevertheless, it is crucial to note that vascular endothelial cells exhibit morphology, physiology, and phenotype variations (Félétou, 2011).

Endothelial cells share a standard set of functions but exhibit significant plasticity in function depending on the vascular bed in which they reside. For example, blood-brain barrier endothelial cells have different functions than those lining the aorta. However, there are conserved molecular mechanisms governing general endothelial function. One of the most critical ones is the nitric oxide signalling pathway due to the potent vasodilatory, anti-inflammatory, and antioxidant properties of nitric oxide, which supports vascular homeostasis (Cyr et al., 2020). Diseases like hypertension, atherosclerosis, and disorders linked to angiogenesis are accompanied or even preceded by anomalies in its production and/or bioavailability. Additionally, NO performs physiological tasks in the neurological and immunological systems, helping to control behaviour, gastrointestinal motility, and tumour and infectious disease defence mechanisms (Zhao et al., 2015). Nitric oxide (NO) can be synthesized by three different types of nitric oxide synthase enzyme (NOS) in the body: the neuronal NOS (nNOS), the inducible NOS (iNOS), and the endothelial NOS (eNOS). However, NO regulation in endothelial cells is more prominently driven by eNOS, a calcium concentration-dependent enzyme activating calcium-activated calmodulin, which modulates its activity and homodimerization. Nitric oxide is mainly synthesized from L-arginine, whose oxidation needs homodimerization of eNOS monomers to catalyse this reaction (Arnau del Valle et al., 2022; Cyr et al., 2020). Its production is usually coupled with intracellular calcium concentrations, but other mechanisms alternatively boost or modulate eNOS activity. eNOS Ser1177 residue phosphorylation leads to a higher calcium sensitivity, which is led by various protein kinase activation pathways, such as VEGF, estrogen, insulin, or shear stress activity. Additionally, under resting conditions, eNOS Thr495 residue phosphorylation by protein kinase C (PKC) can limit calmodulin binding to eNOS and slow NO production. Consistently, dephosphorylation of this residue occurs upon stimulation of intracellular calcium influx mechanisms in endothelial cells (Cyr et al., 2020). By releasing endothelium-derived NO, which activates various effectors in vascular smooth muscle cells to mediate blood vessel dilatation, the endothelium plays a modulator role in regulating blood vessel diameter. In general terms, NO diffusion to smooth muscle cells evokes a series of events leading to a decrease of the free cytosolic calcium through various mechanisms which will ensue in the relaxation of the smooth

muscle cells. These numerous mechanisms include calcium removal from the cell, reuptake into the sarcoplasmic reticulum, and activation of calcium-activated potassium channels. A soluble guanylyl cyclase (sGC) in the cytoplasm of the smooth muscle cells initiates these mechanisms. This guanylyl cyclase will catalyse the conversion of guanosine triphosphate to cyclic guanosine monophosphate, which, in turn, will activate the protein kinase G (PKG). Activation of PKG will lead to a reduction of the cytoplasmic calcium levels of the smooth muscle cells as well through the mentioned mechanisms as well as decreasing the myosin light-chain kinase activity, which also promotes relaxation. On the contrary, blood vessel contraction would involve mechanisms increasing the intracellular calcium concentration in the cytosol in smooth muscle cells (Zhao et al., 2015).

A well-defined nitric oxide production in the endothelium is due to shear stress-dependent-calcium signalling, known as flow-induced vasodilatation (FIV). By increasing shear stress, the concentration of intracellular calcium ($[Ca^{2+}]_i$) increases in the cytosol, leading to the activation of eNOS and, therefore, the production of nitric oxide. As previously described, NO travels from the endothelium to the smooth muscle, causing relaxation and dilatation of the vessels. Once the intracellular calcium increases, the calcium-activated potassium channels open, causing hyperpolarization of the endothelium and the smooth muscle, producing a more robust relaxation of the smooth muscle cells (**Figure 1-b**) (Gerhold et al., 2016). Thus, controlling the intracellular calcium concentration is crucial for regulating vascular tone in both endothelial and smooth muscle cells.

However, the endothelium produces other endothelial factors than nitric oxide that regulate vascular homeostasis. Endothelin, prostacyclin, and the endothelium-derived hyperpolarising factor (EDHF) are some of those relevant endothelial mediators. Endothelin-1 is a vasoconstrictor peptide that binds the endothelin receptors on the smooth muscle cells, increasing vascular resistance and facilitating vasoconstriction. This peptide has also been shown to modulate prostacyclin (PGI₂), an endothelial factor with vasodilatory effects (Victorino et al., 2004). This factor promotes cyclic adenosine monophosphate, therefore leading to vessel relaxation (Webb et al., 1993). The endothelium-derived hyperpolarising factor (EDHF) is also essential to endothelial function. The role of EDHF is to support vasodilation, as in the case of NO and PGI₂. Its role becomes more meaningful when the other vasodilation pathways have been impaired (Lenasi et al., 2008). All these endothelial factors regulate the vascular tone and are necessary to maintain a healthy endothelium. Their study and function are also critical to understanding the different pathological processes that are endothelial-dependent.

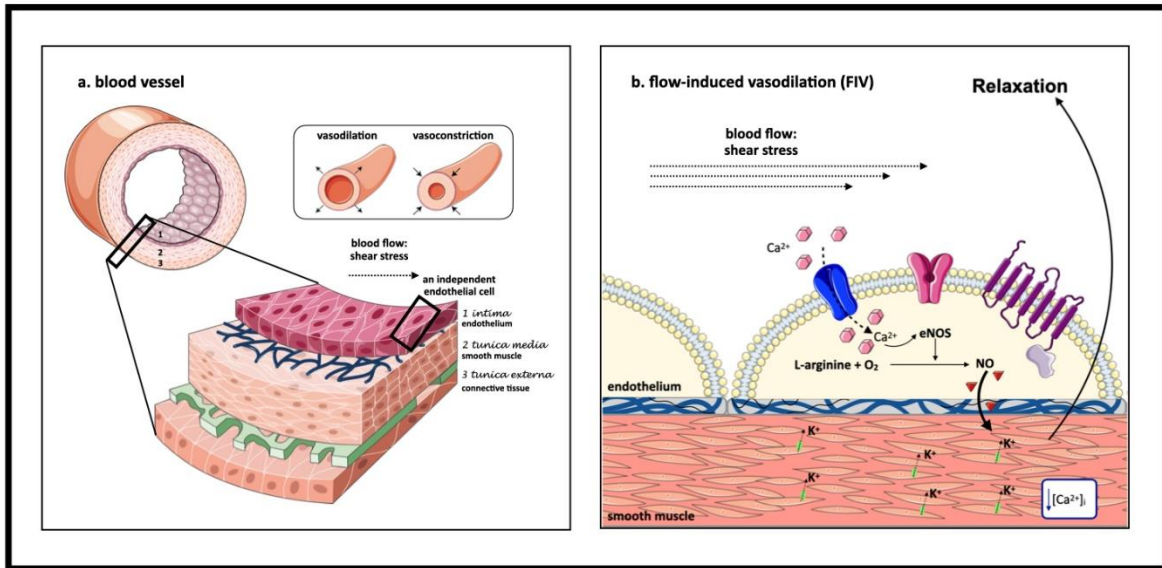


Figure 1. The structure of a vessel wall and the endothelium. **a.** The vessel wall is divided into three main layers, and the endothelium is in direct contact with the blood flow shear stress-induced, mediating processes such as vasodilation or vasoconstriction. **b.** In vascular endothelial cells, calcium influx to the intracellular milieu in response to shear stress increases eNOS activity. This leads to the boosted production of nitric oxide, which diffuses into smooth muscle cells, causing them to dilate and blood pressure to decrease. (Parts of the figure were drawn by using pictures from Servier Medical Art. Servier Medical Art by Servier is licensed under a Creative Commons Attribution 3.0 Unported License (<https://creativecommons.org/licenses/by/3.0/>)).

1.2 Calcium signalling in the endothelium.

Calcium (Ca^{2+}) ions serve as widespread intracellular second messengers, handling various cellular functions such as contractile and secretory activities, cell differentiation, migration, angiogenesis, cell death, and neurotransmission (Berridge et al., 2003; Tsai et al., 2015). Basal or resting cytosolic calcium levels are around 100 nM, significantly increasing upon external stimulation, reaching peak levels at 1 μM . Cytosolic calcium ion signals exceeding 1 μM have been observed on average, but these substantial increases are typically associated with cellular damage and are considered outside the physiological range (Berridge et al., 2003; Berridge et al., 2000; Bootman et al., 2001). It is necessary to highlight that at the opening of an active calcium channel, the calcium concentration can exceed 100 μM . These localized high-concentration areas are determined as having signalling functions (termed Ca^{2+} signalling microdomains) because specific calcium-sensitive effectors near these regions offer a mechanism for brisk and precise cellular responses (Bootman et al., 2020). Cells can be stimulated through various means, including hormonal, neurotransmitter, growth factor, antibody, mechanical, electrical, gasotransmitter, temperature, pH change, osmotic change, cytotoxic reagents, microbial invasion, and the passage of cellular signals through gap junctions. All these stimuli have been demonstrated to increase the cytosolic concentration of calcium ions. A fundamental concept in calcium signalling is that any alteration in the intracellular Ca^{2+} concentration triggers a cellular response. A fine tune exists of the magnitude of calcium rise in the cytosol to control the occurrence and magnitude of calcium-dependent physiological events because excessive, insufficient, or inappropriate calcium ion signalling will inevitably impact cell behaviour and determine its fate (Berridge et al., 2003; Berridge et al., 2000; Bootman et al., 2020; Bootman et al., 2001), the resting calcium concentration might also serve as a signalling mechanism without an increase in calcium ion levels. This is because some cellular processes are hindered when there is a rise in cytosolic calcium concentration (Bootman et al., 2001).

Intracellular calcium levels can increase for two reasons: calcium influx from the extracellular space or calcium release from intracellular stores (Bootman et al., 2001). Calcium influx from the extracellular space, also known as calcium entry, is characterized by the activity of different ion channels that allow ion exchange between the intracellular and the extracellular milieu. Broadly, ion channels are macromolecular pores embedded in the plasma membrane whose response is called gating, which is defined by the opening or closing of the pore (Hille et al., 2012). Different types of ion channels depend on their stimulus-responding mechanism: mechanosensitive ion channels, voltage-gated ion channels, ligand-gated ion channels, and store-operated calcium channels. Firstly, mechanosensitive ion channels respond to cell deformation. Secondly, voltage-gated ion channels are activated by depolarisation of the plasma membrane, while the third, ligand-gated ion channels, allow the passage of ions across the cell membrane in response to a ligand. The last, store-operated calcium channels open upon depletion of intracellular stores (Bootman et al., 2020).

On the other hand, calcium release from the intracellular stores occurs through channels across organelles' membranes, predominantly involving inositol 1,4,5-trisphosphate (IP3) receptors, a product formed together with diacylglycerol (DAG) by the hydrolysis of phosphatidylinositol 4,5-bisphosphate (PIP2) by activation of phospholipase C (Berridge, 1993; Berridge et al., 2003). This mechanism is shared by nonexcitable and excitable cells. IP3Rs-

dependent calcium release occurs from the endoplasmic reticulum (ER), Golgi, and nuclear envelope, and it also activates a limited number of IP3Rs located at the plasma membrane. IP3 is caused in response to various stimuli, such as hormones, growth factors, and neurotransmitters, which bind to cell-surface receptors like G-protein-coupled receptors or receptor tyrosine kinases. The application of these stimuli typically triggers rapid intracellular calcium signals within a few seconds. In addition to IP3 production, DAG is produced and retained within the cell membrane, activating protein kinase C (PKC), which can cooperate with calcium signalling or yield extracellular messengers such as arachidonic acid. Although IP3Rs are the primary mediators of this release, other channels are contributing, such as ryanodine receptors, two-pore channels, and the mucolipin subfamily of transient receptor potential channels (TRPML). Furthermore, even though the ER is the major player in intracellular store calcium signalling, other organelles contribute to this mechanism, including apart from the already mentioned lysosomes, peroxisomes, acidic organelles, and mitochondria (Bootman et al., 2020).

The cells also need different mechanisms to rapidly remove calcium from the cytosol to prevent ion overload, return calcium concentration to resting levels, and maintain cell homeostasis. These mechanisms consist of several pumps, exchangers, and buffers that facilitate calcium extrusion or sequestration at the cell membrane (ex., plasma membrane Ca^{2+} -ATPases, $\text{Na}^+/\text{Ca}^{2+}$ exchanger) and the endoplasmic reticulum (ex., endoplasmic reticulum Ca^{2+} -ATPase pump) (Berridge et al., 2003; Berridge et al., 2000; Brini et al., 2011; Hajnóczky et al., 2003; Periasamy et al., 2007).

Entry and removal of calcium mechanisms are common to all cell types. However, depending on the cell bed, they are discretely modulated and expressed to generate characteristic calcium signalling and cellular outcomes. That is also the case for endothelial cells, whose functionality is significantly influenced by alterations in intracellular calcium concentration.

Alterations in intracellular calcium concentration ensue in response to receptor activation to different agonists (acetylcholine, adenosine triphosphate (ATP), bradykinin, VEGF, among others) and mechanical stimuli, with shear stress being particularly significant for endothelial cell physiology (Félétou, 2011). Additionally, alterations in intravascular pressure, mechanical scraping, and heat can elicit endothelial calcium responses (Moccia et al., 2023). Intracellular calcium increases evoked by agonists generally follow a biphasic pattern, involving an initial phase of calcium release from intracellular stores, largely the endoplasmic reticulum, followed by calcium entry. This is because calcium stores reduction in the endoplasmic reticulum, triggered by receptor stimulation, leads to an elevation in intracellular calcium concentration by activating store-operated calcium entry (SOCE) channels and receptor-operated calcium channels (ROCE). The molecular composition of ROCE and SOCE channels in endothelial cells likely includes transient receptor potential (TRP) channels and the interaction of the stromal interaction molecule (STIM) and Orai proteins, respectively (Félétou, 2011). Furthermore, the entry of calcium ions induced by agonists in endothelial cells may be facilitated by purinergic ionotropic receptors, including P2X receptors and N-methyl-D-aspartate receptors. Calcium mobilisation from the endoplasmic reticulum involves binding agonists to $\text{G}\alpha_q$ -protein coupled receptors or tyrosine kinase receptors on the cell membrane. These receptors are linked to distinct isoforms of phospholipase C, $\text{PLC}\beta$, and $\text{PLC}\gamma$. In the endothelial lineage, IP3 receptors are the predominant family of endoplasmic Ca^{2+} -releasing channels, and three IP3R isoforms,

including InsP3R1, InsP3R2, and InsP3R3, are expressed in vascular endothelial cells (Moccia et al., 2023). Piezo1, a mechanosensitive ion channel, mainly mediates calcium influx upon mechanical stimulation in endothelial cells. However, the role of $G\alpha_q$ -coupled receptors in this process and the contribution of calcium mobilisation from the endoplasmic reticulum have also been described (Sathanoori et al., 2017; Wang et al., 2016; Wang et al., 2015).

Endothelial calcium signalling mediates many cardiovascular functions, such as vasodilation, vascular resistance and permeability, coagulation, leukocyte transmigration, and angiogenesis, and a minimal dysregulation of this signalling can cause significant human diseases, such as atherosclerosis, type 2 diabetes, obesity, hypertension, and cancer (Moccia et al., 2023). Vasodilation is one of the most studied functions regulated by endothelial calcium signalling, as previously mentioned, increasing blood vessel diameter through stimulation of nitric oxide production. It is relevant to mention that small resistance vessels usually benefit from downstream endothelium-dependent hyperpolarization (EDH) via Ca^{2+} -activated K^+ channels to mediate vasodilation than other vascular beds. Flow-induced vasodilation is a shear stress-dependent calcium signalling mechanism, and it is believed to be mediated principally by the mechanosensitive channel Piezo1 but not only as the role of the transient receptors potential vanilloid 4 (TRPV4), two purinergic receptors, one ionotropic P2X4, and other metabotropic P2Y2, have also been pointed as mediators of this mechanism (Ottolini et al., 2021; Swain et al., 2021; Wang et al., 2016; Wang et al., 2015; Yamamoto, Korenaga, Kamiya, Ando, et al., 2000; Yamamoto, Korenaga, Kamiya, Qi, et al., 2000). The following sections will further explore the different contributions and known facts about the endothelial role of the cited membrane receptors.

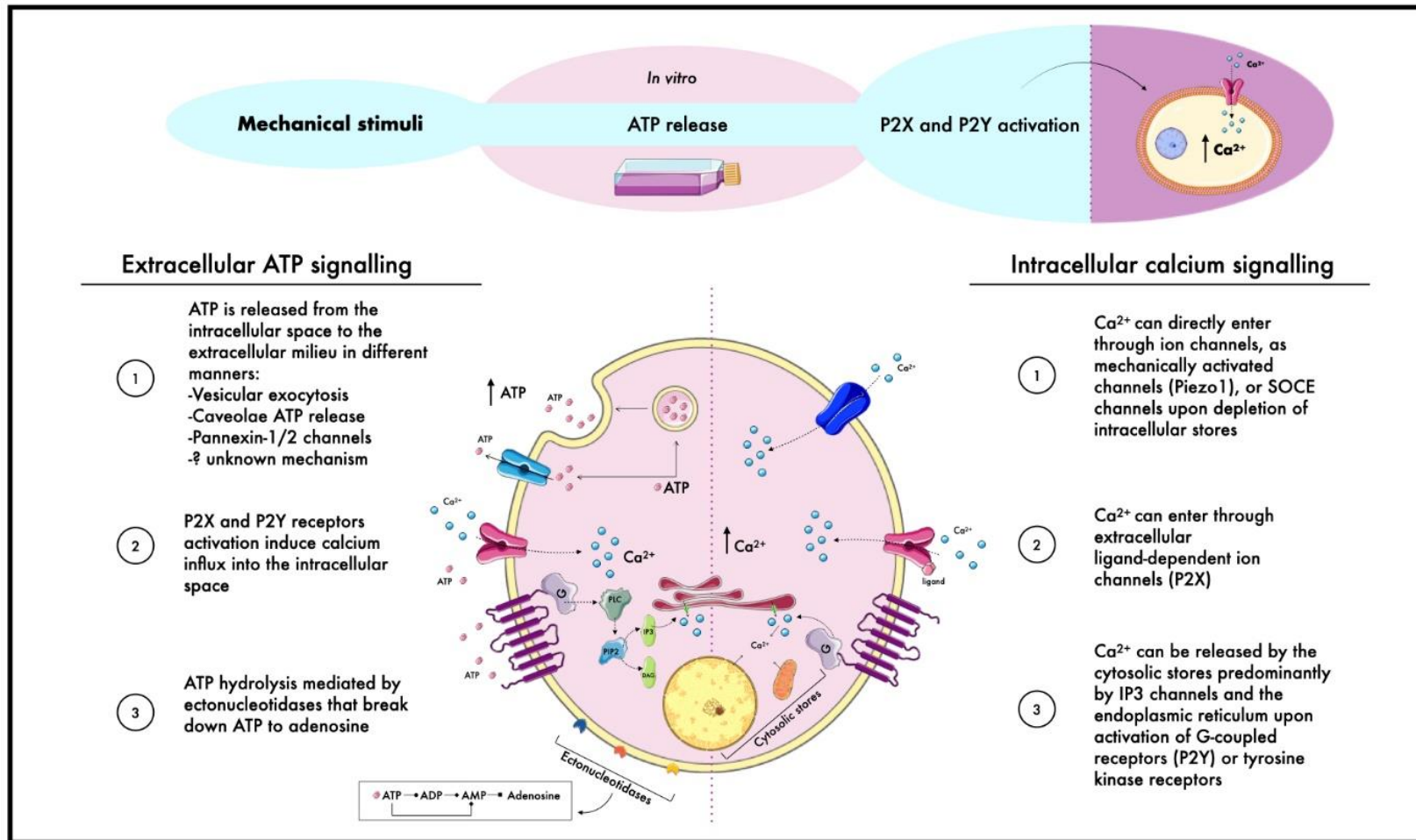


Figure 2. Activation of the purinergic and calcium signalling. *Up.* Effects of mechanical stimuli in the purinergic signalling. *Down.* (Left) Activation of purinergic signalling results in calcium signalling. Three critical components of extracellular ATP signalling and (Right) the three typical intracellular calcium signalling mediators. (Parts of the figure were drawn by using pictures from Servier Medical Art. Servier Medical Art by Servier is licensed under a Creative Commons Attribution 3.0 Unported License (<https://creativecommons.org/licenses/by/3.0/>)).

One of the other most investigated processes in endothelial cells is angiogenesis, a calcium-tuned process. Angiogenesis is a vital process during development. In adults, blood vessels remain resting and quiescent. However, angiogenesis continues to sustain healthy physiological functions and reestablish blood vessels in tissues after injury, in conditions like diabetic retinopathy, or during tumour growth (Folkman, 1989; Karamysheva, 2008; Moccia et al., 2023; Otrrock et al., 2007). The vascular endothelial growth factor (VEGF), considered the primary driver of angiogenesis, can trigger diverse calcium signalling to regulate different steps of the angiogenic response. VEGF evokes calcium signalling in endothelial cells by binding to VEGFR-2, which in turn will induce calcium release from stores via IP3Rs and store calcium operated calcium entry (SOCE), and also possibly by some lysosomal contribution via two-pore channel 2 (TPC2). VEGF can cause specific calcium ion patterns, known as calcium signatures, which can trigger diverse cellular responses, either cell proliferation or migration, by recruiting different calcium-sensitive decoders. Thus, endothelial calcium signalling can modulate endothelial cell functions by recruiting different effectors, evoking selective vascular responses (Moccia et al., 2019; Moccia et al., 2023).

The endothelium is vital as a semipermeable barrier between the blood and the interstitial compartments. However, the inflammatory state modifies the permeability of this barrier, allowing the entry of plasma proteins into the surrounding tissues and contributing to vascular leakage (Filippini et al., 2019). Barrier function can be affected during an acute injury by the release of inflammatory mediators (histamine, bradykinin, thrombin, eicosanoids, leukotrienes, or prostaglandins) that could lead to an intracellular calcium influx by binding receptors on the endothelial cells. VEGF has also been directly implicated in regulating cell permeability through a calcium-dependent pathway. For example, bradykinin and thrombin can activate TRPC6, which is believed to be a determinant for increasing permeability during inflammation. Another example can be that histamine also triggers a calcium-dependent rise in endothelial permeability, and the loss of barrier function induced by histamine is linked to VE-cadherin disassembly. VE-cadherin phosphorylation and disassembly weaken adherens junctions, allowing endothelial cells to separate and forming paracellular gaps that enhance permeability. Thus, inflammatory mediators evoked calcium signalling cause the disassembly of adherens junctions and rearrangements in the cytoskeleton, facilitating endothelial cell retraction and increased permeability (Dalal et al., 2020; Filippini et al., 2019). Endothelial cells are key in the inflammatory process, responding to proinflammatory triggers like lipopolysaccharide (LPS), interleukin 1 α (IL-1 α), and tumour necrosis factor (TNF). TNF operates by binding to TNF receptors (TNFR) 1 and 2. In endothelial cells, the release of soluble TNFR1 is calcium-dependent and crucial for regulating TNF-induced signalling, highlighting the precise control of intracellular calcium concentration in modulating this inflammatory response of the endothelium. Finally, in this concern, TNF α can boost endothelial cells to release multiple cytokines and promote the expression of adhesion molecules, including vascular cell adhesion molecule-1 (VCAM-1) (Xia et al., 1998). VCAM-1, in turn, initiates the recruitment of circulating monocytes, playing a pivotal role in the initial stages of atherosclerosis (Filippini et al., 2019).

1.3 Calcium signalling toolkit in the endothelium.

The calcium signalling toolkit encompasses all the calcium transporters (channels, pumps, and exchangers), calcium-binding proteins, and calcium-dependent effectors found in nature. Cells selectively express components from this extensive toolkit that align with their specific functions (Bootman et al., 2020). Therefore, understanding the calcium signalling toolkit in endothelial cells, which plays a crucial role in a vast range of endothelial functions, is crucial for gaining insights into the intricate signal transduction processes mediated by different receptors and ion channels in this cell type. Comprehending the primary mediators of physiological and pathological endothelial mechanisms is critical to developing modulators of these proteins, which could benefit the health of millions of people. In this section, we will introduce different ion channels and membrane receptors in the scope of our investigation, keeping in mind that the central target is the purinergic receptors. We will also dig into other significant players relevant to understanding the current literature on endothelial calcium homeostasis and the different flanks of our study.

1.3.1. Purinergic signalling and its role in the endothelium.

Adenosine 5'-triphosphate (ATP) is acknowledged for its crucial role in cellular metabolism, serving as a universal enzyme cofactor during biosynthesis and as a source of cellular energy. Professor Geoffrey Burnstock proposed fifty years ago the concept of ATP and extracellular nucleotides functioning as signalling molecules in the purinergic nerve hypothesis (Burnstock, 1977). However, despite previous corroborative evidence (Drury et al., 1929; Emmelin et al., 1948; Holton & 1959; Paton et al., 1963), this concept remained controversial for many years. Nowadays, purine nucleotides and nucleoside signalling have been recognized for a long time. Nonetheless, the hypothesis was not entirely accepted until the receptors were cloned and characterised in the early 1990s (Burnstock, 2006).

ATP is a nonadrenergic-noncholinergic cotransmitter in nerves of the peripheral nervous and central nervous system, acting as a neurotransmitter, neuromodulator, and neurosecretory. In addition, extracellular ATP acts as an autocrine or paracrine signal regulating cellular functions and the communication between neighbouring cells by activating P2 receptors (**Figure 2**) (Gerhold et al., 2016). Despite this, ATP molecules are both large and negatively charged, limiting their simple diffusion across the plasma membrane. In some cases, ATP is uncontrolled released into the extracellular milieu, such as injury to endothelial and smooth muscle cells in the vessel wall, causing homeostatic dysregulation and pathologic purinergic signalling (Cook et al., 2002). In physiological conditions, ATP is constitutively released into the extracellular space, participating in autocrine regulatory signalling (Lazarowski et al., 1995). There are different mechanisms by which ATP can be released in different cell types, such as exocytosis, through ATP-permeable ion channels and transporters, including connexin hemichannels, pannexin channels, calcium homeostasis modulator 1 (CALHM1), volume-regulated anion channels (VRACs), and maxi-anion channels (MACs) (Taruno, 2018; Yegutkin, 2014). P2X7 receptors have been suggested as potential ATP-release channels, but research has been challenging due to the simultaneous activation by ATP itself (Johnsen et al., 2019). In endothelial cells, under mechanical deformation, ATP is released from the intracellular space into the extracellular milieu (Bodin et al., 1991; Burnstock et al., 2014; John et al., 2001; Lohman et al., 2012; Wang et al., 2016; Wang et al., 2015; Wei et al., 2019; Yamamoto et al.,

2011). However, the molecular mechanism that detects the force and mediates, in turn, the release of ATP, needs to be better defined. Vesicular exocytosis and caveolae ATP release have been suggested to mediate ATP release in endothelial cells (Burnstock et al., 2014; Yamamoto et al., 2011), and Wang et al. portrayed pannexin-1/2 channels involvement partially mediating Piezo1 dependent ATP release. However, the release of ATP persisted when genetically muting the pannexin channels. Therefore, there is still some unknown mechanism mediating this ATP release.

Once released to the extracellular milieu, ATP can selectively bind receptors of the P2 receptor family. P2 receptors are among the two groups into which purinoreceptors are divided: those binding purine and pyrimidine nucleosides (P1 receptors) and those binding purine and pyrimidine nucleotides (P2 receptors) (Burnstock et al., 2014) (**Figure 3-a**). These two families have been extensively involved in different endothelial processes, and they will be further discussed in the following sections.

1.3.1.1 P1 receptors.

P1 receptors are considered adenosine G protein-coupled receptors and are divided into four subtypes: A1, A2B, A2B, and A3. Like other G protein-coupled receptors, P1 receptors display seven putative transmembrane spanning regions, with the N-terminus positioned on the extracellular side and the C-terminus on the cytoplasmic side of the membrane. The residues within the transmembrane domains of P1 receptors are implicated in ligand binding, while the intracellular loops of each segment can associate with the respective G protein (Burnstock, 2007). The adenosine receptors are differently G protein coupled. While A1 and A3 couple to a $G\alpha_i$ protein, A2A, and A2B couple to $G\alpha_s$ proteins. $G\alpha_i$ proteins prevent the formation of cyclic adenosine 5'-monophosphate (cAMP), and, on the contrary, $G\alpha_s$ -coupled P1 receptors promote its formation upon adenosine stimulation. The adenosine receptor A2B is the only one that can promiscuously couple to different G proteins, including $G\alpha_i$ and $G\alpha_q$, apart from the already mentioned (Müller et al., 2020). Therefore, it can also induce calcium increase when stimulated.

Adenosine is a purine nucleoside composed of the nucleobase adenine linked to a sugar ribose through a glycosidic linkage (**Figure 3-b**). It is a regular cellular component continuously produced intracellularly and extracellularly. The primary origin of extracellular adenosine is derived from intracellular nucleotides, including ATP, AMP, and ADP, which are released during stress, hypoxia, inflammation, or injury. Different ectonucleotidases can break down ATP and ADP to AMP, followed by an ultimate step involving the dephosphorylation of AMP to generate adenosine. The endothelium powerfully expresses the ectonucleotidase CD39, which mediates the first hydrolysis from ATP to AMP (Effendi et al., 2020).

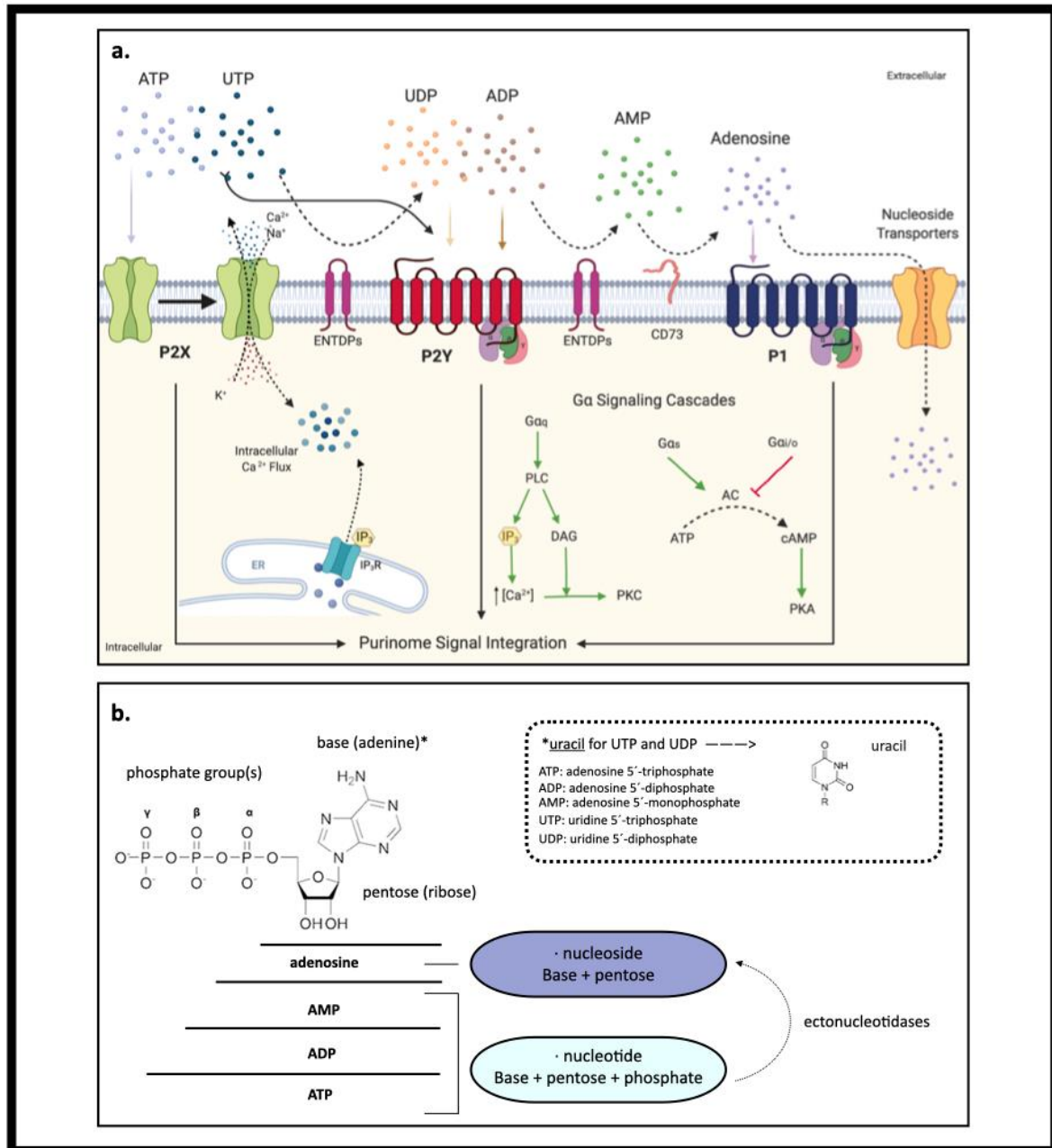


Figure 3. P1, P2X, and P2Y receptors' intracellular signalling pathways and agonists. a. Nucleotides are released into the extracellular space and can bind to P2X and P2Y receptors. They can be enzymatically broken down by ectonucleotidases (ENTDP, CD73) into intermediate metabolites and nucleosides, such as adenosine, that can bind to adenosine receptors (P1). ATP can activate P2X receptors, allowing the entry of Ca²⁺ and Na⁺ ions into the cell, and P2Y receptors, initiating the calcium release from the intracellular stores. Both P1 and P2Y receptors are G protein-coupled and initiate different downstream effects depending on the specific G-protein that binds to them. **b.** General structure of nucleotides and nucleosides agonising purinergic receptors. The main difference between them is, as is represented, that nucleosides are just composed of the sugar (ribose) and the base (adenine or uracil, depending on the receptor to stimulate). At the same time, the nucleotide contains an n number(s) of phosphate groups (n= 1, 2,3). Image **a** obtained from Woods et al, 2021. (Parts of the figure **b** were drawn by using pictures from Servier Medical Art. Servier Medical Art by Servier is licensed under a Creative Commons Attribution 3.0 Unported License (<https://creativecommons.org/licenses/by/3.0/>)).

Adenosine receptors have been shown to be part of the calcium toolkit in endothelial cells in different human models. A2B and A2A receptors have been preferentially reported to be expressed in endothelial cells (Feoktistov et al., 2002; Feoktistov et al., 2004; Lang et al., 2023; Olanrewaju et al., 2000; Tabrizchi et al.), while others reported the four adenosine receptors to be expressed (Deguchi et al., 1998; Fernandez et al., 2012). Some authors reported A2B mediation in VEGF-A upregulation *in vitro* and their role in wound angiogenesis mechanism (Du et al., 2015; Feoktistov et al., 2002; Feoktistov et al., 2004; Ryzhov et al., 2007). Additionally, activating A2A adenosine receptors inhibits the expression of VCAM-1. Moreover, the activation of both A2A and A2B has been linked to a reduction in the permeability of vascular endothelium, suggesting they play a crucial role in preventing and mitigating the inflammatory process of endothelial cells (Blackburn et al., 2009). The release of NO by human endothelial cells has been proposed to contribute to the vasodilator effect of adenosine, as well as the suggestion that cytokines may influence the expression of A2A and A2B adenosine receptors in human endothelium (Burnstock et al., 2014).

1.3.1.2 P2 receptors.

Nucleotides, instead of nucleosides, trigger P2 receptors that are subdivided into two subfamilies named P2X and P2Y receptors (Burnstock et al., 2011). Their sequence homology, topology, and pharmacological profile decided their classification. P2X receptors are ionotropic receptors, while P2Y receptors are metabotropic receptors, sharing with P1 receptors their G protein-coupled receptor nature (Miras-Portugal et al., 2020; Stokes et al., 2017). Ectonucleotidases carefully regulate the concentration of extracellular nucleotides within the physiological nanomolar (nM) to the low micromolar (μ M) range (Woods et al., 2021).

1.3.1.2.1 P2Y receptors.

P2Y receptors are eight metabotropic receptors (P2Y1, P2Y2, P2Y4, P2Y6, P2Y11, P2Y12, P2Y13, P2Y14) associated with different G protein subtypes, providing diverse second messenger system mechanisms upon activation. The first four receptors and P2Y11 were named P2Y1-like receptors (P2Y1, P2Y2, P2Y4, P2Y6, P2Y11) and are primarily linked to $G\alpha_q$ protein. On the other hand, there are the denominated P2Y12-like receptors (P2Y12, P2Y13, P2Y14) mainly coupled to $G\alpha_i$ protein. P2Y1-like $G\alpha_q$ -coupled receptors will act through the PLC β /IP3/DAG pathway, increasing intracellular calcium concentration and activating protein kinase C. On the other hand, P2Y12-like $G\alpha_i$ -coupled receptors, whose activation inhibits adenylyl cyclase activity, decrease intracellular cAMP concentration (Alexander et al., 2019; Woods et al., 2021). The only P2Y promiscuously coupling with $G\alpha_s$ proteins, in addition to the $G\alpha_q$ protein, as mentioned earlier, is P2Y11. That allows the receptor to activate either adenylyl cyclase or PLC β pathways (Kennedy, 2017). P2Y2 and P2Y6 can also couple to $G\alpha_{12/13}$, leading to Rho activation (Alexander et al., 2019; Woods et al., 2021) (**Table 1**). P2Y receptors have seven potential transmembrane-spanning regions, as explained for P1 receptors. The N-terminus of the receptor is located on the extracellular side of the membrane, while the C-terminus is on the cytoplasmic side. The transmembrane domain residues contain the ligand binding pocket, and the intracellular loops enable the corresponding G protein coupling (Erb et al., 2012).

Their preferred agonists can also subdivide them, as P2Ys can be activated by purine and pyrimidine nucleotides with different affinities. As portrayed in **Table 1**, P2Y1, P2Y12, and P2Y13 are preferentially activated by adenosine 5'-diphosphate (ADP), while uridine 5'-diphosphate (UDP) activates P2Y6 and P2Y14. Unlike all P2X receptors, whose preferred agonist is ATP, just P2Y11 and P2Y2 are activated by ATP. Additionally, P2Y2 is activated by uridine 5'-triphosphate UTP, demonstrating an equipotency between both nucleotides. UTP is also the preferentially agonist for P2Y4 (Alexander et al., 2019).

Table 1. P2Y receptor agonist and coupling G protein subunits – human potencies. Table adapted from Alexander et al., 2019 and Woods et al., 2021.

| P2Y receptor subtype | G α Protein subunit | Preferred agonist | Potency (human receptor) |
|----------------------|-----------------------------------|-------------------|--------------------------|
| P2Y1 | G α_q | ADP | 10 nM |
| P2Y2 | G α_q , G α_{12} | ATP = UTP | 0.5-0.3 μ M |
| P2Y4 | G α_q | UTP | 73 nM |
| P2Y6 | G α_q , G $\alpha_{12/13}$ | UDP | 15 nM |
| P2Y11 | G α_q , G α_s | ATP | 38-65 μ M |
| P2Y12 | G α_i | ADP | 60 nM |
| P2Y13 | G α_i | ADP | 60 nM |
| P2Y14 | G α_i | UDP, UDP-glucose | 70-80 nM |

P2Y receptors have also been demonstrated to be components of the calcium signalling toolkit in endothelial cells. The most abundantly expressed and studied P2Y receptor in human endothelium is P2Y2 (Cabou et al., 2022; Ding et al., 2010; Gidlöf et al., 2015; Kukulski et al., 2010; Lang et al., 2023; Mühleder et al., 2020; Sathanoori et al., 2017; Seiffert et al., 2006; Viana et al., 1998; Wang et al., 2016; Wang et al., 2015; Zhang et al., 2014) followed by P2Y1, P2Y4, and P2Y6. P2Y2 is believed to mediate nucleotide-induced vasodilation nitric oxide-dependent (Albarrán-Juárez et al., 2018; Alexander et al., 2019; Cabou et al., 2022; Nishimura et al., 2017; Raqeeb et al., 2011; Wang et al., 2016). Wang et al. showed that Piezo1 activation led to an ATP release which will, in turn, activate P2Y2 receptors during shear stress. P2Y2 was required to activate the mechanosensory complex PECAM-1/VE-cadherin/VEGFR-2. This complex described by Tzima et al. will allow phosphorylation of eNOS and a sustained production of nitric oxide. Some studies also reported transient complexes of P2Y2 and VEGFR-2 in endothelial cell junctions (Erb et al., 2006) and fast tyrosine phosphorylation upon P2Y2 activation (Seye et al., 2004). P2Y2 has been also being involved in endothelial cell alignment and cytoskeleton arrangement in human endothelial cells (Sathanoori et al., 2017), as well as its role in the nucleotide-mediated effects on the proliferation, migration, and spreading of endothelial cells (Cabou et al., 2022). Finally, its function on inflammatory responses in this cell type was proposed in 2004 by Seye et al. who indicated a vascular cell adhesion molecule-1 (VCAM-1) dependency on the activation of P2Y2. P2Y1 is, together with P2Y2, a dominant P2Y receptor in human endothelial cells (Burnstock et al., 2014). As in the case of P2Y2, P2Y1 mediates endothelial vasodilation NO-dependent and has a role in cell proliferation and migration (Cabou et al., 2022; da Silva et al., 2009; Illes et al., 2021). P2Y4 and P2Y6 have also been proposed for endothelial nitric oxide vasorelaxation (Alexander et al., 2019; da Silva et al., 2009) in addition to a function of P2Y4 in endothelial cell migration (Burnstock et al., 2014; Cabou et al., 2022; Nishimura et al., 2017), and P2Y6 in endothelial inflammation (Nishimura et al., 2017; Riegel et al., 2011).

P2Y11 has been broadly reported to be expressed in the endothelium (Cabou et al., 2022; Chadet et al., 2015; Lang et al., 2023; Zhang et al., 2014), but its involvement in endothelial functions have been less studied than the previous ones. Recently, some authors illustrated P2Y11's role as an anti-inflammatory player in the endothelium by modulation of the activity of different factors such as eNOS (Piollet et al., 2021), cytokines (Ng et al., 2018), and VCAM-1 (Kuang et al., 2019). Therefore, agents that modulate P2Y11 could hold protective therapeutic value in addressing atherosclerosis and the inflammation that contributes to the development of the disease (Strassheim et al., 2020). Furthermore, its involvement in cell proliferation (Xiao et al., 2011) and cell migration (Avanzato et al., 2016) has also been signalled. Together with P2Y1, it has been proposed to participate in barrier function promotion (Burnstock et al., 2014).

P2Y12, P2Y13, and P2Y14 expression are being reported to a lower extent (Cabou et al., 2022), and more research is needed on their roles in human endothelial cells. Nonetheless, the role of P2Y12 in cell proliferation (Cabou et al., 2022) and migration (Han, 2022) has been proposed lately.

1.3.1.2.2 P2X receptors.

P2X receptors are seven ionotropic receptors (P2X1, P2X2, P2X3, P2X4, P2X5, P2X6, and P2X7) activated by binding ATP. P2X receptors form non-selective ATP-gated ion channels, whose activation leads to conformational arrangements within the transmembrane domain and Na⁺ and Ca²⁺ influx and K⁺ efflux through the pore, triggering cell membrane depolarization and downstream signalling events (Franklin et al., 2014; Samways et al., 2014; Stokes et al., 2017). Concerning the above-mentioned transmembrane domain, members of this family present a similar three-dimensional structure, consisting of two hydrophobic transmembrane domains (TM1 and TM2), N and C-termini and a large extracellular ectodomain (Dal Ben et al., 2015). Each P2X subunit structure has been compared to the shape of a leaping dolphin. P2X receptors differ from other identified ion channels in sequence and structure (Habermacher et al., 2016). These receptors are trimeric, forming a homotrimeric or heterotrimeric receptor by combining the different peptide subunits (P2X1-7), even though not much is known about heteromeric combinations and their functions (North, 2002; Oken et al., 2022).

ATP is the preferred agonist of the P2X receptors (Kennedy, 2021), but they have different sensitivities to the nucleotide and desensitization kinetics (**Table 2**) (Coddou et al., 2011). Homomeric P2X1 and P2X3 portrayed the fastest desensitization (lower than 1 second), and they are the most sensitive to ATP with submicromolar potency values for human receptors (P2X1: 0.56-0.7 μ M; P2X3: 0.5-1 μ M). The other P2X receptors, except P2X6, considered a silent receptor in humans, demonstrated slower desensitization, greater than 20 seconds. P2X2, P2X4, and P2X5 (exon 10 containing) follow P2X1 and P2X3 in sensitivity, with slightly higher potencies (P2X2: 2-8 μ M; P2X4: 1-10 μ M; P2X5: 0.44-10 μ M), while P2X7 showed potency in the millimolar range (Chessell et al., 1998; Illes et al., 2021; Müller et al., 2020; Stokes et al., 2006).

Table 2. P2X receptor agonist and desensitization profile – human potencies. Table adapted from Illes et al., Müller et al. , Chessell et al., 1998, and Stokes et al., 2006.

| P2X receptor subtype | Preferred agonist | Desensitization | Potency (human receptor) |
|----------------------|-------------------|-----------------|--------------------------|
| P2X1 | ATP | Fast | 0.1-0.7 μ M |
| P2X2 | ATP | Slow | 2-8 μ M |
| P2X3 | ATP | Fast | 1 μ M |
| P2X4 | ATP | Slow | 1-10 μ M |
| P2X5 | ATP | Slow | 0.44-10 μ M |
| P2X6 | ATP | - | - |
| P2X7 | ATP | Slow | 700 μ M-1.8 mM |

P2XRs mediate the regulation of blood vessel tone, and they have a role in the calcium toolkit of endothelial cells. P2X4 and P2X7 are the most expressed P2X receptors in human endothelial cells, and their function is primarily related to the action of shear stress (Korenaga et al., 2001; Sathanoori, Rosi, et al., 2015; Wu et al., 2023; Yamamoto et al., 2018; Yamamoto, Korenaga, Kamiya, Ando, et al., 2000) and inflammatory processes (Aslam et al., 2021; Schmid et al., 2019; Wu et al., 2023). The endothelial shear stress is intimately associated with the physiology, pathophysiology, and development of the blood vessels and can control the form and function of the endothelium (Wu et al., 2023). The main P2X player in this process is P2X4, whose role in mediating ATP-induced responses in endothelial cells and shear stress-dependent responses was demonstrated in early 2000 (Korenaga et al., 2001; Yamamoto, Korenaga, Kamiya, Ando, et al., 2000; Yamamoto, Korenaga, Kamiya, Qi, et al., 2000). In addition, P2X4 transcriptional expression was regulated by applying this stimulus (Korenaga et al., 2001), and P2X4 is also believed to mediate indirect effects, as regulation of Kruppel-like factor 2 (Sathanoori, Rosi, et al., 2015). P2X4 expression has been linked to P2X6 expression in their location in VE-cadherin cell-cell contact at the human endothelial cell adherent junctions (Glass et al., 2002). P2X4's role in vasodilation is backed by genetic analysis that correlates a loss-of-function polymorphism in the hP2X4 with augmented pulse pressure (Schmid et al., 2019). The different expressions of P2X4 between human venous and arterial endothelial cells showed a higher expression of P2X4 in human venous endothelial cells (Aslam et al., 2021). Nonetheless, some studies failed to demonstrate P2X4 functional activity in human endothelial cells and its involvement in ATP-dependent signalling or nitric oxide production, implying the necessity to investigate purinergic signalling in this cell type (Raqeeb et al., 2011; Wang et al., 2015; Wilson et al., 2007). P2X7 involvement in endothelial cells is usually more related to inflammatory processes (Aslam et al., 2021; Burnstock et al., 2014; Schmid et al., 2019; Wu et al., 2023), which does not exclude their activity under shear stress. Under specific shear stresses, ATP can activate P2X7 receptors, inducing E-selectin and IL-1 β secretion that promote endothelial inflammation in atherosclerotic spots (Wu et al., 2023). Additionally, the expression of P2X7 in human carotid artery atherosclerotic plaques is approximately 20 times greater than in non-diseased regions (Schmid et al., 2019). Wilson et al. demonstrated that proinflammatory conditions upregulated P2X7 and P2X4 expression, as Sathanoori et al. did in 2015 in high-glycemic inflammation in human endothelial cells, portraying P2X4 involvement in inflammatory processes (Sathanoori, Swärd, et al., 2015).

Expression of P2X5 has been reported in human endothelial cells (Burnstock et al., 2014; Ralevic, 2012), but its role and functional expression in the endothelium are still to be resolved. It is relevant to mention that the most common form of P2X5 in humans is a splice variant lacking exon 10 that causes loss of function of the P2X5 receptor (Kotnis et al., 2010). Neither P2X2 nor P2X3 are known to be expressed in human endothelial cells. Lastly, expression of P2X1 was demonstrated in human endothelial cells in some reports (Burnstock et al., 2014), but their role in endothelial function still needs to be demonstrated in humans. It is believed that P2X1 is highly specifically expressed in smooth muscle cells, and its vascular function is mainly developed during vasoconstriction (del Carmen Gonzalez-Montelongo et al., 2023; Ralevic, 2012; Wang et al., 2002).

1.3.2. Piezo1 and its role in the endothelium.

Piezo ion channels convert mechanical stimulus into various biological activities through a process called mechanotransduction. Piezo1 and Piezo2 were identified in 2010 as molecular mediators of the mechanically activated current found across multiple cell types (Coste et al., 2010). Piezo proteins are mechanosensitive channels forming a pore force-gated whose opening probability depends on a physical stimulus allowing the entry of cations, slightly preferring calcium over monovalent cations (Ottolini et al., 2021; Prindle et al., 2015). While the primary function of Piezo2 is the mediation of gentle touch sensation, Piezo1 has functions in numerous physiological processes, including sensing shear stress of blood flow for proper blood vessel development, regulating urinary osmotic pressure, controlling blood pressure and exercise performance (Faucherre et al., 2014; Li et al., 2019; Martin-Almedina et al., 2018). Previous studies have shown that over 25 mutations in Piezo1 cause human disease. However, most mutations have yet to be extensively studied (Song et al., 2020). Piezo1 is activated through cell membrane deformations caused by mechanical forces, such as osmotic pressure, fluid shear stress, substrate stiffness, and confinement (Ranade et al., 2014).

Piezo1 presence and function as a critical player in sensing blood flow-induced physiological shear stress have been previously reported (Li et al., 2014; Ranade et al., 2014; Tang et al., 2022). Piezo1 activation leads to vasodilation, endothelial calcium influx and cell alignment shear stress-dependent, and its activation has been directly linked to ATP release upon shear stress stimulation in endothelial cells (Wang et al., 2016). Wang et al. demonstrated P2Y2 downstream signalling due to this ATP release, which in turn favoured activation of the shear stress sensing complex PECAM-1/VE-cadherin/VEGFR-2 (Tzima et al., 2005). Activating this downstream signalling will allow a more sustained eNOS phosphorylation and nitric oxide release. Interestingly, Piezo1's role in endothelial cell alignment was also proposed for P2Y2 (Sathanoori et al., 2017), and deletion of Piezo1 reduced the activation of the Klf-2 factor (Gerhold et al., 2016) as in the case of P2X4 (Sathanoori, Rosi, et al., 2015). In addition to its role in vasodilation, which is believed to be due to proatherogenic and atheroprotective flow-dependent endothelial responses, Piezo1 can mediate vasoconstriction in this cell type during whole-body exercise when the cells are exposed to increased blood flow (Beech, 2018; Ottolini et al., 2021; Rode et al., 2017; Tamargo et al., 2023). Furthermore, Piezo1 mediates pro-atherogenic endothelial responses to disturbed flow, promoting endothelial inflammation. This study also portrayed blocked disturbed flow-induced inflammatory signalling after the knockdown of P2Y2 (Albarrán-Juárez et al., 2018). Finally, Notch receptor 1, a membrane protein expressed in human endothelial cells, has been demonstrated to be activated in

response to fluid flow stimulation. The underlying mechanism remained unknown for a time, but Caolo et al. illustrated in 2020 that the activation of the NOTCH1 response in response to shear stress requires Piezo1 (Caolo et al., 2020).

1.3.3. VEGF and its role in the endothelium.

Vascular endothelial growth factors comprise four VEGFs in vertebrates, from A to D, and the placenta growth factor (PlGF). They bind to the VEGF receptors 1 to 3, but VEGF receptor 2 (VEGFR-2) is the leading player in endothelial VEGF signalling (**Figure 4**). VEGFRs are tyrosine kinases (RTKs), and VEGF binding induces receptor dimerization, which allows the activation of the receptor through autophosphorylation of its tyrosine residues in the intracellular domains of the receptors (Simons et al., 2016).

VEGFR-2 plays a central role in regulating angiogenesis, vascular permeability, and shear stress transduction in the endothelium of blood vessels (Heinolainen et al., 2017; Rahimi, 2006; Tzima et al., 2005; Wang et al., 2016). VEGFR-1 is known to be also involved in angiogenesis, and its function might be limited as a modulator of VEGFR-2 (Rahimi, 2006). VEGFR-1 and R-2 bind to the vascular endothelial growth factor A (VEGF-A). VEGFR-2 can bind VEGF-A and VEGF-C (after proteolytic maturation (Masłowska et al., 2021)) and induce calcium fluxes in the cytosol by activating the PLC pathway and the simultaneous entry of calcium through various channels, such as TRPC5 and Orai channels (Li et al., 2011). The VEGFR-1's lack of ability to evoke VEGF-dependent calcium responses is curious as it has a much higher affinity to VEGF-A than VEGFR-2 (de Vries et al., 1992). Its way to modulate vascular biological responses is limited to its capacity to heterodimerize with VEGFR-2 (Cudmore et al., 2012; Rahimi, 2006; Shibuya, 2011). This is because, unlike most of the tyrosine kinase receptors that activate the Ras pathway or PI3K pathway, it is known that the PLC γ -PKC-MAPK pathway is favourably activated in VEGF-bound VEGFR-2. A domain of PLC γ binds specifically to the 1175-PY site of VEGFR-2. VEGFR-1 exhibits significantly weaker kinase activity than VEGFR-2, and a complete understanding of its signalling cascade is not yet established. The 1169-Y on VEGFR-1, equivalent to 1175-Y on VEGFR-2, serves as a PLC γ activation site for VEGFR-1. Nevertheless, 1169-PY is not a prominent autophosphorylation site on VEGFR-1, and the direct pro-angiogenic activity from VEGFR-1 is usually weak or undetectable (Shibuya, 2011). VEGFR-1 can also bind VEGF-B, which is not the case for VEGFR-2 (Olofsson et al., 1998). VEGFR-2 activation upon VEGF ligands binding is considered the canonical VEGFR-2 activation (Simons et al., 2016). However, a non-canonical activation has also been described. This activation type is based on a non-ligand stimulation, which, in this case, is replaced by mechanical forces such as shear stress that induces tyrosine phosphorylation and activation of the receptor. The previously mentioned mechanosensory complex formed by PECAM-1/VE-cadherin/VEGFR-2 is necessary for the mechanical stimulation of VEGFR-2 and further phosphorylation. The cytoplasmic tyrosine kinase SCR is required to phosphorylate VEGFR-2 and is believed to be dependent on P2Y2 activation (Simons et al., 2016; Tzima et al., 2005; Wang et al., 2016).

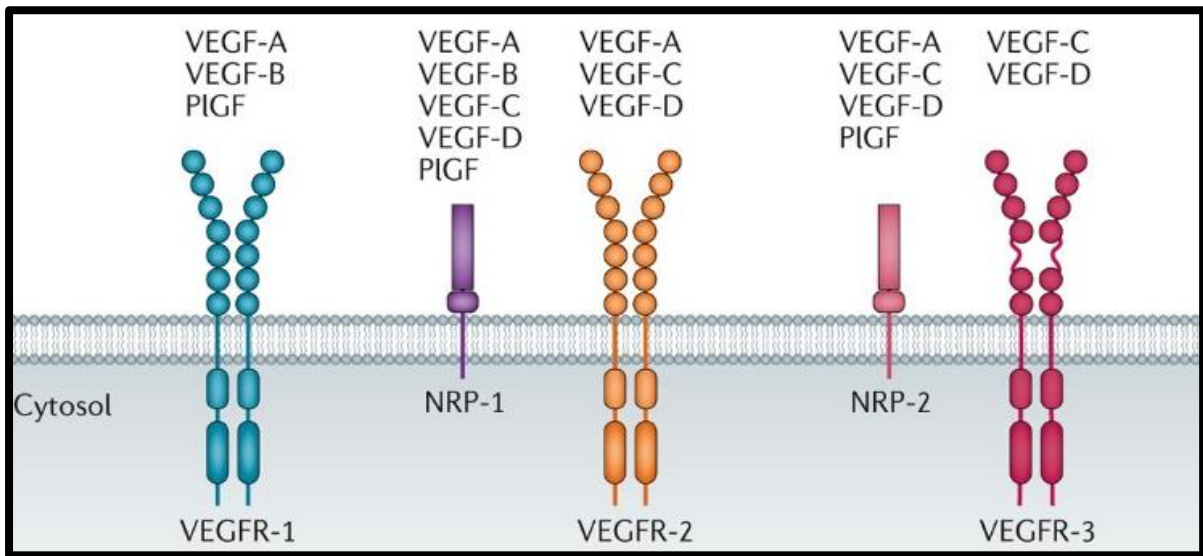


Figure 4. VEGF family: receptors and ligands. The family includes three RTK receptors, VEGFR-1, VEGFR-2, and VEGFR-3, and two neuropilin family members, NRP1 and NRP2. Binding simultaneously to various transmembrane protein types allows the formation of multiprotein complexes that may include not only receptors but also auxiliary proteins such as integrins (Simons et al., 2016). As portrayed, different members of the VEGF family bind to various types of VEGF receptors. Image adapted from (Lange et al., 2016).

VEGFR-2 phosphorylated Y1175 and PLC γ activation results in IP₃ generation and DAG. Classically, IP₃ will induce calcium release from the ER, and DAG will activate calcium-dependent protein kinase C (PKC), activating the ERK1/2 pathway (usually dependent on the Ras pathway). The PLC γ –PKC pathway regulates various elements of endothelial cell biology, including cell fate specification, proliferation, and migration. Calcium signalling plays a crucial role in VEGF biology, mediating the PLC γ -induced activation of the ERK1/2 pathway and contributing to the activation of the nuclear factor of activated T cell (NFAT) family of transcription factors. Calmodulin, which functions as a calcium sensor, and calcineurin, a calcium-dependent serine/threonine phosphatase, regulate the nuclear translocation and transcriptional activation of NFAT proteins. NFAT, in turn, reduces the expression levels of VEGFR-1, leading to increased signalling by VEGFR-2 due to greater availability of VEGFA (Simons et al., 2016).

On the other hand, signals for lymph angiogenesis are transmitted by VEGF-C/D via VEGFR-3 (Heinolainen et al., 2017). VEGFR-3 is initially expressed by both blood and lymphatic endothelial cells during early embryonic development. As development progresses, its expression becomes predominantly confined to the lymphatic system. However, during angiogenesis, there is the potential for reinduction of VEGFR-3 expression in blood endothelial cells (Deng et al., 2015). The signalling pathways of VEGFR-3 do not involve the PLC pathway and affect the PKC pathway and Ras pathway (Hsu et al., 2019; Shibuya, 2011). Recently, research has demonstrated that VEGFR-3 may be a component of the mechanosensory complex and can also be activated non-canonically (Simons et al., 2016).

1.3.4. TRPs and its role in the endothelium.

Transient receptor potential (TRP) channels are a cation ion channel superfamily essential for endothelial calcium fluxes throughout human illnesses and physiological activities (Genova et al., 2020). In humans, TRP channels are divided into six subfamilies: TRPC, TRPM, TRPML, TRPP, TRPA, and TRPV (Moran et al., 2004; Vriens et al., 2014). These six subfamilies have 28 members, but only nine have demonstrated their roles in human endothelial Ca²⁺ signalling and different functions (Thakore et al., 2019). The main members involved, and their functions are summarised in **Table 3**.

Table 3. Functions of human endothelial TRP channel summary. It was modified from Thakore et al., 2019 from references only in human endothelium along the text. TRPV4 role in vasodilation is extracted from Swain et al., 2021.

| TRP subtype | Vasodilation | Permeability | Angiogenesis | Inflammation |
|-------------|--------------|--------------|--------------|--------------|
| TRPA1 | √ | | | √ |
| TRPV1 | √ | | √ | √ |
| TRPV4 | √ | √ | √ | √ |
| TRPC1 | √ | √ | | √ |
| TRPC3 | √ | | √ | √ |
| TRPC4 | | | √ | |
| TRPC5 | | | √ | |
| TRPC6 | | √ | | √ |
| TRPM2 | | √ | | |

*TRPA, ankyrin; TRPV, vanilloid; TRPC, canonical; TRPM, melastatin.

1.4 Shear stress.

Mechanotransduction can be defined as the process by which a mechanical stimulus is translated into a biological response within the cell. Shear stress involves the principal mechanotransductional process in the endothelium, modulating different endothelial processes, including angiogenesis and vascular morphogenesis, remodelling, and tone (Chistiakov et al., 2017; Roux et al., 2020). Endothelial shear stress calcium-induced responses through different receptors have been portrayed in the previous sections, and therefore, an introduction to this stimulus effect in the endothelium is considered relevant.

Shear stress is the frictional force produced by blood flow over the apical cell membrane of the endothelium. The Greek letter τ usually represents this force, measured in dyne/cm^2 (Davies et al., 2019; Davies, 2009; Walshe et al., 2013). *In vivo*, there is a vast range of physiological shear stress values depending on the type of blood vessel. It is typical in human arteries to find values from 2 to 40 dynes/cm^2 , increasing to 100 dynes/cm^2 in branches and bifurcations. As well as the differences in shear stress values, the flow type varies depending on the vascular bed. The straight portions of an artery show a laminar (also called uniaxial) and pulsatile flow pattern, while branches and bifurcations show turbulent (or multidirectional) flow. Different flow types determine different effects on the endothelium. Multidirectional flow has been linked as proinflammatory and proatherogenic, while uniaxial stimuli induce endothelial properties as atheroprotective. On the other hand, changes in the shear stress rate lead to vasoconstriction (decreases in shear stress values) or vasodilation (increases in shear stress values), and fluctuations in shear stress initiate vascular remodelling (an essential factor in the control of vascular development) (Gerhold et al., 2016; Reinhart-King et al., 2008; Warboys et al., 2019). Thus, the physiological role of shear stress in endothelium physiology is undisputed. The different types of blood flow are represented in **Figure 5**, together with the different approaches to studying shear stress effects *in vitro*, for further implications in this investigation.

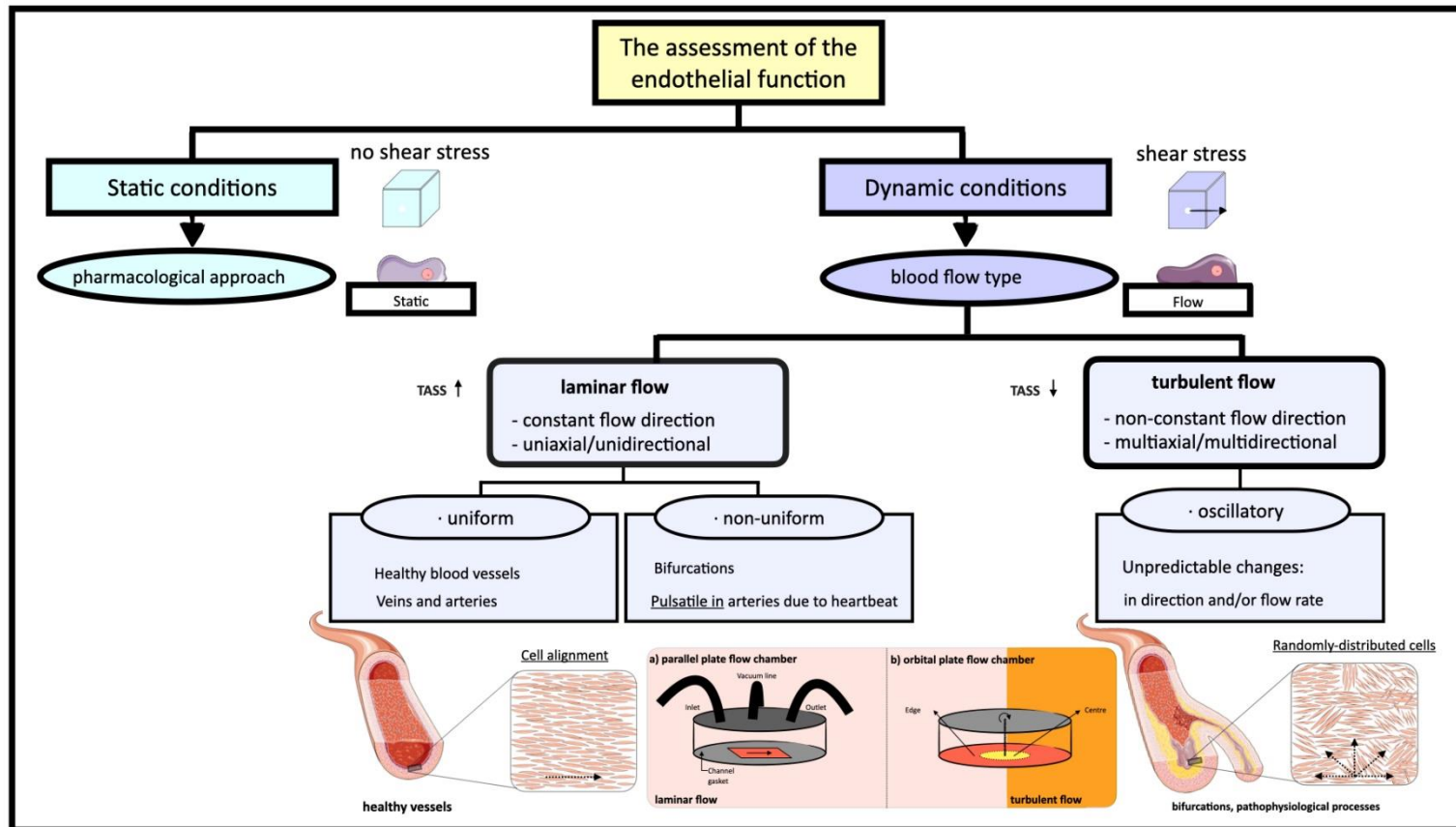


Figure 5. Different in vitro approaches to the endothelial function and flow types. The endothelial function study has two main strategies: static and dynamic conditions. In static conditions, endothelial cells can be pharmacologically stimulated, and the effects of shear stress can be assessed using shear stress-mimic drugs. Dynamic conditions are subdivided into two main physiological blood flow types: laminar and turbulent. Typically, laminar flow is found in healthy vessels, and turbulent flow is characteristic of pathological processes, such as atherosclerosis. Technically, laminar flow can be simulated in parallel plate flow chambers and at the edge of orbital plate flow chambers. Additionally, the orbital plate flow chamber allows the study of the laminar (at the edge) and the turbulent flow chambers (at the centre) simultaneously. (Parts of the figure were drawn by using pictures from Servier Medical Art. Servier Medical Art by Servier is licensed under a Creative Commons Attribution 3.0 Unported License (<https://creativecommons.org/licenses/by/3.0/>)).

1.5 Aims and objectives.

The literature shows that calcium signalling in the endothelium mediates critical physiological processes. Developing drugs and modulators against the molecular players in this signalling can help fight multiple cardiovascular pathologies. Purinergic receptors represent a desirable drug target as they are involved in multiple endothelial functions (vasodilation, vascular permeability, inflammation, cell proliferation, and migration) and interact with other proteins to maintain calcium homeostasis in the endothelium. In addition, some purinergic receptors have been successfully targeted in other cell types for therapeutic gain. For example, the P2Y12 receptor serves as the target for the antiplatelet drug clopidogrel, which is extensively utilized in treating and preventing myocardial infarctions, and the P2Y2 receptor agonist diquafosol is employed in Japan and Korea as a treatment for dry eye.

Through this project, I want to identify the molecular basis of nucleotide-induced calcium responses *in vitro* in immortalised human microvascular endothelial cells and their potential contribution to the vascular endothelial growth factor evoked responses (*Chapter 3*). This analysis will be completed with the purinergic molecular characterization of a human primary endothelial cell line in an attempt to replicate previous observations in the immortalized cell line. Using a similar assay configuration, I also investigate the potential contribution of P2 receptors in the Piezo1-dependent responses (*Chapter 4*), with the primary aim being to compare these results with the possible involvement of P2 receptors in shear stress-dependent calcium responses. In doing so, this work aimed to determine which P2 receptor is the primary mediator of ATP-dependent endothelial calcium signalling and their possible involvement in other receptor signalling.

Chapter 2. Materials and Methods.

2.1 Drugs and reagents

All chemicals used throughout this study were mainly purchased from Thermo Fisher Scientific (Loughborough, UK), Sigma-Aldrich (Gillingham, UK), and Tocris Bioscience (Bristol, UK). The specific suppliers for each used reagent will be detailed throughout this chapter in the following **Tables 1, 2, 3, and 4**.

Table 1. List of exogenous nucleotides and other selective agonists.

| Compound | Target | Supplier | Purity | Vehicle | Concentration | Reference |
|---------------------|--|---------------|--------|---------|---------------|--------------------------|
| ATP | P2XR _s , P2Y _{2,11} | Abcam | >99% | water | 0.01-300 μM | Burnstock (2007) |
| ADP | P2Y _{1,12,13} | Sigma-Aldrich | ≥95% | water | 0.002-300 μM | Chhatiwala et al. (2004) |
| UTP | P2Y _{2,4} | Abcam | ≥96% | water | 0.002-300 μM | Burnstock (2007) |
| UDP | P2Y _{6,Y14} | Sigma-Aldrich | ≥96% | water | 0.01-1000 μM | Burnstock (2007) |
| VEGF ₁₆₅ | VEGFR-1,2 | R&D Systems | >97% | PBS | 0.3-100 ng/mL | Robinson et al. (2001) |
| VEGF ₁₆₇ | VEGFR-1 | R&D Systems | >95% | HCl | 0.3-100 ng/mL | Olofsson et al. (1998) |
| Yoda1 | Piezo1 | Tocris | 99.9% | DMSO | 0.03-30 μM | Syeda et al. (2015) |

Water: deionised water; PBS: phosphate buffered saline; DMSO: dimethyl sulfoxide. Compound stocks were prepared in 100% of the vehicles referred to in the table, stored at -20°C, and serially diluted to the final concentration ranges specified in this study.

Table 2. List of non-selective purinergic receptor antagonists and ATP scavengers (apyrase).

| Compound | Supplier | Concentration | Vehicle | Reference |
|----------|---------------|-----------------|---------|-----------------------|
| Apyrase | Sigma-Aldrich | 0.5, 2, 10 U/mL | water | Kettlun et al. (1982) |
| PPADS | Sigma-Aldrich | 30, 100 μM | water | Jones et al. (2000) |
| Suramin | Sigma-Aldrich | 100 μM | water | Jones et al. (2000) |

Water: deionised water. Compounds stocks were stored at -20°C.

Table 3. List of selective purinergic and adenosine receptors antagonists or modulators.

| Compound | Target | Supplier | Vehicle | Concentration | Reference |
|---------------|-------------------|-----------------------|---------|---------------|-------------------------------|
| BAY-1797 | P2X ₄ | Cambridge Biosciences | DMSO | 3, 10 μM | Werner et al. (2019) |
| 5-BDBD | P2X ₄ | Tocris | DMSO | 10 μM | Bidula et al. (2022) |
| BX430 | P2X ₄ | Tocris | DMSO | 10 μM | Ase et al. (2015) |
| Ivermectin | P2X ₄ | Sigma-Aldrich | DMSO | 3 μM | Khakh et al. (1999) |
| PSB12062 | P2X ₄ | Sigma-Aldrich | DMSO | 10 μM | Hernandez-Olmos et al. (2012) |
| AR-C 118925XX | P2Y ₂ | Tocris | DMSO | 10 μM | Rafehi et al. (2017) |
| NF157 | P2Y ₁₁ | Tocris | water | 5 μM | Ullmann et al. (2005) |

| | | | | | |
|----------|-----|--------|------|--------|------------------|
| MRS 1754 | A2B | Tocris | DMSO | 100 nM | Ji et al. (2001) |
|----------|-----|--------|------|--------|------------------|

Water: deionised water; DMSO: dimethyl sulfoxide. Compounds stocks were stored at -20°C.

Table 4. List of other drugs and inhibitors.

| Compound | Function | Supplier | Vehicle | Concentration | Reference |
|---------------|--------------------------------|---------------|---------|---------------|-------------------------|
| Acetylcholine | Neurotransmitter | Sigma-Aldrich | water | 100 µM | Popot et al. (1984) |
| Carbachol | Acetylcholine receptor agonist | Sigma-Aldrich | water | 100 µM | Scarr et al. (2013) |
| Dooku1 | Yoda1 blocker | Tocris | DMSO | 10 µM | Evans et al. (2018) |
| GsMtx4 | Piezo1 inhibitor | PeptaNova | DMSO | 2.5, 10 µM | Bae et al. (2011) |
| Thapsigargin | SERCA pump inhibitor | Santa Cruz | DMSO | 1, 10 µM | Lyttonsg et al. (1991) |
| SQ 22536 | Adenylyl cyclase inhibitor | Tocris | DMSO | 1, 10 µM | Emery et al. (2013) |
| U-73122 | PLC inhibitor | Santa Cruz | DMSO | 5 µM | Bleasdale et al. (1993) |

Water: deionised water; DMSO: dimethyl sulfoxide; PLC: phospholipase C; SERCA: sarcoendoplasmic reticulum calcium transport ATPase. Compounds stocks were stored at -20°C.

2.2 Cell culture

All cells were cultured in a Class II Microbiology Safety Cabinet and were grown in an incubator with an atmosphere of 5% CO₂ at 37°C. Unless otherwise stated, cells were maintained in uncoated tissue culture flasks from Thermo Fisher. All cells used in this study were adherent and routinely cultured in filtered T25 or T75 flask (Thermo Scientific).

2.2.1. Human microvascular endothelial cells (HMEC-1)

HMEC-1 is a human dermal microvascular endothelial cell line firstly isolated from the male foreskin and a popular alternative to primary endothelial cell lines, with advantages such as growing and expansion time over primary cell lines. HMEC-1 are immortalized cells that were used between passages 1 to 12 because of the response to the vascular endothelial growth factor (VEGF₁₆₅). The lack of VEGF₁₆₅ responsiveness is a sign of them losing their endothelial phenotype.

2.2.1.1 General maintenance

HMECs-1 were maintained in MCDB-131 from Gibco supplemented in-house with 10% of foetal bovine serum (FBS), 1% penicillin/streptomycin solution (20 units·ml⁻¹ penicillin and 50 µg·ml⁻¹ streptomycin), 0.1 µg·mL⁻¹ hydrocortisone (Sigma), 10 ng/mL EGF (Thermo Fisher) and 10 mM L-glutamine (G7513, Sigma). This growth media contains many components not found in traditional basal media, such as trace elements, putrescine, adenine, thymidine, and higher levels of some amino acids and vitamins. It is buffered with sodium bicarbonate, and it has low glucose levels.

2.2.1.2 Cell passage

Cells were sub-cultured when reached 80% confluency. Firstly, cells were washed with 7.5 mL of room temperature sterile and filtered phosphate-buffered saline (PSB, Lonza) twice, followed by treatment of 1.5 mL trypsin EDTA (Lonza) for 3 minutes in the humidifier incubator at 37°C. When required, the cultured vessel was gently tapped, and detaching trypsin reaction was neutralised by adding 3 mL of fresh pre-warmed complete cell growth media. Then, cells were counted using a Neubauer haemocytometer and cells·mL⁻¹ was calculated. For cell line maintenance cells were diluted into a new culture vessel at a density of approximately 2x10⁴ cells·mL⁻¹.

2.2.1.3 Cryopreservation and thawing

First or early passages of HMEC-1s were prepared for cryopreservation as a routine process when receiving a new cell batch from the manufacturer. Cryopreserving solution consisting of 63% complete growth media, 27% foetal bovine serum (FBS), and 10% of dimethyl sulfoxide (DMSO) was used to prepare cryovials with an approximate density of 1x10⁶ cells per vial.

Briefly, in the last step of the cell passage process, and once the trypsin reaction was neutralised with complete cell growth media, the mix was centrifuged at 1200 rpm for 5 minutes at room temperature (RT). Next, the supernatant was aseptically decanted, and the pellet was gently re-suspended in cryopreservation media. Finally, cells were diluted at the appropriate concentration.

For thawing the HMECs from liquid nitrogen, cryovials were directly transferred to dry ice for short transportation, and once in the hood, the cap was twisted to relieve the pressure and retightened again. Then, the vial was quickly immersed in a 37°C warm bath for 5 minutes. Once the vial was disinfected and the supernatant was discarded, the pellet was resuspended in 1 ml of cell growth medium to be transferred to a T75 flask.

2.2.2. Human umbilical vein endothelial cells (HUVECs)

HUVEC is a human endothelial primary cell line commonly used to study important biological processes, including atheroma and shear stress effects in the endothelium. HUVECs were purchased from PromoCell (Heidelberg, Germany) and supplied from pooled donors. Cells were cryopreserved once isolated from the pooled placental large vessel at passage 1 or 2. HUVECs were used between passage 1-12, as the cells stop responding to VEGF₁₆₅, a very characteristic endothelial-like phenotypic response.

2.2.2.1 General maintenance

HUVECs were maintained in PromoCell Endothelial Cell Growth ready to use with the addition of Supplement Mix containing these final concentrations: foetal calf serum 0.02 ml·ml⁻¹, endothelial cell growth supplement 0.004 ml·ml⁻¹, epidermal growth factor (recombinant human) 0.1 ng·ml⁻¹, basic fibroblast growth factor (recombinant human) 1 ng·ml⁻¹, heparin 90 µg·ml⁻¹ and hydrocortisone 0.1 µg·ml⁻¹. 1% penicillin/streptomycin solution (20 units·ml⁻¹

penicillin and 50 $\mu\text{g}\cdot\text{ml}^{-1}$ streptomycin) was also added. The growth medium was kept in a cold room avoiding light, since it is light-sensitive.

2.2.2.2 Cell passage

A standard trypsin neutralization protocol is unsuitable for HUVECs, and a specific Detach Kit is designed for the cell subculture. This kit contains HEPES BSS, Trypsin/EDTA, and Trypsin Neutralizing Solution. Before starting the subcultivation protocol, reagents were warmed at room temperature for at least thirty minutes. Once cell culture reached 70-80% of confluence in a T25 or T75 flasks, the culture medium was carefully aspirated, and cells were washed with 100 μl HEPES BSS solution per cm^2 . Once HEPES was aspirated, 100 $\mu\text{l}\cdot\text{cm}^2$ of Trypsin/EDTA was added. After 5 minutes of treatment at room temperature and gently tapping the side of the vessel, trypsin was neutralized with 100 $\mu\text{l}\cdot\text{cm}^2$ Trypsin Neutralization Solution. The cell suspension was transferred to a centrifugation tube for 3 minutes of spin at 220 x g at RT. The pellet was re-suspended in 1 mL of fresh cell growth media. Cells were counted with the haemocytometer and seeded at the required concentration in a new flask to preserve the cell line or in a 96-well plate for experimental use. Cells were used between passages 1 to 12, and fresh media changes were performed when cells were not passaged for more than two days.

2.2.2.3 Cryopreservation and thawing

First or early passages of HUVECs were prepared for cryopreservation as a routine process when receiving a new cell batch from the manufacturer. In the last step of the cell passage process, once cells were centrifuged in a pellet, a freezing medium (Cryo-SFM from PromoCell) was used to resuspend approximately 1×10^6 cells $\cdot\text{ml}^{-1}$. Cryo-SFM provided excellent results in the cryopreservation of primary human cells and consisted of methylcellulose, DMSO, and other cryoprotectants not specified by the manufacturer. Cryogenic storage vials (Thermo Scientific) with the cell's solution were placed in a cryo-freezing container to reach quickly low temperatures and immediately placed in the liquid nitrogen tank (-196°C). Storage at -80°C is insufficient for preserving HUVECs and causes irreversible cell damage.

For thawing the HUVECs from liquid nitrogen, cryovials were directly transferred to dry ice for short transportation. In the hood, the cap was twisted to relieve the pressure and retightened again. Quickly, the vial was immersed in a 37°C warm bath for 2 minutes, 1 ml of cell medium was added, and, finally, the vial was centrifuged for 3 minutes at 220 x g at RT. Once the vial was disinfected and the supernatant was discarded, the pellet was resuspended in 1 ml of cell growth medium to be transferred to a T25 flask.

2.2.3. Human 1321N1 astrocytoma cells

The human 1321N1 human astrocytoma cell line was isolated from the 1181N1 cell line, previously isolated from a human malignant glioma parental line (Ponten et al., 1968). This cell line lacks the presence of endogenous P2 receptors (Bianchi et al., 1999), making them a good model as a blank control for purinergic receptors when checking protein expression in other cell lines. This cell line will be referred to in this study as the parental 1321N1 cell line. Another human 1321N1 astrocytoma cell line was available in-house, the one stably expressing P2X4,

derived from the first by stable transfection of the human P2X4 gene. This cell line was used as a positive control to test P2X4 antagonists in calcium mobilisation assays.

2.2.3.1 General maintenance

Astrocytoma's cells were maintained in Dulbecco's Modified Eagle Media (DMEM) high glucose from Lonza containing 0.6 g·L⁻¹ L-Glutamine and supplemented with 10% of foetal bovine serum (FBS) and 1% penicillin/streptomycin solution (20 units·ml⁻¹ penicillin and 50 µg·ml⁻¹ streptomycin).

Cell passaging and the cryopreservation and thawing process follow the same procedures previously described in this section for the human microvascular endothelial cells (HMEC-1).

Table 5. Cell lines and culture media specifications summary.

| Cell line | Supplier | Medium |
|---|-----------|---|
| HMEC-1 | ATCC® | MCDB-153 (11513407, Gibco, Fisher Scientific) supplemented with 10% FBS, 1% Pen/strep, 0.1 µg/mL hydrocortisone (H0396, Sigma), 10 ng/mL EGF (E5036, Sigma), 10 mM L-glutamine (G7513, Sigma) |
| HUVEC (cryopreserved, pooled donors) (C12203) | PromoCell | PromoCell Endothelial Cell Growth ready to use prepared with the Supplemental Mix (C-22010) Detach kit from PromoCell was used for cell passaging (C-41210) |
| h1321N1 astrocytoma (parental and hP2X ₄) | ECACC | DMEM High Glucose L-glutamine (11574486, Gibco, Fisher) supplemented with 10% FBS and 1% Pen/Strep |
| HELA | ECACC | DMEM High Glucose L-glutamine (11574486, Gibco, Fisher) supplemented with 10% FBS and 1% Pen/Strep |

Detach solution used was Trypsin 0.25% (25200056, Fisher). Foetal bovine serum (FBS) (F9665) and the penicillin/streptomycin solution (P4458) were acquired from Sigma Aldrich. *HELA cells were cultured following the procedures previously described for h1321N1 astrocytoma cells (Section 2.2.3.1).*

2.3 Calcium mobilisation assays

Intracellular Ca²⁺ concentrations were measured using the fluorescent ratiometric indicator Fura 2-acetoxymethyl ester (Fura 2-AM in DMSO, Abcam Life Technologies) (Grynkiewicz et al., 1985). The dye is selective for calcium other divalent cations, such as, Mg²⁺ or Zn²⁺. Fura 2-AM is permeable through the membrane due to its AM ester group, and once inside the cell, the intracellular esterases cleavage the group trapping the dye in the intracellular milieu and leading to a negative charge fluorescent dye that can bind Ca²⁺ (**Figure 1-C**).

Fura 2-AM measures intracellular calcium ([Ca²⁺]_i) at 340 and 380 nm at two excitation wavelengths, while the emitted light signal is read at 510 nm. The dual excitation of the dye is reached since the absorption peaks of the wavelengths are close to its isosbestic point. Upon binding to free Ca²⁺, the absorption spectrum experiences a shift in a way that Fura-2 is more

efficient at exciting 340 nm when bound to calcium (dye calcium bound form) and, in contrast, at 380 nm, the dye is more efficient when it is nonbound to calcium (dye calcium-free form) (**Figure 1-A, B**). The ratio of these emissions at 510 nm (340/380 nm) is directly proportional to the live intracellular calcium levels in the cytosol. Therefore, the ratiometric nature of this dye will significantly reduce the reading of unspecific calcium signals or artifacts unaffected by conditions such as illumination intensity, probe loading, bleaching, or optical path length (Paredes et al., 2008).

2.3.1. Calcium mobilisation assays buffers

The fluorescence signal was measured in a standard bath solution (SBS) containing 130 mM sodium chloride (NaCl), 5 mM potassium chloride (KCl), 1.5 mM calcium chloride (CaCl₂), 1.2 mM magnesium chloride (MgCl₂), 10 mM (4-(2-hydroxyethyl)-1-piperazineethanesulfonic acid (HEPES), and 8 mM glucose at pH 7.4 adjusted with sodium chloride (NaOH). The free-calcium SBS medium contained 130 mM NaCl, 5 mM KCl, 2.7 mM MgCl₂, 2 mM EGTA, 10 mM HEPES, and 8 mM glucose at pH 7.4. Both solutions were adjusted with D-mannitol (~305 – 310 mOsm/L) to ensure isotonicity (K-7400S Semi-Micro Osmometer, Knauer), meaning the number of solutes is equal between the intracellular and extracellular milieu.

The adjustment of osmolarity follows the next rationale:

$$1 \text{ mM} = 1 \text{ mOsm of D-mannitol, molecular weight (MW)} = 182.17 \frac{\text{g}}{\text{mol}}$$

$$M = \frac{\text{moles}}{V(L)} = \frac{\text{g/MW}}{V(L)}$$

Desired osmolarity = 305 mOsm; desired – calculated osmolarity = **x** g of D-mannitol to add to 1 L of SBS solution.

$$M = \frac{\text{g/MW}}{V(L)}; \text{g} = \mathbf{x} \text{ mM} \cdot \frac{1 \text{ M}}{1000 \text{ mM}} \cdot 1 \text{ L} \cdot 182.17 \frac{\text{g}}{\text{mol}} = \text{g of D-mannitol for 1 L of SBS}$$

In addition, cells were loaded with 2 μM of Fura 2-AM in SBS solution supplemented with a nonionic surfactant 0.01% (w/v) Pluronic (Sigma) called loading buffer (LB). Both buffers were vacuum filtered (Z290424, Sigma) and kept at 4°C to prevent contamination.

2.3.2. Flex Station III assays

Cells were seeded in 96-well clear-bottomed plates (ThermoFisher) at 125.000 cells·mL (25.000 cells per 200 μL of cell growth media) in each independent well 24 h before experimentation in a humidified incubator (37°C, 5% CO₂), allowing cells to adhere and form a confluent monolayer. After washing twice with pre-warmed SBS, cells were incubated with 2 μM Fura 2-AM in 200 μL of loading buffer for 1 hour at 37°C protected from the light. After intensively washing the cells, the loading buffer was replaced with 200 μL of standard bath solution, and measurements were made at 37°C on a 96-well fluorescence plate reader (SoftMax Flex Station 3, Molecular Devices, UK). As detailed above, changes in intracellular calcium were indicated as the ratio of fura-2 emission at 510 nm for 340 and 380 nm excitation wavelengths (F ratio 340/380). The Flex Station 3 can automatically expose the 96-well cell plate to different

concentrations of agonist, injecting a volume of 50 μL to each well, prepared before experimentation in an independent 96-well U bottom plate at the desired concentrations. Readings were taken every 3 seconds over 250 seconds, and every protocol was initiated with 20 seconds of baseline readings. When an antagonist was tested, cells in the 96-well plate were preincubated in their presence at 37°C for 30 minutes, with the same preincubation in the 3-well solvent control (without the antagonist). Exceptionally, thapsigargin was incubated for 5 and 25 minutes instead of 30 for its high impact on the drug's calcium baseline. Then, without washing, the cell plate was ready to run the experiment, as explained previously.

2.3.3. Data analysis for Flex Station III assays

F ratio (340/380) reading values were exported from SoftMax Pro FlexStation software (Molecular Devices) as trace (max-min), peak, and area under the curve (AUC) (**Figure 2**). These three parameters were used to build dose-response curves and characterize the different drug effects. Dose-response data was plotted with the dose function (\log_{10} dose) on the x-axis and the corresponding response on the y-axis. This type of graph illustrates the dose-response relationship independent of time.

OriginPro Software (Origin Lab version 9.95) was used for all data analysis. Data are expressed as mean \pm SEM (standard error of the mean) of experiments performed in five replicates ($N=5$), unless otherwise stated. N represents the number of independent experiments (biological repeats) and n shows the number of technical repeats within an independent experiment. The number of technical repeats in each independent experiment was at least 3. In order to compare the pharmacological activity of a different agonist, data were normalized in each independent experiment to control experimental variation to the response of the agonist in the study (ATP, UTP, Yoda1, or VEGF₁₆₅) or the response of the agonist following pre-treatment. The pharmacological activity was characterised using 2 dose-response curve features: potency and efficacy. Potency refers to the concentration effective in producing 50% of the maximal response. It is commonly expressed as EC_{50} , the half-maximal effective concentration. On the other hand, efficacy is the maximal response a drug can produce, the greatest attainable response.

The Shapiro-Wilk test was used to test if data were normally distributed while equality of variances was validated using Levine's test. For comparisons between two sets of data, when datasets were non-parametric were analysed using Mann-Whitney tests. Contrarily, the datasets following the parametric distribution were assessed using a 2-tailed student's t-test. An asterisk in this work represents statistical significance when the appropriate test calculates that the p-value (p) is lower than 0.05. The higher the degree of statistical significance, the lower the p-value is, as specified: $p^* < 0.05$, $p^{**} < 0.01$, $p^{***} < 0.001$. If the p-value is higher than 0.05, there is no significance between the compared data sets.

Calcium mobilisation assays were plotted as dose-response curves. For EC_{50} (half maximal effective concentration) determinations, curves were fitted using the Hill1 equation:

Hill1 equation

$$y = START + (END - START) \frac{x^n}{k^n + x^n}$$

k = Michaelis constant (EC_{50})
 n = number of cooperative sites (*Hill coefficient that portrays the curve slope*)
 $START$ = baseline; END = maximal, plateau

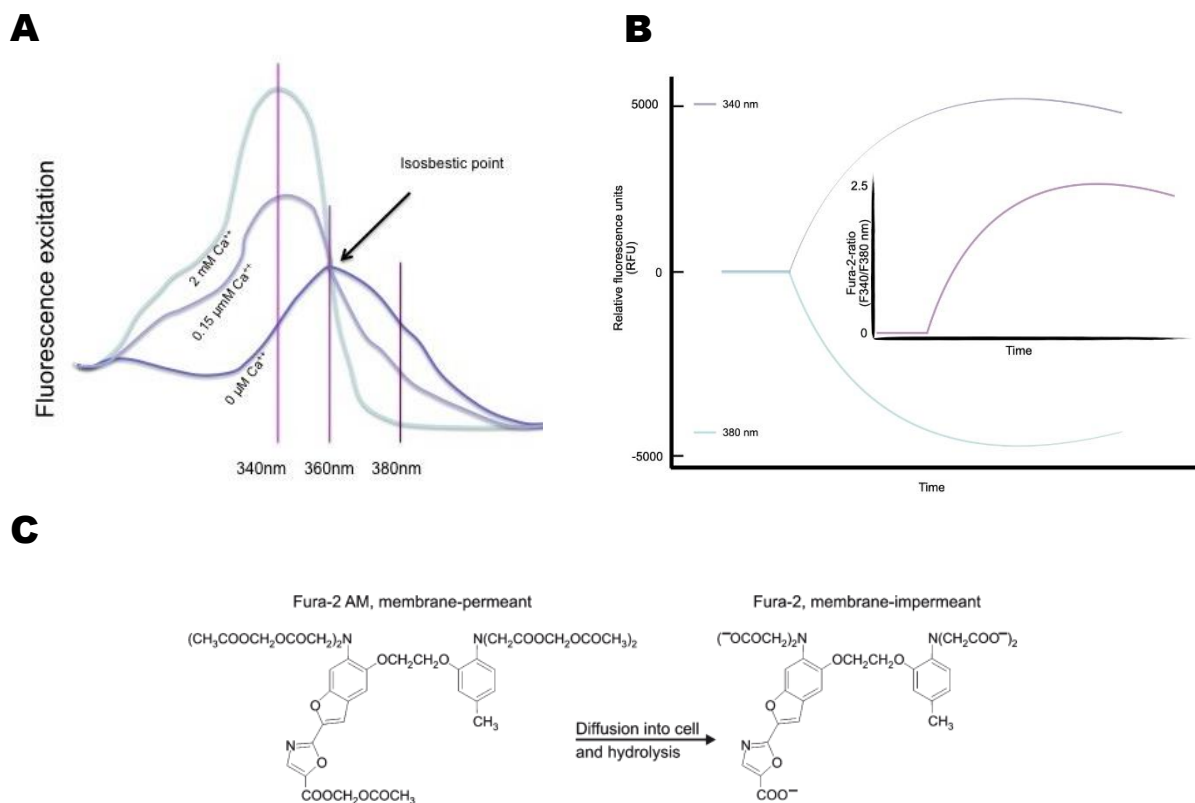


Figure 1. Chemical and fluorescence profile of Fura 2-AM. (A) Fluorescent excitation spectra of Fura-2 at three different concentrations of calcium. The isosbestic point (≈ 360 nm) shows the point where the absorbance is the same for calcium-bound and calcium-free forms, and therefore, the combined fluorescence is the same at any concentration. Image obtained from IonOptix. (B) Change in fluorescence measured at 510 nm after agonist application linked to calcium-bound (340 nm) and calcium-free (380 nm) forms. (C) Representation of the hydrolysis of the FURA 2-AM ester group by esterases, making Fura 2 impermeant to the cell membrane. Structure obtained from Lohr et al. 2010.

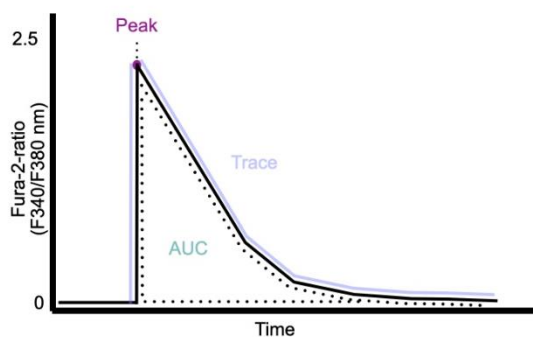


Figure 2. Representative time-resolved intracellular calcium response. F ratios representing the peak, the area under the curve (AUC), and the trace were directly calculated by SoftMax Pro FlexStation software (Molecular Devices). Data is extracted and analysed as described in 2.3.3 methods section.

2.4 Calcium imaging

The ability to image calcium ion fluxes was achieved in the mid-1970s, and from there, different calcium dyes were developed for better performance and specificity of the calcium measurements. Diverse microscopes such as Raman, confocal, or fluorescence microscopy can be used for this type of imaging. In our case, fluorescence time-lapse measurements of intracellular calcium concentrations were obtained using an Olympus IX71 inverted microscope with a 20x objective (LUCPLFLN20x/0.45, Olympus). A Polychrome V monochromator from Till Photonics provided the excitation light (340 and 380 nm), which a dichromatic mirror (model and supplier) applied to the cells. A Hamamatsu recording device acquired the fluorescence images after their passage through an emission filter using the MetaMorph Software version 7.6 (Molecular Devices, California), where fluorescence ratios were extracted for each cell. This technique developed into high-throughput set-ups as the FlexStation III, which was used in this study to perform the pharmacological characterization of the study cells as previously described.

The imaging setup needed previous tuning to ensure appropriate recordings of calcium shifts. ATP was used as an agonist to elicit calcium influx in different cell types. Once this was achieved, two parallel plate flow systems (laminar flow) were used to study flow-mediated calcium responses in 1321N1 hP2X4 astrocytoma and endothelial cells.

2.4.1 Glycotech parallel flow chamber

The Glycotech parallel flow chamber (ref. 31-001) consists of a plexiglass base plate with an inlet and outlet through which media is perfused, a precoated 35-mm standard culture dish on which the cellular monolayer is placed, a gasket that controls the chamber diameter and a vacuum line that allows the structure to be held in place (**Figure 3-A**). Calculating the imposed fluid shear stress in this parallel plate flow chamber is simple. The flow channel length (2 cm) and width (from 0.25 cm to 1 cm) are much greater than the height (from 12.7 μm to 25.4 μm), so it can be considered as flow between infinite parallel plates. It is usually called the plane Poiseuille flow. Considering an incompressible fluid (material density is constant within a fluid parcel) with a constant viscosity (Newtonian fluid), the shear stress is given by the following formula:

$$\text{shear stress } (\tau) = \frac{6Q\mu}{wh^2}$$

Q = flow rate

μ = fluid viscosity

w = channel width

h = channel height (gasket thickness)

Based on this equation, the manufacturer provides a template with predefined data for each gasket (A, B, C, D: referring to different widths and thicknesses) (**Figure 3-B**). To calculate the shear stress ($\text{dynes}\cdot\text{cm}^{-2}$) using a particular gasket, a specific flow rate ($\text{ml}\cdot\text{sec}^{-1}$) must be used (**Figure 3-C**).

The flow rate could be controlled in several ways. In our case, a low-rate peristaltic pump Peri-Star Pro (World Precision Instruments, UK) was used with an internal #14 ID tubing diameter of 1.6 mm. With these characteristics, a range of shear stress from 1 to 20 dynes·cm⁻¹ could be achieved. This pump employed planetary gears for minimal pulsations and greater accuracy.

Twenty-four hours before experimentation, 2mL of growth media with 50,000 cells were seeded in gelatine-coated (2% w/v in PBS for 30 minutes; ref. G1890, Sigma-Aldrich) Corning 35-mm tissue culture dishes in a humidified incubator (37°C, 5% CO₂) to obtain a high confluence in the dish for applying shear stress. After washing twice with room temperature SBS, cells were incubated with 2 μM Fura 2-AM in 500 μL of loading buffer for 30 minutes at 37°C protected from the light. After intensively washing the cells, the loading buffer was replaced with 200 μL of standard bath solution at RT, and then the cells were ready for calcium imaging experimentation. As detailed above, changes in intracellular calcium were indicated as the ratio of fura-2 emission at 510 nm for 340 and 380 nm excitation wavelengths (Ratio 340/380).

2.4.2 Ibidi μ-slides

The Ibidi μ-slide I^{0.4} Luer (ref. 80176; Thistle Scientific) rectangular flow chamber consists of a polymer coverslip with high optical quality, similar to glass. This polymer is prepared with the commercial IbiTreat, a hydrophilic surface modification that improves adherence of all cell types. The channel height of the μ-slide I^{0.4} Luer is 400 μm, and the channel volume is 100 μL. In this case, the shear stress (τ) calculations depended on the dynamical viscosity of the fluid (η) applied, the slide factor (predetermined by the manufacturer; 131.6), and the flow rate (φ):

$$\text{shear stress } (\tau) = \eta * \text{slide factor} * \phi$$

τ = shear stress (dynes · cm⁻¹)

η = dynamical viscosity ((dynes·s)·cm⁻¹)

slide factor = 131.6

φ = flow rate (mL · min⁻¹)

The formula shows a dependency in viscosity for further calculations of the shear stress. Then, the next step was the viscosity calculation of the standard bath solution (SBS) used to perform calcium imaging experiments. Viscosity can be defined as the fluid thickness or resistance to flow. As it depends on temperature, the SBS viscosity was measured at room temperature as experiments were not temperature controlled. A U-tube viscometer was used to calculate the time from A to B (in seconds), and a density bottle was used to calculate SBS density. Then, the final viscosity of the liquid can be calculated following the formula (Figure 3-D, E):

$$\text{dynamical viscosity } (\eta) = \frac{\rho_{SBS} \times t_{SBS}}{\rho_{water} \times t_{water}} \times \eta_{water}$$

ρ = density (g · mL⁻¹)

t = time experimentally calculated (sec)

η = dynamical viscosity of the water (centipoise, ((dyn · s) · cm⁻¹))

However, SBS density is another parameter that needed to be experimentally calculated, and for that, a density bottle was used using water as a reference for this calculation:

$$\text{SBS density } (\rho_{SBS}) = \frac{w_3^{sbs} - w_1}{w_2^{water} - w_1}$$

w_1 = weight of the density bottle
 w_2^{water} = weight of the density bottle full of SBS
 w_3^{sbs} = weight of the density bottle full of water

Following the previously described formulas, the viscosity and density of SBS were calculated:

1st. Calculation of the SBS density (ρ_{SBS}) = $\frac{w_3^{sbs} - w_1}{w_2^{water} - w_1} = \frac{28.4964 - 18.2230}{28.3862 - 18.2230} = 1.011 \frac{\text{g}}{\text{mL}}$

2nd. Experimentally measured SBS and water retention times (averaged N=3) ($t_{SBS} = 111.39 \text{ sec}$; $t_{water} = 104.75 \text{ sec}$) were used to calculate the SBS dynamical viscosity (η) = $\frac{\rho_{SBS} \times t_{SBS}}{\rho_{water} \times t_{water}} \times \eta_{water} = \frac{1.011 \times 111.39}{0.997 \times 104.75} \times 0.997 = 1.075 \text{ centipoise} = 0.01075 \frac{\text{dyn}\cdot\text{s}}{\text{cm}^2}$

3rd. Finally, the flow rate to perform different shear stresses (t from 1 to 20) in the cells was

calculated $\phi = \frac{1 \text{ to } 20 \frac{\text{dyn}}{\text{cm}^2}}{0.01075 \frac{\text{dyn}\cdot\text{s}}{\text{cm}^2} \times 131.6}$ as presented in [Table 6](#).

Table 6. Shear Stress values for μ -slide I⁰⁴ Luer for viscosity $\eta = 1.075$ centipoise.

| τ dynes·cm ² -1 | ϕ mL·min-1 | τ dynes·cm ² -1 | ϕ mL·min-1 |
|---------------------------------|-----------------|---------------------------------|-----------------|
| 1 | 0.706864 | 11 | 7.7755 |
| 2 | 1.413727 | 12 | 8.482364 |
| 3 | 2.120591 | 13 | 9.189227 |
| 4 | 2.827455 | 14 | 9.896091 |
| 5 | 3.534318 | 15 | 10.60295 |
| 6 | 4.241182 | 16 | 11.30982 |
| 7 | 4.948046 | 17 | 12.01668 |
| 8 | 5.654909 | 18 | 13.43041 |
| 9 | 6.361773 | 19 | 14.13727 |
| 10 | 7.068636 | 20 | 14.84414 |

As cited above, the flow rate was controlled using the low-rate peristaltic pump Peri-Star Pro (Word Precision Instruments, UK). In this case, the tubing was replaced with a non-silicone-based tube with low gas permeability and 1.6 mm in diameter (Tygon®, ref. LMT-55; VWR International). The diameter size must be constant as it will directly impact flow speed.

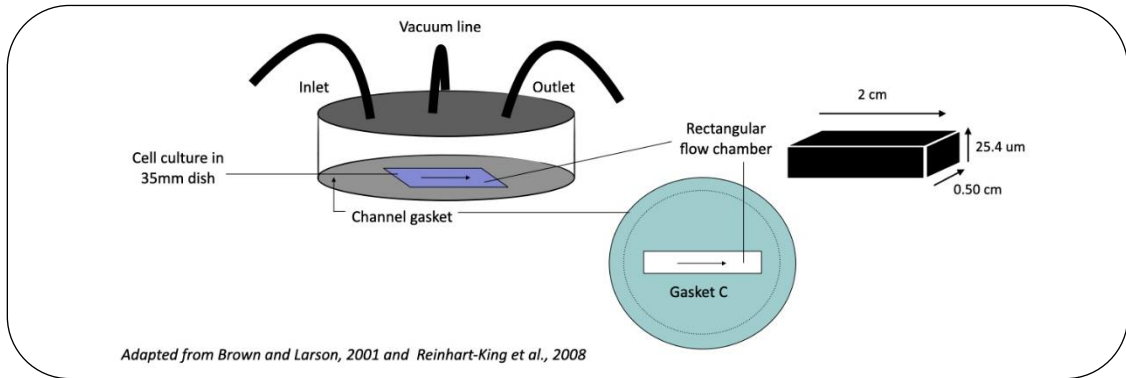
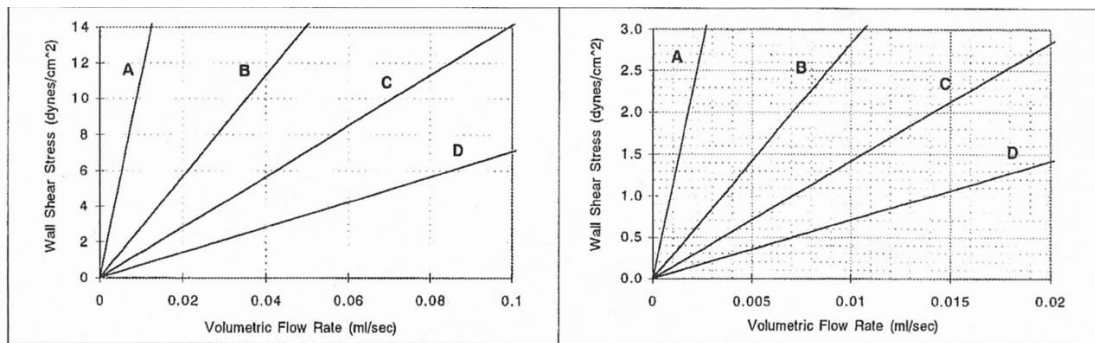
For the Ibidi μ -slide, 3 or 24 hours before experimentation, a range of cell concentrations was seeded in 100 μ L cell growth culture media and cultured in the incubator (37°C, 5% CO₂) once covered the reservoirs with the supplied caps. Each reservoir was filled with 60 μ L cell growth culture media one hour later to ensure better cell adherence in the slide parallel channel. Although the slides were prepared with the commercial IbiTreat, a collagen type I coating (0.5 mg/mL in acetic acid for 30 minutes; C2867, Sigma-Aldrich) was applied before cell seeding, as indicated in Chapter 4, to study the potential effect on the mechanical response of the cells. The day after, after washing twice with room temperature SBS, cells were incubated with 2 μ M Fura 2-AM in 100 μ L of loading buffer for 30 minutes at 37°C protected from the light. After washing the cells, the loading buffer was replaced with 100 μ L of standard bath solution at RT, and the cells were let steady in the microscope for at least ten minutes before experimentation to avoid possible previous stimulation during washing steps. Then, the cells were ready for calcium imaging experimentation. Intracellular calcium recordings were performed using Fura-2AM as described above. Routinely, μ -slides were placed in the incubator for at least 3 hours before cell seeding to avoid emerging bubbles in the slide channel. For medium exchange or washes, reservoirs were emptied, and the channel medium was replaced multiple times without draining the channel, which would cause a complete loss of the cells. The tube was connected to the slide using the Tube adapter set (ref. IB-108301; Thistle Scientific).

Due to previous technical issues during the shear stress assays, the standard bath solution (SBS) used during experimentation was previously degassed for at least 3 hours using a side-arm flask connected to a vacuum system with the help of a stir bar and low-rate stirring.

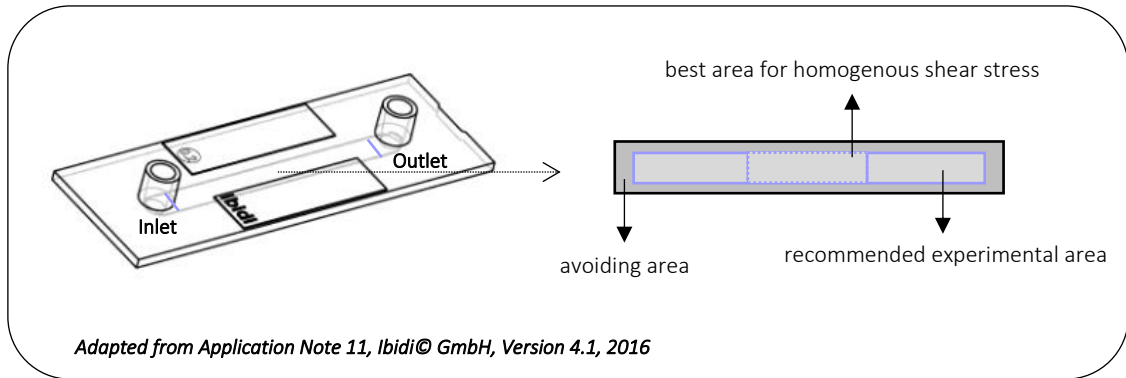
2.4.3 Data analysis for calcium imaging

Intracellular calcium recordings are presented as the ratio of emitted fluorescence after excitation at 340 and 380 nm relative to baseline (1 unit of fluorescence). For that, ratios for independently selected cells (regions of interest, ROIs) of the fluorescence images were extracted using the MetaMorph Software offline tool. This data was then normalised in Excel using the baseline correction previously described by others (Arniges et al., 2004; Pascual et al., 2011; Venturini et al., 2020). Briefly, measurement of basal calcium was obtained along 1 min recording every 5 seconds (10 ratio recordings) before any stimulation for each independent cell. The averaged basal recordings were used to normalise each cell to its baseline. This normalisation allowed us to average and compare the cytosolic calcium concentrations between a batch of cells and between technical repeats.

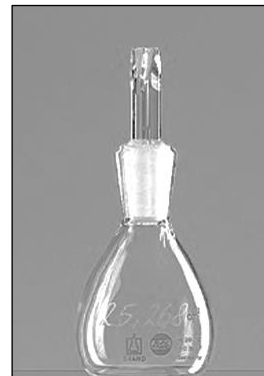
OriginPro Software (Origin Lab version 9.95) was used for plotting the normalised data as mean \pm SEM (standard error of the mean) of cells of the same biological repeat (**N**) or comparison of numerous N of experiments performed.

A**Glycotech parallel flow chamber****B**Wall shear stress relationships for different size gaskets**C**Calculations for Gasket C

| τ dynes-cm ⁻² | ϕ mL-sec-1 | ϕ mL-min-1 |
|-------------------------------|-----------------|-----------------|
| 1 | 0.007 | 0.42 |
| 2.5 | 0.018 | 1.1 |
| 6 | 0.04 | 2.4 |
| 8 | 0.06 | 3.6 |
| 12 | 0.085 | 5.1 |

D**Ibidi μ -slide****E**Dynamical viscosity calculations $t = \text{from A to B in seconds}$ 

U-tube viscometer



Density bottle

Figure 3. Parallel flow chambers specifications. (A) Schematic representation of a Glycotech parallel flow chamber and Gasket C technical specifications. (B) Wall shear stress relationships for the four different-sized gaskets provided by the manufacturer were used to calculate the appropriate (C) flow rate to be applied. (D) Schematic representation of a Ibidi μ -slide with specification of the recommended experimental areas. (E) Calculation of t parameter using a U-tube viscometer and calculation of SBS density (ρ) using a density bottle required for the calculation of the standard bath solution (SBS) dynamical viscosity (image from Sigma-Aldrich website).

2.5 Polymerase chain reaction (PCR)

2.5.1 RNA extraction

Cell lysate for RNA extraction was obtained from a pellet of 1×10^6 cells after a routine cell passage procedure. In a fume hood, the pellet was resuspended in 1 mL of Tri Reagent® (Sigma) (Chomczynski et al., 1987). If not required at collection, stocks of lysed cells in Tri Reagent® were kept at -80°C .

Then, 200 μL of chloroform (Fisher) was added to each sample to separate the homogenate into aqueous and organic phases. Samples were shaken vigorously by hand and allowed to stand at room temperature for 5 minutes before centrifugation at 12,000 rpm for 15 minutes at 4°C . After centrifugation, the upper transparent layer of the sample contained the RNA and was transferred to a fresh 1.5 mL Eppendorf. 0.8X of isopropanol (Fisher) was added to the isolated RNA and mixed vigorously by hand. After 10 minutes of preincubation at room temperature, the mix was centrifuged for 60 minutes at 12,000 rpm at 4°C to pellet the RNA. The supernatant was discarded, and the pellet was washed in 500 μL of ice-cold 80% (v/v). After 5 minutes of centrifugation at 12,000 rpm at 4°C , the ethanol was gently removed from the tube, and the pellet was air-dried for 5 to 10 minutes. Rehydration of RNA was achieved through the addition of an appropriate volume of nuclease-free water and, from here, the sample was kept in ice.

The RNA concentration and quality were checked by adding 1 μL of the RNA sample to a NanoDrop 2000c UV-Vis spectrophotometer instrument (Thermo Scientific). The absorbance ratios of 260/280 nm and 260/230 were used to assess the purity of the RNA. Samples were required to have a ratio value close to 2.00 to be considered pure. When that was not the case, a cleaning process was performed in the samples, as briefly described in the next paragraph.

The RNA sample was exposed to 0.1X volumes of 3 M sodium acetate (NaOAc), and then the mix was treated with 2.5X of ice-cold ethanol (80%) overnight at -80°C . The day after, samples were centrifuged for 30 minutes at 12,000 rpm at 4°C , and the pellet was kept. As previously explained, the pellet was washed in 500 μL of ice-cold 80% (v/v), centrifuged, and air-dried for 5 to 10 minutes. At this point, the RNA was resuspended in nuclease-free water and ready to be quantified again using Nanodrop.

2.5.2 Complementary DNA (cDNA) synthesis

To avoid false positive signals in the subsequent RT-PCR, the extracted RNA was treated with the DNA-free™ DNA Removal Kit (AM1906, Fisher) to degrade possible trace amounts of genomic DNA before the cDNA synthesis. For the DNase digestion, the RNA sample is treated with 1 mL of recombinant DNase I (rDNase I) and 0.1X volume 10X DNase I Buffer at 37°C for 30 minutes. The DNase Inactivation is achieved by vigorously resuspending 0.1X volume of the DNase Inactivation Reagent in the mix and incubating the sample for 2 minutes at room temperature. Lastly, the RNA samples were centrifuged for 1.5 minutes at 10,000 x g, and the supernatant containing the RNA was transferred to a fresh tube.

The extracted RNA from cell lines was ready to be reversed and transcribed into cDNA. In addition to this RNA, human brain RNA (AM7962, Fisher) was used as a positive control for gene expression. Each synthesis reaction was prepared in duplicates where one sample reaction contained reverse transcriptase (RT) enzyme to produce cDNA from the target RNA sequence. In contrast, the other did not contain reverse transcriptase (-RT), ensuring that any PCR amplicon was derived from de novo cDNA rather than genomic DNA.

For each reaction in sterile DNase and RNase free tubes, 1 µg of RNA was primed with 50 ng of random hexamers (C1181, Promega) and 1 µL 10 mM dNTP Mix (BIO39044, SLS) in nuclease-free up to 13 µL. The mix was well mixed by flicking the tube before brief centrifugation and heating to 65°C for 5 minutes to allow the RNA to denature. Then, the reaction was incubated on ice for at least 1 minute allowing the primer to anneal to the RNA. The contents of the tube were collected by a brief centrifugation and transferred into a 1.5 mL sterile DNase/RNase free tube containing 4 µL 5X of First-Strand Buffer, 1 µL of 0.1 M DTT, 1 µL of SuperScript™ III Reverse Transcriptase (for RT reaction, 1 µL nuclease-free water for -RT control reactions) (18080-044, Invitrogen) and 1 µL of RNasin® Ribonuclease inhibitor (N2511, Promega) to limit RNA degradation. All reaction samples were gently flicked before briefly centrifuging and transferred to a PCR machine, where the samples were exposed to three different steps of incubation. To allow transcription to occur, reactions were first incubated at 25°C for 5 minutes and directly after a second incubation step at 50°C for 60 minutes, followed by inactivation of the enzyme at 70 °C for 15 minutes. cDNA reaction samples were stored at -20 °C until required.

2.5.3 Non-quantitative reverse transcription PCR (RT-PCR)

Non-quantitative reverse transcription PCR (RT-PCR) technique was employed to detect gene expression of adenosine, P2X, and P2Y receptors in human umbilical vein endothelial cells (HUVEC).

All primers were previously designed by Dr. Hinnah Campwala, excluding P2X4 and P2Y11. P2X4 inter-spanning primers were manually designed, ensuring the potential amplification of the four transcripts variants for the human P2X4 (NCBI reference sequences: NM_001256796.2, NM_001261397.2, NM_001261398.2 and NM_002560.3). A diverse combination of nucleotides (20-25 bp) with an appropriate percentage of GC between 35-65% were chosen, and the identity of the primers was checked using the Human BLAT search tool from the Genome Institute site of the University of California Santa Cruz. On the other hand, the P2Y11 primer sequence was taken from (Xiao et al., 2011).

New stocks of each primer pair were supplied lyophilized by Sigma-Aldrich. They were reconstituted at 100 µM in nuclease-free water, and working stocks were prepared at 10 µM and used for the PCR sample preparation. Primer and working stocks were kept at -20 °C to ensure their integrity. All forward (F) and reverse (R) primer sequences are listed (5'-3') are shown in **Table 7, 8 and 9**.

As described in the previous section, prepared cDNA samples were used as an experimental template for PCR amplification. Two different PCR master mixes were used in this study due to the difficulty of getting amplicon bands in the positive control (human brain), where these

receptors' expressions have been previously reported in some P2Y receptors. PCR master mix from Promega (Taq polymerase) was the primary polymerase used for this characterization (P1, P2X, and most P2Y receptors), and then the reactions were prepared following manufactured instructions as follows. Reactions for each primer pair were prepared in duplicate in autoclaved nuclease-free microcentrifuge tubes. For a final volume reaction of 25 μ L, 12.5 μ L of the PCR master mix (Promega), 0.5 μ L of working stocks of each primer (F and R), 1 μ L of cDNA (either RT or RT-), and 10.5 μ L nuclease-free water was added. All reaction samples were gently flicked before briefly centrifuging and transferred to a PCR machine, where the samples were thermally cycled to allow selective amplification following three major steps: denaturation, annealing, and extension. The initial denaturation step of the DNA helix lasted 1 minute at 94 $^{\circ}$ C, which was followed by 40 cycles of denaturation at 94 $^{\circ}$ C for 30 seconds, annealing of the primers to the DNA template at the primer-specific annealing temperature (Tables 7, 8, 9) for 30 seconds, and a final extension of the cDNA strand at 72 $^{\circ}$ C for 1 minute. Primer-specific annealing temperatures were determined by previous PCRs, where temperature gradients (55-62 $^{\circ}$ C) were performed to find the optimal reaction conditions. A final extension at 72 $^{\circ}$ C for 5 minutes was needed to ensure proper extension of the cDNA.

One-taq Master Mix from New England BioLabs (a combination of Taq polymerase and Deep Vent[®] DNA Polymerase) was used to study the expression of P2Y2 and P2Y6 (as referred to in Table 9). Reactions were prepared as previously described for the other Master Mix used in this study, with the only difference being that one-third of nuclease-free water (3.5 μ L) was replaced for betaine (1M stock), facilitating the amplification of these genes (Henke et al., 1997). Thermocycling conditions differed from those described, and the steps were configured following manufacturer recommendations. The initial denaturation step of the DNA helix lasted just 30 seconds at 94 $^{\circ}$ C in this case, which was equally followed by 40 cycles of denaturation at 94 $^{\circ}$ C for 30 seconds, annealing of the primers to the DNA template at 58 $^{\circ}$ C for 30 seconds, and a final extension of the cDNA strand at 68 $^{\circ}$ C for 1 minute. Again, a final extension at 68 $^{\circ}$ C for 5 minutes was needed to ensure proper extension of the cDNA.

Table 7. Primer sequences for P1 receptors and housekeeping gene (β -actin).

| Receptor | Sequence | Size (bp) | Annealing temperature ($^{\circ}$ C) |
|----------|-----------------------|-----------|---------------------------------------|
| A1 F | GTGCGAGTTCGAGAAGGTCA | 374 | 55 |
| A1 R | GGATGCGGAAGGCASTAGACA | | |
| A2A F | CTACCGTATCCGCGAGTTCC | 295 | 55 |
| A2A R | GCTAAGGAGCTCCACGTCTG | | |
| A2B F | CAGAACCTGGGATGGAACC | 277 | 55 |
| A2B R | CAGCACAGGGCAAAAATCCC | | |
| A3 F | CTGGTGCCGAGGCTATTTCC | 302 | 55 |
| A3 R | CCTTGCGGACAACCTTGGGA | | |

| | | | |
|------------------|----------------------|-----|-------|
| β -actin F | CACAGAGCCTCGCCTTTGCC | 282 | 55-62 |
| β -actin R | CGATGCCGTGCTCGATGGGG | | |

Table 8. Primer sequences for P2X receptors.

| Receptor | Sequence | Size (bp) | Annealing temperature (°C) |
|----------|-----------------------|-----------|----------------------------|
| P2X1 F | GCTTTCCACGCTTCAAGGTC | 341 | 58 |
| P2X1 R | GAGGTGACGGTAGTTGGTCC | | |
| P2X2 F | GCACAGACGGGTACCTGAAG | 200 | 58 |
| P2X2 R | GGAGTACTTGGGGTTGCACT | | |
| P2X3 F | TGTATCAGACAGCCAGTGCG | 564 | 60 |
| P2X3 R | CGGATGCCAAAAGCCTTCAG | | |
| P2X4 F | TTACGACCAAGGTCAAGGGC | 250 | 55 |
| P2X4 R | CCTGTTGAGACTCCGTTGCT | | |
| P2X5 F | GCAATGTGATGGACGTCAAGG | 263 | 56 |
| P2X5 R | GTACCCGGAGGAGACAGACT | | |
| P2X6 F | GACTTCGTGAAGCCACCTCA | 405 | 56 |
| P2X6 R | TTGTGGTTCATAGCGGCAGT | | |
| P2X7 F | CGGTTGTGTCCCCAGTATCC | 414 | 56 |
| P2X7 R | AATGCCCATATTCCGCCCT | | |

Table 9. Primer sequences for P2Y receptors.

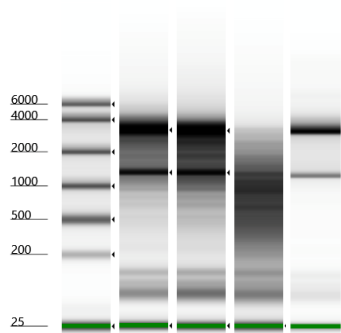
| Receptor | Sequence | Size (bp) | Annealing temperature (°C) |
|----------|---------------------------|-----------|---------------------------------|
| P2Y1 F | GTTCAATTTGGCTCTGGCCG | 326 | 55 |
| P2Y1 R | TTTTGTTTTTGC GGACCCCG | | |
| P2Y2 F | CCGCACCCTCTACTACTCCT | 243 | 58 <i>One-taq Master Mix</i> |
| P2Y2 R | TCAGTTCTGTCGGATCTGCG | | |
| P2Y4 F | CCCCAACCCCTATGGCTCTTC | 427 | 60 |
| P2Y4 R | TGGTCAAACCTCTTCAGGCCG | | |
| P2Y6 F | GCTCTCACTGTCATCGGCTT | 391 | 58 <i>One-taq Master Mix</i> |
| P2Y6 R | TCTGCCATTTGGCTGTGAGT | | |
| P2Y11 F | CTACAGAGCGTATAGCCTGGTGCTG | 365 | 58 |
| P2Y11 R | CCATGTAGAGTAGAGGGTGGACACA | | |
| P2Y12 F | ACTGGGAACAGGACCACTGA | 698 | 55 |
| P2Y12 R | CAGAATTGGGGCACTCAGC | | |
| P2Y13 F | TTCCCAGCCCTCTACACAGT | 461 | 55 |
| P2Y13 R | GGCCCTTTAAGGAAGCACA | | |
| P2Y14 F | CGGAAGTGGCACAAAGCATC | 370 | 60 |
| P2Y14 R | CCCTAAACGGCTGGCATAGA | | |

2.6 RNA sequencing

RNA was extracted as stated in the previous **section 2.4.1**, but RNA quality was double-checked using the RNA ScreenTape® in the 4150 TapeStation (Agilent Technologies). This technology allows the evaluation of total RNA integrity determined by the RNA integrity number equivalent (RIN^e). Traditionally, the integrity was assessed by using electrophoresis in an agarose gel with ethidium bromide showing the two bands for ribosomal RNA subunits (rRNA), 28S and 18S. However, this method is believed to be inconsistent today. The RNA integrity number is more accurate than UV spectrophotometric measurements or ribosomal RNA ratios. In the TapeStation, the sample is separated in the tape channels according to different molecular weights, and a laser detects the small amounts. The system will produce an electropherogram correlating the amount of RNA with the fluorescence change registered, calculating the ratio of the two ribosomal bands. The RIN number is then calculated using a machine-learning algorithm that uses more information than the ratio of ribosomal subunits but is still highly dependent on these two parameters. The range for the RIN score number is 1 to 10, and higher RIN values refer to a higher RNA integrity (Sheng et al., 2017).

Samples from HMEC-1 cells were sent to *Novogen* for Transcriptome Sequencing (Cambridge, UK). The company required a minimum RIN^e of 4, and that was previously checked in-house. For this, samples were prepared using 1 µL of RNA, mixed with 5 µL of RNA ScreenTape Sample Buffer® room temperature equilibrated. The mix was spun down and vortexed for 1 minute at 2000 rpm. Then, the sample was denaturised by a heat shock for 3 minutes at 72°C. Samples were placed in ice for 2 minutes to stop the reaction and directly loaded to the RNA ScreenTape® (Agilent Technologies). The TapeStation Controller Software automatically calculated the RIN^e (**Figure 4**).

Novogen prepared the RNA libraries and sequenced the samples according to the human genome using Illumina PE150 technology. Bioinformatics Analysis provided as the quantification of gene expression level as FPKM (Fragments Per Kilobase of transcript sequence per millions base pairs sequenced), a normalisation of the raw counts which considered the effect of sequencing depth (total read counts, millions) and gene length (kilobase) for the read counts at the same time. This type of normalisation is very well-established in RNA-seq experiments (Mortazavi et al., 2008).

A**B**

| Sample | RIN ^e | 28S/18S (Area) | Conc. (ng·μL) |
|--------|------------------|----------------|---------------|
| 1 | 8.1 | 1.3 | 257 |
| 2 | 7.0 | 1.4 | 311 |
| 3 | 2.0 | - | 367 |
| 4 | 10.0 | 3.1 | 148 |

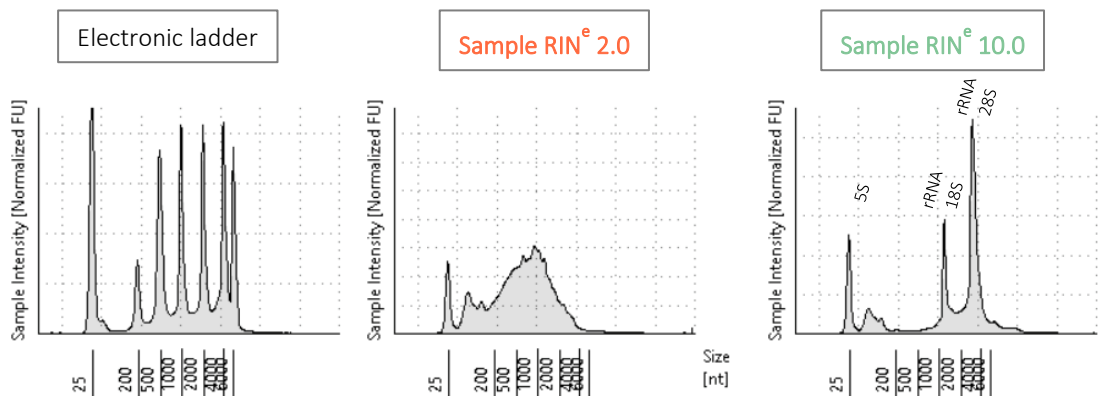
C

Figure 4. Four human microvascular endothelial cell (HMEC-1) samples with different levels of RNA degradation were analysed using the 4150 TapeStation from Agilent Technologies. **(A)** Gel images of the electronic ladder plus the four samples with their respective determined RIN^e values are shown under the gel image. On a scale of 1 to 10, 10 represents intact RNA, while a RIN^e of 1 represents a highly degraded RNA sample. **(B)** Table displaying the four sample results indicating the specific area calculated of the ribosomal subunits and the concentration of the samples tested. **(C)** Representative electropherograms of the electronic ladders, a strongly degraded RNA sample (RIN^e 2), and a highly intact RNA sample (RIN^e 10).

2.7 Western Blotting

Western Blotting technique was employed to detect protein expression of P2X₄, P2Y₂ and P2Y₁₁ receptors in human microvascular endothelial cells (HMEC-1).

2.7.1 Protein extraction and quantification

Cells were washed twice with ice-cold PBS at pH 8 when they reached 70-80% confluency in culture. Cells were scratched on ice in 500 μ L of ice-cold PBS, and cell lysates in the PBS were collected in 1.5mL Eppendorf tubes. Cells were then centrifuged at 4.000 g for 20 minutes at 4°C, and the pellet was resuspended in 20 μ L of ice-cold solubilisation buffer. The buffer contained 150 mM sodium chloride (NaCl), 1 mM magnesium chloride, 1 mM calcium chloride, 2% (v/v) Triton X-100, 20 mM Tris hydrochloric acid at pH 7.6, and protease inhibitor cocktail (Complete™ tablets, Roche). The mix was then homogenised in a rotation wheel for 2 hours in the cold room and centrifuged to pellet the cell debris at 12.000 x g for 20 minutes at 4°C.

The supernatant was collected, and the protein concentration was calculated using a colorimetric Pierce™ BCA protein assay (Sigma-Aldrich, UK). This assay has been extensively used as it is usually less variable than other colorimetric assays, such as the Bradford assay (Bradford, 1976), and can be used in microwell plates. The principle of this assay is the protein capacity to reduce copper (II) (Cu²⁺) to copper (I) (Cu⁺) in a protein concentration-dependent manner. Bicinchoninic acid can form a purple complex with Cu⁺ when chelates with this reduced copper, whose absorbance is maximal at 562nm. The absorbance at this wavelength will be directly proportional to protein concentration (Smith et al., 1985; Wiechelman et al., 1988). The absorbance of the albumin calibration curve is set according to manufacturer instructions, and from there, the protein concentration of the samples can be calculated.

Protein samples were consistently prepared with 25 or 50 μ g of total protein extract in a final volume of 25 μ L sample buffer dithiothreitol (50 mM, DTT) supplemented and boiled for 5 minutes at 96 °C. The sample buffer contained 240 mM Tris-HCl at pH 6.8, 12% (w/v) sodium dodecyl sulphate (SDS), 0.05% (w/v) bromophenol blue and 30% (v/v) glycerol (with a final concentration of 50 mM DTT).

2.7.2 SDS-PAGE and membrane transference

SDS-PAGE (sodium dodecyl sulphate polyacrylamide gel electrophoresis) is a technique used to separate different proteins based on their molecular weight. Proteins have more or less intrinsic electrostatic charge, attracting them to the opposite charge direction and moving through the gel through which an electric current is applied. In this gel electrophoresis type, the SDS detergent will uniform all protein charges after the boiling preincubation. Then, proteins will possess the same mass-charge ratio, and their traveling speed through the gel will be determined by their mass, so heavier proteins will travel slower than lighter ones (Gallagher, 2012).

Precast SDS polyacrylamide (4-12% gradient) Bolt™ Bis-Tris Plus Mini Protein Gels (Invitrogen) were used when available in-house. For these gels, 20X Bolt™ MES SDS Running Buffer was used to ensure the best running conditions. When unavailable, the acrylamide gel was

prepared composed of 5% (v/v) acrylamide stacking and 10% (w/v) acrylamide resolving gel (**Table 10**). In this case, the electrophoresis running buffer consisted of 25 mM Tris, 192 mM glycine, and 0.1% (w/v) SDS. The gels ran at 90V for approximately 90 minutes using the Precision Plus Dual Colour Bio-Rad as a ladder (Bio-Rad Laboratories, UK).

Proteins were then transferred to an Immobilon-P polyvinylidene difluoride (PDVF; 0.45 μ m pore size; Millipore, UK) membrane using ice-cold transfer buffer consisting of 25 mM Tris, 192 mM glycine, and 20% (v/v) methanol in a mini trans tank blot at 90V for 90 minutes in the cold room.

2.7.3 Membrane blocking and protein imaging

Membranes were blocked in blocking solution (**Table 11**) for a minimum of 1 hour at room temperature on a rocking platform. After blocking, membranes were blotted with the specific primary antibody (**Table 12**) at 4 °C overnight when 5% (w/v) semi-skimmed milk blocking solution was used or 3 hours at room temperature in the case of any other blocking solution composition and before the secondary antibody, membranes were washed thrice for 10 minutes at RT on a rocking platform. The washing solution was PBS-T when the milk-based blocking was used, but TBS-T was used in all other cases. Immediately after, membranes were incubated for 1-2 hours at RT with the specific horseradish peroxidase (HRP) conjugated secondary antibody prepared in a blocking solution (containing Tween-20 in all cases). In the case of β -actin detection, the secondary antibody was already conjugated, so the last step wasn't required. The membranes were then washed thrice for 10 minutes at RT and directly incubated in Pierce™ ECL detection reagent (Fisher Scientific, ref. 32106) for 2 minutes. Membranes were imaged on a ChemiDoc™ Imaging System (Bio-Rad Laboratories, UK).

Some membranes were re-probed by stripping the antibodies from the blot for 40 minutes in a 0.2M sodium hydroxide (NaOH) solution, which was sequentially washed thrice, blocked for an hour, and incubated with the additional primary antibody.

Table 10. Stacking and resolving gel composition.

| Stacking acrylamide gel | Resolving acrylamide gel |
|--|---|
| 125 mM Tris pH 6.8, 5 % (v/v) acrylamide 30% 37.5:1, 0.1 % (w/v) SDS, 0.05 % (v/v) ammonium persulphate (APS), 0.1% (v/v) tetramethyl ethylenediamine (TEMED) | 375 mM Tris pH 8.8, 10 % (v/v) acrylamide 30% 37.5:1, 0.1 % (w/v) SDS, 0.05 % (v/v) ammonium persulphate (APS), 0.05 % (v/v) tetramethyl ethylenediamine (TEMED) |

Table 11. Blocking solutions configuration.

| Blocking solution | Washing solution | Primary antibody solution | Secondary antibody solution |
|---|------------------|--|---|
| 5% (w/v) semi-skimmed milk in PBS-T (1X PBS, 0.1% (v/v) Tween-20 (Sigma-Aldrich)) | PBS-T | 5% (w/v) semi-skimmed milk in PBS-T (1X PBS, 0.1% (v/v) Tween-20) | 5% (w/v) semi-skimmed milk in PBS-T (1X PBS, 0.1% (v/v) Tween-20) |
| 1% (w/v) bovine serum albumin, and 10% sucrose in 1X TBS | TBS-T | 1% (w/v) bovine serum albumin in TBS-T (1X TBS, 0.1% (v/v) Tween-20) | 1% (w/v) bovine serum albumin, and 10% sucrose in TBS-T (1X TBS, 0.1% (v/v) Tween-20) |
| 5% sucrose in 1X TBS | | | 5% sucrose in TBS-T (1X TBS, 0.1% (v/v) Tween-20) |
| 10% (w/v) bovine serum albumin in 1X TBS | | | 10% (w/v) bovine serum albumin in TBS-T (1X TBS, 0.1% (v/v) Tween-20) |

Table 12. List of antibodies used for Western Blotting.

| Name | Source | Host | Identifiers | Dilution |
|---------------------------------|---------------|----------------------------------|-------------|--------------|
| anti- β -actin | Sigma-Aldrich | mouse monoclonal- HRP conjugated | A3854 | 1:3000 |
| anti-P2X4 | Alomone Labs | rabbit polyclonal | APR-002 | 1:1000 |
| anti-P2Y2 | Alomone Labs | rabbit polyclonal | APR-010 | 1:1000 |
| | Abcam | mouse polyclonal | ab168535 | |
| anti-P2Y11 | Alomone Labs | rabbit polyclonal | APR-015 | 1:1000 |
| | Abcam | rabbit polyclonal | ab180739 | 1:100-1:1000 |
| anti-rabbit | Invitrogen | goat-HRP conjugated | A16096 | 1:1000 |
| anti-rabbit F(ab') ₂ | Abcam | goat-HRP conjugated | ab6112 | 1:2000 |

2.7.4. Data analysis for western blot imaging

Western blot images were semi-quantified, comparing the relative amount of the protein of interest against the relative expression of β -actin, our loading control, for normalization. Images exported from the ChemiDoc™ Imaging System were saved as a JPEG file and were analysed using Image J (Fiji is Just ImageJ version 1.53; UK).

For each image, a rectangular region of interest (ROI) was defined around the protein of interest band, avoiding the possible surrounding background. This ROI should be of consistent size and shape across all lanes and was used to perform every single measurement in each

independent image. The ROI length was set for the most prominent protein of interest band to ensure a good fit of all the present bands in the blot. The total pixel intensity for each lane's protein of interest bands was measured and saved by moving the ROI between lanes (left-right movement, avoiding changes in ROI height position between lanes). In the same way, background measurements for each lane were taken using the same ROI selecting an area above or below the protein of interest band.

In a total white pixel ROI, the intensity value is 0, as stands for the absence of colour. On the contrary, a total black pixel ROI will have an intensity value of 255, representing this number as the highest intensity of colour possible in the analysis image. Thus, the first step of normalisation of the protein of interest band intensity value is the inversion of each ROI intensity value by subtracting from the highest intensity of colour possible ROI ($255 - \text{ROI}$). The same was done for the background measurements. Then, the amount of net protein was calculated by subtracting the background inverted intensity from the protein of interest inverted intensity previously calculated. The analysis of the relative expression β -actin was performed as previously described, and net β -actin protein loading control value was used to normalised as ratio values of the relative amount of the protein of interest (net protein of interest/net β -actin protein). This ratio normalisation allows us to compare different conditions and technical repeats, as it reduces the variability caused by protein loading error, for instance.

Semi-quantitative results are presented along this thesis in bar charts, indicating the relative expression levels of the protein of interest between different cell lines. Graphs were done using the OriginPro software, and statistical analysis was performed as declared in **section 2.3.3**.

2.8 Nitrite (NO_2^-) measurement

Nitric oxide (NO) is a crucial physiological messenger in the vascular system, regulating vascular tone upon calcium influx. One way to study nitric oxide changes is by measuring one of the two breakdown products of nitric oxide, nitrite (NO_2^-) (Bredt et al., 1994; Dawson et al., 1996). Nitric oxide quickly oxidizes to nitrite, which is much more stable and easier to quantify. For this, the Griess Reagent System is broadly used in biology to measure changes in nitric oxide indirectly. The system is based on the diazotization reaction described by Griess but with multiple modifications. A diazotization reaction consists of two significant steps. First, the nitrite present in the biological sample reacts with sulfanilamide to form a diazonium ion specimen, which, in turn, will react with N-(1-naphthyl) ethylenediamine dihydrochloride (NED) to produce an azo compound. This azo compound results in an azo dye whose absorbance can be measured between 520-550 nm. Both reactions are catalysed under acidic conditions (phosphoric acid specifically) (Green et al., 1982).

This system can be used to test the concentration of NO_2^- in experimental liquid samples. In this study, the quantification of nitrite was quantified in HMEC-1 serum-free culture media (MCDB-153). Sensitivity of the system depends on the liquid matrix in study, so for that comparison of the representative nitrite standard references curves was performed in standard bath solution (SBS) and serum-free culture media (MCDB-153). The standard curve reference showed that serum-free culture media was an equally good matrix to perform the experiments (**Figure 5**). The nitrite concentration detection limit is $2.5 \mu\text{M}$ in ultrapure deionized distilled water, as described by the fabricant (Promega).

Samples came from starved cells that were either drug-treated or unstimulated. 50 μL of experimental samples were freshly transferred and plated in triplicate in a 96-well flat-bottom assay plate. Each well was mixed with the same volume of the sulfanilamide solution and incubated at room temperature, protected from light for 10 minutes. This preincubation is relevant, as sulfanilamide and NED compete for nitrite in the reaction. Following the 10-minute incubation, the same volume of NED solution was added to the sample mix and preincubated again for another 10 minutes in the same conditions. After this time, the sample's absorbances were ready to be measured between 538 nm within 30 minutes, as colour may fade after this time. A standard curve was prepared for each assay in a 0-100 μM range following the same preparation as experimental samples. A nitrite standard reference curve was created with the data extracted from this standard curve performed in each independent experiment. Average absorbance values for the known concentrations were plotted as a Known Y with the known concentrations (0-100 μM) as a function of X. Finally, to determine each experimental sample's nitrite concentration, the average absorbance values for each sample are compared to the nitrite standard reference curve.

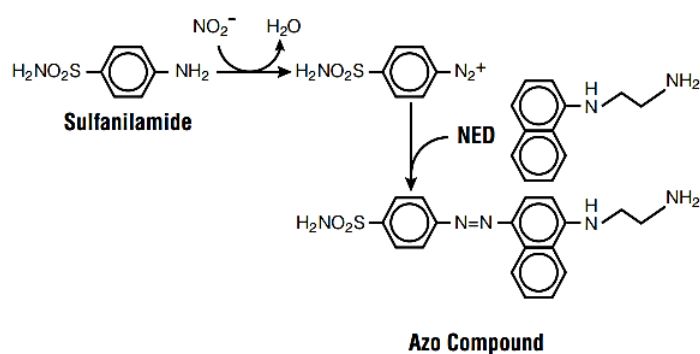
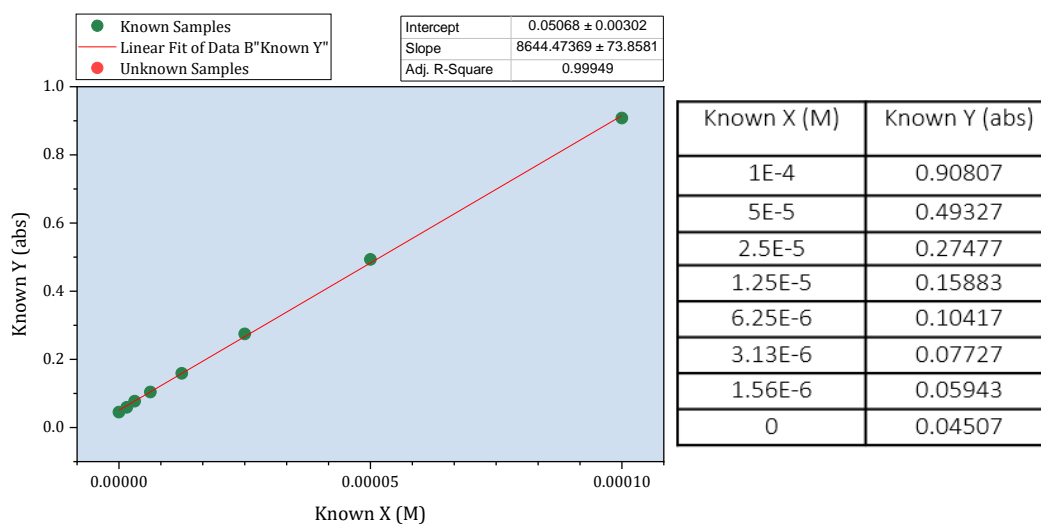
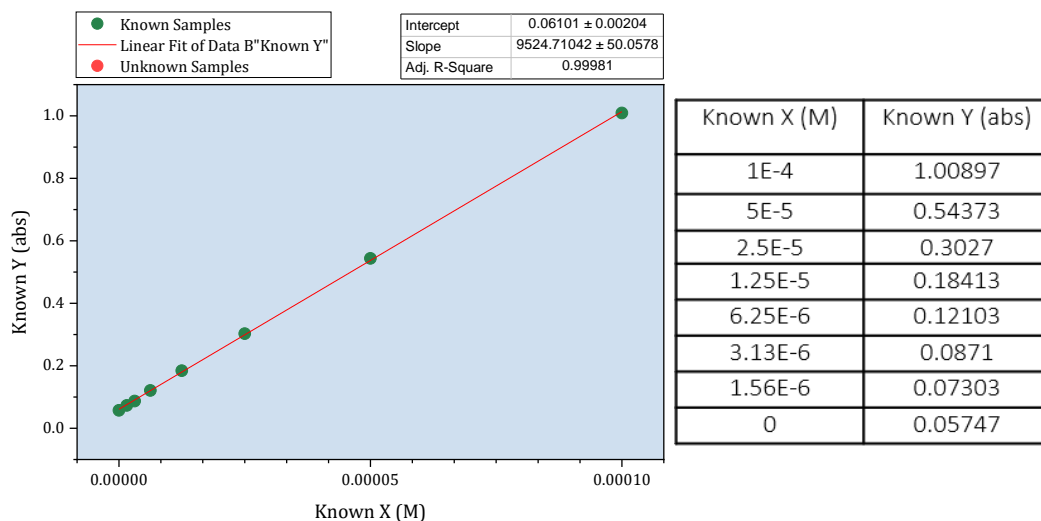
A**B***In SBS***C***In serum-free MCBF medium*

Figure 5. Nitrite measurement specifications.(A) Griess-based diazotization reaction where a *sulfanilamide* reacts with the nitrite in the solution to form a diazonium ion specimen. When this specimen reacts with *NED*, it will produce an *azo compound* whose absorbance can be measured to quantify an experimental sample's nitrite content indirectly. Nitrite standard reference curve performed in (B) standard bath solution (SBS) and (C) serum-free MCBF medium.

Chapter 3. Investigating the contribution of the purinergic receptors in endothelial cells' calcium homeostasis.

3.1 Introduction

The endothelium, the monolayer of specialized cells lining the blood vessels, is recognized not only for its canonical function as a barrier but also for its dynamic participation in regulating vascular tone, blood flow, and various signalling cascades (Félétou, 2011). It plays a crucial role in controlling the trafficking of ions, small and large molecules, and immune cells across the vessel wall, thereby contributing to maintaining tissue homeostasis (Aslam et al., 2021). Calcium is one of these ions and plays an essential role in the endothelium as a second messenger in numerous cell biology processes such as angiogenesis or flow-induced vasodilation (Gerhold et al., 2016; Tsai et al., 2015).

As previously detailed in the **Introduction section 1.3.1**, P2 purinergic receptors have been reported to mediate some of these responses; however, the identity of the receptor contributing to the calcium-induced responses remains in discussion. P2X4 has been proposed as a mediator of shear stress-induced calcium currents in the endothelium and further flow-dependent regulation of vascular tone (Yamamoto, Korenaga, Kamiya, Ando, et al., 2000). In contrast, others fail to prove the contribution of the channel in the calcium-evoked responses (Raqeeb et al., 2011; Wang et al., 2015). P2Y2 can also contribute to high shear stress-induced responses due to the activation of the PLC pathway and, in turn, the release of calcium from the stores (Li et al., 2022; Raqeeb et al., 2011). In addition, purinergic signalling helps maintain the integrity of the endothelial barrier, which is crucial for preventing the passage of harmful substances from the bloodstream into surrounding tissues. ATP and other nucleotides released from vascular cells or applied exogenously can interact with endothelial purinoceptors and influence the barrier function of the endothelium. P2Y1 has been proposed as an endothelial barrier protector through a calcium-dependent pathway (Aslam et al., 2021).

Furthermore, it has been established that endothelial calcium signals are pivotal in promoting angiogenesis by recruiting various calcium-sensitive decoders in response to pro-angiogenic signals, including basic fibroblast growth factor (bFGF) and vascular endothelial growth factor (VEGF) (Moccia et al., 2019). VEGF is the master regulation of angiogenesis. VEGF receptor 2, which is the central signalling VEGF receptor in vascular endothelial cells, recruits PLC β 3 through phosphorylation at serine 537 and 1105 and leads to the PLC activation pathway causing a pro-angiogenic increase in the intracellular calcium (Li et al., 2011; Moccia et al., 2019). Membrane receptors from other families, such as Orai and TRPC channels, have been proposed to contribute to the VEGF calcium-dependent response (J. Li et al., 2015; Li et al., 2011). Of the purinergic receptors family, P2X7 and P2Y11 have been proposed to induce vessel normalisation in a calcium-dependent manner (Avanzato et al., 2016).

3.2 Aims

The aim of this study was to investigate the contribution of the purinergic receptors in endothelial calcium signalling, using both a biomolecular and a pharmacological strategy. The specific objectives were as follows:

1. To identify the purinergic receptors at the transcriptional level and pharmacologically prove the derived candidates' involvement in nucleotide-induced calcium responses in human microvascular endothelial cells (HMEC-1).
2. To elucidate the possible purinergic contribution of purinergic receptors in vascular endothelial growth factor (VEGF) calcium signalling mechanism in HMEC-1 cells.
3. To confirm the protein expression of the proposed pharmacological functional candidates and determine the specificity of the observed responses in HMEC-1 cells.
4. To complement this study with insights into the novel detected mechanism involving P2Y11 and VEGF-dependent responses in a primary cell line, human umbilical vein endothelial cells (HUVEC).

3.3 Results

3.3.1. Membrane receptors RNA sequencing profile of human microvascular endothelial cells (HMEC-1)

RNA sequencing was performed using HMEC-1 cells as a model to elucidate the transcriptional profile of membrane receptors with established roles in endothelial physiology. Although this study focuses on the role of purinergic receptors, the expression of other receptors was considered to have a better understanding of how calcium homeostasis can be regulated in the vascular endothelium.

The data is exposed as normalised gene expression levels for the expected number of fragments per kilobase of transcript sequence per millions of the base pairs sequenced (FPKM) (**Figure 1**). Zero FPKM indicated no gene expression, and greater FPKM values represented higher quantitative gene expression levels. On that basis, the purinergic receptor expression at the mRNA level of two ligand ion channels, P2X4 and P2X5, and the expression of three other G protein coupled receptors, ADORA2B, P2Y2 and P2Y11, was determined. P2Y receptors showed a more prominent expression than P2X4. In contrast, the expression of P2X5 was deficient, and it was not further pursued in the study as there is a lack of pharmacological tools for further characterization (**Figure 1-A**).

In the same way, all the vascular endothelial growth factor receptors (VEGFR1,2,3) were ascertained, and VEGFR2 was detected at grander levels. In the case of the vascular endothelial growth factors, all showed expression in HMEC-1 cells (VEGFA, B, C, D). However, it was a substantial expression of VEGFB, followed by VEGFC and VEGFA. VEGFD was the only undetected (**Figure 1-B**). In the case of mechanosensitive channels, PIEZO1 represented the most evident expression among all the studied, and TRPV4 was detected but at much lower levels if compared, showing a mRNA expression relatively similar to P2X4 (**Figure 1-C**). On the other hand, in the store-operated (CRAC) channels expression, both the pore-forming proteins

ORAI (1-3) and the calcium store sensor (stromal interaction molecule; STIM1,2) were expressed, with ORAI1 being the most extended at the mRNA level (**Figure 1-D**).

The mRNA expression pattern observed in HMEC-1 validated this study's following stages of pharmacological profiling. Only receptors indicating expression were further characterised.

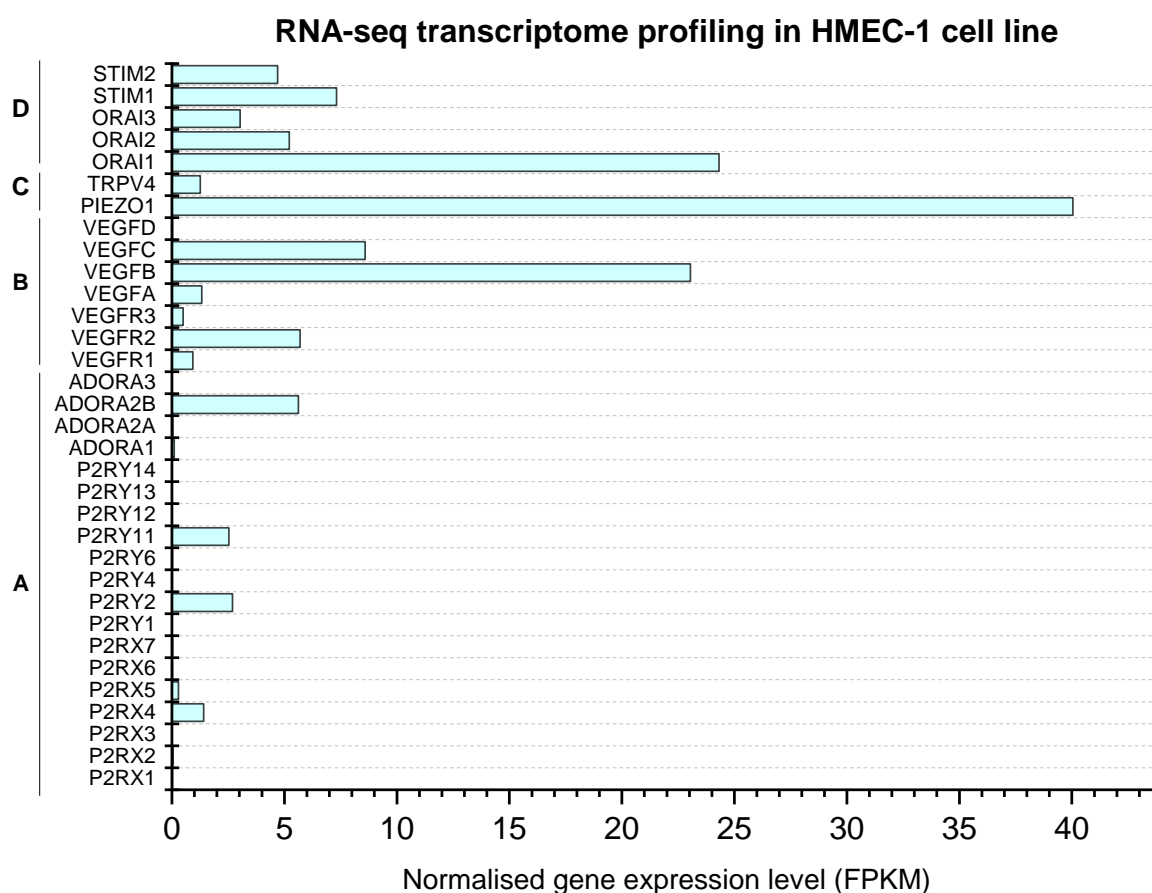


Figure 1. Normalised gene expression for the expected number of FPKM levels in various receptor families in human microvascular endothelial cells (HMEC-1). **(A)** Purinergic receptors of the three main subtypes were expressed in different levels, considering the expression of P2X4, P2X5, P2Y2, P2Y11, and ADORAA2B (the adenosine receptor A2B). **(B)** All vascular endothelial growth factor (VEGF) receptors (R1, R2, R3) and ligands (A, B, C, D) were detected except for the VEGF D ligand subtype. **(C)** In the case of the mechanosensitive channels, both this receptor and TPRV4 expression were detected. **(D)** Similarly, all store-operated (CRAC) channel members were expressed in HMEC-1. Each bar represents an average of three equal samples in FPKM.

3.3.2. Characterisation of the purinergic receptors signalling in human microvascular endothelial cells (HMEC-1).

As indicated in **section 3.3.1**, a range of purinergic receptors are expressed in HMEC-1 cells. P2X4 is an ionotropic permeable non-selective purinergic receptor whose activity can be assessed by recording changes in the intracellular calcium concentration using Fura-2AM dye, as described in the **Methods section 2.3**. In contrast, P2Y2 and P2Y11 are metabotropic purinergic receptors, and their activity can be assessed using the same strategy as both induce an increase in calcium levels upon nucleotide activation.

3.3.2.1 Nucleotide-evoked calcium responses of human microvascular endothelial cells (HMEC-1)

Ionotropic and metabotropic receptors demonstrate different potencies and efficacies, reflecting their respective pathways for increasing calcium levels. ATP is a full agonist of P2X4 (Coddou et al., 2011), P2Y2 (Burnstock, 2014), and P2Y11 (Gruenbacher et al., 2019), and therefore, the early experiments were performed to determine potency and efficacy of ATP in HMEC-1 cells. Estimating these parameters helped to understand the functional expression of the previously reported mRNA-expressed receptors in this cell line. ATP elicited intracellular calcium response in a concentration-dependent manner (0.01 to 300 μ M) with maximal activity at 300 μ M for the peak ($100.27 \pm 2.9\%$) and for the area under the curve (AUC) ($100.68 \pm 3\%$). The half-maximal effective concentration (EC_{50}) for the peak was 568 ± 161 nM and 742 ± 161 nM for the AUC (**Figure 2**). The peak represents the initial rapid calcium response while the area under the curve evaluates the sustained phase response of a drug. **Figure 2-C** depicts time-resolved calcium responses upon ATP stimulation from 0.03 to 300 μ M. This stimulation evoked an initial response followed by a slow and sustained phase that decayed to approximately 65% above baseline. All concentrations showed the same slow, sustained desensitisation phase.

In the absence of extracellular calcium, the maximal responses elicited by ATP were significantly decreased by 54.32% for the peak and 28.86% for the AUC. However, the half-maximal effective concentration did not significantly change when the cells were exposed to ATP in a calcium-free saline bath solution (**Figure 3**). The residual calcium responses indicated at least some contribution dependent on P2Y receptors with a clear dependency on extracellular calcium, which could indicate some P2X activity.

To gain insights into the expression pattern exposed by the RNA sequencing, the effects of exogenous UTP, ADP, and UDP were assessed to provide a more comprehensive characterisation of the pharmacological profile of HMEC-1 cells, as different receptors display different specificity for different nucleotides. Applying these three nucleotides elicited a calcium response in HMEC-1 cells with a considerable rightward shift of ADP and UDP concentration-response curves compared to the ATP curve (**Figure 4**). The four nucleotides were ranked in order of their EC_{50} : ATP = UTP (*ns*) > ADP > UDP, showing, in general, very similar maximal responses. However, UTP exhibited a significantly greater maximal response than ATP. These effects are consistent for the peak and AUC calculated parameters (**Table 1**).

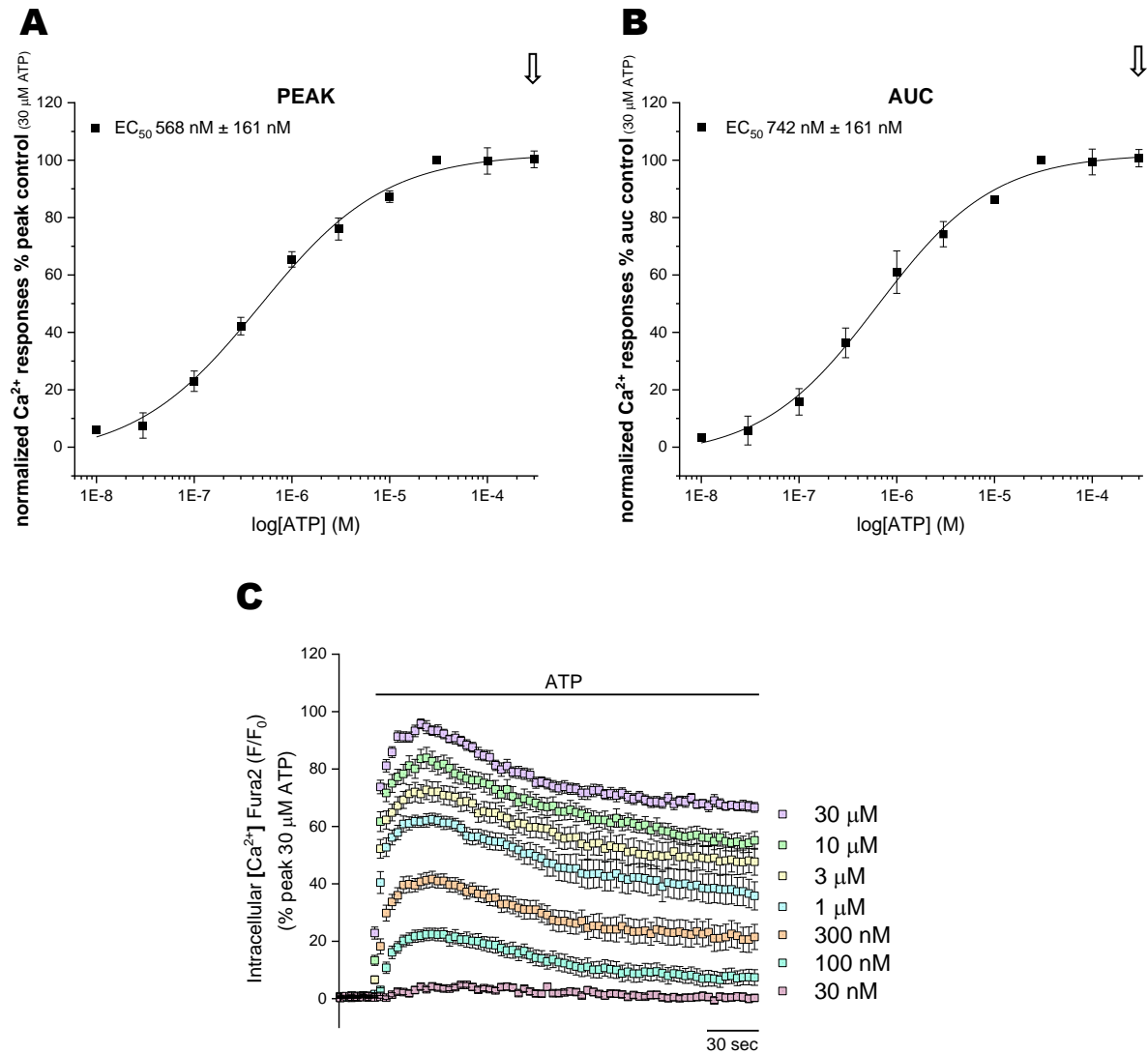
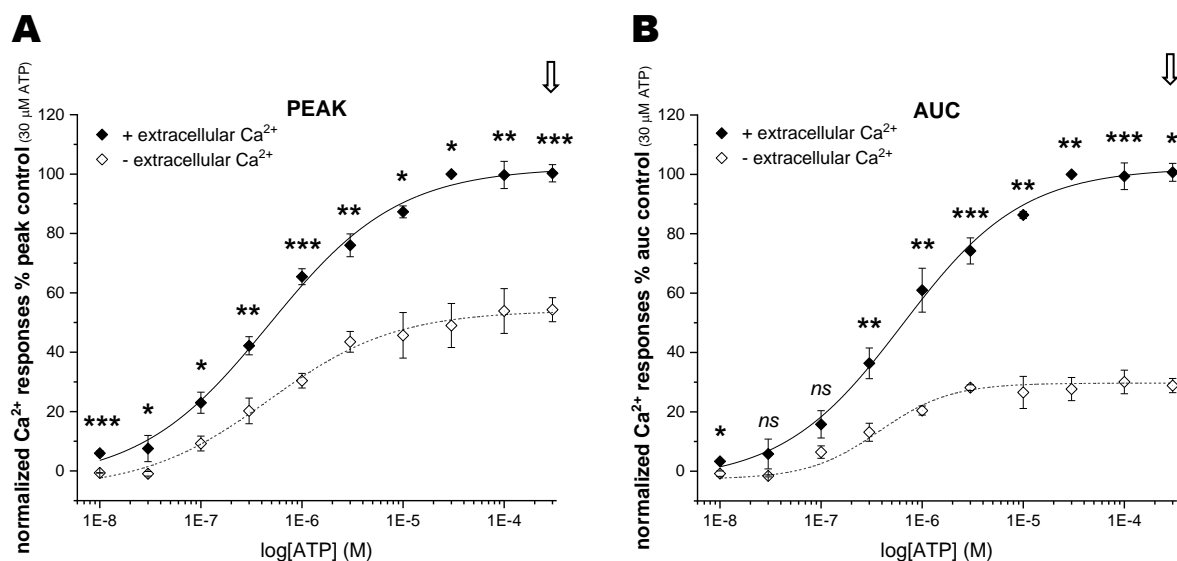


Figure 2. ATP elicits intracellular calcium responses in human microvascular endothelial cells (HMEC-1). Concentration-response curves for the peak (A) and AUC (B) magnitude of intracellular Ca^{2+} responses elicited by ATP (0.01-300 μM ; $N=5$). (C) Averaged time-resolved intracellular Ca^{2+} responses elicited by ATP from 30 μM to 30 nM in HMEC-1 cells over 250 seconds ($N=5$). All data were normalised (*) to 30 μM ATP and fit the Hill1 equation with the EC_{50} values showed in the graphs. Data are represented as mean \pm SEM.

(*) Data normalisation was always done at 30 μM ATP when this agonist was studied.

(**) Arrows (\Downarrow) indicate the maximum response in the control (untreated) curve.

(***) F/F_0 refers to the Fura2 ratio, meaning F340/F380.



C

| | | PEAK | AUC |
|------------------|--------------------------|-------------------------|--------------------------|
| EC ₅₀ | ATP in Ca ²⁺ | 568 ± 161 nM | 742 ± 161 nM |
| | ATP in 0Ca ²⁺ | 1.30 ± 0.9 μM <i>ns</i> | 1.85 ± 1.25 μM <i>ns</i> |
| Maximal response | ATP in Ca ²⁺ | 100.27% | 100.68% |
| | ATP in 0Ca ²⁺ | 54.32% ** | 28.86% * |

Figure 3. Extracellular calcium removal impacted the ATP-evoked response in human microvascular endothelial cells (HMEC-1). Concentration-response curves for the peak (A) and AUC (B) magnitude of intracellular Ca²⁺ responses elicited by ATP (0.01-300 μM; N=5) in the presence (0.01-300 μM; closed rhombus; N=3) or absence (0.01-300 μM; open rhombus; N=5) of extracellular calcium. All data were normalised to 30 μM ATP in the presence of extracellular calcium and fit the Hill1 equation with the EC₅₀ and maximal response values showed in table (C). Asterisks show statistical significance relative to ATP potency and ATP % of maximal response (p *ns* > 0.05, p* < 0.05, p** < 0.01, p*** < 0.001). Data are represented as mean ± SEM.

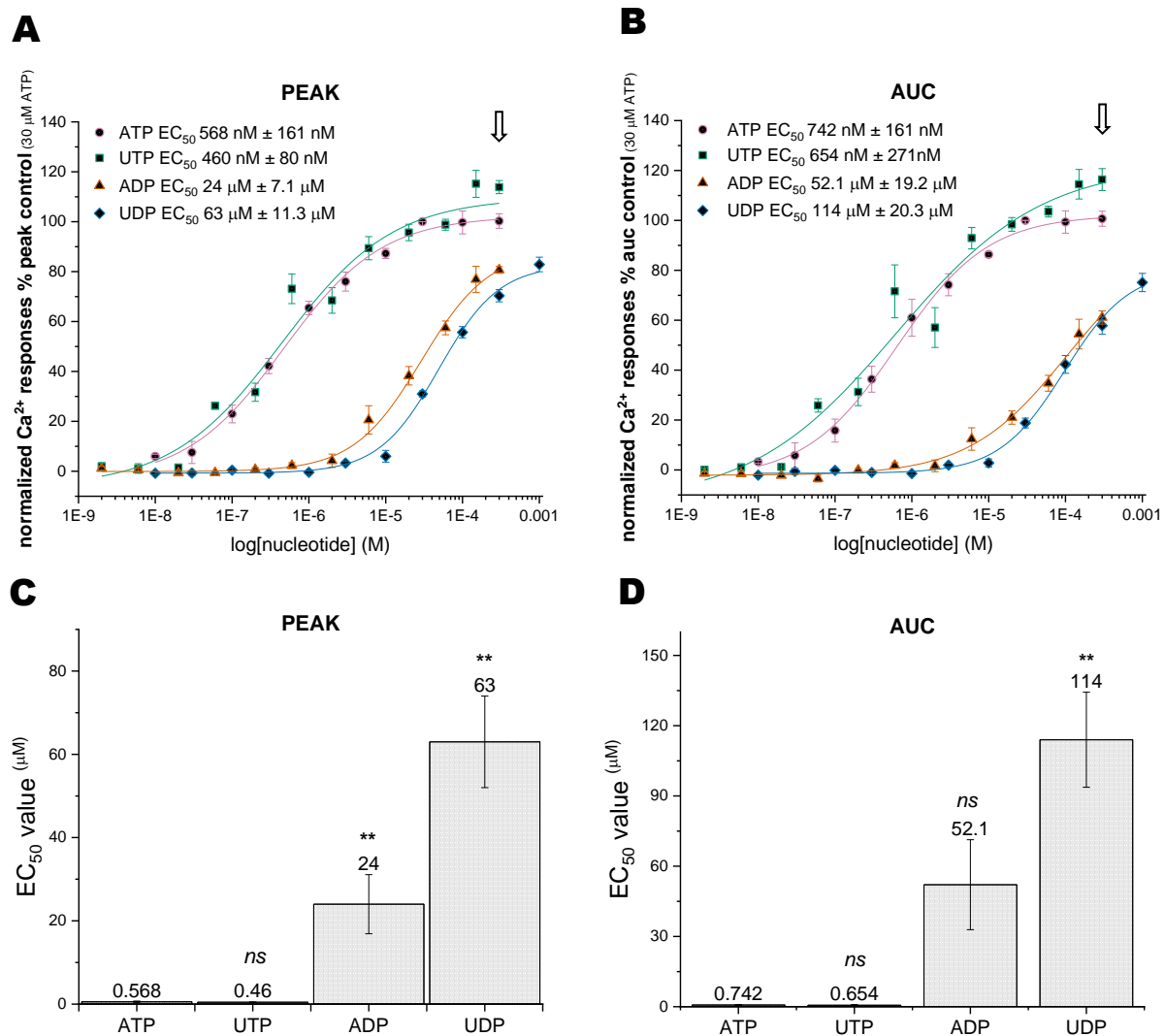


Figure 4. ATP, UTP, ADP and UDP elicit intracellular calcium responses in human microvascular endothelial cells (HMEC-1). Concentration-response curves for the peak (A) and AUC (B) magnitude of intracellular Ca²⁺ responses elicited by ATP (0.01-300 µM; pink closed circles; N=5), UTP (0.002-300 µM; green closed squares; N=5), ADP (0.002-300 µM; orange closed triangles; N=5) and UDP (0.01-1000 µM; blue closed rhombus; N=5). All data were normalised to 30 µM ATP and fit the Hill1 equation with the EC₅₀ values showed in the graphs. Comparison of peak (C) and AUC (D) EC₅₀ values for ATP, UTP, ADP and UDP responses (N=5 for each nucleotide). Asterisks show statistical significance relative to ATP potency (p *ns* > 0.05, p* < 0.05, p** < 0.01, p*** < 0.001). Data are represented as mean ± SEM.

Table 1. Summary of nucleotides-evoked responses in human microvascular endothelial cells (HMEC-1). EC₅₀ statistical analysis was performed against the ATP control curve in saline solution. Efficacy p-value is the statistical comparison between ATP maximal response in saline solution and ATP maximal response in the presence of the applied compound (whose concentration might differ from the previous one).

| Nucleotide | Concentration range, μM | EC ₅₀ PEAK | P value | Maximum response PEAK (μM) | Maximum response PEAK (%) | P value | EC ₅₀ AUC | P value | Maximal response AUC (μM) | Maximal response AUC (%) | P value |
|------------|------------------------------------|-----------------------------|-----------|---|---------------------------|---------|-------------------------------|-----------|--|--------------------------|---------|
| ATP | 0.01-300 | 568 \pm 161 nM | / | 300 | 100.27 \pm 2.9 | / | 742 \pm 161 nM | / | 300 | 100.68 \pm 3.0 | / |
| UTP | 0.002-300 | 460 \pm 80 nM | <i>ns</i> | 150 | 115.19 \pm 5.4 | p<0.05 | 654 \pm 271 nM | <i>ns</i> | 300 | 116.39 \pm 4.4 | p<0.05 |
| ADP | 0.002-300 | 24 \pm 7.1 μM | p<0.01 | 300 | 82.87 \pm 2.9 | p<0.01 | 52.1 \pm 19.2 μM | <i>ns</i> | 300 | 61.1 \pm 2.64 | p<0.001 |
| UDP | 0.01-1000 | 63 \pm 11.3 μM | p<0.01 | 300 | 70.35 \pm 2.4 | p<0.01 | 114 \pm 20.3 μM | p<0.01 | 300 | 75.12 \pm 3.6 | p<0.001 |

Table 2. Effects of broad-spectrum antagonists and ATP scavengers (apyrase) on the ATP-evoked responses in human microvascular endothelial cells (HMEC-1). EC₅₀ statistical analysis was performed against the ATP control curve in saline solution. Efficacy p-value is the statistical comparison between ATP maximal response in saline solution and ATP maximal response in the presence of the applied compound (whose concentration might differ from the previous one).

| Agonist | Agonist range, μM | Antagonist | Antagonist concentration | EC ₅₀ PEAK | P value | Maximal response PEAK (μM) | Maximal response PEAK (%) | P value |
|---------|------------------------------|------------|--------------------------|-------------------------------|-----------|---|---------------------------|-----------|
| ATP | 0.1-300 | / | / | 568 \pm 161 nM | / | 300 | 100.27 \pm 2.9 | / |
| ATP | 0.1-300 | Apyrase | 10 U/mL | 4.98 \pm 1.28 μM | p<0.001 | 100 | 86.1 \pm 3.1 | p<0.01 |
| ATP | 0.1-300 | PPADS | 100 μM | 868 \pm 94 nM | <i>ns</i> | 300 | 77.0 \pm 4 | p<0.01 |
| ATP | 0.1-300 | Suramin | 100 μM | 203 \pm 35 nM | <i>ns</i> | 100 | 93.97 \pm 4.23 | p<0.01 |
| Agonist | Agonist range, μM | Antagonist | Antagonist concentration | EC ₅₀ AUC | P value | Maximal response AUC (μM) | Maximal response AUC (%) | P value |
| ATP | 0.1-300 | / | / | 742 \pm 161 nM | / | 300 | 100.68 \pm 3 | / |
| ATP | 0.1-300 | Apyrase | 10 U/mL | 10.5 \pm 3.63 μM | p<0.001 | 100 | 22.4 \pm 1.7 | p<0.001 |
| ATP | 0.1-300 | PPADS | 100 μM | 1.66 \pm 0.28 μM | <i>ns</i> | 300 | 86.4 \pm 5.7 | <i>ns</i> |
| ATP | 0.1-300 | Suramin | 100 μM | 205 \pm 30 nM | p<0.05 | 10 | 95.3 \pm 4.43 | <i>ns</i> |

3.3.2.2 ATP-evoked calcium responses of human microvascular endothelial cells (HMEC-1) are mediated by phospholipase C (PLC) activation, leading to the subsequent release of calcium from intracellular stores.

To investigate the contribution of the two P2 purinergic receptor families in the ATP-evoked responses, the PLC pathway inhibitor U73122 was applied to check the impact on the intracellular calcium concentration elicited by the nucleotide. The phospholipase C is a component of the downstream signalling pathway initiated by activating G α_q -coupled P2Y receptors. Inhibition of the PLC enzyme compromises the release of inositol triphosphate (IP₃) and diacylglycerol (DAG) and, in turn, the calcium release from stores. The ATP responses were entirely abolished in the presence of 5 μ M of the PLC inhibitor compared with the concentration-response curve in the absence of U73122 (**Figure 5-A, B**), suggesting a predominance of P2Y receptors in the ATP-evoked responses. The representative time-resolved intracellular calcium responses in **Figure 5-C** demonstrated the absence of response upon 30 μ M ATP stimulation.

In addition, thapsigargin (10 μ M) was also used to investigate further the possible role of store-operated calcium responses in HMEC-1. Thapsigargin is a potent non-competitive inhibitor of the calcium ATPase pumps (SERCA), responsible for transporting calcium ions into the sarco/endoplasmic reticulum. It works by obstructing calcium uptake, depleting calcium stores, and raising intracellular calcium levels in the cell (Kijimag et al., 1991). Stores depletion with thapsigargin at two different preincubation times, 5 (**Figure 6-A**) and 25 (**Figure 6-B**) minutes, prevented any ATP-evoked responses, reinforcing the PLC inhibition assay findings. Furthermore, the preincubation with thapsigargin significantly affected the calcium baseline concentration before experimentation, indicating a complete depletion of stores before ATP injection. The drug effect was more prominent when measuring after 5 than 25 minutes of preincubation (**Figure 6-C**). However, the preincubation time did not impact the effect on the dose-response curve (**Figure 6-A, B**).

These two inhibitors and many others used in the following sections were not soluble in deionised water, and DMSO was used as the solvent instead. Strict solvent control was performed to mitigate potential solvent-related influences on the ATP dose-response curve. The presence of DMSO at 0.1% and 0.2% (v/v) did not alter the ATP potencies when compared with EC₅₀ calculated from the ATP dose response curve in saline solution (SBS) (**Figure 7-E**). However, there was a slight effect at 10 μ M in the 0.1% DMSO curve (**Figure 7-A, B**), and a slightly potentiating trend can be found from 3 to 10 μ M in the 0.2% DMSO peak dose-response curve (**Figure 7-C**). Thereby, to ensure consistency in experimental conditions in this study, drugs solved in DMSO will always be compared to their respective dose-response solvent-controlled (0.1 or 0.2% DMSO) curve and derived calculated parameters (potency and efficacy).

It is crucial to note that the PLC inhibitor assay could not be appropriately plotted with its corresponding ATP dose response in 1% DMSO, as it was the only experiment performed in these conditions due to a low stock concentration in 100% DMSO (**Figure 5-A, B**). Therefore, this drug could not be diluted to 0.1 or 0.2% DMSO. Statistical significance is not shown as the experiments were not performed in the same conditions.

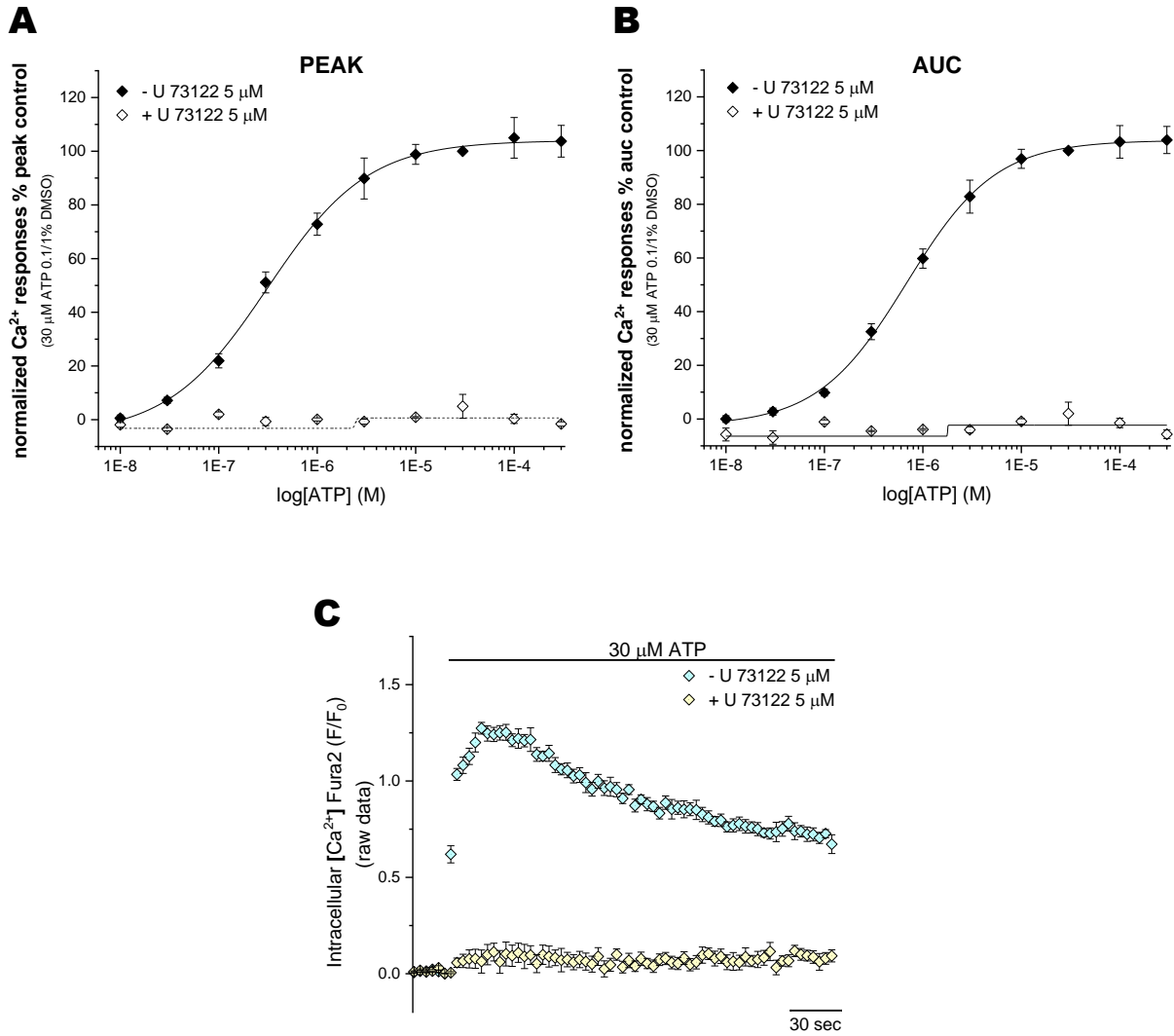


Figure 5. Effects of the phospholipase C (PLC) inhibitor U73122 on the ATP-evoked response in human microvascular endothelial cells (HMEC-1). Concentration-response curves for the peak (A) and AUC (B) magnitude of intracellular Ca^{2+} responses elicited by ATP (0.01-300 μM ; $N=3$) in the presence (0.01-300 μM ; open rhombus; $N=3$) or absence (0.01-300 μM ; closed rhombus; $N=3$) of U 73122 5 μM after 30 minutes preincubation. (C) Averaged time-resolved intracellular Ca^{2+} responses elicited by ATP 30 μM in the presence (light yellow rhombus; $N=3$) or absence (cyan rhombus; $N=3$) of U73122 5 μM over 250 seconds. Data are represented as mean \pm SEM.

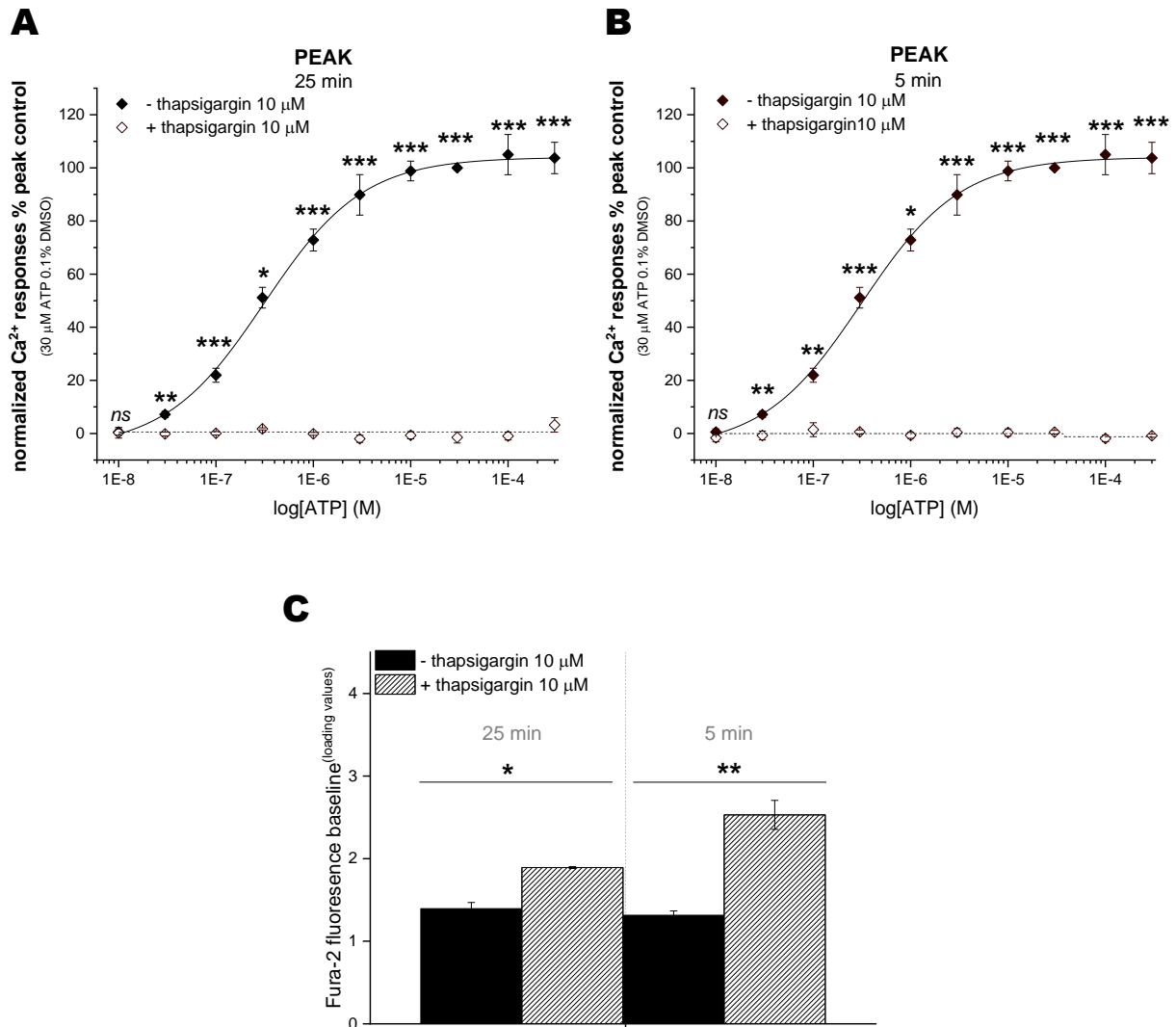
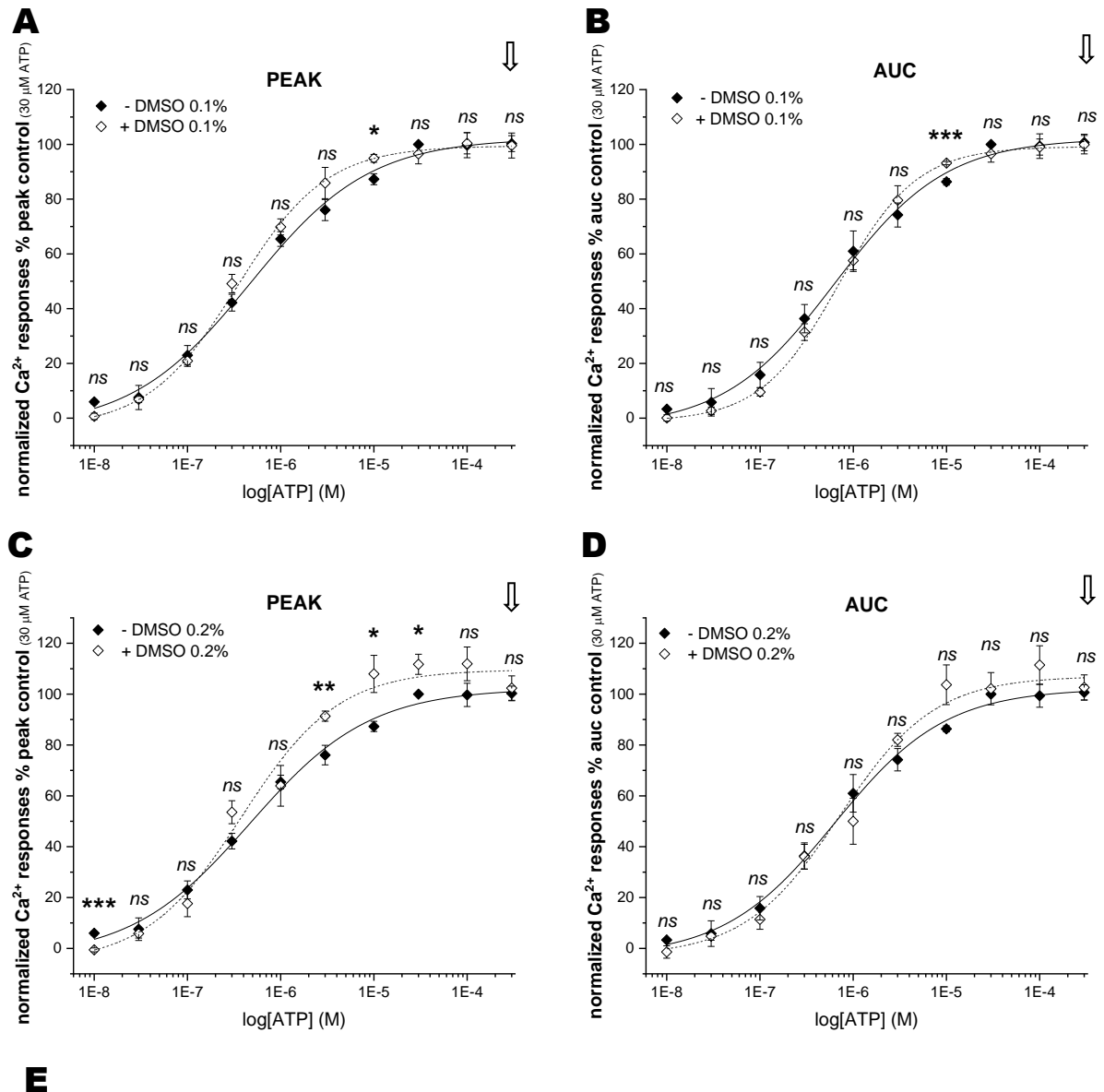


Figure 6. Effects of the sarcoendoplasmic reticulum calcium transport ATPase (SERCA) inhibitor thapsigargin on the ATP-evoked response in human microvascular endothelial cells (HMEC-1). ATP dose-response curve under control conditions (0.01-300 μM; closed rhombus; $N=3$) or following sarcoendoplasmic reticulum Ca²⁺-ATPases inhibition treatment with 10 μM thapsigargin (0.01-300 μM; open rhombus; $N=3$) after 25 (A) or 5 (B) minutes preincubation. All data were normalised to 30 μM ATP and fit the Hill1 equation. (C) Cell loading values under control conditions or in the presence of thapsigargin at two different times. Asterisks show statistical significance relative to control conditions loading values ($p_{ns} > 0.05$, $p^* < 0.05$, $p^{**} < 0.01$, $p^{***} < 0.001$). Data are represented as mean \pm SEM.

Loading values represent a F340/F380 measurement before the FlexStation experiments. We consider a control measurement of the cells for this value to be higher than 1 but lower than 2. The FlexStation is configured to record the pharmacological assays performing a baseline subtraction, and therefore, the traces shown and the raw data presented in this thesis start at 0.



| | EC ₅₀ | |
|------------------------|------------------|--------------|
| | PEAK | AUC |
| ATP in saline solution | 568 ± 161 nM | 742 ± 161 nM |
| ATP in DMSO 0.1% | 338 ± 52 nM | 768 ± 79 nM |
| ATP in DMSO 0.2% | 568 ± 165 nM | 901 ± 232 nM |

Figure 7. Tolerance of the ATP-evoked response in human microvascular endothelial cells (HMEC-1) to 0.1% and 0.2% dimethyl sulfoxide (DMSO). Concentration-response curves for the peak (A) (C) and AUC (B) (D) magnitude of intracellular Ca²⁺ responses elicited by ATP in the presence (0.01-300 μM; open rhombus; N=5) or absence (0.01-300 μM; closed rhombus; N=5) of 0.1% or 0.2% DMSO. All data were normalised to 30 μM ATP in saline solution and fit the Hill1 equation with the EC₅₀ values showed in table (E). Asterisks show statistical significance relative to ATP potency in saline solution (p *ns* > 0.05, p* < 0.05, p** < 0.01, p*** < 0.001). Data are represented as mean ± SEM.

3.3.2.3 The broad-spectrum P2 antagonists affected the ATP-evoked calcium responses of human microvascular endothelial cells (HMEC-1).

Broad-spectrum P2 antagonists were used, as well as apyrase, to continue characterising the P2 receptors' involvement in the ATP-evoked calcium responses in HMEC-1. Pyridoxal-phosphate-6-azophenyl-2',4'-disulfonic acid (PPADS), and suramin broadly target P2X and P2Y receptors in various degrees, and their effects are strictly species-dependent. On the other hand, apyrase is an ATP and ADP scavenger, inhibiting the ATP response by catalysing the hydrolysis of ATP to ADP and ADP to AMP by releasing inorganic phosphate (Kettlun et al., 2005).

The effects of apyrase (10 U/mL) on the ATP dose-response curve control (EC_{50}^{PEAK} : 568 ± 161 nM; EC_{50}^{AUC} : 742 ± 161 nM) were examined to confirm that observed intracellular calcium responses were ATP-dependent. Pre-treatment with apyrase right shifted the ATP dose-response curve and massively reduced the ATP potency for the peak (4.98 ± 1.28 μ M; $p < 0.001$) and the area under the curve (10.5 ± 3.63 μ M; $p < 0.001$) (**Figure 8-D, Table 2**). Furthermore, the control ATP-evoked maximal response at 300 μ M (ATP_{max}^{peak} : $100.27 \pm 2.9\%$; ATP_{max}^{AUC} : $100.68 \pm 3\%$) was significantly affected in the presence of the enzyme for the peak (ATP_{max}^{peak} : $85.44 \pm 4.14\%$; $p < 0.05$) and the AUC (ATP_{max}^{AUC} : $20.22 \pm 1.94\%$; $p < 0.001$) (**Figure 8-A, B**). Accordingly, the maximal response to ATP in the presence of the scavenger was achieved at 100 μ M for the peak (E_{max}^{peak} : $86.1 \pm 3.1\%$; $p < 0.01$) and the AUC (E_{max}^{AUC} : $22.4 \pm 1.7\%$; $p < 0.001$). When comparing these new maximal responses (efficacies, E_{max}) with the maximal response control at 300 μ M ATP in the absence of the apyrase, the response was significantly reduced in both curves, and it never managed to achieve the same level of efficacy as the control, being this fact much more evident in the AUC curve (**Table 2**). The representative time-resolved intracellular calcium responses shown in **Figure 8-C** illustrated apyrase's significant impact on the peak and the massive effect in the area under the curve upon 10 μ M ATP stimulation compared with the control. In the presence of apyrase, the ATP caused a rapid transient increase in the calcium influx with a decay in the response over 30 seconds to the baseline, losing the slow desensitisation kinetics observed in the control response.

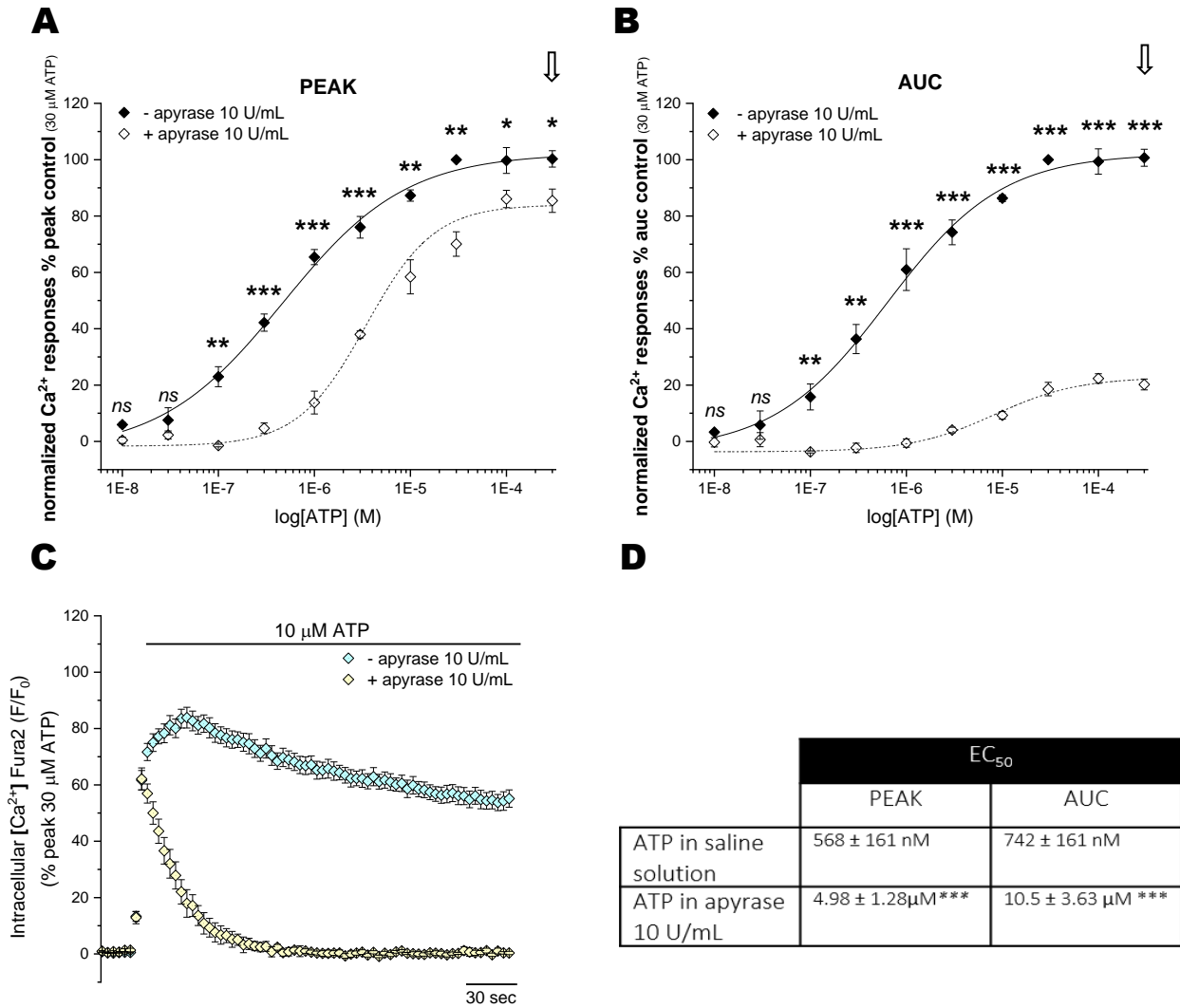


Figure 8. Inhibitory effects of apyrase on the ATP-evoked response in human microvascular endothelial cells (HMEC-1). Concentration-response curves for the peak (A) and AUC (B) magnitude of intracellular Ca^{2+} responses elicited by ATP (0.01-300 μM ; $N=5$) in the presence (0.01-300 μM ; open rhombus; $N=5$) or absence (0.01-300 μM ; closed rhombus; $N=5$) of apyrase 10 U/mL. (C) Averaged time-resolved intracellular Ca^{2+} responses elicited by ATP 10 μM in the presence (light yellow rhombus; $N=5$) or absence (cyan rhombus; $N=5$) of apyrase 10 U/mL over 250 seconds. All data were normalised to 30 $\mu\text{M ATP}$ and fit the Hill1 equation with the EC_{50} values showed in table (D). Asterisks show statistical significance relative to ATP potency ($p_{ns} > 0.05$, $p^* < 0.05$, $p^{**} < 0.01$, $p^{***} < 0.001$). Data are represented as mean \pm SEM.

PPADS is a non-competitive antagonist of all P2X receptors in humans, expecting changes in the efficacy upon application of the drug but not in the potency (Delaune et al., 2023). P2X4 receptor exhibited half-maximal inhibition concentration values in the presence of high concentrations of PPADS (>300 μ M) (Bo, Kim, et al., 2003; Coddou et al., 2011; Jones et al., 2000; Khakh et al., 1999; North et al., 2000). However, lower IC_{50} of 10 μ M has been reported for the human P2X4 receptor (Jones et al., 2000). In contrast, P2X5 demonstrated the highest sensitivity to PPADS with IC_{50} from 200 to 600 nM (Bo, Jiang, et al., 2003; Coddou et al., 2011). Of the P2Y receptors, it has been reported partial inhibition of P2Y1, P2Y4, P2Y6, and P2Y13 when using PPADS concentrations higher than 10 μ M (Charlton et al., 1996a, 1996b; Communi, Motte, et al., 1996; Communi, Parmentier, et al., 1996; Marteau et al., 1995; O'Grady et al., 1996; Robaye et al., 1997). Nevertheless, it is essential to note that no antagonist action was observed in human P2Y2 or P2Y11 receptors (Charlton et al., 1996b; Communi et al., 1999).

The effects of PPADS (100 μ M) on the ATP dose-response curve control (EC_{50}^{PEAK} : 568 ± 161 nM; EC_{50}^{AUC} : 742 ± 161 nM) were examined to investigate if observed intracellular calcium responses could be P2X-dependent, as this antagonist is not meant to inhibit P2Y2 or P2Y11 dependent responses. Pre-treatment with PPADS slightly right-shifted the ATP dose-response curve without influencing the ATP potency for the peak (868 ± 94 nM; *ns*) or the area under the curve (1.66 ± 0.28 μ M; *ns*) (**Figure 9-D, Table 2**). On the contrary, the presence of the antagonist significantly reduced the ATP-evoked maximal control response at 300 μ M (ATP_{max}^{peak} : $100.27 \pm 2.9\%$; ATP_{max}^{AUC} : $100.68 \pm 3\%$) for the peak ($77 \pm 4\%$; $p < 0.01$) but not for the AUC ($86.4 \pm 5.7\%$; *ns*). In this case, the maximal response in the presence of the antagonist was consistently achieved at 300 μ M (**Figure 9-A, B, Table 2**). The representative time-resolved intracellular calcium responses shown in **Figure 9-C** illustrated PPADS' significant impact on the peak and the area under the curve upon 10 μ M ATP stimulation compared with the control. In the presence of PPADS, the activation kinetics at 10 μ M ATP showed a significant decrease of the peak to around 60% above baseline compared to the 80% control response in the absence of the antagonist. The slow desensitisation kinetics was conserved with a significant drop over the last 90 seconds in the sustained calcium that decayed to approximately 20% above baseline, compared to the control that never decayed below 60%.

To further characterise PPADS effects on the ATP-evoked responses, HMEC-1 cells were incubated for 30 minutes in a range of antagonist concentrations (0.1 to 300 μ M) and stimulated with a sub-maximal concentration of ATP (10 μ M), and thereby, IC_{50} was calculated (**Figure 10-A, B**). The half-maximal inhibitory concentration values obtained were 92.5 ± 8.92 μ M for the peak and 136 ± 88 μ M for AUC inhibition curves, not far from what has been previously reported (North et al., 2000).

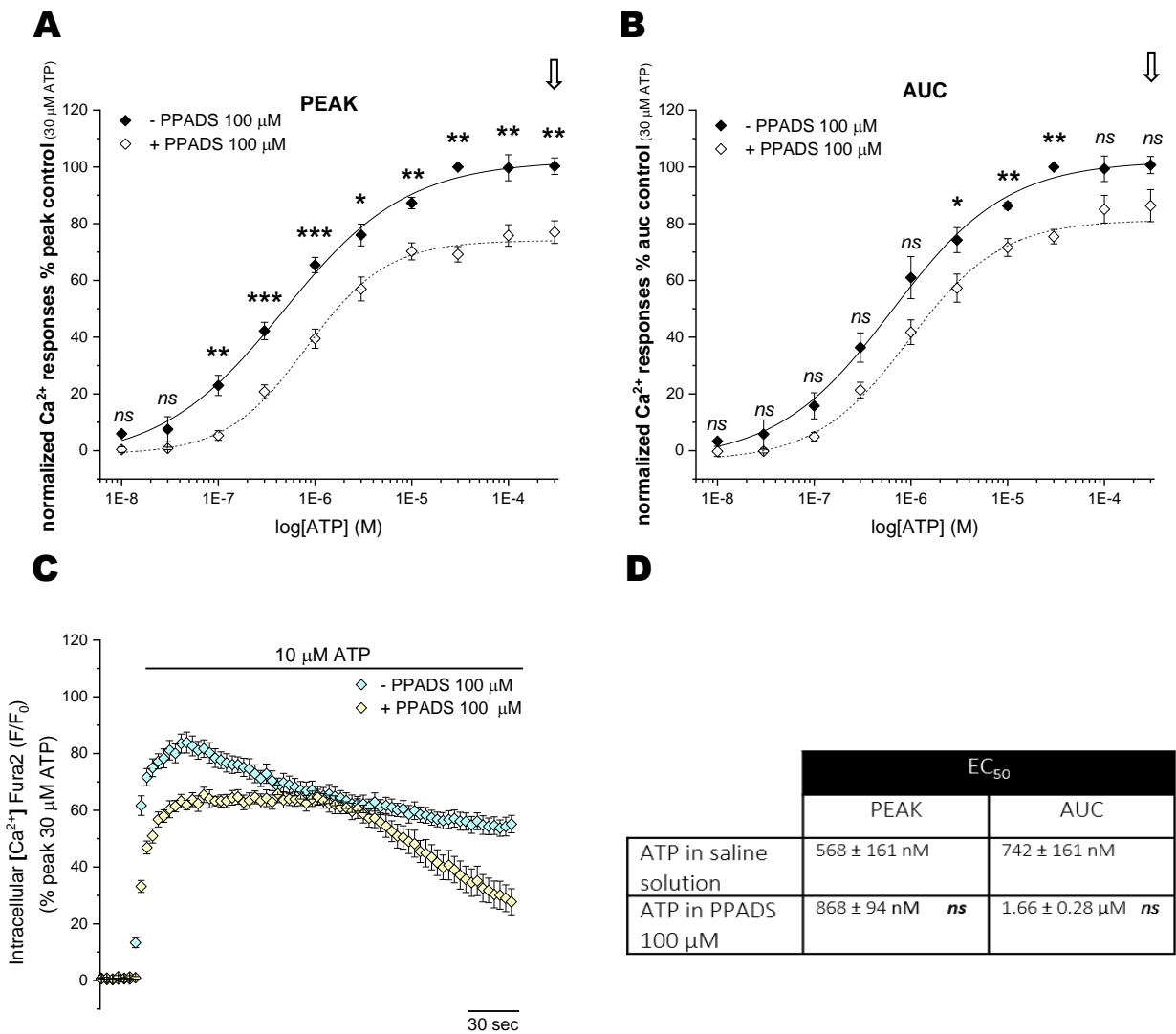


Figure 9. Inhibitory effects of broad-spectrum P2 receptors antagonist PPADS on the ATP-evoked response in human microvascular endothelial cells (HMEC-1). Concentration-response curves for the peak (A) and AUC (B) magnitude of intracellular Ca^{2+} responses elicited by ATP (0.01-300 μM ; $N=5$) in the presence (0.01-300 μM ; open rhombus; $N=5$) or absence (0.01-300 μM ; closed rhombus; $N=5$) of PPADS 100 μM . (C) Averaged time-resolved intracellular Ca^{2+} responses elicited by ATP 10 μM in the presence (light yellow rhombus; $N=5$) or absence (cyan rhombus; $N=5$) of PPADS 100 μM over 250 seconds. All data were normalised to 30 $\mu\text{M ATP}$ and fit the Hill1 equation with the EC_{50} values showed in table (D). Asterisks show statistical significance relative to ATP potency (p *ns* > 0.05, p^* < 0.05, p^{**} < 0.01, p^{***} < 0.001). Data are represented as mean \pm SEM.

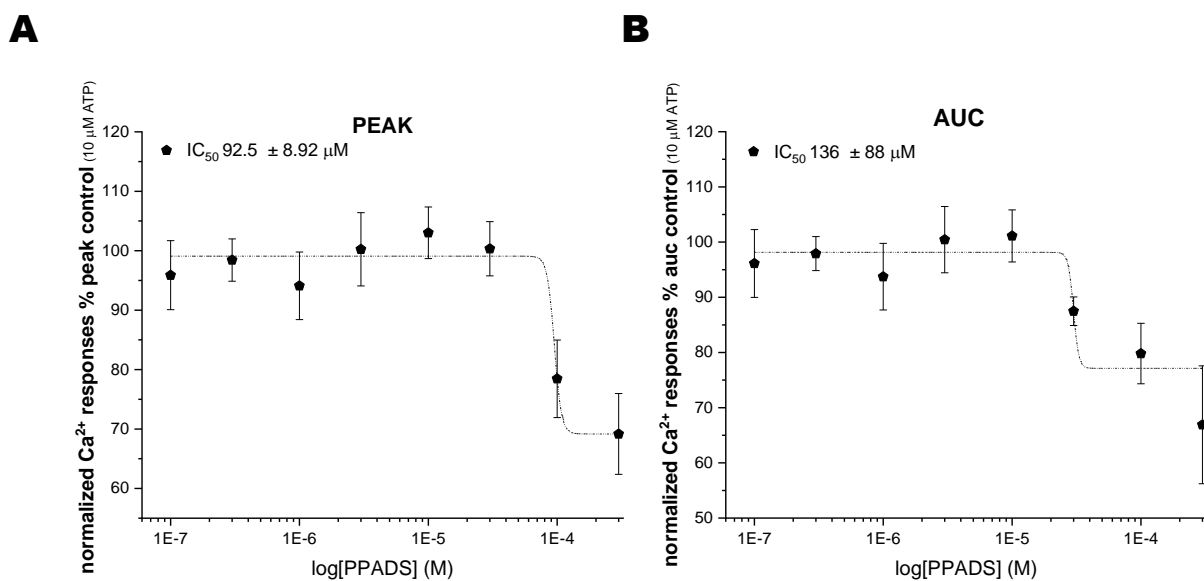


Figure 10. Inhibition concentration-response curves for PPADS on the ATP-evoked response in human microvascular endothelial cells (HMEC-1). Inhibition concentration-response curves for the peak (A) and AUC (B) magnitude of intracellular Ca^{2+} responses elicited by $10 \mu M$ ATP in the presence (0.1 - $300 \mu M$; closed stars; $N=5$) of PPADS $100 \mu M$. All data were normalised to $10 \mu M$ ATP and fit the Hill1 equation with the IC_{50} values showed in the graphs. Data are represented as mean \pm SEM.

Suramin is frequently a non-competitive antagonist of some homomeric P2X receptors in humans (P2X1, P2X3, P2X5 ($\leq 15 \mu\text{M}$)) (Bo, Jiang, et al., 2003; Burnstock et al., 2014; Lambrecht, 2000; Soto et al., 1997), while is weak or inactive for others (P2X2, P2X4, and P2X7) where high concentrations of suramin are required to affect the agonist evoked response ($\geq 78 \mu\text{M}$ -1mM) (Burnstock et al., 2014; George et al., 2019; Lambrecht, 2000; Soto et al., 1997). Of the P2Y receptors, has been characterised as antagonist of P2Y1, P2Y11 and P2Y13 ($\leq 10 \mu\text{M}$) (Abbracchio et al., 2012; Communi et al., 1999; Marteau et al., 2003; O'Grady et al., 1996; Von Kügelgen et al., 2016), while is weak or inactive for P2Y2 ($\geq 40 \mu\text{M}$), P2Y4 and P2Y6 (Charlton et al., 1996a; Rafehi et al., 2018; Ralevic et al., 1998; Von Kügelgen et al., 2016).

The effects of suramin (100 μM) on the ATP dose-response curve control (EC_{50}^{PEAK} : $568 \pm 161 \text{ nM}$; EC_{50}^{AUC} : $742 \pm 161 \text{ nM}$) were examined to investigate if observed intracellular calcium responses could be diminished based on the mRNA expression of P2Y2 and P2Y11. Pre-treatment with suramin slightly left shifted the ATP dose-response curve and increased the ATP potency for the AUC ($205 \pm 30 \text{ nM}$; $p < 0.05$) (**Figure 11-B, Table 2**) while the peak potency remained mainly unchanged ($203 \pm 35 \text{ nM}$; *ns*) (**Figure 11-A, Table 2**). However, there was a significant decrease in net calcium when comparing the ATP control maximal response concentration at 300 μM ($ATP_{\text{max}}^{\text{peak}}$: $100.27 \pm 2.9\%$; $ATP_{\text{max}}^{\text{AUC}}$: $100.68 \pm 3\%$) in the presence of suramin for the peak ($84.60 \pm 2.20\%$; $p < 0.01$) and the AUC ($84.63 \pm 1.90\%$; $p < 0.01$) (**Figure 11-A, B**). Consequently, the maximal response to ATP in the presence of the antagonist was achieved at 100 μM for the peak ($93.97 \pm 4.23\%$; $p < 0.01$) and 10 μM for the AUC ($95.3 \pm 4.43\%$; *ns*). When comparing these new maximal responses with the maximal response control at 300 μM ATP in the absence of the drug, we elucidated that in the case of the AUC, the level of efficacy remained unchanged but shifted to a lower concentration of the agonist 10 μM . In contrast, in the peak curve, the agonist never achieved the same level of efficacy at 100 μM ($93.97 \pm 4.23\%$; $p < 0.01$), but the lower concentration shift for the maximal response was conserved as in the AUC (**Table 2**). The representative time-resolved intracellular calcium responses shown in **Figure 11-C** illustrated the AUC dose-response curve left shift, with a significant increase in the sustained calcium influx upon 300 nM stimulation compared with the control. In the presence of suramin, the ATP caused a rapid transient increase in the calcium influx with a conserved slow desensitisation kinetics influenced by the increase of the sustained net calcium at 300 nM. These results portray unexpected results for a non-competitive antagonist. A decrease in the maximal response could be expected but not an increase in the potency, acting in that case as a positive allosteric modulator of ATP. One alternative explanation for the observed effect can be the performance of suramin as an ectonucleotidase inhibitor. Ectonucleotidase enzymes hydrolyse ATP into ADP, AMP, and adenosine. Suramin can inhibit them (Hourani et al., 1988), preventing the degradation of ATP and increasing its potency, as our data showed.

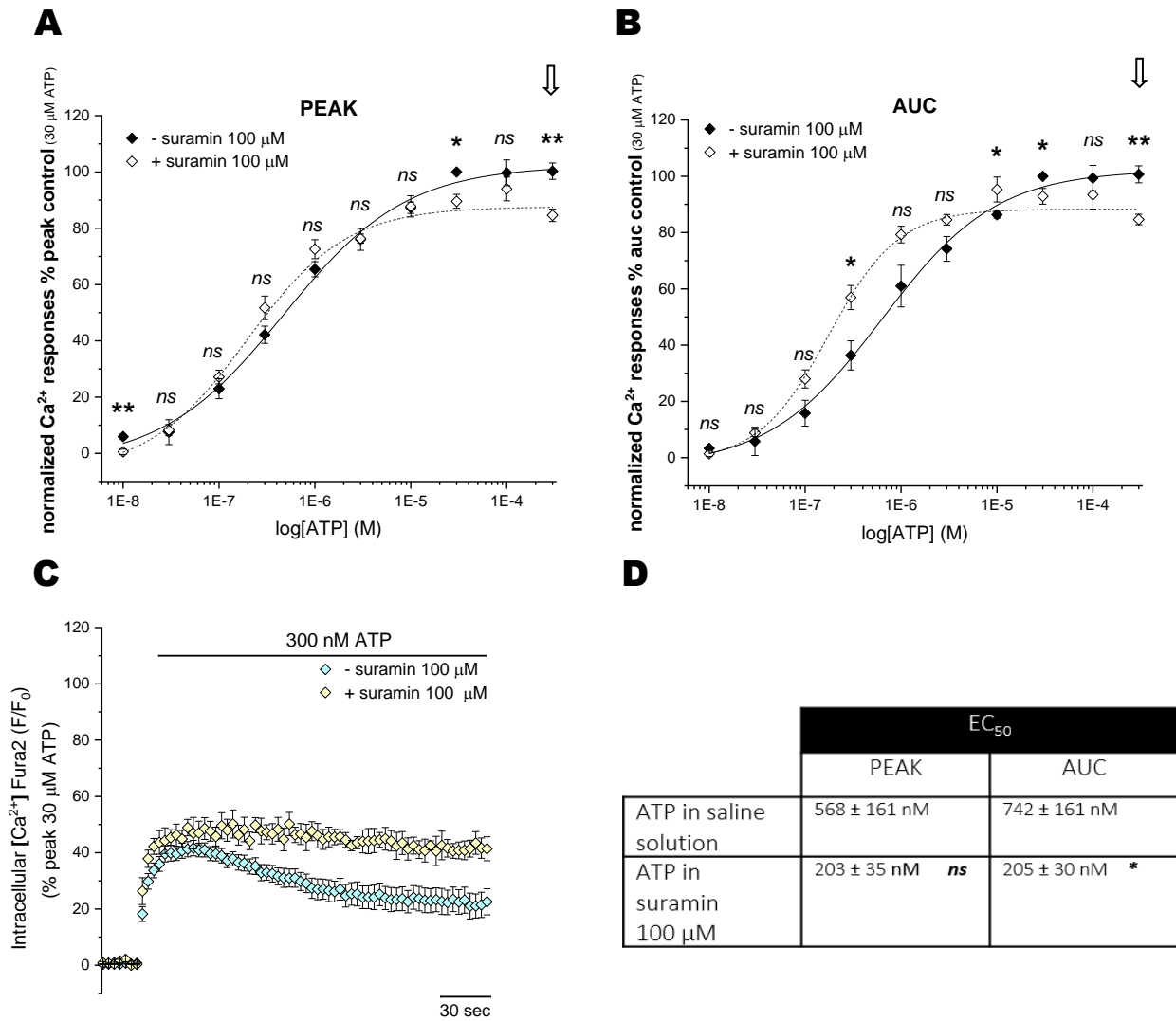


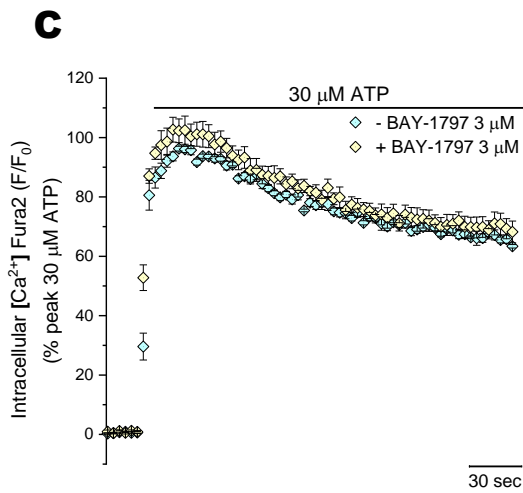
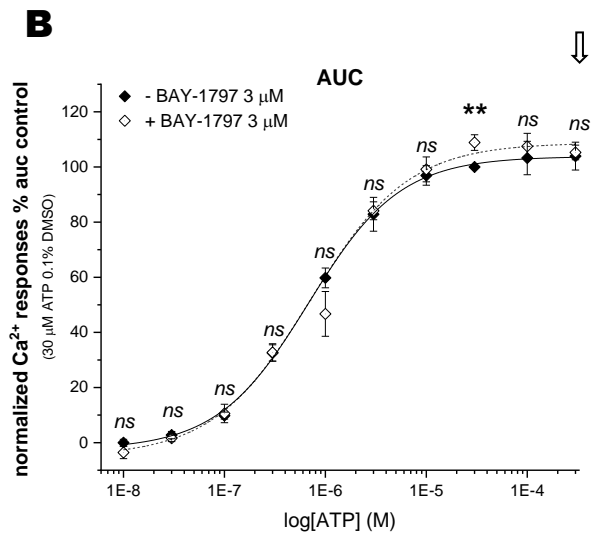
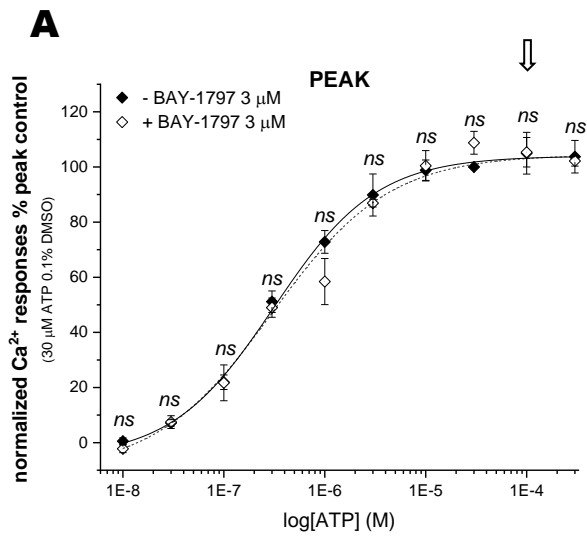
Figure 11. Unexpected effects of broad-spectrum P2 receptors antagonist suramin on the ATP-evoked response in human microvascular endothelial cells (HMEC-1). Concentration-response curves for the peak (A) and AUC (B) magnitude of intracellular Ca²⁺ responses elicited by ATP (0.01-300 μM; N=3) in the presence (0.01-300 μM; open rhombus; N=3) or absence (0.01-300 μM; closed rhombus; N=5) of suramin 100 μM. (C) Averaged time-resolved intracellular Ca²⁺ responses elicited by ATP 300 nM in the presence (light yellow rhombus; N=3) or absence (cyan rhombus; N=5) of suramin 100 μM over 250 seconds. All data were normalised to 30 μM ATP and fit the Hill1 equation with the EC₅₀ values showed in table (D). Asterisks show statistical significance relative to ATP potency (p *ns* > 0.05, p* < 0.05, p** < 0.01, p*** < 0.001). Data are represented as mean ± SEM.

3.3.2.4 P2X4 antagonists inconsistently affected the ATP-evoked calcium responses of human microvascular endothelial cells (HMEC-1).

Nearly all purinergic receptors exhibit a response to ATP, either directly or through ATP breakdown. However, P2X1 to X7, P2Y2, and P2Y11 receptor subtypes demonstrate a higher affinity for ATP than other physiological agonists (Burnstock, 2007). From all P2X receptors, P2X4 was the only candidate depicted from the RNA sequencing to be functionally expressed in HMEC-1 cells, and therefore, its pharmacological characterisation was investigated (**Figure 1**).

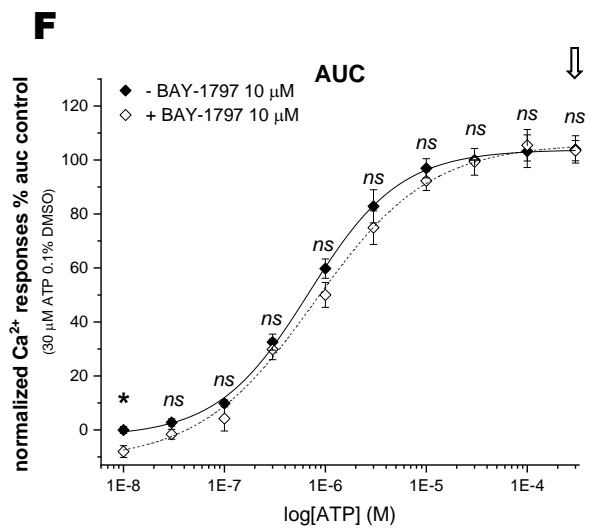
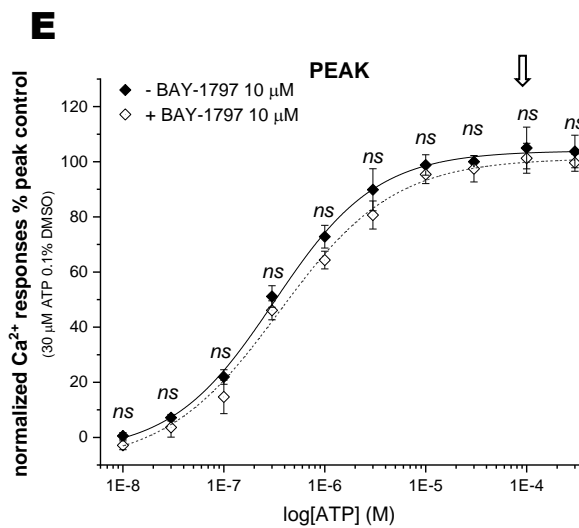
In recent years, advancements in small molecule development techniques enabled the commercialisation of selective P2X4 receptor antagonists. In this study, four different antagonists were tested to elicit the involvement of P2X4 in the ATP-evoked calcium responses in HMEC-1 cells. As previously described in **section 3.3.3**, to ensure consistency in experimental conditions, these four-antagonist solved in DMSO will always be compared to their respective solvent-controlled (0.1 or 0.2% DMSO) dose-response curve and derived calculated parameters (potency and efficacy). Three out of the four antagonists (BAY-1797 (3-10 μ M), 5-BDBD (10 μ M), and BX 430 (10 μ M) failed to significantly alter the ATP dose-response curve.

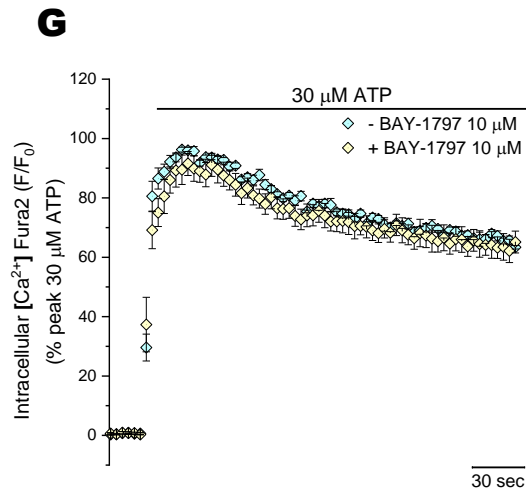
BAY-1797 is a potent and selective hP2X4 antagonist described by Bayer® in 2019 with a half-inhibitory concentration of 211 nM. The displayed activity on other P2X channels exhibited much higher IC₅₀ values in the micromolar range (>50 μ M for the hP2X1, >30 μ M for the hP2X2-3, 8.3 μ M for the hP2X3, and 10.6 μ M for the hP2X7) (Werner et al., 2019). Two different concentrations of BAY-1797 were tested to study the contribution of P2X4 on the ATP-evoked calcium responses (EC₅₀^{PEAK}: 338 \pm 52 nM; EC₅₀^{AUC}: 768 \pm 79 nM) (**Figure 12**). Neither the 3 nor 10 μ M successfully inhibit the calcium responses upon ATP application in the peak and the AUC dose-response curves. Isolated significant effects were found at 30 μ M ATP in the AUC curve when HMEC-1 cells were treated with 3 μ M BAY-1797 (**Figure 12-B**) and at 10 nM ATP in the peak curve when the cells were treated with the 10 μ M BAY-1799 concentration (**Figure 12-F**). Moreover, the potencies for the peak (527 \pm 177 nM; *ns*) and AUC (1.09 \pm 0.307 μ M; *ns*) were unaffected (**Figure 12-D, H**). In addition, no changes were found when comparing the ATP control maximal response concentration at 100 μ M for the peak (ATP_{max}^{peak}: 105 \pm 7.6%) and at 300 μ M for the AUC (ATP_{max}^{AUC}: 103 \pm 5.1%) in the presence of BAY (**Figure 12-A, B, E, F**). The maximal responses for ATP in the peak and AUC curves in the presence of 3 μ M BAY-1797 were found at 30 μ M ATP for the peak and AUC curves, but the level of efficacy remained intact (E_{max}^{peak}: 108.8 \pm 4.1 %; *ns*) and the AUC (E_{max}^{AUC}: 108.9 \pm 2.8%; *ns*) (**Table 3, 4**). These observations align with the isolated significant effect previously mentioned. On the other hand, the maximal responses for ATP in the peak and AUC curves in the presence of 10 μ M BAY-1797 were unchanged for the peak and found at 100 μ M as in the control curve. At the same time, the maximal response of the AUC was achieved at 100 μ M ATP instead of 300 μ M of the AUC control curve, but the level of efficacy was also conserved (E_{max}^{AUC}: 101.3 \pm 5.4%; *ns*). The lack of inhibitory effects was illustrated in the representative time-resolved intracellular calcium responses shown in **Figure 12- C, G**. Therefore, we concluded that BAY-1797 was insufficient to inhibit ATP-evoked responses in HMEC-1 cells.



D

| | EC_{50} | |
|--|----------------------------|---|
| | PEAK | AUC |
| ATP (0.1% DMSO) | 338 ± 52 nM | 768 ± 79 nM |
| ATP in BAY 3 μM (0.1% DMSO) | 527 ± 177 nM <i>ns</i> | $1.09 \mu\text{M} \pm 307$ nM <i>ns</i> |





H

| | EC_{50} | |
|-----------------------------------|----------------------------|----------------------------|
| | PEAK | AUC |
| ATP (0.1% DMSO) | 338 \pm 52 nM | 768 \pm 79 nM |
| ATP in BAY 10 μ M (0.1% DMSO) | 469 \pm 154 nM <i>ns</i> | 718 \pm 123 nM <i>ns</i> |

Figure 12. Lack of inhibitory effects of BAY-1797 P2X4 receptor antagonist on the ATP-evoked response in human microvascular endothelial cells (HMEC-1). Concentration-response curves for the peak (**A**) and AUC (**B**) magnitude of intracellular Ca^{2+} responses elicited by ATP (0.01-300 μ M; $N=5$) in the presence (0.01-300 μ M; open rhombus; $N=5$) or absence (0.01-300 μ M; closed rhombus; $N=5$) of BAY-1797 3 μ M. (**C**) Averaged time-resolved intracellular Ca^{2+} responses elicited by ATP 30 μ M in the presence (light yellow rhombus; $N=5$) or absence (cyan rhombus; $N=5$) of BAY-1797 3 μ M over 250 seconds. All data were normalised to 30 μ M ATP and fit the Hill1 equation with the EC_{50} values showed in table (**D**). Concentration-response curves for the peak (**E**) and AUC (**F**) magnitude of intracellular Ca^{2+} responses elicited by ATP (0.01-300 μ M; $N=5$) in the presence (0.01-300 μ M; open rhombus; $N=5$) or absence (0.01-300 μ M; closed rhombus; $N=5$) of BAY-1797 10 μ M. (**G**) Averaged time-resolved intracellular Ca^{2+} responses elicited by ATP 30 μ M in the presence (light yellow rhombus; $N=5$) or absence (cyan rhombus; $N=5$) of BAY-1797 10 μ M over 250 seconds. All data were normalised to 30 μ M ATP and fit the Hill1 equation with the EC_{50} values showed in table (**H**). Asterisks show statistical significance relative to ATP potency (p *ns* > 0.05, p^* < 0.05, p^{**} < 0.01, p^{***} < 0.001). Data are represented as mean \pm SEM.

Table 3. Effects of selective antagonists on the ATP-evoked peak responses in human microvascular endothelial cells (HMEC-1). EC₅₀ statistical analysis was performed against the ATP control curve in the appropriate vehicle control. Efficacy p-value is the statistical comparison between ATP maximal response in saline solution or saline solution containing 0.1 or 0.2% DMSO and ATP maximal response in the presence of the applied compound.

| Agonist | Agonist range, μ M | Antagonist | Antagonist concentration | Target | EC ₅₀ PEAK | P value | Maximal response PEAK (μ M) | Maximal response PEAK (%) | P value |
|-----------------|------------------------|---------------|--------------------------|-------------------|------------------------|-----------|----------------------------------|---------------------------|-----------|
| ATP (0.1% DMSO) | 0.1-300 | - | - | P2X/P2Y | 338 \pm 52 nM | - | 100 | 105.0 \pm 7.6 | - |
| ATP | 0.1-300 | AR-C 118925XX | 10 μ M | P2Y ₂ | 51.7 \pm 3.1 μ M | p<0.001 | 300 | 70.6 \pm 1.3 | p<0.001 |
| ATP | 0.1-300 | BAY-1797 | 3 μ M | P2X ₄ | 527 \pm 177 nM | <i>ns</i> | 30 | 108.8 \pm 4.1 | <i>ns</i> |
| ATP | 0.1-300 | BAY-1797 | 10 μ M | P2X ₄ | 469 \pm 154 nM | <i>ns</i> | 100 | 101.3 \pm 5.4 | <i>ns</i> |
| ATP | 0.1-300 | BX430 | 10 μ M | P2X ₄ | 392 \pm 100 nM | <i>ns</i> | 100 | 103.3 \pm 3.8 | <i>ns</i> |
| ATP | 0.1-300 | 5-BDBD | 10 μ M | P2X ₄ | 444 \pm 80 nM | <i>ns</i> | 100 | 99.7 \pm 3.2 | <i>ns</i> |
| ATP (0.2% DMSO) | 0.1-300 | - | - | P2X/P2Y | 568 \pm 165 nM | - | 100 | 100.1 \pm 4.2 | - |
| ATP | 0.1-300 | PSB12062 | 10 μ M | P2X ₄ | 160 \pm 50 nM | p<0.05 | 30 | 64.3 \pm 4.4 | p<0.001 |
| ATP (saline) | 0.1-300 | - | - | P2X/P2Y | 568 \pm 161 nM | - | 300 | 100.27 \pm 2.9 | - |
| ATP | 0.1-300 | NF157 | 5 μ M | P2Y ₁₁ | 542 \pm 56 nM | <i>ns</i> | 300 | 107.9 \pm 1.5 | p<0.05 |
| ATP | 0.1-300 | MRS 1754 | 100 nM | A ₂ B | 1.30 \pm 0.9 μ M | <i>ns</i> | 300 | 106.1 \pm 4.0 | <i>ns</i> |

Table 4. Effects of selective antagonists on the ATP-evoked AUC responses in human microvascular endothelial cells (HMEC-1). EC₅₀ statistical analysis was performed against the ATP control curve in the appropriate vehicle control. Efficacy p-value is the statistical comparison between ATP maximal response in saline solution or saline solution containing 0.1 or 0.2% DMSO and ATP maximal response in the presence of the applied compound.

| Agonist | Agonist range, μM | Antagonist | Antagonist concentration | Target | EC ₅₀ AUC | P value | Maximal response AUC (μM) | Maximal response AUC (%) | P value |
|-----------------|------------------------------|---------------|--------------------------|-------------------|---------------------------------|---------|--|--------------------------|---------|
| ATP (0.1% DMSO) | 0.1-300 | / | / | P2X/P2Y | 768 \pm 79 nM | / | 300 | 103 \pm 5.1 | / |
| ATP | 0.1-300 | AR-C 118925XX | 10 μM | P2Y ₂ | 87.5 \pm 1.3 μM | p<0.01 | 300 | 25.4 \pm 2.5 | p<0.001 |
| ATP | 0.1-300 | BAY-1797 | 3 μM | P2X ₄ | 1.09 μM \pm 307 nM | ns | 30 | 108.9 \pm 2.8 | ns |
| ATP | 0.1-300 | BAY-1797 | 10 μM | P2X ₄ | 718 \pm 123 nM | ns | 100 | 105.5 \pm 5.8 | ns |
| ATP | 0.1-300 | BX430 | 10 μM | P2X ₄ | 1.02 μM \pm 153 nM | ns | 100 | 104.9 \pm 3.2 | ns |
| ATP | 0.1-300 | 5-BDBD | 10 μM | P2X ₄ | 909 \pm 80 nM | ns | 100 | 98.6 \pm 5.3 | ns |
| ATP (0.2% DMSO) | 0.1-300 | / | / | P2X/P2Y | 901 \pm 232 nM | / | 100 | 109.4 \pm 4.8 | / |
| ATP | 0.1-300 | PSB12062 | 10 μM | P2X ₄ | 184 \pm 55 nM | p<0.05 | 300 | 53.3 \pm 4.8 | p<0.05 |
| ATP (saline) | 0.1-300 | / | / | P2X/P2Y | 742 \pm 161 nM | / | 300 | 100.68 \pm 3 | / |
| ATP | 0.1-300 | NF157 | 5 μM | P2Y ₁₁ | 1.05 μM \pm 83 nM | ns | 300 | 107.7 \pm 1.8 | ns |
| ATP | 0.1-300 | MRS 1754 | 100 nM | A ₂ B | 1.85 \pm 1.25 μM | ns | 300 | 106.4 \pm 3.1 | ns |

The second P2X4 antagonist investigated was 5-BDBD. It was the first described hP2X4 antagonist by Bayer® in 2004, and it is 17 times less potent ($IC_{50} = 3710$ nM) than BAY-1797 (Werner et al., 2019). 10 μ M of 5-BDBD was applied to study the contribution of P2X4 on the ATP-evoked calcium responses (**Figure 13**). 5-BDBD could not inhibit any calcium responses upon ATP application in the peak and the AUC dose-response curves (**Figure 13-A, B**), and both potencies were unaffected by the presence of the antagonist (EC_{50}^{PEAK} : 444 ± 80 nM, *ns*; EC_{50}^{AUC} : 909 ± 80 nM, *ns*) (**Fig 13-D**). No change was found when comparing the ATP control maximal response concentration at 100 μ M for the peak (ATP_{max}^{peak} : $105 \pm 7.6\%$) and at 300 μ M for the AUC (ATP_{max}^{AUC} : $103 \pm 5.1\%$) in the presence of 5-BDBD for the peak (99.7 ± 3.2 , *ns*) and the AUC (98.6 ± 5.3 , *ns*) (**Figure 13-A, B**). Nevertheless, in the case of the AUC, the maximal response for ATP in the presence of 10 μ M 5-BDBD was found at 100 μ M ATP instead of 300 μ M. Consistently, the level of efficacy remained intact (**Table 4**). The representative time-resolved intracellular calcium responses depicted in **Figure 13-C** demonstrated the described absence of inhibitory effects. As a result, we have concluded that 10 μ M 5-BDBD was not effective in inhibiting ATP-induced responses in HMEC-1 cells.

The third P2X4 antagonist examined was BX 430. It was described by Ase et al. in 2015, and it is 4 times less potent ($IC_{50} = 780$ nM) than BAY-1797 (Ase et al., 2015; Werner et al., 2019). As previously reported for the previous antagonist, 10 μ M of BX430 could not impede any calcium responses upon ATP application in the peak and the AUC dose-response curves (**Figure 14-A, B**), and both potencies were unaffected by the presence of the antagonist (EC_{50}^{PEAK} : 392 ± 100 nM, *ns*; EC_{50}^{AUC} : 1.02 ± 0.153 μ M, *ns*) (**Fig 14-D**). When comparing the ATP control maximal response, there was no change at 100 μ M for the peak (ATP_{max}^{peak} : $105 \pm 7.6\%$) and at 300 μ M for the AUC (ATP_{max}^{AUC} : $103 \pm 5.1\%$) in the presence of BX 430 (ATP_{max}^{peak} : 103.3 ± 3.8 , *ns*; ATP_{max}^{AUC} : $104.9 \pm 3.2\%$, *ns*) (**Figure 14-A, B**). However, in the case of the AUC, the maximal response for ATP in the presence of 10 μ M BX430 was observed at 100 μ M ATP instead of the 300 μ M ATP concentration in the control curve. Nonetheless, the level of efficacy remained unaffected (**Table 4**). The representative time-resolved intracellular calcium responses exemplified in **Figure 14-C** demonstrated the absence of inhibitory effects. Therefore, we have concluded that 10 μ M BX 430 did not have any inhibitory effects on the ATP-induced responses in HMEC-1 cells.

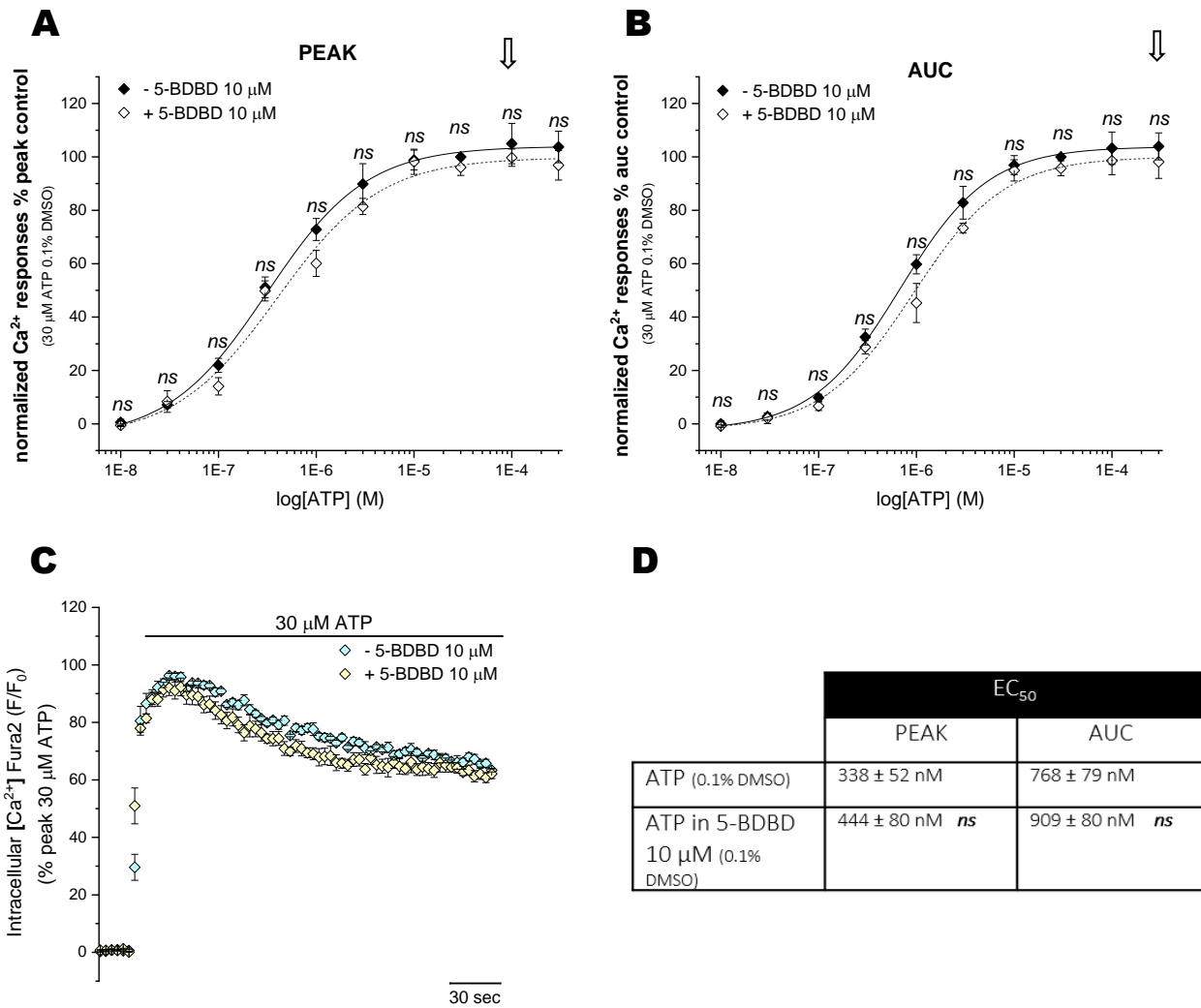


Figure 13. Lack of inhibitory effects of 5-BDBD P2X4 receptor antagonist on the ATP-evoked response in human microvascular endothelial cells (HMEC-1). Concentration-response curves for the peak (A) and AUC (B) magnitude of intracellular Ca^{2+} responses elicited by ATP (0.01-300 μM ; $N=5$) in the presence (0.01-300 μM ; open rhombus; $N=5$) or absence (0.01-300 μM ; closed rhombus; $N=5$) of 5-BDBD 10 μM . (C) Averaged time-resolved intracellular Ca^{2+} responses elicited by ATP 30 μM in the presence (light yellow rhombus; $N=5$) or absence (cyan rhombus; $N=5$) of 5-BDBD 10 μM over 250 seconds. All data were normalised to 30 μM ATP and fit the Hill1 equation with the EC_{50} values showed in table (D). Asterisks show statistical significance relative to ATP potency ($p_{ns} > 0.05$, $p^* < 0.05$, $p^{**} < 0.01$, $p^{***} < 0.001$). Data are represented as mean \pm SEM.

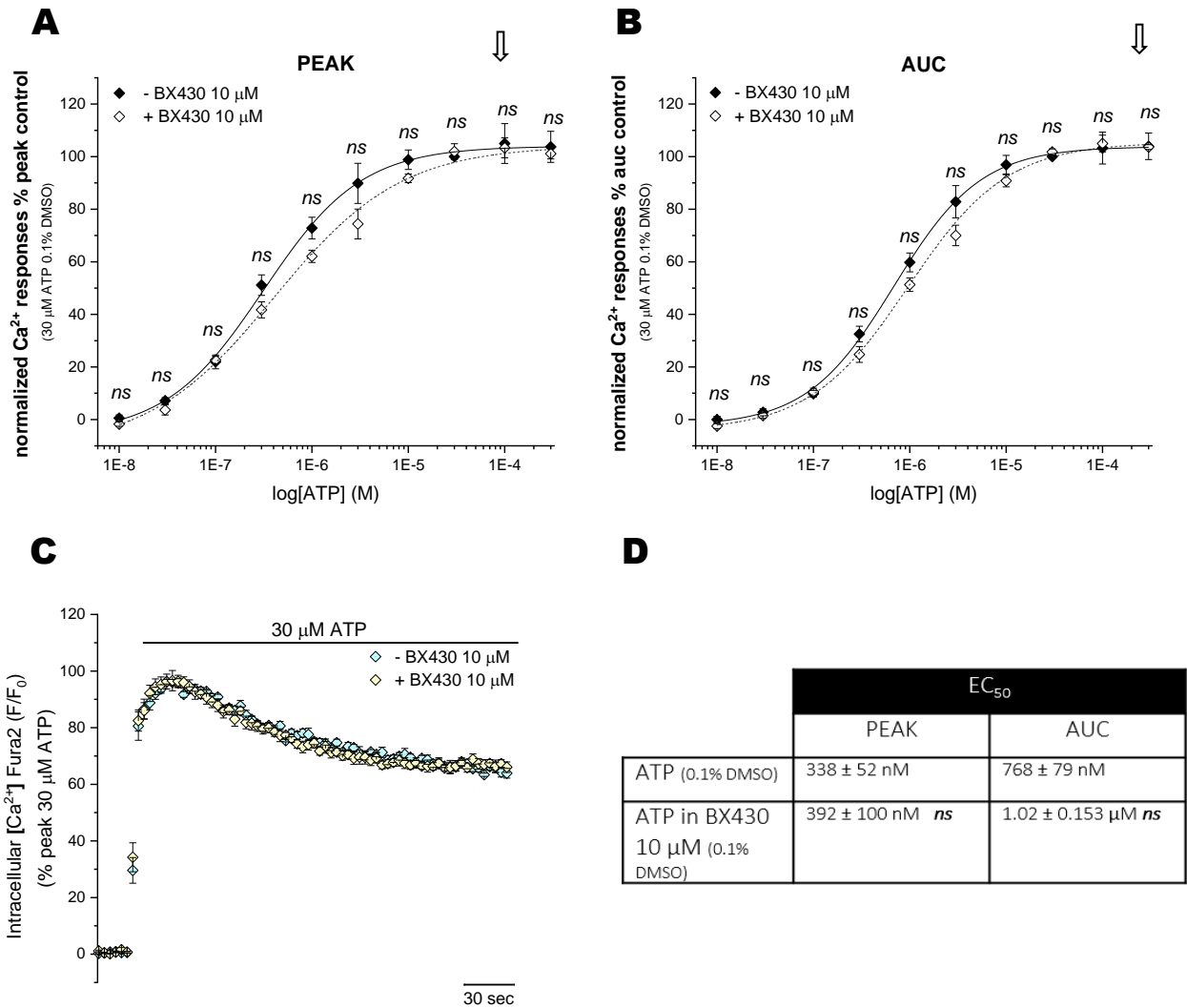


Figure 14. Lack of inhibitory effects of BX 430 P2X4 receptor antagonist on the ATP-evoked response in human microvascular endothelial cells (HMEC-1). Concentration-response curves for the peak (**A**) and AUC (**B**) magnitude of intracellular Ca^{2+} responses elicited by ATP (0.01-300 μM ; $N=5$) in the presence (0.01-300 μM ; open rhombus; $N=5$) or absence (0.01-300 μM ; closed rhombus; $N=5$) of BX430 10 μM . (**C**) Averaged time-resolved intracellular Ca^{2+} responses elicited by ATP 30 μM in the presence (light yellow rhombus; $N=5$) or absence (cyan rhombus; $N=5$) of BX430 10 μM over 250 seconds. All data were normalised to 30 μM ATP and fit the Hill1 equation with the EC₅₀ values showed in table (**D**). Asterisks show statistical significance relative to ATP potency (p *ns* > 0.05, p^* < 0.05, p^{**} < 0.01, p^{***} < 0.001). Data are represented as mean \pm SEM.

To further complement this pharmacological profiling and given the lack of effects using hP2X4 selective antagonists, 1321N1 astrocytoma cells stably expressing the human P2X4 receptor, were utilised to double-check the known ability of one of the selective antagonists, BX 430 in this case, to inhibit hP2X4 ATP-dependent evoked responses. In this way, we could exclude any concern of unexpected antagonist behaviour.

ATP was applied to confirm whether the human P2X4 receptor was functionally active in this model. ATP elicited intracellular calcium response in a concentration-dependent manner (30 to 0.3 μM ; dark blue square) (**Figure 15**). Contrarily, ATP did not cause an endogenous calcium response in parental 1321N1 astrocytoma cells (**Figure 16-A**), proving that the ATP calcium responses were due to human P2X4 receptors. 30 μM ATP calcium response was not significantly different than the vehicle control-induced response (**Figure 16-B**). Cell viability was confirmed using ionomycin 1 μM , that effectively evoked a robust intracellular calcium response (**Figure 16-C**). Ionomycin is a well-known intracellular calcium-inducer. It is an ionophore that increases calcium concentration in the intracellular space by directly facilitating the transport of calcium ions across the plasma membrane (Dedkova et al., 2000).

10 μM BX 430 significantly blocked the ATP-evoked responses at 30 and 3 μM 1321N1 astrocytoma cells stably expressing the human P2X4 receptor, confirming the canonical antagonist effect of the molecule. The representative time-resolved intracellular calcium responses exemplified in **Figure 15-A, B** demonstrated these inhibitory effects. Therefore, we agreed that 10 μM BX 430 is an effective tool for inhibiting the P2X4 ATP-dependent calcium responses in human cells.

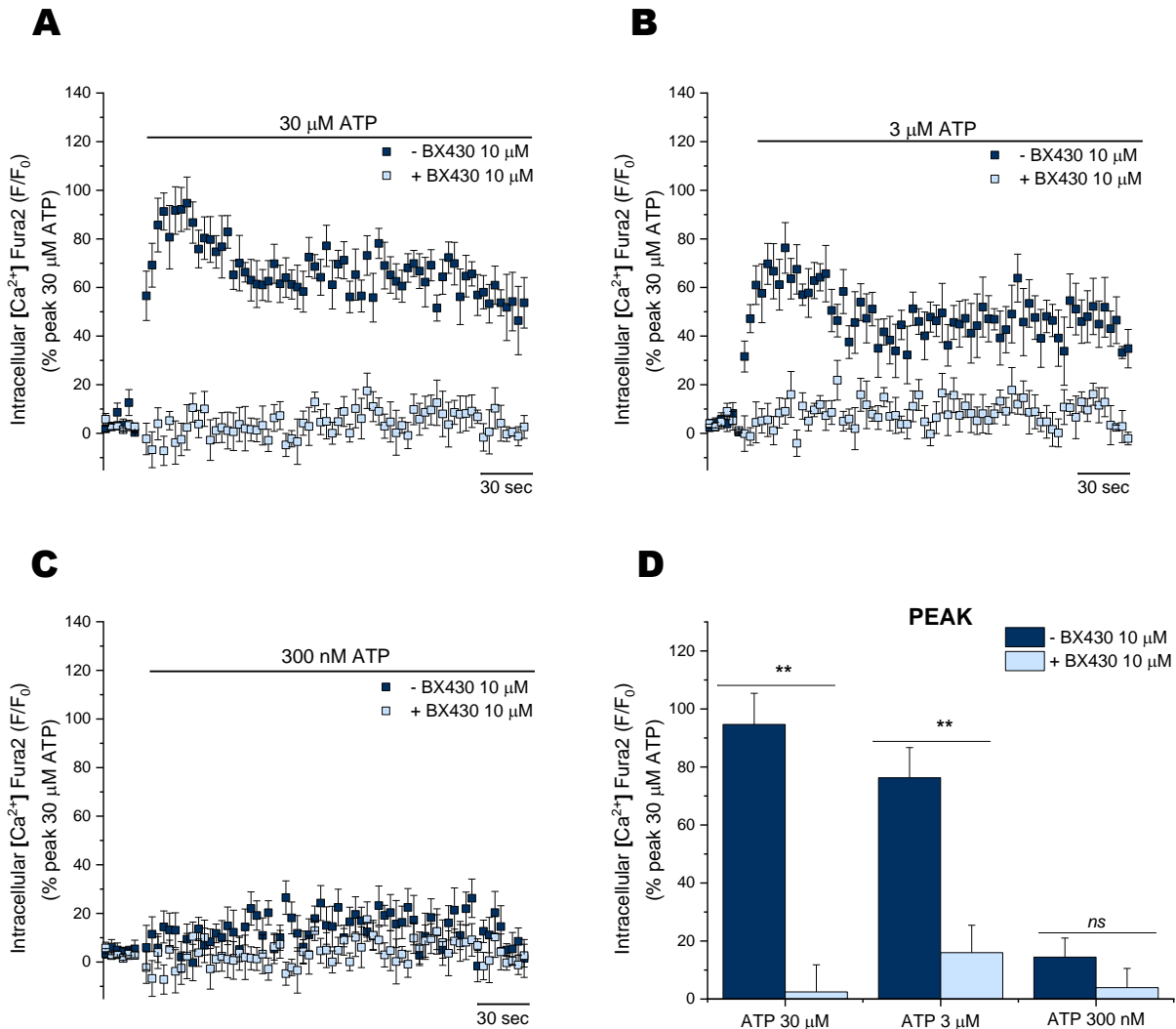


Figure 15. Inhibitory effects on ATP-evoked Ca²⁺ responses after treatment with BX 430 selective human P2X4 receptor antagonist in 1321N1 human P2X4 stable astrocytoma cells. Averaged time-resolved intracellular Ca²⁺ responses elicited by ATP 30 μM (**A**), 3 μM (**B**) and 300 nM (**C**) in the presence (light blue square; N=3) or absence (dark blue square; N=3) of BX430 10 μM over 250 seconds. (**D**) Comparison of peak magnitude of intracellular Ca²⁺ responses induced by ATP at three different concentrations in the presence (light blue square; N=3) or absence (dark blue square; N=3) of BX430 10 μM. All data were normalised to 30 μM ATP. Asterisks show statistical significance relative to ATP peak (p *ns* > 0.05, p* < 0.05, p** < 0.01, p*** < 0.001). Data are represented as mean ± SEM.

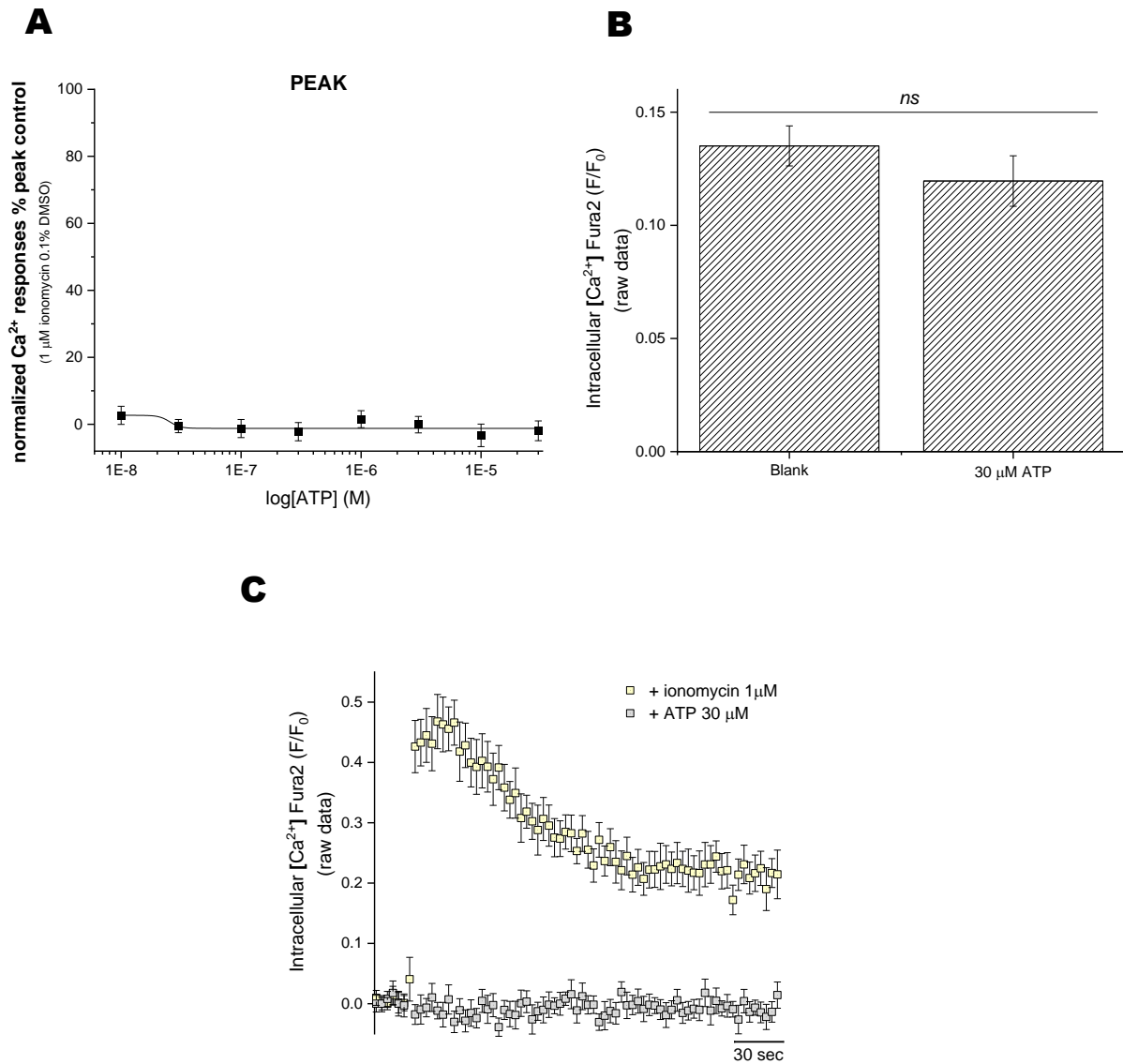


Figure 16. ATP did not cause an endogenous calcium response in 1321N1 parental astrocytoma cells. (A) Concentration-response curves for the peak magnitude of intracellular Ca^{2+} responses elicited by ATP (0.03-30 μM ; $N=5$). **(B)** Comparison of peak magnitude of intracellular Ca^{2+} responses induced by the injection of vehicle control (*blank*) or 30 μM ($N=5$). **(C)** Averaged time-resolved intracellular Ca^{2+} responses elicited by ATP 30 μM (grey square; $N=5$) and ionomycin 1 μM (light yellow rhombus; $N=5$) over 250 seconds. Asterisks show statistical significance relative to ATP 30 μM (p *ns* > 0.05, p^* < 0.05, p^{**} < 0.01, p^{***} < 0.001). Data are represented as mean \pm SEM.

The fourth P2X4 antagonist examined was PSB12062. It was described by Hernandez-Olmos et al. in 2012, and it is 7 times less potent ($IC_{50}= 1.38 \mu\text{M}$) than BAY-1797 (Hernandez-Olmos et al., 2012; Werner et al., 2019). In contrast with the three previous antagonists, $10 \mu\text{M}$ of PSB12062 impacted the ATP dose-response curve control (EC_{50}^{PEAK} : $568 \pm 165 \text{ nM}$; EC_{50}^{AUC} : $901 \pm 232 \text{ nM}$). The presence of the antagonist significantly increased the ATP potency for the peak ($160 \pm 50 \text{ nM}$, $p < 0.05$) and the area under the curve ($184 \pm 55 \text{ nM}$, $p < 0.05$) (**Figure 17-D, Table 3, 4**). Furthermore, the presence of the antagonist led to a substantial reduction in calcium responses at all consecutive ATP concentrations from $300 \mu\text{M}$ to $3 \mu\text{M}$, after which the effect diminished (**Figure 17-A, B**). Accordingly, the ATP control maximal response to ATP at $100 \mu\text{M}$ ($ATP_{\text{max}}^{\text{peak}}$: $100.1 \pm 4.2 \%$; $ATP_{\text{max}}^{\text{AUC}}$: $109.4 \pm 4.8\%$) in the presence of PSB12062 was significantly reduced ($ATP_{\text{max}}^{\text{peak}}$: $59.42 \pm 4.43\%$, $p < 0.001$; $ATP_{\text{max}}^{\text{AUC}}$: $50.64 \pm 4.07 \%$, $p < 0.001$). Consequently, the maximal response in the presence of the inhibitor was achieved at $30 \mu\text{M}$ for the peak ($64.3 \pm 4.4 \%$; $p < 0.001$) and the at $300 \mu\text{M}$ for the AUC ($53.3 \pm 4.8 \%$; $p < 0.05$). When comparing these new maximal responses with the maximal response control at $100 \mu\text{M}$ ATP in the absence of the PSB12062, the cells never managed to achieve the same level of efficacy as the control (**Table 3, 4**). The representative time-resolved intracellular calcium responses shown in **Figure 17-C** illustrated PSB12062's significant impact on the peak and the area under the curve upon $30 \mu\text{M}$ ATP stimulation compared with the control. In the presence of this antagonist, the activation kinetics at $30 \mu\text{M}$ ATP showed a significant decrease of the peak to around 60% above baseline compared to the 100 % control response in the absence of the antagonist. The slow desensitisation kinetics was conserved, but the decay, in this case, reached approximately 20% above baseline, compared to the control, which never decayed below 60%. These results portray unexpected results for a non-competitive negative allosteric modulator (Hernandez-Olmos et al., 2012). A decrease in the efficacy could be expected but not an increase in the potency, acting in that case as a positive allosteric modulator of ATP.

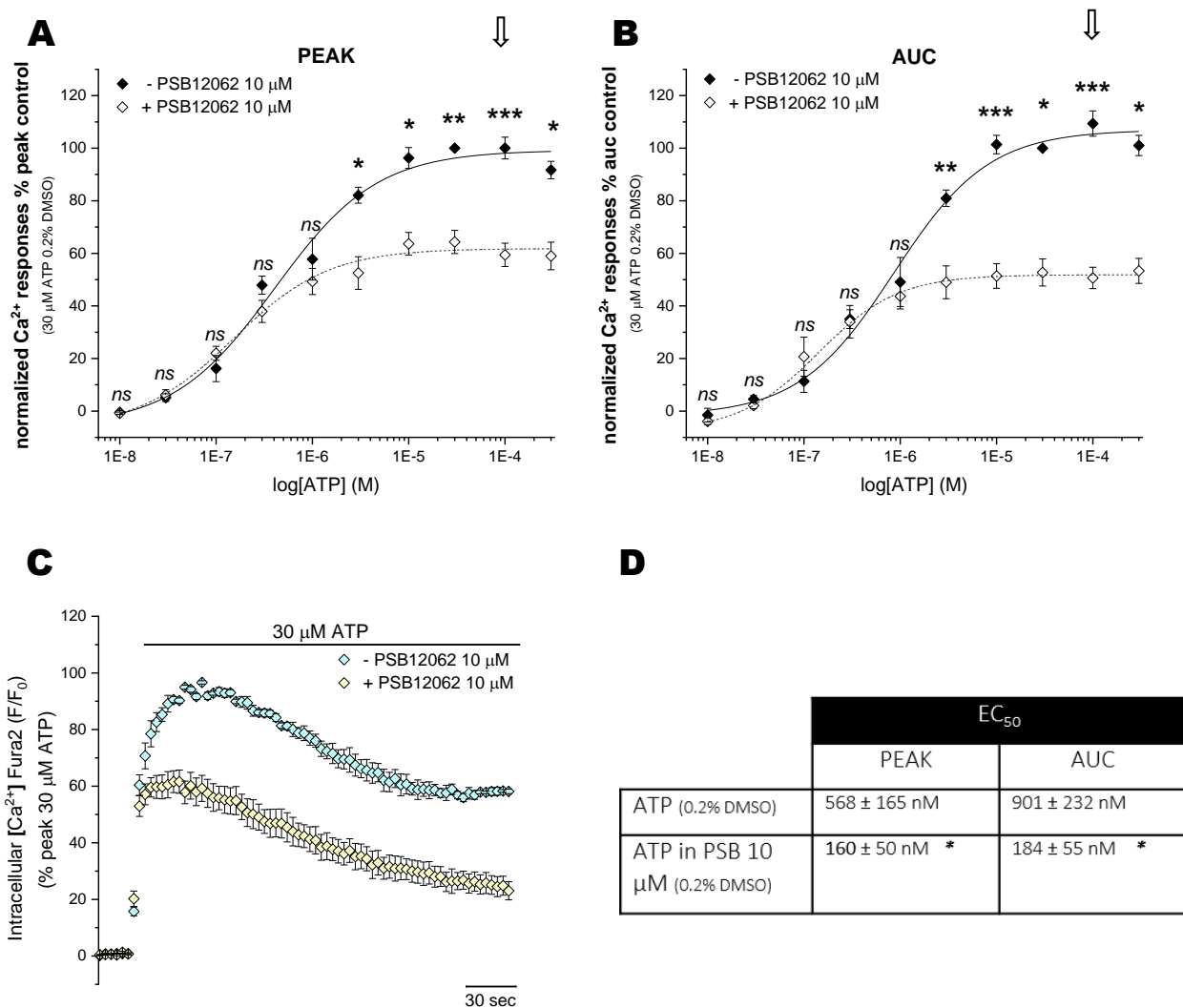


Figure 17. Inhibitory effects of PSB12062 P2X4 receptor antagonist on the ATP-evoked response in human microvascular endothelial cells (HMEC-1). Concentration-response curves for the peak (A) and AUC (B) magnitude of intracellular Ca^{2+} responses elicited by ATP (0.01-300 μ M; $N=5$) in the presence (0.01-300 μ M; open rhombus; $N=5$) or absence (0.01-300 μ M; closed rhombus; $N=5$) of PSB12062 10 μ M. (C) Averaged time-resolved intracellular Ca^{2+} responses elicited by ATP 30 μ M in the presence (light yellow rhombus; $N=5$) or absence (cyan rhombus; $N=5$) of PSB12062 10 μ M over 250 seconds. All data were normalised to 30 μ M ATP and fit the Hill1 equation with the EC_{50} values showed in table (D). Asterisks show statistical significance relative to ATP potency (p $ns > 0.05$, $p^* < 0.05$, $p^{**} < 0.01$, $p^{***} < 0.001$). Data are represented as mean \pm SEM.

3.3.2.5 P2X4 positive allosteric modulator, ivermectin, had an unexpected impact on the ATP-evoked calcium responses of human microvascular endothelial cells (HMEC-1).

Ivermectin is a selective positive allosteric modulator of the human and rodent P2X4 receptor, which acts by potentiating the ATP-evoked currents and slowing the rate of receptor deactivation (Gao et al., 2015; Khakh et al., 1999; Priel et al., 2004; Stokes et al., 2020; Weinhausen et al., 2022). This modulator has been defined as type I/II (mixed) of the positive allosteric modulators, meaning it left-ward shifts the dose-response curve and increases the maximum response (Stokes et al., 2020).

In an attempt to isolate possible P2X4 contribution to the ATP-evoked responses, cells were treated with 3 μ M ivermectin, and the rise in intracellular calcium response was measured when stimulating with three different concentrations of ATP (3 μ M, 0.3 μ M, and 0.1 μ M) in the presence and the absence of the modulator. Ivermectin significantly decreased, instead of potentiating, the ATP-induced calcium response at 3 μ M, while the other 2 concentrations in the study were unaffected (**Figure 18-A, D**). In **Figure 18-E** a representative calcium-response trace revealed this significant impact on the peak and the area under the curve upon 3 μ M ATP stimulation compared with the control. In the presence of ivermectin, the activation kinetics at 3 μ M ATP showed a significant decrease of the peak to around 90% response above baseline compared to the 100 % control response in the absence of the modulator. The slow desensitisation kinetics persisted, but the decay reached approximately 20% above baseline, compared to the control, which never decayed below 60%. In these assays, either potentiation or non-affected of the ATP response was anticipated. However, the reduction observed opened the door to decipher the unexpected outcome further.

Ivermectin has been shown to inhibit at the micromolar range calcium ATPase (SERCA) channels, responsible for the calcium reuptake in the endoplasmic reticulum. As thapsigargin is a potent non-competitive SERCA inhibitor, it leads to the depletion of the calcium stores by blocking calcium uptake (Pimenta et al., 2010). In these assays, cells were again treated with 3 μ M ivermectin, and the rise in intracellular calcium response was measured when stimulated with 200 nM thapsigargin. Ivermectin significantly decreased the thapsigargin-induced calcium response at 200 nM (**Figure 18-B, D**), which portrayed its cited effect in the SERCA channels and indirectly assessed the effect in the previously described ATP-induced responses. As shown in **Figure 18-F**, thapsigargin trace kinetics, in the absence of ivermectin, presented a sustained calcium response characterised by the prolonged increase in intracellular calcium over approximately four minutes, reaching its highest peak as the response progressed. This fashion was conserved in the presence of ivermectin but illustrated the significant reduction in the peak and the AUC in the presence of the modulator. Therefore, ivermectin is an effective tool for regulating the depletion of the calcium responses in human cells, and the inhibitory effects observed are probably due to one of its noncanonical effects.

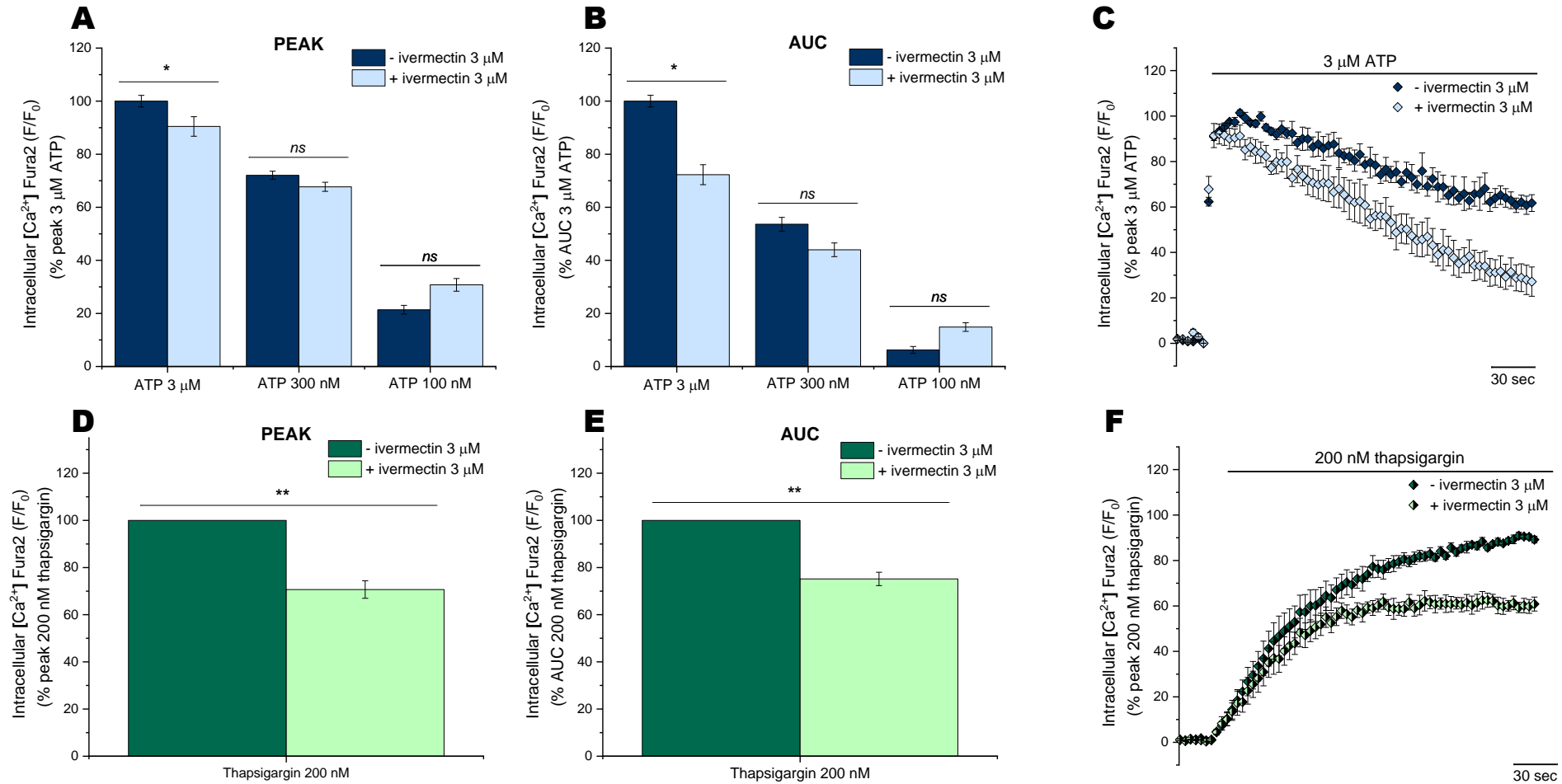


Figure 18. Unexpected effects of ivermectin in human microvascular endothelial cells (HMEC-1). Comparison of peak (A) and AUC (C) magnitude of intracellular Ca^{2+} responses induced by ATP at three different (3 μ M, 300 nM and 100 nM) concentrations in the presence (light blue; $N=4$) or absence (dark blue; $N=4$) of ivermectin 3 μ M. (E) Averaged time-resolved intracellular Ca^{2+} responses elicited by ATP 3 μ M, 300 nM and 100 nM in the presence (light blue rhombus; $N=4$) or absence (dark blue rhombus; $N=4$) of ivermectin 3 μ M over 250 seconds. All data were normalised to 3 μ M ATP. Comparison of peak (B) and AUC (D) magnitude of intracellular Ca^{2+} responses induced by thapsigargin at 200 nM in the presence (light green; $N=5$) or absence (dark green; $N=5$) of ivermectin 3

μM . (F) Averaged time-resolved intracellular Ca^{2+} responses elicited by thapsigargin 200 nM in the presence (light green rhombus; $N=4$) or absence (dark green rhombus; $N=4$) of ivermectin 3 μM over 250 seconds. All data were normalised to 200 nM thapsigargin. Asterisks show statistical significance relative to ATP peak ($p_{ns} > 0.05$, $p^* < 0.05$, $p^{**} < 0.01$, $p^{***} < 0.001$). Data are represented as mean \pm SEM.

3.3.2.6 P2Y2 selective antagonist significantly affected the ATP and UTP-evoked calcium responses of human microvascular endothelial cells (HMEC-1).

Of the P2Y metabotropic receptors, P2Y2 and P2Y11 proved a higher affinity for ATP than other physiological agonists (Burnstock, 2007). Furthermore, as previously stated, both P2Y2 and P2Y11 were identified as potential candidates for functional expression in HMEC-1 cells based on RNA sequencing data (**Figure 1**).

P2Y2 is equally sensitive to ATP and UTP. Therefore, both nucleotides are valuable tools to investigate this receptor functional activity. The selective and competitive antagonist, AR-C 118925XX, was utilised to determine if P2Y2 was involved in the ATP and UTP-evoked calcium responses in HMEC-1. AR-C 118025XX half maximal inhibitory concentrations for the human P2Y2 were described by Rafehi et al., 2017. The antagonist inhibited ATP-induced calcium responses with an IC_{50} value of 57.4 nM. The potency decreased when inhibiting UTP-evoked calcium responses with an IC_{50} value of 72.1 nM when P2Y2 receptors were recombinantly expressed in 1321N1 astrocytoma cells. However, these values were notably increased when reported in endothelial cells (Muoboghare et al., 2019).

First, the effects of AR-C 118925XX (10 μ M) on the ATP dose-response curve control (EC_{50}^{PEAK} : 338 ± 52 nM; EC_{50}^{AUC} : 768 ± 79 nM) were explored. As AR-C was not soluble in deionised water, DMSO was used as the solvent. As described in **section 3.3.3**, this antagonist was always compared to its respective solvent-controlled 0.1 % DMSO ATP dose-response curve (**Figure 7-A, B**) and derived calculated parameters (potency and maximal response) (**Table 3, 4**) to ensure consistency in experimental conditions. Pre-treatment with AR-C 118925XX (10 μ M) right-shifted the ATP dose-response curve and significantly reduced the ATP potency for the peak (51.7 ± 3.1 μ M, $p < 0.001$) and the area under the curve (87.5 ± 1.3 μ M, $p < 0.001$), diverting the potencies to the micromolar scale. (**Figure 19-A, B, Table 3, 4**). Furthermore, the presence of the antagonist significantly affected the control ATP maximal response (ATP_{max}^{peak} : 105.0 ± 7.6 %; ATP_{max}^{AUC} : 103 ± 5.1 %) at 100 μ M for the peak (ATP_{max}^{peak} : 53.03 ± 2.62 %, $p < 0.001$) and at 300 μ M for the AUC (ATP_{max}^{AUC} : 25.4 ± 2.5 %, $p < 0.001$) (**Figure 19-A, B**). Accordingly, the maximal response to ATP in the presence of AR-C was achieved at 300 μ M for the peak (70.6 ± 1.3 %; $p < 0.001$). When comparing this new maximal response with the control response in the absence of the antagonist, the level of efficacy was significantly reduced in both curves, and it never managed to achieve the same level of efficacy as the control being this fact much more evident in the AUC curve (**Table 4**). The representative time-resolved intracellular calcium responses shown in **Figure 19-C** illustrated AR-C's significant impact on the peak and the massive effect in the area under the curve upon 30 μ M ATP stimulation compared with the control. In the presence of AR-C, the ATP caused a rapid transient increase in the calcium influx. However, it was much weaker (25%) than the control response (100%). There was a quick decay in the response over approximately 60 seconds to the baseline, losing the slow desensitisation kinetics observed in the control response.

To further characterise AR-C 118925XX effects on the ATP-evoked responses, HMEC-1 cells were incubated for 30 minutes in a range of antagonist concentrations (0.312 to 10 μ M) and stimulated with a sub-maximal concentration of ATP (10 μ M) and thereby, IC_{50} was calculated (**Figure 20-A, B**). The half-maximal inhibitory concentration values obtained were 1.77 ± 0.73 μ M for the peak and 559 ± 173 nM for AUC inhibition curves. The representative time-resolved

intracellular calcium responses shown in **Figure 20-C** depicted 1.25 μM AR-C's significant impact on the peak and the area under the curve upon 10 μM ATP stimulation compared with the control. In the presence of AR-C, the ATP caused a rapid transient increase in the calcium influx, but it was weaker (60%) than the control response (100%). There was a relatively quick decay in the response over approximately 2 minutes to the baseline, losing the slow desensitisation kinetics observed in the control response. These results were not far from what has been previously reported in endothelial cells.

Secondly, the effects of AR-C 118925XX (10 μM) on the UTP dose-response curve control ($\text{EC}_{50}^{\text{PEAK}}$: 450 ± 241 nM; $\text{EC}_{50}^{\text{AUC}}$: 673 ± 198 nM) were investigated. As in the case of the ATP control dose-response curves, strict solvent control was performed to mitigate potential solvent-related influences on the UTP dose-response curve (**Figure 21**). The presence of DMSO at 0.1% (v/v) did not alter the UTP potencies when compared with EC_{50} calculated from UTP in saline solution (SBS) (**Figure 21-C**). However, to guarantee consistency in experimental conditions, drugs solved in DMSO will always be compared to their respective dose-response solvent-controlled (0.1 % DMSO) curve. Pre-treatment with AR-C 118925XX (10 μM) right-shifted the UTP dose-response curve and significantly reduced the UTP potency for the peak (14.3 ± 3.7 μM ; $p < 0.05$) and the area under the curve (22.2 ± 8.3 μM , $p < 0.05$), diverting the potencies to the micromolar scale, precisely in the same fashion seen in the ATP dose-response (**Figure 22-A, B**). Similarly, the presence of the antagonist significantly affected the control UTP-evoked maximal response at 200 μM ($\text{UTP}_{\text{max}}^{\text{peak}}$: 106.37 ± 3.65 %; $\text{UTP}_{\text{max}}^{\text{AUC}}$: 111.6 ± 3.02 %) for the peak (35.18 ± 1.48 %, $p < 0.001$) and the AUC (10.63 ± 1.26 %, $p < 0.001$) (**Figure 22-A, B**). The representative time-resolved intracellular calcium responses shown in **Figure 22-C** illustrated AR-C's massive impact on the peak and the area under the curve upon 30 μM UTP stimulation compared with the control. Likewise, the influence on the trace kinetics resembles what was observed in the time-resolved intracellular calcium responses to ATP (**Figure 19-C**).

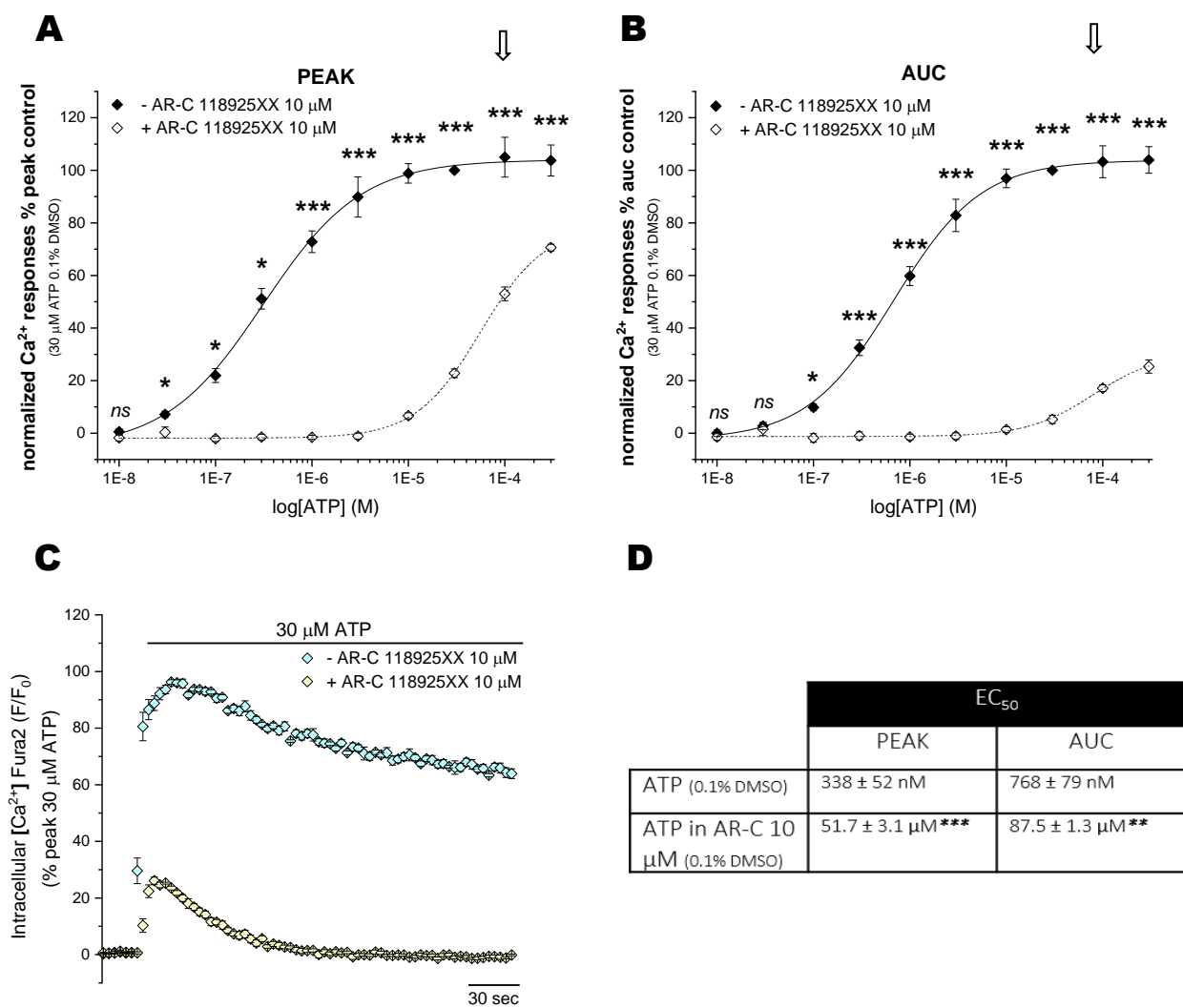


Figure 19. Inhibitory effects of AR-C 118925XX P2Y2 receptor antagonist on the ATP-evoked response in human microvascular endothelial cells (HMEC-1). Concentration-response curves for the peak (A) and AUC (B) magnitude of intracellular Ca^{2+} responses elicited by ATP (0.01-300 μM ; $N=5$) in the presence (0.01-300 μM ; open rhombus; $N=5$) or absence (0.01-300 μM ; closed rhombus; $N=5$) of AR-C 118925XX 10 μM . (C) Averaged time-resolved intracellular Ca^{2+} responses elicited by ATP 30 μM in the presence (light yellow rhombus; $N=5$) or absence (cyan rhombus; $N=5$) of AR-C 10 μM over 250 seconds. All data were normalised to 30 μM ATP and fit the Hill1 equation with the EC_{50} values showed in table (D). Asterisks show statistical significance relative to ATP potency ($p_{ns} > 0.05$, $p^* < 0.05$, $p^{**} < 0.01$, $p^{***} < 0.001$). Data are represented as mean \pm SEM.

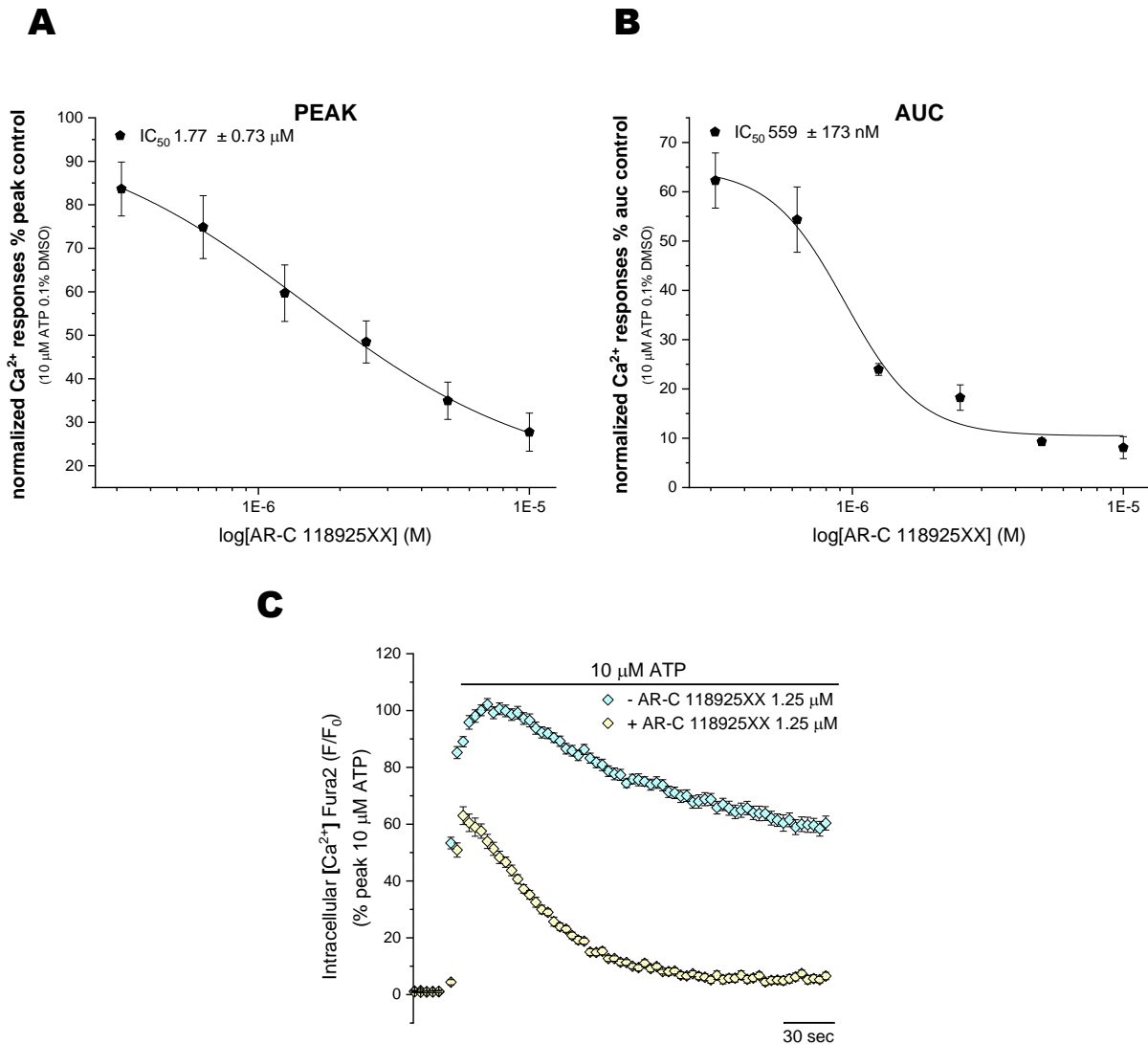


Figure 20. Inhibition concentration-response curves for AR-C 118925XX (P2Y2 receptor antagonist) on the ATP-evoked response in human microvascular endothelial cells (HMEC-1). Inhibition concentration-response curves for the peak (A) and AUC (B) magnitude of intracellular Ca^{2+} responses elicited by 10 μM ATP in the presence (0.312-10 μM ; closed stars; $N=5$) of AR-C. All data points showed statistical significance $p^{**}<0.01$ compared to ATP 10 μM control concentration. (C) Averaged time-resolved intracellular Ca^{2+} responses elicited by ATP 10 μM in the presence (light yellow rhombus; $N=5$) or absence (cyan rhombus; $N=5$) of AR-C 1.25 μM over 250 seconds. All data were normalised to 10 μM ATP and fit the Hill1 equation with the IC_{50} values showed in the graphs. Data are represented as mean \pm SEM.

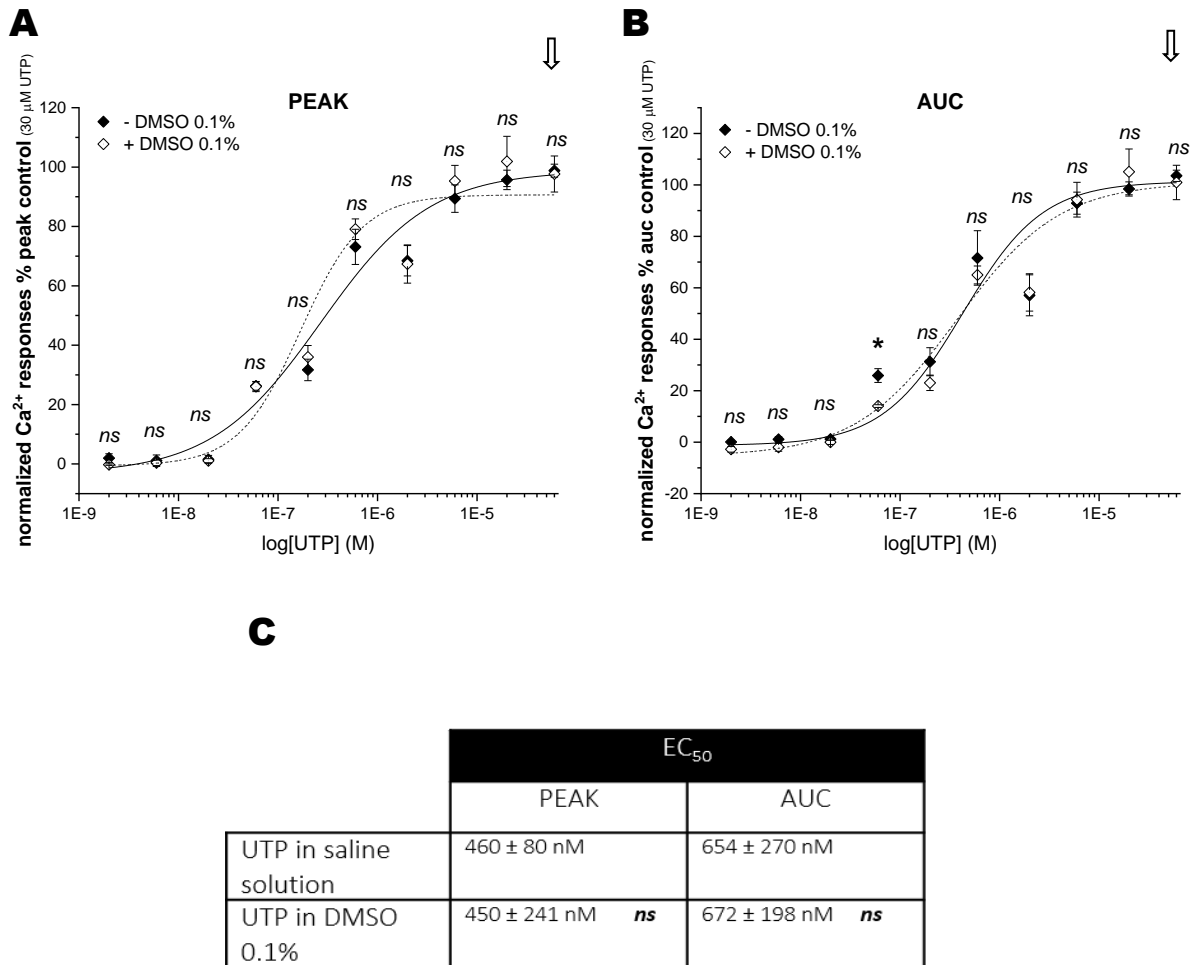


Figure 21. Tolerance of the UTP-evoked response in human microvascular endothelial cells (HMEC-1) to 0.1% dimethyl sulfoxide (DMSO). Concentration-response curves for the peak (A) and AUC (B) magnitude of intracellular Ca^{2+} responses elicited by UTP in the presence (0.002-60 μM ; open rhombus; $N=5$) or absence (0.002-60 μM ; closed rhombus; $N=5$) of 0.1% DMSO. All data were normalised to 30 μM UTP in saline solution and fit the Hill1 equation with the EC_{50} values showed in table (C). Asterisks show statistical significance relative to UTP potency ($p_{ns} > 0.05$, $p^* < 0.05$, $p^{**} < 0.01$, $p^{***} < 0.001$). Data are represented as mean \pm SEM.

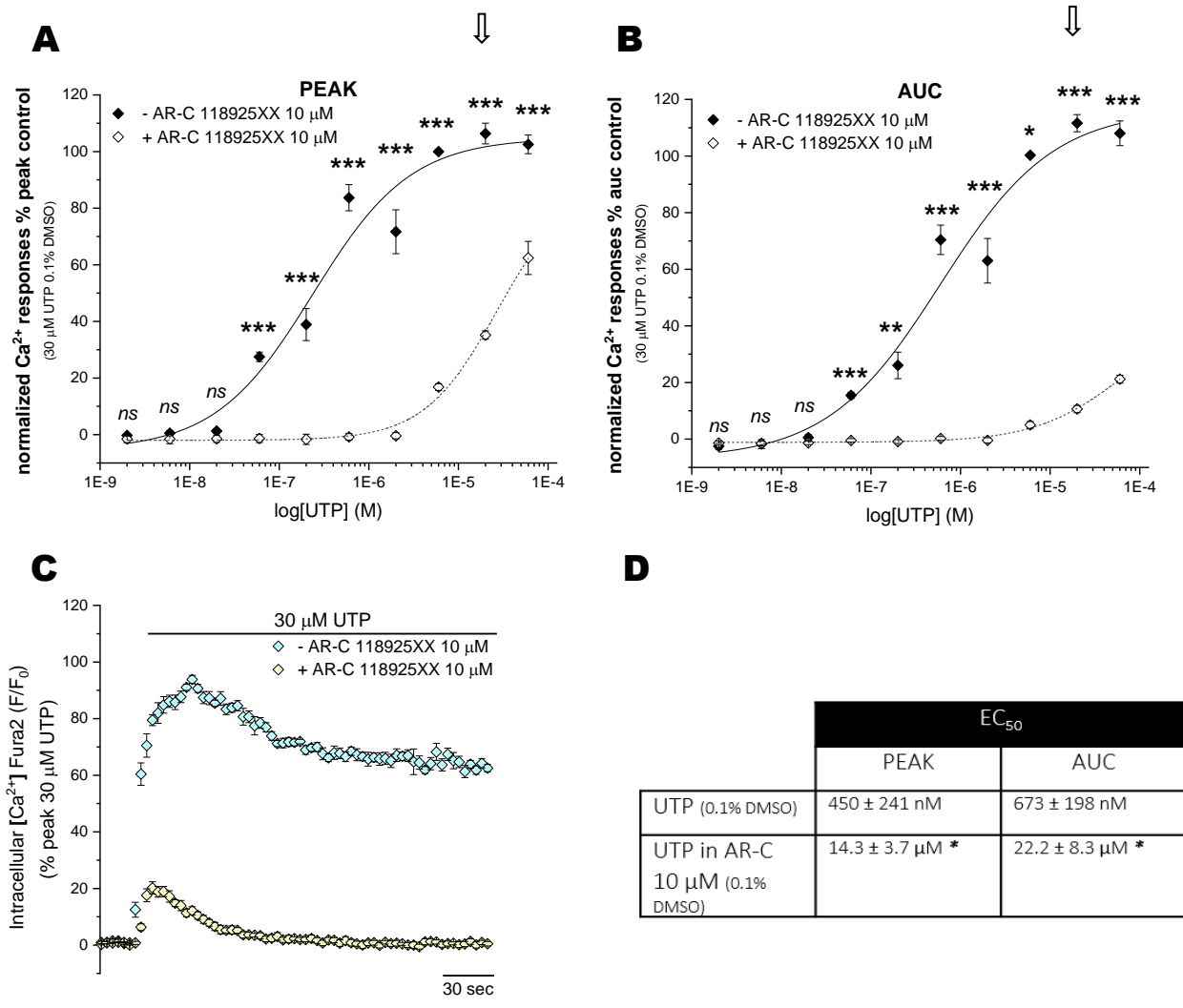


Figure 22. Inhibitory effects of AR-C 118925XX P2Y2 receptor antagonist on the UTP-evoked response in human microvascular endothelial cells (HMEC-1). Concentration-response curves for the peak (A) and AUC (B) magnitude of intracellular Ca²⁺ responses elicited by UTP (0.002-60 μM; N=5) in the presence (0.002-60 μM; open rhombus; N=5) or absence (0.002-60 μM; closed rhombus; N=5) of AR-C 118925XX 10 μM. (C) Averaged time-resolved intracellular Ca²⁺ responses elicited by UTP 30 μM in the presence (yellow light rhombus; N=5) or absence (cyan rhombus; N=5) of AR-C 10 μM over 250 seconds. All data were normalised to 30 μM UTP and fit the Hill1 equation with the EC₅₀ values showed in table (D). Asterisks show statistical significance relative to UTP potency (p *ns* > 0.05, p* < 0.05, p** < 0.01, p*** < 0.001). Data are represented as mean ± SEM.

3.3.2.7 P2Y11 selective antagonist did not affect the ATP-evoked calcium responses of human microvascular endothelial cells (HMEC-1).

P2Y11 is the last P2 receptor candidate for functional expression in HMEC-1 cells, as indicated by the RNA sequencing data (**Figure 1**). Signalling through P2Y11 can be mediated by $G\alpha_q$ or $G\alpha_s$ -type G proteins. $G\alpha_q$ -type G proteins activate the PLC pathway, depleting intracellular calcium stores and inducing a detectable change in cytosolic calcium levels. In contrast, $G\alpha_s$ -type G proteins activate the adenylate cyclase pathway, leading to cAMP production (Communi et al., 1997; Qi et al., 2001). The selective competitive antagonist, NF157, was utilised to determine if P2Y11 was involved in the ATP-evoked calcium responses in HMEC-1 (IC_{50} 463 ± 59 nM; P2Y11 receptors recombinantly expressed in 1321N1 astrocytoma cells) (Ullmann et al., 2005).

The effects of NF157 (5 μ M) on the ATP dose-response curve control (EC_{50}^{PEAK} : 568 ± 161 nM; EC_{50}^{AUC} : 742 ± 161 nM) were examined. Isolated significant effects were found at 0.01 μ M ATP in the AUC curve (**Figure 23-B**) and at 300 and 10 μ M ATP in the peak curve (**Figure 23-A**), when comparing the cells in the presence or the absence of the P2Y11 inhibitor. However, these changes represented potentiation effects, did not follow a trend, and were minimal. In addition, upon treatment, the potencies were unaffected (EC_{50}^{PEAK} : 542 ± 56 nM, *ns*; EC_{50}^{AUC} : 1.05 ± 83 nM, *ns*) (**Figure 23-D, Table 3, 4**). The representative time-resolved intracellular calcium responses in **Figure 23-C** documented the described absence of inhibitory effects. As a result, we concluded that 5 μ M NF157 was ineffective in inhibiting ATP-induced responses in HMEC-1 cells.

3.3.2.8 A2B selective antagonist did not affect the ATP-evoked calcium responses of human microvascular endothelial cells (HMEC-1).

Adenosine, but not ATP, activates four subtypes of G protein-coupled adenosine receptors (A1, A2A, A2B, and A3). However, exogenous ATP can be hydrolysed by a cascade of ectonucleotidases converting ATP to adenosine, which could activate them (Yegutkin, 2014). Just one candidate was present at the RNA sequencing performed in HMEC-1 cells, the A2B receptor. A2B can couple with a $G\alpha_q$ and $G\alpha_s$ -type G protein receptor. Even so, for further implications of A2B later in this study, the lack of effect in the ATP-evoked response was double-checked using the selective antagonist, MRS 1754.

Then, the effects of MRS 1754 (100 nM) on the ATP dose-response curve control (EC_{50}^{PEAK} : 568 ± 161 nM; EC_{50}^{AUC} : 742 ± 161 nM) were examined. MRS 1754 could not inhibit any calcium responses upon ATP application in the peak and the AUC dose-response curves (**Figure 24-A, B**), and both potencies were unaffected (EC_{50}^{PEAK} : 1.30 ± 0.9 μ M, *ns*; EC_{50}^{AUC} : 1.85 ± 1.25 μ M, *ns*) by the presence of the antagonist (**Figure 24- D**). No change was found when comparing the ATP control maximal response at 300 μ M (ATP_{max}^{peak} : 100.27 ± 2.9 %; ATP_{max}^{AUC} : 100.68 ± 3 %) in the presence of the antagonist for the peak (106.1 ± 4 %; *ns*) and the AUC (106.4 ± 3.1 %; *ns*) (**Figure 24-A, B, Table 3, 4**). The representative time-resolved intracellular calcium responses in **Figure 24-C** confirmed the described absence of inhibitory effects. As a result, we confirmed that 100 nM MRS 1754 was ineffective in inhibiting ATP-induced responses in HMEC-1 cells.

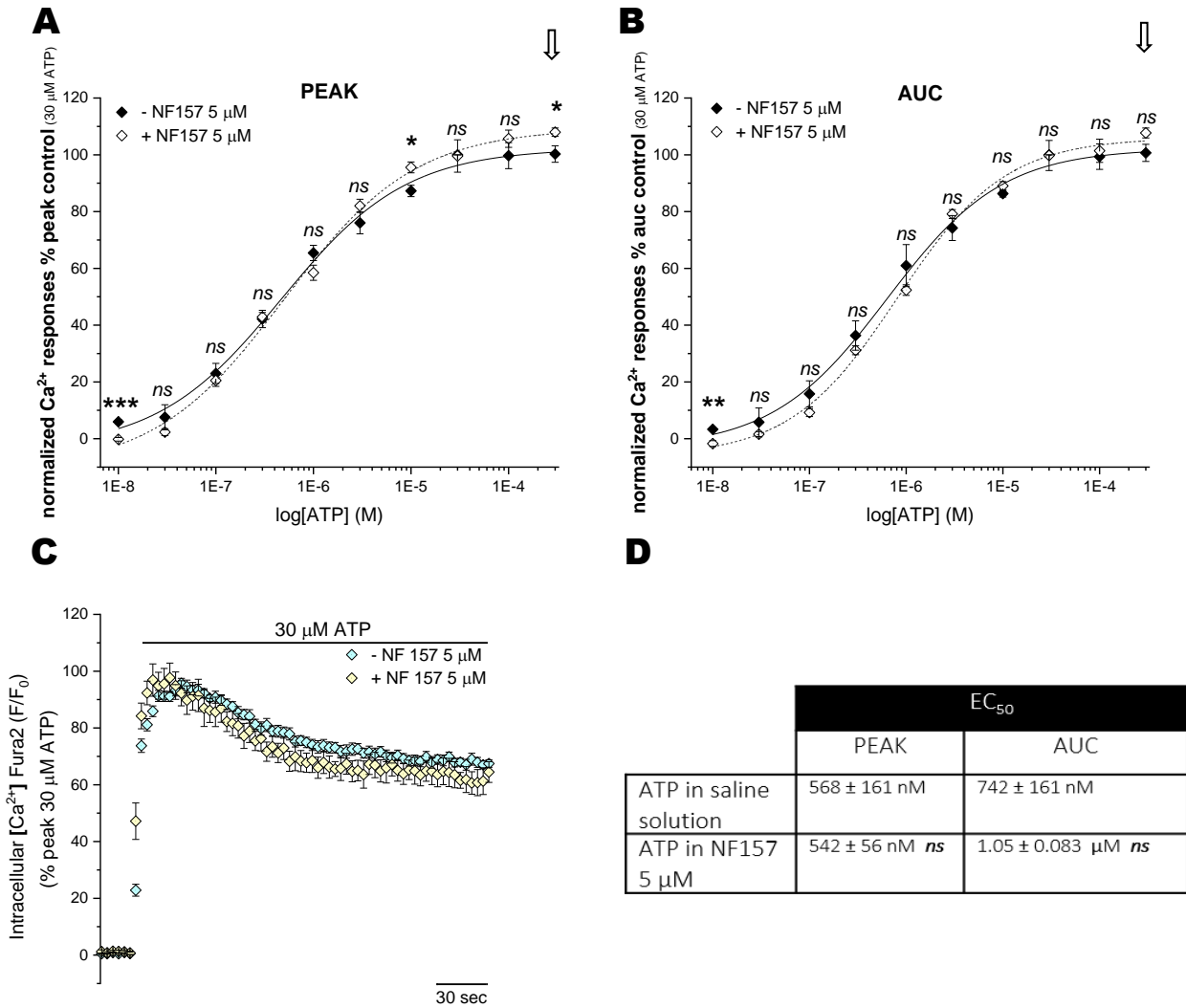


Figure 23. Lack of inhibitory effects of NF157 P2Y11 receptor antagonist on the ATP-evoked response in human microvascular endothelial cells (HMEC-1). Concentration-response curves for the peak (**A**) and AUC (**B**) magnitude of intracellular Ca^{2+} responses elicited by ATP (0.01-300 μM ; $N=5$) in the presence (0.01-300 μM ; open rhombus; $N=5$) or absence (0.01-300 μM ; closed rhombus; $N=5$) of NF157 5 μM . (**C**) Averaged time-resolved intracellular Ca^{2+} responses elicited by ATP 30 μM in the presence (light yellow rhombus; $N=5$) or absence (cyan rhombus; $N=5$) of NF157 5 μM over 250 seconds. All data were normalised to 30 μM ATP and fit the Hill1 equation with the EC₅₀ values showed in table (**D**). Asterisks show statistical significance relative to ATP potency (p *ns* > 0.05, p^* < 0.05, p^{**} < 0.01, p^{***} < 0.001). Data are represented as mean \pm SEM.

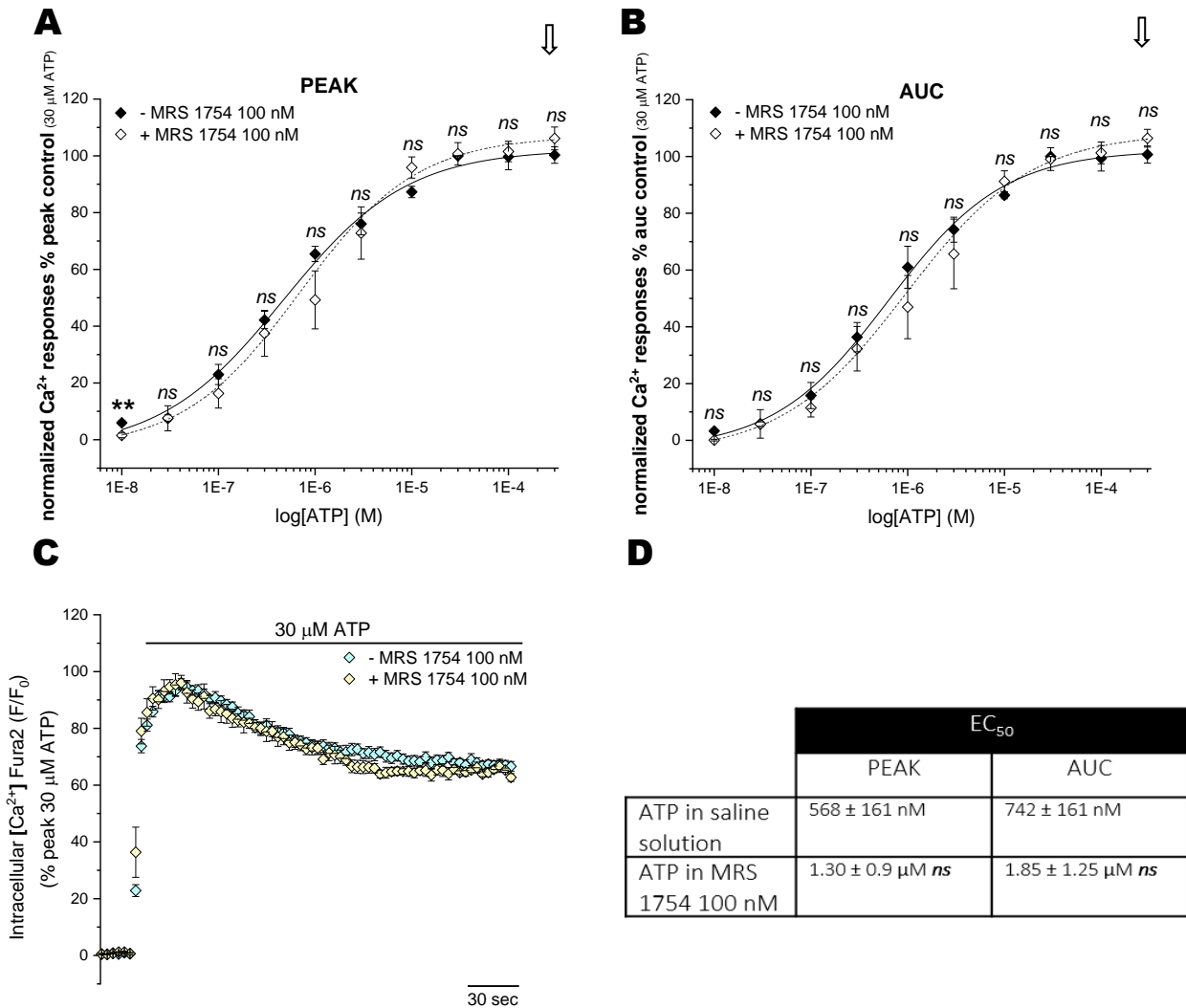


Figure 24. Inhibitory effects of MRS 1754 A2B receptor antagonist on the ATP-evoked response in human microvascular endothelial cells (HMEC-1). Concentration-response curves for the peak (A) and AUC (B) magnitude of intracellular Ca^{2+} responses elicited by ATP (0.01-300 μM ; $N=5$) in the presence (0.01-300 μM ; open rhombus; $N=5$) or absence (0.01-300 μM ; closed rhombus; $N=5$) of MRS 1754 100 nM. (C) Averaged time-resolved intracellular Ca^{2+} responses elicited by ATP 30 μM in the presence (light yellow rhombus; $N=5$) or absence (cyan rhombus; $N=5$) of MRS 1754 100 nM over 250 seconds. All data were normalised to 30 μM ATP and fit the Hill1 equation with the EC_{50} values showed in table (D). Asterisks show statistical significance relative to ATP potency (p ns > 0.05, $p^* < 0.05$, $p^{**} < 0.01$, $p^{***} < 0.001$). Data are represented as mean \pm SEM.

3.3.3. Characterisation of the vascular endothelial growth factor calcium signalling in human microvascular endothelial cells (HMEC-1).

As pointed out in **section 3.3.1**, the three vascular endothelial growth factor receptors (VEGFR-1, 2, and 3) were expressed in HMEC-1 cells. VEGFR-1 and 2 are the principal members of the family involved in endothelial function. VEGFR-1 and VEGFR-2 are closely related receptor tyrosine kinases (RTKs) that share common and distinct ligands. VEGFR-1 is considered a kinase-impaired RTK, with its kinase activity inhibited by a single amino acid substitution in its kinase domain and carboxyl terminus. In contrast, VEGFR-2 is a highly active kinase that triggers various signalling pathways, including intracellular calcium release in endothelial cells (Rahimi, 2006).

Both receptors bind to the vascular endothelial growth factor A (VEGF-A). VEGF-A serves as a fundamental inducer of endothelial cell activities, notably in controlling vascular permeability and promoting angiogenesis (Li et al., 2011). VEGFR-1 binds VEGF-A with a much higher affinity than VEGFR2 (de Vries et al., 1992), but VEGFR-2 is the only one capable of eliciting a calcium response VEGF-A-dependent (Cudmore et al., 2012). The VEGFR-1's ability to modulate this biological response is limited to its capacity to heterodimerize with VEGFR-2 (Cudmore et al., 2012; Rahimi, 2006). The VEGF-A-induced calcium increase through VEGFR-2 occurs due to calcium release from intracellular stores and the simultaneous entry of calcium through various channels, collectively maintaining the elevated cytosolic calcium levels (Li et al., 2011).

3.3.3.1 VEGF₁₆₅-evoked calcium responses of human microvascular endothelial cells (HMEC-1)

In humans, various alternatively spliced isoforms of the VEGF-A are expressed, including those consisting of 121, 145, 165, 183, 189, and 206 amino acids (aa) in length. Among these isoforms, VEGF₁₆₅ (165 aa) is considered the most abundant and potent (Robinson et al., 2001), thereby, the one used to characterize the VEGFR-2 evoked response in this cell line.

VEGF₁₆₅ elicited intracellular calcium response in a concentration-dependent manner (0.3 to 100 ng/mL) with maximal activity at 30 ng/mL for the peak (111.6 ± 4.3 %) and at 100 ng/mL for the area under the curve (AUC) (100 %). The peak's calculated half-maximal effective concentration (EC₅₀) was 2.85 ± 1 ng/mL and the AUC EC₅₀ was 3.5 ± 1.3 ng/mL (**Figure 25**). **Figure 25-C** depicts time-resolved calcium responses upon VEGF₁₆₅ stimulation from 0.3 to 100 ng/mL. This stimulation did not elicit a rapid or transient response but is characterised by a delayed, slower, and more sustained calcium release over four minutes. Calcium levels continue to rise over time and reach their highest point as the response progresses, and, therefore, the peak response is observed towards the end of the response period in almost all concentrations applied. In general, rapid increases in intracellular calcium correlate to Ca²⁺ release from intracellular stores, whereas slower increases in intracellular calcium result from calcium influx from the extracellular space. The trace kinetics shown in **Figure 25-C** could then indicate some ion channel-mediated calcium entry contribution from the extracellular milieu.

In the absence of extracellular calcium, the VEGF₁₆₅ control maximal responses elicited were significantly decreased at 30 ng/mL by 48.5 ± 4.3 % ($p < 0.001$) for the peak and at 100 ng/mL

41.6 ± 56.2 % ($p < 0.05$) for the AUC. Despite an increased tendency in the half-maximal effective concentrations, the absence of extracellular Ca^{2+} did not significantly alter VEGF₁₆₅ potency ($\text{EC}_{50}^{\text{PEAK}}$: 6.44 ± 2.9 ng/mL, *ns*; $\text{EC}_{50}^{\text{AUC}}$: 10 ± 3.2, *ns*) (**Figure 26-E**). The impact of the absence of extracellular calcium in the VEGF₁₆₅ response is major, as illustrated in the time-resolved calcium responses shown in **Figure 26-C, D**. At 3 ng/mL, VEGF₁₆₅ lost its ability to elicit calcium response, and at 10 ng/mL, the response was reduced from 80% to approximately 20% above baseline. This significant effect on the calcium responses indicated at least some ion channel-mediated calcium entry contribution from the extracellular milieu. On the other hand, the residual calcium responses indicated some contribution dependent on calcium release from intracellular stores.

A double-check was performed to ensure the lack of VEGFR-1 calcium response using its selective ligand, VEGF-B. Two isoforms of mature VEGF-B containing 167 or 186 amino acid (aa) residues exist, VEGF₁₆₇ and VEGF₁₈₆. Both VEGF-B isoforms bind VEGFR-1 but not VEGFR-2 (Olofsson et al., 1998), so if any calcium responses were observed, we could attribute some of the VEGF₁₆₅ calcium responses to this receptor activity.

VEGF₁₆₇ did not evoke intracellular calcium responses when HMEC-1 cells were exposed to a range of ligand concentrations (1 to 100 ng/mL) (**Figure 27**). Recorded intracellular calcium at 100 ng/mL VEGF₁₆₇ responses were not significantly different from the vehicle control injection-derived recording, inferring the inability of this factor to cause any event in this cell line (**Figure 27-B**). In **Figure 27-C**, time-resolved intracellular Ca^{2+} responses representative traces clearly illustrated the lack of this response compared to the VEGF₁₆₅ evoked response in the same vehicle control.

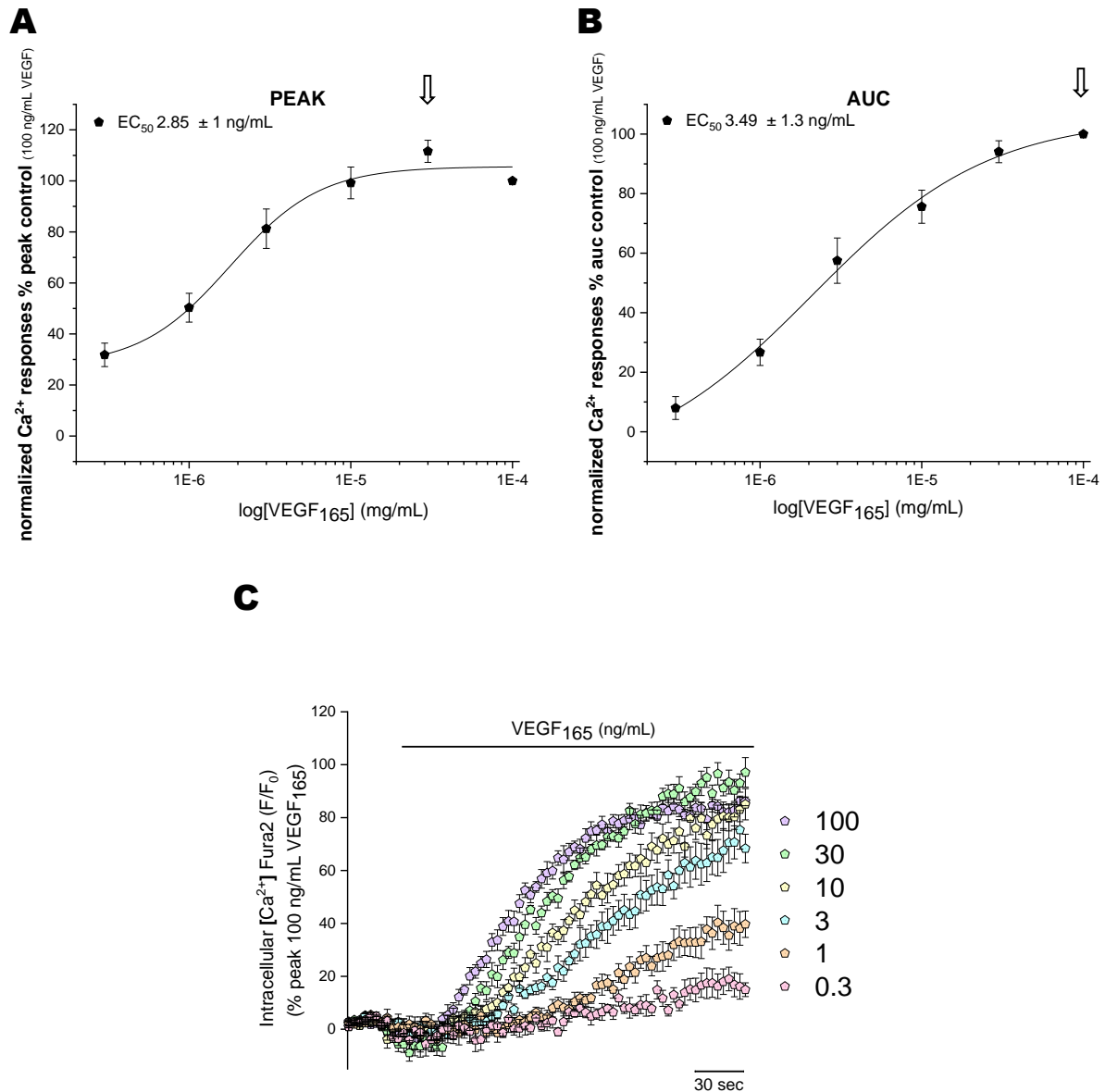
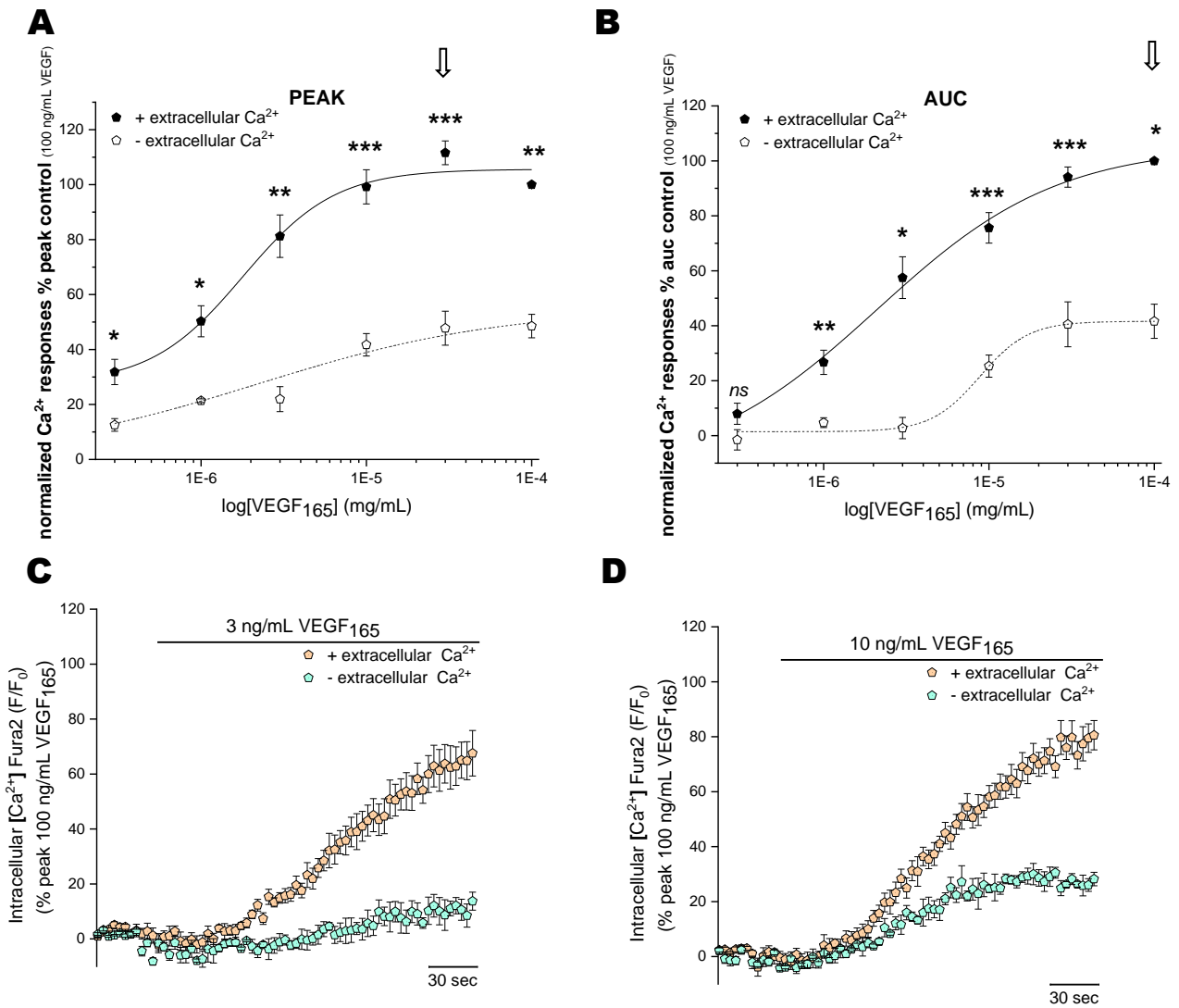


Figure 25. VEGF₁₆₅ elicits intracellular calcium responses in human microvascular endothelial cells (HMEC-1). Concentration-response curves for the peak (A) and AUC (B) magnitude of intracellular Ca²⁺ responses elicited by VEGF₁₆₅ (0.3-100 ng/mL; N=8). (C) Averaged time-resolved intracellular Ca²⁺ responses elicited by VEGF₁₆₅ from 0.3 ng/mL to 100 ng/mL in HMEC-1 cells over 250 seconds (N=8). All data were normalised to 100 ng/mL VEGF₁₆₅ and fit the Hill1 equation with the EC₅₀ values showed in the graphs. Data are represented as mean ± SEM.

(*) Data normalisation was always done at 100 ng/mL VEGF₁₆₅ when this agonist was studied.

(**) Arrows (⇓) indicate the maximum response in the control (untreated) curve.

(***) F/F₀ refers to the Fura2 ratio, meaning F340/F380.



E

| | | PEAK | AUC |
|------------------|--|----------------------------|--------------------|
| EC ₅₀ | VEGF ₁₆₅ in Ca^{2+} | 2.85 ± 1 ng/mL | 3.49 ± 1.3 ng/mL |
| | VEGF ₁₆₅ in 0Ca^{2+} | 6.44 ± 2.9 ng/mL <i>ns</i> | 10 ± 3.2 <i>ns</i> |
| Maximal response | VEGF ₁₆₅ in Ca^{2+} | 111.6 ± 4.3 % | 100 % |
| | VEGF ₁₆₅ in 0Ca^{2+} | 48.5 ± 4.3 % *** | 41.6 ± 6.2 %* |

Figure 26. Extracellular calcium removal impacted the VEGF₁₆₅-evoked response in human microvascular endothelial cells (HMEC-1). Concentration-response curves for the peak (A) and AUC (B) magnitude of intracellular Ca^{2+} responses elicited by VEGF₁₆₅ in the presence (0.3-100 ng/mL; closed pentagon; $N=8$) or absence (0.3-100 ng/mL; open pentagon; $N=3$) of extracellular calcium. (C) Averaged time-resolved intracellular Ca^{2+} responses elicited by VEGF₁₆₅ 3 ng/mL (C) or 10 ng/mL (D) in the presence (orange pentagon; $N=8$) or absence (cyan pentagon; $N=3$) of extracellular calcium over 250 seconds. All data were normalised to 100 ng/mL VEGF₁₆₅ and fit the Hill1 equation with the EC₅₀ and maximal response values showed in table (E). Asterisks show statistical significance relative to VEGF₁₆₅ potency and VEGF₁₆₅ % of maximal response ($p_{ns} > 0.05$, $p^* < 0.05$, $p^{**} < 0.01$, $p^{***} < 0.001$). Data are represented as mean ± SEM.

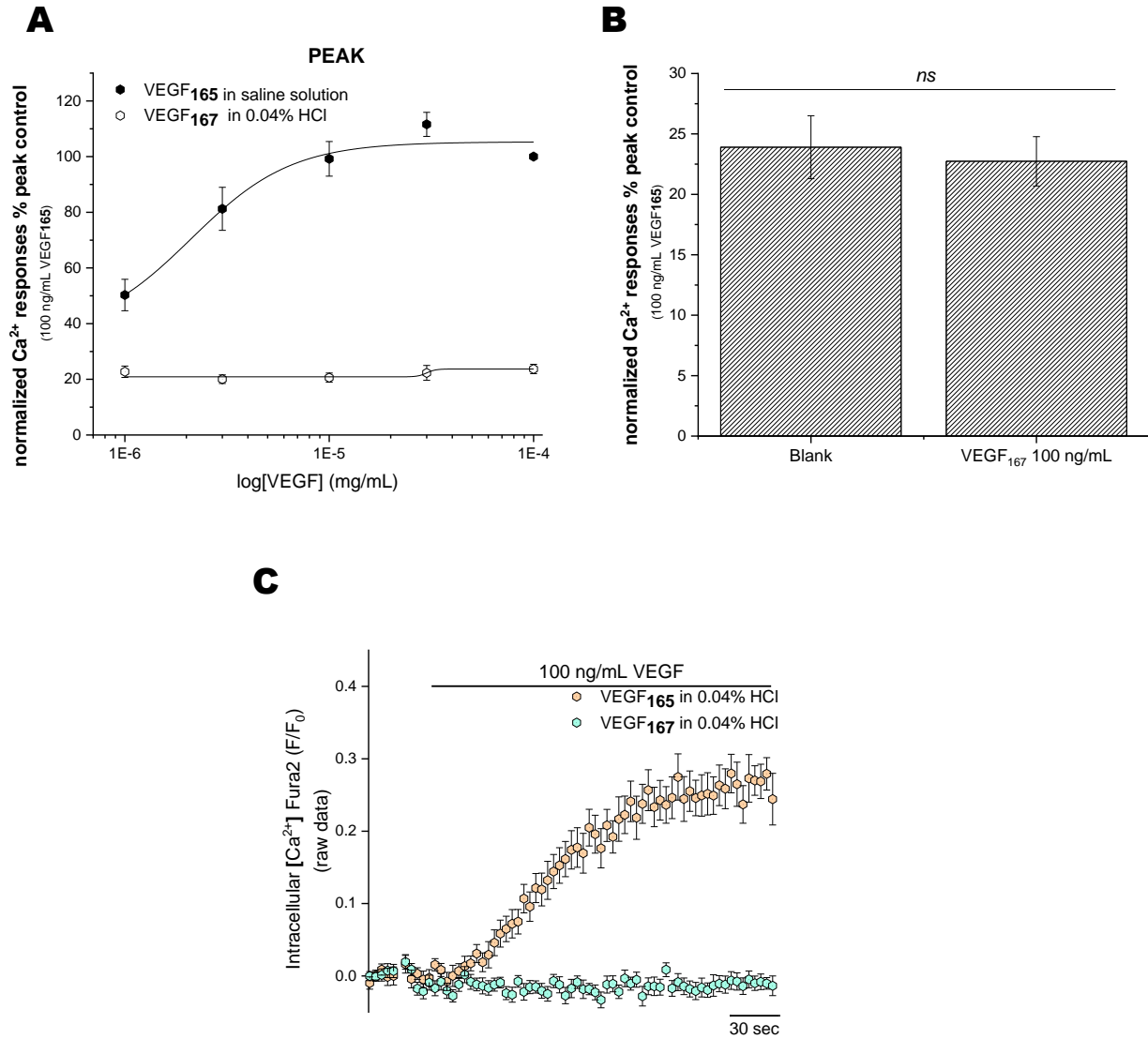


Figure 27. VEGF₁₆₇ did not elicit intracellular calcium response in human microvascular endothelial cells (HMEC-1). Concentration-response curve for the peak (**A**) magnitude of intracellular Ca²⁺ responses elicited by VEGF₁₆₇ (1-100 ng/mL in 0.04% HCl; *N*=5) and VEGF₁₆₅ (1-100 ng/mL in saline solution; *N*=8). (**B**) Comparison of peak magnitude of intracellular Ca²⁺ responses induced by the injection of vehicle control (*blank*) or 100 ng/mL VEGF₁₆₇ (*N*=5) in saline solution containing 0.04% of HCl. (**C**) Averaged time-resolved intracellular Ca²⁺ responses elicited by VEGF₁₆₅ (orange pentagon) and VEGF₁₆₇ (cyan pentagon) from 0.3 ng/mL to 100 ng/mL over 250 seconds (*N*=5). All data were normalised to 100 ng/mL VEGF₁₆₅ in 0.04% HCl where indicated and fit the Hill1 equation. Data are represented as mean ± SEM.

3.3.3.2 VEGF₁₆₅-evoked calcium responses are mediated by phospholipase C (PLC) activation in human microvascular endothelial cells (HMEC-1)

As cited above, one of the pathways in the VEGFR-A-evoked calcium responses through VEGFR-2 occurs due to calcium release from intracellular stores. Therefore, the phospholipase C route should be implicated.

The PLC pathway inhibitor U73122 was applied to check the impact on the intracellular calcium concentration elicited by the VEGF₁₆₅. The VEGF₁₆₅ responses were entirely abolished in the presence of 5 μ M of the PLC inhibitor compared with the concentration-response curve in the absence of U73122 (**Figure 28**), suggesting a dependency on intracellular stores of calcium release in the VEGF₁₆₅-evoked responses. As in the case of the ATP dose response in the presence of U73122, statistical significance is not shown as the experiments were not performed in the same conditions due to a different percentage of DMSO in the vehicle control.

As in the case of the ATP dose-response, thapsigargin was also used to investigate further the possible role of VEGF₁₆₅ store-operated calcium responses. Stores depletion with 1 μ M thapsigargin caused an unexpected disruption in the VEGF₁₆₅ dose-dependent curve (**Figure 29-A**). Not just for the significant increase caused by the two lower concentrations (**Figure 29-A, B**) but the random nature of the responses in the presence of the drug within the same biological repeat (**Figure 29-C, D**), thapsigargin was then considered a useless tool to characterise this response further.

As previously described in **section 3.3.2.2.**, to ensure consistency in experimental conditions, all drugs solved in DMSO in this section will always be compared to their respective solvent-controlled VEGF₁₆₅ 0.1 % DMSO dose-response curve (**Figure 30-A, B**) and derived calculated parameters (potency and efficacy) (**Figure 30-C**).

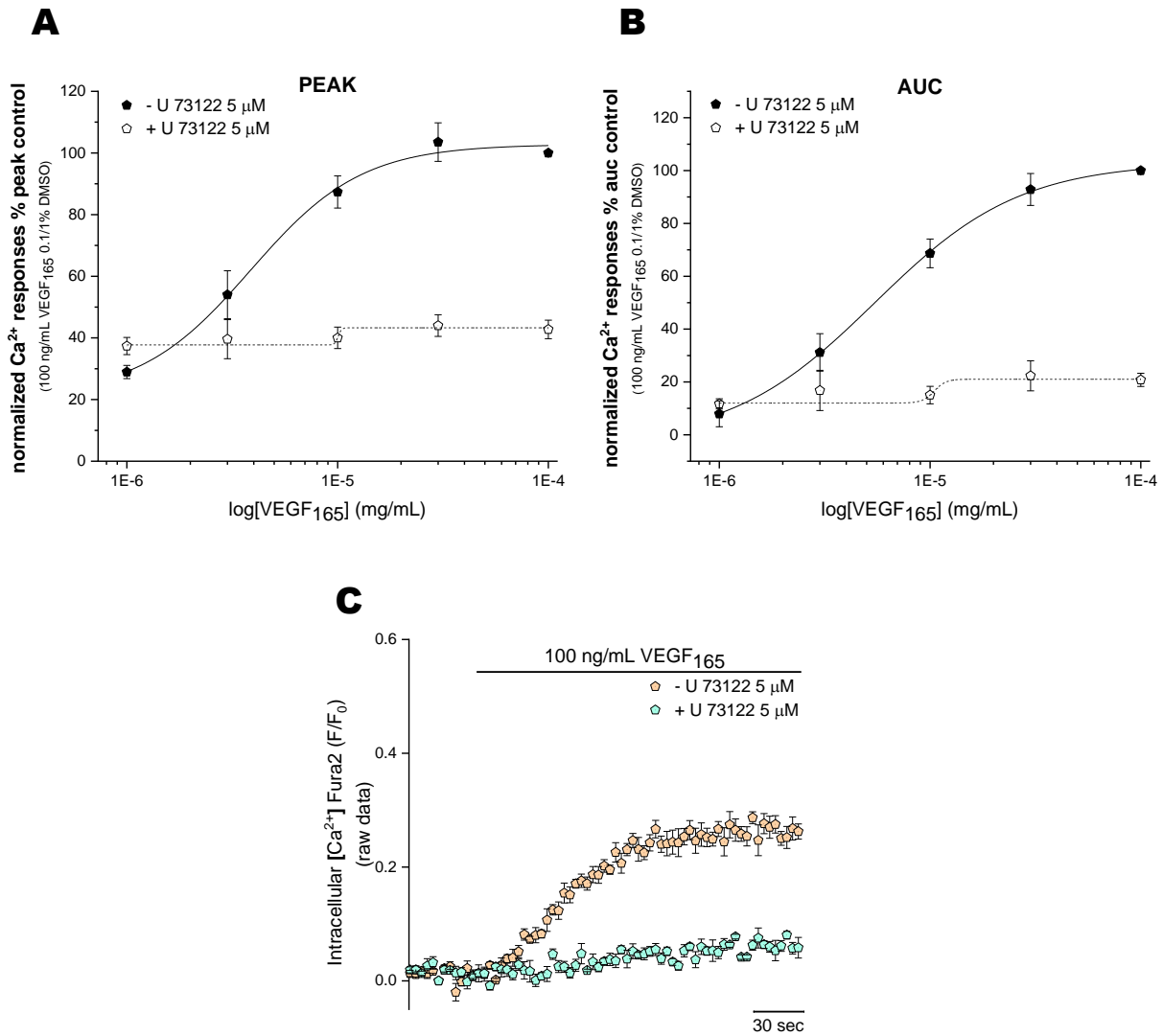


Figure 28. Effects of the phospholipase C (PLC) inhibitor U73122 on the VEGF₁₆₅-evoked response in human microvascular endothelial cells (HMEC-1). Concentration-response curves for the peak (A) and AUC (B) magnitude of intracellular Ca^{2+} responses elicited by VEGF₁₆₅ in the presence (0.3-100 ng/mL; open pentagon; $N=5$) or absence (0.3-100 ng/mL; closed pentagon; $N=5$) of U 73122 5 μM . (C) Averaged time-resolved intracellular Ca^{2+} responses elicited by VEGF₁₆₅ 10 ng/mL in the presence (cyan pentagon; $N=5$) or absence (orange pentagon; $N=5$) of U 73122 5 μM over 250 seconds. All data were normalised to 100 ng/mL VEGF₁₆₅ and fit the Hill1 equation. Data are represented as mean \pm SEM.

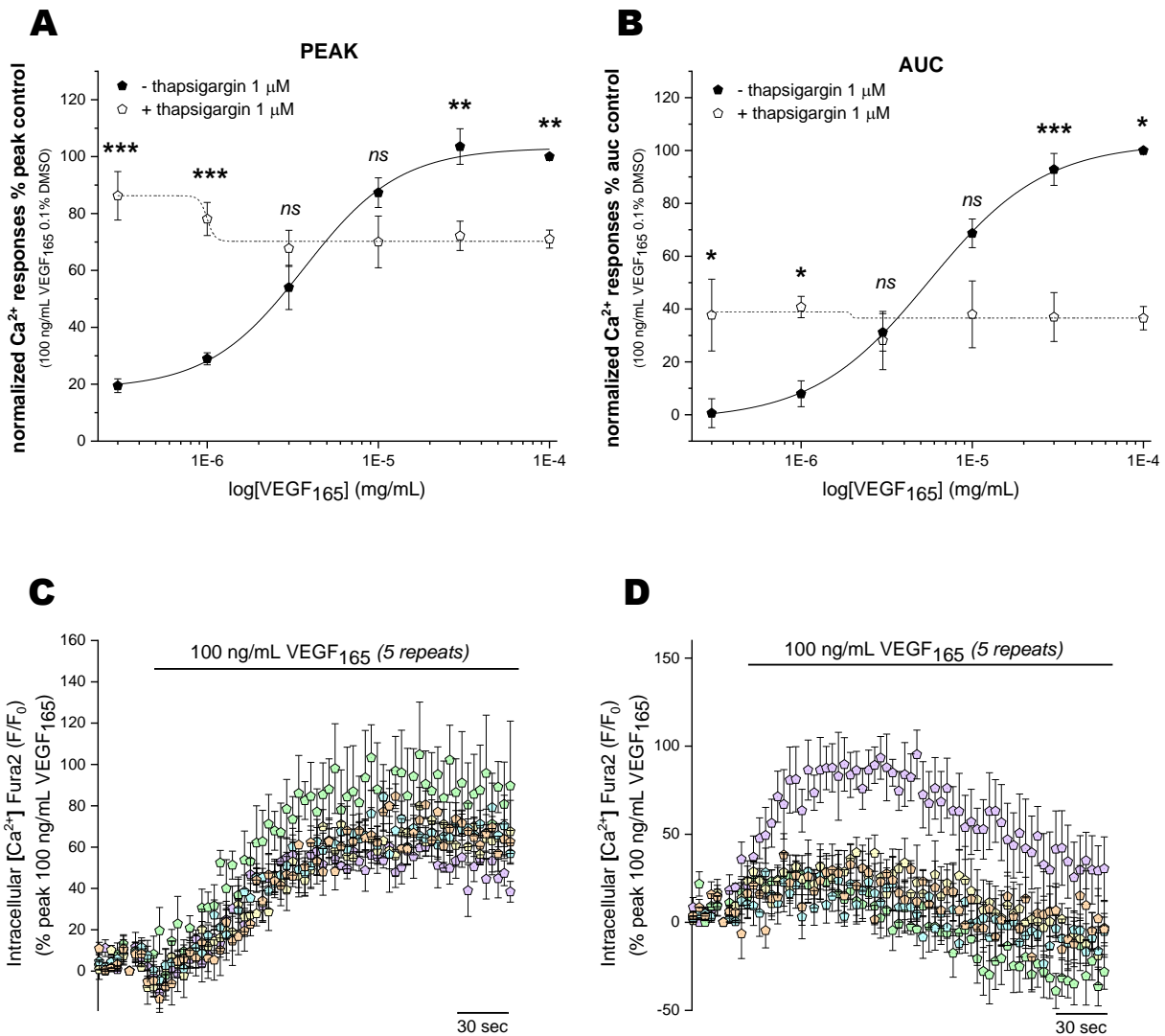
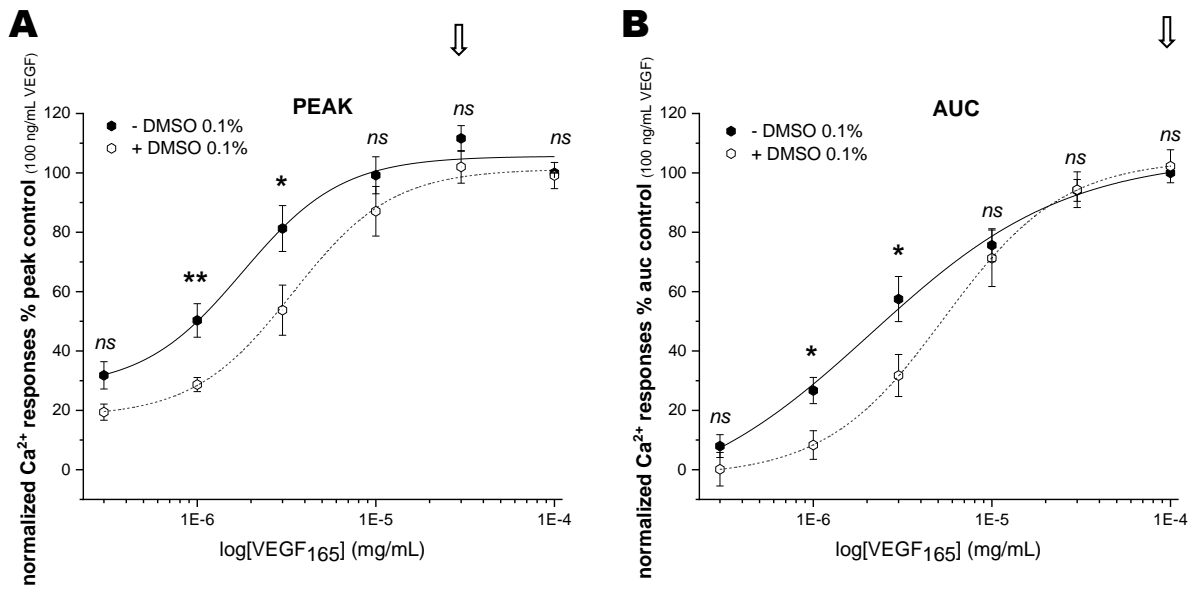


Figure 29. Effects of the sarcoendoplasmic reticulum calcium transport ATPase (SERCA) inhibitor, thapsigargin, on the VEGF₁₆₅-evoked response in human microvascular endothelial cells (HMEC-1). Concentration-response curves for the peak (A) and AUC (B) magnitude of intracellular Ca²⁺ responses elicited by VEGF₁₆₅ in the presence (0.3-100 ng/mL; open pentagon; N=5) or absence (0.3-100 ng/mL; closed pentagon; N=5) of thapsigargin 1 μM. (C, D) Representative time-resolved intracellular Ca²⁺ responses elicited by VEGF₁₆₅ 100 ng/mL of the five repeats of the same biological repeat in the presence (N=1) of thapsigargin 1 μM over 250 seconds. All data were normalised to 100 ng/mL VEGF₁₆₅ in 0.1% DMSO and fit the Hill1 equation. Asterisks show statistical significance relative to VEGF₁₆₅ potency (p *ns* > 0.05, p* < 0.05, p** < 0.01, p*** < 0.001). Data are represented as mean ± SEM.



C

| | EC ₅₀ | |
|--|-----------------------------|-----------------------------|
| | PEAK | AUC |
| VEGF ₁₆₅ in saline solution | 2.85 ± 1 ng/mL | 3.49 ± 1.3 ng/mL |
| VEGF ₁₆₅ in DMSO 0.1% | 4.20 ± 0.99 ng/mL <i>ns</i> | 6.16 ± 1.16 ng/mL <i>ns</i> |

Figure 30. Tolerance of the VEGF₁₆₅-evoked response in human microvascular endothelial cells (HMEC-1) to 0.1% dimethyl sulfoxide (DMSO). Concentration-response curves for the peak (A) and AUC (B) magnitude of intracellular Ca²⁺ responses elicited by VEGF₁₆₅ in the presence (0.3-100 ng/mL; open pentagon; *N*=5) or absence (0.3-100 ng/mL; closed pentagon; *N*=8) of 0.1% DMSO. All data were normalised to 100 ng/mL VEGF₁₆₅ in saline solution and fit the Hill1 equation with the EC₅₀ values showed in table (C). Asterisks show statistical significance relative to VEGF₁₆₅ potency (*p ns* > 0.05, *p** < 0.05, *p*** < 0.01, *p**** < 0.001). Data are represented as mean ± SEM.

3.3.3.3 The broad-spectrum P2 antagonists affected the VEGF₁₆₅-evoked calcium responses of human microvascular endothelial cells (HMEC-1).

Apyrase and PPADS were used to investigate the P2 receptors' involvement in the VEGF₁₆₅-evoked calcium responses in HMEC-1.

The effects of apyrase (10 U/mL) on the VEGF₁₆₅ dose-response curve control (EC_{50}^{PEAK} : 2.85 ± 1 ng/mL; EC_{50}^{AUC} : 3.49 ± 1.3 ng/mL) were examined to study the hypothetical purinergic regulation of the VEGF₁₆₅-dependent calcium responses. Pre-treatment with apyrase slightly right shifted the VEGF₁₆₅ dose-response curve without a significant impact on the VEGF₁₆₅ potency for the peak (6.17 ± 2.7 ng/mL; *ns*) and the area under the curve (4.19 ± 2.5 ng/mL; *ns*) (**Figure 31-D, Table 5**). On the contrary, the presence of the enzyme significantly affected the control VEGF₁₆₅ maximal response ($VEGF_{165 \text{ max}}^{peak}$: 111.59 ± 4.32 %; $VEGF_{165 \text{ max}}^{AUC}$: 100%) at 30 ng/mL for the peak (76.69 ± 8.28 %; $p < 0.01$) and at 100 ng/mL the AUC (50.1 ± 5.66 %; $p < 0.01$). (**Figure 31-A, B**). Therefore, the level of efficacy was diminished in the presence of apyrase (**Table 5**). The representative time-resolved intracellular calcium responses shown in **Figure 31-C** illustrated apyrase's significant impact on the peak and the area under the curve upon 10 ng/mL VEGF₁₆₅ stimulation compared with the control. In the presence of apyrase, the VEGF₁₆₅ conserved its slow and delayed calcium increase kinetics. However, it depicted a significant decrease in the late peak, which reached approximately 40% above baseline compared to the VEGF response in the absence of the enzyme, which reached almost 90% of the control response.

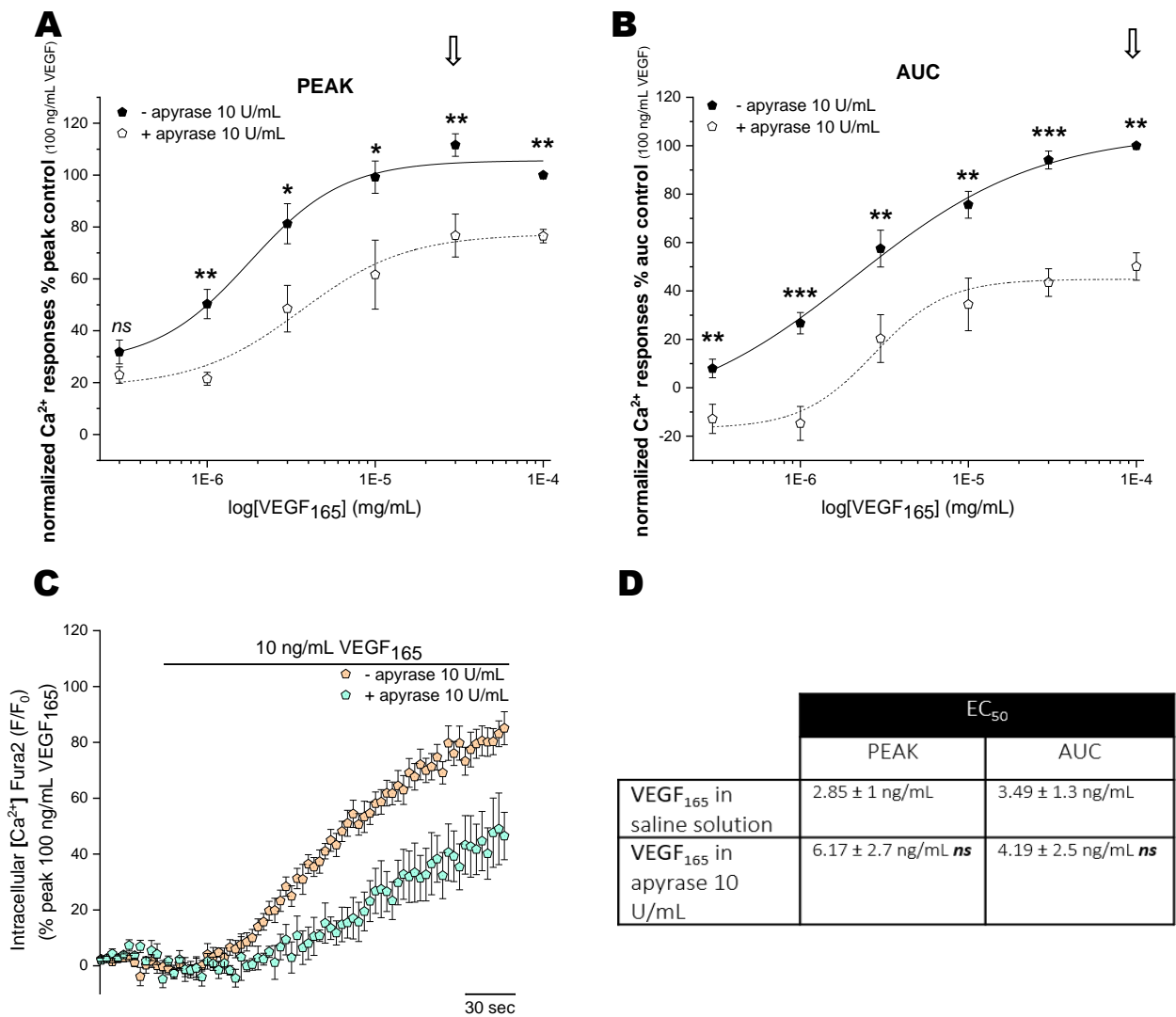


Figure 31. Inhibitory effects of apyrase on the VEGF₁₆₅ -evoked response in human microvascular endothelial cells (HMEC-1). Concentration-response curves for the peak (**A**) and AUC (**B**) magnitude of intracellular Ca²⁺ responses elicited by VEGF₁₆₅ in the presence (0.3-100 ng/mL; open pentagon; N=5) or absence (0.3-100 ng/mL; closed pentagon; N=8) of apyrase 10 U/mL. (**C**) Averaged time-resolved intracellular Ca²⁺ responses elicited by VEGF₁₆₅ 10 ng/mL in the presence (cyan pentagon; N=5) or absence (orange pentagon; N=8) of apyrase 10 U/mL over 250 seconds. All data were normalised to 100 ng/mL VEGF₁₆₅ in saline solution and fit the Hill1 equation with the EC₅₀ values showed in table (**D**). Asterisks show statistical significance relative to VEGF₁₆₅ potency (p *ns* > 0.05, p* < 0.05, p** < 0.01, p*** < 0.001). Data are represented as mean ± SEM.

Pre-treatment with PPADS also right-shifted the VEGF₁₆₅ dose-response curve (EC_{50}^{PEAK} : 2.85 ± 1 ng/mL; EC_{50}^{AUC} : 3.49 ± 1.3 ng/mL) but more consistently than apyrase, significantly influencing the VEGF₁₆₅ potency for the peak (17.6 ± 4.8 ng/mL, $p < 0.01$) or the area under the curve (363 ± 312 ng/mL, $p < 0.01$) (**Figure 32-D, Table 5**). In addition, the presence of PPADS significantly reduced the VEGF₁₆₅ control maximal response ($VEGF_{165 \text{ max}}^{peak}$: 111.59 ± 4.32 %; $VEGF_{165 \text{ max}}^{AUC}$: 100%) at 30 ng/mL for the peak (73.80 ± 4.37 %; $p < 0.001$) and at 100 ng/mL for the AUC 76.73 ± 5.93 %; $p < 0.01$). In this case, the peak maximal response in the presence of the antagonist was shifted and achieved at 100 ng/mL (**Figure 32-A, Table 5**). When comparing this new maximal response with the maximal response control at 30 ng/mL VEGF₁₆₅ in the absence of the PPADS, the efficacy was significantly reduced (87.21 ± 6.65 %; $p < 0.01$), and it never managed to achieve the same level of efficacy as the control, as in the case of the AUC (**Table 5**). The representative time-resolved intracellular calcium responses shown in **Figure 32-C** illustrated PPADS' significant impact on the peak and the area under the curve upon 10 ng/mL VEGF₁₆₅ stimulation compared with the control. In the presence of PPADS, the activation kinetics at 10 ng/mL VEGF₁₆₅ conserved its slow and delayed calcium increase kinetics, as in the case of the apyrase, but with a much bigger significant decrease in the late peak, which reached approximately 20% above baseline compared to the VEGF response in the absence of the antagonist, which reached almost 90%.

To further characterise PPADS effects on the VEGF₁₆₅-evoked responses, HMEC-1 cells were incubated for 30 minutes in a range of antagonist concentrations (0.01 to 300 μ M) and stimulated with 30 ng/mL VEGF₁₆₅, and thereby, IC_{50} was calculated. The half-maximal inhibitory concentration values obtained were 67.6 ± 18.9 μ M for the peak and 57.7 ± 22.9 μ M for the AUC inhibition curves (**Figure 33-A, B**).

Hence, we concluded that both molecules had a significant impact on the VEGF₁₆₅ dose-dependent curve, and these effects should be further explored by utilising selective antagonists of the P2 purinergic receptors proposed candidates in HMEC-1, as previously systematically performed in the ATP response curve.

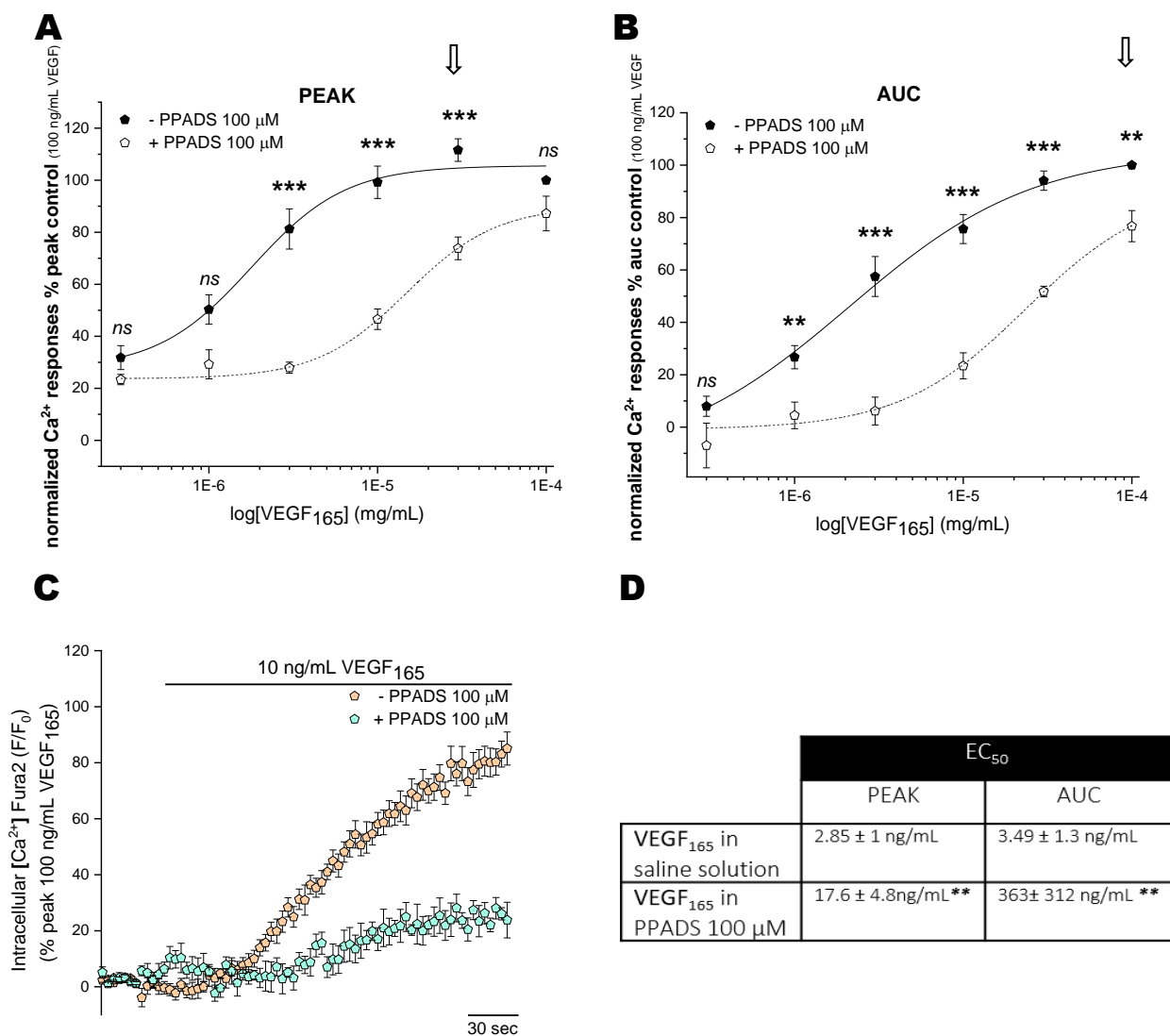


Figure 32. Inhibitory effects of broad-spectrum P2 receptors antagonist PPADS on the VEGF₁₆₅-evoked response in human microvascular endothelial cells (HMEC-1). Concentration-response curves for the peak (A) and AUC (B) magnitude of intracellular Ca²⁺ responses elicited by VEGF₁₆₅ in the presence (0.3-100 ng/mL; open pentagon; N=5) or absence (0.3-100 ng/mL; closed pentagon; N=8) of PPADS 100 μM. (C) Averaged time-resolved intracellular Ca²⁺ responses elicited by VEGF₁₆₅ 10 ng/mL in the presence (cyan pentagon; N=5) or absence (orange pentagon; N=8) of PPADS 100 μM over 250 seconds. All data were normalised to 100 ng/mL VEGF₁₆₅ in saline solution and fit the Hill1 equation with the EC₅₀ values showed in table (D). Asterisks show statistical significance relative to VEGF₁₆₅ potency (p *ns* > 0.05, p* < 0.05, p** < 0.01, p*** < 0.001). Data are represented as mean ± SEM.

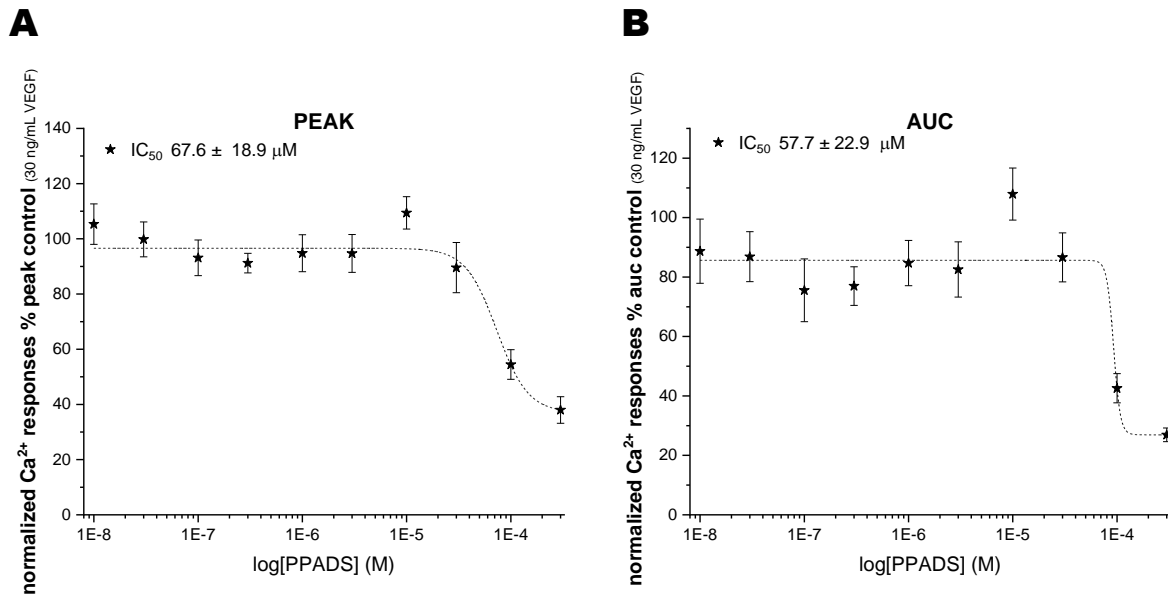


Figure 33. PPADS inhibition dose-response curves for VEGF₁₆₅ in human microvascular endothelial cells (HMEC-1). Inhibition concentration-response curves for the peak (A) and AUC (B) magnitude of intracellular Ca²⁺ responses elicited by 30 ng/mL VEGF₁₆₅ in the presence (0.01-300 μM; closed stars; N=5) of PPADS 100 μM. All data were normalised to 30 ng/mL VEGF₁₆₅ and fit the Hill1 equation with the IC₅₀ values showed in the graphs. Data are represented as mean ± SEM.

3.3.3.4 P2X4 antagonists inconsistently affected the VEGF₁₆₅-evoked calcium responses of human microvascular endothelial cells (HMEC-1).

Of all the P2X receptors, P2X4 was the candidate identified from the RNA sequencing data to be functionally expressed in HMEC-1 cells whose participation in the ATP-dependant responses was previously described. As the responses were ambiguous and just one of the selective antagonists, PSB12062, impacted the calcium responses, its potential role in the VEGF₁₆₅ response was investigated using this molecule, and the most potent P2X4 selective antagonist described, BAY-1797, that could not modify the ATP control responses. Thereby, we could have a better understanding of the possible P2X4 involvement in VEGF₁₆₅-dependent effects.

10 μ M of BAY-1797 was applied to study the contribution of P2X4 on the VEGF-evoked calcium responses (**Figure 34**). The antagonist could not inhibit any calcium responses upon VEGF₁₆₅ application in the peak and the AUC dose-response (**Figure 34-A, B**), and both potencies curves (EC_{50}^{PEAK} : 4.20 ± 0.99 ng/mL; EC_{50}^{AUC} : 6.2 ± 1.2 ng/mL) were unaffected by the presence of the antagonist (peak: 4.96 ± 0.58 ng/mL; *ns*; AUC: 9.2 ± 1.7 ng/mL; *ns*) (**Figure 34-D**). An isolated significant effect was found at 0.30 ng/mL VEGF in the peak curve when HMEC-1 cells were treated with 10 μ M BAY-1797 (**Figure 34-A**), but the change showed potentiation and was an isolated effect. No change was found when comparing the VEGF₁₆₅ control maximal response (30 ng/mL VEGF_{165 max}^{peak}: 103.5 ± 6.3 %; 100 ng/mL VEGF_{165 max}^{AUC}: 100%) in the presence of BAY-1797 for the peak (109.4 ± 6.3 %; *ns*) and the AUC (110.5 ± 7.5 %; *ns*) (**Figure 34-A, B**), and therefore, the level of efficacy remained intact (**Table 6, 7**). The representative time-resolved intracellular calcium responses in **Figure 34-C** demonstrated the described absence of inhibitory effects. As a result, we have concluded that 10 μ M BAY-1797 was ineffective in inhibiting VEGF₁₆₅-induced responses in HMEC-1 cells.

The other selective antagonist investigated it was PSB12062. Contrarily as previously reported for BAY-1797, 10 μ M of PSB12062 somehow impeded calcium responses upon VEGF₁₆₅ application in the peak and the AUC dose-response curves (**Figure 35-A, B**), but both potencies were unaffected by the presence of the antagonist (peak: 2.97 ± 1.8 ng/mL; *ns*; AUC: 2.94 ± 1.79 ng/mL; *ns*) (**Figure 35-D**). When comparing the VEGF₁₆₅ control maximal response in the presence of 10 μ M PSB12062, there was a significant change for both peak (68.5 ± 1.3 %; $p < 0.01$) and AUC (\pm ; $p < 0.05$) **Figure 35-A, B**. Nevertheless, in the case of the AUC, the maximal response for VEGF₁₆₅ in the presence of 10 μ M PSB12062 was found at 30 ng/mL VEGF₁₆₅ instead of 100 ng/mL. When comparing this new maximal response with the maximal response control at 100 ng/mL in the absence of the PSB12062, the response was significantly reduced (treated 30 ng/mL VEGF₁₆₅, 55 ± 2.5 %; $p < 0.01$) and, consistently, it never achieved the same level of efficacy as the control (**Table 6, 7**). The representative time-resolved intracellular calcium responses shown in **Figure 35-C** illustrated PSB12062's significant impact on the peak and the area under the curve upon 10 ng/mL VEGF₁₆₅ stimulation compared with the control. In the presence of PSB12062, the VEGF₁₆₅ response conserved its slow and delayed calcium increase kinetics. However, it depicted a significant decrease in the late peak, which reached approximately 30% above baseline compared to the VEGF response in the absence of the enzyme, which reached almost 90%. Accordingly, we have determined that 10 μ M PSB12062 unexpectedly inhibited VEGF₁₆₅-induced responses in HMEC-1 cells.

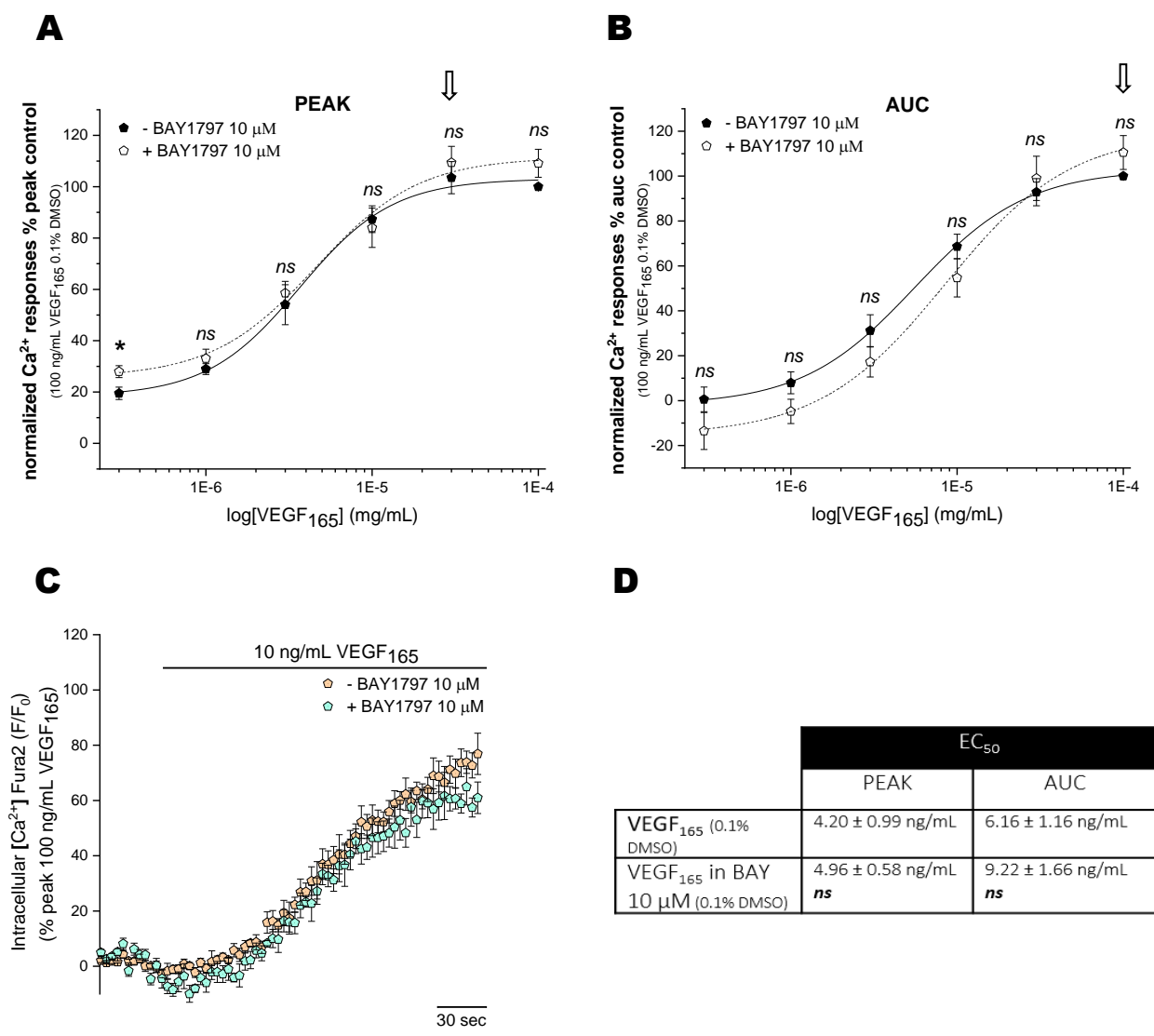


Figure 34. Lack of inhibitory effects of BAY-1797 P2X4 receptor antagonist on the VEGF₁₆₅-evoked response in human microvascular endothelial cells (HMEC-1). Concentration-response curves for the peak (A) and AUC (B) magnitude of intracellular Ca²⁺ responses elicited by VEGF₁₆₅ in the presence (0.3-100 ng/mL; open pentagon; N=5) or absence (0.3-100 ng/mL; closed pentagon; N=5) of BAY1797 10 μM . (C) Averaged time-resolved intracellular Ca²⁺ responses elicited by VEGF₁₆₅ 10 ng/mL in the presence (cyan pentagon; N=5) or absence (orange pentagon; N=5) of BAY1797 10 μM over 250 seconds. All data were normalised to 100 ng/mL VEGF₁₆₅ in 0.1% DMSO and fit the Hill1 equation with the EC₅₀ values showed in table (D). Asterisks show statistical significance relative to VEGF₁₆₅ potency (p *ns* > 0.05, p* < 0.05, p** < 0.01, p*** < 0.001). Data are represented as mean \pm SEM.

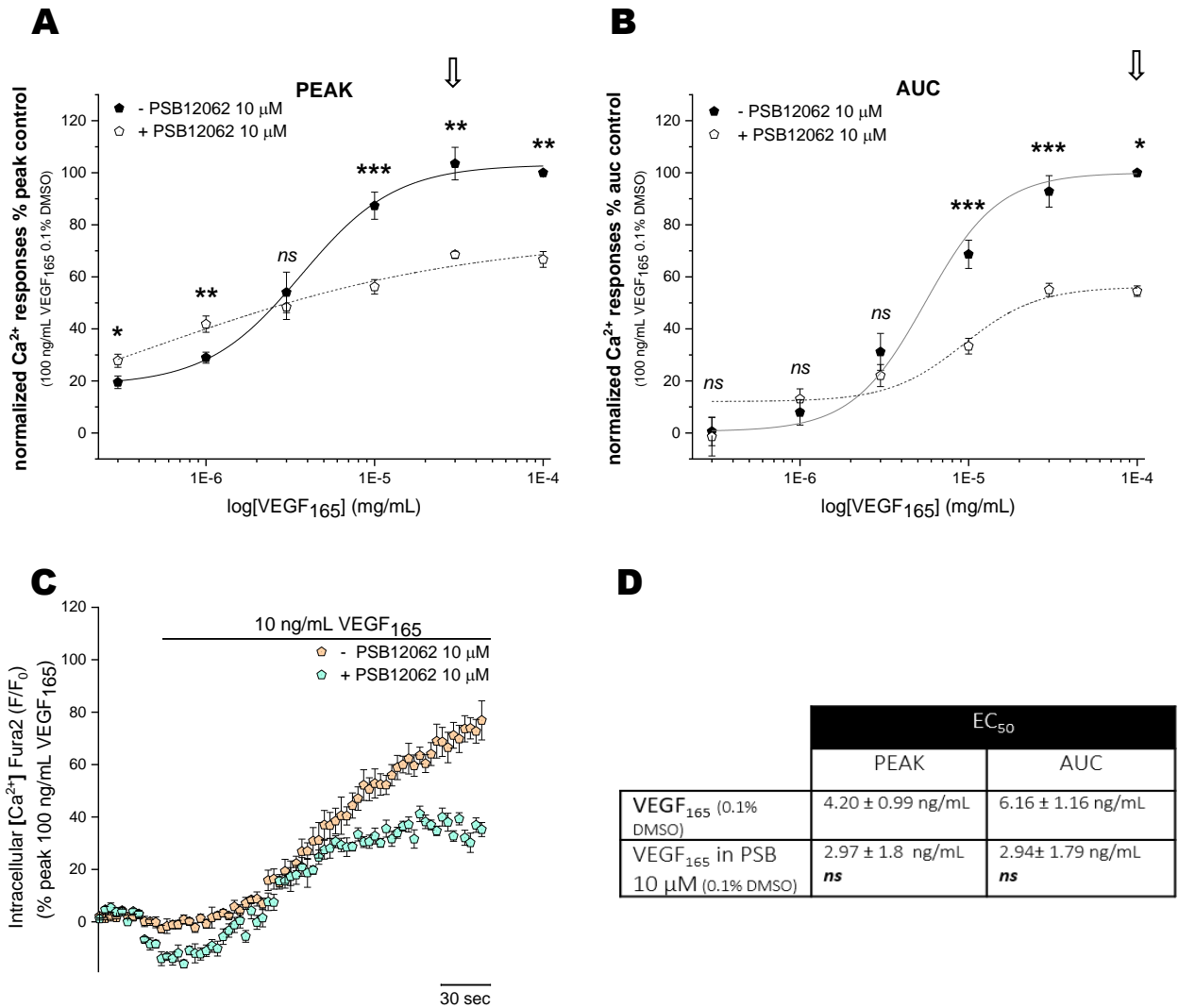


Figure 35. Inhibitory effects of PSB12062 P2X4 receptor antagonist on the VEGF₁₆₅-evoked response in human microvascular endothelial cells (HMEC-1). Concentration-response curves for the peak (A) and AUC (B) magnitude of intracellular Ca^{2+} responses elicited by VEGF₁₆₅ in the presence (0.3-100 ng/mL; open pentagon; N=5) or absence (0.3-100 ng/mL; closed pentagon; N=5) of PSB12062 10 μM . (C) Averaged time-resolved intracellular Ca^{2+} responses elicited by VEGF₁₆₅ 10 ng/mL in the presence (cyan pentagon; N=5) or absence (orange pentagon; N=5) of PSB12062 10 μM over 250 seconds. All data were normalised to 100 ng/mL VEGF₁₆₅ in 0.1% DMSO and fit the Hill1 equation with the EC₅₀ values showed in table (D). Asterisks show statistical significance relative to VEGF₁₆₅ potency (p *ns* > 0.05, p* < 0.05, p** < 0.01, p*** < 0.001). Data are represented as mean ± SEM.

3.3.3.5 P2Y2 selective antagonist did not affect the VEGF₁₆₅-evoked calcium responses of human microvascular endothelial cells (HMEC-1).

Of all the P2Y receptors, P2Y2 was the candidate identified from the RNA sequencing data to be functionally expressed in HMEC-1 cells whose inhibition impacted the ATP dose-response curve. As the ATP responses were undoubtedly inhibited by AR-C 118925XX, its potential role in the VEGF₁₆₅ response was investigated using this antagonist.

10 μ M AR-C 118925XX could not inhibit any calcium responses upon VEGF₁₆₅ application in the peak and the AUC dose-response curves (EC_{50}^{PEAK} : 4.20 ± 0.99 ng/mL; EC_{50}^{AUC} : 6.2 ± 1.2 ng/mL) (**Figure 36-A, B**), and both potencies were unaffected by the presence of the antagonist (peak: 5.81 ± 1.1 ng/mL; *ns*; AUC: 24.1 ± 15.3 ng/mL; *ns*) (**Figure 36-D**). No change was found when comparing the VEGF₁₆₅ control maximal response (30 ng/mL VEGF₁₆₅ max^{peak} : 103.5 ± 6.3 %; 100 ng/mL VEGF₁₆₅ max^{AUC} : 100%) in the presence of AR-C for the peak (95.15 ± 7.26 %; *ns*) or the AUC (90.6 ± 9.9 %; *ns*) (**Figure 36-A, B**). However, in the case of the peak, the maximal response for VEGF₁₆₅ in the presence of 10 μ M AR-C was found at 100 ng/mL VEGF₁₆₅ instead of 30 ng/mL of the control curve (88.4 ± 6.7 %; *ns*). Once again, the efficacy remained intact (**Table 6, 7**). The representative time-resolved intracellular calcium responses in **Figure 36-C** confirmed the described absence of inhibitory effects. As a result, we have concluded that 10 μ M AR-C was ineffective in inhibiting VEGF₁₆₅-induced responses in HMEC-1 cells.

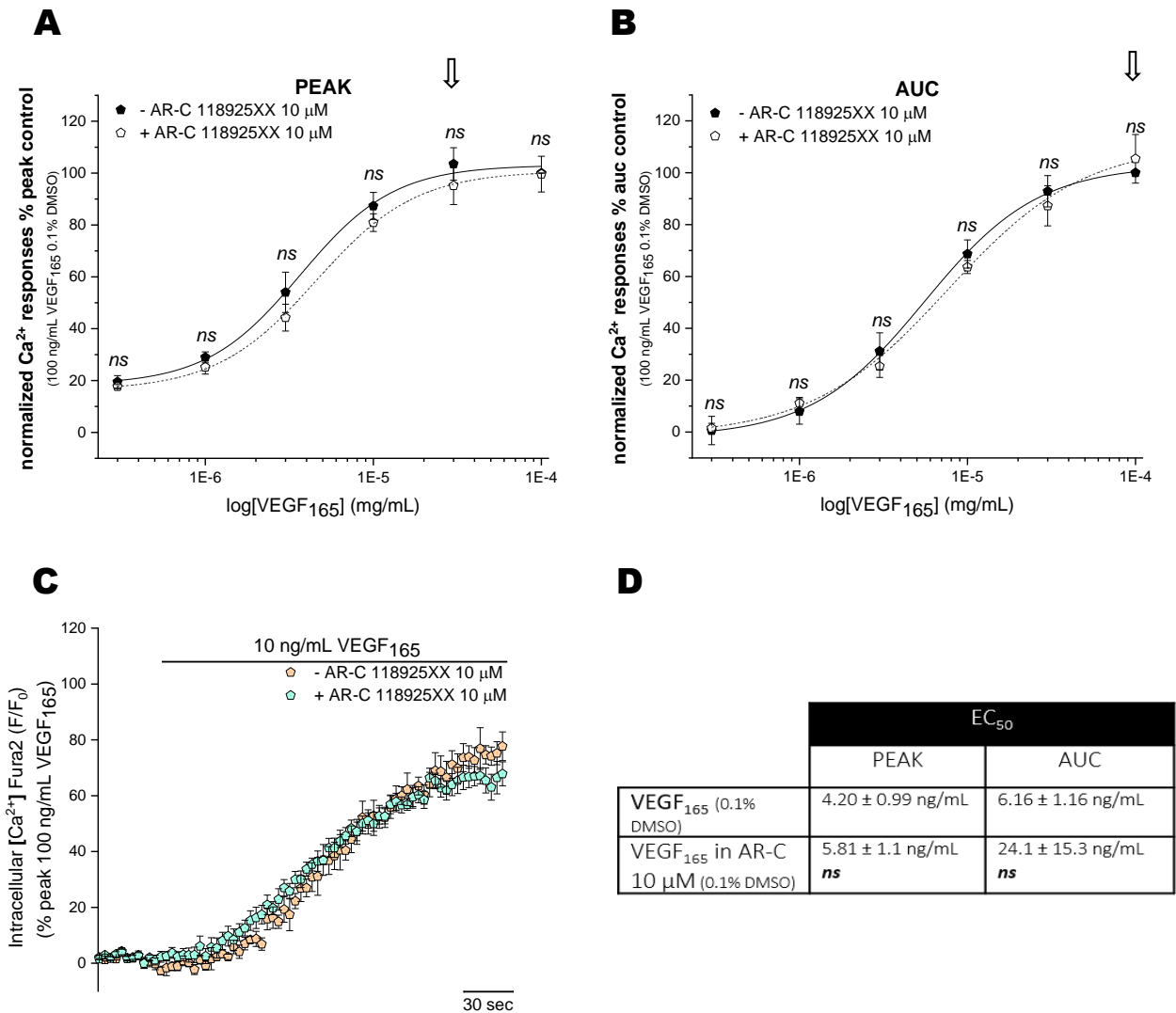


Figure 36. Lack of inhibitory effects of AR-C 118925XX P2Y2 receptor antagonist on the VEGF₁₆₅ - evoked response in human microvascular endothelial cells (HMEC-1). Concentration-response curves for the peak (A) and AUC (B) magnitude of intracellular Ca^{2+} responses elicited by VEGF₁₆₅ in the presence (0.3-100 ng/mL; open pentagon; $N=8$) or absence (0.3-100 ng/mL; closed pentagon; $N=5$) of AR-C 118925XX 10 μ M. (C) Averaged time-resolved intracellular Ca^{2+} responses elicited by VEGF₁₆₅ 10 ng/mL in the presence (cyan pentagon; $N=8$) or absence (orange pentagon; $N=5$) of AR-C 118925XX 10 μ M over 250 seconds. All data were normalised to 100 ng/mL VEGF₁₆₅ in 0.1% DMSO and fit the Hill1 equation with the EC₅₀ values showed in table (D). Asterisks show statistical significance relative to VEGF₁₆₅ potency ($p_{ns} > 0.05$, $p^* < 0.05$, $p^{**} < 0.01$, $p^{***} < 0.001$). Data are represented as mean \pm SEM.

Table 5. Effects of broad-spectrum antagonists on the VEGF₁₆₅-evoked responses in human microvascular endothelial cells (HMEC-1). EC₅₀ statistical analysis was performed against the VEGF₁₆₅ control curve in saline solution. Efficacy p-value is the statistical comparison between VEGF₁₆₅ maximal response in saline solution and VEGF₁₆₅ maximal response in the presence of the applied compound (whose concentration might differ from the previous one).

| Agonist | Agonist range, μM | Antagonist | Antagonist concentration | EC ₅₀ PEAK | P value | Maximal response PEAK (μM) | Maximal response PEAK (%) | P value |
|---------------------|------------------------------|------------|--------------------------|-----------------------------|-----------|---|---------------------------|---------|
| VEGF ₁₆₅ | 0.3-100 | / | / | 2.85 \pm 1 | / | 30 | 111.6 \pm 4.3 | / |
| VEGF ₁₆₅ | 0.3-100 | Apyrase | 10 U/mL | 6.17 \pm 2.7 | <i>ns</i> | 30 | 76.69 \pm 8.28 | p<0.01 |
| VEGF ₁₆₅ | 0.3-100 | PPADS | 100 μM | 17.6 \pm 4.8 | p<0.01 | 100 | 50.10 \pm 5.66 | p<0.01 |
| Agonist | Agonist range, μM | Antagonist | Antagonist concentration | EC ₅₀ AUC | P value | Maximal response AUC (μM) | Maximal response AUC (%) | P value |
| VEGF ₁₆₅ | 0.3-100 | / | / | 3.5 \pm 1.3 | / | 100 | 100 | / |
| VEGF ₁₆₅ | 0.3-100 | Apyrase | 10 U/mL | 4.19 \pm 2.5 | <i>ns</i> | 100 | 50.10 \pm 5.66 | p<0.01 |
| VEGF ₁₆₅ | 0.3-100 | PPADS | 100 μM | 363 \pm 312 μM | p<0.01 | 100 | 87.21 \pm 6.65 | p<0.01 |

Table 6. Effects of selective antagonists on the VEGF₁₆₅-evoked peak responses in human microvascular endothelial cells (HMEC-1). EC₅₀ statistical analysis was performed against the VEGF₁₆₅ control curve in the appropriate vehicle control. Efficacy p-value is the statistical comparison between VEGF₁₆₅ maximal response in saline solution and VEGF₁₆₅ maximal response in the presence of the applied compound (whose concentration might differ from the previous one).

| Agonist | Agonist range, ng/mL | Antagonist | Antagonist concentration | Target | EC ₅₀ PEAK, ng/mL | P value | Maximal response, ng/mL | Maximal response (%) | P value |
|---------------------------------|----------------------|-----------------|--------------------------|-------------------------------------|------------------------------|-----------|-------------------------|----------------------|-----------|
| VEGF ₁₆₅ (0.1% DMSO) | 0.3-100 | / | / | VEGR-1,2 | 4.20 ± 0.99 | / | 30 | 103.5 ± 6.3 | / |
| VEGF ₁₆₅ | 0.3-100 | AR-C 118925XX | 10 μM | P2Y ₂ | 5.81 ± 1.1 | <i>ns</i> | 100 | 88.4 ± 6.7 | <i>ns</i> |
| VEGF ₁₆₅ | 0.3-100 | BAY-1797 | 10 μM | P2X ₄ | 4.96 ± 0.58 | <i>ns</i> | 30 | 109.4 ± 6.3 | <i>ns</i> |
| VEGF ₁₆₅ | 0.3-100 | PSB12062 | 10 μM | P2X ₄ | 2.97 ± 1.8 | <i>ns</i> | 30 | 68.5 ± 1.3 | p<0.01 |
| VEGF ₁₆₅ | 0.3-100 | SQ 22536 | 1 μM | Adenylyl cyclase | 1.92 ± 0.6 | <i>ns</i> | 30 | 102.8 ± 4 | <i>ns</i> |
| VEGF ₁₆₅ | 0.3-100 | SQ 22536 | 10 μM | Adenylyl cyclase | 3.86 ± 0.7 | <i>ns</i> | 30 | 107.3 ± 5.2 | <i>ns</i> |
| VEGF ₁₆₅ | 0.3-100 | SQ 22536, NF157 | 10 μM | Adenylyl cyclase, P2Y ₁₁ | 16.4 ± 2.8 | p<0.01 | 100 | 112.1 ± 5.3 | <i>ns</i> |
| VEGF ₁₆₅ (saline) | 0.3-100 | / | / | VEGR-1,2 | 2.85 ± 1 | / | 30 | 111.6 ± 4.3 | / |
| VEGF ₁₆₅ | 0.3-100 | NF157 | 5 μM | P2Y ₁₁ | 19.9 ± 2.9 | p<0.001 | 100 | 109.4 ± 3.5 | <i>ns</i> |
| VEGF ₁₆₅ | 0.3-100 | MRS 1754 | 100 nM | A ₂ B | 9.28 ± 2.9 | p<0.05 | 30 | 101.6 ± 5 | <i>ns</i> |

Table 7. Effects of selective antagonists on the VEGF₁₆₅-evoked AUC responses in human microvascular endothelial cells (HMEC-1). EC₅₀ statistical analysis was performed against the VEGF₁₆₅ control curve in the appropriate vehicle control. Efficacy p-value is the statistical comparison between VEGF₁₆₅ maximal response in saline solution and VEGF₁₆₅ maximal response in the presence of the applied compound (whose concentration might differ from the previous one).

| Agonist | Agonist range, ng/mL | Antagonist | Antagonist concentration | Target | EC ₅₀ AUC, ng/mL | P value | Maximal response, ng/mL | Maximal response (%) | P value |
|---------------------------------|----------------------|-----------------|--------------------------|-------------------------------------|-----------------------------|-----------|-------------------------|----------------------|-----------|
| VEGF ₁₆₅ (0.1% DMSO) | 0.3-100 | / | / | VEGR-1,2 | 6.2 ± 1.2 | / | 100 | 100 | / |
| VEGF ₁₆₅ | 0.3-100 | AR-C 118925XX | 10 µM | P2Y ₂ | 24.1 ± 15.3 | <i>ns</i> | 100 | 90.6 ± 9.9 | <i>ns</i> |
| VEGF ₁₆₅ | 0.3-100 | BAY-1797 | 10 µM | P2X ₄ | 9.2 ± 1.7 | <i>ns</i> | 100 | 110.5 ± 7.5 | <i>ns</i> |
| VEGF ₁₆₅ | 0.3-100 | PSB12062 | 10 µM | P2X ₄ | 2.9 ± 1.8 | <i>ns</i> | 30 | 55 ± 2.5 | p<0.01 |
| VEGF ₁₆₅ | 0.3-100 | SQ 22536 | 1 µM | Adenylyl cyclase | 3.1 ± 0.9 | <i>ns</i> | 30 | 94.4 ± 5.7 | <i>ns</i> |
| VEGF ₁₆₅ | 0.3-100 | SQ 22536 | 10 µM | Adenylyl cyclase | 6.1 ± 1 | <i>ns</i> | 30 | 107 ± 12.9 | <i>ns</i> |
| VEGF ₁₆₅ | 0.3-100 | SQ 22536, NF157 | 10 µM | Adenylyl cyclase, P2Y ₁₁ | 13 ± 2.1 | p<0.05 | 100 | 125.3 ± 6.4 | p<0.05 |
| VEGF ₁₆₅ (saline) | 0.3-100 | / | / | VEGR-1,2 | 3.5 ± 1.3 | / | 100 | 100 | / |
| VEGF ₁₆₅ | 0.3-100 | NF157 | 5 µM | P2Y ₁₁ | 51.6 ± 21.1 | p<0.001 | 100 | 117.2 ± 5.6 | p<0.05 |
| VEGF ₁₆₅ | 0.3-100 | MRS 1754 | 100 nM | A ₂ B | 11.6 ± 5.8 | <i>ns</i> | 100 | 100.5 ± 2.8 | <i>ns</i> |

3.3.3.6 P2Y11 selective antagonist significantly inhibited the VEGF₁₆₅-evoked calcium responses of human microvascular endothelial cells (HMEC-1).

Of all the P2 purinergic receptors, P2Y11 is the last candidate identified from the RNA sequencing that could have a potential impact on the VEGF₁₆₅ calcium-induced responses. None of the other P2 receptors selective antagonists affected the VEGF₁₆₅ response, including AR-C 118925XX, which dramatically reduced the ATP-evoked calcium responses. Therefore, P2Y11 is the last candidate that could be involved in the VEGF₁₆₅ response.

The effects of NF157 (5 μ M), the selective P2Y11 antagonist, on the VEGF₁₆₅ dose-response curve control (EC₅₀ PEAK: 2.85 \pm 1 ng/mL; EC₅₀ AUC: 3.49 \pm 1.3 ng/mL) were investigated. Pre-treatment with NF157 right shifted the VEGF₁₆₅ dose-response curve (**Figure 37-A, B**), and massively reduced the VEGF₁₆₅ potency for the peak (19.9 \pm 2.9 ng/mL; $p < 0.001$) and the area under the curve (51.6 \pm 21.1 ng/mL; $p < 0.001$) (**Figure 37-D, Table 6, 7**). Furthermore, the presence of the inhibitor significantly affected the control VEGF₁₆₅-evoked maximal response (30 ng/mL VEGF₁₆₅ max^{peak}: 111.6 \pm 4.3 %; 100 ng/mL VEGF₁₆₅ max^{AUC}: 100 %) for the peak (94.62 \pm 4.54 %; $p < 0.05$) and the AUC (117.2 \pm 5.6 %; $p < 0.05$). Interestingly, in the AUC, the presence of the inhibitor caused an increase in the maximal response (**Figure 37-B, Table 7**). In addition, the maximal response to VEGF₁₆₅ in the presence of NF157 was achieved at 100 ng/mL for the peak (109.4 \pm 3.5 %; *ns*) instead of 30 ng/mL as the control curve, but the level of efficacy remained unaffected for the peak (**Table 6**). It is remarkable, in this case, the powerful effect of the drug on the calcium evoked responses from 1 to 10 ng/mL (**Figure 37-A, B**). As shown in **Figure C**, at 10 ng/mL, in the presence of the antagonist, the response was reduced from 80% in control conditions to approximately 20% above baseline.

To further characterise NF157 effects on the VEGF₁₆₅-evoked responses, HMEC-1 cells were incubated for 30 minutes in a range of antagonist concentrations (0.1875 to 5 μ M) and stimulated with a sub-maximal concentration of VEGF₁₆₅ (10 ng/mL) and thereby, IC₅₀ was calculated (**Figure 38-A, B**). The half-maximal inhibitory concentration values obtained were 1.23 \pm 0.4 ng/mL for the peak and 1.25 \pm 0.3 ng/mL for AUC inhibition curves, not far from what has been previously described. The representative time-resolved intracellular calcium responses shown in **Figure 38-C** depicted 1.25 μ M NF157's significant impact on the peak and the area under the curve upon 10 ng/mL VEGF₁₆₅ stimulation compared with the control. In the presence of the antagonist, the response was reduced from 80% in control conditions to approximately 40% above baseline. As a result, we have concluded that NF157 was effective in inhibiting VEGF₁₆₅-induced responses in HMEC-1 cells.

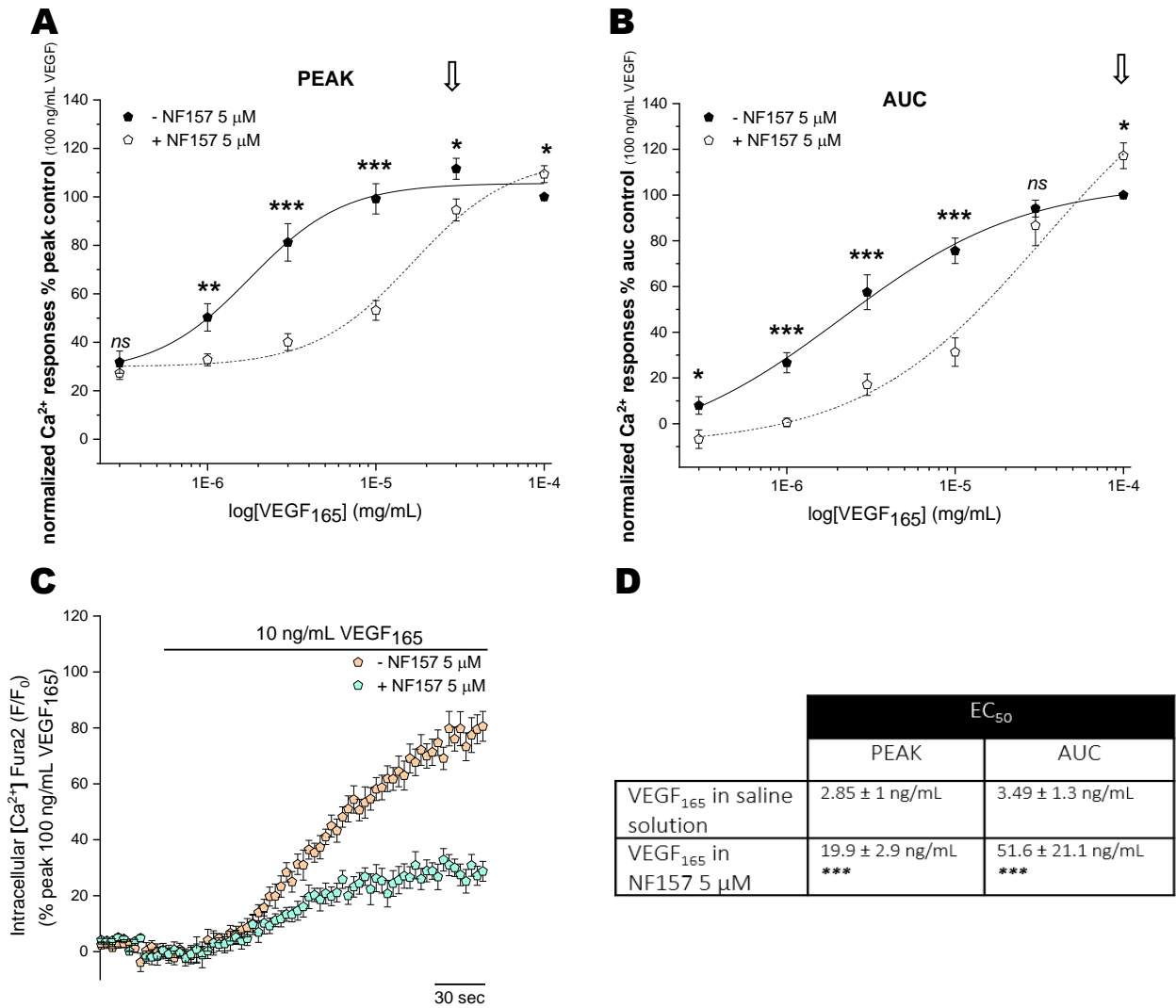


Figure 37. Inhibitory effects of NF157 P2Y11 receptor antagonist on the VEGF₁₆₅-evoked response in human microvascular endothelial cells (HMEC-1). Concentration-response curves for the peak (A) and AUC (B) magnitude of intracellular Ca^{2+} responses elicited by VEGF₁₆₅ in the presence (0.3-100 ng/mL; open pentagon; $N=10$) or absence (0.3-100 ng/mL; closed pentagon; $N=8$) of NF157 5 μM . (C) Averaged time-resolved intracellular Ca^{2+} responses elicited by VEGF₁₆₅ 10 ng/mL in the presence (cyan pentagon; $N=10$) or absence (orange pentagon; $N=8$) of NF157 5 μM over 250 seconds. All data were normalised to 100 ng/mL VEGF₁₆₅ and fit the Hill1 equation with the EC₅₀ values showed in table (D). Asterisks show statistical significance relative to VEGF₁₆₅ potency ($p_{ns} > 0.05$, $p^* < 0.05$, $p^{**} < 0.01$, $p^{***} < 0.001$). Data are represented as mean \pm SEM.

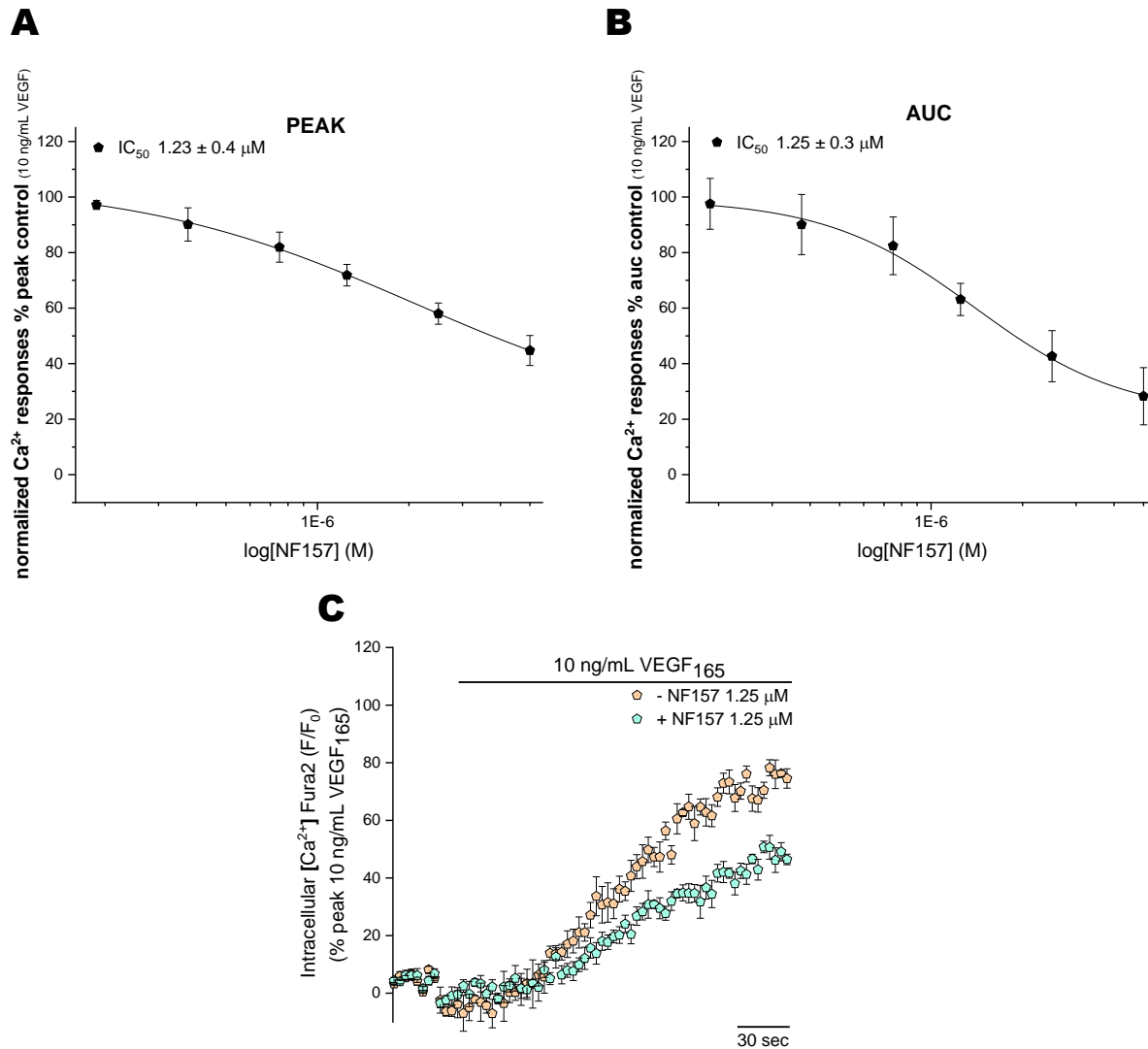
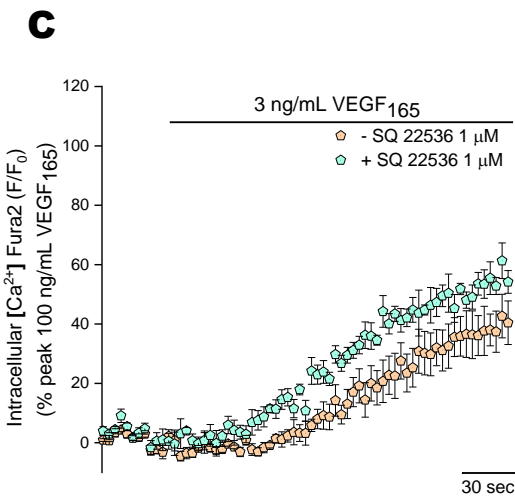
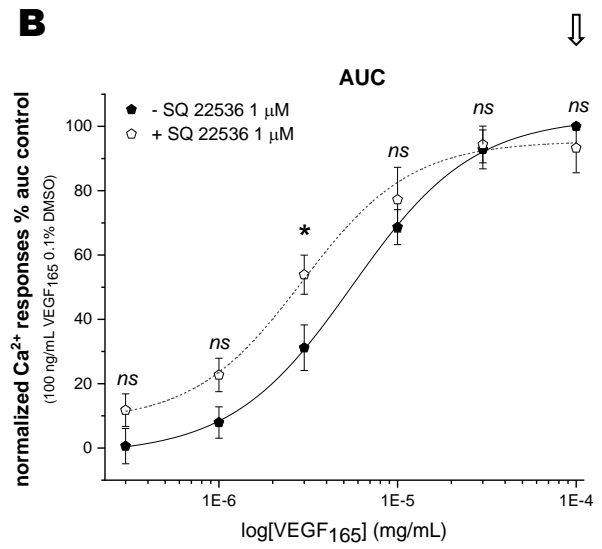
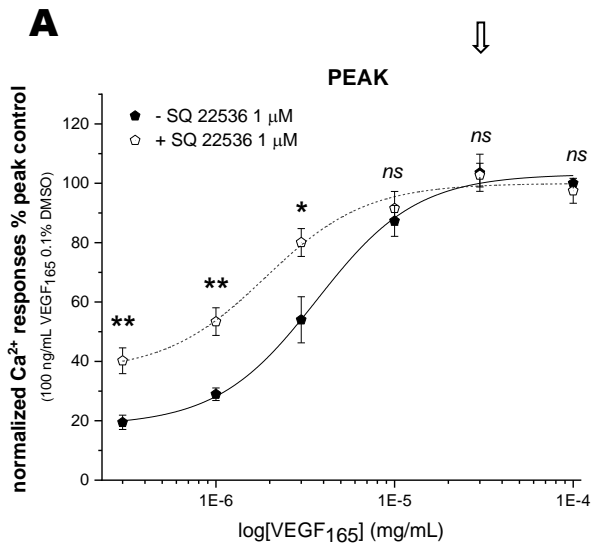


Figure 38. VEGF₁₆₅ inhibition dose-response curves for NF157 in human microvascular endothelial cells (HMEC-1). Inhibition concentration-response curves for the peak (A) and AUC (B) magnitude of intracellular Ca²⁺ responses elicited by 10 ng/mL VEGF₁₆₅ in the presence (0.1875-5 μM ; closed stars; $N=5$) of NF157. (C) Averaged time-resolved intracellular Ca²⁺ responses elicited by VEGF₁₆₅ 10 ng/mL in the presence (cyan start; $N=5$) or absence (orange start; $N=5$) of NF157 1.25 μM over 250 seconds. All data were normalised to VEGF₁₆₅ 10 ng/mL and fit the Hill1 equation with the IC_{50} values showed in the graphs. Data are represented as mean \pm SEM.

3.3.3.7 VEGF₁₆₅-evoked calcium responses P2Y11-dependent are mediated by the adenylyl cyclase pathway in human microvascular endothelial cells (HMEC-1).

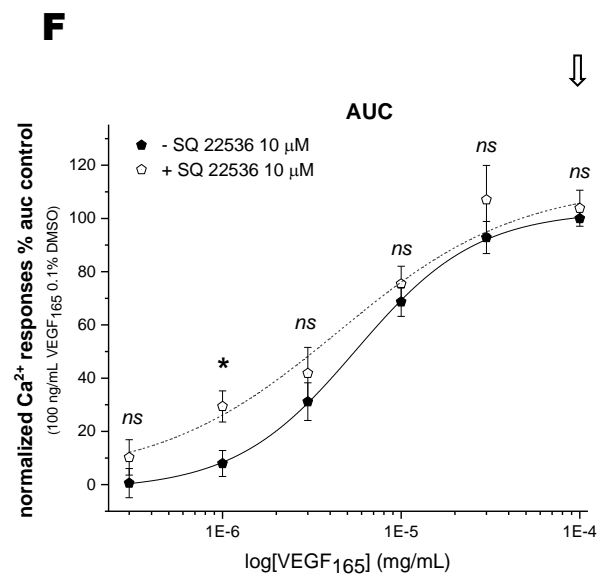
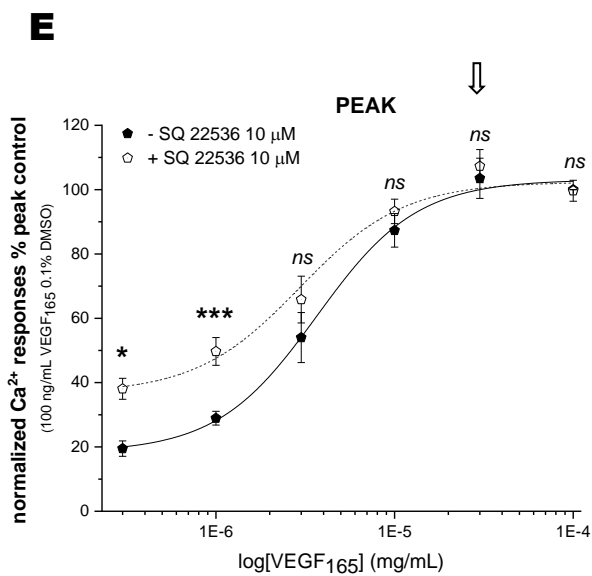
As explained in **section 3.3.2.7**, P2Y11 signalling can be mediated by the PLC or the adenylyl cyclase pathway. That is the case because P2Y11 can be a G α_q -type or G α_s -coupled receptor. When studying the effects of NF157 in the ATP dose-response curve, no significant effects were observed, and therefore, there were two direct interpretations. The first was that P2Y11 is not expressed in HMEC-1 at the protein level, and the second, G α_s -type G proteins mediate P2Y11 signalling. The NF157 impact in the VEGF₁₆₅ calcium responses proposed expression of P2Y11 at the protein level, then we hypothesised if the adenylyl cyclase signalling pathway could mediate the previously reported effects in the VEGF₁₆₅ responses. For that, SQ 22536, a selective AC pathway inhibitor (IC₅₀=1 μ M) (Harris et al., 1979), was used to test this hypothesis.

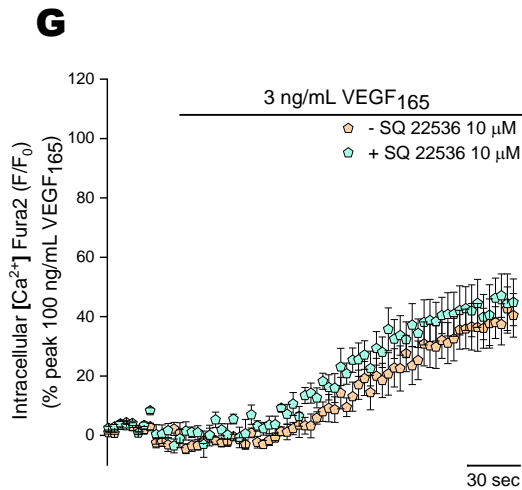
Two different concentrations of SQ 22536 were tested to study the contribution of the AC pathway on the VEGF₁₆₅-evoked calcium responses (EC₅₀^{PEAK}: 4.20 \pm 0.99 ng/mL; EC₅₀^{AUC}: 6.2 \pm 1.2 ng/mL) (**Figure 39**). Neither the 1 nor 10 μ M successfully inhibit the calcium responses upon VEGF₁₆₅ application and the potencies were unaffected (**Figure 39-D, H**). No change was found either when comparing the VEGF₁₆₅-evoked maximal responses (30 ng/mL VEGF₁₆₅ max^{peak}: 103.5 \pm 6.3 %; 100 ng/mL VEGF₁₆₅ max^{AUC}: 100%) in the presence of SQ 22536 under both treatments (**Figure 39-A, B, E, F, and Table 6,7**). However, both dose-response curves presented a subtle leftward shift that was demonstrated with significant potentiation effects from 0.3 to 3 ng/mL responses in both curves and treatments, more intensified this effect at the lower concentration of SQ 22536 (1 μ M). Furthermore, the time-resolved intracellular calcium responses in **Figure 39-C** illustrated this slight potentiation effect at 3 ng/mL when the cells were treated with 1 μ M SQ 22536. This effect was not conserved at 10 μ M SQ 22536 (**Figure 39-G**), whose potentiation trend is less obvious.



D

| | EC ₅₀ | |
|---|----------------------------|----------------------------|
| | PEAK | AUC |
| VEGF ₁₆₅ (0.1% DMSO) | 4.20 ± 0.99 ng/mL | 6.16 ± 1.16 ng/mL |
| VEGF ₁₆₅ in SQ 1 μM (0.1% DMSO) | 1.92 ± 0.6 ng/mL <i>ns</i> | 3.13 ± 0.9 ng/mL <i>ns</i> |





H

| | EC ₅₀ | |
|---|----------------------------|-------------------------|
| | PEAK | AUC |
| VEGF ₁₆₅ (0.1% DMSO) | 4.20 ± 0.99 ng/mL | 6.16 ± 1.16 ng/mL |
| VEGF ₁₆₅ in SQ 10 μM (0.1% DMSO) | 3.86 ± 0.7 ng/mL <i>ns</i> | 6.1 ± 1 ng/mL <i>ns</i> |

Figure 39. Unexpected effects of SQ 22536 adenylyl cyclase inhibitor on the VEGF₁₆₅-evoked response in human microvascular endothelial cells (HMEC-1). Concentration-response curves for the peak (A) and AUC (B) magnitude of intracellular Ca²⁺ responses elicited by VEGF₁₆₅ in the presence (0.3-100 ng/mL; open pentagon; N=5) or absence (0.3-100 ng/mL; closed pentagon; N=5) of SQ 22536 1 μM. (C) Averaged time-resolved intracellular Ca²⁺ responses elicited by VEGF₁₆₅ 3 ng/mL in the presence (cyan pentagon; N=5) or absence (orange pentagon; N=5) of SQ 22536 1 μM over 250 seconds. All data were normalised to 100 ng/mL VEGF₁₆₅ and fit the Hill1 equation with the EC₅₀ values showed in table (D). Concentration-response curves for the peak (E) and AUC (F) magnitude of intracellular Ca²⁺ responses elicited by VEGF₁₆₅ in the presence (0.3-100 ng/mL; open pentagon; N=5) or absence (0.3-100 ng/mL; closed pentagon; N=5) of SQ 22536 10 μM. (G) Averaged time-resolved intracellular Ca²⁺ responses elicited by VEGF₁₆₅ 3 ng/mL in the presence (cyan pentagon; N=5) or absence (orange pentagon; N=5) of SQ 22536 10 μM over 250 seconds. All data were normalised to 100 ng/mL VEGF₁₆₅ and fit the Hill1 equation with the EC₅₀ values showed in table (H). Asterisks show statistical significance relative to VEGF₁₆₅ potency (p *ns* > 0.05, p* < 0.05, p** < 0.01, p*** < 0.001). Data are represented as mean ± SEM.

These results were difficult to interpret, and potentiation of the calcium response was not expected. Trying to gain a better understanding of the hypothetical involvement of the AC pathway in the P2Y11-dependent VEGF₁₆₅-evoked calcium responses, the effect of a combined pre-treatment with NF157 5 μ M and SQ 022536 10 μ M was investigated. This combined treatment right shifted the VEGF₁₆₅ dose-response curve (EC_{50}^{PEAK} : 4.20 ± 0.99 ng/mL; EC_{50}^{AUC} : 6.2 ± 1.2 ng/mL) more obviously for the peak but consistently also for the AUC (**Figure 40-A, B**), reducing the VEGF₁₆₅ potency for the peak (16.4 ± 2.8 ng/mL; $p < 0.01$) and the AUC (13 ± 2.1 ng/mL; $p < 0.05$). Furthermore, the presence of both drugs significantly affected the control VEGF₁₆₅-evoked maximal response at 100 ng/mL (100%) for the AUC (125.3 ± 6.4 ; $p < 0.05$), showing an improved efficacy than in the absence of the drugs. The peak maximal control response observed at 30 ng/mL remained unchanged (\pm ; *ns*). In addition, the maximal response to VEGF₁₆₅ in the presence of both drugs for the peak was achieved at 100 ng/mL (112.1 ± 5.3 %; *ns*), but when comparing this new maximal response with the maximal response at 30 ng/mL in the absence of the treatment, the level of efficacy was conserved. There was an evident impact on the time-resolved trace kinetics (**Figure 40-C**). Compared to the control, in the absence of treatment, the stimulation with VEGF₁₆₅ did elicit a rapid response. It was a much lower sustained response with the difference that reached its maximum peak early after the agonist injection at approximately 20% above baseline. In comparison, the control showed a late sustained peak response of around 80%.

The VEGF₁₆₅ potency fold change comparison between the co-application of both drugs and the effect of the NF157 is shown in **Figure 41**. A fold change comparison was required as both assays were conducted using different vehicle controls. SQ 22536 stock required solubilisation in DMSO, while NF157 was prepared in deionised water. Therefore, the combined assay statistical significance was calculated compared to the dose-response control parameters at 0.1% DMSO. In contrast, the NF157 assay was calculated compared to the dose-response control parameters in saline solution (SBS). Following a 30-minute incubation with the NF157 P2Y11 antagonist, there was a 7-fold increase in VEGF₁₆₅ peak EC_{50} , directly translated as a 7-fold decrease in potency. However, when the NF157 P2Y11 antagonist was co-incubated with the SQ 22536 adenylyl cyclase inhibitor, the effect was partially mitigated, resulting in a 3.9-fold decrease in potency compared to the control. The effect was much more pronounced in the area under the curve. After a 30-minute incubation with the NF157 P2Y11 antagonist, there was a robust 14.8-fold increase in VEGF₁₆₅ EC_{50} . Yet, when the NF157 P2Y11 antagonist was co-incubated with the SQ 22536 adenylyl cyclase inhibitor, the effect was partially prevented, resulting in a 2.1-fold decrease in potency compared to the control. As a result, we concluded that there is an involvement of the AC pathway in the P2Y11 involvement NF157-dependent VEGF₁₆₅-induced responses.

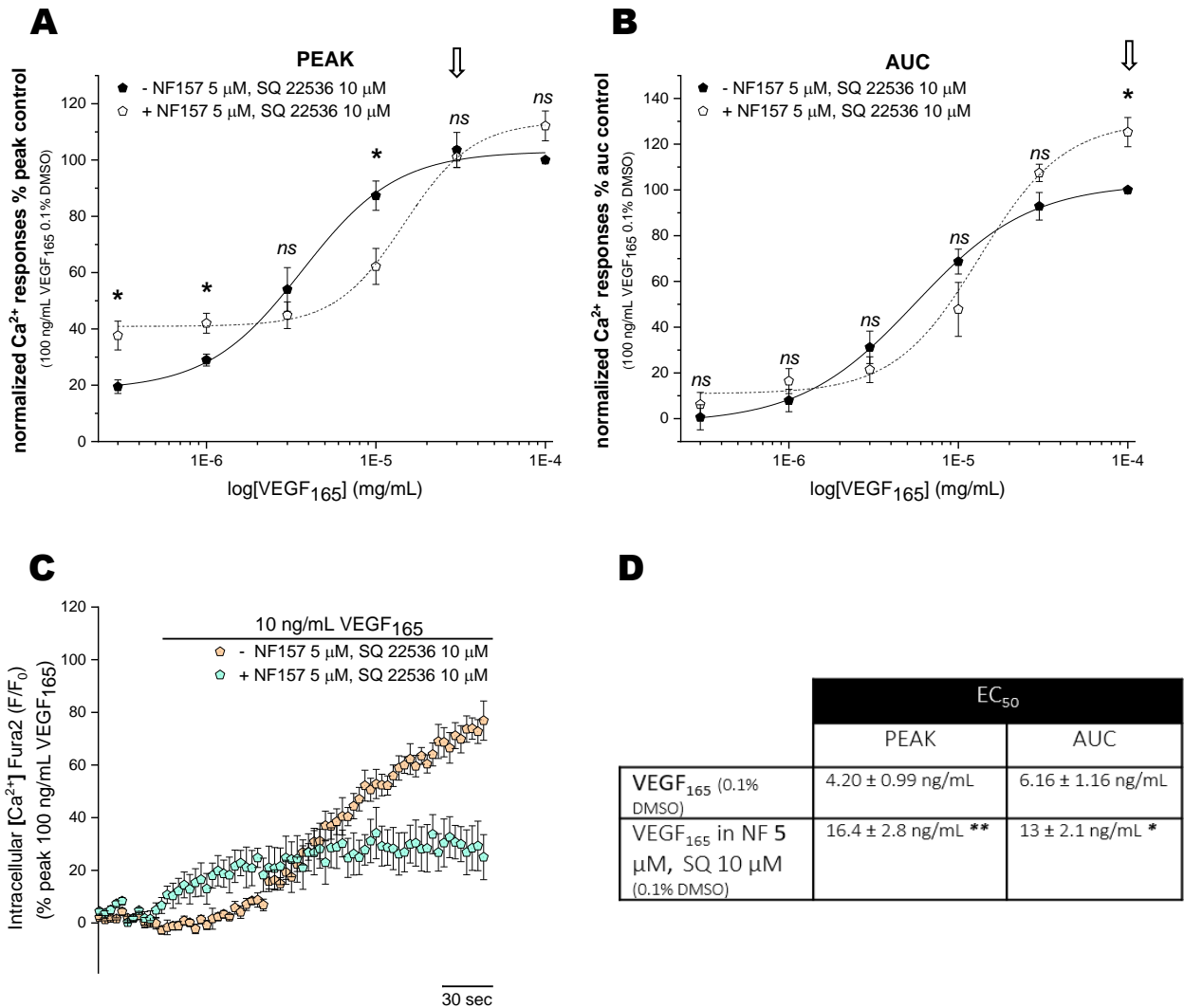


Figure 40. Effects of the combination of NF157 P2Y11 antagonist and SQ 22536 adenylyl cyclase inhibitor on the VEGF₁₆₅-evoked response in human microvascular endothelial cells (HMEC-1). Concentration-response curves for the peak (**A**) and AUC (**B**) magnitude of intracellular Ca²⁺ responses elicited by VEGF₁₆₅ in the presence (0.3-100 ng/mL; open pentagon; N=5) or absence (0.3-100 ng/mL; closed pentagon; N=5) of NF157 5 μ M and SQ 22536 10 μ M. (**C**) Averaged time-resolved intracellular Ca²⁺ responses elicited by VEGF₁₆₅ 10 ng/mL in the presence (cyan pentagon; N=5) or absence (orange pentagon; N=5) of NF157 5 μ M and SQ 22536 10 μ M over 250 seconds. All data were normalised to 100 ng/mL VEGF₁₆₅ in 0.1% DMSO and fit the Hill1 equation with the EC₅₀ values showed in table (**D**). Asterisks show statistical significance relative to VEGF₁₆₅ potency (p *ns* > 0.05, p* < 0.05, p** < 0.01, p*** < 0.001). Data are represented as mean \pm SEM.

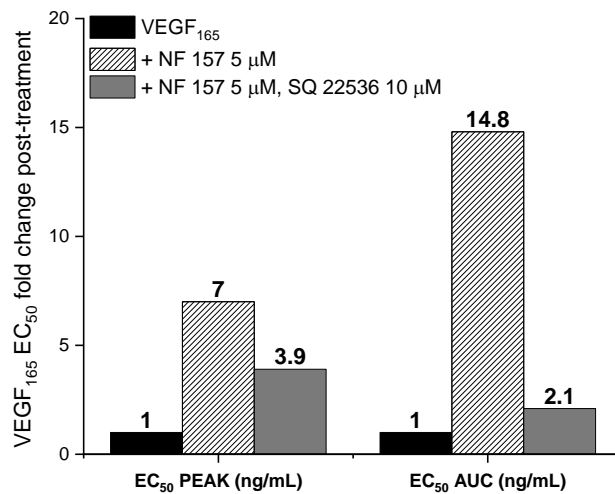


Figure 41. VEGF₁₆₅ potency fold change comparison between the effects of NF157 P2Y11 antagonist and the co-application with SQ 22536 adenylyl cyclase inhibitor in human microvascular endothelial cells (HMEC-1). *(Left)* There was a 7-fold change increase in the VEGF₁₆₅ peak EC₅₀ after 30 minutes of incubation with the NF157 P2Y11 antagonist while the co-preincubation of NF157 P2Y11 antagonist and SQ 22536 adenylyl cyclase inhibitor partially prevented the effect leading to 3.9-fold change potency decrease compared to the control. *(Right)* There was a 14.8-fold change increase in the VEGF₁₆₅ AUC EC₅₀ after 30 minutes of incubation with the NF157 P2Y11 antagonist while the co-preincubation of NF157 P2Y11 antagonist and SQ 22536 adenylyl cyclase inhibitor partially prevented the effect leading to 2.1-fold change potency decrease compared to the control.

3.3.3.8 A2B selective antagonist significantly affected the VEGF₁₆₅-evoked calcium responses of human microvascular endothelial cells (HMEC-1).

As explained in **section 3.3.2.8**, A2B can couple with a G α_q and G α_s -type G protein receptor. When studying the effects of MRS 1754 in the ATP dose-response curve, no significant effects were observed. However, as we just explained in the case of P2Y₁₁, a potential involvement of the AC pathway can be involved in the VEGF₁₆₅-induced calcium responses. Here, we tested the potential inhibition of VEGF₁₆₅-evoked responses using MRS 1754 to elicit any matching behaviour, as seen in the P2Y₁₁ selective inhibition.

The effects of MRS 1754 (100 nM), the selective A2B antagonist, on the VEGF₁₆₅ dose-response curve control (EC₅₀ PEAK: 2.85 ± 1 ng/mL; EC₅₀ AUC: 3.49 ± 1.3 ng/mL) were investigated. Pre-treatment with MRS 1754 right shifted the VEGF₁₆₅ dose-response curve (**Figure 42-A, B**), and reduced the VEGF₁₆₅ potency for the peak (9.28 ± 2.9 ng/mL; p<0.05) but not for the area under the curve (11.6 ± 5.8 ng/mL; *ns*) (**Figure 42-D, Table 6, 7**). Furthermore, the presence of the inhibitor did not affect the control VEGF₁₆₅-evoked maximal response (30 ng/mL VEGF₁₆₅ max^{peak}: 111.6 ± 4.3 %; 100 ng/mL VEGF₁₆₅ max^{AUC}: 100 %) for the peak (101.6 ± 5%; *ns*) or the AUC (100.5 ± 2.8 %; *ns*). As shown in **Figure 42-C**, at 10 ng/mL, in the presence of the antagonist, the response was reduced from 80% in control conditions to approximately 40% above baseline. As a result, we have concluded that MRS 1754 effectively inhibited VEGF₁₆₅-induced responses in HMEC-1 cells.

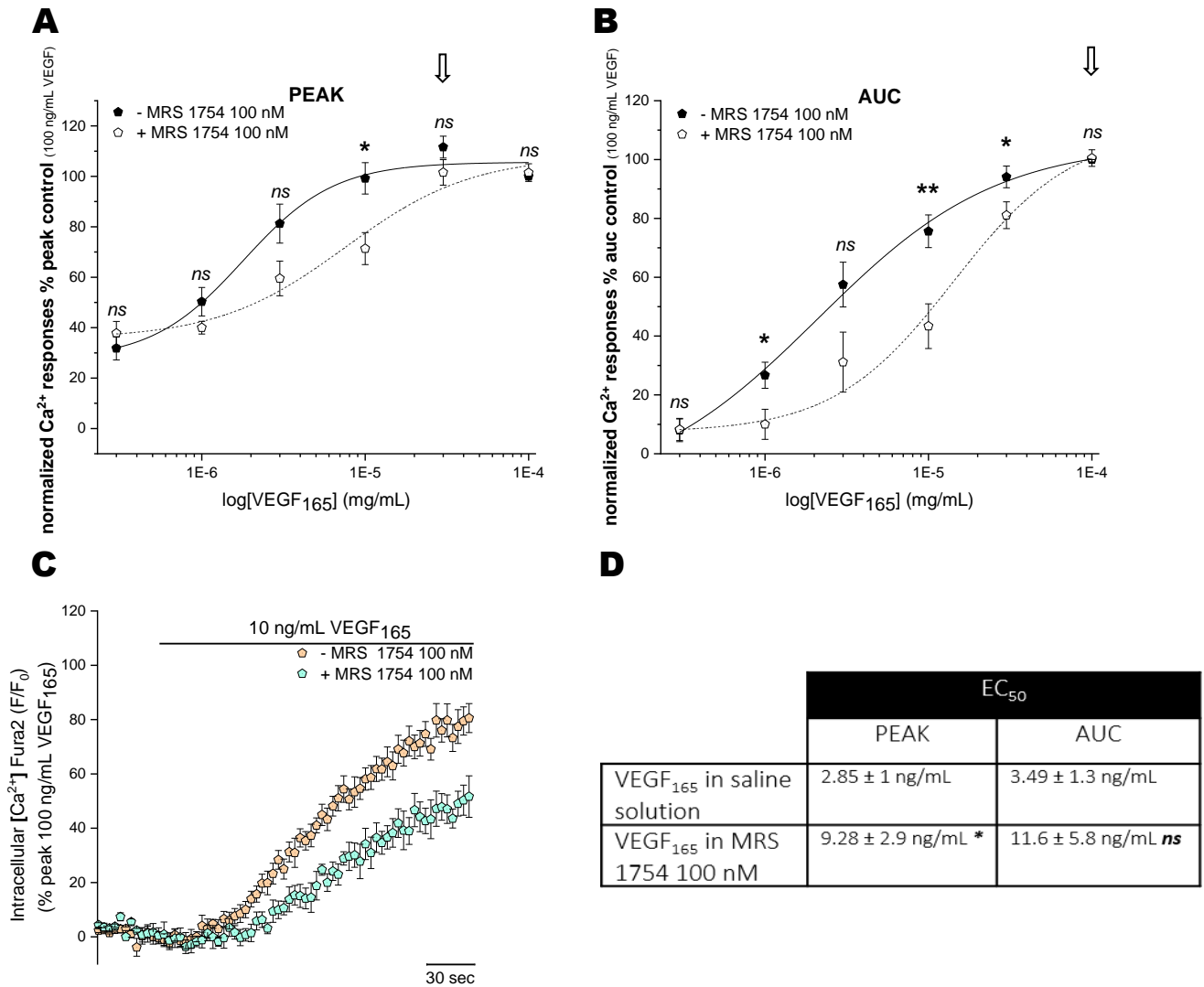


Figure 42. Inhibitory effects of MRS 1754 A2B receptor antagonist on the VEGF₁₆₅-evoked response in human microvascular endothelial cells (HMEC-1). Concentration-response curves for the peak (**A**) and AUC (**B**) magnitude of intracellular Ca^{2+} responses elicited by VEGF₁₆₅ in the presence (0.3-100 ng/mL; open pentagon; $N=10$) or absence (0.3-100 ng/mL; closed pentagon; $N=8$) of MRS 1754 100 nM. (**C**) Averaged time-resolved intracellular Ca^{2+} responses elicited by VEGF₁₆₅ 10 ng/mL in the presence (cyan pentagon; $N=5$) or absence (orange pentagon; $N=8$) of MRS 1754 100 nM over 250 seconds. All data were normalised to 100 ng/mL VEGF₁₆₅ and fit the Hill1 equation with the EC₅₀ values showed in table (**D**). Asterisks show statistical significance relative to VEGF₁₆₅ potency ($p_{ns} > 0.05$, $p^* < 0.05$, $p^{**} < 0.01$, $p^{***} < 0.001$). Data are represented as mean ± SEM.

3.3.4. P2 purinergic receptors protein profile of human microvascular endothelial cells (HMEC-1).

In the previous sections, we described the P2 receptors transcriptome profile in HMEC-1 cells (**section 3.3.1**), as well as tried to gain insights into the four purinergic receptors candidates (P2X4, P2Y2, P2Y1, and A2B) contribution to the ATP- and VEGF₁₆₅-dose response with the pharmacological characterisation described in the previous sections (**sections 3.3.2 and 3.3.3**). Immunoblotting was used to confirm which P2 receptor was expressed at the protein level in HMEC-1 and, thereby, have a tool to interpret the previous results.

3.3.4.1 P2X4 protein expression was not detected in human microvascular endothelial cells (HMEC-1).

RNA sequencing depicted the presence of P2X4 at the mRNA level. However, an ambiguous contribution to the calcium responses was reported. The majority of the P2X4 selective antagonist did not impact either the ATP-evoked calcium responses, but PSB12062 did. Then, to ascertain the protein expression of P2X4, whole-cell P2X4 levels in HMEC-1 were investigated by western blot.

Along with whole-cell lysates of HMEC-1 cells (25 µg), lysates from parental (negative control, -) and stable expressing hP2X4 1321N1 astrocytoma cells (positive control, +) were used to elucidate the presence of P2X4 (**Figure 43**). Parental astrocytoma cells are void of any ATP-induced responses, as shown in **Figure 16** and other previously reported (Bianchi et al., 1999) Therefore, they should be a reasonable negative control of the absence of P2X4. Contrastingly, 1321N1 astrocytoma cells stably expressing hP2X4 demonstrated their ability to evoke ATP responses (**Figure 15**), responses not detected in the untransfected parental cells, giving assurance the response is P2X4 dependent, and the receptor was expressed at the protein level in that cell line.

The expected P2X4 specific band at 60KDa was detected in hP2X4 astrocytoma cells (**Figure 43; Lane 2, + sample**), and that was not the case of the parental astrocytoma cells, where just unspecific banding at lower molecular weights was detected (**Figure 43-Lane 1, - sample**), confirming the ability of the anti-P2X4 antibody (*Alomone, APR-002*) to detect specific P2X4 protein expression. The unspecific banding in the parental astrocytoma was also detected in hP2X4 astrocytoma cells (50 KDa, 30 KDa), but it did not comprise the specific protein detection. HMEC-1 cells sample lane was void of banding, proving the lack of P2X4 protein expression in this cell line (**Figure 43-Lane 3, ? sample**). β-Actin was also immunoblotted as a positive loading control and used to perform the hP2X4 densitometric analysis in the different cells investigated (**Figure 43-B**), as described in the **methods section 2.7.4**. The statistical analysis reported significant differences between the protein expression levels of human P2X4 in hP2X4 astrocytoma cells and parental astrocytoma ($p < 0.05$) and HMEC-1 cells ($P < 0.05$), illustrating the absence of P2X4 protein in HMEC-1 cells.

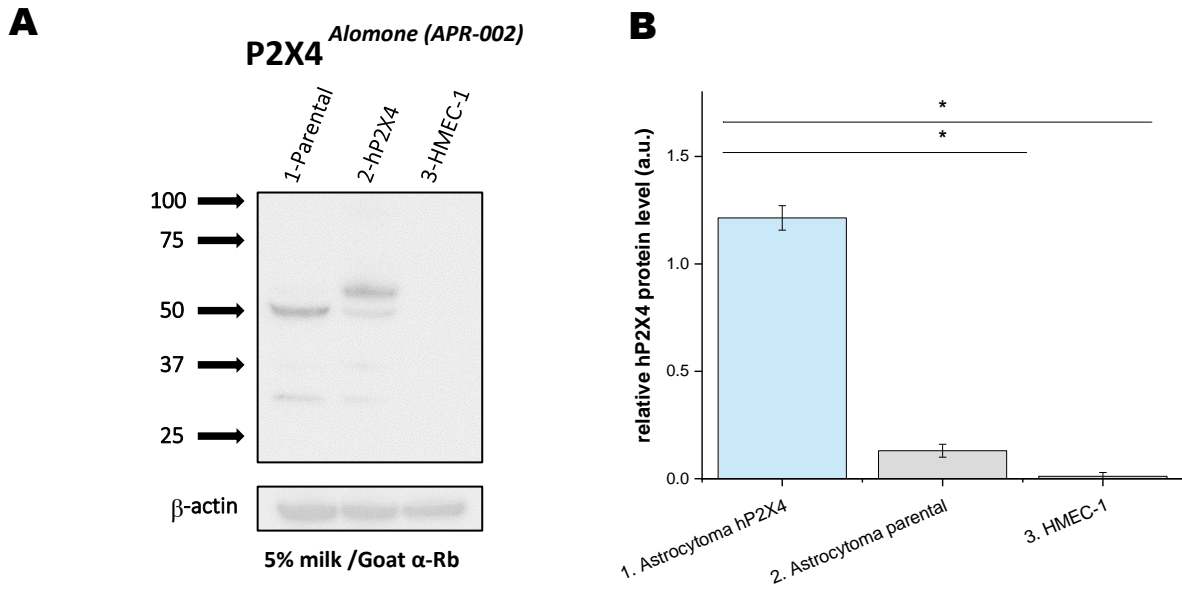


Figure 43. P2X4 is not expressed in human microvascular endothelial cells (HMEC-1) at the protein level (60 KDa). (A) Representative immunoblot for hP2X4 in 1321N1 parental astrocytoma cells (1-Parental, - sample), 1321N1 stable transfected hP2X4 astrocytoma cells (2-hP2X4, + sample) and human microvascular endothelial cells (3-HMEC-1, sample ?). (B) Semi-quantitative immunoblot analysis of relative expression of hP2X4 in studied cells lines. Asterisks show statistical significance relative to P2X4 expression in 1321N1 stable transfected hP2X4 astrocytoma cells (p *ns* > 0.05, p^* < 0.05, p^{**} < 0.01, p^{***} < 0.001). Data are represented as mean \pm SEM ($N=5$).

3.3.4.2 P2Y2 protein expression was ambiguously detected in human microvascular endothelial cells (HMEC-1).

RNA sequencing described the presence of P2Y2 at the mRNA, and AR-C 118925XX, its selective antagonist, impacted the ATP and UTP-evoked calcium responses in a significant manner. Then, to ascertain the protein expression of P2Y2, whole-cell protein levels in HMEC-1 were studied by western blot. As well as whole-cell lysates of HMEC-1 cells (25 µg), lysates from 1321N1 stable expressing hP2X4 or parental astrocytoma cells (negative control, -) were employed to investigate the presence of P2Y2.

The expected P2Y2 specific band at 50KDa was detected in HMEC-1 (**Figure 44; Lane 3 and 4, + sample**) at two different denaturalisation conditions. Nonetheless, that was also the case of the stable expressing hP2X4 1321N1 astrocytoma cells (**Figure 44; Lane 1 and 2, - sample**), illustrating the inability of the anti-P2Y2 antibody (*Alomone*, *APR-010*) to detect specific P2Y2 protein expression. β -Actin was also immunoblotted as a positive loading control and used to perform the hP2Y2 densitometric analysis in the different cells investigated. In this case, relative protein levels were not compared as the western blots simultaneously for both cell lines were repeated twice (N=2; mean \pm SEM) (**Figure 44-B**). The first blot was performed using just HMEC-1 cells (N=1).

Considering these results, a second anti-P2Y2 antibody (*Abcam*, *ab168535*) was tested to prove the protein expression of P2Y2. In the initial phase, different blocking solutions were tested to ensure the best conditions for protein detection using HMEC-1 and parental 1321N1 astrocytoma cells. No bands were detected in HMEC-1 or parental 1321N1 astrocytoma cells (40 µg) (**Figure 45-A, B; N=1**) at two different blocking conditions (10% BSA or 5% milk-based solution). The β -Actin positive loading control confirmed that the Western blot proceeded successfully and the presence of the protein in the PVDF membrane (**Figure 45-A**). However, the expected P2Y2-specific but very faint band at 42 KDa was detected in a non-mammalian 5% sucrose-based blocking solution in both cell lines (**Figure 45-A, B; N=1**).

Then, the sucrose-based blocking solution was the selected one to try to elucidate the specific expression of P2Y2 in HMEC-1, as it was the only one giving bands at the appropriate weight. As in the case of the *Alomone* anti-P2Y2 antibody, the expected P2Y2 specific band at 42KDa was detected in HMEC-1 (**Figure 45-C**) and this it was also the case of the parental 1321N1 astrocytoma cells (**Figure 45-C**). The statistical analysis did not report significant differences between the protein expression levels of human P2Y2 in HMEC-1 and parental astrocytoma cells (*ns*) (**Figure 45-D**), complicating the assessment of P2Y2 protein expression in HMEC-1 cells.

Because of the unexpected protein expression of P2Y2 in parental astrocytoma cells, a third cell line was used to check the antibody specificity one more last time. Non-transfected 293T HEK cell lysate (40 µg) was used as a negative control to test the lack of banding when probing with the P2Y2 *Abcam* antibody, as the manufacturer described in the product datasheet (**Figure 45-E**). Three HEK lysate samples were probed and showed a much fainter banding pattern at the specific P2Y2 expected weight (**Figure 45-E**). The statistical analysis showed significant differences between the protein expression levels of human P2Y2 in non-transfected 293T HEK and HMEC-1 cells ($p < 0.05$), inferring the possibility of the antibody's

ability to detect P2Y2. Furthermore, there was also a statistical difference between non-transfected 293T HEK and parental 1321N1 astrocytoma cells ($p < 0.01$) (**Figure 45-F**), being this result much more challenging to justify.

It is important to note that this last statistical analysis refers to the comparison of 6 different HMEC-1, 4 parental astrocytoma, and 3 non-transfected 293T HEK cell lysates samples (technical repeats) and not biological repeats, as being through this whole study due to the lack of time in the laboratory.

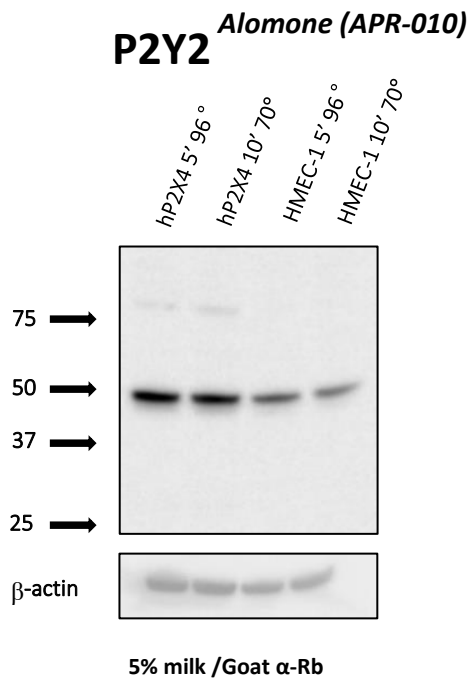
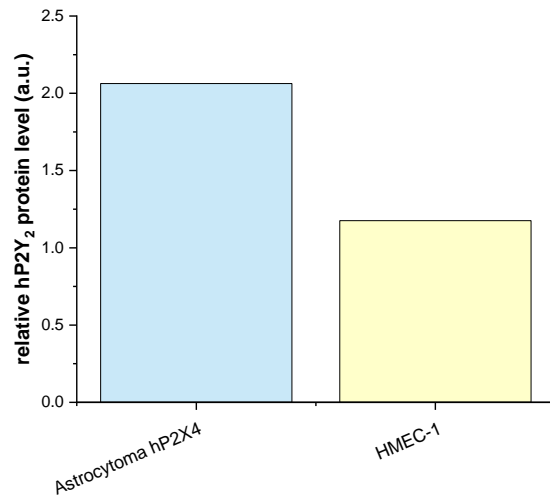
A**B**

Figure 44. Ambiguous P2Y₂ protein expression levels comparison of whole-cell extracts of human microvascular endothelial cells (HMEC-1) and human P2X₄ 1321N1 parental astrocytoma cells using milk-based blocking solution and anti-P2Y₂ antibody from *Alomone (APR-015)* (50 KDa). (A) Representative immunoblot for P2Y₂ in P2X₄ 1321N1 parental astrocytoma cells and human microvascular endothelial cells (HMEC-1). (B) Semi-quantitative immunoblot analysis of relative expression of P2Y₂ in both cell lines. Data are represented as mean ± SEM (N=3).

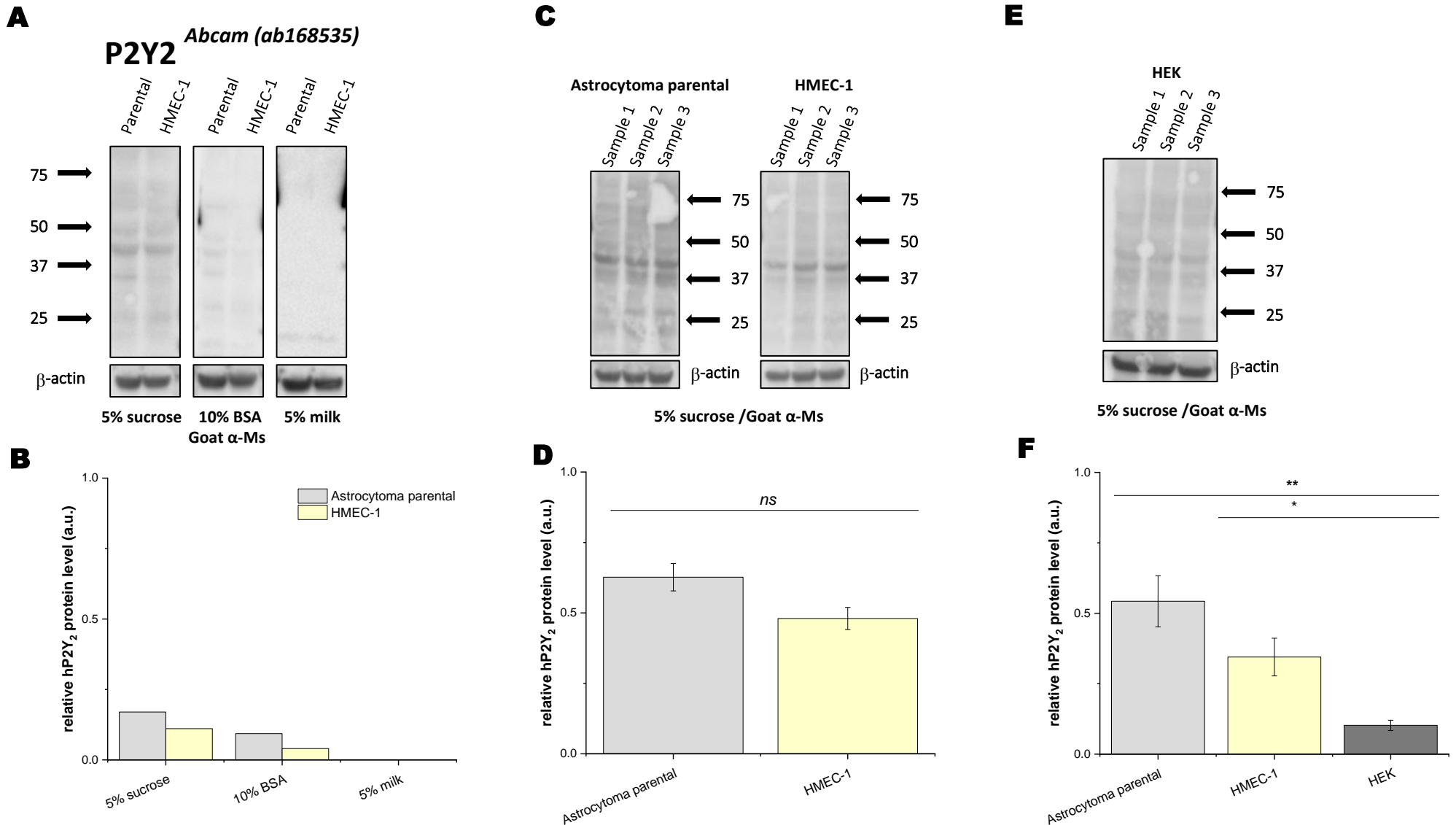


Figure 45. Determination of the blocking solution to use for P2Y₂ protein expression levels comparison of whole-cell extracts of human microvascular endothelial cells (HMEC-1) and human P2X₄ 1321N1 parental astrocytoma cells using anti-P2Y₂ antibody from *Abcam (ab168535)* (42 KDa). (A) Representative immunoblot for P2Y₂ in P2X₄ 1321N1 parental astrocytoma cells and human microvascular endothelial cells (HMEC-1) comparing three different blocking

solutions ($N=1$). **(B)** Semi-quantitative immunoblot analysis of relative expression of P2Y2 in both cell lines for the three different blocking solutions ($N=1$). **(C)** Sucrose-based blocking solution performed better than BSA/sucrose or BSA-based blocking solutions showing bands at the expected weight. **(D)** Semi-quantitative immunoblot analysis of relative expression of P2Y2 in both cell lines in sucrose-based blocking solution ($N=3$). **(E)** Representative immunoblot for P2Y2 in untransfected HEK cells ($N=3$). **(F)** Semi-quantitative immunoblot analysis of relative expression of P2Y2 in the three cell lines in sucrose-based blocking solution ($N=3$). Data are represented as mean \pm SEM ($N=3$).

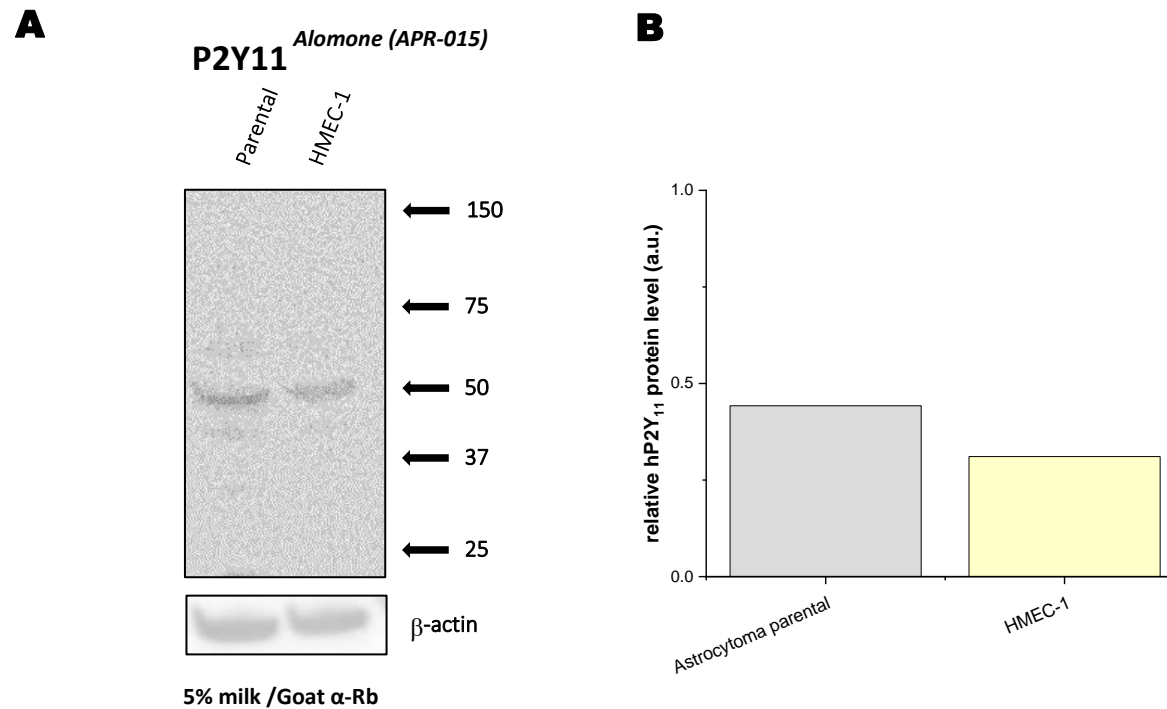


Figure 46. Ambiguous P2Y11 protein expression levels comparison of whole-cell extracts of HMEC-1 and 1321N1 parental astrocytoma cells using milk-based blocking solution and anti-P2Y11 antibody from Alomone (APR-015) (50 KDa). **(A)** Representative immunoblot for P2Y11 in 1321N1 parental astrocytoma cells and human microvascular endothelial cells (HMEC-1). **(B)** Semi-quantitative immunoblot analysis of relative expression of P2Y11 in both cell lines. Data are represented as mean \pm SEM ($N=3$).

3.3.4.3 P2Y11 protein expression was detected in human microvascular endothelial cells (HMEC-1).

RNA sequencing also described the presence of P2Y11 at the mRNA, and NF157, its selective antagonist, impacted significantly the VEGF₁₆₅ but not the ATP-evoked calcium responses. Then, to verify the protein expression of P2Y11, whole-cell protein levels in HMEC-1 cells were investigated by immunoblot. As well as whole-cell lysates of HMEC-1 cells (25 µg), lysates from 1321N1 parental astrocytoma cells (negative control, -) were utilized to explore the presence of the receptor.

Firstly, as previously described for P2Y2, the anti-P2Y11 *Alomone* (APR-015) antibody was probed due to its availability in-house. The expected P2Y11-specific band at 50KDa was detected in HMEC-1 and this was also the case in the 1321N1 astrocytoma parental cells (**Figure 46**), depicting again the incapability of the anti-P2Y11 antibody (*Alomone*, APR-015) to detect specific P2Y11 protein expression. In this case, relative protein levels were not compared as the western blots simultaneously for both cell lines were repeated twice. The first blot used hP2X4 1321N1 astrocytoma cells instead of parentals as a theoretical negative control. Therefore, the comparison shown in **Figure 46-B** is a representative plot of an independent technical repeat. Again, as in the case of P2Y2, these results complicated the assessment of P2Y11 protein expression in HMEC-1 cells.

A second anti-P2Y11 antibody (*Abcam*, ab180739) was tested to prove the protein expression of P2Y11. In the initial phase, different blocking solutions were tested to ensure the best conditions for protein detection using HMEC-1 and parental 1321N1 astrocytoma cells. No bands were detected in HMEC-1 or parental 1321N1 astrocytoma cells using a milk-based blocking solution at two different denaturalisation conditions and total protein lysate concentrations (**Figure 47-A**). That was the case, too, when using two different BSA-based blocking solutions (1% BSA/10% sucrose and 10% BSA solution) (**Figure 47-B, C**) and the commercial EveryBlot® blocking buffer from Bio-Rad (**Figure 47-E**). The β-Actin positive loading controls confirmed that the Western blot proceeded successfully and the presence of the protein in the PVDF membrane. Surprisingly, the expected P2Y11-specific but faint band at 43 KDa was detected in a non-mammalian 5% sucrose-based blocking solution in both cell lines (**Figure 47-B, C**). Therefore, the sucrose-based blocking solution was the selected one to clarify the specific expression of P2Y11 in HMEC-1, as it was the only one giving bands at the appropriate weight. Using fresh lysate samples (50 µg), the expected P2Y11-specific band at 43 KDa was detected in HMEC-1 (**Figure 48-A**), and this was also the case in the parental 1321N1 astrocytoma cells but in a significantly lower fashion when using fresh lysate samples. The statistical evaluation of the densitometric analysis reported significant differences between the protein expression levels of human P2Y11 in HMEC-1 and parental astrocytoma cells ($p < 0.05$) (**Figure 48-B**), figuring a specific significant P2Y11 protein expression in HMEC-1 cells.

An anti-rabbit HRP conjugated secondary antibody was used in these western blots. This antibody detects heavy and light chains of the primary antibody. To investigate further the presence of bands in the astrocytoma parental negative control, we hypothesised that the unexpected banding could be derived from non-specific secondary antibody detection. To test that, two lysate samples, one for HMEC-1 and the other for parental astrocytoma cells, were

probed with the secondary antibody directly after blocking. In this way, the membrane was never exposed to a primary antibody, and no banding should be detected. However, non-specific signals were detected in both lysate samples (**Figure 48-C, D**). Therefore, some detected signals in these conditions might come from the secondary antibody non-specific signalling. Suppose we subtract this signalling (**Figure 48-D**) from the primary antibody probed blot (**Figure 48-B**), the remaining signals will illustrate a minimal banding presence for astrocytoma parental cells and a detectable remaining banding for HMEC-1 cells.

Another type of HRP-conjugated secondary antibody (anti-rabbit F(ab')₂) was available in-house, and it was also tested to check if it could reduce the non-specific secondary antibody previously detected. Again, two lysate samples of each cell line were probed with the secondary antibody directly after 5% sucrose-based blocking. Anti-rabbit F(ab')₂ antibody detected low molecular weight bands of approximately 30 KDa, as well as non-specific bands at approximately 40 and 50 KDa, that could be misinterpreted as P2Y₁₁-specific 43 KDa band (**Figure 47-D**). Therefore, this secondary antibody was not further considered an alternative to the regular HRP-conjugated secondary antibody.

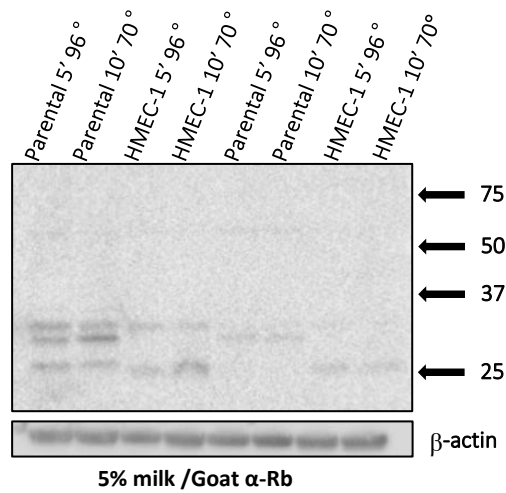
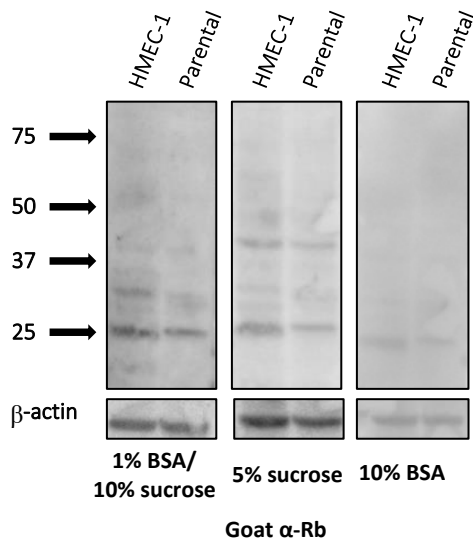
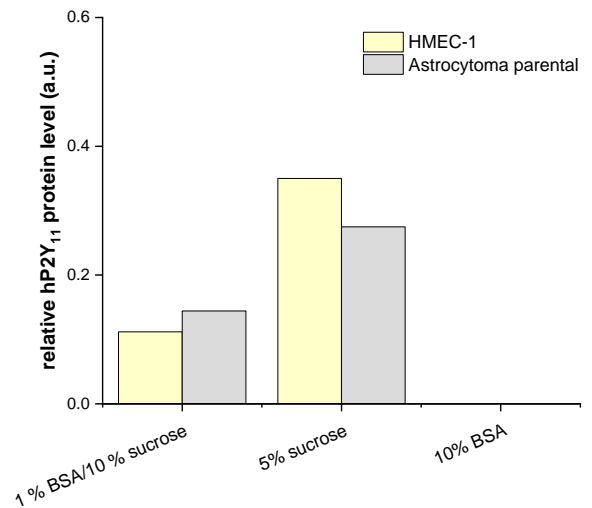
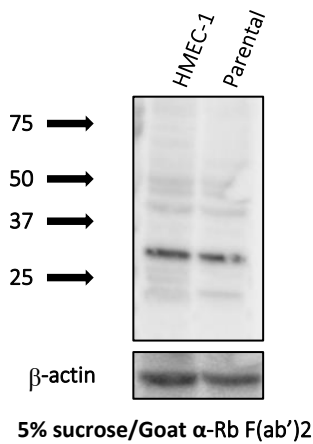
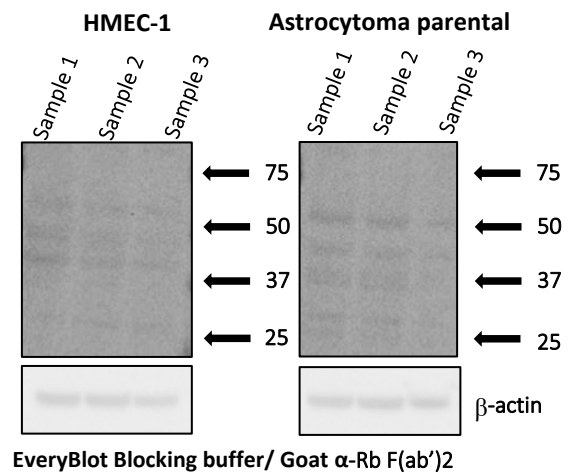
A**P2Y₁₁** *Abcam (ab180739)***B****C****D****E**

Figure 47. Determination of which blocking solution to use for P2Y₁₁ protein expression levels comparison of whole-cell extracts of HMEC-1 and 1321N1 parental astrocytoma cells with anti-P2Y₁₁

antibody from Abcam (ab180739) (43 KDa). (A) Lack of specificity for P2Y11 Abcam antibody when using milk-based blocking solution and goat anti-rabbit secondary antibody at different boiling conditions in 1321N1 astrocytoma and HMEC-1 cells. (B) Sucrose-based blocking solution performed better than BSA/sucrose or BSA-based blocking solutions showing bands at the expected weight. (C) Semi-quantitative immunoblot analysis of relative expression of P2Y11 in these previous blocking solutions, being sucrose-based solution the one showing desired relative expression of P2Y11. (D) Lack of specificity for P2Y11 in 1321N1 parental astrocytoma and human microvascular endothelial (HMEC-1) cells in sucrose-based blocking solution and goat anti-rabbit F(ab')₂ secondary antibody. (E) Lack of specificity for P2Y11 Abcam antibody when using EveryBlot blocking solution and goat anti-rabbit F(ab')₂ secondary antibody in 3 samples of 1321N1 astrocytoma and HMEC-1 cells.

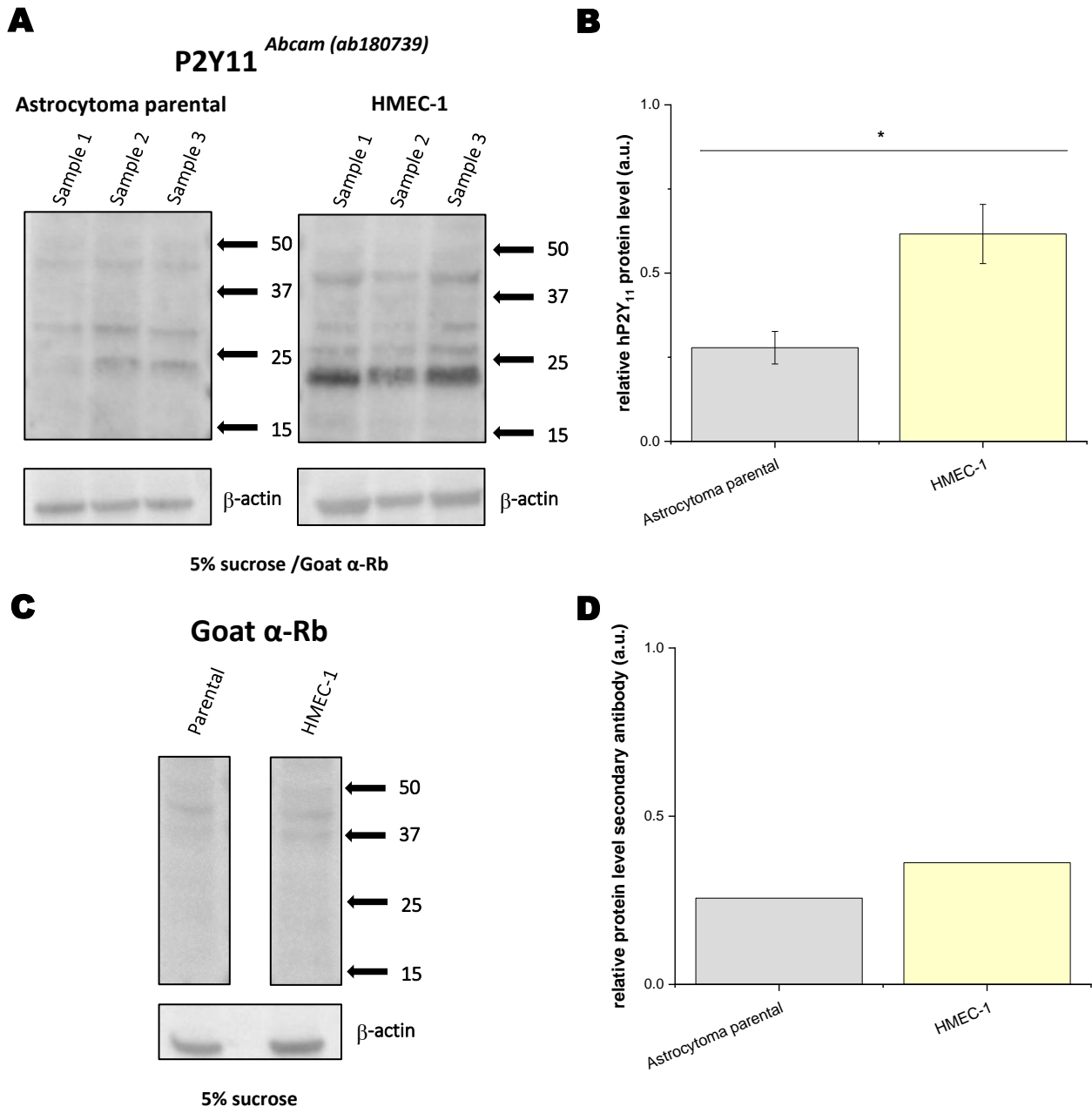


Figure 48. P2Y11 is expressed in human microvascular endothelial cells (HMEC-1) at the protein level (43 KDa). (A) Representative immunoblot of the P2Y11 protein expression levels comparison of 3 different biological whole-cell extracts of human microvascular endothelial cells (HMEC-1) and 1321N1 parental astrocytoma cells using sucrose-based blocking solution and anti-P2Y11 antibody from *Abcam (ab180739)*. (B) Semi-quantitative immunoblot analysis of relative expression of P2Y11 in both cells lines. (C) Representative immunoblot of protein sample in secondary antibody for studying unspecific background bands. (D) Semi-quantitative immunoblot analysis of relative expression of secondary antibody-derived bands. Asterisks show statistical significance relative to P2Y11 expression in 1321N1 astrocytoma cells ($p_{ns} > 0.05$, $p^* < 0.05$, $p^{**} < 0.01$, $p^{***} < 0.001$). Data are represented as mean \pm SEM ($N=3$ technical repeats).

3.3.5. Purinergic receptor mRNA expression profile of human umbilical vein endothelial cells (HUVECs).

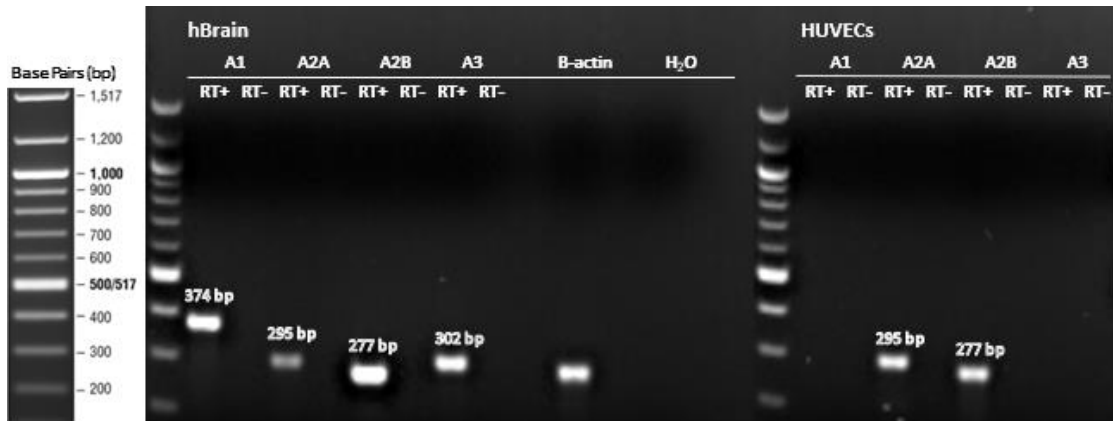
Human umbilical vein endothelial cells (HUVECs) are primary cells isolated from the umbilical cord, and they are considered a good in-vitro model for studying human vascular endothelial physiology. HUVECs have been previously used as a tool to characterise VEGF-dependent calcium responses and the relevance of other membrane receptors to vascular endothelial growth factor (VEGF) physiology (J. Li et al., 2015; Li et al., 2011). We found interesting to investigate the VEGF P2Y₁₁-dependent responses, as previously documented in HMEC-1 cells, in a primary cell line as the next stage in this study. For this, the first step was to characterise at the mRNA level the presence of P2Y₁₁ and the other purinergic receptors in HUVECs, as the expression pattern might affect the output of the investigating responses.

Initial studies were performed in human brain to confirm specificity and functionality of the primers. Once the primers were validated as useful tool for this study, every technical repeat was designed to run in parallel a known positive human brain cDNA sample with a HUVEC sample for each gene in study. In addition, β -Actin, the housekeeping gene served as a positive control for all the PCR reactions. β -Actin detection was even more relevant in the assays where the interrogated gene was not detected since detecting the housekeeping gene in HUVECs demonstrated a good quality cDNA and not just the well-performed PCR reaction. A non-reverse transcriptase enzyme control was performed for each gene to control cDNA-specific derived band and not genomic DNA contamination. Besides this control, negative water control was done in every PCR run, where the cDNA was substituted by water and exposed to the transcriptase enzyme as the interrogated samples to ensure the sampling was not contaminated with an unknown and non-desired cDNA.

Following the validation of the primers, the expression of purinergic receptors mRNA transcripts was examined. **Table 8** and **Figures 49** and **50** summarize the results obtained for this profiling.

Table 8. Non quantitative RT-PCR expression profile of purinergic receptors in human brain and umbilical vein endothelial cells (HUVEC). A ✓ means gene was detected, a (✓) means the gene is detected but not consistently, and × means the gene was not detected, as shown in Figures 49 and 50.

| Gene | Human brain | Human umbilical vein endothelial cells, HUVEC |
|-------|-------------|---|
| A1 | ✓ | × |
| A2A | ✓ | ✓ |
| A2B | ✓ | ✓ |
| A3 | ✓ | × |
| P2X1 | (✓) | × |
| P2X2 | ✓ | × |
| P2X3 | (✓) | × |
| P2X4 | ✓ | ✓ |
| P2X5 | ✓ | ✓ |
| P2X6 | ✓ | × |
| P2X7 | ✓ | ✓ |
| P2Y1 | ✓ | ✓ |
| P2Y2 | ✓ | ✓ |
| P2Y4 | ✓ | ✓ |
| P2Y6 | ✓ | ✓ |
| P2Y11 | ✓ | (✓) |
| P2Y12 | ✓ | ✓ |
| P2Y13 | ✓ | × |
| P2Y14 | ✓ | ✓ |

A**B****C**

*hBrain (B); HUVECs (H)

Figure 49. Non-quantitative RT-PCR expression profile of adenosine and P2X receptors in human brain and HUVEC cells. (A) Detection of adenosine (P1) receptors expression showing bands detected for ADORA1 (A1) (374 bp), ADORA2A (A2A) (295 bp), ADORA2B (A2B) (277 bp) and ADORA3 (A3) (302 bp) in human brain and ADORA2A (A2A) (295 bp) while ADORA2B (A2B) (277 bp) were detected in HUVEC ($N=5$). **(B)** Detection of P2X1-3 expression showing bands for P2X1 (341 bp), P2X2 (200 bp) and P2X3 (564 bp) in human brain. None of these receptors were detected in HUVECs. **(C)** Detection of P2X4-7 expression showing bands for P2X4 (250 bp), P2X5 (263 bp), P2X6 (405 bp) and P2X7 (414 bp) in human brain while P2X4 (250 bp), P2X5 (263 bp) and P2X7 (414 bp) were detected in HUVECs ($N=3$). Primers amplify all splicing variants of the selected gene. *RT+*, reverse transcriptase cDNA samples; *RT-*, no reverse transcriptase enzyme control samples.

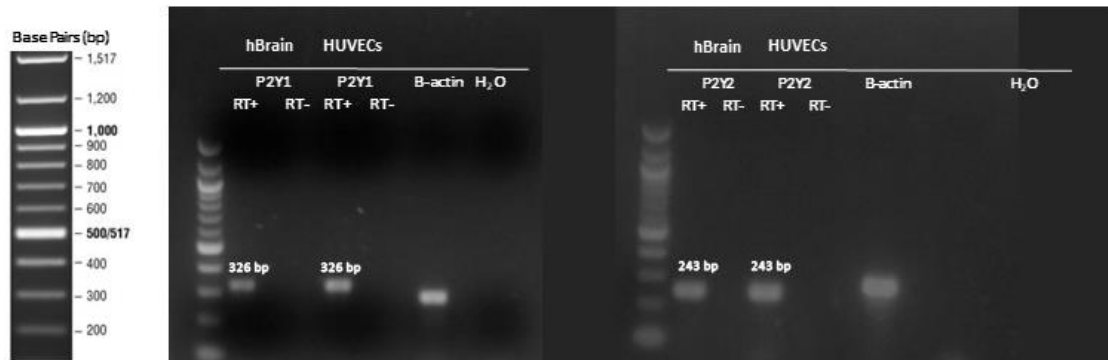
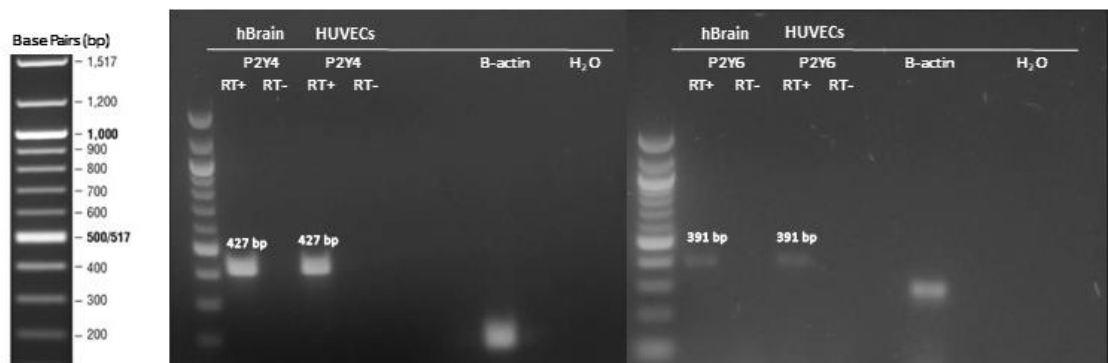
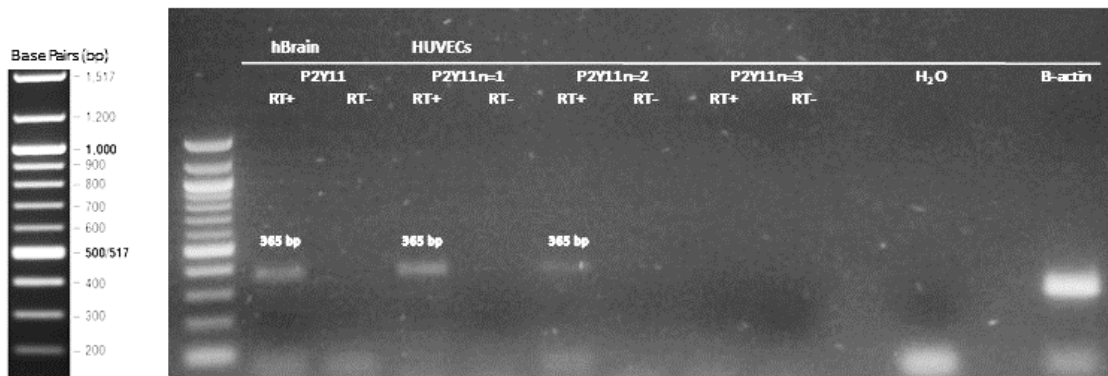
A**B****C****D**

Figure 50. Non-quantitative RT-PCR expression profile of P2Y receptors in human brain and umbilical vein endothelial cells (HUVEC). (A) Detection of P2Y1 and P2Y2 purinoreceptors expression showing bands for P2Y1 (326 bp) and P2Y2 (243 bp) in human brain and HUVECs. (B) Detection of P2Y4 and P2Y6 purinoreceptors expression showing bands for P2Y4 (427 bp) and P2Y6 (391 bp) in human brain and HUVECs. (C) Detection of P2Y11 expression showing a band (365 bp) in human brain. In HUVECs, two out of three independent samples showed a band (365 bp). (D) Detection of P2Y12-13 purinoreceptors expression showing bands detected for P2Y12 (698 bp), P2Y13 (461 bp) and P2Y14 (370 bp) in human brain while P2Y12 (698 bp) and P2Y14 (370 bp) were detected in HUVECs (*N*=3). Primers amplify all splicing variants of the selected gene. *RT+*, reverse transcriptase cDNA samples; *RT-*, no reverse transcriptase enzyme control samples.

As shown in **Table 8** and **Figure 49**, non-quantitative analysis of mRNA transcripts revealed that HUVEC cells expressed two P1 receptor subtypes, A2A and A2B (**Figure 49-A**), and three P2X receptors, P2X4, P2X5 and P2X7 (**Figure 49-B, C**). Remarkably, P2X1 and P2X3 were not consistently detected, meaning the detection of the band in the human brain fluctuated. However, a band in a HUVEC sample was never detected in P2X1 or P2X3 positive human brain assays.

Almost all P2Y receptors but P2Y13 were detected (**Table 8, Figure 50**). However, P2Y11 demonstrated an inconsistent expression pattern in HUVEC cells. Two technical repeats with three distinct biological samples each showed specific bands for P2Y11 in 2 out of the 3 biological repeats (**Figure 50-C**). This lack of consistency suggests low receptor expression even though P2Y11 could yet potentially contribute to the VEGF calcium responses.

3.3.6. Characterisation of the vascular endothelial growth factor calcium signalling in human umbilical vein endothelial cells (HUVECs).

The mRNA expression profile of the vascular endothelial growth factor receptors could not be performed in HUVECs due to the lack of time for this study. However, there is substantial literature supporting VEGFR-2 as the mediator of the VEGF-dependent calcium responses in this cell line (J. Li et al., 2015; Li et al., 2011). Thus, we directly performed the pharmacological profiling upon VEGF₁₆₅ stimulation.

3.3.6.1 VEGF₁₆₅-evoked calcium responses in human umbilical vein endothelial cells (HUVECs).

VEGF₁₆₅ elicited intracellular calcium response in a concentration-dependent manner (0.3 to 100 ng/mL) with maximal activity at 10 ng/mL for the peak ($148.85 \pm 17.9\%$) and at 30 ng/mL for the area under the curve (AUC) ($125.89 \pm 10.45\%$). The peak's calculated half-maximal effective concentration (EC₅₀) was 1.7 ± 0.4 ng/mL for the peak and 2.4 ± 0.4 ng/mL for the AUC (**Figure 51-A, B**). **Figure 51-C** depicts time-resolved calcium responses upon VEGF₁₆₅ stimulation from 0.3 to 100 ng/mL. This stimulation elicited a relatively rapid and sustained response at high ligand concentrations (10 to 100 ng), but this kinetic fashion was lost at concentrations lower than 10 ng/mL. From 0.3 to 3 ng/mL, VEGF₁₆₅ did not elicit a rapid response. However, it was characterised by a delayed, slower, and more sustained calcium release over four minutes, with the peak response observed towards the end of the response. Thereby, we confirmed the ability of HUVECs to respond to the ligand and evoke VEGF₁₆₅-dependent calcium responses.

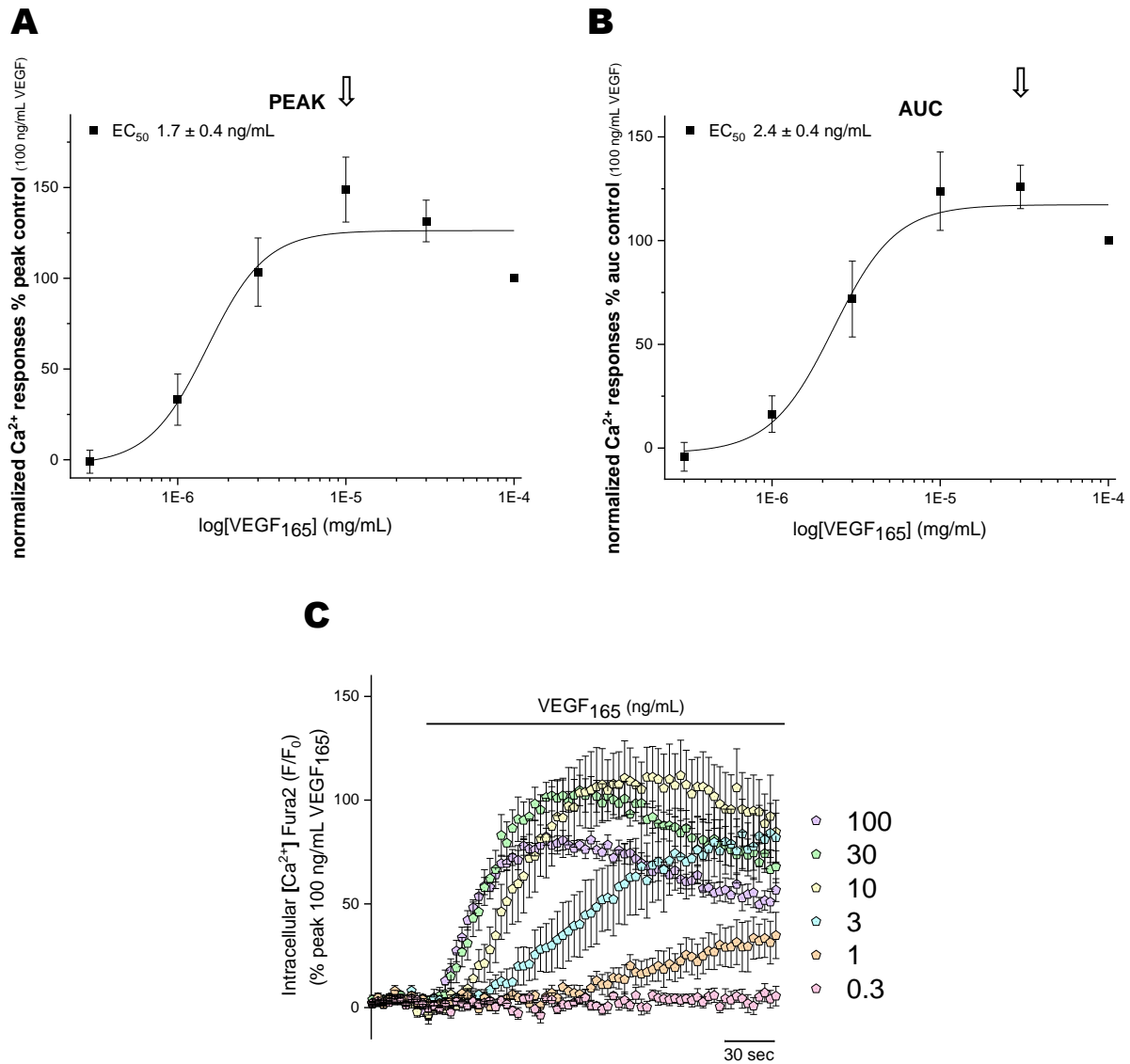


Figure 51. VEGF₁₆₅ elicits intracellular calcium responses in human umbilical vein endothelial cells (HUVEC). Concentration-response curves for the peak (A) and AUC (B) magnitude of intracellular Ca²⁺ responses elicited by VEGF₁₆₅ (0.3-100 ng/mL; *N*=6). (C) Averaged time-resolved intracellular Ca²⁺ responses elicited by VEGF₁₆₅ from 0.3 ng/mL to 100 ng/mL in HUVEC cells over 250 seconds (*N*=6). All data were normalised to 100 ng/mL VEGF₁₆₅ and fit the Hill1 equation with the EC₅₀ values showed in the graphs. Data are represented as mean ± SEM.

(*) Data normalisation was always done at 100 ng/mL VEGF₁₆₅ when this agonist was studied.

(**) Arrows (↓) indicate the maximum response in the control (untreated) curve.

(***) F/F₀ refers to the Fura2 ratio, meaning F340/F380.

3.3.6.2 The broad-spectrum P2 antagonist, PPADS, affected the VEGF₁₆₅-evoked calcium responses of human umbilical vein endothelial cells (HUVECs).

In HMEC-1 cells, the broad-spectrum P2 antagonist, PPADS, had a significant impact on the VEGF₁₆₅-evoked calcium responses, and therefore, it was proposed to investigate the potential same effect in HUVECs. Due to the difficulties in the HUVECs' availability and their culturing times, this assay was performed just once as a proof of concept.

Pre-treatment with PPADS also right-shifted the VEGF₁₆₅ dose-response curve as in the case of the HMEC-1 cells (**Figure 52**). Preliminarily, the presence of PPADS reduced the VEGF₁₆₅-evoked maximal control response for the peak at 10 ng/mL (VEGF_{max}^{PEAK} 58.20 ± 6.61) but not for the AUC at 30 ng/mL VEGF_{max}^{AUC} 112.23 ± 14.4). The representative time-resolved intracellular calcium responses shown in **Figure 52-C** illustrated PPADS' impact on the peak and the area under the curve upon 10 ng/mL VEGF₁₆₅ stimulation compared with the control. In the presence of PPADS, the activation kinetics at 10 ng/mL VEGF₁₆₅ conserved its relatively rapid calcium increase kinetics but with a larger decrease in the peak, which reached approximately 50% above baseline compared to the VEGF response in the absence of the antagonist, which reached almost 110%.

Considering these results as a positive proof of concept, we moved forward to investigate the possible involvement of P2Y11.

3.3.6.3 P2Y11 selective antagonist did not affect the VEGF₁₆₅-evoked calcium responses of human umbilical vein endothelial cells (HUVECs).

In the same way as in **section 3.3.2** and **3.3.3**, the selective competitive antagonist, NF157, was utilised to determine if P2Y11 was involved in the VEGF₁₆₅-evoked calcium responses in HUVECs.

The effects of NF157 (5 µM) on the VEGF dose-response curve control (EC₅₀^{PEAK}: 1.7 ± 0.4 ng/mL; EC₅₀^{AUC}: 2.4 ± 0.4 ng/mL) were examined. Isolated significant effects were found at 100 ng/mL in the peak and the area under the curve when comparing the cells in the presence or the absence of the P2Y11 inhibitor and the control VEGF-evoked maximal response at 10 ng/mL for the peak and 30 ng/mL for the AUC were unchanged (**Figure 52-A, B**). In addition, upon treatment, the potencies were also unaffected (EC₅₀^{PEAK}: 1.55 ± 0.17 ng/mL; *ns*; EC₅₀^{AUC}: 1.6 ± 0.2 ng/mL; *ns*) (**Figure 52-D**). The representative time-resolved intracellular calcium responses in **Figure 52-C** documented the described isolated potentiation effects at the higher concentration of 100 ng/mL. These changes represented potentiation effects and did not follow a trend, considering them challenging to interpret. As a result, we concluded that 5 µM NF157 was ineffective in inhibiting VEGF-induced responses in HUVECs as it did in HMEC-1 cells.

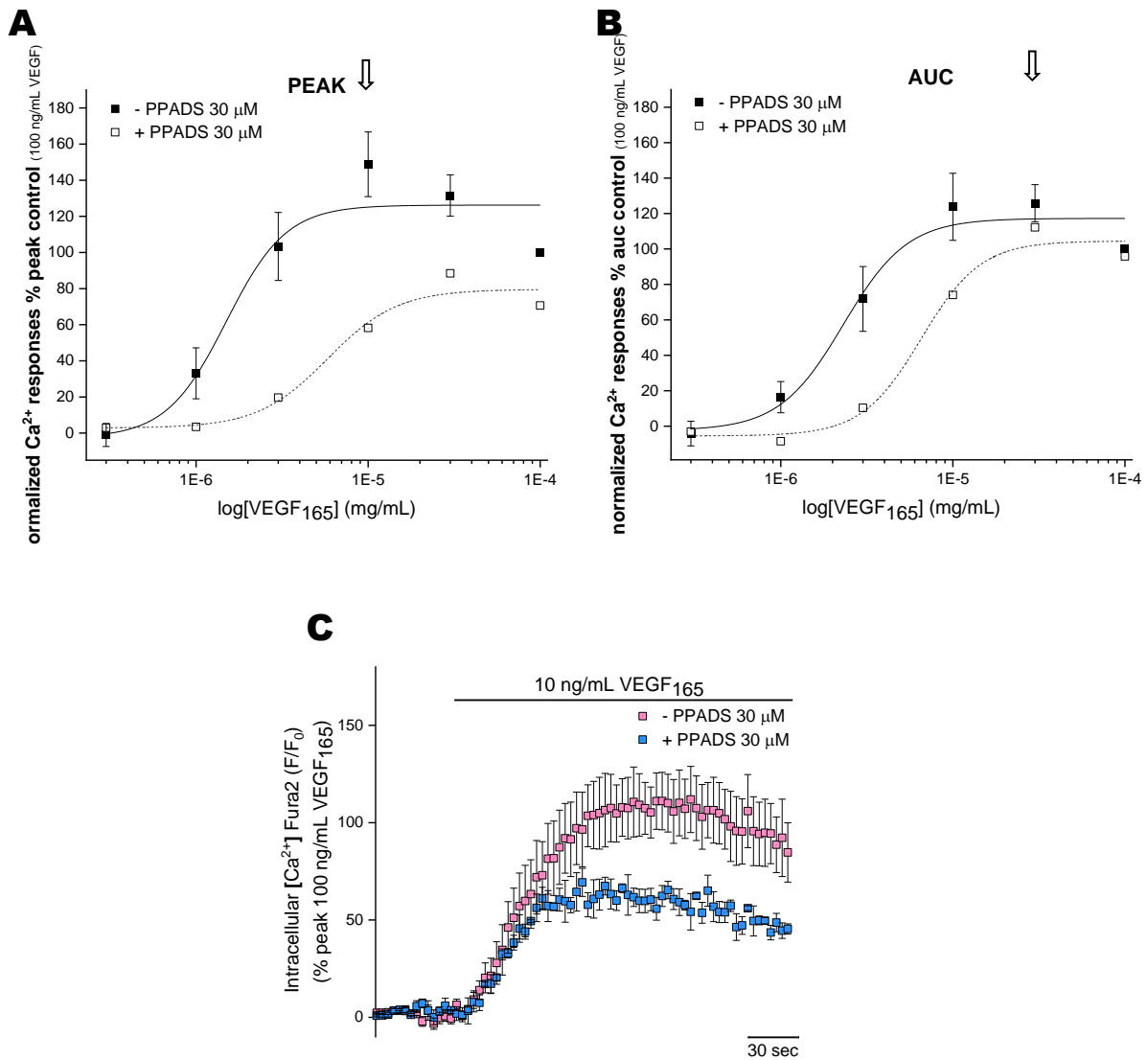


Figure 52. Preliminary inhibitory effects of broad-spectrum P2 receptors antagonist PPADS on the VEGF₁₆₅-evoked response in human umbilical vein endothelial cells (HUVEC). Concentration-response curves for the peak (A) and AUC (B) magnitude of intracellular Ca^{2+} responses elicited by VEGF₁₆₅ in the presence (0.3-100 ng/mL; open pentagon; $N=1$) or absence (0.3-100 ng/mL; closed pentagon; $N=6$) of PPADS 100 μM . (C) Averaged time-resolved intracellular Ca^{2+} responses elicited by VEGF₁₆₅ 10 ng/mL in the presence (blue square; $N=1$) or absence (pink square; $N=6$) of PPADS 100 μM over 250 seconds. All data were normalised to 100 ng/mL VEGF₁₆₅ in saline solution and fit the Hill1 equation. Data are represented as mean \pm SEM.

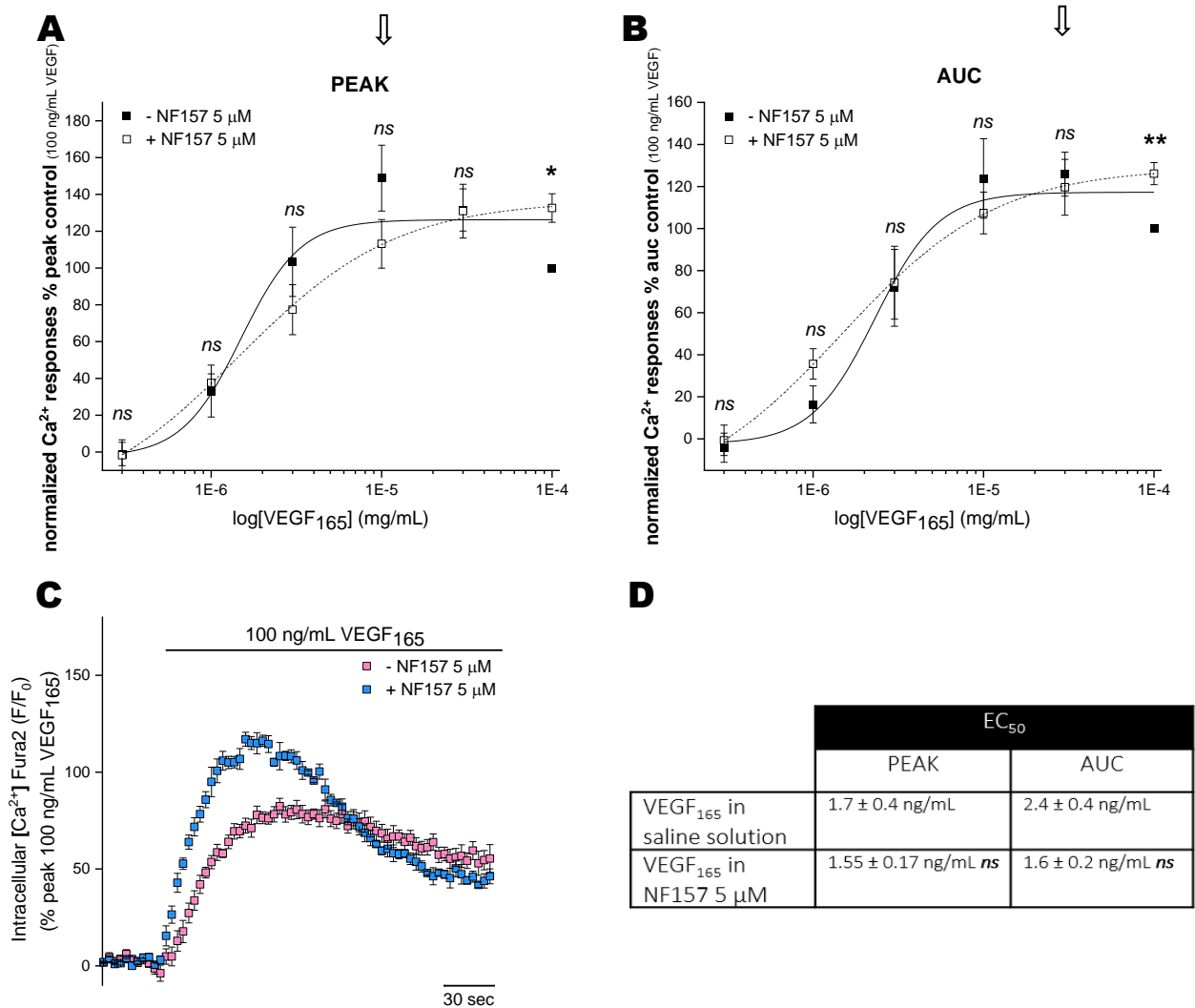


Figure 53. Lack of inhibitory effects of NF157 P2Y11 receptor antagonist on the VEGF₁₆₅-evoked response in human umbilical vein endothelial cells (HUVEC). Concentration-response curves for the peak (A) and AUC (B) magnitude of intracellular Ca²⁺ responses elicited by VEGF₁₆₅ in the presence (0.3-100 ng/mL; open pentagon; N=3) or absence (0.3-100 ng/mL; closed pentagon; N=6) of NF157 5 μM . (C) Averaged time-resolved intracellular Ca²⁺ responses elicited by VEGF₁₆₅ 10 ng/mL in the presence (blue square; N=3) or absence (blue square; N=6) of NF157 5 μM over 250 seconds. All data were normalised to 100 ng/mL VEGF₁₆₅ and fit the Hill1 equation with the EC₅₀ values showed in table (D). Asterisks show statistical significance relative to VEGF₁₆₅ potency (*p ns* > 0.05, *p** < 0.05, *p*** < 0.01, *p**** < 0.001). Data are represented as mean ± SEM.

3.3.6.4 VEGF₁₆₅ kinetics profile differed between human umbilical vein endothelial cells (HUVECs) and human microvascular endothelial cells (HMEC-1), and this response is characteristic of endothelial cells.

Considering the recent findings, a comparative analysis of the VEGF₁₆₅ responses of the two distinct endothelial cell lines was conducted in an attempt to identify differences that might elucidate their disparate behaviour.

Figure 54-A, B showed the concentration-response curve for VEGF₁₆₅ in HUVEC and HMEC-1 cells. As was already portrayed, VEGF₁₆₅ elicited a concentration-dependent increase in intracellular calcium levels in both cell lines, but there were the HUVEC cells the ones demonstrating higher potency (EC₅₀ PEAK: 1.71 ± 0.35 ng/mL; EC₅₀ AUC: 2.20 ± 0.46 ng/mL) and efficacy (maximal response at 10 ng/mL significantly higher; $p < 0.05$) than HMEC-1 cells (EC₅₀ PEAK: 2.87 ± 1 ng/mL; EC₅₀ AUC: 3.55 ± 1.32 ng/mL). When comparing the potencies between cell lines, significance was not achieved; however, a higher sensitivity pattern can be observed in **Figure 54-E**. Raw data comparisons are tough as errors tend to be higher and demonstrate significance become intricate. The slope compares the steepness of the dose-response curves. HUVEC dose responses illustrated steeper curves than HMEC-1, also suggesting greater sensitivity to changes in VEGF₁₆₅ concentration. The representative calcium time-responses curves at 10 ng/mL (**Figure 54-C**) and 30 ng/mL (**Figure 54-D**) illustrated the difference in the trace kinetics in the cell lines. HUVECs presented a much more rapid but sustained response, while HMEC-1 showed a sustained calcium response characterised by its late peak. This data portrayed the idea that HUVEC responses have a more outstanding contribution to the calcium release from the stores than HMEC-1 cells, even though previous results suggest the involvement of this pathway in both cell lines' VEGF₁₆₅-dependent responses.

VEGF₁₆₅ dependent biological responses are meant to be characteristic of endothelial cells. To confirm these responses are cell type specific, a double-check was performed exposing 1321N1 human P2X4 stably expressing astrocytoma cells to this agonist (**Figure 55**). At 100 ng/mL VEGF₁₆₅, this cell line could not induce any intracellular calcium responses. In contrast, the response to 30 μ M ATP demonstrated the cells' viability and responsiveness, confirming their ability to respond to an agonist (**Figure 55-A**). The responses to VEGF₁₆₅ did not differ from the vehicle control response control, illustrating the cells' incapacity to respond to the ligand (**Figure 55-B**). Statistical significance is not shown as the experiments were performed just twice.

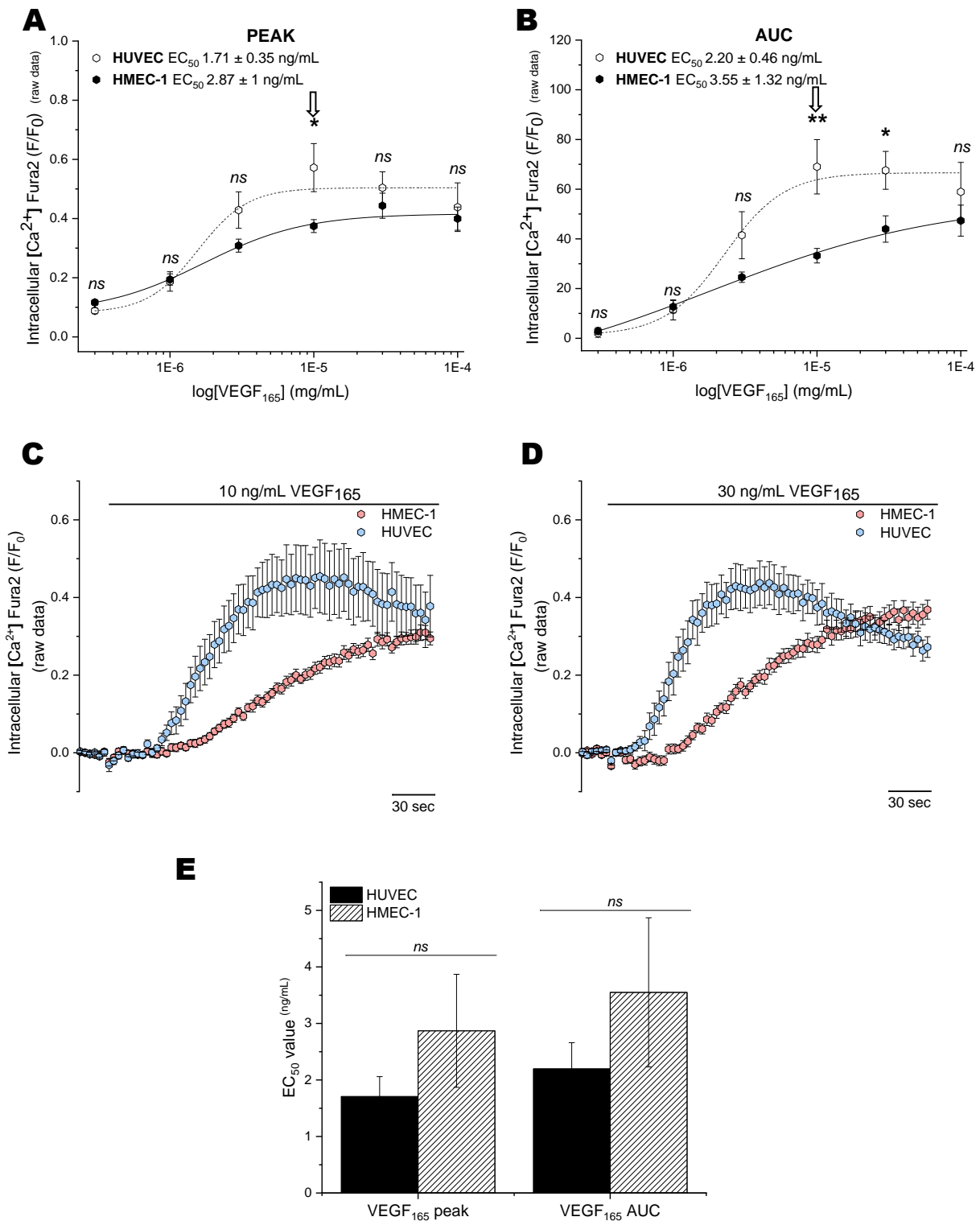


Figure 54. VEGF₁₆₅'s kinetics profile varied between human umbilical vein endothelial cells (HUVECs) and human microvascular endothelial cells (HMEC-1). Concentration-response curves for the peak (A) and AUC (B) magnitude of intracellular Ca²⁺ responses elicited by VEGF₁₆₅ in HUVEC cells (0.3-100 ng/mL; open circles; N=6) and HMEC-1 (0.3-100 ng/mL; closed circles; N=8). All data fit the Hill1 equation with the EC₅₀ values showed in the graphs. Averaged time-resolved intracellular Ca²⁺ responses elicited by VEGF₁₆₅ (C) 10 ng/mL and (D) 30 ng/mL in HMEC-1 (pink hexagon; N=8) and HUVEC (blue hexagon; N=6) cells. (E) Comparison of EC₅₀ values for VEGF₁₆₅ responses in HUVEC (N=6) and HMEC-1 (N=8) cells.

Asterisks show statistical significance where p *ns* > 0.05, p^* < 0.05, p^{**} < 0.01, p^{***} < 0.001 Data are represented as mean \pm SEM.

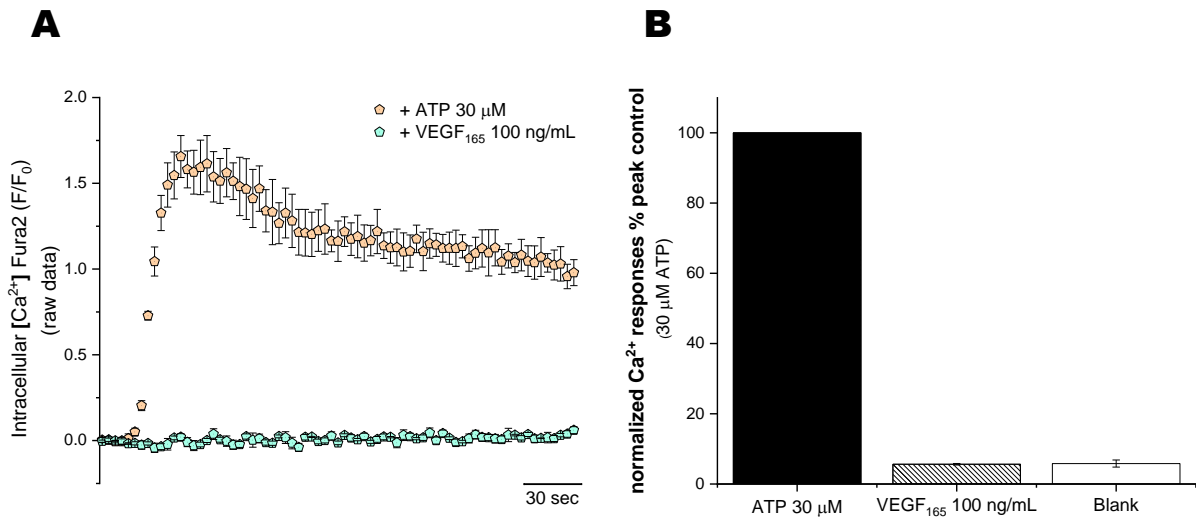


Figure 55. VEGF₁₆₅ did not elicit intracellular calcium response in 1321N1 human P2X4 stable astrocytoma cells. (A) Averaged time-resolved intracellular Ca^{2+} responses elicited by ATP 30 μ M (orange pentagon) and 100 ng/mL VEGF₁₆₅ (cyan pentagon) over 250 seconds ($N=2$). (B) Comparison of peak magnitude of intracellular Ca^{2+} responses induced by the injection of ATP 30 μ M, 100 ng/mL VEGF₁₆₅ and vehicle control (*blank*) ($N=2$) in saline solution. Data are normalised to 30 μ M ATP when indicated and represented as mean \pm SEM.

3.3.7. Characterisation of the ATP calcium signalling in human umbilical vein endothelial cells (HUVECs).

Biomolecular profiling at the mRNA level of the HUVECs was portrayed in **section 3.3.5**, but the ability of HUVECs to respond to ATP still needs to be proven. Furthermore, understanding the ATP signalling in this cell line might help us better interpret the latest observations.

3.3.7.1 ATP-evoked calcium responses in human umbilical vein endothelial cells (HUVECs).

ATP elicited intracellular calcium response in a concentration-dependent manner (0.03 to 30 μM) with a maximal attainable response at 30 μM for the peak and the area under the curve (AUC) (100%). The half-maximal effective concentration (EC_{50}) for the peak was $1.77 \pm 0.28 \mu\text{M}$ and $6.58 \pm 0.20 \mu\text{M}$ for the AUC (**Figure 56-A, B**). **Figure 56-C** depicts time-resolved calcium responses upon ATP stimulation from 0.03 to 30 μM . This stimulation evoked a rapid and transient initial response followed by a sustained phase that decayed to approximately 50% above baseline for 30 μM stimulation. However, this decay is more dramatic at lower concentrations. From 0.03 to 3 μM , the responses returned to the baseline level over 4 minutes.

To complement this data, thapsigargin was used to investigate further the possible store-operated calcium release contribution in the ATP-dependent response in HUVEC. Preincubation with 5 μM thapsigargin prevented any ATP-induced responses (**Figure 57**), suggesting the dependency on the intracellular stores to evoke calcium increase in the cytosol.

Finally, the P2X4 contribution to the ATP-evoked calcium responses was briefly studied. As described for HMEC-1, we could not observe any contribution to the 30 μM ATP response when preincubating the cells with 10 μM BX430 (**Figure 58**). That agreed with what was previously reported in the laboratory, as Dr. Jessica Meades reported the same lack of effects and the SERCA inhibition when applying ivermectin using the same cell model, similarly as we reported for HMEC-1 cells (*unpublished data*).

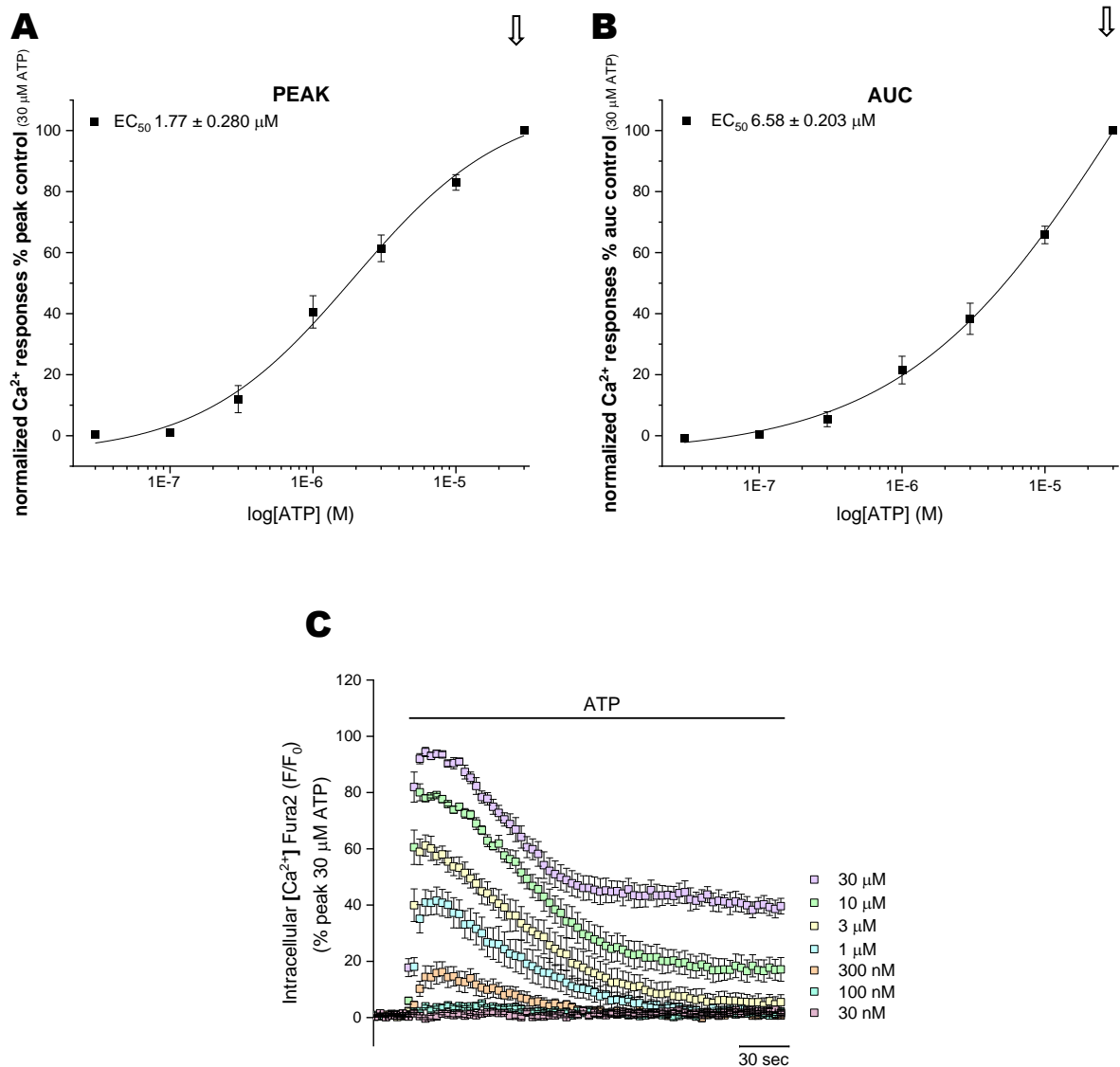


Figure 56. ATP elicits intracellular calcium responses in human umbilical vein endothelial cells (HUVEC). Concentration-response curves for the peak **(A)** and AUC **(B)** magnitude of intracellular Ca^{2+} responses elicited by ATP (0.03-30 μM ; $N=5$). **(C)** Averaged time-resolved intracellular Ca^{2+} responses elicited by ATP from 30 μM to 30 nM in HUVEC cells over 250 seconds ($N=5$). All data were normalised to 30 μM ATP and fit the Hill1 equation with the EC_{50} values showed in the graphs. Data are represented as mean \pm SEM.

(*) Data normalisation was always done at 30 μM when this agonist was studied.

(**) Arrows (\Downarrow) indicate the maximum response in the control (untreated) curve.

(***) F/F_0 refers to the Fura2 ratio, meaning F_{340}/F_{380} .

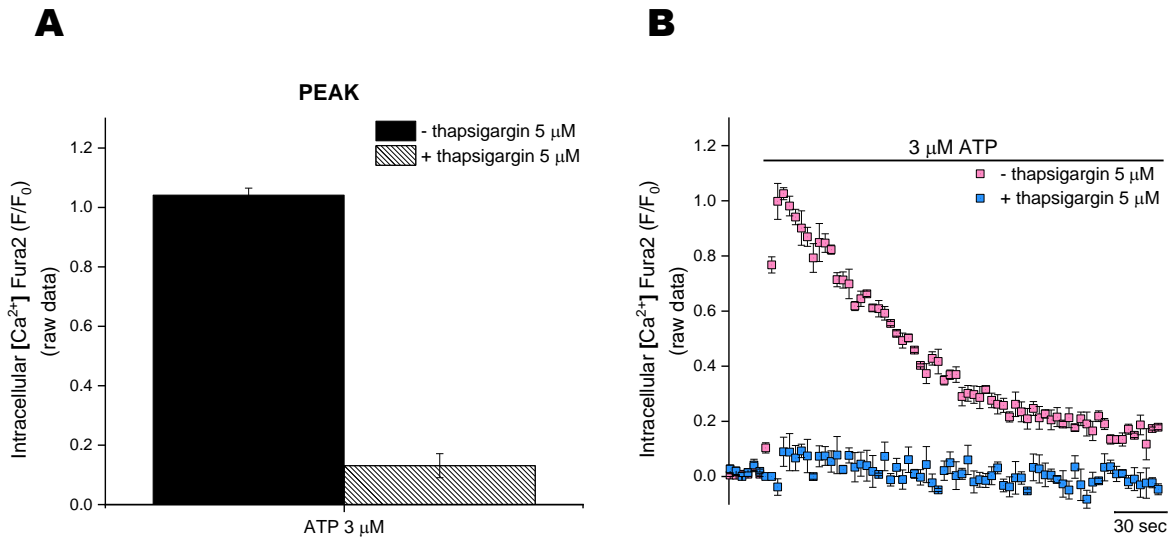


Figure 57. Effects of the sarcoendoplasmic reticulum calcium transport ATPase (SERCA) inhibitor thapsigargin on the ATP-evoked response in human umbilical vein endothelial cells (HUVEC). **(A)** Comparison of peak magnitude of intracellular Ca^{2+} responses induced by ATP at 3 μ M in the presence ($N=1$) or absence ($N=1$) of thapsigargin 5 μ M. **(B)** Averaged time-resolved intracellular Ca^{2+} responses elicited by ATP 3 μ M in the presence (blue square; $N=1$) or absence (pink square; $N=1$) of thapsigargin 5 μ M over 250 seconds. Data are represented as mean \pm SEM of the n replicates within the same technical experiment.

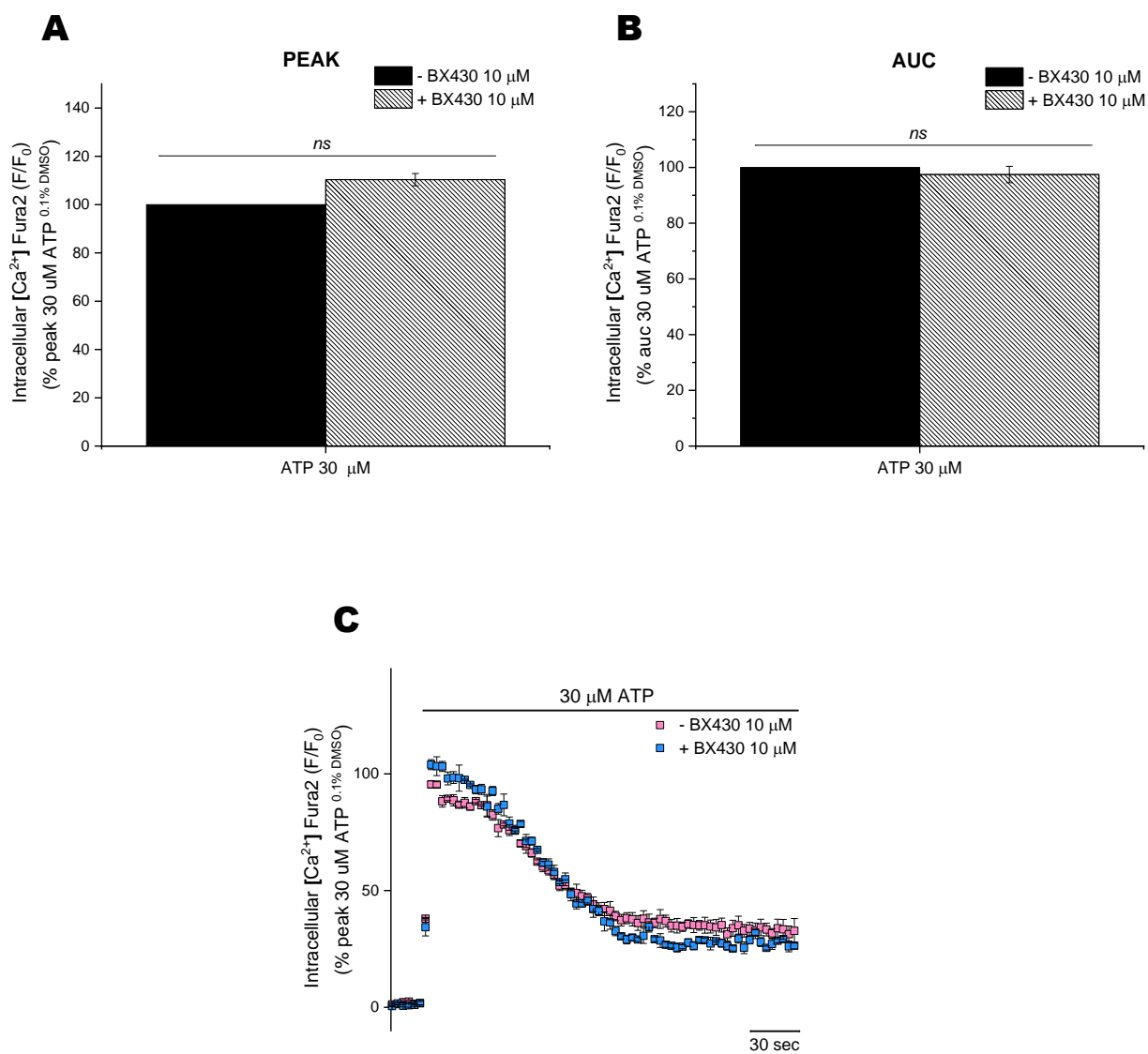


Figure 58. Lack of inhibitory effects of BX430 P2X4 receptor antagonist on the ATP-evoked response in human umbilical vein endothelial cells (HUVEC). Comparison of peak (A) and AUC (B) magnitude of intracellular Ca^{2+} responses induced by ATP at 30 μ M in the presence ($N=3$) or absence ($N=3$) of BX430 10 μ M. (F) Averaged time-resolved intracellular Ca^{2+} responses elicited by ATP 30 μ M in the presence (blue square; $N=3$) or absence (pink square; $N=3$) of BX430 10 μ M over 250 seconds. All data were normalised to 30 μ M ATP. Asterisks show statistical significance relative to ATP 30 μ M in saline solution containing 0.1% DMSO (p ns > 0.05, p^* < 0.05, p^{**} < 0.01, p^{***} < 0.001). Data are represented as mean \pm SEM.

3.3.7.2 ATP kinetics profile differed between human umbilical vein endothelial cells (HUVECs) and human microvascular endothelial cells (HMEC-1).

If we compared HUVEC and HMEC-1 cells ATP concentration-response curves, contrarily to what we reported for the VEGF₁₆₅ response, HMEC-1 cells demonstrated higher potency (**Figure 59-A, B, E**) (EC_{50}^{PEAK} : 427 ± 64 nM; EC_{50}^{AUC} : 1.16 ± 0.52 μ M) and efficacy (maximal comparable response at 30 μ M for the AUC; $p < 0.01$) than HUVEC cells (EC_{50}^{PEAK} : 1.59 ± 0.296 μ M; EC_{50}^{AUC} : 9.22 ± 2 μ M). The representative calcium time-responses curves at 1 μ M (**Figure 59-C**) and 10 μ M (**Figure 59-D**) illustrated the difference in the trace kinetics in the cell lines. Both cell lines presented an initial rapid response. However, HMEC-1 presented a much more sustained response. At the same time, HUVECs showed a more transient response, whose response decayed to baseline after approximately 2 minutes at 1 μ M ATP. The response dramatically dropped also at 10 μ M ATP, even though it did not reach baseline in this case. This sustained characteristic response in HMEC-1 is why efficacy was significantly increased in their AUC and not in the peak, whose parameter was achieved with the same efficacy in both cell lines, as they had their rapid initial responses conserved. This data depicted the idea that HUVEC responses have a more remarkable contribution to the calcium release from the stores than HMEC-1 cells, as late sustained responses are thought to be more membrane ion-channel dependent. That might imply the involvement of a different pattern of P2 receptor functional expression in both cell lines. The transcriptome comparison profile elicited remarkable differences at the mRNA level (**Figure 60**). However, it is worth noting that other essential families of ion channels, such as ORAI channels, also rely on store-dependent mechanisms and could impact ATP-dependent trace kinetics.

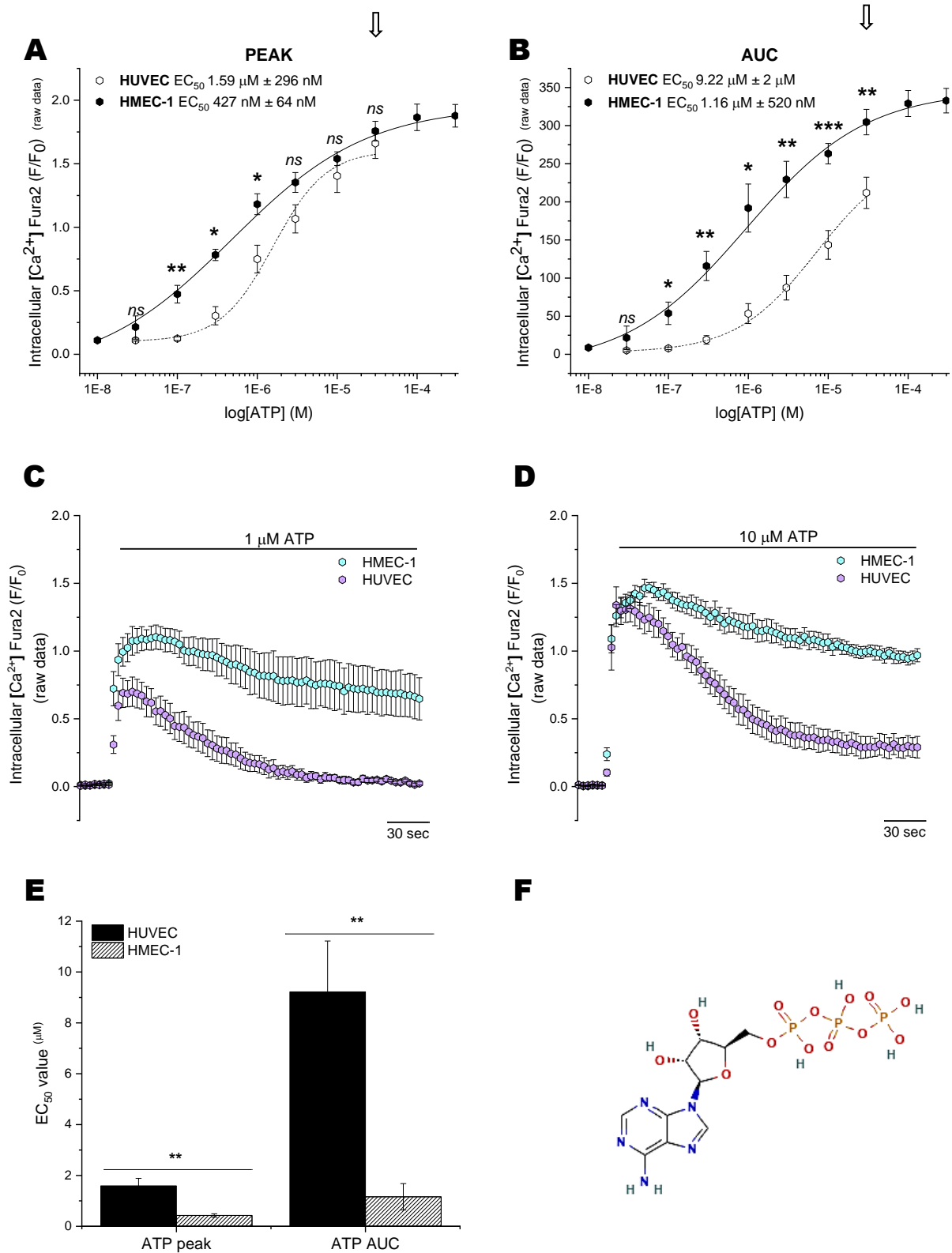


Figure 59. ATP's kinetics profile varied between human umbilical vein endothelial cells (HUVECs) and human microvascular endothelial cells (HMEC-1). Concentration-response curves for the peak (A) and AUC (B) magnitude of intracellular Ca^{2+} responses elicited by ATP in HUVEC cells (0.03–30 μ M; open circles; $N=6$) and HMEC-1 (0.01–300 μ M; closed circles; $N=8$). All data fit the Hill1 equation with the EC_{50} values showed in the graphs. Averaged time-resolved intracellular Ca^{2+} responses elicited by ATP (C) 1 μ M and (D) 10 μ M in HMEC-1 (cyan hexagon; $N=8$) and HUVEC (purple hexagon; $N=6$) cells. (E) Comparison of EC_{50} values for ATP responses in HUVEC ($N=6$) and HMEC-1 ($N=8$) cells. Asterisks show

statistical significance where $p_{ns} > 0.05$, $p^* < 0.05$, $p^{**} < 0.01$, $p^{***} < 0.001$ (F) ATP chemical structure (National Center for Biotechnology Information (2023)). Data are represented as mean \pm SEM.

Purinergic receptors expression profile comparison (%)

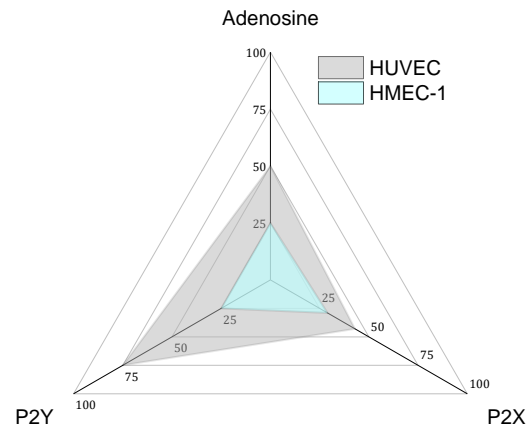


Figure 60. Comparison of purinergic receptor expression profile between human umbilical vein endothelial cells (HUVEC) and human microvascular endothelial cells (HMEC-1). Graphical representation of the percentage of purinergic receptors expression from reverse transcription polymerase chain reaction (RT-PCR) in HUVEC cell line or RNA sequencing data in HMEC-1 cell line. HUVEC cells expressed a higher percentage of the three purinergic receptors family at the mRNA level.

3.4 Discussion

3.4.1. Human dermal microvascular endothelial cells (HMEC-1) express various purinergic receptors at the transcriptional level.

This study's principal *in vitro* model was the human dermal microvascular endothelial cell line (HMEC-1). As previously stated, P2 receptors have been proposed as mediators of the endothelial calcium responses in various physiological processes (Aslam et al., 2021; Li et al., 2022; Raqeeb et al., 2011; Wang et al., 2015; Yamamoto, Korenaga, Kamiya, Qi, et al., 2000). This immortalised cell model, established by Ades et al., has been broadly used in endothelial research (Del Carratore et al., 2012; Ding et al., 2010; Du et al., 2015; Feoktistov et al., 2004; H. Li et al., 2015; Ryzhov et al., 2007). They conserve the main morphological, phenotypical, and functional characteristics of endothelial cells (VEGF responsiveness, expression of von Willebrands factor (vWF), cell adhesion molecules such ICAM-1, and process the LDL uptake) (Belair et al., 2015; Bouđè et al., 2001; Muñoz-Vega et al., 2018). Furthermore, HMEC-1 cells exhibit many features of primary microvascular endothelial cells. As our investigation did not specifically focus on either macro- or microvasculature, the cell line was considered representative, given that most of the endothelium in our body constitutes the microvasculature (Bouđè et al., 2001).

Expression of purinergic receptors in HMEC-1 cells was investigated by RNA sequencing. Five different purinergic receptors were found at the transcriptional level (P2X4, P2X5, P2Y2, P2Y11, and A2B), which agrees with the RNA sequencing output from Bastounis (2021). While the results of this study are relevant, it is essential to bear in mind that the cells were cultured in slightly different conditions (glass substrates coated with 0.25 mg/mL collagen I), whereas we did not coat the plastic growing flask. Matrix rigidity promotes different expression patterns in endothelial cells (Hubbi et al., 2012; Zhang et al., 2022), which might explain the different receptors' subtle relative expression levels in that study. Most literature agrees with the expression of P2Y2 at the mRNA level in HMEC-1, which is by far the most studied P2 receptor using these cells (Ding et al., 2010; Gidlöf et al., 2015; Seiffert et al., 2006; Zhang et al., 2014). Seiffert et al. reported using RT-PCR the same expression pattern in HMEC-1 except for adding P2X7 expression. No specific study showing P2X7 in the cell line was found except from Y. Zhang et al., who reported even more P2 receptors in HMEC-1 (P2X3, P2X4, P2X5, P2X7, P2Y1, P2Y2, P2Y4, P2Y11, and P2Y12; RT-PCR). Notably, in this case, cells were cultured in a completely different media, whereas in Seiffert et al. work, the media composition slightly varied (higher concentrations of hydrocortisone and absence of L-glutamine). Regarding adenosine receptors, Feoktistov et al. showed that HMEC-1 preferentially expressed A2B than A2A. Then, our findings agree with most current literature and confirm the expression of P2X4, P2X5, P2Y2, P2Y11, and A2B in HMEC-1 cells.

3.4.2. Purinergic receptors contribute to the endothelial calcium homeostasis in HMEC-1.

ATP can bind to different P2 receptors with different affinities (Burnstock, 2007). To evaluate which receptor is involved in the ATP-evoked calcium responses, we measured intracellular calcium increases for nucleotides, ATP, UTP, ADP, and UDP. ATP and UTP evoked almost

identical calcium responses in HMEC-1 cells with equal potency for the peak (EC_{50}^{ATP} : 568 ± 161 nM; EC_{50}^{UTP} : 460 ± 80 nM; *ns*) and the area under the curve (EC_{50}^{ATP} : 742 ± 161 nM; EC_{50}^{UTP} : 654 ± 271 nM; *ns*), being the UTP slightly more efficient than ATP (higher maximal response peak and AUC; $p < 0.05$). The potency for ADP and UDP were significantly lower than the previous nucleotides for the peak (EC_{50}^{ADP} : 27 ± 7.1 μ M; EC_{50}^{UDP} : 63 ± 11.3 μ M; $p < 0.01$) and the AUC (EC_{50}^{ADP} : 52.1 ± 19.2 μ M, *ns*; EC_{50}^{UDP} : 114 ± 20.3 μ M; $p < 0.01$). Consistently the maximal responses were significantly reduced for both nucleotides for the peak and the AUC ($p < 0.01$). It is relevant to mention that our calculated EC_{50} for ADP and UDP is far higher than others reported. ADP is an agonist of P2Y1, P2Y12, and P2Y13, with lower than 100 nM potencies. Similarly, UDP is an agonist of P2Y6 and P2Y14, and their potencies are in the same range as the previous ones (Woods et al., 2021). Furthermore, none of the previous P2 referred were detected in the RNA sequencing. Therefore, it is unlikely these results portrayed a specific nucleotide evoked response. Instead, those responses could be due to ATP or UTP contamination, whose reported manufacturer purity never ensures 100%. The ATP and UTP agonist profiles are consistent with an involvement of P2Y2 that is activated equipotently by ATP and UTP (Ding et al., 2010; Nicholas et al., 1996; Parr et al., 1994; Woods et al., 2021). Ding et al. reported the same nucleotide responses in HMEC-1 with similar potencies to ATP and UTP in the nanomolar range (EC_{50}^{ATP} : 364 ± 65 nM; EC_{50}^{UTP} : 170 ± 32 nM). Furthermore, the EC_{50} values for ADP and UDP (EC_{50}^{ADP} : 16.8 ± 2.6 μ M; EC_{50}^{UDP} : 3.8 ± 1.5 μ M) were also in the micromolar range. In general, their responses show a lower concentration fashion in all the potencies reported; however, even though they used a similar fluorometric imaging plate reader, the preparation for the experiment slightly differed from ours, and the data extraction and treatment were different too, meaning some impact in the extrapolated parameters. Using a different immortalised vascular endothelial cell line, EAhy926, Muoboghare et al., 2019 showed EC_{50}^{AUC} for UTP of 670 nM that is almost identical of our calculated potency (673 ± 198 nM) in HMEC-1 cells. However, Raqeeb et al. reported slightly higher EC_{50} using HUVECs for UTP (1.26 μ M) and significantly decreased potency for ATP (3.07 μ M).

Removing extracellular calcium had no significant effect on ATP potency, but it had in the maximal responses (peak, $p < 0.01$; AUC, $p < 0.05$). Implicitly, this result infers the contribution of at least one P2Y receptor in response to ATP stimulation. The recorded calcium increase could only come from the intracellular stores in a calcium-free media. Removing extracellular calcium is applied in calcium mobilisation assays when intracellular contribution to calcium responses wants to be isolated (Li et al., 2011; Liu et al., 2010). The observed residual calcium responses suggest extracellular calcium entry through ion channels, which could indicate P2X activity. However, as we will discuss later, we know it is unlikely to be true in our model. Alternatively, this result could also indicate store-operated calcium entry (SOCE). SOCE (store-operated calcium entry) is the process in which the depletion of endoplasmic reticulum (ER) calcium stores leads to calcium influx across the plasma membrane. The store-operated channels (SOCs) responsible for this phenomenon are known as calcium release-activated calcium (CRAC) channels, characterized by their high calcium selectivity. Activation of these channels occurs by binding ER calcium sensors, specifically stromal interaction molecule 1 (STIM1) and STIM2, to CRAC channel proteins (Orai1, Orai2, and Orai3). STIM proteins bind to and directly activate Orai channels. Both families of molecules can completely restore SOCE in heterologous expression systems, demonstrating that these proteins are essential and sufficient for the SOCE process. Our data from the RNA sequencing suggests the transcriptional expression of both families in HMEC-1, which again agrees with the RNA sequencing output

from Bastounis, 2021. Nonetheless, it is complicated to find studies using these cells exploring the functional expression of CRAC channels as the vast majority of investigations were performed using human umbilical vein endothelial cells (HUVEC) (Beech, 2012; Li et al., 2015; Li et al., 2011; Moccia et al., 2023). Following the proposed involvement of P2Y, treatment with the PLC pathway inhibitor (U73122) and the SERCA inhibitor thapsigargin prevented any ATP-evoked responses, reaffirming the predominance of P2Y receptors in the ATP-evoked responses. Others have suggested using different endothelial cell models to the involvement of P2Y2 in their ATP-induced responses that were further blocked by the preincubation of U73122 (Kamouchi et al., 1999; Viana et al., 1998). The specific phospholipase C inhibitor blocked the two phases of the agonist-evoked calcium response, as we observed in HMEC-1 cells. However, these results need to be taken cautiously as unexpected side effects (Foufelle et al., 2016; Horowitz et al., 2005) have been reported using these two pharmacological tools and the involvement of P2X was still in the table when this initial characterisation was performed.

3.4.2.1 The broad-spectrum P2 antagonists impair ATP calcium influx in HMEC-1.

Before the systematic pharmacological characterisation performed with the P2 propose candidates at the transcriptional level, three broad-spectrum inhibitors of the ATP response were used to gain insight into the primary mediators of the ATP-dependent calcium response in HMEC-1 cells. Apyrase was the one that significantly impacted the ATP dose-response kinetics, inferring the ATP dependency nature of the observed responses. The drug massively decreased the ATP potency and reduced the maximal responses, an ability not demonstrated either for PPADS or suramin. However, apyrase is not a receptor antagonist but diminishes the ATP-evoked responses by its ability to catalyse the hydrolysis of ATP to ADP and ADP to AMP (Kettlun et al., 2005). The scavenger has been broadly used to pharmacologically diminish the ATP-evoked responses in electrophysiology or calcium mobilisation assays (Jiang et al., 2017; Madry et al., 2018; Newman, 2005; Ollivier et al., 2006; Thuringer, 2004; Toma et al., 2008).

The lack of effect in the ATP potency upon PPADS application was expected as the antagonist acts as a non-competitive antagonist of all P2X receptors as a partial antagonist of some P2Y receptors in humans (Burnstock et al., 2014; Delaune et al., 2023; Ralevic et al., 1996) but not for the P2Y2 or P2Y11 receptors (Charlton et al., 1996b; Communi et al., 1999). Therefore, observed effects in the maximal responses were interpreted as a potential involvement of P2X4 in the ATP-evoked response. P2X4 showed very high IC₅₀ values in various reports (Bo et al., 2003; Coddou et al., 2011; Jones et al., 2000; Khakh et al., 1999; North et al., 2000), in agreement with our experimental calculated IC₅₀ that was around 100 µM for the peak and the AUC. Nonetheless, the hypothetical role of P2X4 and PPADS action will be further discussed in the following sections (**Chapter 5, Section 5.1**).

Suramin is considered weak or inactive at inhibiting human P2X4 and P2Y2 (Lambrecht, 2000; Rafehi et al., 2018; Ralevic et al., 1998; Soto et al., 1997). However, some investigations reported effects at high concentration of the antagonist, and it has been used to characterise P2Y2 responses (Charlton et al., 1996b; Rafehi et al., 2018). In addition, it was commonly used as a P2Y11 antagonist (Kennedy, 2017). As a non-competitive antagonist, the slight left shift for the AUC curve with the increasing significant impact on the ATP potency (p<0.05) was then

unexpected, profiling the typical effect of a positive allosteric modulator of ATP. Contrastingly, the maximal response was diminished in both curves. The results are considered atypical, and others have reported non-specific effects at high concentrations of the inhibitor (Jones et al., 2000; North et al., 2000; Soto et al., 1997), which was the configuration used for this inhibition assay. Nonetheless, suramin can inhibit ectonucleotidases (enzymes that hydrolyse ATP into ADP, AMP, and adenosine), leading to prolonged availability and elevated levels of extracellular ATP. By inhibiting ectonucleotidases, ATP degradation would be slowed down, lowering its EC₅₀, as observed in our data.

3.4.2.2 P2X4 is unlikely to play a role in the ATP-evoked calcium responses in HMEC-1.

The systematic pharmacological characterisation performed with the P2 transcriptional proposed candidates was initiated by investigating the effects of P2X4 selective antagonists and ivermectin, its positive allosteric modulator. This was the only P2X receptor characterised in this study. As was already mentioned, P2X5 pharmacology is limited, and its relevance in humans might be restricted to heterodimerization for forming a functional channel (Müller et al., 2020). Furthermore, P2X5 can be found as two different isoforms determined by substituting a thymidine for guanine (non-functional channel lacking exon 10), and just 14% of the population is known to have functional homomeric channels (Bo, Jiang, et al., 2003; King, 2023). This and the deficient mRNA expression of P2X5 in the RNA sequencing made us avoid further investigating its involvement in the ATP-evoked response. However, future work might focus on genetically profiling the P2X5 isoform presented in HMEC-1 and consistently conclude its potential ability to contribute to endothelial ATP-induced responses.

Four different P2X4 selective antagonists (BAY-1797, BX430, 5-BDBD, and PSB12062) were used to investigate the potential channel contribution to the ATP responses in HMEC-1. In general, pharmacological characterization reported no effect in the ATP dose-response potency, maximal response, or trace kinetics when cells were pre-treated with the inhibitors, including the most potent and novel selective antagonist, BAY-1797 (Werner et al., 2019). However, strikingly, the last antagonist tested, PSB12062, impaired the ATP responses. This antagonist is seven times less potent than BAY-1797 and usually works non-competitively (Hernandez-Olmos et al., 2012). In our study, PSB12062 significantly increased ATP potency ($p < 0.05$) and reduced the maximal response in both curves ($p < 0.001$). That portrays unexpected behaviour for a non-competitive allosteric modulator, and despite being considered potentially non-P2X4 dependent, it is taken into account as this modulator has been broadly used to characterise P2X4 responses selectively (He et al., 2020; Layhadi et al., 2017; Layhadi et al., 2018; Müller et al., 2020; Orriss et al., 2023; Xiang et al., 2021).

To complement this observation, ivermectin was used to explore the possible positive allosteric modulation of P2X4 in HMEC-1, but it was not a valuable tool in this case. Ivermectin potentiates ATP-evoked responses and slows the rate of receptor deactivation (Stokes et al., 2020; Weinhausen et al., 2022). Nonetheless, that was not the output observed upon ivermectin preincubation in HMEC-1 cells. Ivermectin reduced the ATP response ($p < 0.05$) and also reduced in the same fashion the thapsigargin evoked response. Thapsigargin is a non-competitive SERCA (calcium ATPase channels) inhibitor that depletes calcium stores by impairing calcium uptake. As Pimenta et al. previously reported, ivermectin can inhibit SERCA

channels and, therefore, impact the thapsigargin-evoked response, explaining the noncanonical effects observed in the ATP-evoked responses that clearly showed a dependency in store-released calcium. That agreed with what was previously reported in the laboratory, as Dr. Jessica Meades reported the same inhibition pattern in another endothelial model (*unpublished data*).

3.4.2.3 P2Y2 mediates ATP-dependent responses in HMEC-1.

The second investigated candidate was P2Y2, which is known to be equally sensitive to ATP and UTP (Ding et al., 2010; Nicholas et al., 1996; Parr et al., 1994; Woods et al., 2021). As we previously stated, the ATP and UTP agonist profiles we reported are consistent with an involvement of P2Y2 that is activated equipotently by ATP and UTP. Furthermore, our data agrees with Ding et al., values reported in HMEC-1 cells. The selective and competitive antagonist AR-C 118925XX has been used to identify and characterise P2Y2 in endogenous systems as human vascular endothelial cells and, therefore, was used in this study to complement the indications we had about P2Y2 involvement in the ATP-induced responses in HMEC-1 cells (Muoboghare et al., 2019). AR-C 118925XX significantly impacted the ATP and UTP dose-response curves, causing a massive rightwards in both curves and chasing their potencies that were consistently shifted to the micromolar range. Muoboghare et al. showed EC_{50}^{peak} for UTP of 670 nM in EAhy926 immortalised human vascular endothelial cells, that is very close to our calculated potency (450 ± 241 nM) in HMEC-1 cells. Their calculated potency was consistently moved to the micromolar range when treated with 30 nM AR-C 118925XX for five minutes ($EC_{50}^{peak} = 7.6$ μ M). The major difference with their study is the lack of effect in their maximum responses. Contrarily, our assays using ATP and UTP powerfully illustrated the significant effect in the maximal response when the cells were exposed to the inhibitor. Methodological differences between our study and theirs might cause that. They used coverslips in a recording chamber whose fluorescence was recorded using a spectrophotometer whose cells were continuously perfused with buffer and exposed to different concentrations of UTP. Additionally, the 30 nM of the inhibitor was just applied for 5 minutes, whereas our treatment is much longer and more robust (10 μ M). As a competitive antagonist, AR-C 118925XX does not affect agonist maximal response but decreases potency. Thus, a normal maximal response to the agonist may be reached in its presence, albeit at higher agonist concentrations. That means the reduction in our control maximal response can be expected, and if exposing the cells to higher nucleotide concentrations, the same efficacy level could be reached. We found it challenging to find any other work showing the impact of the inhibitor in either an ATP or UTP dose response to gain more insights into the effect of the maximal response apart from Muoboghare et al.

The half maximal inhibitory concentration (IC_{50}) reported by Rafehi et al. in 1321N1 astrocytoma cells recombinantly expressing P2Y2 was potent for ATP (57.4 nM) and UTP (72.1 nM). Similarly, Muoboghare et al. showed a similar IC_{50} of 80 nM for UTP. However, our calculated potencies were weaker than those published in a heterologous system (IC_{50}^{PEAK} : 1.77 ± 0.73 μ M; IC_{50}^{AUC} : 559 ± 173 nM). That is not uncommon when comparing ion channels' heterogeneous expression to an endogenous system since the receptor expression level greatly influences agonist potency (Alexander et al., 2019; Alexander et al., 2021; Kennedy, 2017). In addition, others have shown in different assays the inhibitor reported an IC_{50} around 1 μ M in epithelial cells (Kemp et al., 2004).

We considered this data consistent to propose P2Y2 as the primary mediator of the ATP-evoked responses in HMEC-1. However, we will gain more insights later in the study by investigating protein expression and receptor presence.

Notably, the residual calcium influx in both nucleotide dose responses in the presence of the antagonist could indicate a slight participation of P2X4 or P2Y11 to the ATP responses and UTP, and therefore, P2Y11 participation was interrogated using its selective antagonist NF157. Although most P2Y11 studies showed a lack of response to UTP, White et al. reported unexpected UTP dose-dependent in a heterologous system expressing the receptor.

3.4.2.4 P2Y11 and A2B receptors do not mediate ATP responses in HMEC-1.

Signalling through P2Y11 can occur via G α s or G α q-type proteins, and the receptor couples more efficiently with the G α q signalling pathway than with the G α s pathway (Kennedy, 2017). G α q-type G proteins trigger the PLC pathway, depleting intracellular calcium stores and, thereby, inducing a detectable change in cytosolic calcium levels (Communi et al., 1997; Qi et al., 2001). P2Y11 signalling through the G α q-type G protein has been reported in an endogenous (Fruscione et al., 2011; Meis et al., 2010) and heterologous system (Communi et al., 1997; Qi et al., 2001). ATP is one of its agonists, and therefore, the selective antagonist NF157 was used to determine P2Y11 hypothetical G α q coupling and involvement in the ATP-induced responses in HMEC-1. In general, pretreatment with NF157 reported no effect on the ATP dose-response potency or trace kinetics. Some minimal effects were reported in the dose responses upon treatment but did not follow a trend and represented slight potentiation effects, while the potencies stayed unchanged. The suramin analogue, NF157, is a competitive antagonist whose significant action reflects in a potency reduction (Ullmann et al., 2005), so we conclude the inhibitor was ineffective in inhibiting ATP-induced responses in HMEC-1 cells.

The only adenosine receptor expressed at the mRNA level was A2B (ADORAA2B), which can couple with the G α q and G α s-type G protein receptor. A2B signalling through the G α q-type G protein has been reported in an endogenous system (Cohen et al., 2010; Gao et al., 2018; Müller et al., 2020). ATP cannot activate A2B, but different ectonucleotidases can hydrolyse ATP to adenosine, activating A2B. Upon pretreatment with MRS 1754, no effects were observed in the ATP dose response, inferring the antagonist's inability to impair the responses.

3.4.3. Human dermal microvascular endothelial cells (HMEC-1) express various vascular endothelial growth factors receptors and ligands at the transcriptional level.

The vascular endothelial growth factor's mRNA expression pattern in HMEC-1 cells was investigated by RNA sequencing of the cell line. The three VEGF receptors were found at the transcriptional level (VEGFR-1, VEGFR-2, VEGFR-3), while VEGFR-2 was detected at higher levels. Regarding the vascular growth factors, VEGF-B was substantially more expressed than the others but still a robust expression of VEGF-C followed by VEGF-A. In this case, VEGF-D was

not detected. These results agree with the RNA sequencing output from Bastounis, 2021. For both receptors and growth factors, the expression fashion is conserved.

The Human Protein Atlas is a Swedish initiative that seeks to comprehensively map all human proteins within cells, tissues, and organs. Analysis of the transcriptome in The Human Protein Atlas reveals that 68% (n=13,807) of all human proteins (n=20,162) are identified in endothelial cells. Among these, 554 genes exhibit elevated expression in endothelial cells (blood and lymphatic vessels) compared to other cell types. The three VEGF receptors are included in those 554 elevated genes, as well as VEGF-C. If checking RNA single-cell type specificity for the other ligands in the same source, VEGF-A and VEGF-B are found but not at comparable levels as VEGF-C, which is enhanced in endothelial cells (**Appendix I**). In agreement with our data, VEGF-D was rarely expressed in endothelial cells. In general terms, our data report the expected RNA single-cell type specificity for endothelial cells with the main difference of the higher expression of VEGF-B than VEGF-C. The elevated levels of VEGF receptors in endothelial cells make them a reference for the phenotypic endothelial marker.

Most studies using HMEC-1 cells reported functional expression of VEGF receptors or vascular endothelial growth factor actions in physiological processes (Bodnar et al., 2006; Butler et al., 2017). However, it is challenging to find investigations proving the mRNA presence of the VEGF family. Chen et al. and Del Carratore et al., showed mRNA selective expression of VEGF-A and VEGFR-2 using PCR, in agreement with what we reported.

3.4.4. VEGF receptors contribute to the endothelial calcium homeostasis in HMEC-1.

VEGF-A is a fundamental inducer of endothelial cell activities, notably in controlling vascular permeability and promoting angiogenesis (Li et al., 2011). VEGF-A was selected to characterise the VEGF-induced calcium responses in HMEC-1 cells based on the assumption that VEGFR-2 is its primary mediator (Simons et al., 2016). Although both A and C can bind to the receptor, VEGF-C reported higher affinity for VEGFR-3 than VEGFR-2. Consistently, VEGF-A has been broadly used to characterised VEGFR-2 calcium evoked responses (Li et al., 2011). Different alternative spliced isoforms of VEGF-A can be found in humans (121, 145, 165, 183, 189, and 206 aa in length), but it is VEGF₁₆₅ considered to be the most abundant and potent (Robinson et al., 2001).

VEGF₁₆₅ elicited intracellular calcium response in a concentration-dependent manner with a half-maximal effective concentration of 2.85 ± 1 ng/mL for the peak and 3.5 ± 1.3 ng/mL for the AUC. Studies on VEGF-A signalling have primarily utilized fixed concentrations of the ligand rather than complete concentration-response profiles. This approach makes it challenging to directly compare the relative activity of VEGF receptors across various studies (Peach et al., 2018). VEGF-evoked calcium influx has been poorly characterised in HMEC-1 cells. We exceptionally found Jho et al. (2005) investigation showing some VEGF-dependent calcium responses using fixed concentrations of the agonist. The vast majority of investigations reporting isolated VEGF-dependent calcium responses were done using HUVEC cells (Byzova et al., 2000; Cerezo et al., 2017; Favot et al., 2003; J. Li et al., 2015; Li et al., 2011; Sulpice et al., 2009). Yet, based on estimations of binding affinity, it is observed that all VEGF-A isoforms can bind to VEGFR-2 with nanomolar affinity (Peach et al., 2018). Suppose we transform our

calculated EC₅₀ to the nanomolar scale. In that case, they are translated as EC₅₀^{peak} ≈ 79nM and EC₅₀^{AUC} ≈ 94 nM (considering VEGF-A mol. weight as 36 KDa) and then in agreement with the limited data available.

The stimulation observed did not trigger a rapid response. Instead, it is characterised by a delayed, slower, and prolonged calcium release over four minutes. Calcium levels continuously rise throughout the response period, reaching their highest point towards the end. Consequently, the peak response is consistently observed toward the end of the response period. Typically, rapid increases in intracellular calcium are associated with the release from intracellular stores, while slower increases suggest calcium influx from the extracellular space (Parekh et al., 2005; Prakriya, 2013; Prakriya et al., 2015). This may suggest a potential contribution of ion channel-mediated calcium entry from the external environment.

Without extracellular calcium, the VEGF₁₆₅ potency was not significantly affected, but maximal responses were (peak, p<0.001; AUC, p<0.05). Despite an increased tendency in the half-maximal effective concentrations, the absence of extracellular calcium did not significantly alter VEGF₁₆₅ potency. This might be explained by the difficulties in fitting the Hill1 sigmoidal curve in the absence of the ion, which inferred a higher error when calculating the average potency for the curves. Despite this fact, the impact is still prominent. This result implies the contribution of at least some ion channel-mediated calcium entry, while the residual responses indicate some assistance dependent on calcium release from intracellular stores. It has been shown that VEGF₁₆₅ induces calcium increase through VEGFR-2 due to calcium release from intracellular stores and the simultaneous entry of calcium through various channels, collectively maintaining elevated cytosolic calcium levels (Li et al., 2011). Therefore, our data portrays expected calcium responses. It is essential to bear in mind that the comparison is mainly performed with data extracted from human umbilical vein cells (HUVEC), the most used model in this area of investigation.

Let us compare the trace kinetics of VEGF₁₆₅ response in HMEC-1 in the presence of extracellular calcium to the one described by Li et al., in HUVEC cells. There is one main difference that is remarkable. Their response showed a kinetic calcium response with a remarkable transient phase followed by a long and sustained phase (Appendix II), and that is clearly not the case in our trace kinetics. In the absence of extracellular calcium their trace kinetics is conserved, as in our case, reporting lower transient and sustained response. Jho et al. reported traces in HUVEC cells in the presence or absence of extracellular calcium, similar to Li et al. Additionally, some traces were reported in HMEC-1 cells in the absence of extracellular calcium, where the kinetics showed a very transient response still, very similar to the HUVEC cell, which disagrees with our observations. Our VEGF₁₆₅ evoked response seems less dependent in the calcium release from stores than other reported both in the absence or the presence of extracellular calcium.

Li et al. showed the role of Orai1 and CRAC channels in the VEGF₁₆₅ response, whose recorded calcium response in HUVEC cells depended on the functionality of Orai1. The deletion of Orai1 and the chemical impairment of the channel implicated a reduction of the Ca²⁺ in the cytosol upon VEGF₁₆₅ stimulation. Furthermore, Jho et al. showed TRPC1 could also contribute to VEGF-induced sustained calcium in HMEC-1 cells, and Orai1 may constitutively interact with TRPC4 and potentially with TRPC1 upon intracellular calcium release from the endoplasmic

reticulum (Moccia et al., 2023). However, is relevant to say that Li et al. could not replicated the involvement of TRPC1 in HUVEC cells. On the other hand, Hamdollah Zadeh et al. (2008) have demonstrated TRPC6 mediation of VEGF-dependent extracellular calcium entry in microvasculature but not the same model as ours. Finally, Li et al. showed later in 2015 that Orai3 could modulate VEGF response by a process implicating the arachidonic acid metabolism not previously described with VEGF signalling. This is an independent SOCE route, as endogenous Orai3 does not contribute to store depletion-evoked calcium entry in the vasculature.

It is known that the PLC γ -PKC-MAPK pathway is favourably activated in VEGF-bound VEGFR-2, and further events involved IP3 generation for the endpoint of calcium release from intracellular stores, so the action of the PLC pathway inhibitor (U73122) was pursued. U73122 prevented any VEGF₁₆₅-evoked responses, reaffirming the mechanism of VEGF-evoked calcium. This result agrees with the reported HUVEC cells, whose calcium responses were also abolished in the presence of the inhibitor (Li et al., 2011, 2015). Despite the difference in the response kinetics, the initial phase of the VEGF-dependent response in endothelial cells appears comparable.

Finally, the ability of VEGF-B, that binds VEGFR-1 and not VEGFR-2 (Olofsson et al., 1998), to evoke calcium response in HMEC-1 was tested. VEGFR-1 exhibits significantly weaker kinase activity than VEGFR-2. The 1169-Y on VEGFR-1, equivalent to 1175-Y on VEGFR-2, serves as a PLC γ activation site for VEGFR-1. Nevertheless, 1169-PY is not a prominent autophosphorylation site on VEGFR-1 (Shibuya, 2011). Not surprisingly, VEGF-B₁₆₇ did not evoke any calcium increase in the cytosol, inferring a possible inability of the VEGFR-1 to contribute by itself to the calcium-mediated responses in endothelial cells.

3.4.4.1 The broad-spectrum P2 antagonists impair VEGF₁₆₅ calcium influx in HMEC-1.

In the previous section, we recalled the involvement of different proteins in the VEGF₁₆₅-induced calcium responses in a dependent or independent SOCE manner. The possible involvement of purinergic receptors in this process has been poorly documented, and thereby, we performed a systematic pharmacological characterisation of the proposed P2 candidates from the RNA sequencing in VEGF₁₆₅-induced calcium responses as aforementioned for ATP. Consistently, the first step was gaining some insight into this possible contribution by studying the broad-spectrum P2 antagonist impact in VEGF₁₆₅-induced calcium responses.

In this case, PPADS significantly impacted the VEGF₁₆₅ dose-response more than apyrase. Still, both affected the curves similarly and right shifted them in a different gradient. On the other hand, apyrase right shifted the curves modestly but consistently affected both maximal responses for the peak and the AUC. This result might imply an ATP release upon VEGF₁₆₅ stimulation, which could also contribute to the calcium release in the cytosol upon applying the vascular factor. PPADS inhibition dose-response curves for VEGF₁₆₅ showed the effects of the inhibitor at very high concentrations of the drug. However, they would still be consistent with the high concentration of PPADS needed for blocking P2X4-mediated responses.

Comparing these results with previous studies is very challenging because no investigations have been published illustrating the possible effects of these drugs in the VEGF calcium-dependent response in humans or other mammalian models. Thuringer portrayed an indirect calcium measurement of the effect of a combined treatment of VEGF plus PPADS in the cell-to-cell propagation of mechanically evoked calcium waves. Still, it is not considered experimentally close enough to extrapolate the data to our system. PPADS's impact on VEGF-A expression at the protein level has been previously reported in rats (Mancini et al., 2018; Zhang et al., 2019). In humans, no further approaches were found. In the case of apyrase, Doktor et al. (2018), showed the impact of apyrase on VEGF-A mRNA levels upon treatment with the enzyme, and Morrone et al. (2006) reported an impairment of VEGF-A release in a glioma model in rats.

3.4.4.2 P2X4 selective antagonists inconsistently impair VEGF₁₆₅ calcium influx in HMEC-1.

Despite our suspicions about the effect of PSB12062 and given its high use as a selective P2X4 inhibitor, it was used together with BAY1797, its most potent inhibitor, to ascertain a possible contribution of P2X4 to VEGF₁₆₅ responses.

BAY1797 did not impact the VEGF₁₆₅ dose responses in any way, but PSB12062 did in the same fashion described for the ATP dose response. Nonetheless, in this case, the potencies were unaffected in the presence of the antagonist, whereas the maximal responses were significantly diminished. Again, no investigations have been found describing the possible effects of these drugs in the VEGF calcium-dependent response (or any other experimental setting) in humans or other mammalian models. Considering these results and the difficulties in interpreting them, P2X4 protein expression was characterised by western blot as the next step after this systemic pharmacological characterisation. Thereby, ATP and VEGF₁₆₅ antagonism effects will be further discussed in **section 3.4.5.1**.

3.4.4.3 P2Y2 selective antagonist did not impair the VEGF₁₆₅ calcium influx in HMEC-1.

The selective and competitive P2Y2 antagonist AR-C 118925XX undoubtedly decreased the ATP-evoked responses. However, this effect is not conserved when referring to the VEGF₁₆₅ calcium response. The inhibitor was ineffective in inhibiting any response or affecting the potencies or maximal responses.

Some studies reported transiently complex of P2Y2 and VEGFR-2 in cell junctions of endothelial cells (Erb et al., 2006; Liao et al., 2014) as well as rapid tyrosine phosphorylation of VEGFR-2 in human coronary endothelial cells upon activation of P2Y2 (Seye et al., 2004). Nonetheless, these effects were not translated to our experimental setting upon antagonism with AR-C 118925XX. In some way, the lack of effect of this antagonist, given the observed impact on the ATP responses, reaffirms other possible inhibitions observed, such as those of PSB12062 for P2X4 or the following section observations using the P2Y11 antagonist NF157.

3.4.4.4 P2Y11 selective antagonist impaired the VEGF₁₆₅ calcium influx in an adenylyl cyclase-dependent manner in HMEC-1.

P2Y11 is the last P2 receptor candidate as a possible contributor to the VEGF₁₆₅-induced responses. Its selective and competitive antagonist, NF157, showed no effects on the ATP-evoked response. This lack of response could mean different things. In the first option, the receptor is not expressed at the protein level, and therefore, any response observed should not show any P2Y11 dependency. The second option is that the receptor is not at the membrane in a resting cell state, so its physiological role is mute. The third and last option, its signalling is mediated by G α_s -type G proteins instead of G α_q -type proteins, not leading to the depletion of the intracellular stores but an increase in the cyclic AMP.

To our surprise, the antagonist affected the VEGF₁₆₅-evoked Ca²⁺ response; therefore, the second and third options were considered a possible mechanism. NF157 firmly right-shifted the curves and massively compromised the VEGF₁₆₅ potency with a 7-fold decrease in the peak and an approximately 15-fold decrease in the AUC potency. Additionally, a higher concentration is required to achieve the maximal response in the presence of NF157. In this case, the level of efficacy remained constant. However, in the AUC, the maximal response is conserved at the highest concentration of VEGF₁₆₅, but the level of efficacy was significantly improved. To gain insights into the P2Y11 inhibition dependency, the IC₅₀ of NF157 in the presence of 10 ng/mL of VEGF₁₆₅ was calculated, resulting in an inhibitory potency of 1.25 μ M. Ullman et al. reported an IC₅₀ of 463 \pm 59 nM in 1321N1 astrocytoma recombinantly expressing P2Y11. Our calculated IC₅₀s are close enough to this value to be P2Y11 dependent, considering we work in an endogenous system.

Some studies illustrated in monocytes and macrophages a gene upregulation of VEGF-A P2Y11 dependent (Bles et al., 2007; Dănilă et al., 2020; Klaver et al., 2022). Additionally, Piollet et al. (2021) showed the impairment of VEGF secretion in human coronary artery smooth muscle cells also dependent of P2Y11. However, these experimental settings are considered very far from ours, based on the calcium-dependent responses upon exogenous VEGF₁₆₅ stimulation.

The first step to interpreting better this inhibition was to dig further into the mechanism mediating the significant inhibitory effects observed. Our first hypothesis was that P2Y11 is not G α_q -coupled in HMEC-1, as backed up by the lack of effect of NF157 in the ATP dose-response curves. Then, the effect we observed could be mediated by downstream signalling from P2Y11 G α_s -couple receptors, hypothesising that the adenylyl cyclase signalling pathway is mediating the previously reported effects. Even though SQ22536 alone did not impact the VEGF₁₆₅ potency, it portrayed slight potentiation effects at lower concentrations of VEGF₁₆₅ and caused a significant recovery of the VEGF₁₆₅ calcium-evoked after NF157 inhibition, meaning at least some involvement of the adenylyl cyclase pathway. The most common pathway for cyclic adenosine monophosphate (cAMP) synthesis is through G α_s -couple G protein receptors linked to one of the nine described isoforms of transmembrane adenylyl cyclase (AC isoform), and different isoforms can be expressed simultaneously. The resting cAMP in the absence of stimulation is typically low, and it is highly controlled by enzymes that degrade cAMP, cAMP phosphodiesterases. G α_s -dependent cAMP production via ACs occurs upon agonist stimulation of the G-coupled receptor. For P2Y11, the G α_s -dependent cAMP production via ACs occurs, leading to activation of protein kinase A (PKA). However, this production is modulated by

inositol lipid hydrolysis (PLC pathway), which is dependent on the activation of protein kinase C (PKC) and intracellular calcium mobilisation (Hofer, 2012; Kennedy, 2017; Qi et al., 2001).

The nine different adenylyl cyclase isoforms are highly conserved, with differences determining their individual properties. Their complexity as a transmembrane architecture is comparable to those known for ion channels and other membrane receptors (Cooper, 2015). Different calcium concentration ranges inhibit some of them, but all the ACs are commonly inhibited by high concentrations of calcium ($\approx 25 \mu\text{M}$). Interestingly, physiological concentrations of calcium regulate ACs in a different manner. AC5 and AC6 are inhibited by submicromolar concentrations of calcium but has not effect on AC2, AC4, AC7 and AC9 (Cooper, 2015; Halls et al., 2011; Sanchez-collado et al., 2020). The physiological concentration of calcium activates AC1, AC3, and AC8 via the calmodulin ($\text{Ca}^{2+}/\text{CaM}$). Nonetheless, the process is mediated via SOCE for AC1 and AC8 while becoming more intricate for AC3. For the adenylyl cyclase 3, the activation can be mediated then by $\text{Ca}^{2+}/\text{CaM}$ and via PKC at submicromolar concentrations but inhibited by calmodulin-dependent enzymes (CAMKII) at supramicromolar Ca^{2+} concentrations (Hofer, 2012; Sanchez-collado et al., 2020).

There is a store-operated process involving the recruitment of adenylyl cyclases and, therefore, an enhanced production of cAMP. This process is meant to be independent of cytosolic calcium concentrations but dependent on the calcium-free concentration in the endoplasmic reticulum (ER) through a process involving STIM1, illustrating additional functions for STIM1 in the reticulum that, when in punctae near the plasma membrane modulates not only calcium entry but cyclic AMP independently of Orai channels activity (Hofer, 2012; Lefkimmiatis et al., 2009). Maiellaro et al. (2012) pointed AC3 isoform as the main mediator of this store-operated cAMP production process. Other authors also referred to the potential involvement of AC1, AC5, AC6, and AC8 in this process (Hofer, 2021). In addition to this cAMP production regulation by calcium, calcium signalling is also highly impacted by cyclic AMP (Hofer, 2012). Protein kinase A (PKA) can modulate calcium signalling in different ways, including (1) alteration of inositol trisphosphate (IP_3) production by phosphorylation of PLC_β , (2) alteration of IP_3 receptors which in turn impact the intracellular store's release, and (3) alteration of ryanodine receptors and SERCA pump activity (Hofer, 2012; Sanchez-collado et al., 2020).

It is relevant to mention the existence of a tenth AC isoform, AC 10. This is a soluble AC usually found in microtubules and centrioles. It is highly expressed in testis, and it is activated by calcium as AC1, AC8, and AC3. One of the most relevant features of this AC is its lack of sensitivity to SQ22536, the adenylyl cyclase inhibitor used in this study (Hofer, 2012; Sanchez-collado et al., 2020).

Then, going back to P2Y₁₁ and assuming it is $\text{G}\alpha_s$ -coupled, SQ22536, the adenylyl cyclase inhibitor, was used to study the possible direct impact of cAMP production in the VEGF calcium-induced response. AC3 showed a higher mRNA level in our RNA sequencing in HMEC-1 cells (**Figure 1**), followed by AC6 and AC9. AC3 is the less sensitive to be modulated by $\text{Ca}^{2+}/\text{CaM}$ compared to AC1 and AC8, however has been postulated as a mediator of the store-operated cAMP production (Hofer, 2012; Sanchez-collado et al., 2020). Additionally, its activation is improved when mediated by $\text{G}\alpha_s$ -couple receptors activation (Choi et al., 1992).

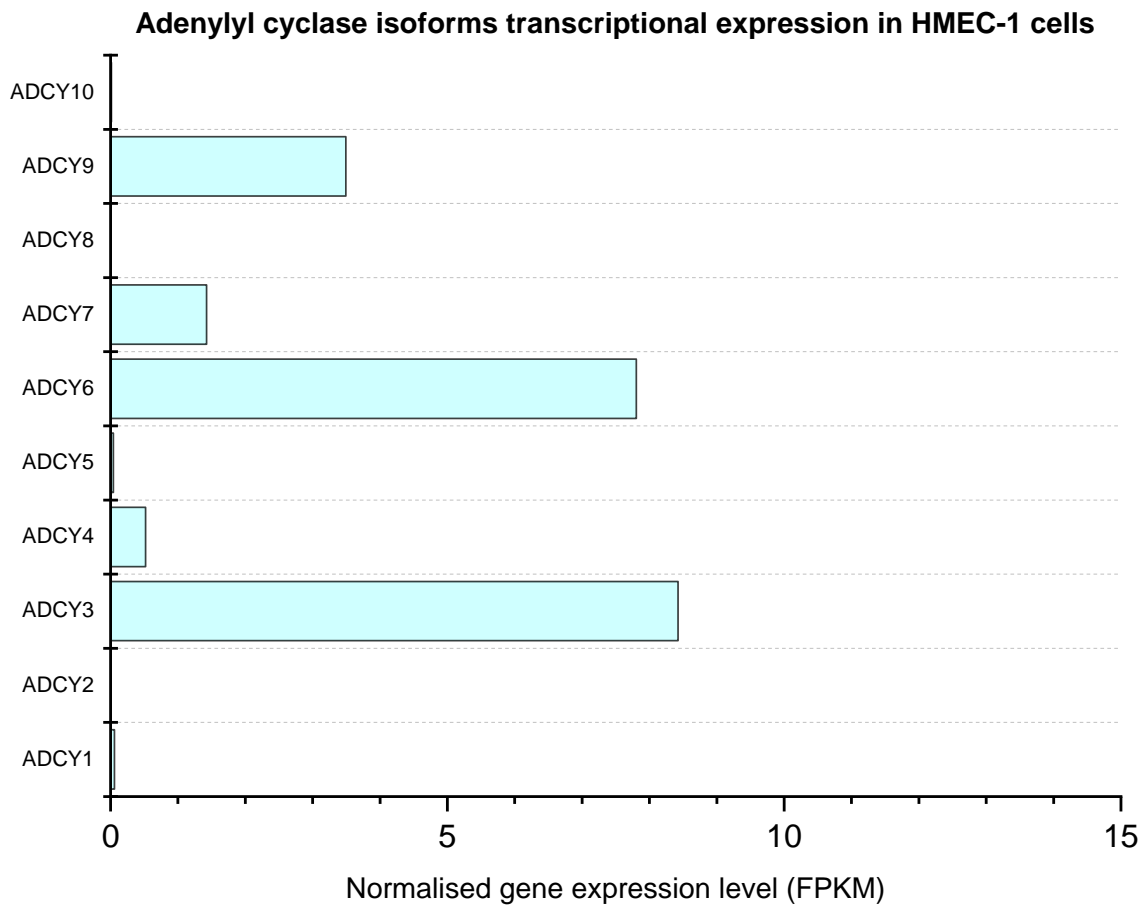


Figure 1. Normalised gene expression for the expected number of FPKM levels for the different adenylyl cyclase isoforms in human microvascular endothelial cells (HMEC-1). AC3 (ADCY3) showed a higher mRNA level, followed by AC6 (ADCY6) and AC9 (ADCY9). AC7 (ADCY7) and AC4 (ADCY4) demonstrated some expression but at a deficient level.

*This data is part of the RNA sequencing described in **Chapter 2, Section 2.6**, and it was independently plotted from the data in **Chapter 3, Section 3.3.1**, to ease the reading of this discussion.*

As our system portrays a favourable scenario for AC3 to mediate the observed responses, we want to understand how the explanation could be. However, it became intensely complicated due to the effects of SQ22536.

In a situation where upon VEGF₁₆₅ addition, P2Y11 G α_s -coupled and VEGFR-2 activate, resulting in an increase in cAMP through AC3 P2Y11-dependent and an increase of calcium via PLC with the Ca²⁺ release from the intracellular stores mediated by VEGFR-2. As previously described, emptying the ER stores could lead to a store-operated process enhancing cAMP production. Additionally, as a downstream event of PLC pathway activation, PKC favours cAMP production, also through AC3. cAMP production leads to activating one of its major effectors, PKA, which can modulate the PLC/IP3 pathway and derived intracellular calcium concentration. This describes a mechanism where these modulations favour an increase of calcium in the cytosol. In this scenario, P2Y11 blocking will avoid one of the biggest cAMP production vias and reduce the calcium increase PKA-dependent regulation, which will explain the impact in the VEGF₁₆₅ dose response upon NF157 treatment. Then, when selectively blocking the adenylyl cyclase using SQ22536, the same effect was expected, the calcium cAMP- dependent inhibition, but that was not the case. To further clarify the possible involvement of adenylyl cyclase in the VEGF₁₆₅ calcium-dependent response, a combined treatment of NF157 and SQ22536 was investigated. This combined treatment reversed NF157 effects in a significant way, meaning a much lower inhibition of the response was observed. That portrays a complex explanation if hypothesising P2Y11 is G α_s -coupled if all the effects observed are directly cAMP mediated by AC3. If this was the case, treatments with NF157 and SQ5523 should reproduce similar effects. If imagining the opposite scenario, where PKA modulates the calcium response negatively, AC3 activation would lead to PKA production, causing a decrease in the calcium influx. The effect of NF157 and SQ22536 should lead to increased calcium, which was not the case.

Another scenario where P2Y11 G α_s -coupled could mediate these responses is possible if the AMP cyclic-dependent calcium effects are not mediated by one of their known main effectors (PKA or Epac). Shen et al. (2011) described a unique direct effect of cAMP leading to the activation of TRPC6 and its derived calcium entry through a pathway involving stimulation of phosphatidylinositol 3-kinase (PI3K) and MAP kinase pathways. However, there is still a dependency on direct cAMP for the initial firing of TRPC6; therefore, the same effects will be expected when blocking P2Y11 or AC3. Additionally, the expression of TRPC6 is insignificant in HMEC-1. If this observed inhibition occurs through AC3 and P2Y11 G α_s -coupled receptor and cAMP production pathway, it is via a mechanism not previously described that involves a third effector collaborating to create the observed response.

Given the difficulties in understanding a possible mechanism through P2Y11 G α_s -coupled, the idea of P2Y11 G α_q -coupled and present in the membrane upon VEGF₁₆₅ exposition was introduced. This idea came from Li et al. who reported that VEGF₁₆₅ is required for Orai3 to be located in the plasma membrane. Trafficked to the membrane is the only way P2Y11 could be G α_q -couple, as we have already reported the NF157 lack of effect in the ATP-evoked calcium response. Then, the hypothetical mechanism would consist of a synergic PLC pathway activation with the established calcium release from the ER, which will lead to a store-operated process enhancing cAMP production (socAMP). PKC will also favour cAMP production through AC3 as a downstream event of PLC pathway activation. In addition, AC3 is considered a Ca²⁺/CaM-activated adenylyl cyclase isoform, which, in this case, will be activated by the

release of ER calcium. cAMP production leads to the activation of PKA, which can modulate the PLC/IP3 pathway and its derived intracellular calcium concentration. Suppose activation of PKA leads to negative regulation of the intracellular stores of calcium release. In that case, in the presence of VEGF₁₆₅ in basal conditions, cAMP will downregulate the activity of the PLC pathway.

When inhibiting P2Y11 with NF157, the VEGF₁₆₅-dependent response is blocked, indicating a massive decrease in the intracellular calcium recorded. That will reduce the cAMP (sacAMP and PKC induced) and the activation of AC3 and PKA, and therefore, a decrease in the level activity of this adenylyl cyclase. At this level, the effect in the recorded calcium might be minimal, based on a less intense negative regulation that is masked by the massive effect of NF157. Then, the second scenario is when pretreating the cells with SQ22536. Following the previous rationale, upon VEGF stimulation, P2Y11 and VEGFR-2 will induce calcium release from the stores (high calcium levels). AC3 blocking SQ-dependent will avoid the PLC pathway's negative regulation, leading to slight increases in calcium. That is shown in our results, where significant increases of Ca²⁺ were observed at low concentrations of VEGF₁₆₅. Finally, the last scenario consists of the combined blocking of NF157 and SQ22536. Once P2Y11 G_{αq}-coupled is blocked, the calcium decreases. As before, there is an impact on the cAMP levels, which is massively supported by the combined effect of SQ22536, giving rise to AC3 blocking and, in that way, blocking the negative regulation of the PLC pathway and rescuing the levels of calcium signalling as portrayed in the effects in the potencies when comparing treatments. This mechanism does not describe perfectly the observed effects but closely does. The major criticism would be the insignificant effect in the potencies when treating with SQ22536. However, we consider for this VEGF mechanism to be AC-dependent, the modulation of P2Y11 is required. Somehow, the synergic effects of inhibiting both proteins led to a significant recovery of the VEGF₁₆₅ calcium-evoked response.

The involvement of AC6, the second most expressed AC at the transcriptional level, should be considered as Ca²⁺ inhibits it, and it has been suggested as a mediator of the mediate store-operated process enhancement of the cAMP production. Then, the hypothetical mechanism, as proposed for AC3, would consist again of a synergic PLC pathway activation with the established calcium release from the ER. However, in this case, the calcium increase in the cytosol will block AC6 activity and cAMP-dependent PKA effects at some level. Suppose activation of PKA leads to negative regulation of the intracellular stores of calcium release. In that case, in the presence of VEGF₁₆₅ in basal conditions, cAMP will downregulate the activity of the PLC pathway but in a very minimal way.

When inhibiting P2Y11 with NF157, the VEGF₁₆₅-dependent response is blocked, indicating a massive decrease in the intracellular calcium recorded, favouring the expression of AC6. That will cause a reduction of calcium in the cytosol and synergic AC6 inhibitory activity through PKA in the intracellular calcium levels. Then, pretreating the cells with SQ22536, P2Y11, and VEGFR-2 will induce calcium release from the stores (high calcium levels) upon VEGF stimulation. AC6 block will avoid the PLC pathway's negative regulation, leading to slight increases in calcium, as AC6 will be more inhibited than in basal conditions. That is shown in our results, where significant increases of Ca²⁺ were observed at low concentrations of VEGF₁₆₅, as previously described. Finally, the last step consists of the combined blocking of NF157 and SQ22536. Once P2Y11 G_{αq}-coupled is blocked, the calcium decreases, but the concomitant treatment with

SQ22536, blocking AC6, rescues the calcium response due to the block of the negative effect of PKA in the PLC pathway. As before, this mechanism does not describe perfectly the observed effects but closely explains the major effects observed. As in the case of AC3, the hypothesis of AC6 involvement through P2Y11 $G\alpha_q$ -coupled G protein effects would illustrate a complex explanation of the effects of SQ22536 alone or in combination with NF157, that should show similar effects, and that is not the case. All the proposed mechanisms assume that VEGF₁₆₅ mediates P2Y11 activation, possibly through ATP release VEGF₁₆₅-dependent. As apyrase can inhibit VEGF₁₆₅ response, this is the most likely scenario. AC7 and AC9 are not considered mediators of this process as they are not calcium-regulated and have not been described as mediating store-operated process enhancement of cAMP production.

A well-established modulation of Ca^{2+} influx is regulated by cAMP involving the Orai1 channel and AC8. Willoughby et al. (2012), from the Cooper group, showed a direct binding between Orai1 and AC8. The described interaction is between the amino termini of AC8 and Orai1 and leads to a reciprocal crosstalk between the calcium influx and cAMP production (Hofer, 2012; Sanchez-collado et al., 2020). This interaction is favoured by the spatial arrangement where the proteins are found in the plasma membrane. Ca^{2+} /CaM sensitive adenylyl cyclases (AC1, AC3, AC5, AC6 and AC8) are located in membrane lipid rafts, PM areas rich in cholesterol and sphingolipids instead of glycerophospholipids. This membrane area has also been proposed to harbour other signalling proteins such as TRPCs, G proteins, and Orai channels (Willoughby et al., 2007). The lipid rafts are possibly dynamic structures that arrange their activity due to physiological cell demands and the AC's compartmentalization in these areas can give them a physiological advantage as they will be isolated from the broad cytosolic process and close to potential interaction proteins (Cooper et al., 2014; Halls et al., 2011; Willoughby et al., 2007). The mechanism described for this interaction of Orai1 and AC8 is based on the activation of SOCE. STIM1 is positioned close to the PM upon depletion of the intracellular stores. It leads to the activation of the pore-forming Orai1, which, in turn, will facilitate calcium influx in these located lipid rafts. Ca^{2+} influx via Orai1 activates AC8 and the production of cAMP. cAMP, through a process involving PKA, will modulate Orai1 inactivation via phosphorylation at Ser34 (Sanchez-collado et al., 2020). In non-excitabile cells, one of the main effects of SOCE is this reciprocal regulation of calcium sensitive adenylyl. Of the calcium sensitive ACs, AC1 and AC8 are activated via SOCE while that was not the case for AC3. There is a need for additional studies to investigate the regulation of AC3 and explore its potential implications in this process. Although its activation has been told to be calcium-dependent, this area has been underexplored, possibly due to the intricate nature of its activation and inhibition (Halls et al., 2011). In the same way, AC5 and AC6 are inhibited via SOCE (Cooper et al., 2014).

It is currently unclear whether other calcium-sensitive adenylyl cyclases (ACs) form similar complexes, aside from the identified interaction between Orai1 and AC8 in non-excitabile cells. Since AC8 is not expressed in HMEC-1 cells, a mechanistic gap exists in understanding the potential Orai1 interactions with another adenylyl cyclase that might be involved in this process. The existence of an AC isoform in HMEC-1 cells with the same type of interaction with Orai1 (or other CRAC channels involved in SOCE) would smoothly explain our results. As illustrated in **Table 1** and **2**, in a scenario involving P2Y11 $G\alpha_q$ -coupled presence in the membrane upon VEGF stimulation, in basal conditions, VEGF₁₆₅ will evoke calcium release in the cytosol via ER, which in turn will activate calcium influx via Orai1. As previously described, Orai1-dependent calcium influx will activate AC8 and produce cAMP, inactivating Orai1. When

we pre-treat the cells with NF157, there is a negative effect on the intracellular calcium release, leading to a decrease in the calcium influx via Orai1. AC will produce lower levels of cAMP, which would be sufficient to inactivate Orai1. In general, the calcium levels upon VEGF₁₆₅ stimulation should be highly reduced, per our experimental data. However, when pre-treating the cell with SQ22536, the PLC pathway, and Orai1 influx will be fully activated again to basal levels, but AC8 will be blocked, so Orai1 will not be inactivated. That explains ideally the slight increase we see upon preincubation with the AC inhibitor. Finally, when using these two inhibitors in combination, there is a recovery in the calcium levels; they do not go back to basal levels but considerably recover. Calcium levels are reduced due to P2Y11 blocking, which will lead to lower levels of calcium influx via Orai1 but conserved, as in this case AC8 is blocked and there is no production of cAMP, Orai1 will not inactivate and allow more significant calcium influx, recovering the cytosol calcium levels and see a lower impact compared to control. If we substitute AC8 for AC3 (**Table 1**), as the higher expressed in our model, hypothesizing it could work as SOCE dependent, we could accurately explain our observed results. As mentioned, the adenylyl cyclase 3 activation is calcium-dependent and has been underinvestigated, so we keep its role in this process. Again, if P2Y11 were G α_s -coupled instead of G α_q -coupled, the results based on this mechanism would be hard to explain because of the differences in SQ22536 and NF157 inhibition.

If we substitute AC8 for AC6, as the second higher expressed in our model, whose inhibition has been classified as SOCE (Ca²⁺) dependent. The mechanism will follow a very close rationale as previously described, considering the main difference as cAMP is regulated oppositely in this case as AC6 is blocked in basal conditions (after control VEGF₁₆₅ stimulation) and, therefore, Orai1 is not inactive. From there, the mechanism follows the same rationale but in the opposite way, as explained in **Table 2**. The potential interaction between SOCE-regulated ACs, as AC6, with Orai1, has been hypothesized as AC6 has a long N-termini as AC8. In addition, it has been shown that the role of regulating adenylyl cyclases by SOCE, as in the case of the endothelial gap formation, strongly depends on the inhibition of AC6 SOCE dependent (Cooper, 2015). This positions AC6 as an excellent candidate to be the mediator in our proposed mechanism.

AC6 has been involved in a regulatory complex with an L-type channel. Briefly, AC6 activity will produce cAMP, favouring calcium influx via the L-type channel (Ca_v1.2), subsequently inhibiting AC6 (Cooper et al., 2014). This scenario was not considered in this discussion, as RNA sequencing revealed the absence of CACNAC1 gen at the mRNA level.

SQ22536 has been previously used as a tool to report indirect effects of adenylyl cyclase inhibition impact in intracellular calcium recordings (Daniel et al., 2004; Skeberdis et al., 2006; Sprague et al., 1996; Wang et al., 2009). Still, finding any study where this inhibitor reported effects in the VEGF-evoked calcium response needed to be more attainable. However, SQ22536 has shown some effects in different assays involving VEGF-A release-cAMP dependent in microvasculature and other cell types (Cao et al., 2006; Kim et al., 2012). Finally, it is important to mention that SQ22536 has been demonstrated to interact with adenosine receptors except for A2B, the only one expressed in HMEC-1s. Then, no effects should be aroused in this case (Klotz et al., 2016; Ostrom et al., 2022).

Table 1. Proposed mechanism involving adenylyl cyclase 3 (AC3) isoform.

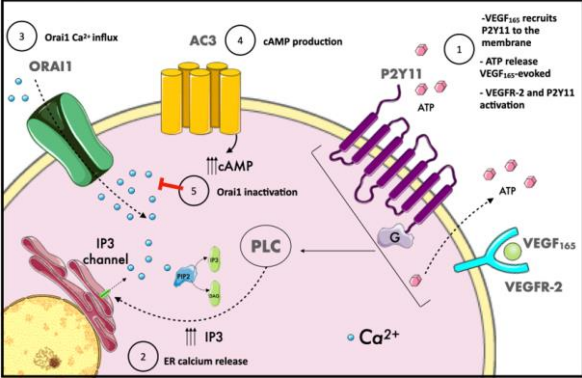
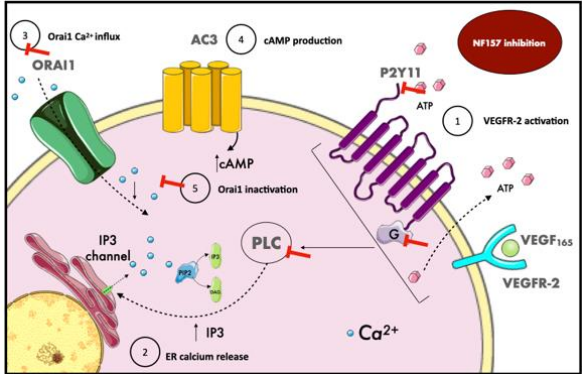
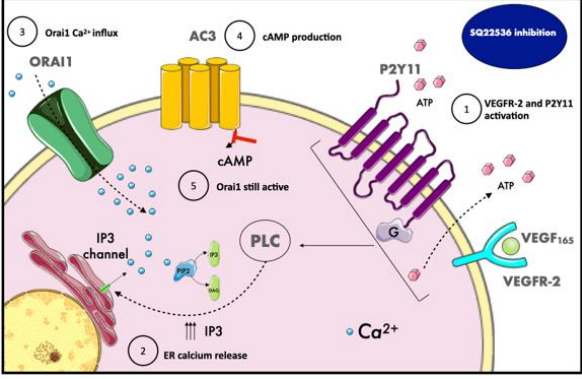
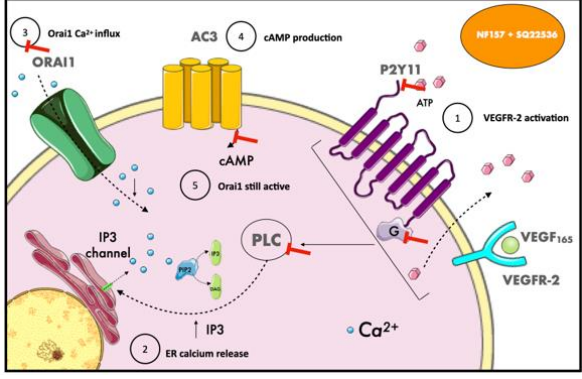
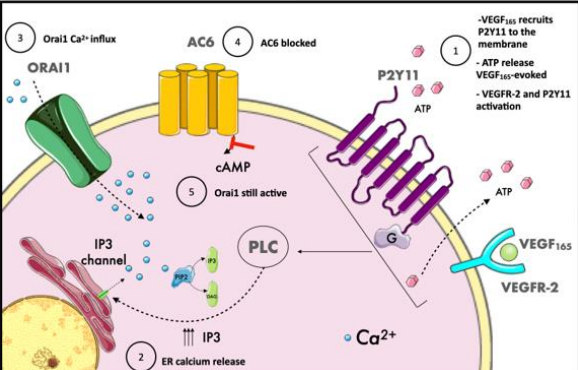
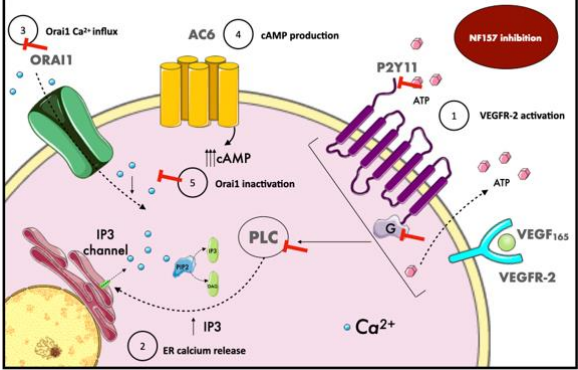
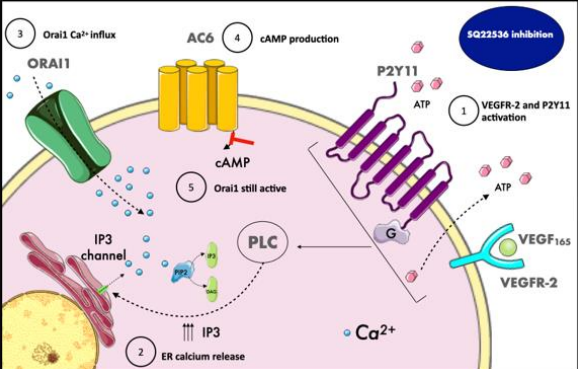
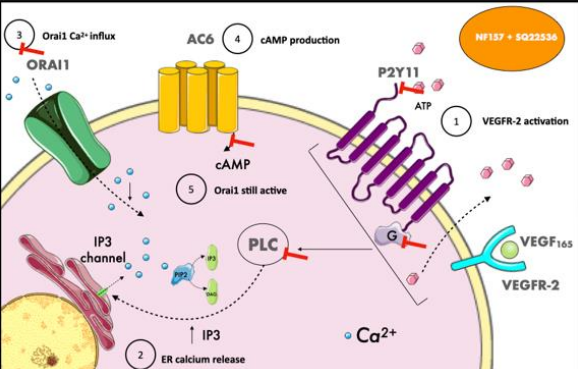
| P2Y11 $G\alpha_q$ -coupled | Mechanism |
|--|--|
| <p>VEGF₁₆₅ stimulation</p> <ol style="list-style-type: none"> 1. VEGF₁₆₅ recruits P2Y11 to the membrane and evokes ATP release to the extracellular milieu. Both receptors activate 2. ER calcium release \uparrow 3. Orai1 Ca²⁺ influx 4. AC8/AC3 activation, cAMP production 5. Orai1 inactivation |  <p> - VEGF₁₆₅ recruits P2Y11 to the membrane - ATP release VEGF₁₆₅-evoked - VEGFR-2 and P2Y11 activation </p> |
| <p>NF157 inhibition</p> <ol style="list-style-type: none"> 1. VEGF₁₆₅ activates while P2Y11 is inhibited 2. Decreased ER calcium release 3. Decreased Orai1 Ca²⁺ influx 4. Decreased AC8/AC3 activation, cAMP production 5. Orai1 inactivation |  <p> - NF157 inhibition </p> |
| <p>SQ22536 inhibition</p> <ol style="list-style-type: none"> 1. VEGF₁₆₅ recruits P2Y11 to the membrane and evokes ATP release to the extracellular milieu. Both receptors activate 2. ER calcium release \uparrow 3. Orai1 Ca²⁺ influx 4. AC8/AC3 blocked, no cAMP production 5. Orai1 still active |  <p> - SQ22536 inhibition </p> |
| <p>NF157 + SQ22536 inhibition</p> <ol style="list-style-type: none"> 1. VEGF₁₆₅ activates while P2Y11 is inhibited 2. Decreased ER calcium release 3. Decreased Orai1 Ca²⁺ influx 4. AC8/AC3 blocked, no cAMP production 5. Orai1 still active |  <p> - NF157 + SQ22536 </p> |

Table 2. Proposed mechanism involving adenylyl cyclase 6 (AC6) isoform.

| P2Y11 G α_q -coupled | Intracellular calcium concentration |
|--|--|
| <p style="text-align: center;">VEGF₁₆₅ stimulation</p> <ol style="list-style-type: none"> 1. VEGF₁₆₅ recruits P2Y11 to the membrane and evokes ATP release to the extracellular milieu. Both receptors activate 2. ER calcium release \uparrow 3. Orai1 Ca²⁺ influx 4. AC6 blocked 5. Orai1 still active |  |
| <p style="text-align: center;">NF157 inhibition</p> <ol style="list-style-type: none"> 1. VEGF₁₆₅ activates while P2Y11 is inhibited 2. Decreased ER calcium release 3. Decreased Orai1 Ca²⁺ influx 4. Increase AC6 activation, cAMP production 5. Orai1 inactivation |  |
| <p style="text-align: center;">SQ22536 inhibition</p> <ol style="list-style-type: none"> 1. VEGF₁₆₅ recruits P2Y11 to the membrane and evokes ATP release to the extracellular milieu. Both receptors activate 2. ER calcium release \uparrow 3. Orai1 Ca²⁺ influx 4. AC6 blocked, no cAMP production 5. Orai1 still active |  |
| <p style="text-align: center;">NF157 + SQ22536 inhibition</p> <ol style="list-style-type: none"> 1. VEGF₁₆₅ activates while P2Y11 is inhibited 2. Decreased ER calcium release 3. Decreased Orai1 Ca²⁺ influx 4. AC6 blocked, no cAMP production 5. Orai1 still active |  |

3.4.4.5 A2B selective antagonist impaired the VEGF₁₆₅ calcium influx in HMEC-1.

Adenosine receptor A2B can promiscuously couple to different G protein types ($G\alpha_s$, $G\alpha_q$, and $G\alpha_i$) (Cohen et al., 2010; Gao et al., 2018). ATP cannot directly activate this receptor, but it could be if hydrolysed to adenosine by ectonucleotidases (Yegutkin, 2014). No effects were observed in the ATP-dependent dose-response curves when incubating HMEC-1 cells in the presence of its selective antagonist, MRS 1754. Due to this indirect way of studying its possible contribution to the ATP-evoked response, it is challenging to make conclusions about its possible coupling nature. Contrary to the observed effects in the ATP dose response, MRS 1754 impaired the VEGF-evoked responses. The antagonist significantly increased the VEGF₁₆₅ peak EC₅₀, and the right shifting fashion is also conserved in the AUC dose-response.

Du et al. (2015) and Ryzhov et al. (2007) showed in HMEC-1 cells transcriptional upregulation of VEGF-A was blocked by MRS 1754. Similarly, Feoktistov et al. (2002) who compared HUVEC and HMEC-1 cells, reported predominantly expression of A2B in HMEC-1, whose stimulation increased the expression of VEGF-A. This effect was not conserved in HUVEC cells, which preferentially express A2A. Furthermore, this work indicated that A2B receptors in HMEC-1 couple to $G\alpha_q$ proteins instead of $G\alpha_s$. Cárdenas et al. (2013) and Patel et al. (2014) illustrated A2B mediation in VEGF overproduction in different kidney cells in rodents, presenting a diabetic physiopathologic state. That overproduction was inhibited *in vivo* using MRS 1754.

Finding works portraying the effects of MRS 1754 in VEGF-dependent evoked responses is very challenging and complicates the interpretation of our data. However, taking all the data describing a specific dependency between A2B activity and VEGF expression together, the observed inhibition does not sound incoherent. Following Feoktistov et al., A2B appears to be $G\alpha_q$ and contributes to the upregulation of VEGF₁₆₅ release. That does not contradict the reported results observed in the ATP dose response, as it was an indirect way of testing activity. In addition, we consider a scenario where A2B translocates to the membrane in the presence of VEGF₁₆₅, which is also based on Li et al. (2011), as we previously suggested for P2Y11. Despite our first hypothesis that A2B might be coupled to $G\alpha_s$ and observed results could agree with P2Y11 inhibition assays if $G\alpha_s$ couple, we consider the possibilities for interpreting this inhibition to be too broad. We cannot directly assume the process involved is the same as the one observed in P2Y11. This inhibition needs to be further explored to reach any conclusion.

3.4.5. Human dermal microvascular endothelial cells (HMEC-1) express different purinergic receptor patterns at the protein level.

3.4.5.1 P2X4 is not expressed in HMEC-1 at the protein level.

Despite the mRNA expression of P2X4 in HMEC-1, most P2X4 antagonists used in this study did not affect the ATP or VEGF-evoked responses. However, PSB12062 did, so protein expression investigation was performed by western blot to document the presence or absence of the receptor.

Whole-cell lysates of three cell lines were used to control the experiment better. As previously described, 1321N1 astrocytoma cells are void of purinergic receptors and ATP-induced responses, and therefore, they portray an ideal model to ascertain the absence of hP2X4. Consistently, stably transfected hP2X4 1321N1 astrocytoma cells that demonstrated their ability to evoke ATP-dependent responses are considered a perfect model to determine the presence of hP2X4. HMEC-1 lysates were run together with these models to conclude whether hP2X4 is expressed in this cell line. The representative immunoblot showed a positive band at 60 kDa for the hP2X4 1321N1 astrocytoma cells, while neither parental nor HMEC-1 cells did. That was confirmed by the semi-quantitative analysis of the relative expression, whose statistical analysis confirmed the significant presence of this band compared to the other two cell lines. This immunoblot was repeated $N=5$ times. As the previously mentioned in the **Results section 3.3.4.1**, unspecific banding was detected in both 1321N1 astrocytoma cells (50 kDa, 30 kDa). However, they do not compromise the detection of the specific weight protein band. We conclude that the anti-P2X4 Alomone (*APR-002*) antibody can detect specific hP2X4 in experimental lysates.

Given these results, we deduced that hP2X4 is not expressed at the protein level in HMEC-1 and, therefore, the PSB12062 effects cannot be P2X4 dependent. That brings some concerns about the selectivity of this antagonism, which has been broadly used to illustrate P2X4-dependent effects in different cells and models. We already mentioned our concerns about the selectivity of the antagonist in both ATP and VEGF responses, as the observed impact in the dose-response curve did not match its theoretical way of action. Hernandez-Olmos et al., who discovered and synthesized this antagonist, described PSB12062 as a non-competitive negative allosteric modulator whose impact on the efficacy was expected but not an increase in the potency, as in the case of the ATP dose responses. Regarding the VEGF responses, PSB12062 did not impact VEGF EC_{50} but impacted the dose-response kinetics and maximal response. Furthermore, as represented in the average time-resolved intracellular calcium responses, the antagonist caused a decrease in calcium upon VEGF injection, something not observed in the control responses. The antagonist was tested in Hernandez-Olmos work against different P2Xs and species, and nonselective effects were observed. This unexpected response does not indicate others' P2 inhibition but probably something else. Reviewing the literature did not bring any other study showing the unexpected effects of PSB12062. Even after considering all our results together, we conclude that PSB12062 is not a reliable tool for studying P2X4 in microvasculature.

There are various reasons why mRNA might not translate to a functional protein within the cell. From the RNA sequencing analysis, we already excluded the ones that are not protein-coding mRNA, so the transcriptional P2X4 expression reported excludes all of those (pseudogenes, long noncoding RNA (lincRNA), etc.). Additionally, we can exclude the presence of antisense P2X4 RNA (asRNA) from the RNA sequencing, which would block its transcription. Even if mRNA is present, regulatory mechanisms can prevent the translation of that mRNA into a functional protein. Some of these regulatory mechanisms include the presence of microRNAs, RNA-binding proteins (Jackson et al., 2010; Sonenberg et al., 2009), or secondary structures (ex., hairpins) that can void ribosomes doing their function (Kozak, 1989). At this point and after a review of the published literature, we need more information to hypothesize what could be the mechanism preventing the protein expression of P2X4.

On the other hand, it is relevant to mention another possibility. The immunoreactive segment of P2X4 receptors may be blurred due to interactions with other macromolecules. The intracellular C-terminal is crucial for interactions among P2X receptors and other proteins and interactions with antibodies targeting this segment. These interactions could potentially lead to false-negative immunoreactivity (Nieto Pescador et al., 2013). Although it is a possibility, and given all the data presented, it is doubtful that this is the case.

Moreover, the location of a protein within a cell can affect its detectability. P2X4 exhibits a distinctive subcellular distribution, showing a preference for localization within lysosomes (Kanellopoulos et al., 2021). However, the anti-P2X4 receptor antibody used in this investigation recognised an epitope localized in the intracellular C-terminus of the protein. Therefore, it could be detected either at the cell membrane or intracellular organelles. Conserved motifs at the C-terminus favour the localization of P2X4 in lysosomes instead of the cell membrane (Kanellopoulos et al., 2021).

Finally, reviewing the published literature did not bring any other work reporting P2X4 expression at the protein level in HMEC-1. Nonetheless, this is not a shared characteristic with other endothelial cell lines, as numerous works reported P2X4 expression at the protein level in HUVEC cells (Lv et al., 2015; Sathanoori, Rosi, et al., 2015; Tang et al., 2008; Yamamoto, Korenaga, Kamiya, Ando, et al., 2000; Yamamoto, Korenaga, Kamiya, Qi, et al., 2000).

3.4.5.2 P2Y2 protein detection is ambiguous in HMEC-1 cells.

P2Y2 demonstrated the highest mRNA expression of the expressed P2 purinergic receptors in HMEC-1, and its selective antagonist, AR-C 118925XX, significantly impacted the ATP and UTP-evoked dose-response curves. Western blot performed a P2Y2 protein expression investigation to document its presence at the protein level.

The first antibody used was the Alomone *APR-010*, using a milk-based blocking solution that is the most commonly used in-house. This antibody binds the epitope localised in its third intracellular loop. Whole-cell lysates of stably transfected hP2X4 1321N1 astrocytoma and HMEC-1 cells were used. As previously described, 1321N1 astrocytoma cells (stably transfected with P2X4 or not) are void of P2Y2 receptors. Therefore, they portray an ideal model to ascertain the absence of hP2Y2. HMEC-1 lysates were run together with this model to conclude whether hP2Y2 is expressed in this cell line. Strikingly, the representative immunoblot showed a positive band at 50 KDa for the hP2X4 1321N1 astrocytoma cells and HMEC-1 cells. We did not expect to see any band in the astrocytoma lysates, and we thought the antibody was not specific and was an invaluable tool for studying the P2Y2 expression in these two cell lines. However, the manufacturer claims the antibody is knock-out validated. Sathanoori et al. (2017) previously reported expression of P2Y2 using this antibody, but nonnegative cell line control is shown. They report a significant decrease of the detected band when siRNA P2Y2 in HUVEC cells. Nonetheless, the band was still detectable and visible after this siRNA. It was unattainable to find any work reporting the use of this antibody or any other anti-P2Y2 in HMEC-1 cells. The P2Y2 expression in HMEC-1 cells at the protein level has yet to be previously reported to our understanding. Contrarily, Martinez et al. (2016) illustrated the lack of band when using an Alomone antibody in parental astrocytoma cells. However, it is relevant to mention that there is no mention of the antibody reference, and we cannot ensure it was the same one we used.

In his master's thesis, Wenker (2005), using the same antibody, reported a lack of banding when testing parental astrocytomas. However, this was not the case when probing the antibody in astrocytomas stably transfected with P2Y₁; unspecific banding appeared. As previously mentioned in this thesis, Gendron et al. (2003) reported by RT-PCR the lack of any P2Y receptors in 1321N1 parental cells. Additionally, we tested the responsiveness of these cells, and no ATP-evoked responses were observed.

The second antibody used was the Abcam *ab168535*, firstly using a milk-based blocking solution that is the most commonly used in-house. Surprisingly, no bands were reported at the appropriate weight (42 kDa). Thus, two other blocking solution configurations were tested. The one 5% sucrose-based showed more prominent bands in the preliminary tests. Therefore, it was used to examine further the presence of P2Y₂ in parental astrocytoma and HMEC-1 cells. In this case, we decided to use parental astrocytoma (not stably transfected) to avoid any indirect possible effect in detecting different P2 receptors. When repeating the western blot with three fresh lysates of astrocytoma parental and HMEC-1 cells, bands at the appropriate weight were detected. However, the detection in astrocytoma parental cells was conserved, as in the case of the Alomone antibody. The manufacturer probed the specificity of the antibody using lysates of non-transfected 293T HEK and stably transfected P2Y₂ 293T HEK cells as a positive control. Their representative immunoblot showed a clear lane in non-transfected 293T cells, detecting bands in the P2Y₂ 293T cells. We decided to extract protein lysates of non-transfected HEK cells available in-house and check whether the band was persistent. The band at the three freshly extracted sample lysates was conserved, but, in this case, the detection level was shallow. When statistically comparing the relative expression of P2Y₂ in non-transfected 293T and HMEC-1 cells, the last ones reported significantly higher levels of the human P2Y₂, presuming the possibility of the antibody's ability to detect the receptor. However, the statistical significance was higher when compared to the parental astrocytoma, making this fact much more challenging to justify. It is tough to believe that astrocytoma expresses P2Y₂ at the protein level at higher levels, as the cells are void of any ATP-evoked response, and P2Y₂ is a very sensitive receptor to this nucleotide. Further investigation of why the antibodies detects something at a specific weight must be executed. Sequencing of this cell line should be performed to isolate high homology regions that might be mimicking the receptor sequence. The manufacturer does not offer a blocking peptide option, so the experimental test to mask the P2Y₂-specific bands was discarded. However, the blocking peptide could hinder off-target binding of the antibody to antigens sharing the same epitope, creating an illusion of specificity (Pillai-Kastoori et al., 2020).

Let us leave aside the unexpected astrocytoma results and consider the data in this study together. P2Y₂ functional evidence concludes that this receptor is functionally expressed in HMEC-1 cells: the RNA sequencing reported the highest value of expression, both ATP and UTP elicited dose responses in values previously reported to be P2Y₂ dependent, and AR-C 118925XX, its selective antagonist, effectively blocked its response. In addition, when comparing the relative protein expression of non-transfected 293T cells and HMEC-1 cells, the latter reported significantly higher levels.

The sucrose-based buffer had better performance when probing the anti-P2Y₂ Abcam antibody. The choice of blocking buffer is critical for the success of immunoassays. Blockers are crucial in enhancing sensitivity by diminishing background interference, improving the signal-

to-noise ratio, facilitating specific binding of the primary antibody, and decreasing non-specific interactions (Ambroz et al., 2008; Licor, 2008; Pillai-Kastoori et al., 2020). Specific blocking buffers, such as milk-based ones, have been seen to mask and interfere with detecting specific target proteins (Denhollander et al., 1989; Pillai-Kastoori et al., 2020). That might be the case we observed with this antibody. The observation was practically identical when using a 10% BSA blocking buffer. The blocking buffer selection was run in parallel with the anti-P2Y11 antibodies, where we faced the same issue when first probing the Abcam antibodies. At the time, we found Paz Prada et al. work, where certain specifications were cited. In that investigation, five primary antibodies were probed, and all of them but anti-P2Y11 were diluted in milk-based blocking solutions, and membranes were blocked in the same way. In the particular case of the P2Y11 antibody, they specified using a nonmammalian blocking buffer for the blocking step and diluting the primary antibody in 1% bovine serum albumin. We understood they might have faced similar problems when using milk-based buffers. They used Odyssey blocking buffer, which was unavailable in-house when performing these assays. The Odyssey blocking buffer composition is confidential, so we decided to use sucrose-based blocking, as it was the only alternative we found when avoiding any mammalian component, as other members of the laboratory use sucrose in their routine immunohistochemistry procedures.

A blocking buffer refers to a solution containing a protein, a mixture of proteins, or other compounds that passively adsorb to all remaining binding surfaces of the plate. Sucrose is not commonly used as a blocker buffer in western blot, but its use in another protein-related blocking process has been described. Dubrow et al. (2022) found that saccharides act as an excellent blocker of nonspecific binding in quantitative analysis of protein-protein interactions. Similarly, Yazdani et al. (2015) pointed out that disaccharides can be a good tool to maintain the stability of antibodies and decrease background noise in ELISAs. We have probed sucrose-based buffers as a good alternative to studying the protein expression of P2Y receptors.

3.4.5.3 P2Y11 is expressed in HMEC-1 at the protein level.

P2Y11 demonstrated the second highest mRNA expression, after P2Y2, of the expressed P2 purinergic receptors in HMEC-1, and its selective antagonist, NF157, significantly impacted the VEGF₁₆₅-evoked dose-response curves. We have hypothesized different mechanisms by which P2Y11 might be mediating this inhibition. Western blot performed a P2Y11 protein expression investigation to document its presence at the protein level and gain more evidence of the P2Y11 possible involvement in the mentioned mechanisms.

The first antibody used was Alomone *APR-015*, using a milk-based blocking solution. This antibody binds the epitope localized in the intracellular C-terminus. Whole-cell lysates of parental 1321N1 astrocytoma and HMEC-1 cells were used. HMEC-1 and parental lysates were run to conclude whether hP2Y2 is expressed in this cell line. Again, the representative immunoblot showed a detectable band at 50 KDa for both cell lines, as observed when studying P2Y2 expression. No band was expected in the astrocytoma lysates, and we moved forward to study the P2Y11 expression in these two cell lines using an Abcam antibody. These assays were run in parallel with P2Y2. Hence, we moved to a new antibody in both cases, needing more time to return and reprobe Alomone antibodies in different conditions. Bátori et al. (2019) previously reported the expression of P2Y11 using this antibody. They report a significant

decrease of the detected band when siRNA P2Y11 in HLMVEC, another type of microvasculature endothelial model. Similarly, Chadet et al. (2015) showed expression of the receptor whose band was significantly decreased when siRNA-treated in human dendritic cells. No works reported this antibody's use in parental astrocytoma cells. It is hard to accept that astrocytoma expresses P2Y11 at the protein level, and additional investigation of why the antibodies detect something at a specific weight must be performed, as previously discussed for P2Y2.

The second antibody used was Abcam ab180739, which was first probed in a milk-based blocking solution. Again, no bands were reported at the appropriate weight (43 kDa). Consequently, four other blocking solution configurations were tested. We replicated what Paz Prada et al. (2019) did using these buffers instead of the Odyssey blocking buffer. The 5% sucrose-based buffer was the only buffer showing bands in the correct weight in the preliminary tests, and it was used to examine further the presence of P2Y11 in parental astrocytoma and HMEC-1 cells. In the preliminary test, the relative expression of P2Y11 in HMEC-1 was already higher than in the astrocytoma cells. When repeating the western blot with three fresh lysates of astrocytoma parental and HMEC-1 cells, bands at the appropriate weight were detected. In this case, the detection in astrocytoma parental cells significantly decreased compared to HMEC-1 cells. The 5% sucrose-based blocking solution is then the suitable blocking buffer to investigate the presence of P2Y11 in these two cell lines.

Despite the band shallowed in the astrocytoma parental, we wanted to investigate if that band could be due to non-specific secondary antibody detection. Anti-rabbit HRP conjugated secondary antibody was used in most western blots presented in this thesis. When the antibody was directly probed after the blocking step as a negative control only, residual non-specific banding was detected in HMEC-1 and parental astrocytoma cell lysates, contributing to the 43 kDa P2Y11 specific band. The detected bands are residual but could contribute to the bands we observed when probing with the primary antibody. Anti-rabbit HRP conjugated secondary antibody can bind the heavy and light chains of the IgG molecule, or in other words, the crystallized fragment of the IgG (Fc) or the two antigen-binding fragments (F(ab')₂) (Novus Biologicals, 2017). In trying to find an alternative option, the same secondary negative control was performed using an anti-rabbit F(ab')₂ antibody available in-house. F(ab')₂ secondary antibodies do not bind the Fc of the IgG, avoiding the non-specific binding between Fc portions of antibodies. In the same way, this antibody will prevent non-specific binding to the Fc receptor in live cells (Jackson ImmunoResearch Laboratories, 2017). However, this possibility is unlikely as Fc receptors are usually expressed in immunological cells as macrophages. Again, this negative control illustrated non-specific banding between 37-50 kDa and strong binding between 25-37 kDa. Both anti-rabbit (H+L) and F(ab')₂ secondary antibodies showed non-specific banding at 50 kDa. Therefore, we can conclude that the bands are not Fc portion dependent but non-specific banding due to the secondary antibody picking up something in the sample. Anti-rabbit (H+L) showed less relative expression of this unexpected banding, so it was chosen to proceed with the experiments. Although some of the detected bands when probing the anti-P2Y11 Abcam antibody could be increased by this secondary non-specific banding, if subtracting this signalling from the primary antibody probed blot, the remaining signals will demonstrate a very residual banding in the astrocytoma parental cells and a detectable remaining banding for HMEC-1 cells. All these data together confirm the presence of P2Y11 in HMEC-1 cells at the protein level.

3.4.6. Human umbilical vein endothelial cells (HUVEC) express various purinergic receptors at the transcriptional level.

HUVEC cells have been previously reported as an excellent model for investigating VEGF-dependent calcium responses in the endothelium and the relevance of other receptors to the VEGF receptor responses (Li et al., 2011, 2015). Using a primary cell model was considered relevant to test the observed P2Y11 contribution to the VEGF responses but before that, we needed to confirm the purinergic transcriptional profile in this cell line using RT-PCR.

A higher percentage of the purinergic receptors were found in HUVECs compared with the HMEC-1 purinergic profile. Two adenosine receptors were found at the transcriptional level, A2A and A2B. This profile pattern was previously described by others (Feoktistov et al., 2002; Feoktistov et al., 2004; Lang et al., 2023). Some authors have reported the expression of the four adenosine receptors in HUVECs (Deguchi et al., 1998; Fernandez et al., 2012). HUVEC cells can be cultured in different manners, and isolation in-house or in a manufactured batch might affect the expressed pattern of these cells. Feoktistov et al. reported a preferable expression of A2A above A2B in this cell line, but our data is not quantitative, so further comparison is unattainable. Interestingly, they showed adenosine dependency for VEGF modulation in HMEC-1 cells, but this dependency was not conserved in HUVEC cells.

Of the P2X receptors, P2X4, P2X5, and P2X7 were detected in HUVECs. Lang et al. (2023) reported the expression of P2X4 and P2X7 in their RNA sequencing. Consistently, Tang et al. (2008); Wilson et al. (2007), and Yamamoto, Korenaga, Kamiya, Qi, et al. (2000) reported the same pattern profile as the one we observed in this study. P2X6 expression in HUVEC cells has been previously reported (Glass et al., 2002; Ralevic, 2012), but that was never the case in our $N=5$ repetitions, while it was consistently detected in the positive control.

Most literature agrees with the expression of P2Y2 at the mRNA level in HUVECs, which is one of the most studied P2 receptors using these cells (Cabou et al., 2022; Kukulski et al., 2010; Lang et al., 2023; Mühleder et al., 2020; Sathanoori et al., 2017; Wang et al., 2015). Additionally, we showed expression of P2Y1, P2Y4, P2Y6, P2Y12, P2Y14 and, in some level, of P2Y11. P2Y1, P2Y2, P2Y6, and P2Y11 have been previously shown to be expressed in HUVECs (Cabou et al., 2022; Lang et al., 2023), while P2Y4 and P2Y14 have been reported to a lower extent (Cabou et al., 2022). Induction of P2Y12 in HUVECs has also been previously shown (Shanker et al., 2006). P2Y11 demonstrated an inconsistent expression pattern in our transcriptional investigation. If we compared our data with HUVECs RNA sequencing by Lang et al., P2Y11 showed a higher expression level than any other P2Y receptor in HUVECs. This substantial difference in P2Y11 expression might be due to technical variations when culturing HUVECs and the isolation method. Lang et al. HUVEC cells were freshly isolated from human umbilical veins of a donated placenta, while ours, for example, were bought from PromoCell. One of the main differences in the isolation/culturing process is the variation of supplemented factors in the culturing media. Some groups used endothelial media supplemented with VEGF (Lang et al., 2023; Li et al., 2011, 2015), and others, as in our case, without VEGF (Swain et al., 2021). These differences could affect the mRNA pattern expression observed in the cell line. Indirectly, this data could indicate a dependency of VEGF-A in this cell line for P2Y11.

3.4.7. VEGF receptors contribute to endothelial calcium homeostasis in HUVECs, and their trace kinetics differ from those observed in HMEC-1 cells.

Most investigations illustrating VEGF₁₆₅ responses were performed in HUVECs, as previously mentioned. In this work, we have confirmed the ability of these cells to respond to this ligand by building a dose-response curve using six different concentrations. VEGF₁₆₅ elicited intracellular calcium response in a concentration-dependent manner with a half-maximal effective concentration of 1.7 ± 0.4 ng/mL for the peak and 2.4 ± 0.4 ng/mL for the AUC. Although these potencies are not significantly different from the ones reported in HMEC-1 cells, there is an apparent difference in dose-response kinetics between the two cell lines, showing HUVECs as the steepest curve. Additionally, the efficacy was significantly higher for the peak and the AUC in HUVECs. VEGF₁₆₅ responses are more prominent in HUVECs than HMEC-1.

We previously compared VEGF₁₆₅ (100 ng/mL) trace kinetics in HMEC-1 in the presence of extracellular calcium to the one described by Li et al. in HUVEC cells. Let us now compare that HUVEC trace kinetics to our HUVEC data. Oppositely to what we reported in HMEC-1, HUVEC illustrated two distinct phases, the transient and sustained, described by them with some noticeable differences. The two phases in their trace are much more distinguished than in our data. Their response is characterized by a remarkable transient peak, which deeply decays, followed by the sustained phase. In our case, the peak is quickly reached at high concentrations after VEGF₁₆₅ application, but a deep decay of the recorded calcium does not precede the sustained phase. These calcium responses appear to be less dependent on the calcium release from stores of the ones reported by Li et al. but more than our HMEC-1 ones. If we compared our culturing conditions of HUVECs with Li et al., we could see a clear difference that might affect the expression of VEGF₁₆₅ receptors. Our culture media does not contain VEGF₁₆₅, while theirs does contain this supplementation. That could explain differences in trace kinetics observed in the same assay conditions.

Generally, the magnitude of the calcium responses evoked by VEGF₁₆₅ in both cell lines is always vastly lower than the ones evoked by ATP. If we talk in peak raw data terms, VEGF₁₆₅ maximal responses are around $F_{\text{ratio}} \approx 0.5-0.6$, while ATP responses can evoke much higher calcium responses around $F_{\text{ratio}} \approx 1.5-2$ in endothelial cell lines. This tendency is translatable to AUC values.

3.4.7.1 P2Y11 selective antagonist did not impair the VEGF₁₆₅ calcium influx in HUVECs.

Following the rationale maintained in this thesis, an inhibitory preliminary test was first done with PPADs. This was performed as a proof of concept to evaluate if the observed effect in the HMEC-1 cell was conserved. Directly after that, we tested the effects of the P2Y11 selective inhibitor in the VEGF₁₆₅ evoked response in HUVECs. In this case, NF157 was ineffective in inhibiting VEGF-induced responses. That does not directly mean the contribution of P2Y11 to the VEGF₁₆₅ is not consistent because there are some reasons why we could not see any inhibitory effects. When discussing the transcriptional expression of P2Y11, we already mentioned the inconsistency in detecting P2Y11 bands in the PCR. That observation could

suggest deficient expression of P2Y11 in this cell line; therefore, isolating P2Y11 effects would be very tricky. Due to this inconsistent detection, we consider it relevant to perform our RNA sequencing of this cell line and protein expression assays to confirm the relevance of using HUVECs for understanding the proposed mechanisms. In addition, P2Y11 could be coupled to the opposite G protein to the one it does in HMEC-1 cells, meaning it could not be mediation of the response by the exact mechanism. Further experimental assays are needed to reach any conclusion of the observed effects in HUVECs.

3.4.8. Purinergic receptors contribute to the endothelial calcium homeostasis in HUVECs, and their trace kinetics differ from those observed in HMEC-1 cells.

Profiling the ATP pharmacological response in HUVECs was needed to investigate the mechanistic differences between HMEC-1 and HUVEC cells. As in the case of HMEC-1 cells, HUVECs responded to ATP dose-dependently with a half-maximal effective concentration of $1.77 \pm 0.28 \mu\text{M}$ for the peak and $6.58 \pm 0.2 \mu\text{M}$ for the AUC. These potencies are significantly lower than the ones reported in HMEC-1 cells. If we look at HUVECs traces kinetics, there is a clear difference when compared to HMEC-1 cells. The sustained response phase to ATP in HUVECs is vastly lower than observed in the other model, while the transient phase is the primary mediator in the response in HUVECs. The transient dependency of the response is portrayed in the cited potencies, as peak potency is almost four times lower than the AUC. This data shows a greater dependency of the HUVECs response in the intracellular store's calcium release and less contribution of ion-channel influx, as late sustained responses are thought to be more membrane influx dependent. Our data agrees with that of Cortés et al. (2013) and Raqeeb et al. (2011), who previously showed similar trace kinetics in HUVECs. Both reported potencies in the micromolar range in agreement with what we observed, $3.04 \mu\text{M}$ and $8.4 \mu\text{M}$, respectively. Oppositely to the observed with the VEGF₁₆₅ responses, ATP responses are more prominent in HMEC-1 than HUVECs. This data illustrates a different functional expression of P2 and VEGF receptors.

3.4.8.1 The SERCA inhibitor thapsigargin impaired the ATP calcium influx in HUVECs, while BX430 could not inhibit the studied responses.

As in the case of HMEC-1 cells, thapsigargin abolished the ATP-evoked responses in HUVECs. This block suggests an explicit dependency on metabotropic P2Y receptors for the ATP-dependent response. P2Y2 has been previously reported as the P2 primary mediator of the purinergic regulation homeostasis in HUVECs (Liao et al., 2014; Raqeeb et al., 2011; Sanabria et al., 2008; Tanaka et al., 2004; Wang et al., 2016). To confirm this fact, we consider it relevant to use its selective inhibitor, AR-C 118925XX, to confirm its involvement in our ATP-evoked response as the next step in this study. Additionally, characterisation of UTP responses and potency calculations could help us to complement the pharmacological study as others have done before (Raqeeb et al., 2011; Sanabria et al., 2008).

On the other hand, P2X4 has also been pointed out as a relevant mediator of ATP-evoked responses in HUVECs. Lang et al. RNA sequencing demonstrated P2X4 as the most expressed P2 receptor in HUVECs, which agrees with previous reports (Tang et al., 2008; Wilson et al., 2007; Yamamoto, Korenaga, Kamiya, Ando, et al., 2000; Yamamoto, Korenaga, Kamiya, Qi, et

al., 2000). However, the selective P2X4 antagonist, BX430, could not block the ATP-evoked response at 30 μ M. We tested only a single concentration, and we consider it relevant to dig further into the P2X4 dependent responses in HUVECs, as a *nonpublished* protein expression analysis done in collaboration with Dr. Fortuny-Gomez confirmed P2X4 expression in HUVECs. As previously mentioned, P2X4 prefers localization within lysosomes (Kanellopoulos et al., 2021). We performed the pharmacological characterisation in static conditions. Still, others have shown P2X4 activity under shear stress (Yamamoto, Korenaga, Kamiya, Ando, et al., 2000), meaning the membrane localization of the receptor could vary depending on the stimulus source and its physical characteristics.

Chapter 4. Exploring the contribution of purinergic receptors in mechanosensitive evoked calcium responses.

4.1 Introduction

Piezo ion channels convert mechanical stimulus into various biological activities through a process called mechanotransduction. Piezo1 is activated through cell membrane deformations caused by mechanical forces, such as osmotic pressure, fluid shear stress, substrate stiffness, and confinement (Coste et al., 2010; Ranade et al., 2014). When Piezo1 is activated, it induces calcium influx, transducing mechanical forces into biochemical responses (Dombroski et al., 2021). Piezo1 has broad roles in multiple physiological processes, including sensing shear stress of blood flow for proper blood vessel development, regulating red blood cell function, and controlling cell migration and differentiation (Ge et al., 2015). Piezo1 is considered the central blood flow sensor and transducer of shear-stress-evoked calcium influx in endothelial cells (Li et al., 2014).

Multiple experimental manipulations can stimulate Piezo1. The most used are “stretch” and “poke” combined with patch-clamp electrophysiology. High-pressure perfusion is an alternative method to deform the cell without physically contacting the membrane. By contrast, shear flow achieved through microfluidic channels applies parallel stress to the substrate surface (Wu et al., 2017). In addition to these methods, Syeda et al. discovered a chemical agonist called Yoda1. In HEK cells overexpressing the channel, Yoda 1 slows the inactivation phase of transient currents, sensitizes Piezo1 to activation by a mechanical stimulus, and partially activates channels (Botello-Smith et al., 2019). Furthermore, Yoda1 is considered a tool to mimic laminar flow *in vitro* (Davies et al., 2019).

Various studies show the dependency of ATP release upon mechanical stimulation in the shear stress-induced calcium response. The purinergic receptors have been classified as shear stress-sensitive, and different subunits may contribute to the calcium influx shear stress-dependent. The two purinergic subtypes investigated to have a role in this process are P2Y2 and P2X4 (Gerhold et al., 2016). However, their role in the shear stress sensing process must be better understood.

4.2 Aims

This chapter aimed to interrogate the contribution of the purinergic receptors in the shear stress-dependent calcium signalling using pharmacological and mechanical methods.

The specific goals were as follows:

1. To determine the functional expression of Piezo1 in HMEC-1 and HUVEC cells using a pharmacological strategy.
2. To elucidate the possible contribution of purinergic receptors in Piezo1 calcium signalling using the P2 broad-spectrum antagonist in HMEC-1 and HUVEC cells.
3. To set up a functional parallel flow system to mechanically stimulate endothelial cells *in vitro* and study the purinergic contribution of purinergic receptors in the shear-stress evoked responses.
4. To explore the utility of the Griess reagent system to measure nitric oxide release in endothelial cells.

4.3 Results

4.3.1. Characterisation of Piezo1 signalling in human microvascular endothelial cells (HMEC-1) and human umbilical vein cells (HUVEC).

Yoda1, the Piezo1 selective agonist, was used in the early experiments to determine its potency and efficacy in human microvascular endothelial cells (HMEC-1) and human umbilical vein endothelial cells (HUVECs). This data was complemented with some selective antagonism assays to characterise better the possible Piezo1-dependent response. Both models were considered relevant in this study as they have been demonstrated to respond to a mechanical stimulus (Carrillo-Garcia et al., 2021; Li et al., 2014), and they were used to set up the parallel flow system to stimulate the cells mechanically *in vitro*.

4.3.1.1 Yoda1 evoked calcium responses in human microvascular endothelial cells (HMEC-1), and this response was inhibited in the presence of GsMTx4.

Yoda1 elicited intracellular calcium response in a dose-dependent manner (0.03 to 30 μM) with a maximal response at 20 μM for the peak ($105.35 \pm 4.1\%$) and the area under the curve (AUC) ($109.1 \pm 3.6\%$). The half-maximal effective concentration for the peak was $\text{EC}_{50}^{\text{peak}} = 559 \pm 83$ nM and $\text{EC}_{50}^{\text{AUC}} = 623 \pm 91$ nM for the AUC (**Figure 1-A, B**). **Figure 1-C** depicts time-resolved calcium responses upon Yoda1 stimulation from 0.03 to 30 μM . This stimulation evoked an extremely rapid initial response at high concentrations (3-30 μM) followed by a sustained phase that barely decayed over approximately four minutes. At lower concentrations, 300 nM and 1 μM , the responses lost their ability to induce such a quick response, and they portrayed a more sustained trace kinetics.

GsMTx4, a spider venom peptide, was used to characterise the Piezo1 involvement in the Yoda1-induced calcium responses in HMEC-1. GsMTx4 inhibits cationic mechanosensitive channels from the Piezo and transient receptor potential (TRP) channel families (Bae et al., 2011; Bowman et al., 2007; Suchyna et al., 2000) and it has been used to inhibit Yoda1-evoked responses (Venturini et al., 2020; Wadud et al., 2020). Therefore, the venom was used as a tool to further investigate Piezo1 functional expression in HMEC-1 cells.

Cells were treated with 2.5 and 10 μM of GsMTx4, and the rise in intracellular calcium was measured when stimulating with three different concentrations of Yoda1 (3 μM , 1 μM , and 300 nM) in the presence and the absence of the inhibitor. GsMTx4 decreased the Yoda1-induced calcium response both at 1 μM and 300 nM when using the highest venom concentration (10 μM) (**Figure 2-D, E, F**). The effect was more evident at 300 nM for the peak and the AUC, and that was represented in **Figure 2-F**, where the representative calcium-response trace revealed the impact of the inhibitor compared with the control in the absence of the venom. In the presence of GsMTx4, the activation kinetics at 300 nM Yoda1 showed a decrease of the response that decayed approximately to baseline ($F_{\text{ratio}} \approx 0.2$) compared to the six times bigger response in the absence of the modulator ($F_{\text{ratio}} \approx 0.8$). In comparison, that was not the case at the venom's lowest concentration (2.5 μM), where effects could not be found at any of the Yoda1 concentrations applied (3 μM , 1 μM , and 300 nM) (**Figure 2-A, B, C**). It is relevant to mention that statistical significance is not performed as the experiments were not done thrice because of the unavailability of the drug in-house, so a definitive statement about the venom effects cannot be made. However, the inhibition pattern is illustrated in the previously described assays at 10 μM .

It is relevant to note that the GsMTx4 assays were done in a slightly different manner than all of the other inhibition assays presented in this study. In this particular case, besides preincubate the HMEC-1 cells in the presence of 10 μM Gsmtx4, the inhibitor was also present in the agonist injection solution to compensate for the concentration in the cell plate and ensure a constant concentration of the venom throughout the experiment. A decrease in the venom's final concentration impaired the inhibition effects (data not shown). Therefore, the configuration that helped study this inhibition was the same as in electrophysiological assays.

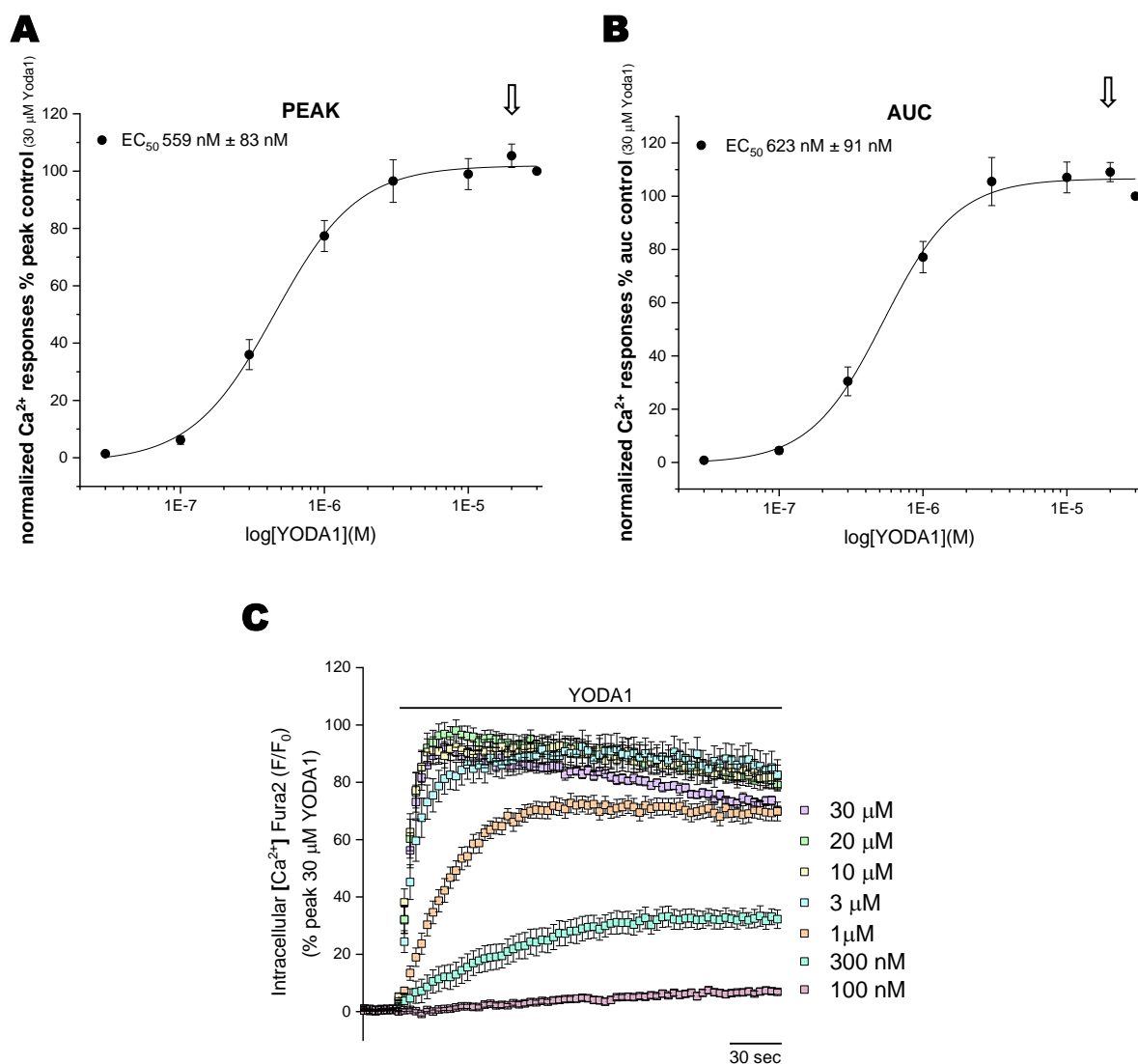


Figure 1. Yoda1 elicited intracellular calcium responses in human microvascular endothelial cells (HMEC-1). Concentration-response curves for the peak (A) and AUC (B) magnitude of intracellular Ca^{2+} responses elicited by Yoda1 (0.03-30 μM ; $N=5$). (C) Averaged time-resolved intracellular Ca^{2+} responses elicited by Yoda1 from 30 μM to 100 nM in HMEC-1 cells over 250 seconds ($N=5$). All data were normalised to 30 μM Yoda1 and fit the Hill1 equation with the EC_{50} values showed in the graphs. Data are represented as mean \pm SEM.

(*) Data normalisation was always done at 30 μM Yoda1 when this agonist was studied.

(**) Arrows (\Downarrow) indicate the maximum response in the control (untreated) curve.

(***) F/F_0 refers to the Fura2 ratio, meaning F340/F380.

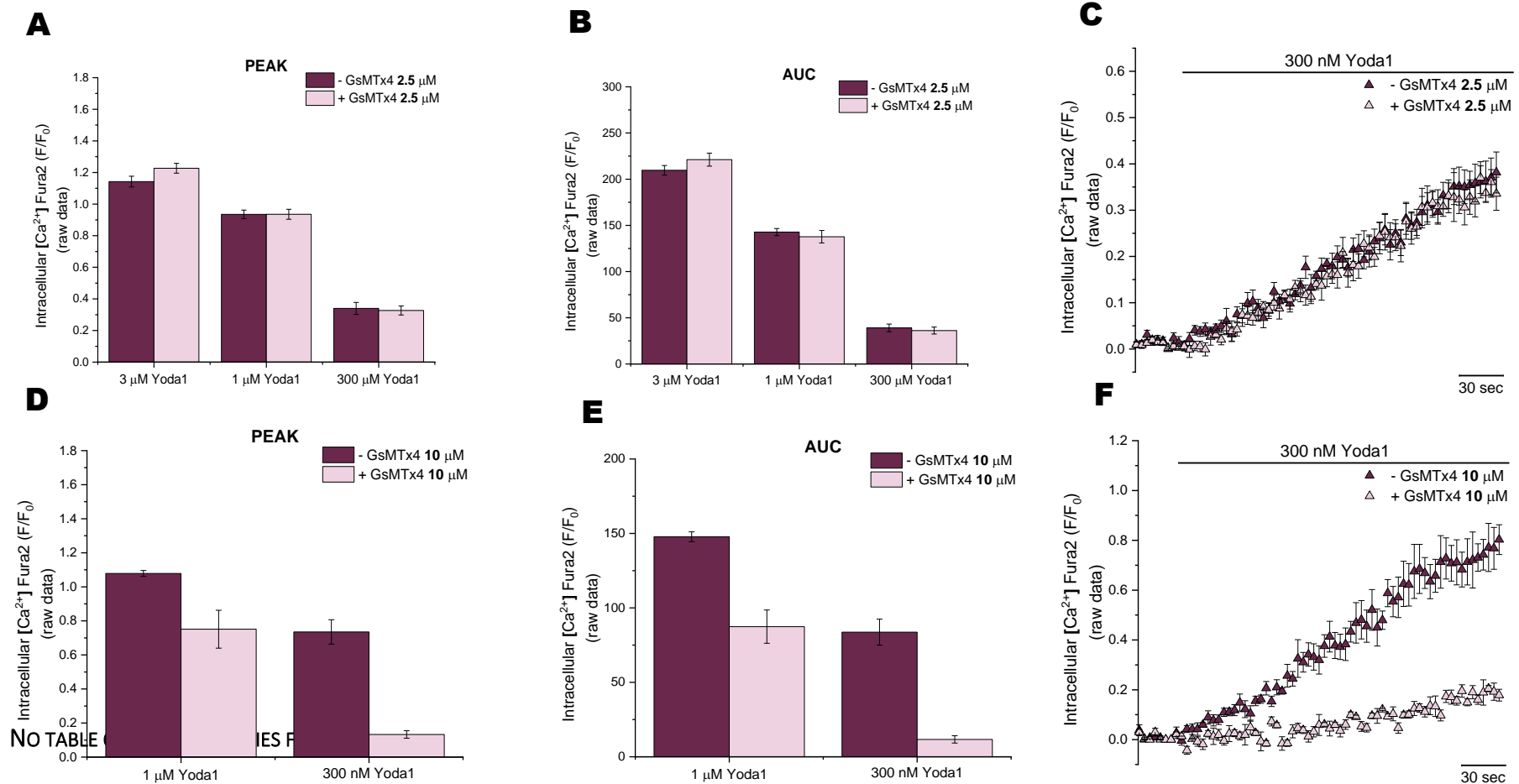


Figure 2. GsMTx4, the spider venom peptide, inhibited Yoda1-induced Ca²⁺ response in human microvascular endothelial cells (HMEC-1). Comparison of peak (A) and AUC (B) magnitude of intracellular Ca²⁺ responses induced by Yoda1 at three different (3 μM, 1 μM and 300 nM) concentrations in the presence (light pink; N=2) or absence (dark pink; N=2) of GsMTx4 2.5 μM. (C) Averaged time-resolved intracellular Ca²⁺ responses elicited by Yoda1 300 nM in the presence (light pink triangle; N=2) or absence (dark pink triangle; N=2) of GsMTx4 2.5 μM over 250 seconds. Comparison of peak (D) and AUC (E) magnitude of intracellular Ca²⁺ responses induced by Yoda1 at three different (3 μM, 1 μM and 300 nM) concentrations in the presence (light pink; N=2) or absence (dark pink; N=2) of GsMTx4 10 μM. (F) Averaged time-resolved intracellular Ca²⁺ responses elicited by Yoda1 300 nM in the presence (light pink triangle; N=2) or absence (dark pink triangle; N=2) of GsMTx4 10 μM over 250 seconds. Data are represented as mean ± SEM.

4.3.1.2 Yoda1 evoked calcium responses in human umbilical vein endothelial cells (HUVEC), and this response was inhibited in the presence of Dooku1.

Yoda1 elicited intracellular calcium response in a concentration-dependent manner (0.03 to 30 μ M) with a maximal response at 20 μ M for the peak ($111.5 \pm 8.95\%$) and for the area under the curve (AUC) ($116.2 \pm 8.6\%$). The half-maximal effective concentration for the peak was $EC_{50}^{peak} = 1.24 \pm 0.109 \mu$ M and $EC_{50}^{AUC} = 1.41 \pm 0.29 \mu$ M for the AUC (**Figure 3-A, B**), **Table 2**). **Figure 3-C** illustrates time-resolved calcium responses upon Yoda1 stimulation from 0.03 to 30 μ M. This stimulation evoked a rapid initial response at high concentrations (3-30 μ M) followed by a sustained phase humbly decayed over approximately four minutes. At lower concentrations, specifically 300 nM and 1 μ M, the responses lost their capacity to elicit a rapid reaction and instead sustained more prolonged trace kinetics.

In the absence of extracellular calcium, the maximal responses elicited by Yoda1 were significantly decreased to $5.5 \pm 0.5\%$ ($p < 0.001$) for the peak and $7.2 \pm 0.8\%$ ($p < 0.001$) for the AUC of response in the presence of calcium (**Figure 4-A, B, E**). Furthermore, the half-maximal effective concentration did significantly change for the peak $EC_{50}^{peak} = 171.23 \pm 155.3 \text{ M}$ ($p < 0.05$) and the AUC $EC_{50}^{AUC} = 19.49 \pm 19.37 \text{ M}$ ($p < 0.05$) when the cells were exposed to Yoda1 in a calcium-free saline bath solution (**Figure 4-E**). In the absence of calcium, 3 μ M Yoda1 did not evoke any calcium response, being the same as the baseline (**Figure 4-C**). However, at 20 μ M Yoda1, there is a residual calcium increase that was illustrated in **Figure 4-D**. That might indicate activation of the Piezo1 channel in the intracellular stores.

Dooku1 was used to antagonise Yoda1 responses. Dooku1 effectively reversibly inhibits Yoda1 effects, with an IC_{50} of approximately 1.5 μ M in endothelial cells. The inhibitor does not impact constitutive Piezo1 channel activity. However, it acts as an antagonist against Yoda1-induced Piezo1 activation in endothelial cells and delays Yoda1-induced Ca^{2+} entry *in vitro* (Evans et al., 2018). Hence, Dooku1 was employed as a tool to examine the expected canonical behaviour of Yoda1-induced Piezo1 responses and assess the potential inhibition of these responses by the drug.

HUVEC cells were incubated for 30 minutes in a range of antagonist concentrations (0.25 to 10 μ M) and stimulated with 8 μ M Yoda1, and thereby, IC_{50} was calculated (**Figure 5-A, B**). The half-maximal inhibitory concentration values obtained were $IC_{50}^{peak} = 716 \pm 124 \text{ nM}$ for the peak and $IC_{50}^{AUC} = 753 \pm 139 \text{ nM}$ for the AUC inhibition curves. The representative time-resolved intracellular calcium responses shown in **Figure 5-C** depicted 1 μ M Dooku1's significant impact on the peak and the AUC upon 8 μ M Yoda1 stimulation compared with the control in the absence of the antagonist. In the presence of Dooku1, Yoda1 profiled the same trace kinetics, but the peak response was significantly decreased to 40% above baseline. These results were not far from what has been previously reported in endothelial cells.

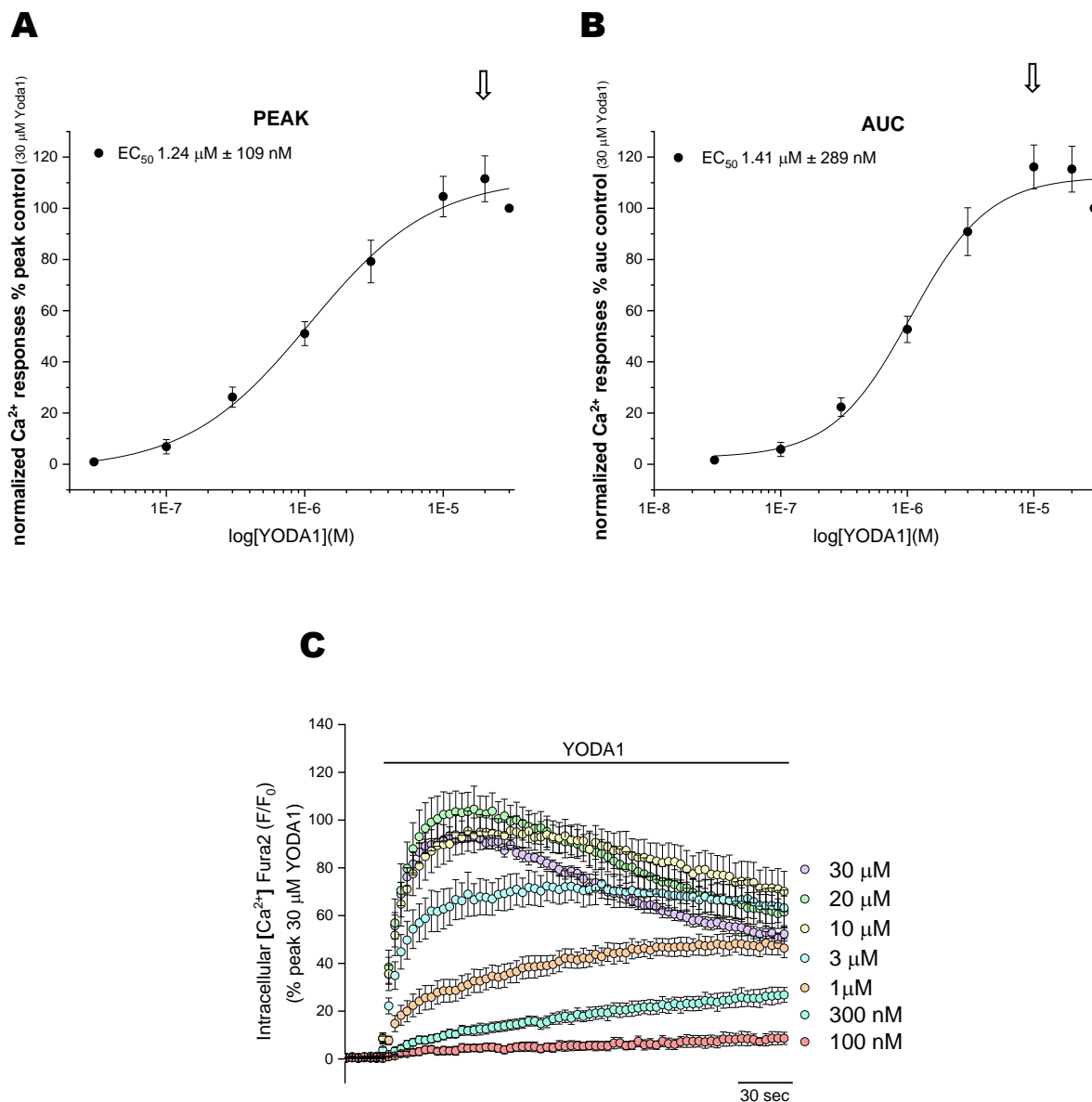


Figure 3. Yoda1 elicited intracellular calcium responses in human umbilical vein endothelial cells (HUVEC). Concentration-response curves for the peak (**A**) and AUC (**B**) magnitude of intracellular Ca^{2+} responses elicited by Yoda1 (0.03-30 μM ; $N=5$). (**C**) Averaged time-resolved intracellular Ca^{2+} responses elicited by Yoda1 from 30 μM to 100 nM in HUVEC cells over 250 seconds ($N=5$). All data were normalised to 30 μM Yoda1 and fit the Hill1 equation with the EC_{50} values showed in the graphs. Data are represented as mean \pm SEM.

(*) Data normalisation was always done at 30 μM Yoda1 when this agonist was studied.

(**) Arrows (\Downarrow) indicate the maximum response in the control (untreated) curve.

(***) F/F_0 refers to the Fura2 ratio, meaning F_{340}/F_{380} .

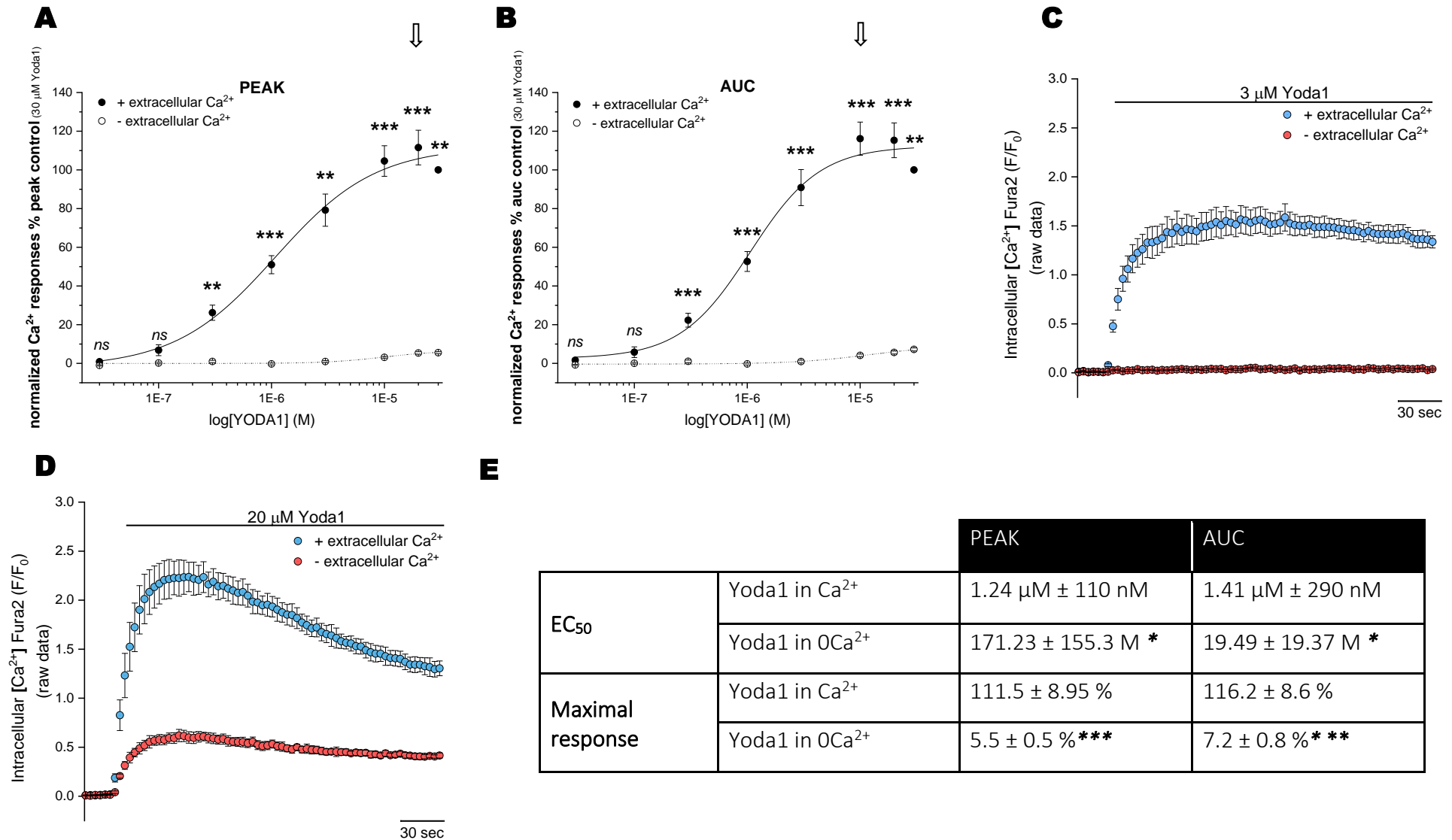


Figure 4. Removing extracellular calcium diminished the Yoda1-evoked response in human umbilical vein endothelial cells (HUVEC). Concentration-response curves for the peak (A) and AUC (B) magnitude of intracellular Ca^{2+} responses elicited by Yoda1 (0.03–30 μM ; $N=5$) in the presence (0.03–30 μM ; closed circles; $N=5$) or absence (0.03–30 μM ; open circles; $N=5$) of extracellular calcium. Averaged time-resolved intracellular Ca^{2+} responses elicited by Yoda1 3 μM (C) or 20

μM (D) in the presence (blue circle; $N=5$) or absence (red circle; $N=5$) of extracellular calcium over 250 seconds. Data in A and B were normalised to 30 μM Yoda1 in the presence of extracellular calcium and fit the Hill1 equation with the EC_{50} and maximal response values showed in table (E). Asterisks show statistical significance relative to Yoda1 potency and Yoda1 % of maximal response ($p_{ns} > 0.05$, $p^* < 0.05$, $p^{**} < 0.01$, $p^{***} < 0.001$). Data are represented as mean \pm SEM.

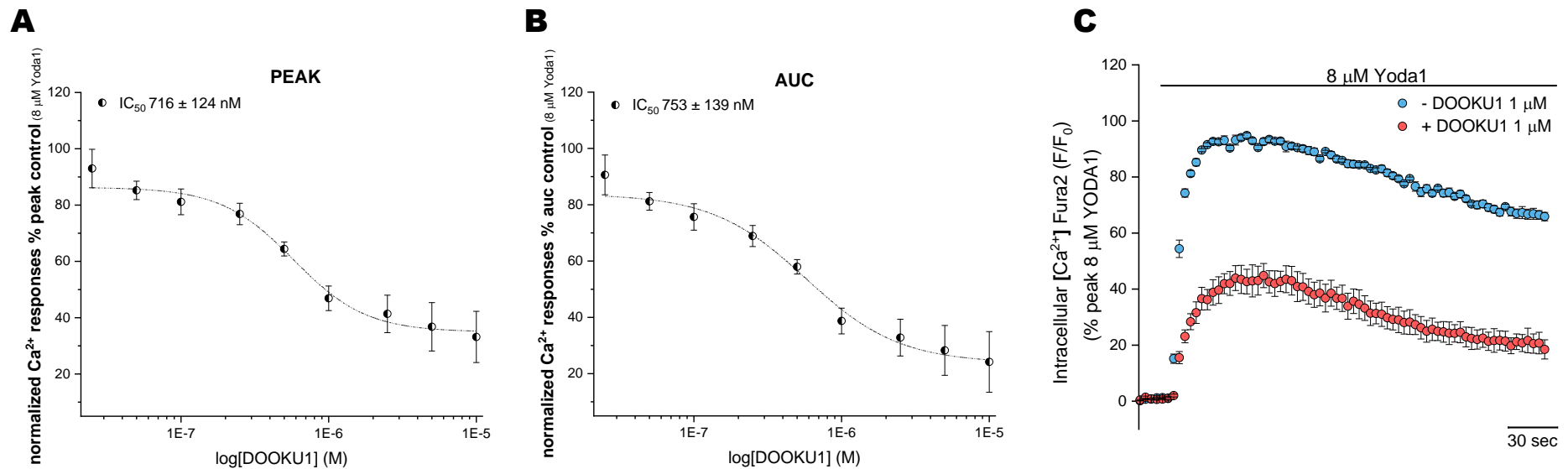


Figure 5. Inhibition concentration-response curves in the presence of Dooku1 on the Yoda1-evoked response in human umbilical vein endothelial cells (HUVEC). Inhibition concentration-response curves for the peak (A) and AUC (B) magnitude of intracellular Ca^{2+} responses elicited by 8 μM Yoda1 in the presence (closed stars; $N=5$) of Dooku1 from 10 μM to 25 nM. (C) Averaged time-resolved intracellular Ca^{2+} responses elicited by Yoda1 8 μM in the presence (red circle; $N=5$) or absence (blue circle; $N=5$) of Dooku1 1 μM over 250 seconds. All data were normalised to 8 μM Yoda1 and fit the Hill1 equation with the IC_{50} values showed in the graphs. Data are represented as mean \pm SEM.

4.3.1.3 Yoda1 kinetics profile differed between human umbilical vein endothelial cells (HUVECs) and human microvascular endothelial cells (HMEC-1).

If we compared HUVEC and HMEC-1 cells Yoda1 concentration-response curves, similarly as we reported for the ATP response, HMEC-1 cells demonstrated higher potency (**Figure 6-A, B, E**) (EC_{50}^{PEAK} : 539 ± 67 nM; EC_{50}^{AUC} : 573 ± 63 nM) than HUVEC cells (EC_{50}^{PEAK} : 1.24 ± 0.109 μ M; EC_{50}^{AUC} : 1.13 ± 0.067 μ M) ($p < 0.001$). Their lower response at 1 μ M determines the right shift in the Yoda1 dose-response curve in HUVEC while their maximal response remained constant (**Figure 6-C**). The representative calcium time-resolved responses at 3 μ M (**Figure 6-D**) portrays the lack of differences at higher concentration. However, the trace kinetics at these two concentrations in both cell lines remain conserved.

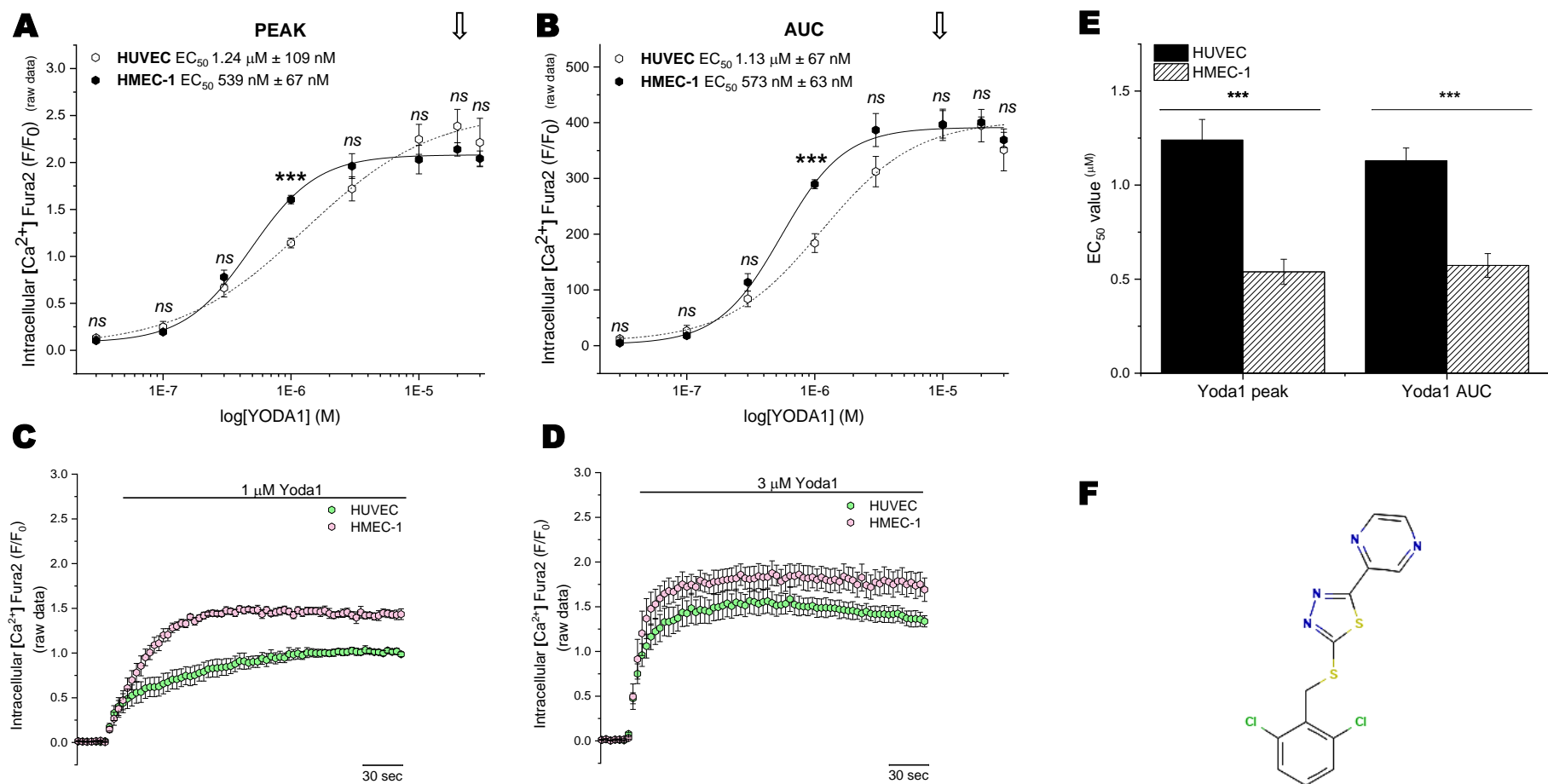


Figure 6. Yoda1's kinetics profile varied between human umbilical vein endothelial cells (HUVECs) and human microvascular endothelial cells (HMEC-1). Concentration-response curves for the peak (**A**) and AUC (**B**) magnitude of intracellular Ca^{2+} responses elicited by Yoda1 (0.03–30 μ M) in HUVEC cells (open circles $N=5$) and HMEC-1 (closed circles $N=5$). All data fit the Hill1 equation with the EC_{50} values showed in the graphs. Averaged time-resolved intracellular Ca^{2+} responses elicited by Yoda1 (**C**) 1 μ M and (**D**) 3 μ M in HMEC-1 (green hexagon; $N=8$) and HUVEC (pink hexagon; $N=6$) cells. (**E**) Comparison of EC_{50} values for Yoda1 responses in HUVEC ($N=6$) and HMEC-1 ($N=8$) cells. Asterisks show statistical significance where $p_{ns} > 0.05$, $p^* < 0.05$, $p^{**} < 0.01$, $p^{***} < 0.001$ (**F**) Yoda1 chemical structure (National Center for Biotechnology Information, 2023). Data are represented as mean \pm SEM.

4.3.2. Characterisation of broad-spectrum P2 antagonist effects in Yoda1-induced responses in human microvascular endothelial cells (HMEC-1) and human umbilical vein cells (HUVEC).

As previously described for the VEGF₁₆₅ response, apyrase, the ATP and ADP scavenger, and PPADS, the broad-spectrum antagonist, were used to investigate the P2 receptors' involvement in the Yoda1-evoked calcium responses in HMEC-1 and HUVEC cells.

4.3.2.1 The broad-spectrum P2 antagonists did not affect the Yoda1-evoked calcium responses of human microvascular endothelial cells (HMEC-1).

The effects of apyrase (10 U/mL) on the Yoda1 dose-response curve control ($EC_{50}^{peak} = 559 \pm 83$ nM; $EC_{50}^{AUC} = 623 \pm 91$ nM) were examined to investigate any P2 dependency in Yoda1-evoked calcium responses.

Pre-treatment with apyrase did not affect the Yoda1 dose response potency ($EC_{50}^{peak} = 567 \pm 71$ nM; $EC_{50}^{AUC} = 708 \pm 55$ nM; *ns*). Furthermore, the control Yoda1-evoked maximal response at 20 μ M (Yoda1 control peak: 105.3 ± 4.1 %; control AUC: 109.1 ± 3.6 %) was unaffected in the presence of the scavenger (peak: 98.95 ± 2.5 %; AUC: 102.51 ± 2.3 %; *ns*) (**Figure 7-A, B**). However, two concentrations, 300 and 100 nM, showed statistically significant differences in the peak or the AUC. The representative time-resolved intracellular calcium responses shown in **Figure 7-C** illustrated apyrase's significant impact on the trace kinetics upon 300 nM Yoda1 stimulation. In the absence of the inhibitor, Yoda1 caused a rapid but sustained calcium increase, reaching a peak approximately 30% above baseline. However, in the presence of apyrase, even with the peak percentage being conserved (*ns*), the evoked calcium response is much slower, characterised by a much slower sustained calcium increase. Thereby, the AUC in this case was significantly reduced ($p < 0.05$). Nevertheless, this effect was observed at only two concentrations, and no additional effects were evident, so it cannot be concluded that apyrase influences Yoda1-dependent calcium responses.

Pre-treatment with PPADS did not impact either the Yoda1 dose response potency ($EC_{50}^{peak} = 570 \pm 47$ nM; $EC_{50}^{AUC} = 674 \pm 51$ nM; *ns*) or the Yoda1-evoked maximal response at 20 μ M (peak: 114 ± 3.65 %; AUC: 115.96 ± 3.15 %; *ns*) (**Figure 8-A, B**). In contrast with the previous inhibitor, no concentration showed statistically significant differences in the presence of PPADS. Although there was a slight impact on the trace kinetics in the presence of PPADS, the peak and the AUC remained consistent, and no statistically significant differences were observed (**Figure 8-C**).

Based on these findings, we can conclude that the involvement of P2 receptors is not evident under the described experimental conditions.

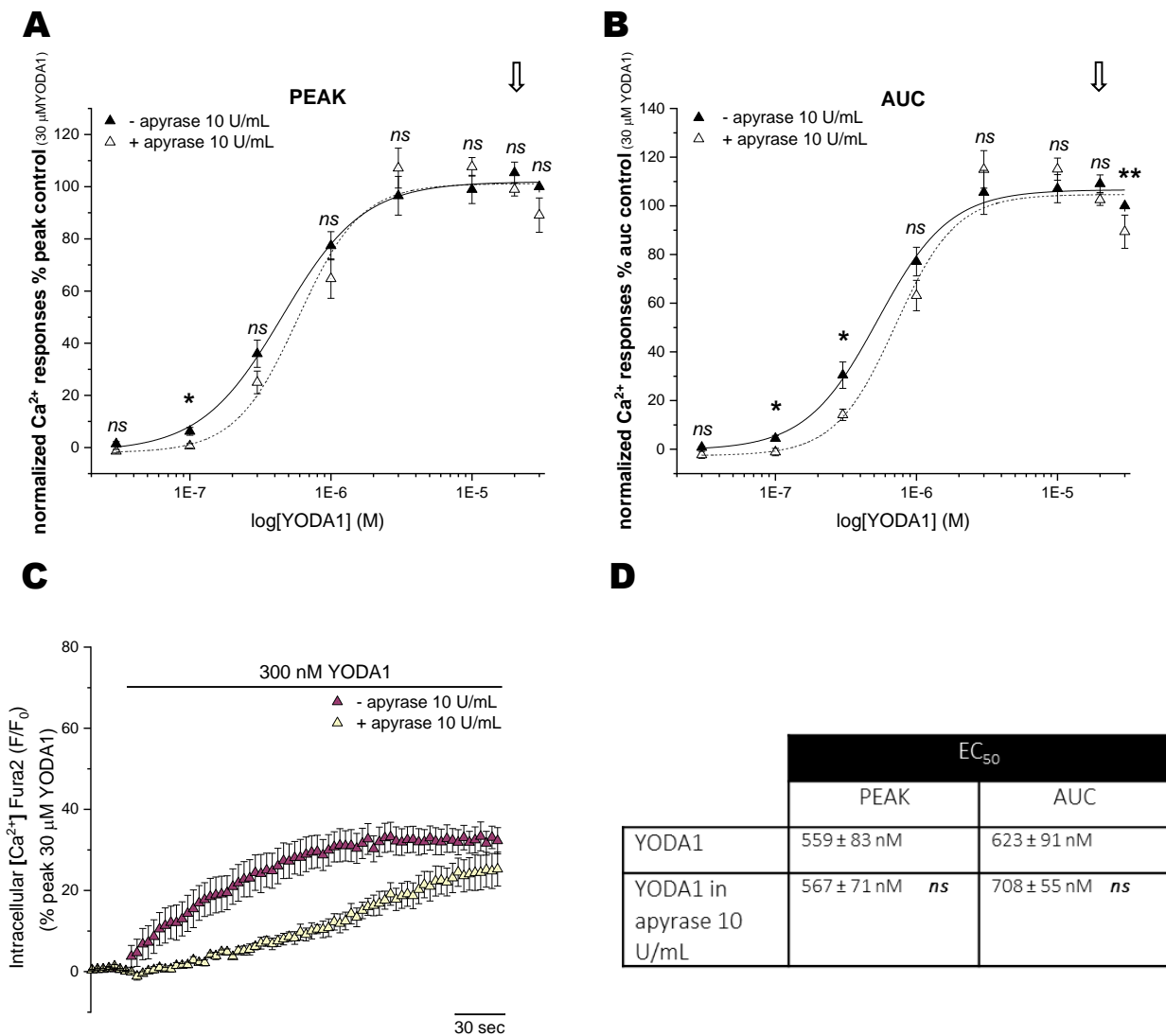


Figure 7. Minimal and isolated effects of the ATP and ADP scavenger apyrase on the Yoda1-evoked response in human microvascular endothelial cells (HMEC-1). Concentration-response curves for the peak (A) and AUC (B) magnitude of intracellular Ca^{2+} responses elicited by Yoda1 (0.03-30 μM ; $N=5$) in the presence (0.01-30 μM ; open triangle; $N=5$) or absence (0.03-30 μM ; closed triangle; $N=5$) of apyrase 10 U/mL. (C) Averaged time-resolved intracellular Ca^{2+} responses elicited by Yoda1 300 nM in the presence (light yellow triangle; $N=5$) or absence (dark pink triangle; $N=5$) of apyrase 10 U/mL over 250 seconds. All data were normalised to 30 μM Yoda1 and fit the Hill1 equation with the EC_{50} values showed in table (D). Asterisks show statistical significance relative to Yoda1-induced calcium responses (p *ns* > 0.05, p^* < 0.05, p^{**} < 0.01, p^{***} < 0.001). Data are represented as mean \pm SEM.

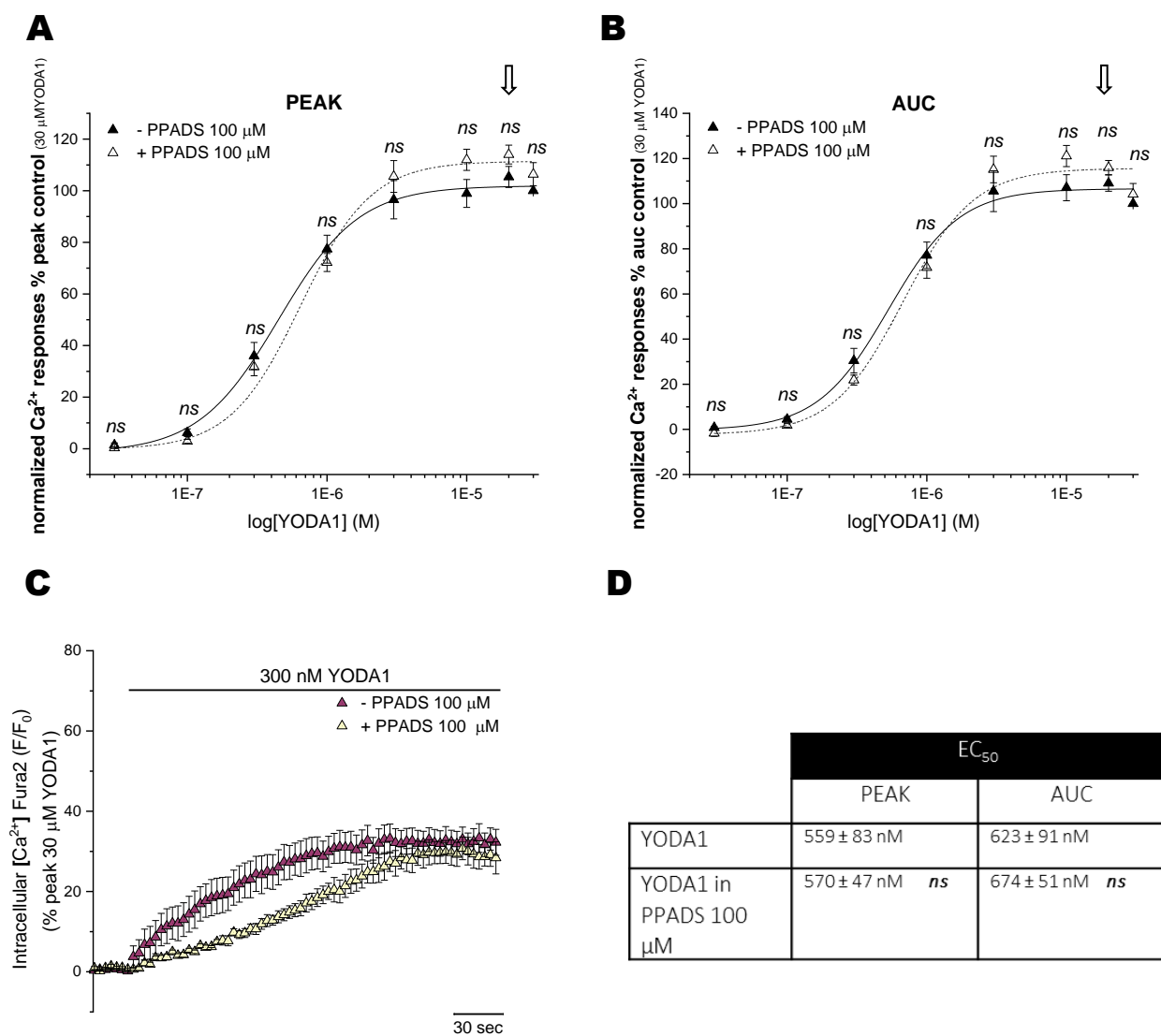


Figure 8. Lack of inhibitory effects of broad-spectrum P2 receptors antagonist PPADS on the Yoda1-evoked response in human microvascular endothelial cells (HMEC-1). Concentration-response curves for the peak (A) and AUC (B) magnitude of intracellular Ca^{2+} responses elicited by Yoda1 (0.03–30 μM ; $N=5$) in the presence (0.01–30 μM ; open triangle; $N=5$) or absence (0.03–30 μM ; closed triangle; $N=5$) of PPADS $100 \mu\text{M}$. (C) Averaged time-resolved intracellular Ca^{2+} responses elicited by Yoda1 300 nM in the presence (light yellow triangle; $N=5$) or absence (dark pink triangle; $N=5$) of over 250 seconds. All data were normalised to 30 μM Yoda1 and fit the Hill1 equation with the EC_{50} values showed in table (D). Asterisks show statistical significance relative to Yoda1-induced calcium responses ($p \text{ ns} > 0.05$, $p^* < 0.05$, $p^{**} < 0.01$, $p^{***} < 0.001$). Data are represented as mean \pm SEM.

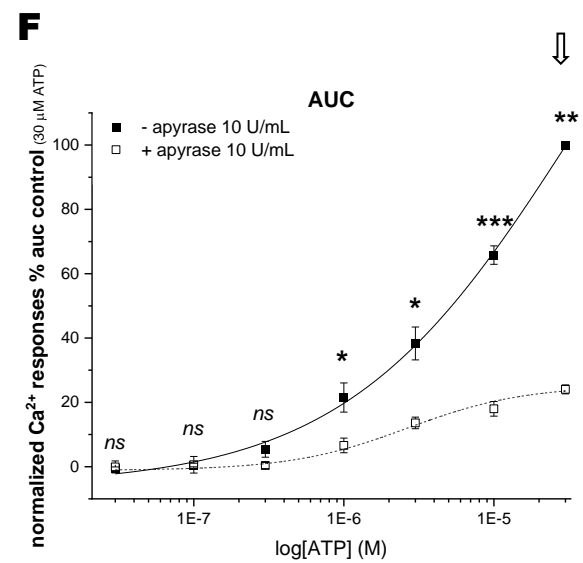
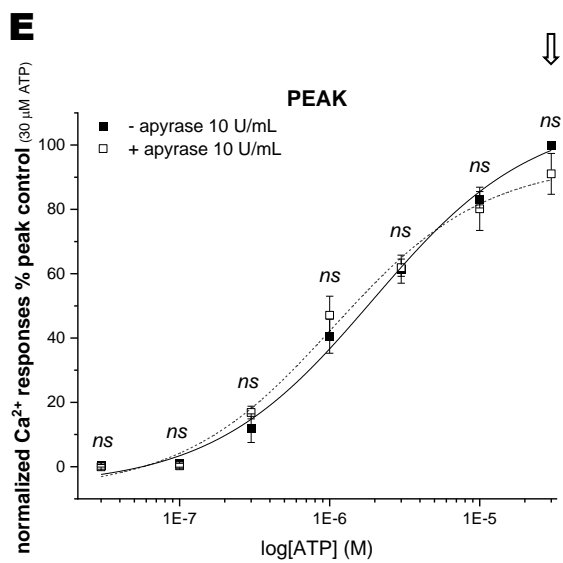
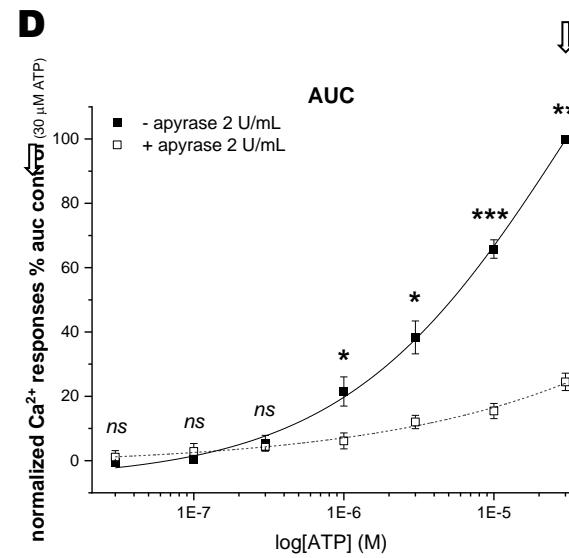
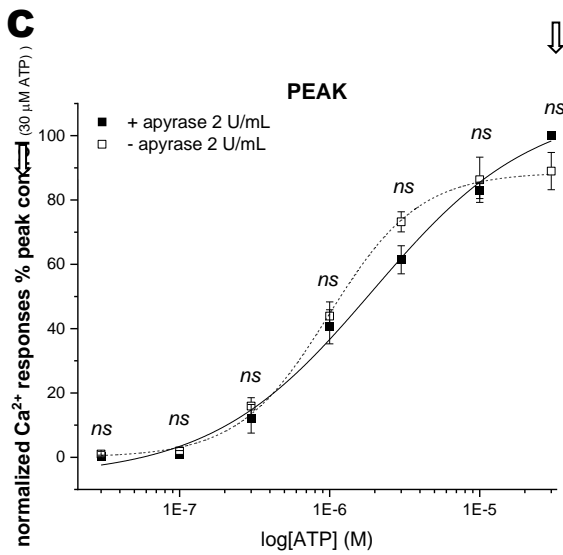
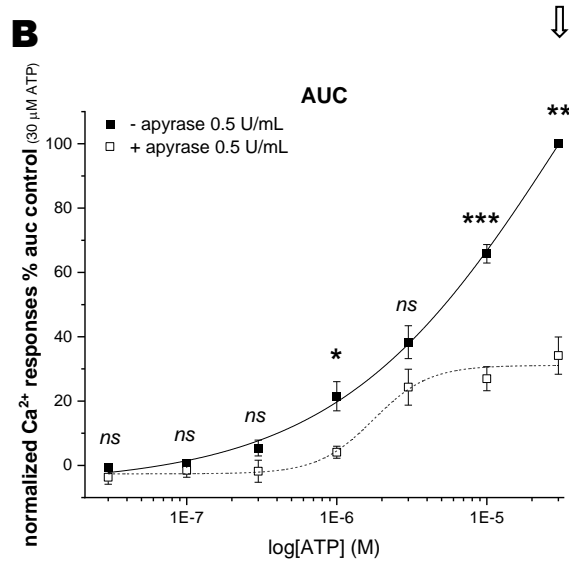
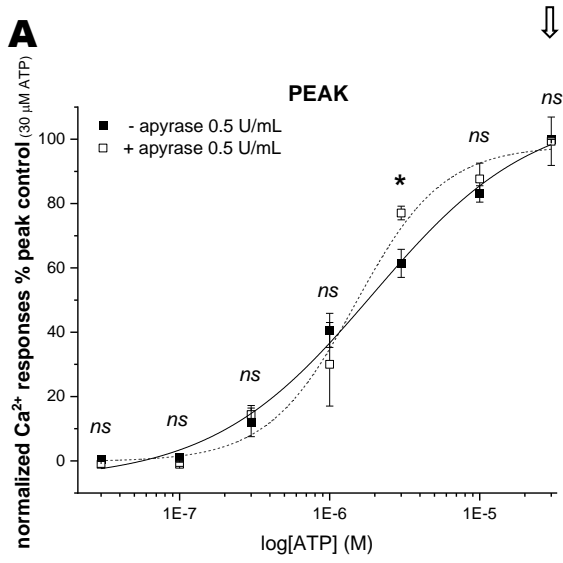
4.3.2.2 *The broad-spectrum P2 antagonists affected the Yoda1-evoked calcium responses of human umbilical vein endothelial cells (HUVEC).*

The same type of assays was designed to evaluate the impact of the broad-spectrum P2 antagonist in the Yoda1-evoked responses in HUVEC. However, an initial characterisation of the effects of these antagonists in the ATP dose response was required as that had not yet been fulfilled.

The effects of three different concentrations of apyrase (0.5, 2, and 10 U/mL) were examined to confirm that ATP evoked calcium responses could be inhibited using this compound. Pre-treatment with apyrase did not affect the peak, but it significantly impacted the AUC dose-response curves (**Figure 9, Table 1**). These constant effects in the AUC were conserved through different concentrations of the inhibitor, as shown in **Figure 9-J**, but that was not the case for the peak (**Figure 9-I**). Consistently, the control ATP-evoked maximal response for AUC was significantly decreased for all the concentrations of apyrase applied (**Table 1**). These effects in the AUC were illustrated in the time-resolved intracellular calcium responses at 3 μM (**Figure 9-G**) and 30 μM ATP (**Figure 9-H**). In the presence of the scavenger, the sustained calcium response was voided, and the transient ATP responses decayed to baseline approximately one minute after stimulation.

Then, the effects of two concentrations of PPADS (30 and 100 μM) were also investigated. Pre-treatment with PPADS affected the peak and AUC dose-response curves, and the control ATP-evoked maximal response for both curves was significantly decreased for all the concentrations of PPADS applied (**Figure 10, Table 1**). These constant effects were conserved through different inhibitor concentrations, as shown in **Figure 10-G, H**. In the presence of PPADS, the trace kinetics were conserved but significantly impacted the amplitude of response of all conditions studied (**Figure 10-E, F**). The time-resolved responses portrayed decreased intracellular calcium response when the inhibitor was onboard.

Therefore, we considered these two inhibitors an adequate tool to study the possible P2 contribution in the Yoda1-evoked response.



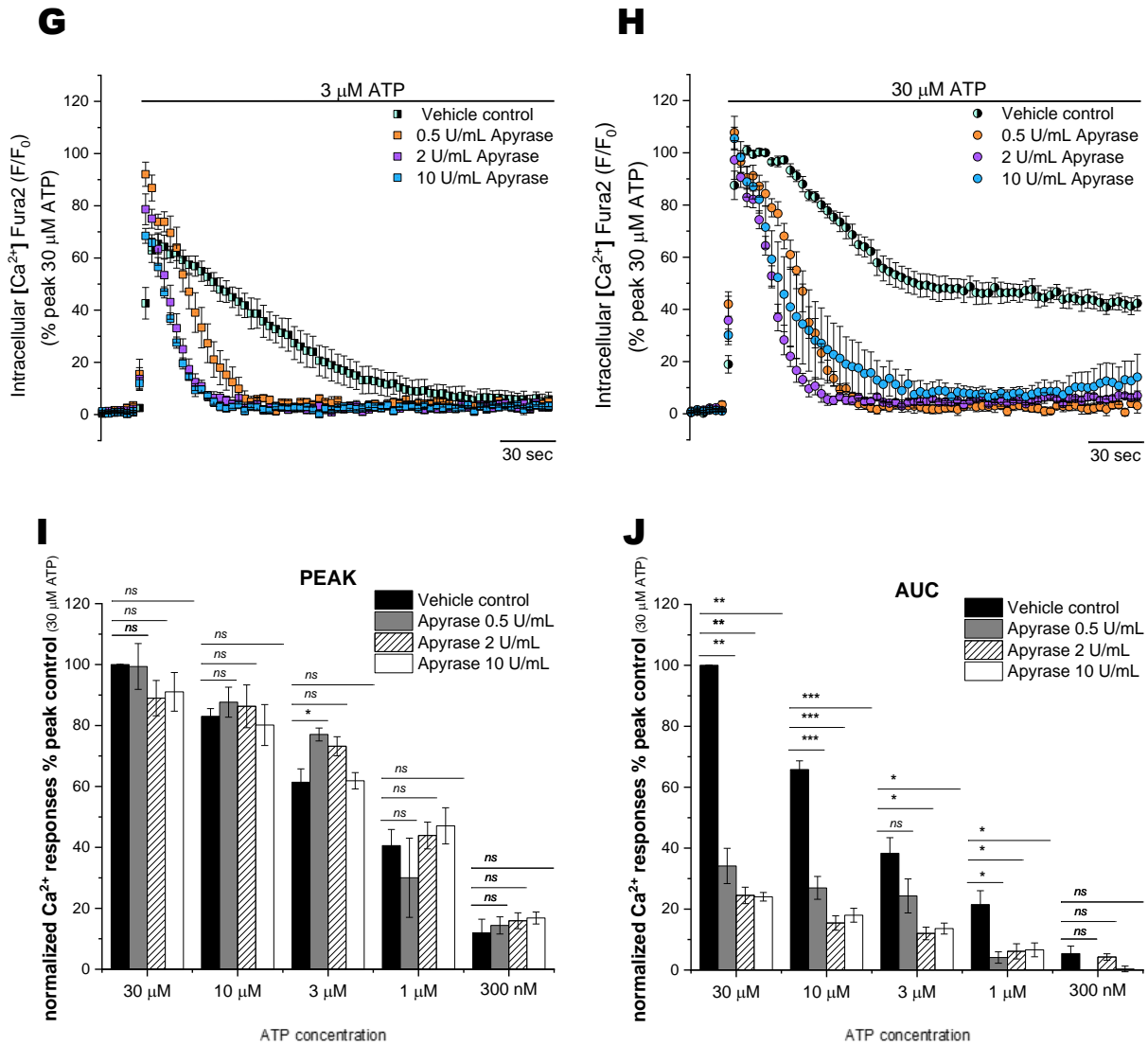
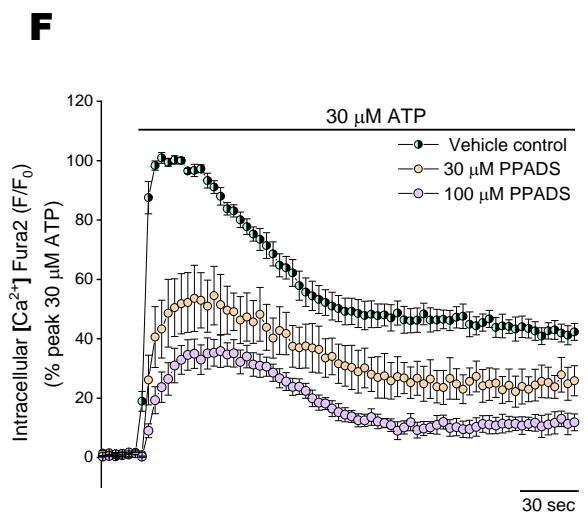
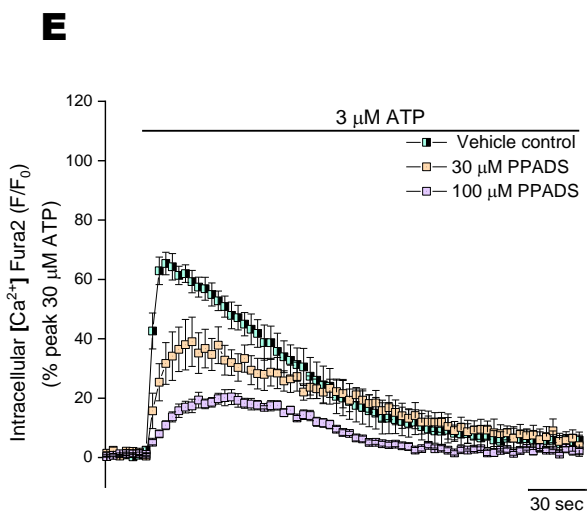
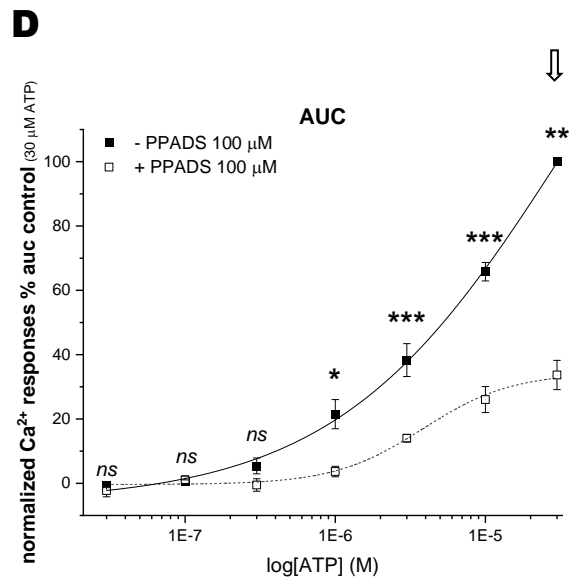
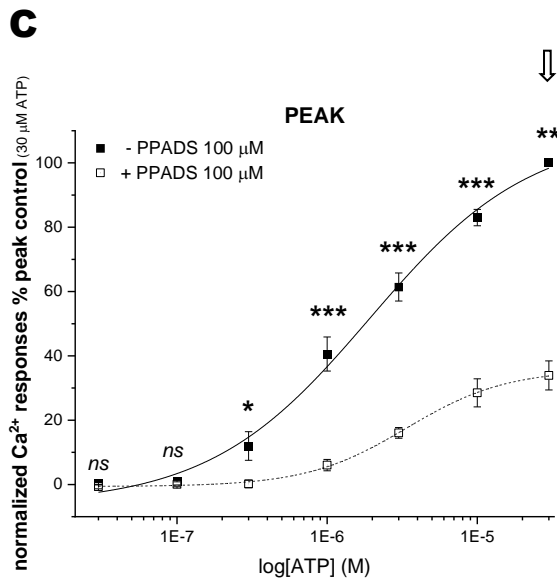
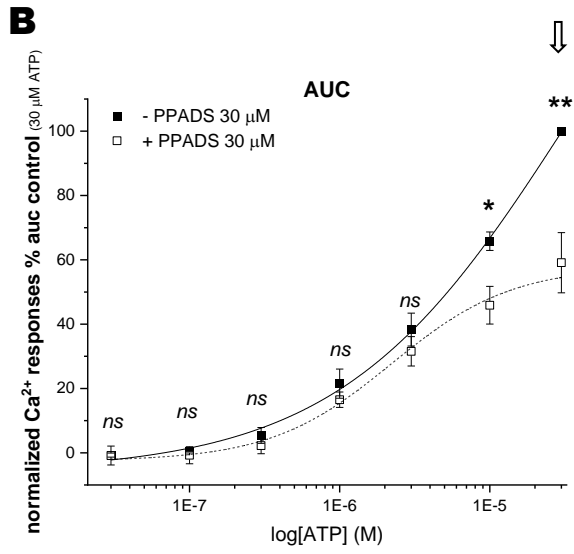
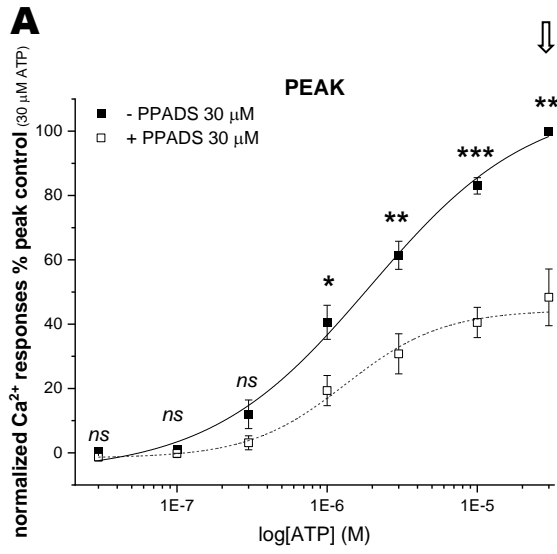


Figure 9. Inhibitory effects of the ATP and ADP scavenger apyrase on the ATP-evoked response in human umbilical vein endothelial cells (HUVEC). Concentration-response curves for the peak (A) (C) (E) and AUC (B) (D) (F) magnitude of intracellular Ca^{2+} responses elicited by ATP (0.03-30 μ M; $N=5$) in the presence (0.03-30 μ M; open square; $N=5$) or absence (0.03-30 μ M; closed square; $N=5$) of apyrase 0.5, 2, and 10 U/mL. Averaged time-resolved intracellular Ca^{2+} responses elicited by ATP 3 μ M (G) or ATP 30 μ M (H) in the presence ($N=5$) or absence ($N=5$) of apyrase 0.5, 2, and 10 U/mL over 250 seconds. Comparison of peak (I) and AUC (J) magnitude of intracellular Ca^{2+} responses induced by ATP at five different concentrations (30 μ M, 10 μ M, 3 μ M, 1 μ M and 300 nM) in the presence ($N=5$) or absence ($N=5$) of apyrase 0.5, 2 and 10 U/mL. All data were normalised to 30 μ M ATP and fit the Hill1 equation with the EC₅₀ values showed in Table 1. Asterisks show statistical significance relative to ATP control concentration (p ns > 0.05, p * < 0.05, p ** < 0.01, p *** < 0.001). Data are represented as mean \pm SEM.



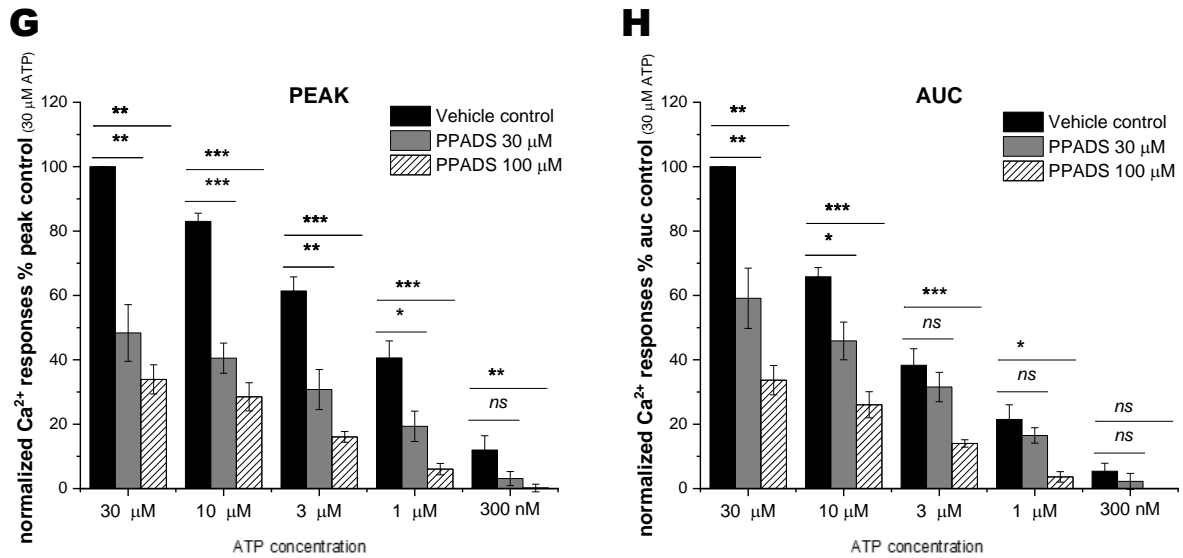


Figure 10. Inhibitory effects of broad-spectrum P2 receptors antagonist PPADS on the ATP-evoked response in human umbilical vein endothelial cells (HUVEC). Concentration-response curves for the peak (A) (C) and AUC (B) (D) magnitude of intracellular Ca^{2+} responses elicited by ATP (0.03-30 μM ; $N=5$) in the presence (0.03-30 μM ; open square; $N=5$) or absence (0.03-30 μM ; closed square; $N=5$) of PPADS 30 and 100 μM . Averaged time-resolved intracellular Ca^{2+} responses elicited by ATP 3 μM (E) or ATP 30 μM (F) in the presence ($N=5$) or absence ($N=5$) of PPADS 30 and 100 μM over 250 seconds. Comparison of peak (G) and AUC (H) magnitude of intracellular Ca^{2+} responses induced by ATP at five different concentrations (30 μM , 10 μM , 3 μM , 1 μM and 300 nM) in the presence ($N=5$) or absence ($N=5$) of PPADS 30 and 100 μM . All data were normalised to 30 μM ATP and fit the Hill1 equation with the EC_{50} values showed in **Table 1**. Asterisks show statistical significance relative to ATP control concentration ($p_{ns} > 0.05$, $p^* < 0.05$, $p^{**} < 0.01$, $p^{***} < 0.001$). Data are represented as mean \pm SEM.

Table 1. Effects of broad-spectrum antagonists on the ATP-evoked responses in human umbilical endothelial cells (HUVEC).

EC₅₀ statistics were performed against the control ATP dose-response curve (0.03-30 μM). Maximal response p-value is the statistical comparison between ATP maximal response in saline solution and ATP maximal response in the presence of the applied compound.

| Agonist | Antagonists | Antagonist concentration, μM | EC ₅₀ PEAK, μM | P value | EC ₅₀ AUC, μM | P value | Maximal response PEAK (μM) | Maximal response PEAK (%) | P value | Maximal response AUC (μM) | Maximal response AUC (%) | P value |
|---------|-------------|------------------------------|---------------------------|-----------|--------------------------|-----------|----------------------------|---------------------------|-----------|---------------------------|--------------------------|---------|
| ATP | / | / | 1.77 ± 0.28 | / | 6.58 ± 0.2 | / | 30 | 100 | / | 30 | 100 | / |
| ATP | Apyrase | 0.5 U/mL | 1.25 ± 0.39 | <i>ns</i> | 10.3 ± 7.31 | <i>ns</i> | 30 | 99.4 ± 7.53 | <i>ns</i> | 30 | 34.2 ± 5.79 | p<0.01 |
| ATP | Apyrase | 2 U/mL | 1.07 ± 0.16 | <i>ns</i> | 5.61 ± 3.59 | <i>ns</i> | 30 | 88.9 ± 5.80 | <i>ns</i> | 30 | 24.5 ± 2.70 | p<0.01 |
| ATP | Apyrase | 10 U/mL | 0.99 ± 0.15 | p<0.05 | 4.61 ± 3.05 | <i>ns</i> | 30 | 91.0 ± 6.34 | <i>ns</i> | 30 | 24.0 ± 1.40 | p<0.01 |
| ATP | PPADS | 30 μM | 1.96 ± 0.31 | <i>ns</i> | 4.05 ± 1.11 | <i>ns</i> | 30 | 48.3 ± 8.81 | p<0.01 | 30 | 59.1 ± 9.40 | p<0.01 |
| ATP | PPADS | 100 μM | 6.30 ± 3.52 | <i>ns</i> | 11.5 ± 5.01 | <i>ns</i> | 30 | 33.9 ± 4.52 | p<0.01 | 30 | 33.7 ± 4.6 | p<0.01 |

Table 2. Effects of broad-spectrum antagonists on the Yoda1-evoked responses in human umbilical endothelial cells (HUVEC).

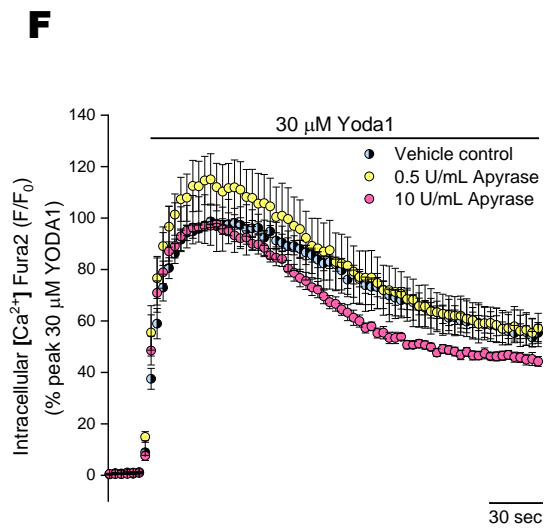
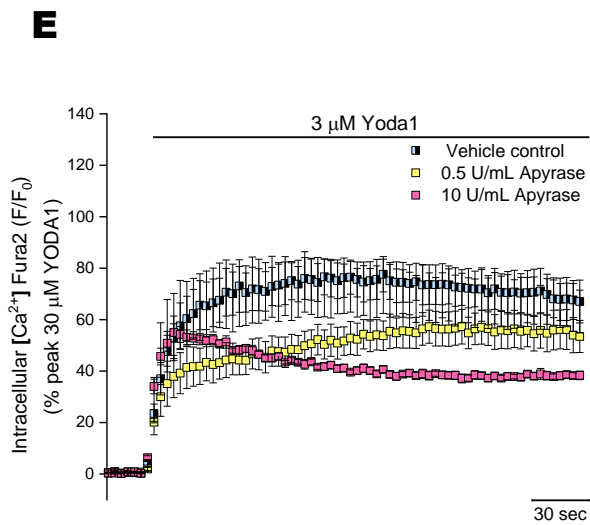
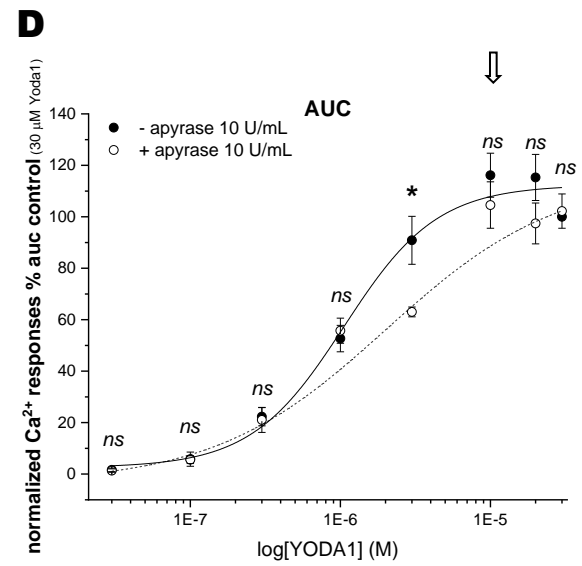
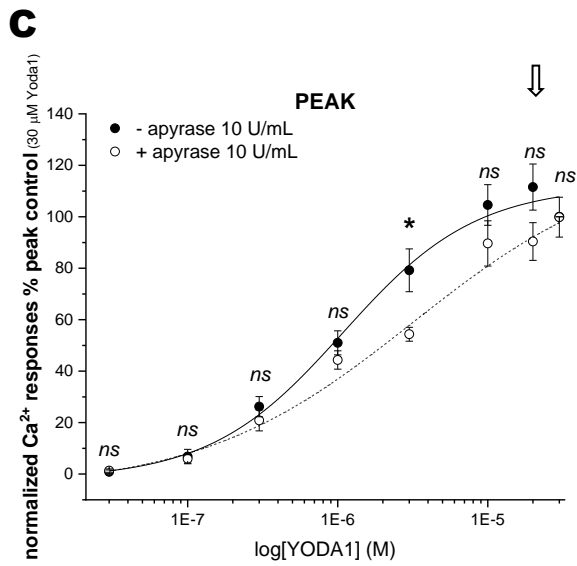
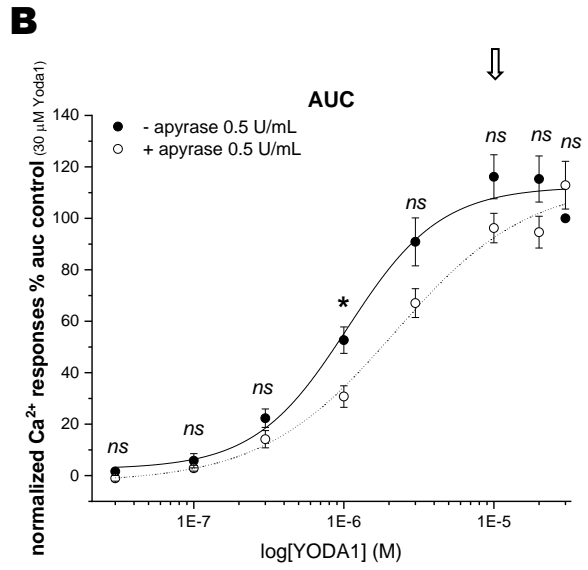
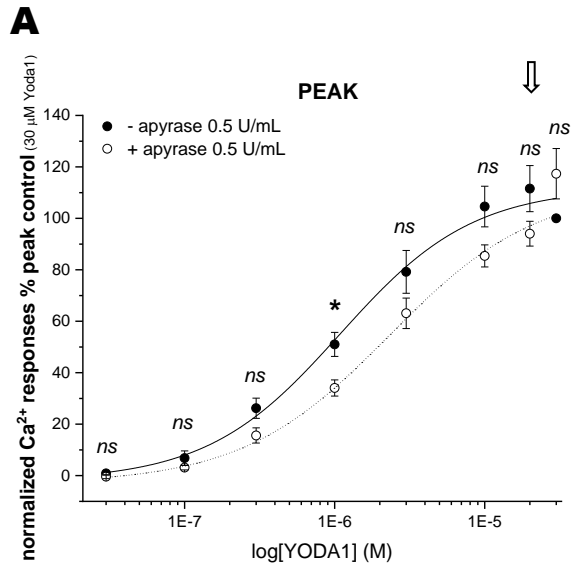
EC₅₀ statistics were performed against the control Yoda1 dose-response curve (0.03-30 μM). Efficacy p-value is the statistical comparison between Yoda1 maximal response and Yoda1 maximal response in the presence of the applied compound (whose concentration might differ from the previous one).

| Agonist | Antagonists | Antagonist concentration, μM | EC ₅₀ PEAK, μM | P value | EC ₅₀ AUC, μM | P value | Maximal response PEAK (μM) | Maximal response PEAK (%) | P value | Maximal response AUC (μM) | Maximal response AUC (%) | P value |
|---------|-------------|------------------------------|---------------------------|-----------|--------------------------|-----------|----------------------------|---------------------------|-----------|---------------------------|--------------------------|-----------|
| Yoda1 | / | / | 1.24 ± 0.11 | / | 1.41 ± 0.29 | / | 20 | 111.5 ± 8.95 | / | 10 | 116.2 ± 8.6 | / |
| Yoda1 | Apyrase | 0.5 U/mL | 3.14 ± 1.35 | <i>ns</i> | 2.45 ± 0.36 | p<0.05 | 30 | 117.3 ± 9.80 | <i>ns</i> | 30 | 112.9 ± 9.3 | <i>ns</i> |
| Yoda1 | Apyrase | 2 U/mL | 1.20 ± 0.19 | <i>ns</i> | 1.04 ± 0.13 | <i>ns</i> | 10 | 109.6 ± 10.9 | <i>ns</i> | 10 | 124.7 ± 11 | <i>ns</i> |
| Yoda1 | Apyrase | 10 U/mL | 1.29 ± 0.43 | <i>ns</i> | 1.06 ± 0.35 | <i>ns</i> | 30 | 99.85 ± 7.74 | <i>ns</i> | 10 | 104.6 ± 9 | <i>ns</i> |
| Yoda1 | PPADS | 30 μM | 5.62 ± 2.30 | p<0.05 | 4.82 ± 2.06 | <i>ns</i> | 30 | 103.6 ± 3.65 | <i>ns</i> | 20 | 101.3 ± 1.5 | <i>ns</i> |
| Yoda1 | PPADS | 100 μM | 2.37 ± 0.54 | <i>ns</i> | 1.52 ± 0.40 | <i>ns</i> | 20 | 110.2 ± 5.48 | <i>ns</i> | 20 | 107.6 ± 6.7 | <i>ns</i> |

As previously described, the effects of two different concentrations of apyrase (0.5 and 10 U/mL) were investigated in the Yoda1 concentration-response curve ($EC_{50}^{peak} = 1.24 \pm 0.109 \mu\text{M}$ and $EC_{50}^{AUC} = 1.41 \pm 0.29 \mu\text{M}$). Pre-incubation with apyrase slightly right shifted the dose-response for the peak and the AUC at both concentrations; however, the potency was significantly decreased just in the treatment at 0.5 U/mL ($EC_{50}^{AUC} = 2.45 \pm 0.36 \mu\text{M}$; $p < 0.05$) while the control Yoda1-evoked maximal response (Yoda1 20 μM control peak: $111.5 \pm 8.95 \%$; 10 μM control AUC: $116.2 \pm 8.6 \%$) was unaffected in the presence of the scavenger (**Figure 11**). The significant decrease at 1 μM mainly caused this effect at 0.05 U/mL, while at 10 U/mL, this effect is observed at 3 μM Yoda1 (**Figure 11-I, J**). The representative time-resolved intracellular calcium responses shown in **Figure 11-E** illustrated the 10 U/mL apyrase's significant impact on the peak and the AUC at 3 μM Yoda1 and the decreased pattern at 0.5 U/ml of the ATP scavenger. However, these inhibitory effects were lost at higher concentrations, as represented in **Figure 11-H**.

The effects of the two different concentrations of PPADS (30 and 100 μM) were then studied in the Yoda1 concentration-response curve. Pre-treatment with the inhibitor similarly slightly right shifted the dose-response for the and the AUC at both concentrations, but the EC_{50} was significantly decreased in the treatment at 30 μM ($EC_{50}^{peak} = 5.62 \pm 2.3 \mu\text{M}$; $p < 0.05$) (**Figure 12, Table 2**). The control Yoda1-evoked AUC maximal response was significantly decreased in the presence of 30 μM of the antagonist (Yoda1 10 μM AUC: $\pm \%$), while the peak remained unchanged (Yoda1 20 μM AUC: $\pm \%$). Accordingly, the maximal response to Yoda1 for the AUC in the presence of PPADS was achieved at 20 μM Yoda1. When comparing this new maximal response with the maximal response control at 10 μM Yoda1 in the absence of PPADS, no significant difference was observed ($101.3 \pm 1.5 \%$, *ns*). Thus, the level of efficacy remained intact (**Table 2**). No significant changes were observed in terms of potency or efficacy when 100 μM was applied. Nonetheless, at both concentrations of the inhibitor, the significant decrease at 3 and 10 μM caused this rightward shift effect (**Figure 12-G, H**). The representative time-resolved intracellular calcium responses in **Figure 12-E** illustrated the significant effect on the peak and the AUC at 3 μM Yoda1. However, these inhibitory effects were lost at higher concentrations, as represented in **Figure 12-F**.

Together, these results suggest a potential modest contribution of P2 receptors to Yoda1-induced calcium responses.



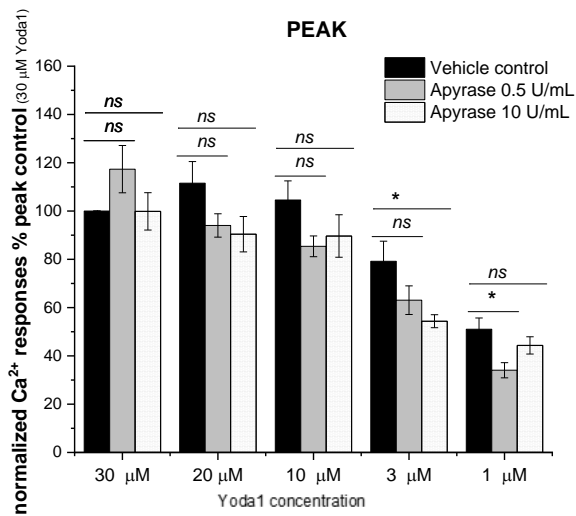
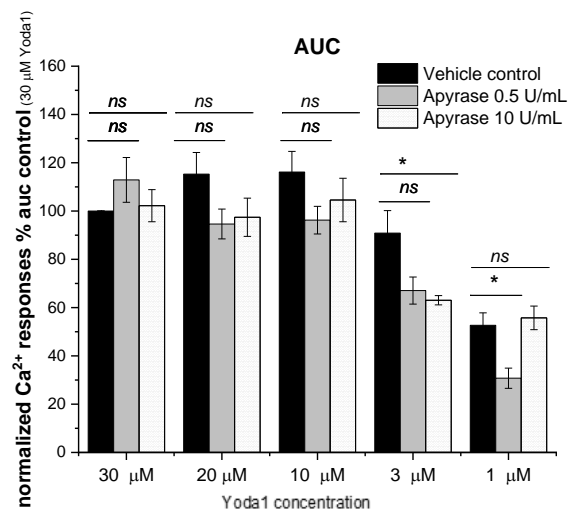
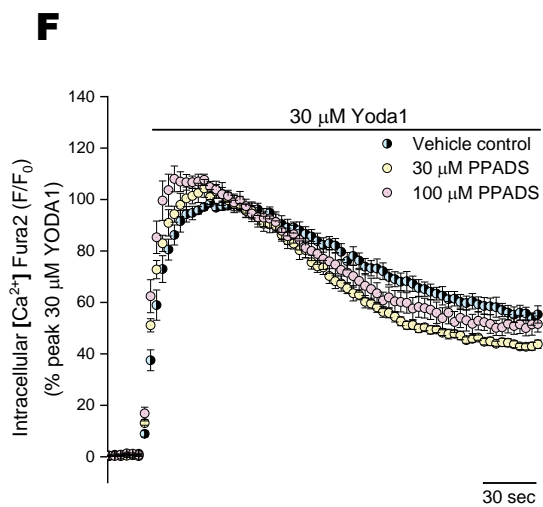
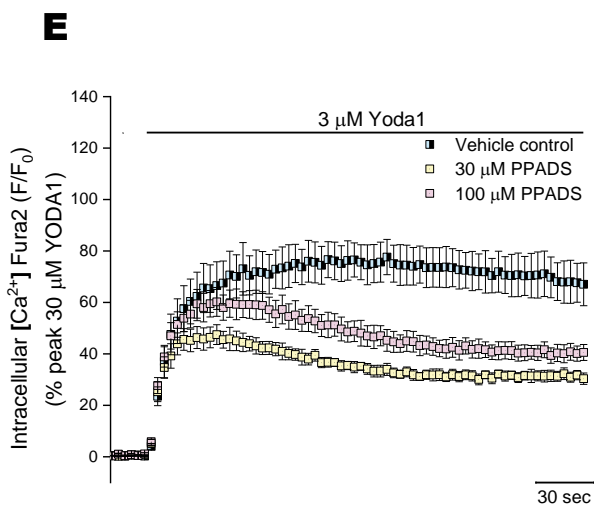
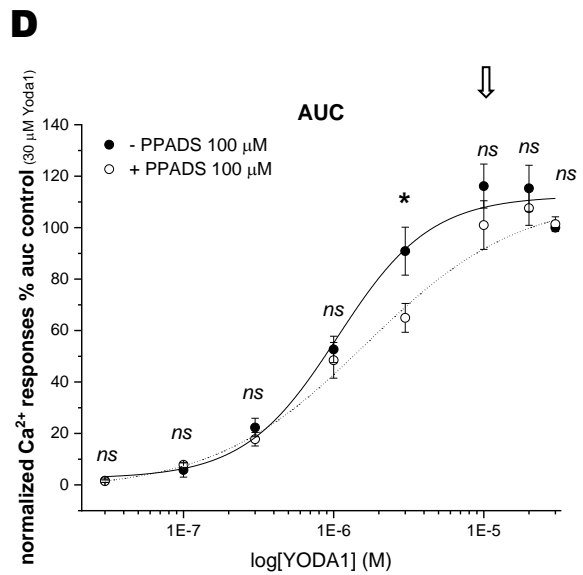
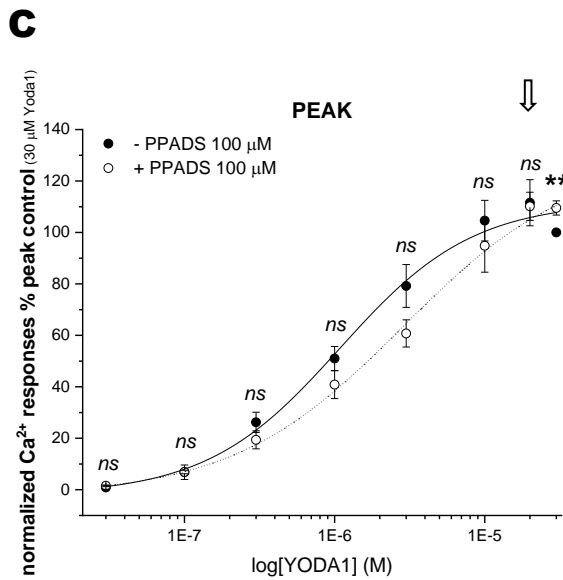
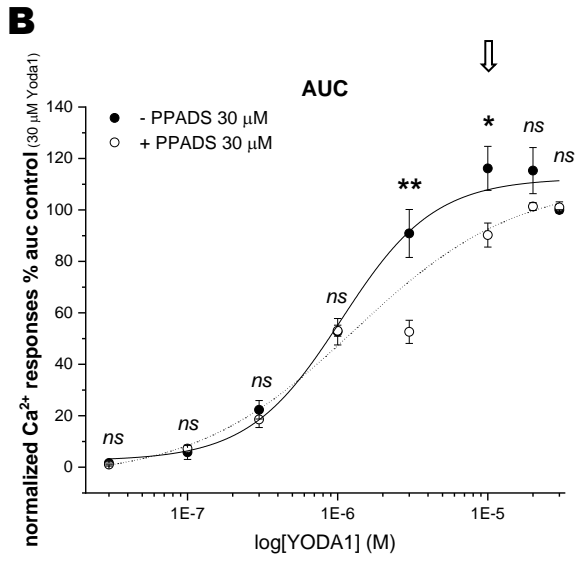
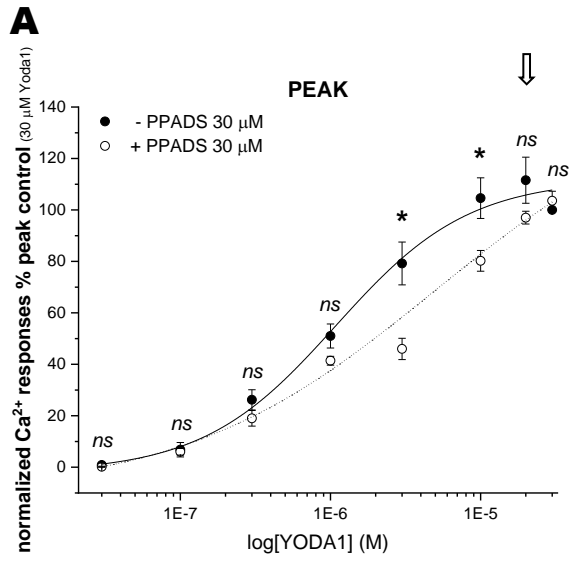
G**H**

Figure 11. Inhibitory effects of the ATP and ADP scavenger apyrase on the Yoda1-evoked response in human umbilical vein endothelial cells (HUVEC). Concentration-response curves for the peak (A) (C) and AUC (B) (D) magnitude of intracellular Ca²⁺ responses elicited by Yoda1 (0.03-30 μM; *N*=5) in the presence (0.03-30 μM; open circle; *N*=5) or absence (0.03-30 μM; closed circle; *N*=5) of apyrase 0.5 and 10 U/mL. Averaged time-resolved intracellular Ca²⁺ responses elicited by Yoda1 3 μM (E) or 30 μM (F) in the presence (*N*=5) or absence (*N*=5) of apyrase 0.5 and 10 U/mL over 250 seconds. Comparison of peak (G) and AUC (H) magnitude of intracellular Ca²⁺ responses induced by Yoda1 at five different concentrations (30 μM, 20 μM, 10 μM, 3 μM and 1 μM) in the presence (*N*=5) or absence (*N*=5) of apyrase 0.5 and 10 U/mL. All data were normalised to 30 μM Yoda1 and fit the Hill1 equation with the EC₅₀ values showed in **Table 2**. Asterisks show statistical significance relative to Yoda1 control concentration (*p* *ns* > 0.05, *p* * < 0.05, *p* ** < 0.01, *p* *** < 0.001). Data are represented as mean ± SEM.



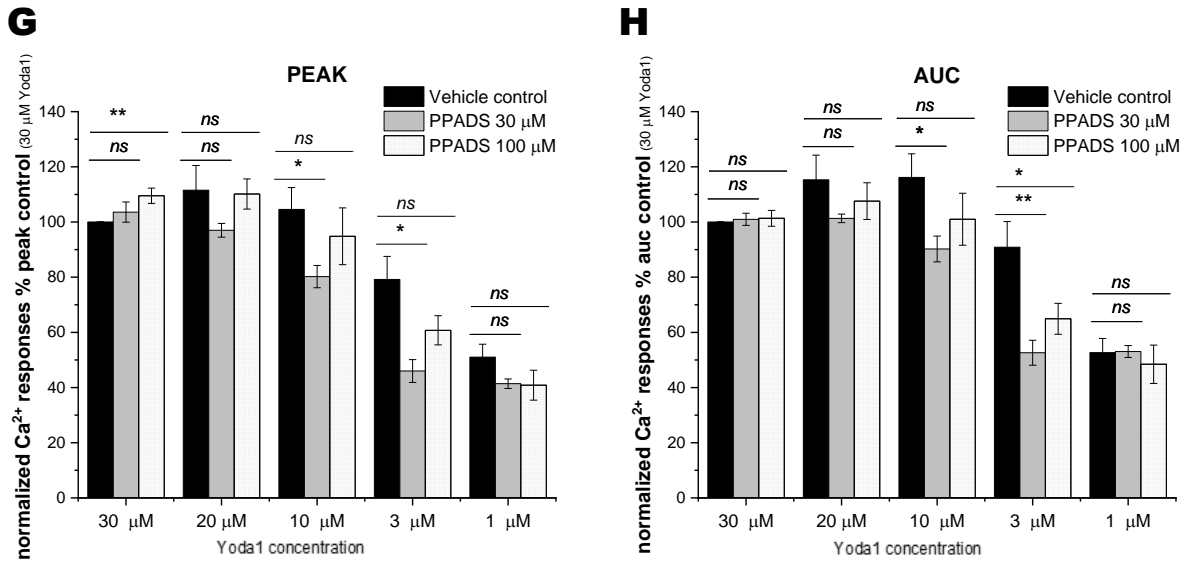


Figure 12. Inhibitory effects of broad-spectrum P2 receptors antagonist PPADS on the Yoda1-evoked response in human umbilical vein endothelial cells (HUVEC). Concentration-response curves for the peak (A) (C) and AUC (B) (D) magnitude of intracellular Ca²⁺ responses elicited by Yoda1 (0.03-30 μM; N=5) in the presence (0.03-30 μM; open circles; N=5) or absence (0.03-30 μM; closed circles; N=5) of PPADS 30 and 100 μM. Averaged time-resolved intracellular Ca²⁺ responses elicited by Yoda1 3 μM (E) or 30 μM (F) in the presence (N=5) or absence (N=5) of PPADS 30 and 100 μM over 250 seconds. Comparison of peak (G) and AUC (H) magnitude of intracellular Ca²⁺ responses induced by Yoda1 at five different concentrations (30 μM, 20 μM, 10 μM, 3 μM and 1 μM) in the presence (N=5) or absence (N=5) of PPADS 30 and 100 μM. All data were normalised to 30 μM Yoda1 and fit the Hill1 equation with the EC₅₀ values showed in **Table 2**. Asterisks show statistical significance relative to Yoda1 control concentration (p *ns* > 0.05, p* < 0.05, p** < 0.01, p*** < 0.001). Data are represented as mean ± SEM.

4.3.3. Insights into the suitability of two different parallel flow chambers for mechanical stimulation of cells *in vitro*.

The main goal of this chapter was to set up a functional parallel flow system to mechanically stimulate endothelial cells *in vitro* and study the purinergic contribution in the shear-stress evoked responses. As we previously did with the Yoda1, in static conditions, we hypothesised that when subjected to shear stress in a dynamic and more physiological situation, the role of P2 receptors could be isolated, potentially unveiling an impact on the Piezo1 mechanosensitive response.

However, first, to approximate the role of mechanosensitive channels in endothelial cells, a tuning of the calcium imaging setup was required to ensure the reliability and quality of the calcium-recorded images. Several issues were detected in the early stages of the imaging process between the coupling of the different setup parts, such as the camera's connectivity with the software or the non-recognition of the monochromator. Once these inconveniences were solved and the optical transmission was improved, the focus area was delimited to a stable field of study where the whole sample was exposed equally. Then, ATP was used to activate HUVEC cells and confirm the reproducibility of the assays using the microscope (**Figure 13**). These initial experiments were performed traditionally, using coverslips to grow the cells and expose them to the agonist. **Figure 13-A** depicts the time-resolved calcium response upon 30 μM ATP stimulation, characterised by an initial rapid response followed by a sustained phase that decayed to baseline calcium levels over eight minutes. On the other hand, **Figure 13-B** showed representative images for unstimulated cells with baseline fluorescence (left) and stimulated cells with higher fluorescence levels (right) upon 30 μM ATP stimulation.

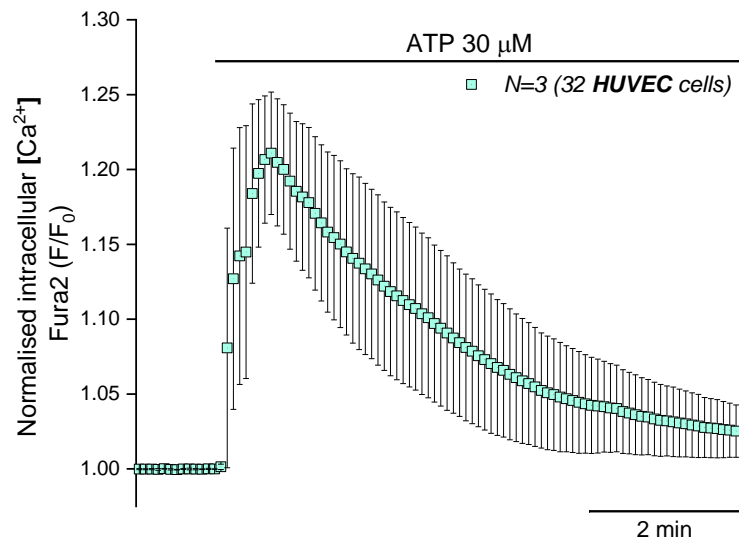
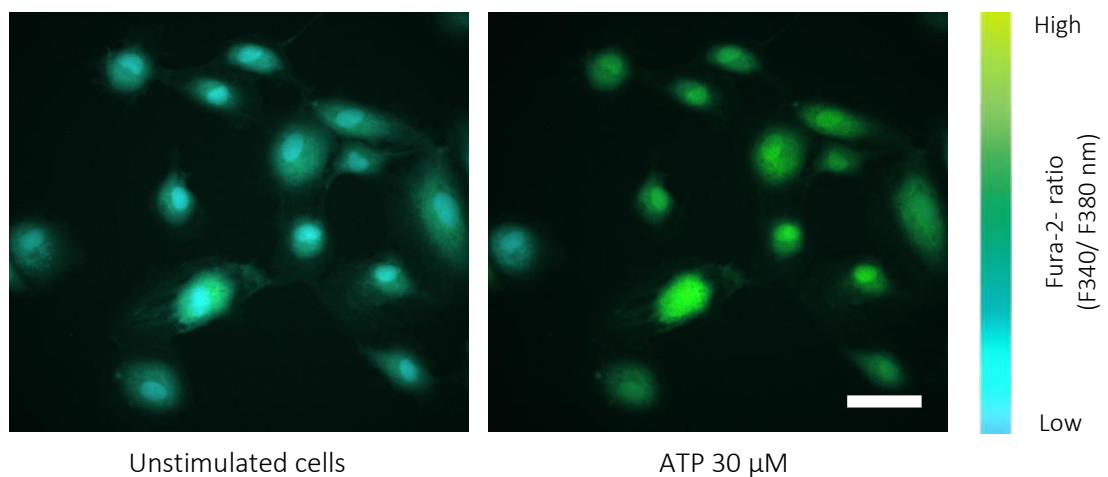
A**B**

Figure 13. ATP evoked detectable intracellular calcium responses using the calcium imaging setup. **(A)** Averaged time-resolved intracellular Ca^{2+} response elicited by ATP 30 μ M over 8 minutes. **(B)** Representative images for unstimulated (baseline fluorescence) and stimulated cells with ATP 30 μ M ($N=3$; $n=32$). Scale bar represents 10 μ M.

^(*)In this section (4.3.3), F/F_0 exceptionally refers to the baseline normalisation of each cell.

4.3.3.1 *The Glycotech parallel flow chamber was discarded as an option to stimulate cells in vitro mechanically.*

The first parallel flow chamber used to investigate the shear stress stimulation was the Glycotech parallel flow chamber (**Methods section, Figure 3-A**). All assays using the Glycotech system were performed using 24 hours-seeded cells and high confluences. As HUVEC cells are traditionally recognised to respond to shear stress, they were used as the preferred model to isolate mechanical responses (**Figure 14-A, B**). Despite the high expectations in this experiment, no response could be isolated at 12 dynes/cm² (**Figure 14-A**), and some technical challenges started appearing in our way. Cells struggled to survive attached to the dish upon shear stress stimulation, and the assay replicate was limited by the technical problems occurring. That resulted in 50% of the experiments failing due to technical issues (**Figure 14-B**). As already mentioned, HUVEC cells are a complicated and expensive model to grow, so because of the above technical problems, we decided to use as an alternative model 1321N1 human P2X4 astrocytoma cells, as they could respond to Yoda1, and they are a much handier model (**Figure 14-F**). Unfortunately, the rate of failings was conserved using these cells. Just 35.3% of the experiments made it to the end (5.9% responded; 29.4% did not respond). Contrarily, 64.7% of the trials failed due to technical issues (**Figure 14-C, D, E**). **Figure 14-C** illustrates the lack of responsiveness assays (29.4%) when stimulating the cells with 2.5 or 8 dynes/cm². In contrast, shear stress-induced responses were achieved just once (5.9%), as represented in **Figure 14-D**, when applying 1 and 8 dynes/cm². This shear stress-dependent response appeared genuine, as the kinetics of mechanical activation through Piezo1 were reported to be as rapid and transient as the one we show (Swain et al., 2021). However, that was never replicated, and a vast range of technical issues disrupt and complicate these assays. A representative range of the experienced technical issues is illustrated in **Figure 15**. The first technical issue shown in **Figure 15-A** stands for an unexpected preactivation of the hP2X4 astrocytoma cells before applying the stimulus. Once applied 1 or 2.5 dyne/cm², the cells' intracellular calcium decreased. This effect might be caused by the pressure from the vacuum line, which maintains the gasket into the dish to create a parallel flow. The second technical issue reported, and one of the most concerning was the spontaneous activation of the cells when any shear-stress force was applied (0 dyne/cm²) because of the similarity of this response to the shear-stress expected ones (**Figure 15-B**). We hypothesised that this activation might be caused again by fluctuations in the pressure vacuum line that could spontaneously mechanically activate the cells. The third technical limitation and the most disruptive was the bubble presence in the bath solution used to produce the shear stress. After applying 1 dyne/cm², and therefore, saline solution flow in the parallel chamber, cells reported high levels of Ca²⁺. That caused the loss of more than half of the initial cells in the dish (**Figure 15-C**). The plotted trace kinetics for this disruption could be understood as a shear stress-induced response if not interpreted with the calcium imaging. Similarly, to this effect is the one shown in **Figure 15-D**, which illustrates a less disruptive bubble effect after applying 2.5 dyne/cm². The response could again be confused with a specific activation, but the slight cell wash in the right image after stimulation reveals the opposite. This image illustrates the loss of some cells and the presence of cellular debris remaining after the cells were subjected to the bubble induced mechanical stress. Because of these technical deficiencies, a different parallel flow chamber was tested.

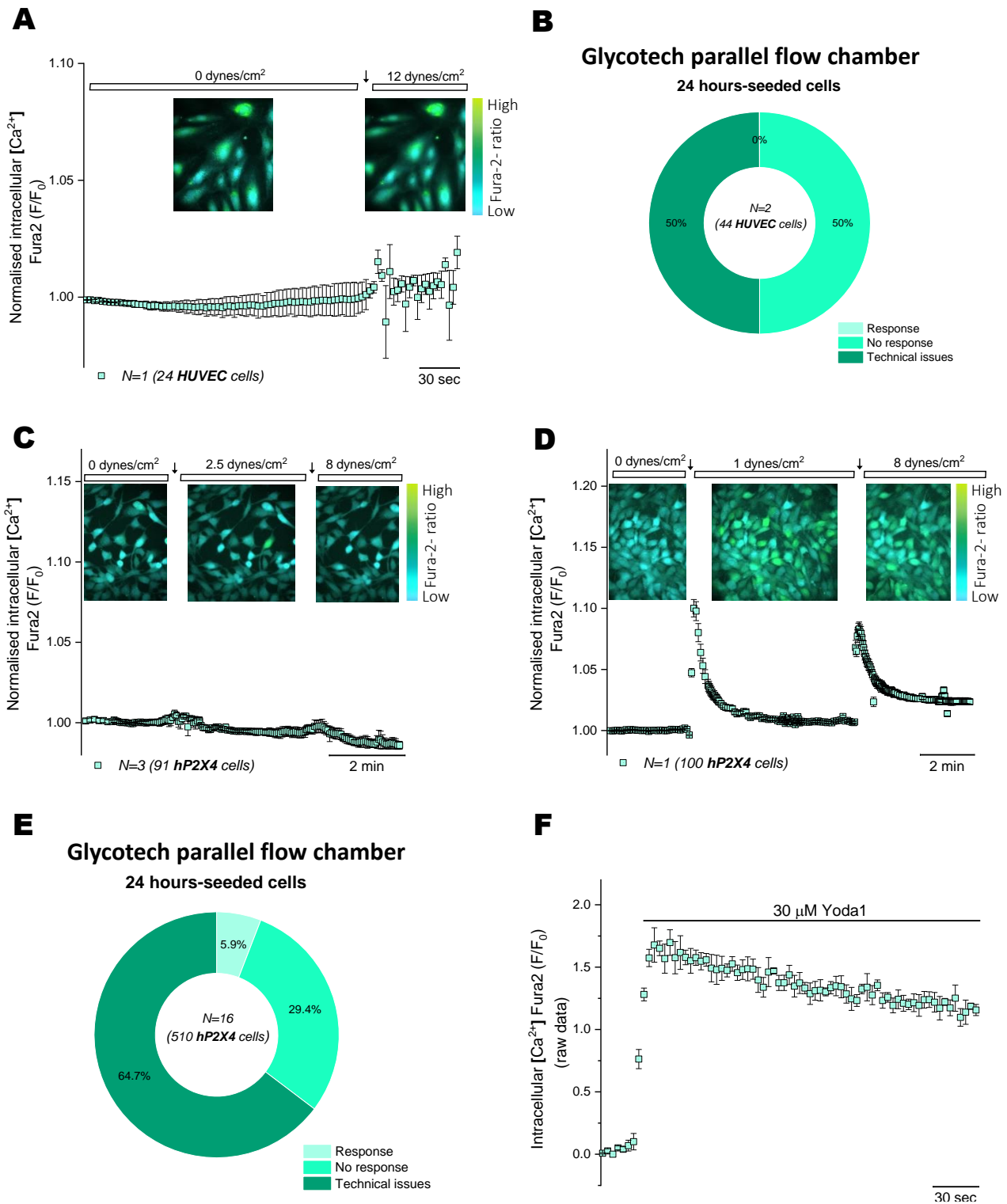
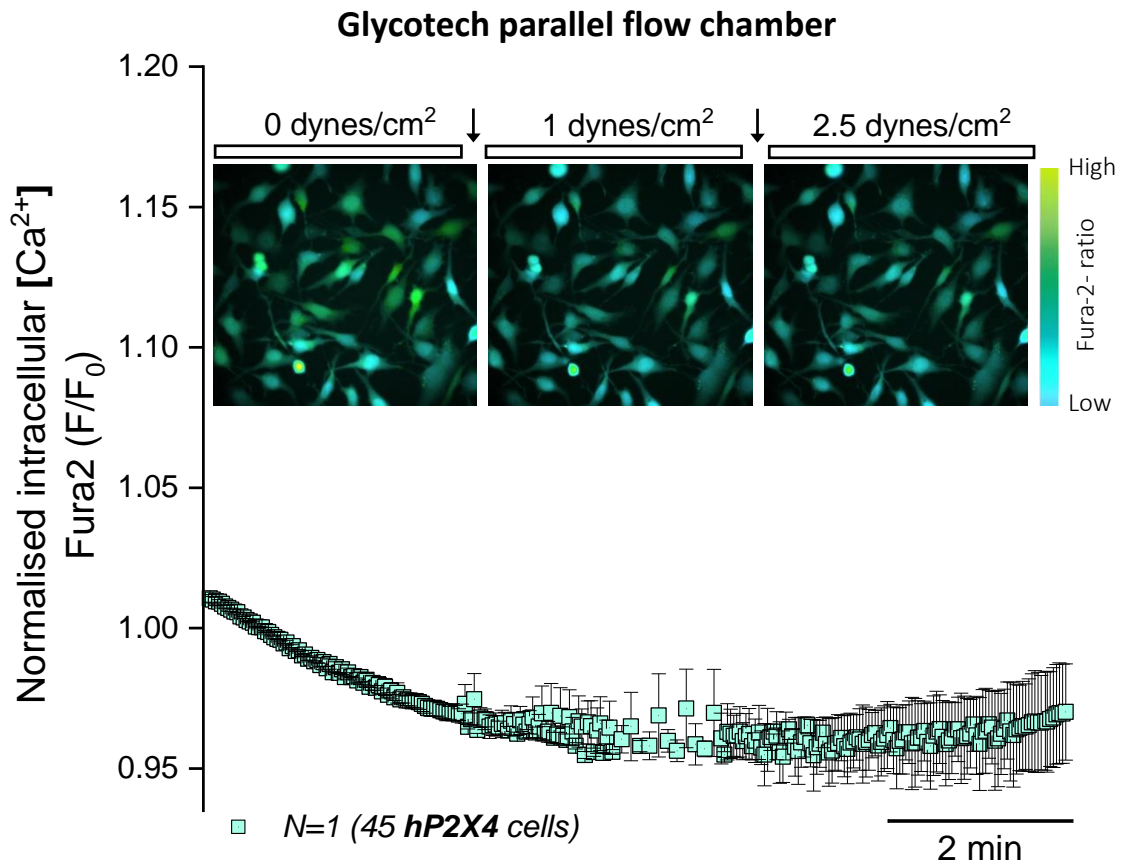
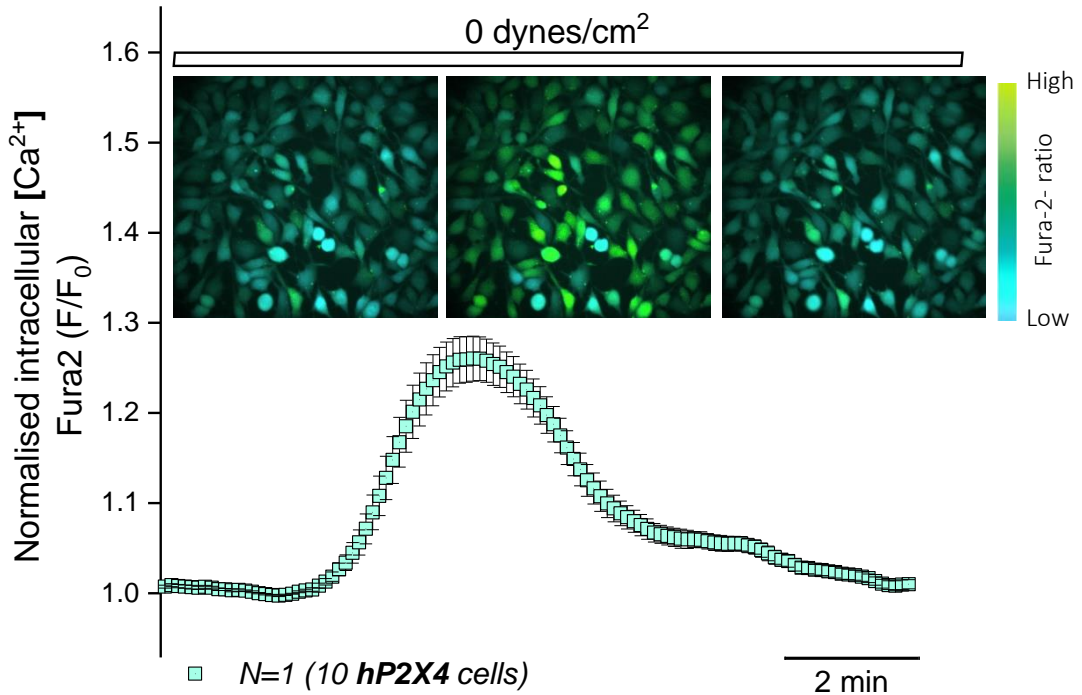


Figure 14. Shear stress stimulation assays using the Glycotech parallel flow chamber. (A) Shear stress did not elicit any calcium response when applying 12 dynes/cm² in 24 hours-seeded HUVEC cells ($N=2$; $n=44$). (B) In addition, half of the trials failed due to technical issues. (C) Shear stress did not elicit any calcium response when applying 2.5 or 8 dynes/cm² in 24 hours-seeded hP2X4 astrocytoma cells ($N=3$; $n=91$), but stimulation was achieved (D) when applying 1 and 8 dynes/cm² ($N=1$; $n=100$). (E) In this case, 64.7% of the experiments failed due to technical issues. (F) Time-resolved intracellular Ca^{2+} responses elicited by Yoda1 30 μ M (blue square) over 250 seconds ($N=1$) using the Flex Station III. Data are represented as mean \pm SEM. Percentage calculations were performed using total N numbers as 100%.

Arrows (↓) indicate the application of the mechanical stimulus.

A**B**

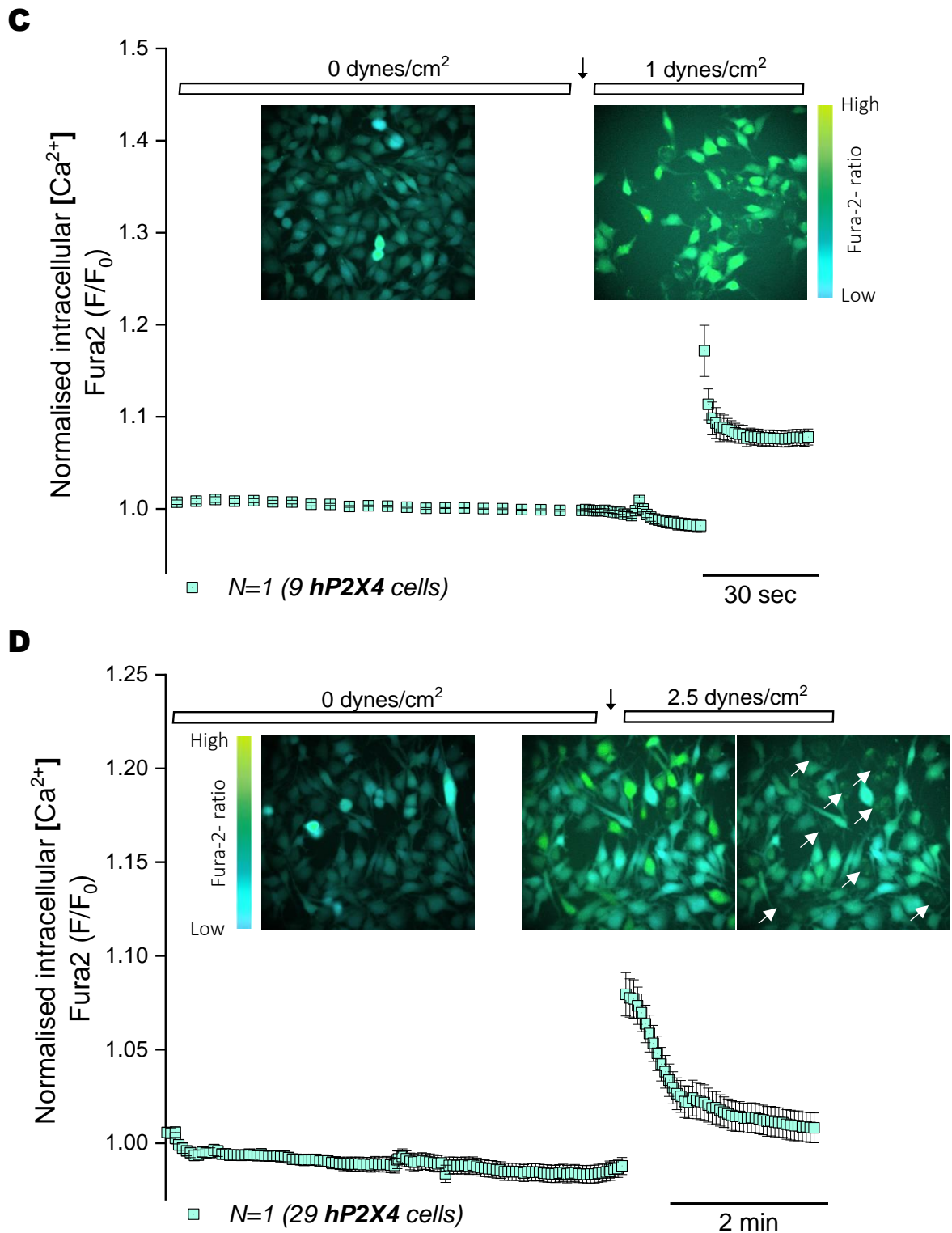


Figure 15. Representative technical issues when performing shear stress assays using the Glycotech parallel flow chamber. (A) Shear stress did not elicit any calcium response when applying 1 or 2.5 dynes/cm² in 24 hours-seeded hP2X4 stable astrocytoma cells due to an unexpected preactivation before application of the stimulus ($N=1$; $n=45$). (B) 24 hours-seeded hP2X4 astrocytoma cells were spontaneously activated in the chamber when they were subjected to any stimulus ($N=1$; $n=10$). (C) Disruptive bubble effect when applying 1 dyn/cm² in 24 hours-seeded hP2X4 astrocytoma cells ($N=1$; $n=9$). (D) The bubble effect when applying 2.5 dyn/cm² in 24 hours-seeded hP2X4 astrocytoma cells could be confused with a specific activation, but slight cell wash reveals the opposite ($N=1$; $n=29$). Data are represented as mean \pm SEM.

4.3.3.2 The Ibidi μ -slide was an inconsistent but potentially valuable tool to stimulate cells in vitro mechanically.

The following parallel flow chamber used to investigate the shear stress stimulation was the Ibidi μ -slide (**Methods section, Figure 3-D**). Different seeding times and confluency levels, as indicated, were used to perform the experimental trials with this device. In the initial experiment, hP2X4 astrocytoma cells at high confluences were used to stimulate shear stress-dependent calcium responses (**Figure 16-A, B**). However, the seeding cell time in these trials was 3 hours instead of 24 hours, as previously reported for the Glycotech chamber, as we hypothesised it could help in the mechanical stimulation of the cells. Despite the new conditions, no response could be isolated at 3 or 6 dyne/cm² (**Figure 16-A**). However, in this case, failure due to technical issues was decreased to 25% of experiments, whereas 75% were not responsive using these new settings (**Figure 16 -B**). Because of their availability in-house, HeLa cells were also used as a cheap model to check the shear stress responsiveness using the Ibidi μ -slide. Nonetheless, shear stress did not elicit any calcium response when applying 12 dynes/cm² in 24-hours seeded high confluent HeLa cells (**Figure 16-C**). The success rate using these cells was improved compared to the rates observed using the Glycotech system, as in the case of the hP2X4 astrocytoma cells. These experiments reported 40% failure due to technical issues, while the resting 60% assays could not successfully stimulate the cells (**Figure 16-D**). To ensure cells were viable and healthy to respond to shear stress mechanically, the same cell slide was exposed to an agonist, such as Yoda1, to verify their responsiveness condition afterward. This was the case for every nonresponsive assay shown in this study. **Figure 16-E** illustrates a representative experiment of the previously reported mechanically nonresponsive slide (**Figure 16-C**) when exposed to Yoda1 3 μ M. The cells elicited Yoda1-dependent calcium influx, confirming the capacity of the cell to respond normally to chemical stimuli.

As these two models did not allow us to observe any shear stress-dependent response, even when the success rates improved, we decided to invest in some HUVEC cells to conclude if these slides were helpful for our study. Both seeding times were investigated. Firstly, HUVEC cells 3-hours seeded were exposed to 4 and 12 dynes/cm² (**Figure 17-A, B**). Shear stress-evoked calcium responses were observed in both conditions, illustrating a sustained trace kinetics response. When applying 4 dynes/cm², the variability of the responses was notable, as portrayed in **Figure 17-B**. The success rate using HUVEC cells 3 hours seeded was the best compared to the rates observed using the Glycotech system or in any other Ibidi μ -slide conditions studied. These experiments reported just 14.3% failure due to technical issues, while the resting 71.4% assays successfully stimulated the cells (**Figure 17-D**). As some spiking signals were observed before the mechanical stimulation when performing the experiments, a control assay testing spontaneous activation was performed to discard any unspecific activation that could occur, as in the case of the Glycotech chambers (**Figure 16-B**). In **Figure 17-C** the arrow indicates the average response represented as mean \pm SEM while the other traces illustrate every single cell's behaviour without mechanical stimulus. In a sample of 45 HUVEC cells, just 3 isolated cells spontaneously spiked, which did not impact the average output of the experiment, as confirmed in the average response.

The second seeding time investigated was 24 hours. Surprisingly, this change in the seeding time had a significant impact on the HUVEC cells' ability to respond to mechanical stimuli. Shear

stress did not elicit any calcium response when applying 4 (**Figure 18-A**), 12 (**B**), or 20 (**C**) dynes/cm². Although there is a slight sustained increase after shear stress application, it is not considered a response because of the magnitude. The success rate using HUVEC cells 24 hours seeded was worse than the one observed at 3 hours but comparable with the ones seen with the same slides in hP2X4 and HeLa cells. These experiments reported 28.6% failure due to technical issues, while the resting 71.4% assays could not successfully stimulate the cells (**Figure 18-D**). Nonetheless, the cells exhibited responsiveness to 100 μM ATP (**Figure 18-E**) or 30 μM Yoda1 (**Figure 18-F**) following the attempted mechanical stimulation, eliciting typical calcium responses.

Due to unpublished observations of the impact of the confluence in the mechanical stimulation of Piezo1, we decided to perform these assays at lower confluences. Due to a lack of HUVEC availability, HMEC-1 cells were used as an endothelial model to corroborate the hypothesis. HMEC-1 cells 24-hours seeded were exposed to 15 dynes/cm² (**Figure 19-A, B**). The seeding time was this because it has been traditionally reported in papers using the μ-slides (Reinhart-King et al., 2008; Sedlak et al., 2023). Shear stress elicited calcium responses when applying 15 dynes/cm² in 38.5% of the trials, whereas 23.1% were nonresponsive. Additionally, the failure rate was higher in this case, reporting 38.5% failed trials due to technical issues (**Figure 19-C**).

These experimental conditions, together with 3-hour seeding times in the Ibidi μ-slide, demonstrated the best mechanical stimulation performance. However, more time was required to find the ideal setting configuration. We consider both cell lines capable of being stimulated mechanically, but an improvement of the system is required to characterise the contribution of P2 receptors to this response pharmacologically. Success rates need to be improved regarding technical feasibility, and cell responsiveness must reach at least 70% of the trials.

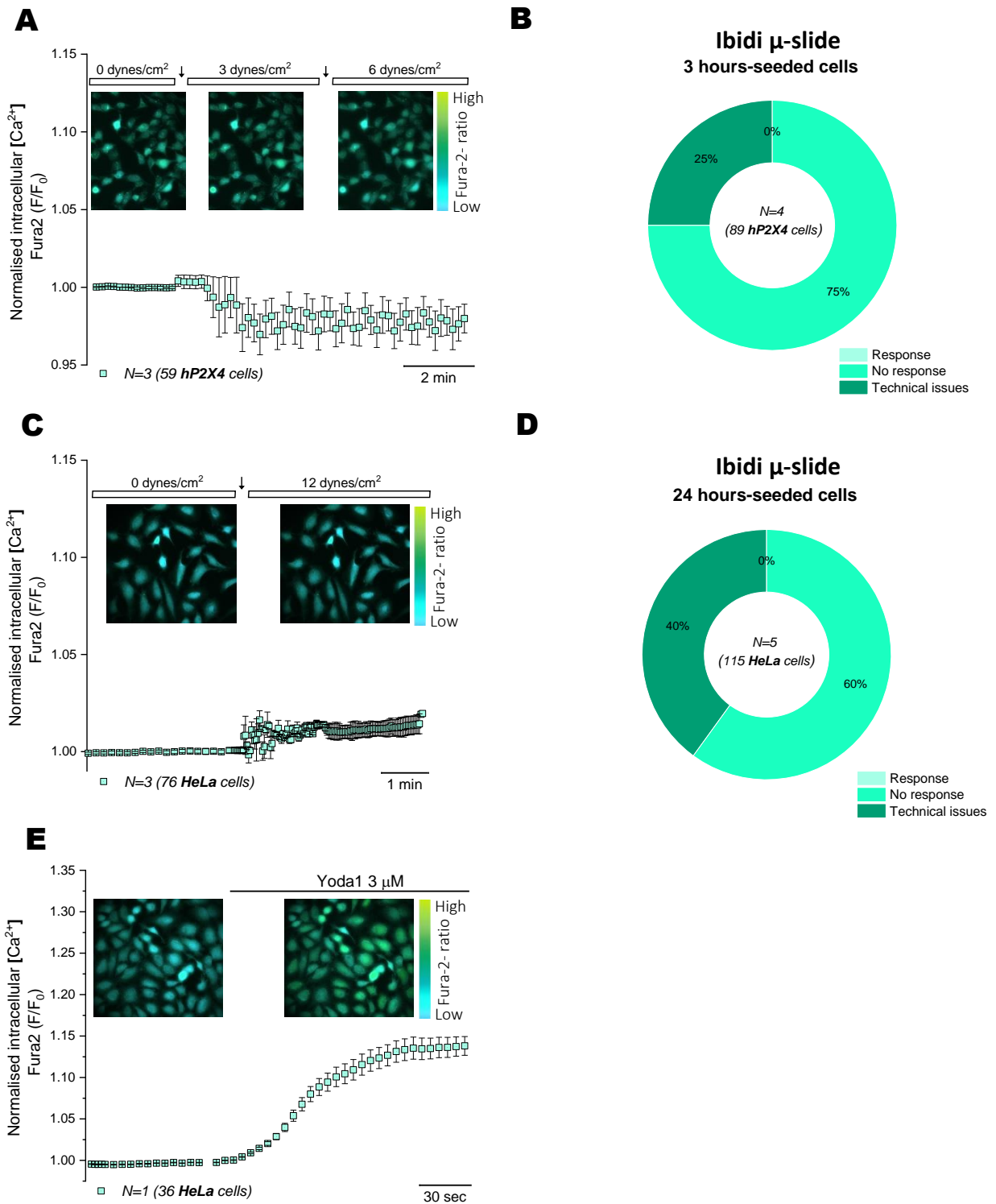


Figure 16. Shear stress stimulation assays using the Ibidi μ -slide. (A) Shear stress did not elicit any calcium response when applying 3 or 6 dynes/cm² in 3 hours-seeded 1321N1 human P2X4 stable astrocytoma (hP2X4) cells ($N=3$; $n=59$). (B) In addition, 25% of the trials failed due to technical issues. (C) Shear stress did not elicit any calcium response when applying 12 dynes/cm² in 24 hours-seeded HeLa cells ($N=3$; $n=76$), and (D) 40% of the trials failed due to technical issues. (E) However, the same cell slide (representative experiment) was exposed to 3 μ M Yoda1, and the cells elicited regular calcium responses ($N=1$; $n=36$). Data are represented as mean \pm SEM. Percentage calculations were performed using total N numbers as 100%.

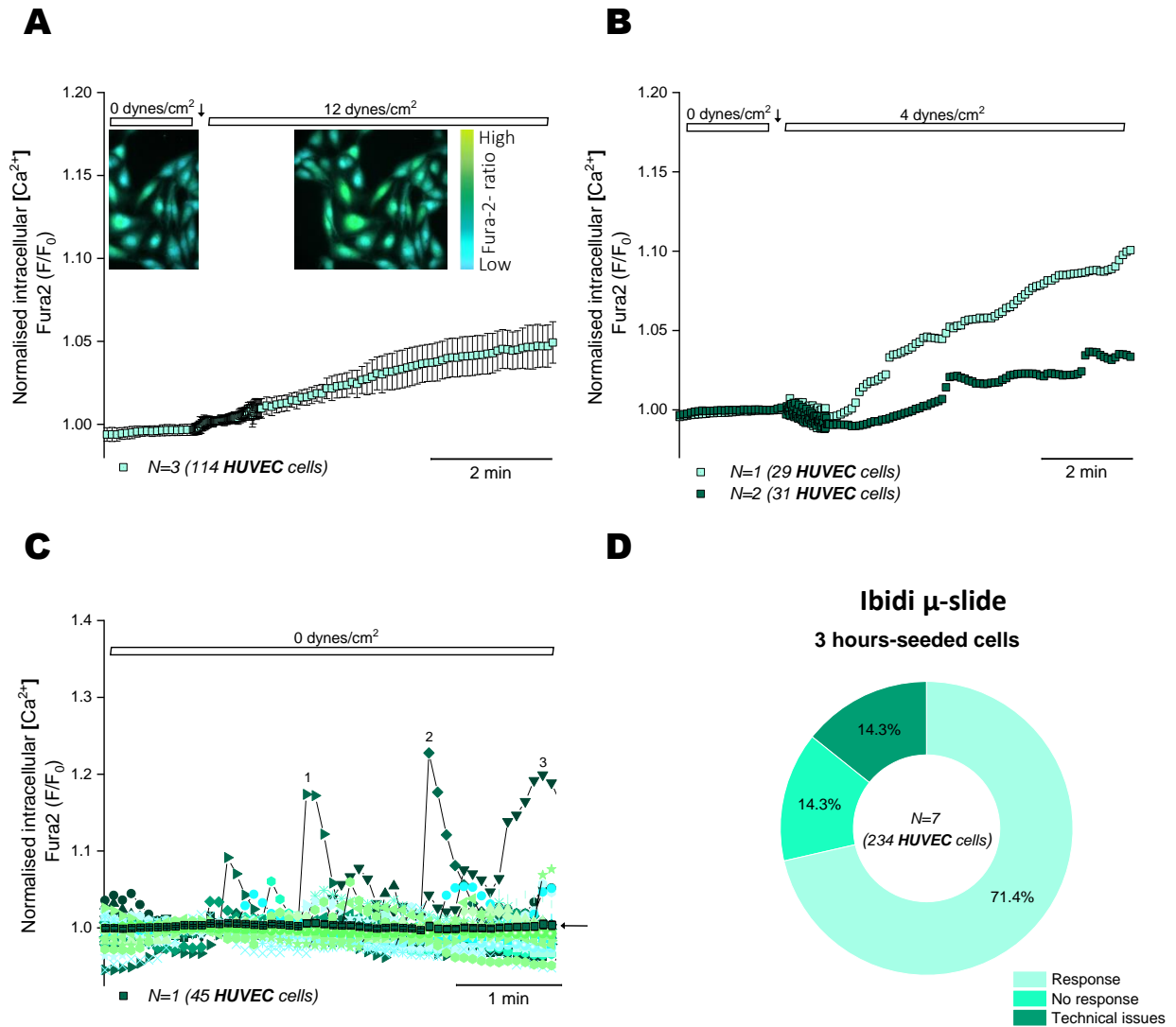


Figure 17. Shear stress stimulation assays in 3 hours-seeded human umbilical vein endothelial (HUVEC) cells using the Ibidi μ -slide. (A) Shear stress elicited a calcium response when applying 12 dynes/cm² in 3 hours-seeded human umbilical vein endothelial (HUVEC) cells ($N=3$; $n=114$). (B) Shear stress elicited a calcium response when applying 4 dynes/cm² in 3 hours-seeded human umbilical vein endothelial (HUVEC) cells ($N=2$; $n=60$). (C) Control assay testing spontaneous activation in 3 hours-seeded HUVEC cells over 4 minutes. The arrow indicates the average response, while the graph represents calcium flickerings for each cell in the slide ($N=1$; $n=45$). (D) In this case, just 14% of the trials failed due to technical issues. Data are represented as mean \pm SEM. Percentage calculations were performed using total N numbers as 100%.

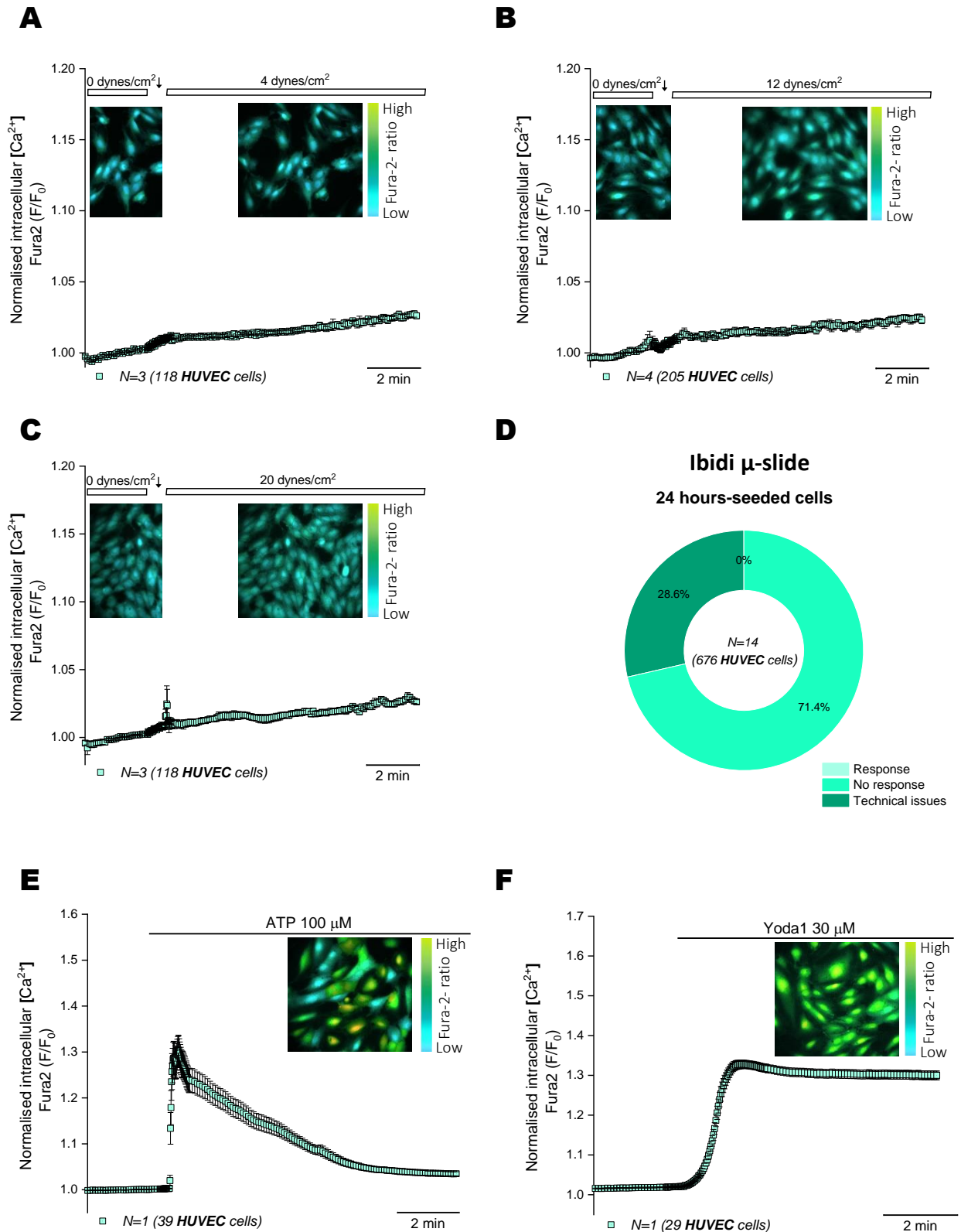


Figure 18. Shear stress stimulation assays in 24 hours-seeded human umbilical vein endothelial (HUVEC) cells using the Ibidi μ-slide. Shear stress did not elicit any calcium response when applying (A) 4 ($N=3$; $n=118$), (B) 12 ($N=4$; $n=205$), or (C) 20 ($N=3$; $n=118$) dynes/cm² in 24 hours-seeded HUVEC cells. (D) In addition, 28.6 % of the trials failed due to technical issues. However, cells were responsive to (E) 100

μM ATP ($N=1$; $n=39$) and (F) $30 \mu\text{M}$ Yoda1 ($N=1$; $n=29$), eliciting regular calcium responses after mechanical stimulation tentative. Data are represented as mean \pm SEM. Percentage calculations were performed using total N numbers as 100%.

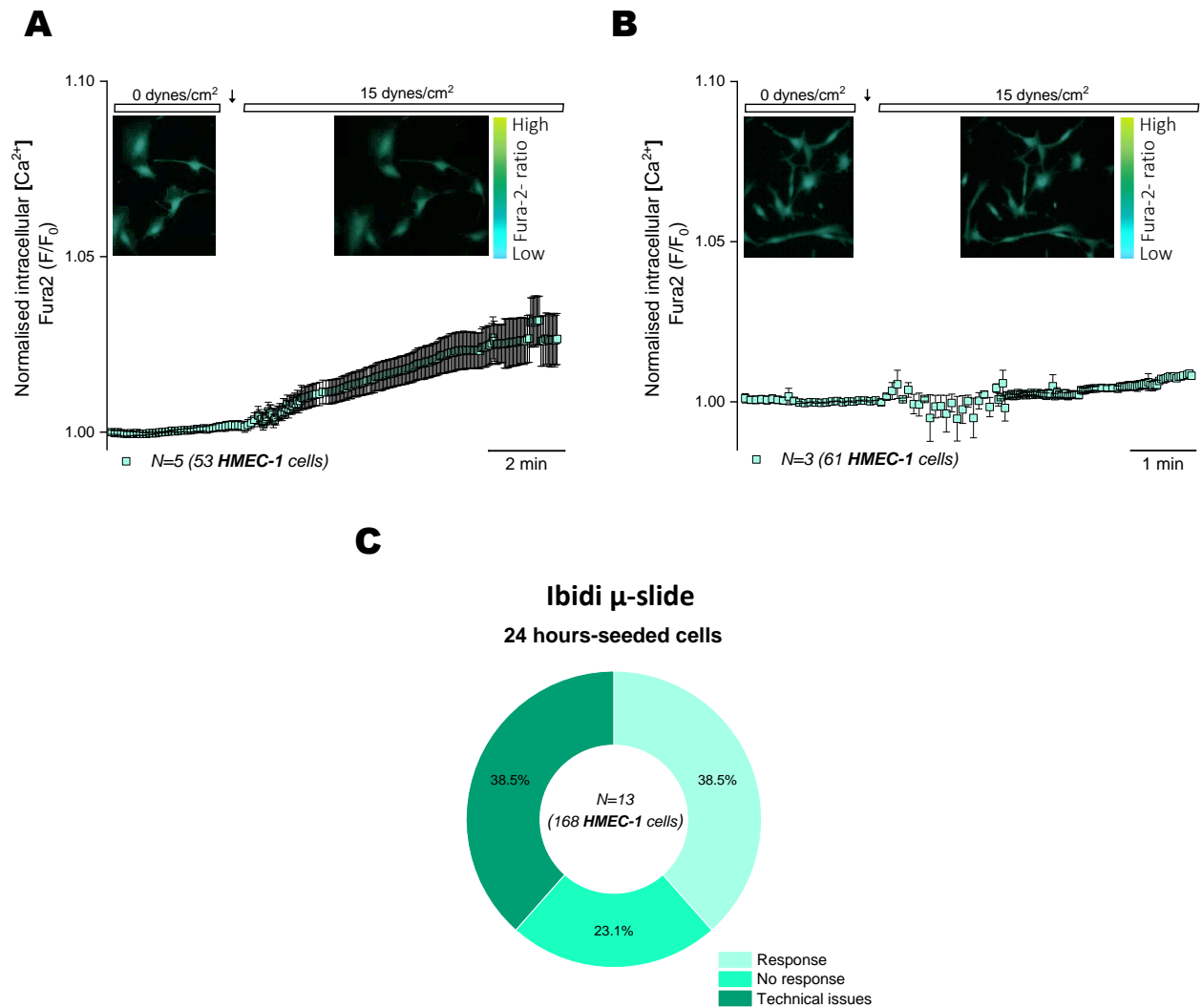


Figure 19. Shear stress stimulation assays in 24 hours-seeded human microvascular endothelial (HMEC-1) cells using the Ibidi μ -slide. (A) Shear stress elicited a calcium response when applying 15 dynes/cm^2 in 24 hours-seeded HMEC-1 cells ($N=5$; $n=53$). **(B)** However, this wasn't consistent as shear stress didn't elicit any calcium response when applying the same stimulus in other technical repeats. **(C)** In addition, 38.5% of the trials failed due to technical issues. Data are represented as mean \pm SEM. Percentage calculations were performed using total N numbers as 100%.

4.3.4. Investigation of the benefit of the Griess reagent for quantifying nitric oxide in endothelial cells *in vitro*.

Vascular endothelial cells produce a relaxing agent known as nitric oxide (NO), which plays a role in various physiological processes. One approach to assess nitric oxide production is measuring nitrite accumulation (NO₂-), one of the breakdown products upon nitric oxide formation, which can be measured using the Griess reagent.

The significance of measuring nitric oxide emanated from previous studies that explored the dependence of nitric oxide release on mechanical stimulation and the resulting calcium-induced vasodilation (Wang et al., 2016). The goal of this investigation was to explore the utility of the Griess reagent as a way to measure nitric oxide release shear stress-induced and, in addition, to further study the involvement of VEGF^A₁₆₅ in its release, as well as the potential role of P2Y₁₁ in the VEGF^A₁₆₅ dependent effects in the endothelium. Yoda1, ATP and carbachol stimulation have been demonstrated to induce nitric oxide production *in vitro* (Lockwood et al., 2014; Miyashita et al., 2002.; Wang et al., 2016); therefore, they were used as theoretical positive controls in these assays. ATP-γ-S was used in these trials instead of ATP because it hydrolyses much slower in the presence of phosphatases or ATPases. Its ability to induce a calcium concentration-response curve is shown in **Figure 20-A**, and the response to 30 μM ATP-γ-S versus 30 μM ATP is represented in **Figure 20-B**. Because of their similarity, ATP-γ-S was selected for these experiments in which the cells needed a more prolonged nucleotide availability than usual.

Different starvation times were applied as they might simulate more physiological conditions, as cells in the human body are exposed to lower levels of nutrients and growth factors. Additionally, serum-starved cells have often reduced their proliferation rates, which is beneficial to investigate the cellular response to stimuli as it is believed to decrease the basal activity of the cells. After 4 hours of starvation in the absence of L-arginine, none of the agonists (30, 10, 1 μM Yoda1; 300, 100, 30 μM ATP; 100, 30 ng/mL VEGF₁₆₅ or 100 μM carbachol) caused an increase in nitrite levels (**Figure 21-A**). L-arginine favours nitric oxide release *in vitro* (Privat et al., 1997). In addition, S-nitroso acetyl penicillamine (SNAP), a nitric oxide donor, was used as a positive control to ensure the Griess reagent's capacity to detect nitrite (Arnau del Valle et al., 2022). Thereby, the subsequent assay trial was performed in the presence SNAP at two different concentrations (200 and 500 μM) in cells starved and exposed to L-arginine (200 and 400 μM) for 24 hours prior to experimentation (**Figure 21-B**). In the presence of 200 μM SNAP and 200 μM L-arginine, 4.1 μM of nitrite was detected. Consistently, 500 μM SNAP and 400 μM L-arginine caused a nitrite release of 8 μM (**Figure 21-E**). To understand better these effects, a third condition was designed consisting of a more exhaustive starvation of 48 hours where SNAP at two different concentrations was again tested, as well as ATP and Yoda1 at different concentrations in the presence or absence of L-arginine (**Figure 21-C**). In the presence of 200 μM SNAP, independently of the presence or absence of L-arginine, nitrite was detected, and that was also the case at 500 μM SNAP, where a dose-dependent increase was detected, being the amount of nitrite considerably higher, ≈ 28 μM, compared to the lower concentration of NO donor (≈ 14 μM) (**Figure 21-E**). Unfortunately, a nitrite increase after stimulation with any other agonist (ATP and Yoda1) in the presence of L-arginine after 48 hours of starvation remained undetectable. The last starvation condition was done for 96 hours, where SNAP at the highest concentration, 500 μM, was again tested, as well as ATP and Yoda1

at different concentrations in the presence or absence of L-arginine (**Figure 21-D**). In the presence of 500 μM SNAP, independently of the presence or absence of L-arginine, nitrite was detected in a slightly higher concentration ($\approx 36 \mu\text{M}$) compared to the same conditions after 48 hours of starvation ($\approx 28 \mu\text{M}$) (**Figure 21-E**). Unfortunately, a nitrite increase after stimulation with any other agonist (ATP and Yoda1) in the presence of L-arginine after 96 hours of starvation remained undetectable.

It is crucial to mention that these experiments represent a single biological repeat ($N=1$ per condition) where each drug was tested in triplicates ($n=3$), and the reason was the lack of experimental time. However, these preliminary results suggest that the Griess reagent range of detection depends on the cells' starvation state but not on their exposure to L-arginine. Any tested drugs (ATP, Yoda1, VEGF₁₆₅, or carbachol) did not evoke a detectable amount of nitrite, and just an artificial donor of nitric oxide at high concentrations, SNAP, was able to induce detectable nitrite using the Griess reagent. All of the tested drugs previously demonstrated their ability to evoke a calcium response, but carbachol effects in the HMEC-1 cells' calcium responses had been tested previous to these assays. Surprisingly, 100 μM did not evoke any intracellular Ca^{2+} response in HMEC-1 cells (**Figure 20-C**), and no nitric oxide release should be expected. To complement the understanding of HMEC-1 cells' possible nitric oxide synthesis pathways, a calcium mobilisation assay was performed in the presence of 100 μM acetylcholine, a neurotransmitter that mediates the activation of endothelial nitric oxide synthase (Kellogg et al., 2005). Again, 100 μM acetylcholine did not evoke any intracellular Ca^{2+} response in HMEC-1 cells (**Figure 20-D**).

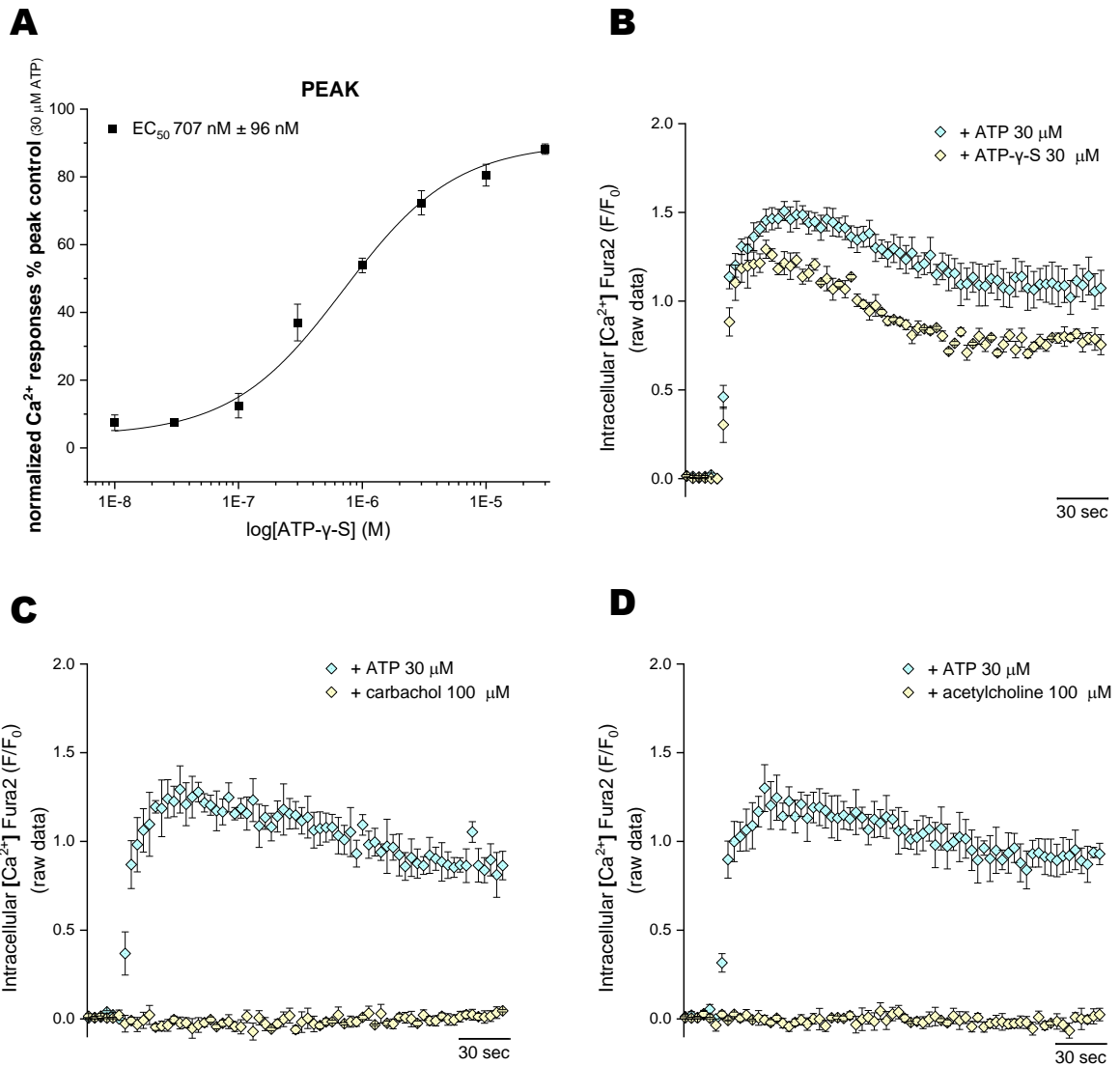


Figure 20. Investigation of calcium-induced responses from relevant agonists in the study of nitric oxide release in human microvascular endothelial cells (HMEC-1). **(A)** Concentration-response curves for the peak magnitude of intracellular Ca^{2+} responses elicited by ATP- γ -S (0.1-30 μ M; closed square; $N=1$). All data were normalised to 30 μ M ATP and fit the Hill1 equation with the EC_{50} value showed in the graph. **(B)** Averaged time-resolved intracellular Ca^{2+} responses elicited by ATP 30 μ M (cyan rhombus; $N=1$) and ATP- γ -S 30 μ M (light yellow rhombus; $N=1$) over 250 seconds. **(C)** Averaged time-resolved intracellular Ca^{2+} responses elicited by ATP 30 μ M (cyan rhombus; $N=1$) and carbachol 100 μ M (light yellow rhombus; $N=1$) over 250 seconds. **(D)** Averaged time-resolved intracellular Ca^{2+} responses elicited by ATP 30 μ M (cyan rhombus; $N=1$) and acetylcholine 100 μ M (light yellow rhombus; $N=1$) over 250 seconds. Data are represented as mean \pm SEM.

(*) F/F_0 refers to the Fura2 ratio, meaning F340/F380

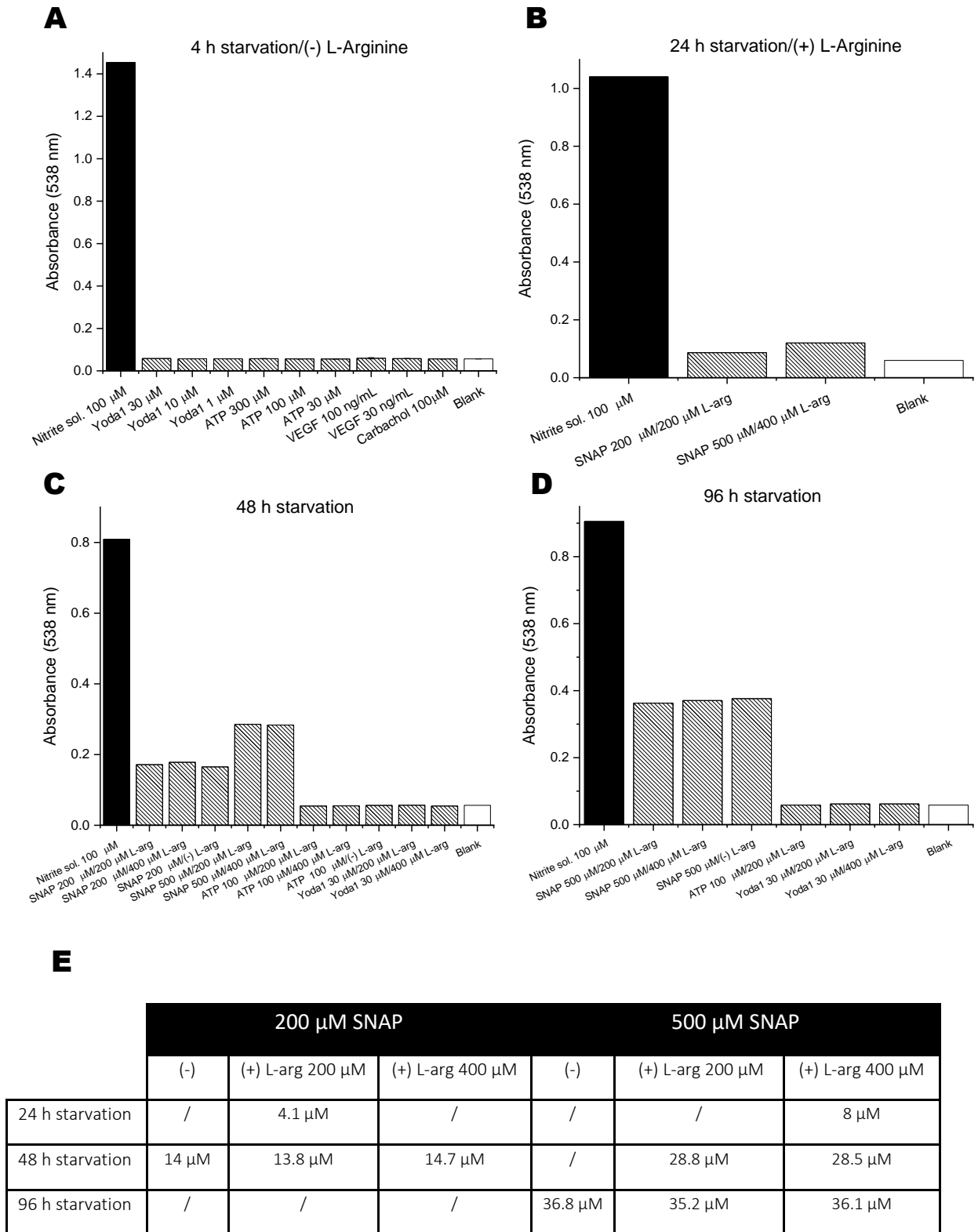


Figure 21. Accumulated Nitrite (NO_2^-) measurement upon different agonist stimulation in Human Microvascular Endothelial Cells (HMEC-1). **(A)** After 1 h ATP, Yoda1, VEGF₁₆₅, or carbachol treatment, the nitrite content in the media of 4-hour starved cells was measured by Griess reagents. Cells were not previously exposed to L-arginine (-). **(B)** After 1- hour SNAP treatment, the nitrite content in the media of 24-hour starved cells was measured by Griess reagents. Cells were previously exposed to 200 and 400 μ M L-arginine (+). **(C)** After 1 h SNAP, ATP, or Yoda1 treatment, the nitrite content in the media

of 48-hour starved cells was measured by Griess reagents. Some conditions were exposed to L-arginine, as indicated in the graph. **(D)** After 4 h SNAP, ATP, or Yoda1 treatment, the nitrite content in the media of 96-hour starved cells was measured by Griess reagents. Some conditions were exposed to L-arginine, as indicated in the graph. *Black chart*: Standard nitrite solution 100 μ M; *Stripe chart*: drug treated samples; *White chart*: no treated samples, vehicle control.

4.4 Discussion

4.4.1. Piezo1 is transcriptionally and functionally expressed in human dermal microvascular endothelial cells (HMEC-1) and human umbilical vein cells (HUVEC).

HUVEC and HMEC-1 cells have been previously used to study the effects of shear stress effects in the endothelium. However, calcium influx shear-induced has been reported in HUVECs (Li et al., 2014; Swain et al., 2021; Wang et al., 2016; Yoshikawa et al., 1997), which is not the case for HMEC-1 cells. In the last cell line, shear stress effects were always studied from an expression change point of view (Goedicke-Fritz et al., 2015; Nguyen et al., 2001), and it is also challenging to find studies showing morphological changes upon stimulus (Polk et al., 2022), something very documented in HUVECs. Nonetheless, HMEC-1 responded to another mechanical stimulus, such as stretching through the activation of Piezo1 (Carrillo-Garcia et al., 2021). Piezo1 is the primary mediator of the shear stress stimulus, and its impairment led to the morphological and functional changes in the endothelium. HUVECs have been by far the preferred cell line to study Piezo1 functional expression (Li et al., 2014; Ranade et al., 2014; Swain et al., 2021; Wang et al., 2016). Piezo1's mRNA expression in HMEC-1 was investigated by RNA sequencing, as shown in **Chapter 3.3.1**. It was by far the most expressed receptor of our analysis, which agrees with the RNA sequencing output from Bastounis (2021), and siRNA expression by Carrillo-Garcia et al. (2021). On the other hand, the transcriptional expression of Piezo1 was not performed in-house for the lack of time, but others have previously reported (Li et al., 2014; Ranade et al., 2014; Wang et al., 2016).

To study the functional expression of Piezo1, we used Yoda1, its selective agonist. Yoda1 was first described in 2015 by Syeda et al., who showed its effect on the sensitivity and inactivation kinetics of Piezo1-evoked currents. Later, Botello-Smith et al. showed that Yoda1 can bind directly to the channel, acting as a "molecular wedge," facilitating its opening probability at a lower activation threshold. Yoda1 evoked dose-dependent responses in HMEC-1 cells with a potency in the nanomolar range (EC_{50}^{PEAK} : 559 ± 83 nM; EC_{50}^{AUC} : 623 ± 91 nM). Carrillo-Garcia et al. reported traces of 20 μ M Yoda1 stimulation in agreement with our data. However, finding more studies showing this stimulation was challenging, and we could not find reports illustrating dose response stimulations or Yoda1 potency calculations in HMEC-1.

GsMTx4, the spider venom, was used to inhibit Piezo1-dependent responses by affecting cell membrane mechanics (Bae et al., 2011), as others have previously reported using different cell models (Venturini et al., 2020; Wadud et al., 2020). The venom at its higher concentration (10 μ M) impacted the Yoda1 evoked calcium responses, but not at lower inhibitor concentrations. We cannot compare these effects with other HMEC-1 cell effects as they have not been previously reported. However, their high sensitivity to Yoda1 might explain the necessity of the higher concentration of GsMtx4.

Similarly, as observed in HMEC-1 cells, Yoda1 also evoked dose-dependent responses in HUVECs. Nonetheless, the channel needed more Yoda1 to reach 50% of activation in this case. That is portrayed in the potency in this cell line (EC_{50}^{PEAK} : 1.24 ± 0.11 μ M; EC_{50}^{AUC} : 1.41 ± 0.29 μ M), which is in the micromolar range and significantly lower than the one observed in HMEC-

1 cells. If comparing trace kinetics in both cell lines, the most significant difference is the modestly decayed sustained phase observed in HUVECs. However, the trace kinetics are still conserved between cell lines. Our illustrated trace kinetics in HUVECs agreed with what has been shown earlier by Evans et al. and Jiang et al. Nonetheless, Evans et al. calculated potency was much lower than ours (0.23 μM). Various factors might explain the difference. They strictly used passages lower than six, while our cells were subcultured to passage ten. Additionally, their cells were provided by Lonza instead of PromoCell, which might affect the isolation process and supplementation. Thereby, the culture media used differed from ours (**Table 1**).

Table 1. Composition of growth media supplement for Lonza and Promo Cell. In both cases, information was extracted using the manufacturer's website and can be found under the specified reference number for Lonza (CC-3162) and Promo Cell (C-22010).

| | EGM-2 (Lonza) | Endothelial Cell Growth Medium (Promo Cell) |
|------------------|---|--|
| media supplement | hEPG (Epidermal Growth Factor), hydrocortisone, GA-100 (Gentamicin, Amphotericin-B), FBS (Fetal Bovine Serum), VEGF (Vascular Endothelial Growth factor) , hFGF-B (Fibroblast Growth Factor), R ³ -IGF-1 (Insulin-like Growth Factor), Ascorbic acid, Heparin | hEPG (Epidermal Growth Factor), hydrocortisone, FCS (Fetal Calf Serum), ECGS (Endothelial Cell Growth Supplement), hFGF (Fibroblast Growth Factor), Heparin |

Yoda1 potency and maximal responses were dramatically reduced when the same assays were investigated without calcium. A very minimal entry of calcium can be observed at high concentrations that might infer the contribution of Piezo1 activation in the intracellular stores. This dramatic reduction of the response makes sense as the Piezo1 is present in the cell membrane, more localized in its dynamic protrusions (Koser et al., 2016; Li et al., 2014; Sugimoto et al., 2017). Others have also shown a possible Piezo1 localization in the RE (McHugh et al., 2010; Zhang et al., 2017), but this is still in debate.

Dooku1, the Yoda1-evoked effects antagonist (Evans et al., 2018), was used to investigate whether Yoda1-evoked responses behave canonically, as others have previously reported using different cell models (Barnett et al., 2023; Deivasikamani et al., 2019; Hatem et al., 2023; Matsunaga et al., 2021; Szabó et al., 2022; Wadud et al., 2020). Dooku1 did not exhibit a direct effect on PIEZO1. However, it demonstrated its ability to inhibit 2 μM Yoda1 calcium responses, with an IC₅₀ of 1.5 μM in HUVECs. Evans et al., suggested a competitive effect on the same or a binding site similar to Yoda1. Our calculated IC₅₀ was close to what they reported but is lower (≈ 700 nM), and the dose-response trace kinetics differ. Despite the range of Dooku1 concentrations being very similar, in our case, 10 μM Dooku1 inhibits Yoda1 response to 30% of its basal response. In contrast, in their assay, the inhibition at the same antagonist concentration decreases the control response to around 60%. The investigation reported the earlier mentioned Yoda1 potency in HUVECs of 0.23 μM . As their umbilical endothelial cells showed greater sensitivity to Yoda1, it sounds reasonable for their cells to need more concentration of Dooku1 to obtain the same level of inhibition.

4.4.2. The broad-spectrum P2 antagonist impacted the Yoda1 calcium influx differently in HMEC-1 and HUVEC cells.

Piezo1 is found in the endothelium and senses the blood flow-induced physiological shear stress, leading to endothelial calcium influx and cell alignment (Li et al., 2014; Ranade et al., 2014; Tang et al., 2022). ATP release upon shear stress-induced activation is known to be a primary step in the mechanotransduction of this stimulus (Bodin et al., 1991; Burnstock et al., 2014; John et al., 2001; Lohman et al., 2012; Wang et al., 2016; Wang et al., 2015; Wei et al., 2019; Yamamoto et al., 2011). The activation of Piezo1 led to an ATP release, partially by pannexin channels, which will activate P2Y2 receptors downstream. This P2Y2 downstream calcium activation will favour the shear stress sensing complex described by Tzima et al. (PECAM-1/VE-cadherin/VEGFR-2), whose activity will allow phosphorylation of NO synthase (eNOS) and a sustained contribution to nitric oxide release (**Figure 1**) (Wang et al., 2016). It has been noted that only a small portion of the increase in intracellular calcium concentration resulting from PIEZO1 activation is attributed to PIEZO1-mediated influx (Lee et al., 2014; Retailleau et al., 2016). Most recorded Piezo1 calcium influx is believed to stem from downstream amplification mechanisms, such as P2Y2 activation. In line with this observation, it was shown that the loss of Gq/G11 in endothelial cells significantly inhibited Yoda1-induced rises in intracellular calcium (Wang et al., 2016). They stated that Yoda1 replicated the impact of fluid shear stress (also supported by Davies et al., 2019) on endothelial cells and induced vasorelaxation in a manner dependent on PIEZO1. Therefore, it can be used to study downstream signalling pathways. P2Y2 has also been shown to impair cell alignment and impact the cytoskeleton arrangement (Sathanoori et al., 2017).

How ATP is released to the extracellular space is still in debate. Wang et al., (2016) showed that pannexin-1/2 channels partially mediate Piezo1-dependent ATP release. However, when losing the channels, the ATP released persisted even when significantly reduced. Vesicular exocytosis and caveolae ATP release have also been suggested to mediate ATP release in endothelial cells (Burnstock et al., 2014; Yamamoto et al., 2011). In 2018, Yamamoto et al. proposed mitochondrial ATP generation shear stress-dependent, leading to release in the caveolae or lipid rafts.

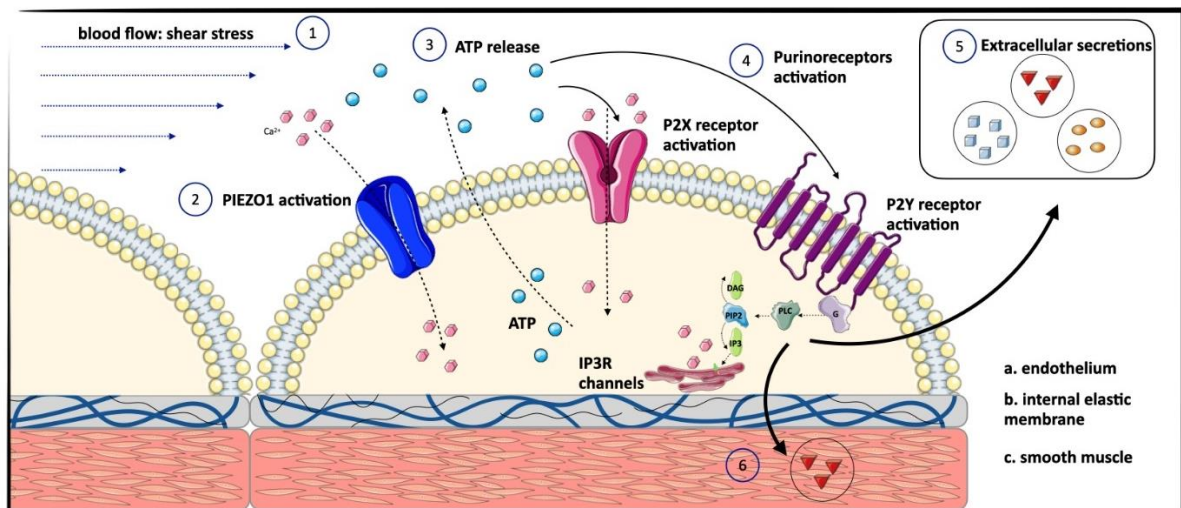


Figure 1. Proposed Piezo1 activation mechanism and downstream events upon shear stress stimulation.

1. Blood flow evokes shear stress mechanical stimulation in the endothelium, 2. leading to Piezo1 activation and its dependent calcium influx into the cytosol, and 3. ATP release to the blood vessel lumen. 4. Released ATP can activate, in turn, P2 purinergic receptors, evoking direct calcium influx from P2Xs or increasing cytosolic calcium concentration through the activation of the PLC pathway. 5. This process will also cause different extracellular secretions to the blood vessel lumen, and 6. diffusion of biomolecules such as nitric oxide from the endothelium to the smooth muscle, provoking vasodilation (Parts of the figure were drawn by using pictures from Servier Medical Art. Servier Medical Art by Servier is licensed under a Creative Commons Attribution 3.0 Unported License (<https://creativecommons.org/licenses/by/3.0/>)).

Yamamoto et al. were the first to portray the central role of P2X4 mediating ATP-induced responses in HUVECs. That was followed by a work illustrating the involvement of P2X4 in the shear stress-dependent responses that were not PLC pathway-dependent but required ATP exogenous application (Yamamoto, Korenaga, Kamiya, Ando, 2000). In human pulmonary endothelial cells, the same group demonstrated upon shear stress stimulation that P2X4 mediates calcium influx, and the action of apyrase blocked this effect, the ATP and ADP scavenger (Yamamoto et al., 2003). In addition, in mice endothelial cells, P2X4 knockout demonstrated reduced dilation in response to shear stress-dependent ATP release and lower release levels of nitric oxide (Yamamoto et al., 2006). The mediation of shear stress by P2X4 is supported by reported changes in mRNA P2X4 expression in HUVEC cells exposed to shear stress (Korenaga et al., 2001). Also, this ion channel is believed to mediate the indirect effects of shear stress in expressing the Kruppel-like factor 2 (KLF2) (Sathanoori, Rosi, et al., 2015). It was unclear whether P2X4 acted in the endothelium as a mechanosensory channel *per se*, and Kessler et al. interrogated it. The idea was supported by similar structural features with ENAC channels, whose evidence of being mechanosensitive is growing (Althaus et al., 2007). They concluded that shear stress does not affect P2X4 currents but modulates the channel's response to ATP, suggesting a stabilization of the open state of the receptor and not a mechanosensitive action of P2X4. Recent studies failed to demonstrate P2X4 activity in HUVEC cells regarding calcium signalling or mediation of nitric oxide production and concluded the predominant action of P2Y2 in the mediation of endothelial responses (Raqeeb et al., 2011; Wang et al., 2015). As previously mentioned, we could not see any antagonism effect when testing P2X4 selective inhibitor BX430 in the ATP-evoked responses in HUVECs.

This chapter's rationale is based on the already known events of shear stress dependents. To our understanding, a mechanistic link between Piezo1 effects and downstream signalling of P2X4 effects has yet to be previously investigated in endothelial cells. Although we could not see any effect of BX430 in the ATP evoked response in HUVEC in static conditions, using the Flex Station III, we consider it interesting to evaluate in dynamic conditions under shear stress stimulation inhibition of P2X4, as P2X4 showed expression by western blotting. This assay setting would more accurately replicate physiological conditions and could elicit different functional expressions and contributions of P2X4 to shear stress-dependent calcium responses. In addition, Wang et al. characterised P2Y2 Piezo1 downstream signalling in static conditions using Yoda1, and they also reported independently Piezo1 effects in the shear stress calcium evoked responses in dynamic conditions when blocking P2Y2 (Wang et al., 2015). So, it will be interesting to dig further into the possible mechanism and downstream events upon Piezo1 activation under dynamic conditions for the proposed involvement of P2Y2 and P2X4 in endothelial cells with a different P2 expression profile. How ATP is released is still under investigation. Comparing the effects in static vs dynamic conditions could create some understanding of the biomolecular pathway in which ATP shear stress-induced release occurs and which P2 receptor contributes to this response. Thus, the first step in this chapter was to analyse the impact in static conditions, the effects of apyrase and PPADs in the Yoda1 evoked response and see any contribution to the Piezo1 response in HMEC-1 and HUVEC cells.

PPADs and apyrase could not significantly affect the Yoda1-evoked responses in HMEC-1 cells, and therefore, we cannot suggest any P2 receptor involvement in this response using this experimental setting. However, that was not the case when applying these broad inhibitors in HUVEC Yoda1-evoked responses. The effects were modest but significantly relevant for both

inhibitors. Apyrase affected the peak potency with a conserved slightly right shift marked by the effects observed at Yoda1 1 or 3 μM at 0.5 and 10 U/mL, respectively. Similarly, PPADS affected the peak potency also with a conserved slightly right shift determined by the effects at Yoda1 3 μM . The effects of these inhibitors at relatively lower concentrations (1 and 3 μM) could indicate ATP release concentration Yoda1 dependent (supported by Wang et al., 2016), in a way that at higher concentrations, the ATP release is so high that the inhibitors cannot impair that contribution. However, those concentrations still contribute in a more modest way that can be observed. That effect is illustrated in the traces upon both antagonist treatments, where minimal or not effects can be observed at 30 μM while the inhibition is evident at 3 μM .

Finding other works to complement these observations is challenging, as few have reported the effects of either apyrase or PPADS in Yoda1-evoked responses in endothelial cells. The closest observations were done by Wang et al., who showed apyrase inhibition of Yoda1-induced effects in eNOS phosphorylation in HUAECs (human umbilical arterial endothelial cells), and apyrase inhibition of nitrite release Yoda1-induced in HUVECs (Wang et al., 2015). In other cell types, the apyrase effects in Yoda1 responses look conserved, as recently reported by Malko et al. (2023) in microglial cells. Yoda1 exposure inhibited TNF- α production, and the inhibition was prevented in the presence of the ATP scavenger. Desplat et al. (2021) showed apyrase could inhibit Yoda1 calcium evoke responses in cholangiocytes. Parallel effects of apyrase and PPADS have been portrayed by Mousawi et al. (2020) in mesenchymal stem cells. In a mechanism involving Piezo1 activation, PPADS, and apyrase could prevent Yoda1-dependent cell migration, but they did not have an effect on their own in this process. Gerrie (2018) was unique reporting potentiation effects of treatment with PPADS in the Yoda1-induced calcium responses in microglia. These reports suggest a consistent impairment of Piezo1-dependent responses upon apyrase and PPADS treatment. Then, our data and others suggest that HUVEC cells are a better model to study this interaction, at least in static conditions. Given that P2X4 is expressed in this cell line and not in HMEC-1, a direct hypothesis could be that P2X4 might be responsible for this mediation even though we could not inhibit ATP-evoked responses with BX430, its selective antagonist. Studying the inhibition with BX430 and other selective inhibitors in dynamic conditions would be interesting. However, any other P2 receptors should not be disregarded as candidates at this point. In static conditions, an appropriate next step for this study could be the pretreatment of HUVECs with ATP and after stimulation with Yoda1 to see if there is any effect in the dose-response curves. If there is any effect, it will support the contribution of P2 receptors to this response. Additionally, selective inhibition of the expressed P2 receptors must be performed to isolate the main contributor to this interaction. We cannot discard a possible direct effect of PPADS or apyrase in Piezo1 responses through, for example, effects in the membrane tension. Further investigation is also needed in this area.

In this chapter, we also portrayed the broad spectrum P2 antagonist effects in the ATP-evoked response prior to their effect in the Yoda1 response to ensure their action. In the case of apyrase, the effects were more significant in the AUC than in the peak, where minimal effects were reported. If comparing these effects with the ones observed in HMEC-1 cells, there were more prominent effects in potencies and maximal effects for both the peak and the AUC than in HUVECs. In the case of PPADS, the impact is conserved between cell lines, but the inhibition is more dramatic in HUVECs than in HMEC-1 cells. These differences may be inferred from the functional expression of P2 receptors profile in these cell lines. PPADS inhibition could indicate

the involvement of P2X4 or P2X7 in the ATP response. P2X7 is also sensitive to this broad-spectrum antagonist (Chessell et al., 1998; Michel, Chambers, et al., 2008; Michel, Clay, et al., 2008), but its EC₅₀ in human cells is extremely high, between 700 μ M-1.8 mM (Chessell et al., 1998; Stokes et al., 2006). Thus, any contribution of P2X7 to the ATP dose response should be observed in our concentration range of study. Preliminary data not shown in this study when investigating the effects of AZ11645373, a P2X7 selective antagonist, demonstrated no impact on the ATP response. In addition, we cannot rule out PPADS nonspecific inhibition observed in HMEC-1 cells.

4.4.3. The parallel flow system for mechanically stimulating endothelial cells *in vitro* still needs time to investigate the P2 contribution in the shear stress-dependent responses.

After tuning the calcium imaging setup, an ATP pharmacological assay confirmed the rig's ability to record intracellular calcium changes and reproducibility. Immediately after, the first parallel flow chamber was tested as an option to stimulate HUVEC cells *in vitro* mechanically. HUVECs have been broadly used as a shear stress model and as the preferred model to isolate the mechanical response (Korenaga et al., 2001; Li et al., 2014; Swain et al., 2021; Wang et al., 2015, 2016; Yamamoto, Korenaga, Kamiya, Ando, 2000). Physiological ranges for shear stress are diverse fluctuating from 0.5 dyne/cm² in post-capillary venules (Brown et al., 2001) to 100 dyne/cm² in branches and bifurcations (Reinhart-King et al., 2008). In arteries, the values are in a range of 2-20 dyne/cm² (Cheng et al., 2003; Chiu et al., 2011; Gerhold et al., 2016; Jackson et al., 2023; Reinhart-King et al., 2008), and HUVECs have demonstrated their ability to respond to shear stress in a range from 0.44 to 25 dyne/cm² (**Table 2**) (Kraiss et al., 2003; Kraiss et al., 2000; Ley et al., 1989; Li et al., 2014; Pearce et al., 1996; Swain et al., 2021; Walshe et al., 2013; Wang et al., 2016; Yamamoto, Korenaga, Kamiya, Ando, et al., 2000). Therefore, the first shear stress applied was 12 dyne/cm². Note that even though HUVECs are vein cells, they are considered an arterial model for the characteristic way of the placenta vessels configuration (Lau et al., 2021). Many technical challenges prevented further investigation of this cell line. We decided to use a convenient and affordable source of Piezo1, 1321N1 human P2X4 stable astrocytoma cells, available in-house. This cellular line has not been used as a model for shear stress stimulations. Exceptionally, we found the work of Khan et al. (2013), who used 1321N1 astrocytoma cells to investigate astrocyte cellular stiffness using a microfluidic manometer device. Although these cells do not express some receptors relevant to our study, such as P2Y₂, Ranade et al. demonstrated that only the presence of Piezo1 in a heterologous system is enough to evoke shear stress-dependent calcium responses. I had the opportunity to probe myself the same ability of Piezo1 to elicit shear stress-dependent responses (Paz et al., 2023), agreeing with what was previously reported. Therefore, this cell line was considered appropriate to evaluate the feasibility of the Glycotech parallel flow chamber to stimulate Piezo1 mechanically. The failing rate with HUVECs was around 50%, which was conserved and even more dramatic when using hP2X4 astrocytoma cells (64.7%). We found several technical issues even when applying lower shear stress (0-8 dyne/cm²) to decrease the mechanical stress applied to the cells and better control the inconveniences. There were two main technical challenges using this parallel chamber: the cells' preactivation prior to voluntary mechanical stimulation and bubbling disruption. We believe the first type of activation is due to pressure from holding the gasket into the dish, which is needed to create a parallel flow channel. The vacuum needed to hold together the system was applied using an automatic vacuum line

whose magnitude was not adjustable, limiting the test of this hypothesis. The vacuum line could also produce fluctuations in the pressure strong enough to activate the cells mechanically before shear stress application. The bubbling disruption was the second issue we faced and made to improve the experiment's technical settings, adding one step in the saline solution preparation. When moving to Ibidi slides, all solutions were degassed correctly, as described in the methods section. 35.3% of the experiments culminated, but most portrayed no response upon shear stress stimulation. Just one highly confluent dish showed shear stress-induced responses with mechanical response kinetics similar to those illustrated by Swain et al. However, that was never replicated, and all outputs suggested a change in the parallel flow chamber.

Table 2. Published physiological values of shear stress in different vascular beds and HUVEC cells.

| | System/tissue/cell type | Shear stress (dyne/cm ²) | Reference |
|---|-------------------------|--------------------------------------|--|
| reported physiological ranges | Cardiovascular system | 10 | Chiu and Chien, 2011 |
| | Aorta | 1-22 | Cheng et al., 2003 |
| | Arteries | 2-20 | Reinhart-King et al., 2008 |
| | | 10-40 | Gerhold and Schwartz, 2016 |
| | | 10-70 | Chiu and Chien, 2011; Cheng et al., 2003 |
| | | 10-17 | Jackson et al., 2023 |
| | Veins | 1-6 | Chiu and Chien, 2011; Malek et al., 1999 |
| | Capillaries | 3-95 | Koutsiaris et al., 2007 |
| Post-capillary venules | 0.5-5 | Brown and Larson, 2001 | |
| Branches and bifurcations | 30-100 | Reinhart-King et al., 2008 | |
| reported applied effective shear stress <i>in vitro</i> | HUVEC | 0.44 (30 min) | Ley et al., 1989 |
| | | 1.04-8.3 (5-60 min) | Pearce et al., 1996 |
| | | 12 (0.5-24h) | Kraiss et al., 2000; Kraiss et al., 2003 |
| | | 3-15 (< 100 sec) | Yamamoto et al., 2000 |
| | | 10 (24-72 h) | Walshe et al., 2013 |
| | | 5-20 (up to 60h) | Li et al., 2014 |
| | | 5-25 (50 sec) | Wang et al., 2016 |
| 4-12 (5-60 sec) | Swain & Liddle, 2021 | | |

The Glycotech parallel flow chamber is sold to perform well-controlled shear stress assays combined with immune cell-endothelial cell adhesion (Patton, 1996), as demonstrated on their website in the only reference (Brown et al., 2001). Other authors, such as Taite et al. (2006), have previously made this use. None of them reported unique culture details for cell monolayers exposed to shear stress, so we assumed they used technical specifications provided by the manufacturer. Glycotech indicates culturing the endothelial monolayer in 35-mm coated/uncoated dishes until it reaches the confluence (\pm 24 hours in culture). We followed the instructions in both coated and uncoated dishes, but either alternative improved the setup. Kaur et al. are the only authors referring to this type of chamber to study shear stress effects directly in endothelial cell responses and phenotype. Although they did not use the one provided by Glycotech, it is very interesting that they designed almost an identical chamber that does not need a vacuum holding system, believed to be one of our main sources of issues. To surpass this, they designed an adaptation where the dish, gasket, and flow desk are held inside a metallic microscope support. The inlet and outlet are still accessible precisely in the same configuration as our Glycotech flow chamber. Additionally, they proposed the endothelial cell culture in dish plates with an incorporated coverslip to see the cells and strict

control of the temperature and CO₂ during the assays. These modifications sound reasonable and needed for Glycotech to be a suitable system for mechanically stimulating endothelial cells *in vitro*. One constant limitation of this chamber and the Glycotech ones is the assumption of the flow media as a Newtonian fluid, which eases shear stress calculations with constant viscosity and density. However, this is a nonphysiological assumption, as blood is a non-Newtonian fluid (Jackson et al., 2023). Sedlak et al. (2023) illustrated a method protocol to stimulate the cells using a Glycotech chamber mechanically. Unfortunately, this chapter refers to the rectangular parallel flow chamber, which differs far from ours and is not considered comparable.

Given these technical challenges with the Glycotech chamber, we invested in a new parallel flow chamber type, the Ibidi μ -slide I^{0.4}. This rectangular flow chamber is made of a polymer coverslip that is ready to use and can be precoated as needed. In this case, this type of slide does not need a vacuum system because the manufacturer already assembles the parallel chamber to create the experimental area, with the only need to culture the cell by adding a suspension directly to the slide. In addition, the fluid is not treated as Newtonian but as physiological non-Newtonian blood flow (Ibidi, 2019). The same peristaltic pump was used, as in the case of the Glycotech chamber, as it is one of the most recommended and used types of pump for these assays (Kaur et al., 2012; Sedlak et al., 2023). A peristaltic pump incorporates a rotor with multiple contact points that compress the inserted tubing, creating a squeezing action to propel the medium forward (Ibidi, 2019). Peristaltic pumps have been contraindicated in flow adhesion assays (Jackson et al., 2023), but as this is not our case, it appears to be the most adequate system to produce the desired shear stress. The tubing provided by Peri-Start Pro, the pump manufacturer, was replaced with a non-silicone-based tube with low gas permeability to try to avoid as many bubbling issues as possible. With the same aim, the saline solution used to perfuse was always degassed prior to experimentation. A male elbow Luer connector was also used to ensure perfect coupling between the tubing and the slide and prevent any possible derived bubbling. The manufacturer explicitly suggested this connector and its impact on the shear stress applied should be negligible. Two generic cell models were used in the initial testing of these slides: 1321N1 astrocytoma hP2X4, as with the Glycotech chamber, and HeLa cell, which have been proposed to be shear stress-responsive (Schwachtgen et al., 1998) and they endogenously express Piezo1 (Pardo-Pastor et al., 2023). Using these two models was worthwhile as we observed improved success rates despite having no shear stress-dependent response. However, they could not induce shear stress calcium influx, so we invested in more HUVEC cells to evaluate the utility of these slides. As three hours-seeded cells were the best in terms of success rate when using hP2X4 astrocytoma, this time point was used to determine its benefit in HUVEC cell assays. The idea of a lower seeding time was taken from Li et al. and Swain et al., whose calcium imaging recording were taken after 1-4 h seeded HUVEC cells, as typically cells are allowed 24 hours or more to sit in the plates before experimentation (Sedlak et al., 2023; Reinhart-King et al., 2008). This configuration's success rate massively improved, with 71.4% of assays successfully stimulated and just 14.3% of failure, which was much better than the ones obtained at 24 hours-seeded cells for HUVECs (no responsive cells recorded) and HMEC-1 cells (38.5% success rate), portraying the significant impact of the seeding time in the success of these assays. As HMEC-1 cells were seeded at much lower confluency due to unpublished observations of the impact of the confluence in the mechanical stimulation of Piezo1, improving the successful rate might be a benefit by lower seeding confluences. We consider both cell lines capable of stimulating

mechanically, but HUVECs demonstrated to be a better model, at least with the applied settings. This agrees with Bastounis et al., who suggested after a transcriptional analysis of both cell lines that HUVECs showed upregulation of vascular tone and shear stress-related genes while downregulated in HMEC-1, profiling a model that might be more sensitive to mechanical cues and perturbations than HMEC-1 cells. As a next step, we propose further experimentation using the Ibidi μ -slide at 3-hour seeding times at a different confluence to ensure the highest degree possible in these cells. Additionally, a lower passage of cells is required; we should not use passages higher than five, as others have previously reported (Swain et al., 2021), and a bubble trapper to prevent as many inconveniences as possible.

Nonetheless, there is an essential observed feature to comment on the mentioned responsive assays. The trace kinetics observed did not portray the rapid response, characterized by a peak that decays, and it is followed by a lower sustained phase observed in hP2X4 astrocytoma cells and others such as Swain et al. and Wang et al., but a slow, sustained phase which reaches the peak at the end of the recording. This is not a Piezo1 characteristic response, as the initial firing usually causes that initial peak with a more or less sustained phase. Although some papers show these very nice and clear Piezo1-dependent responses from 4 to 12 dynes/cm² (Swain et al., 2021), others have shown a more complex response pattern when stimulating HUVECs *in vitro* from 3 to 25 dynes/cm² (Li et al., 2014; Wang et al., 2015, 2016). Li et al. portrayed HUVECs shear stress responses in the Extended Data Figure 4, which also differed from those shown by Swain et al. Li et al. illustrated trace kinetics with a clear initial peak and a sustained response of the same magnitude that does not decay at 20 dynes/cm². In addition, Wang et al. struggled to show any shear stress dependent in shear stresses lower than 15 dynes/cm². They could illustrate shear kinetics at this magnitude, characterized by a rapid peak followed by a decayed sustained phase. They could not represent magnitude-dependent shear stress calcium responses, being the highest and mainly the only response at 15 dynes/cm². However, something they all have in common, and we lack it, is the initial rapid response reaching a peak after the shear stress application. There is a main difference between our study and theirs: the HUVECs' source and cultivation conditions. In the cited published studies, cells were bought from Lonza, while ours were bought from Promo Cell. In the same way, cells were cultured using the Bullet kit EGM-2 to supplement their endothelial basal medium (EBM-2). The relevant point is the different supplementation content of the media where the cells were isolated and cultivated. One immediately observed difference was that their medium contained VEGF, and ours did not. In informal conversations with some authors, they referred to the critical point of the media supplementation for HUVECs' proper activation. That could be because VEGF could boost shear responses if VEGF receptors are integral components of the broader shear sensing machinery, as Tzima et al. proposed. Therefore, we considered the modification of culture conditions and, possibly, the change in HUVECs source manufacturer critical to try and replicate what others did to perform the P2 receptors characterization in dynamic conditions as we initially proposed.

4.4.4. The Griess reagent was not valuable for measuring nitric oxide release in HMEC-1 cells in the tested conditions.

In response to homeostatic stimuli, small quantities of nitric oxide (NO) are generated by neurons, endothelial cells, platelets, and neutrophils. Human endothelial cells line blood

vessels and are versatile cells capable of secreting various biologically active mediators. Nitric oxide is one of them, and a reduction in endothelial expression of NO commonly characterizes endothelial dysfunction. Various biological systems produce varying amounts of NO, and *in vivo*, the primary end products of NO oxidation are nitrite (NO_2^-) and nitrate (NO_3^-). The proportions of nitrite and nitrate generated from these reactions vary and cannot be reliably predicted. Given that the half-life of NO in plasma and other body fluids is only 4 seconds, the most reliable indicator of total NO production is considered to be the sum of nitrite and nitrate (Yucel et al., 2012). In endothelial cells, NO is mainly synthesized from L-arginine by endothelial nitric oxide synthase (eNOS), a calcium-dependent enzyme (Arnau del Valle et al., 2022). However, it can also be produced by an induced nitric oxide synthase (iNOS) in proinflammatory situations, which, on the contrary, is a calcium-independent enzyme (Arnau del Valle et al., 2022; Hemmrich et al., 2003). eNOS in endothelial cells produced low concentrations of nitric oxide, at the nanomolar scale, for short periods of time (Arnau del Valle et al., 2022). HMEC-1 cells have demonstrated their ability to evoke nitric oxide release (Lin et al., 2002; Nasoni et al., 2022; Vassalle et al., 2003), as well as HUVECs (Ashpole et al., 2014; Joshi et al., 2007; Lee et al., 2000; B. Yang et al., 2015; Z. Yang et al., 2015). However, since this type of assay had never been performed before, we decided to test it using the most economical cell line.

The Griess reagent is an indirect measurement of nitric oxide based on the assessment of the nitrite accumulation (Tsikas, 2007). This study aimed to assess the applicability of the Griess reagent for measuring nitric oxide release shear stress-induced and further investigate the role of VEGF₁₆₅ in this release. To preliminary test the utility of the reagent, known NO agonists were used. Others have proven the NO release upon Yoda1 (Wang et al., 2016), ATP (Lockwood et al., 2014), carbachol (Berkels et al., 2008; Miyashita et al., 2002), and VEGF₁₆₅ (Dulak et al., 2003; Hood et al., 1998; Kimura et al., 2003; Kroll et al., 1999; Mohammadi et al., 2022) stimulation *in vitro*. In the first attempt, responses to the cited agonist did not differ from blank (non-treated samples). Thus, a nitric oxide donor, SNAP, was used to corroborate Griess reagent's capacity to detect nitrite (Arnau del Valle et al., 2022; Lee et al., 2000). SNAP induced dose-dependent nitrite accumulation, which was benefited by longer starvation times in HMEC-1 cells. The measured amounts of nitrite are high (lower detected at 4 μM) for expected eNOS activity, reported to be in the nanomolar range. Additionally, Griess reagent has a technical limitation of 2.5 μM of nitrite. Although some authors showed the benefit of using it in HUVECs (Ashpole et al., 2014; Lee et al., 2000) and HMEC-1 (Lin et al., 2002) cells, many others preferred a modified and more sensitive version of this reagent to quantify NO release in endothelial cells *in vitro* (Joshi et al., 2007; Miyashita et al., 2002; Wang et al., 2016; B. Yang et al., 2015; Z. Yang et al., 2015). For this reason, we consider using the improved Griess reagent, which would measure nitrite and nitrate (Miyashita et al., 2002), as an alternative with higher sensitivity as the next step of this investigation. L-arginine did not impact the NO production in these preliminary tests. However, the external supply of the amino acid should favour nitric production (Joshi et al., 2007) and still be considered for further experimentation. One could argue that the detected NO in almost all the previously cited endothelial studies is in the micromolar range, and the Griess reagent should be sensitive enough to quantify changes in HMEC-1, as it was for Lin et al. Nevertheless, we know cells behave differently in different culture rooms, and we believe the basal release in our HMEC-1 could be lower than theirs, and then any change will be more challenging to quantify. In HUVECs, Lee et al. showed blank values of the medium without cells of 4 μM NO and in the presence of 100 μM SNAP of

20-25 μM NO after 18 hours plated. In contrast, we quantified 4 μM NO after 24 hours of starvation and 200 μM SNAP. We needed to use five times more SNAP to reach levels of NO similar to their levels, portraying the lower production of nitric oxide of HMEC-1 cells compared to others reported. Finally, the lack of carbachol and acetylcholine responsive to calcium in HMEC-1 is worth mentioning. While finding published carbachol-dependent calcium responses was challenging, Miyashita et al. compared nitric oxide production carbachol-induced in cardiac macrovascular and microvascular endothelial cells, where the microvasculature demonstrated their lack of ability to evoke NO release. Nonetheless, this release was upregulated and significantly increased in the presence of specific pharmacological tools. That could indicate low expression of muscarinic receptors in the microvasculature that could be regulated in certain situations. On the other hand, Lisec et al. (2023) showed a very low calcium-evoked acetylcholine-dependent trace in HMEC-1 when using 200 μM . Therefore, our lack of response could be due to the concentration rather than the absence of the muscarinic receptors in this cell line.

Chapter 5. General discussion.

5.1 Key findings and concluding remarks.

Endothelial calcium signalling is one of the main processes governing vascular endothelium function and mediates various cardiovascular functions such as vasodilation, vascular permeability, angiogenesis, and inflammation (Moccia et al., 2023). Changes in intracellular calcium concentrations occur in response to the activation of receptors by various agonists and mechanical stimuli in endothelial cells. One of these receptor families is the purinergic receptors, whose endothelial role and functional activity were the main focus of this investigation (Félétou, 2011). P2 receptors respond to ATP, eliciting intracellular calcium increase, both by calcium entry from the extracellular milieu (P2X ligand-gated ion channels) and through activation of the PLC pathway and subsequently cytosolic stores calcium release (P2Y receptors) (Miras-Portugal et al., 2020; Stokes et al., 2017, 2020). P2Y2 has been the most studied P2Y receptor in endothelial cells; its activity is linked to nitric oxide-dependent vasodilation, inflammatory responses, proliferation, and cell migration (Alexander et al., 2019; Cabou et al., 2022; Seye et al., 2004; Wang et al., 2015, 2016). However, it has not been the only one, as P2Y1, P2Y4, and P2Y6 have also been proposed to mediate these endothelial responses. P2Y11's function in the endothelium has been less investigated than the others. However, its involvement in inflammatory responses, cell proliferation, and cell migration has also been pointed out (Avanzato et al., 2016; Ng et al., 2018; Strassheim et al., 2020; Xiao et al., 2011). Of the P2X ion channels, P2X4 and P2X7 have been demonstrated to lead the function of this subfamily in endothelial cells. While P2X4 function is mainly believed to mediate flow-induced vasodilation (Korenaga et al., 2001; Sathanoori, Rosi, et al., 2015; Yamamoto, Korenaga, Kamiya, Ando, 2000; Yamamoto, Korenaga, Kamiya, Qi, et al., 2000), P2X7's role is portrayed in inflammatory conditions (Aslam et al., 2021; Burnstock et al., 2014; Schmid et al., 2019). Relevantly, the role of P2X4 has been challenged as some investigations failed to demonstrate its activity in human endothelial cells (Raqeeb et al., 2011; Wang et al., 2015; Wilson et al., 2007). P2 receptors varied endothelium functions and involvement in physiological and pathophysiological processes make them promising targets for developing new therapeutic agents in cardiovascular disease. Many investigations have shown their roles independently in different endothelial cell types. However, a complete pharmacological and biomolecular characterization of the purinergic receptors in endothelial cells is challenging to find in the literature, which could help better understand their contribution to the endothelial calcium signalling and derived physiological process.

This thesis's principal aim was to systematically characterise the purinergic signalling's transcriptional, functional, and expressional profile in endothelial cells, using immortalized human microvascular endothelial cells (HMEC-1) as our primary model, contributing original knowledge to the current literature. Our experimental strategy enclosed i) transcriptional characterization of the cell line using RNA sequencing, ii) pharmacological tools to investigate the previously determined P2 candidate's contribution to the ATP-dependent calcium responses by intracellular calcium mobilisation assays, and iii) western blotting assessment of the protein expression of the demonstrated P2 candidates which previously showed pharmacological effects. Following the previous rationale, the vascular endothelial growth

factor (VEGF) and Piezo1 evoked responses were also pharmacologically depicted following the same methodology, and some mechanical assays for Piezo1 investigation, with the primary goal of finding a potential contribution of purinergic signalling to their response. Some pharmacological assays were also replicated in an endothelial primary cell line, human endothelial umbilical vein cells (HUVECs), to complement our findings and better understand some endothelial mechanisms.

In the first part of this thesis (Chapter 3), we provided the transcriptional expression profile of the relevant calcium signalling toolkit in HMEC-1, allowing us to efficiently focus our pharmacological study on three different P2 receptors: P2X4, P2Y2, and P2Y11. The expression of the A2B receptor was also detected, and it was also sought when characterizing ATP and VEGF evoked responses for a complete understanding of the studied calcium influx. Our results evidenced P2Y2's significant contribution to the ATP-evoked responses in HMEC-1 cells, supported by ATP and UTP equipotency and the inhibition of the responses using its selective antagonist, AR-C 118925XX. Its role was also backed up by the impact on the ATP responses in the absence of extracellular calcium, the PLC inhibitor effects, and the SERCA inhibitor thapsigargin. Although the protein expression studies did not ease the confirmation at the protein level of P2Y2, we consider demonstrated P2Y2 functional expression in HMEC-1 cells. The unexpected parental astrocytoma results when probing the P2Y2 antibodies is a limitation challenging to surpass, and it should be further studied to understand better why, as this cell line has been demonstrated to be void of any P2 receptors. Still, residual responses upon this channel inhibition and PPADS observed effects could indicate slight participation of P2X4 or P2Y11 to the ATP response. Three P2X4 selective antagonists in this study did not inhibit ATP-induced responses. However, PSB12062 impacted the ATP dose response, resulting in difficult-to-interpret and complicated results that delayed our other studies. Because of this observation, we investigated the effects of ivermectin for possible positive allosteric modulation of P2X4. These results did not ease the situation, as ivermectin reduced the ATP response, possibly inhibiting SERCA activity. Another possibility for the residual responses observed upon P2Y2 inhibition was a contribution from P2Y11 to the ATP-induced responses. However, the P2Y11 selective antagonist, NF157, did not affect the response, opening the possibility for P2Y11 to be coupled to a $G\alpha_s$ -type protein instead of a $G\alpha_q$ -type, leading to the activation of the adenylyl cyclase pathway instead of the PLC pathway.

Immediately after this characterisation, we studied the VEGF dose dependency calcium responses. VEGF receptor 2 is vital in regulating angiogenesis, vascular permeability, and shear stress transduction in the endothelium (Heinolainen et al., 2017; Rahimi, 2006; X. Wang et al., 2020). Its capacity to evoke calcium responses is due to its tyrosine kinase nature, whose stimulation induces dimerization and autophosphorylation, activating the PLC pathway (Li et al., 2011, 2015; Simons et al., 2016). The role of Orai1, CRAC channels, and various TRPC channels in contributing to the VEGF response (Hamdollah Zadeh et al., 2008; Jho et al., 2005; J. Li et al., 2015; Li et al., 2011) hypothesised that a purinergic contribution could also exist, as others have suggested some functional interaction between the two receptor families (Erb et al., 2006; Liao et al., 2014; Seye et al., 2004). In the same way as previously done for the ATP evoked response, and after demonstrating the concentration-response profile to VEGF₁₆₅ in HMEC-1 cells, systematic calcium mobilisation inhibition assays were performed targeting the purinergic candidates previously tested. The VEGF₁₆₅ concentration-response calcium profile

in endothelial cells had yet to be well reported, so our investigation contributes to a better understanding of VEGF activity in endothelial cells.

P2Y2 selective antagonist did not impair the VEGF-evoked calcium influx, while P2Y11, ineffective in inhibiting any ATP-evoked responses, significantly diminished the calcium responses. At the same time, PSB12062 could impair the VEGF₁₆₅ responses, while BAY1797, the most potent P2X4 antagonist, did not affect the dose responses. Given these results and to finally conclude the possible P2X4 involvement in the ATP and VEGF response, protein expression was performed, with the immunoblots clearly showing the lack of hP2X4 in HMEC-1 cells. This result portrays one of the main limitations of our study, as the PSB12062 effects in the dose responses were unspecific. Our efforts during this time focused on understanding why this selective antagonist, broadly used to inhibit P2X4 but not the others, had an effect. In addition to this effect, the PPADS effects also supported the P2X4 hypothetical contribution. PPADS is a non-competitive antagonist of all P2X receptors and a partial agonist of some P2Ys in humans but not for the P2Y2 and P2Y11 receptors (Charlton et al., 1996; Communi et al., 1999; Delaune, 2023; Ralevic et al., 1996). Thus, the only possibility for this PPADS effect was to impact P2X4 activity, concluding that both PSB12062 and PPADS have non-specific effects in either ATP or VEGF₁₆₅ responses, and they are unreliable for studying P2 contribution in the microvasculature.

Once P2X4 was discarded as a possible contribution to the ATP and VEGF response, P2Y11 was the only candidate portraying a contribution to the VEGF calcium-dependent responses. Because of the lack of effect of the P2Y11 selective antagonist, NF157, in the ATP dose response, our first hypothesis, and what drove our investigation around the adenylyl cyclase pathway, was the possibility of P2Y11 to be G α_s -coupled instead of G α_q . To study the involvement of cyclic AMP production observed effects, SQ22536, an adenylyl cyclase inhibitor, was used. This inhibitor was used alone or in combination with NF157 to understand the AC involvement better. SQ22536 did not reproduce what we saw when using the P2Y11 inhibitor alone (a pronounced calcium inhibition) but caused a slight potentiation effect at lower concentrations of VEGF₁₆₅. Because of our results and the explained hypothesis in the Chapter 3 discussion, a situation where P2Y11 is G α_s -coupled sounds unlikely and complex, and the pharmacological effects become difficult to justify. However, the possibility of P2Y11 being G α_q -coupled and present at the membrane upon VEGF stimulation could explain our results following the described Willoughby et al. system between Orai1 and AC8. The compartmentalization in the lipid rafts of G proteins, Orai channels, and ACs is the basis of the rationale for this hypothesis (Willoughby et al., 2007). Briefly, the mechanisms they described consisted of a reciprocal regulation between Orai1 calcium influx and cAMP production. Upon ER depletion, Orai1 activates and, in turn, facilitates localized calcium influx, activating AC8 localized in the same lipid raft. AC8 will produce cAMP modulating Orai1 inactivation (Sanchez-collado et al., 2020). HMEC-1 cells lack expression of AC8, which portrays a mechanistic gap as another isoform could interact with Orai1 in this fashion. This hypothetical interaction will smoothly explain our results, as **Table 1 and 2 in Chapter 3 (Discussion)** illustrate. The RNA sequencing showed a great expression of AC3, followed by AC6 and AC9. The last was not considered in our hypothesis as it is not calcium-regulated. AC3 activity is calcium-dependent, but its intricate nature and inhibition patterns make it difficult to understand this isoform's roles in calcium-dependent mechanisms and its activation via SOCE (Halls et al., 2011). On the other hand, AC6 is calcium-dependent, but its activity is inhibited in response to calcium

increase and via SOCE. Whether other calcium-sensitive AC can form similar complexes in non-excitabile cells is unclear but sounds plausible given our results and proposed mechanisms. P2Y11's contribution to VEGF₁₆₅ calcium-evoked responses may illustrate a novel mechanism involving AC activity and Orai1 activation to modulate the VEGF primary response. Nonetheless, we know further characterization of this mechanism needs to be performed to confirm our hypothesis. We consider demonstrated P2Y11 protein expression as specific bands were detected significantly higher in HMEC-1 cells than in parental astrocytoma cells. Remarkably, both tested antibodies had difficulty directly detecting the receptor, and diverse blocking solutions testing was required until 5% sucrose-based blocking was determined suitable to investigate P2Y11 protein expression (and P2Y2).

Once we observed the contribution effect of P2Y11 to the VEGF₁₆₅ response, we believed it relevant to investigate if that was conserved in HUVECs, as it is the most characterized primary endothelial cell model, also in terms of VEGF calcium responses. Once the purinergic receptors transcriptional characterisation was performed, VEGF concentration response dependency assays were also completed. However, in this case, the P2Y11 antagonist did not impair the VEGF calcium responses as it did in HMEC-1 cells. There are multiple reasons for the mechanism not to be conserved, the most prominent one being the inconsistency when investigating the transcriptional levels of P2Y11 in HUVECs. Future research is needed to understand if P2Y11 is functionally expressed in HUVEC and, from there, try to understand the lack of P2Y11 involvement in the VEGF responses. HUVECs showed more prominent responses than HMEC-1 with different trace kinetics, indicating possible different contributors to the VEGF-evoked response. On the contrary, ATP responses were more prominent in HMEC-1 cells, with HUVEC responses much more transient than the others. These observations support the different transcriptional patterns observed in both cell lines, which could mean a different P2 contribution to the ATP and VEGF₁₆₅ responses.

In the second part of this thesis (Chapter 4), we explored the functional expression of the Piezo1 channel in HMEC-1 and HUVECs to perform a pharmacological characterisation using the broad-spectrum purinergic antagonist and investigate the possible P2 involvement in the Piezo1 evoked responses. Piezo1 senses the blood flow-induced shear stress in the blood vessels, and its activation leads to ATP release and downstream activation of P2Y2, favouring the activity of the shear stress sensing complex and a sustained nitric oxide production (Tzima et al., 2005; Wang et al., 2015, 2016). The ATP released upon shear stress stimulation could also activate other P2 receptors functionally expressed in the endothelial cells, such as P2X4. P2X4 involvement in shear stress events has also been broadly published (Ando et al., 2013; Sathanoori, Rosi, et al., 2015; Yamamoto, Korenaga, Kamiya, Ando, et al., 2000; Yamamoto, Korenaga, Kamiya, Qi, et al., 2000). However, recent studies failed to demonstrate its participation in endothelial calcium signalling or nitric oxide production (Raqeeb et al., 2011; Wang et al., 2015). P2X4 participation is discarded in HMEC-1 cells, but exploring its possible involvement in HUVECs-induced Piezo1-dependent responses is still interesting. In addition, the effects of the broad-spectrum inhibitors in HMEC-1 were not significant, considering HUVEC cells a much more interesting model to further study purinergic involvement in Piezo1 responses. Given the fact P2X4 is expressed at the protein level in HUVECs (*unpublished data*) and not in HMEC-1 cells, a direct interpretation could be that P2X4 might be active in this cell line. Even though we could not inhibit the ATP response at 30 μ M, more efforts are needed to understand the functional expression or activity of P2X4 in HUVECs. Nonetheless, as previously

reported unspecific effects of PPADS also limit the interpretation of this data and selective antagonist assays should be done to evaluate specific P2 contribution to the Piezo1 response. Furthermore, we wanted to set up a functional parallel flow system to mechanically stimulate both cell types in vitro and study the possible contributions to the shear stress calcium-evoked responses of the P2 receptors in both cell lines in dynamic conditions. The dynamic characterization was challenging even though we tried two different parallel flow chambers and different conditions. The second parallel flow chamber, the Ibidi slide, was the best and technically friendly approach and the success rates started improving thanks to the lack of a vacuum line, its derived pressure, and lower cell seeding times. Although the responsive rates increased, the shear stress evoked response kinetics did not represent a typical Piezo1 response in HUVECs nor HMEC-1 cells, characterized by a rapid initial peak followed by a more or less sustained phase. Taken all data together, we conclude that HUVECs were a better model, as portrayed in more promising responsive success rates. Nonetheless, efforts are still needed to clarify if different culture conditions might be affecting the mechanical stimulation of this cell line. Therefore, we could not perform the dynamic conditions investigation, and this specific goal is still an open study. Similarly, in the tested settings, we failed to demonstrate the Griess reagent capacity to measure nitric oxide release in HMEC-1 cells.

5.2 Future directions.

The research presented in this thesis provides an extensive description of purinergic receptors contribution to the ATP-evoked calcium response in human microvasculature endothelial cells (HMEC-1) and a possible novel mechanism of how P2Y11 contributes to the VEGF-dependent responses in the endothelium. However, this mechanism needs to be validated, potentially involving a knockdown model, to ensure the P2Y11 attribution of the responses. In addition, as two different adenylyl cyclases (AC3/AC6) have been proposed as potential candidates for this mechanism, further efforts should focus on confirming their expression and propose one of them as the mediator of the mechanism. As no selective AC isoform inhibitors exist, a similar strategy with a knockdown model could help investigate their involvement and protein expression characterisation that might involve western blotting and immunofluorescence. The protein expression studies should also involve VEGFR-2, P2Y11, and Orai1, another critical piece of the proposed mechanism. We proposed a $G\alpha_q$ -coupled P2Y11, which is not present in the membrane until VEGF stimulation, following the rationale proposed by Li et al. when studying Orai3's contribution to the VEGF response. Immunofluorescence could be useful to demonstrate that P2Y11 is not at the membrane unless VEGF is involved. Orai1 is proposed to mediate the SOCE calcium influx upon VEGF-P2Y11 calcium release stimulation in HMEC-1. In HUVECs, others have portrayed its role as a significant contributor to the VEGF-evoked calcium influx. As a player in the proposed mechanism, pharmacology characterization of the Orai1 calcium contribution is also considered very relevant. A short-interfering RNA strategy and a pharmacological inhibition using S66, a CRAC selective blocker, will illustrate how this channel contributes to the VEGF response in the microvasculature and if the effects are comparable to those observed in HUVECs. Furthermore, in the absence of Orai1, it would be fascinating to investigate the levels of cAMP as we proposed AC activation dependent on this channel. That will demonstrate the direct dependency of adenylyl cyclases in the CRAC channel, and all together, with the confirmation of P2Y11's presence in the membrane and role in the firing calcium response, it will nicely support the proposed mechanism.

A potential future direction for this project is to determine an endothelial function where this mechanism can impact. Both receptors have been involved in vasodilation and angiogenesis; therefore, efforts could be focused on performing assays to determine their potential involvement. We already showed the preliminary assay trying to measure nitric oxide production using the Griess reagent, an indirect measurement of the nitric oxide based on nitrite accumulation. However, we considered it not sensitive enough and proposed using the improved Griess reagent as an alternative. We also consider using DAF-FM, a nonfluorescent reagent, until it reacts with nitric oxide, forming a fluorescent product (Agrawal et al., 2019; Bevers et al., 2006; Li et al., 2021; Li et al., 2003; Xu et al., 2007) or the two-photon fluorescent molecular probe, DANPY-NO (Arnau del Valle et al., 2022). A modulable nitric oxide release dependent on the mechanism proposed will show the utility of this mechanism to modulate vasodilation in HMEC-1. Furthermore, their role in cell migration and tube formation could portray some involvement in angiogenesis. As Li et al. did before, cell migration assays using Boyden chambers or an analysis of the tube formation using Matrigel in studies involving certain players' knockdown would illustrate the potential role of these proteins in angiogenesis.

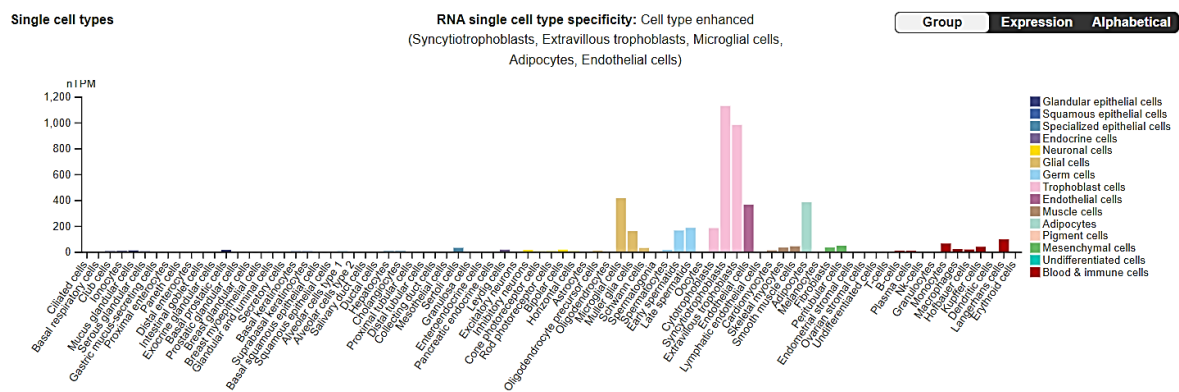
Piezo1 responses in static conditions were affected by purinergic broad-spectrum antagonists in HUVEC cells, while HMEC-1 cells were not. This and the better success rates in shear stress assays make HUVECs a more suitable cell line to study this possible contribution in both static and dynamic conditions. Furthermore, we consider it critical to evolve the HUVEC's pharmacological characterisation in the same way we performed the HMEC-1 cells, as it might help to understand better the shear stress responses and also the lack of translation for the mechanism above between HMEC-1 and HUVECs. Relevantly, P2X4 was demonstrated to be at the protein level in HUVECs. Pursue its expression and function in endothelial cells because the controversial beliefs about the channel would favour general knowledge. Finally, we do not underestimate the value of characterising the shear stress calcium responses in HMEC-1 cells, as this model has not been previously studied. Decoding the shear stress mechanism in another vascular model and its potential purinergic involvement would benefit the human endothelium's functional knowledge.

Appendix.

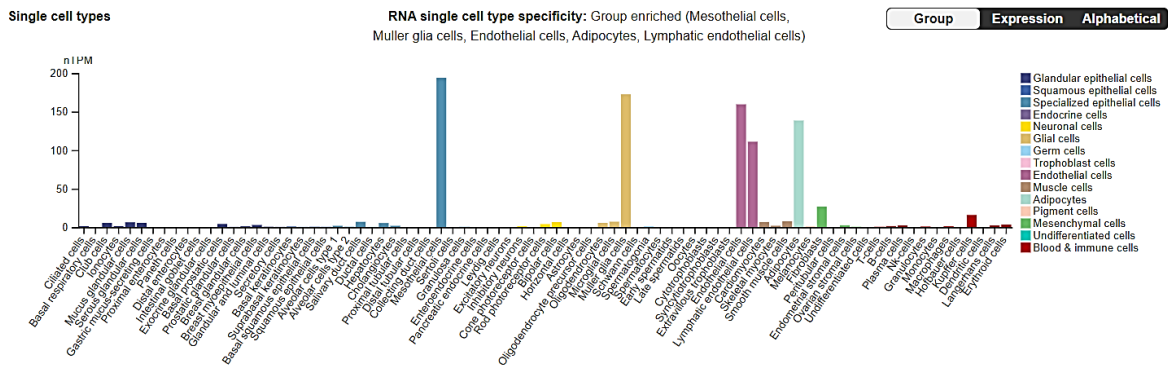
Appendix I. VEGF receptors and ligands expression from The Human Protein Atlas.

A summary of normalised single cell RNA from all single cell types. Colour-coding is based on cell type groups, each consisting of cell types with functional features in common.

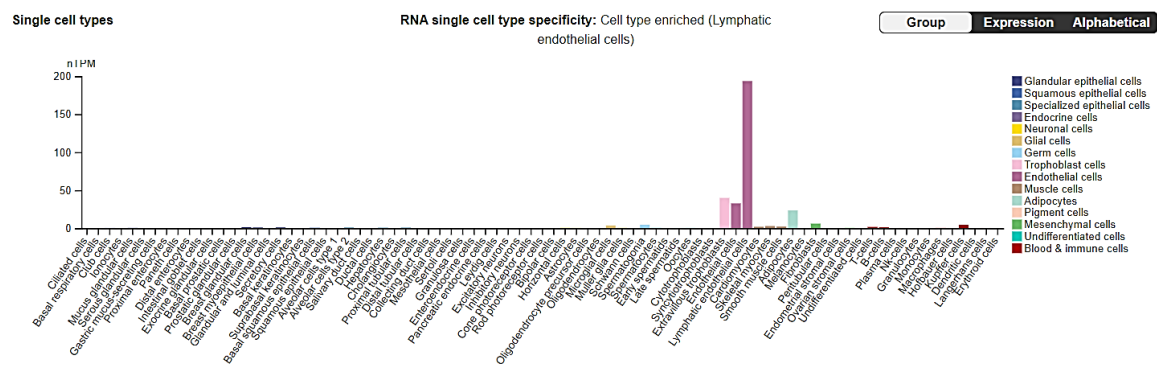
FLT1-VEGFR-1



KDR-VEGFR-2



FLT4-VEGFR-3

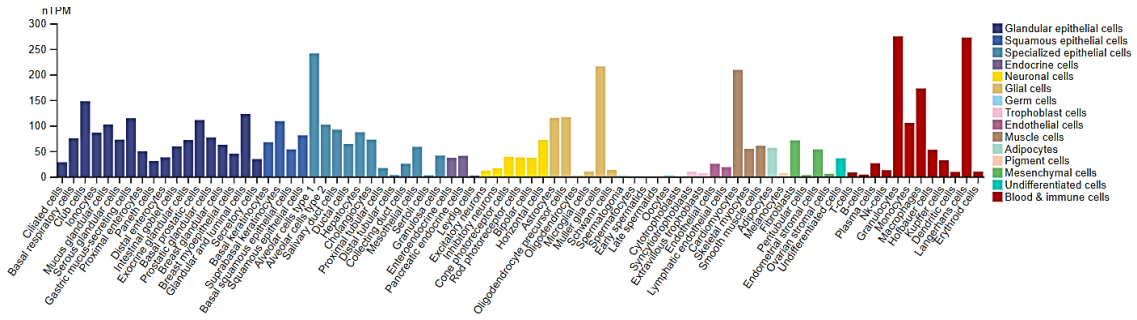


VEGFA

Single cell types

RNA single cell type specificity: Cell type enhanced (Granulocytes, Langerhans cells, Alveolar cells type 1)

Group Expression Alphabetical

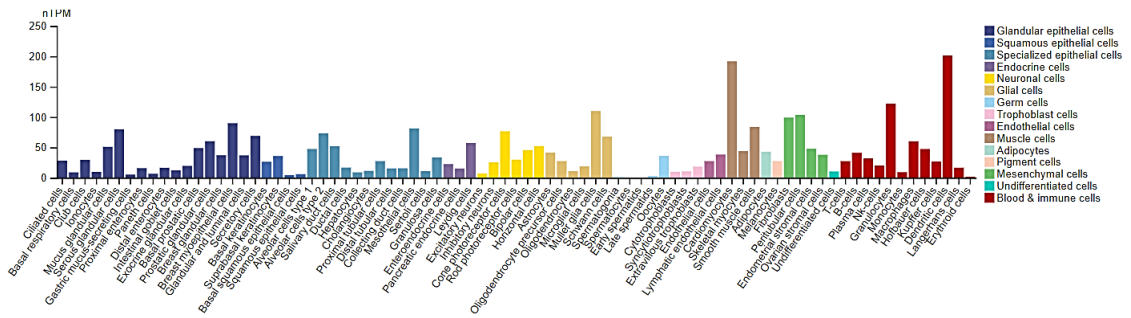


VEGFB

Single cell types

RNA single cell type specificity: Cell type enhanced (Dendritic cells, Cardiomyocytes)

Group Expression Alphabetical

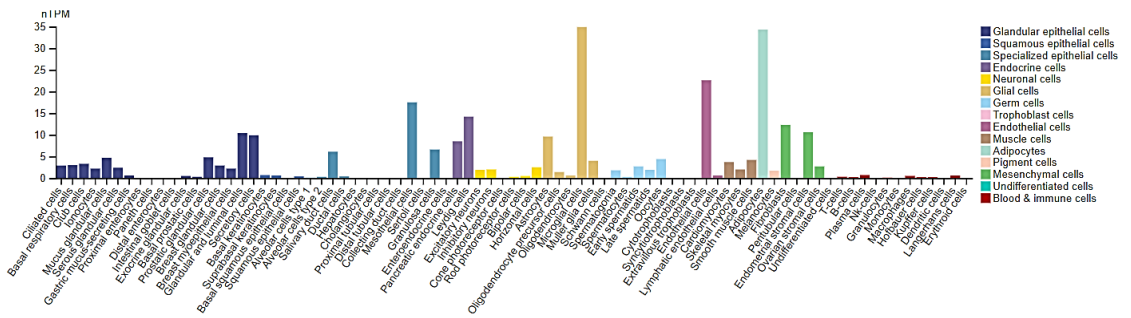


VEGFC

Single cell types

RNA single cell type specificity: Cell type enhanced (Microglial cells, Adipocytes, Endothelial cells, Mesothelial cells, Leydig cells)

Group Expression Alphabetical

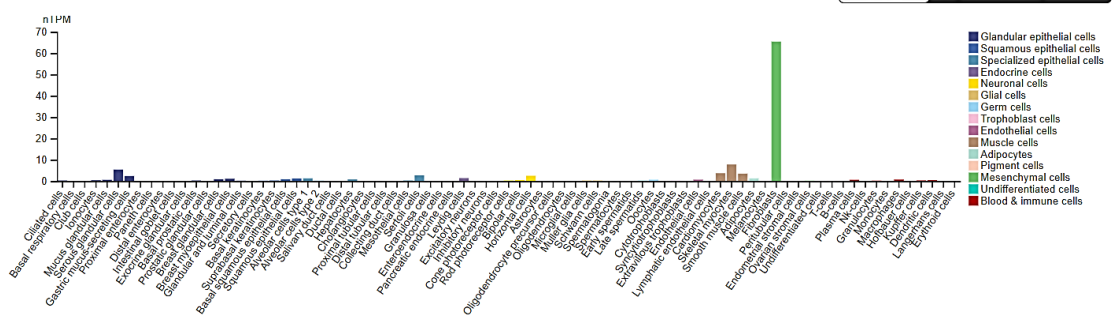


VEGFD

Single cell types

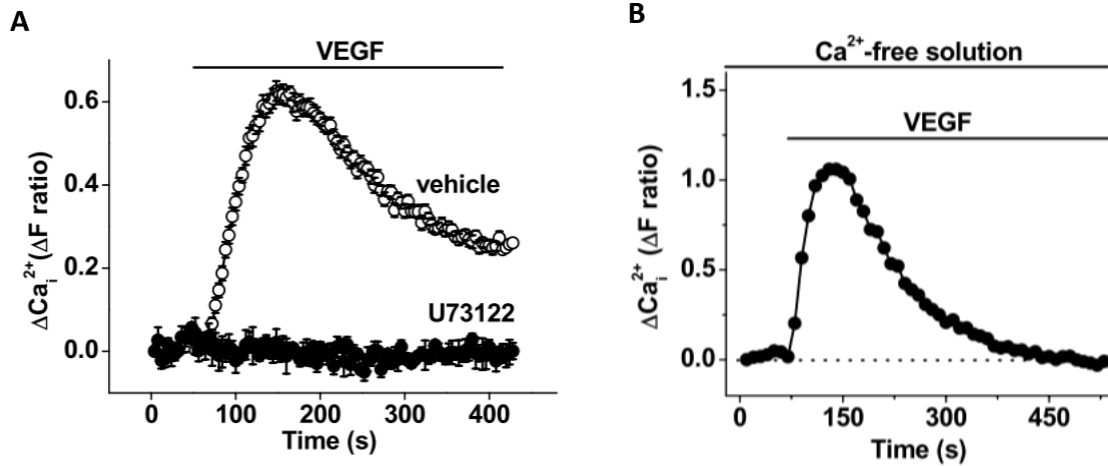
RNA single cell type specificity: Cell type enriched (Fibroblasts)

Group Expression Alphabetical



Appendix II. Li et al., 2011 VEGF₁₆₅ trace kinetics in HUVECs.

A. Example traces showing the VEGF response and the effects U73122 on the VEGF response in the presence of extracellular Ca²⁺ (1.5 mmol/L). B. Example trace showing the VEGF response in the absence of extracellular Ca²⁺.



References.

- Abbracchio, M. P., Burnstock, G., Boeynaems, J.M., Eric, A., Boyer, J. L., Kennedy, C., Knight, G. E., Gachet, C., Jacobson, K. A., Weisman, G. A. (2012). International Union of Pharmacology LVIII: update on the P2Y G protein-coupled nucleotide receptors: from molecular mechanisms and pathophysiology to therapy. In (Vol. 58, pp. 281-341): Pharmacological reviews.
- Agrawal, S., Kumari, R., Luthra, P. M. (2019). A reliable fluorimetric method to screen the nitric oxide synthase inhibitors in 96 well plate. In (Vol. 577, pp. 42-44): Analytical biochemistry.
- Albarrán-Juárez, J., Iring, A., Wang, S., Joseph, S., Grimm, M., Strilic, B., Wettschureck, N., Althoff, T. F., Offermanns, S., & (2018). Piezo1 and Gq/G11 promote endothelial inflammation depending on flow pattern and integrin activation. In (Vol. 215, pp. 2655-2672): Journal of Experimental Medicine.
- Alexander, S. P. H., Christopoulos, A., Davenport, A. P., Kelly, E., Mathie, A., Peters, J. A., Veale, E. L., Armstrong, J. F., Faccenda, E., Harding, S. D., Pawson, A. J., Sharman, J. L., Southan, C., Davies, J. A., Abbracchio, M. P., Alexander, W., Al-hosaini, K., Bäck, M., Beaulieu, J. M. (2019). The concise guide to pharmacology 2019/20: G protein-coupled receptors. In (Vol. 176, pp. S21-S141): British journal of pharmacology.
- Alexander, S. P. H., Mathie, A., Peters, J. A., Veale, E. L., Striessnig, J., Kelly, E., Armstrong, J. F., Faccenda, E., Harding, S. D., Pawson, A. J. (2021). The Concise Guide to pharmacology 2021/22: Ion channels. In (Vol. 178, pp. 157-245): British journal of pharmacology.
- Althaus, M., Bogdan, R., Clauss, W. G., Fronius, M. (2007). Mechano-sensitivity of epithelial sodium channels (ENaCs): laminar shear stress increases ion channel open probability. In (Vol. 21, pp. 2389-2399): The FASEB Journal.
- Ambroz, K. L. H., Zhang, Y., Schutz-Geschwender, A., Olive, D. M. (2008). Blocking and detection chemistries affect antibody performance on reverse phase protein arrays. In (Vol. 8, pp. 2379-2383): Proteomics.
- Ando, J., Yamamoto, K. (2013). Flow detection and calcium signalling in vascular endothelial cells. In (Vol. 99, pp. 260-268): Cardiovascular research.
- Arnau del Valle, C., Williams, L., Thomas, P., Johnson, R., Raveenthiraraj, S., Warren, D., Sobolewski, A., Muñoz, M. P., Galindo, F., Marín, M. J. (2022). A highly photostable and versatile two-photon fluorescent probe for the detection of a wide range of intracellular nitric oxide concentrations in macrophages and endothelial cells. In (Vol. 234): Journal of Photochemistry and Photobiology B: Biology.
- Arniges, M., Vázquez, E., Fernández-Fernández, J. M., Valverde, M. A. (2004). Swelling-activated Ca²⁺ entry via TRPV4 channel is defective in cystic fibrosis airway epithelia. In (Vol. 279, pp. 54062-54068): Journal of Biological Chemistry.
- Ase, A. R., Honson, N. S., Zaghdane, H., Pfeifer, T. A., Séguéla, P. (2015). Identification and characterization of a selective allosteric antagonist of human P2X4 receptor channels. In (Vol. 87, pp. 606-616): American Society for Pharmacology and Experimental Therapy.
- Ashpole, N. E., Overby, D. R., Ethier, C. R., Stamer, W. D. (2014). Shear stress-triggered nitric oxide release from Schlemm's canal cells. In (Vol. 55, pp. 8067-8076): Association for Research in Vision and Ophthalmology.

- Aslam, M., Gündüz, D., Troidl, C., Heger, J., Hamm, C. W., Schulz, R. (2021). Purinergic Regulation of Endothelial Barrier Function. In (Vol. 22): International journal of molecular sciences.
- Avanzato, D., Genova, T., Fiorio Pla, A., Bernardini, M., Bianco, S., Bussolati, B., Mancardi, D., Giraud, E., Maione, F., Cassoni, P. (2016). Activation of P2X7 and P2Y11 purinergic receptors inhibits migration and normalizes tumor-derived endothelial cells via cAMP signaling. In (Vol. 6): Scientific Reports.
- Bae, C., Sachs, F., Gottlieb, P. A. (2011). The mechanosensitive ion channel Piezo1 is inhibited by the peptide GsMTx4. In (Vol. 50, pp. 6295-6300): Biochemistry.
- Banerjee, S., Mwangi, J. G., Stanley, T. K., Mitra, R., Ebong, E. E. (2021). Regeneration and Assessment of the Endothelial Glycocalyx to Address Cardiovascular Disease. In (Vol. 60, pp. 17328-17347): American Chemical Society.
- Barnett, S. D., Asif, H., Buxton, I. L. O. (2023). Novel identification and modulation of the mechanosensitive Piezo1 channel in human myometrium. In (Vol. 601, pp. 1675-1690): The Journal of Physiology.
- Barrs, R. W., Jia, J., Silver, S. E., Yost, M., Mei, Y. (2020). Biomaterials for Bioprinting Microvasculature. In (Vol. 120, pp. 10887-10949: Chemical reviews.
- Bastounis, E. E. (2021). NCBI GEO database. In Sample GSM5319358.
- Bátori, R., Kumar, S., Bordán, Z., Cherian-Shaw, M., Kovács-Kása, A., MacDonald, J. A., Fulton, D. J. R., Erdődi, F., Verin, A. D. (2019). Differential mechanisms of adenosine- and ATPγS-induced microvascular endothelial barrier strengthening. In (Vol. 234, pp. 5863-5879): Journal of cellular physiology.
- Beech, D. J. (2012). Orai1 calcium channels in the vasculature. In (Vol. 463, pp. 635-647): Pflügers Archiv-European Journal of Physiology.
- Beech, D. J. (2018). Endothelial Piezo1 channels as sensors of exercise. In (Vol. 596, pp. 979-984): The Journal of Physiology.
- Belair, D. G., Whisler, J. A., Valdez, J., Velazquez, J., Molenda, J. A., Vickerman, V., Lewis, R., Daigh, C., Hansen, T. D., Mann, D. A. (2015). Human Vascular Tissue Models Formed from Human Induced Pluripotent Stem Cell Derived Endothelial Cells. In (Vol. 11, pp. 511-525): Stem cell reviews and reports.
- Berkels, R., Purol-Schnabel, S., Roesen, R. (2008). Nitric oxide protocols In Hassid (Eds.). In (Vol. 279, pp. 1-9): Springer Science & Business Media.
- Berridge, M. J. (1993). Inositol trisphosphate and calcium signalling. In (Vol. 361, pp. 315-325): Nature.
- Berridge, M. J., Bootman, M. D., Roderick, H. L. (2003). Calcium signalling: dynamics, homeostasis and remodelling. In (Vol. 4, pp. 517-529): Nature reviews Molecular cell biology.
- Berridge, M. J., Lipp, P., Bootman, M. D. (2000). The versatility and universality of calcium signalling. In (Vol. 1, pp. 11-21): Nature reviews Molecular cell biology.
- Bevers, L. M., Braam, B., Post, J. A., van Zonneveld, A. J., Rabelink, T. J., Koomans, H. A., Verhaar, M. C., Joles, J. A. (2006). Tetrahydrobiopterin, but Not L -Arginine, Decreases NO Synthase Uncoupling in Cells Expressing High Levels of Endothelial NO Synthase. In (Vol. 47, pp. 87-94): Hypertension.
- Bianchi, B. R., Lynch, K. J., Touma, E., Niforatos, W., Burgard, E. C., Alexander, K. M., Park, H. S., Yu, H., Metzger, R., Kowaluk, E. (1999). Pharmacological characterization of recombinant human and rat P2X receptor subtypes. In (Vol. 376, pp. 1999-1127): European Journal of Pharmacology.

- Bidula, S., Nadzirin, I. B., Cominetti, M., Hickey, H., Cullum, S. A., Searcey, M., Schmid, R., Fountain, S. J. (2022). Structural Basis of the Negative Allosteric Modulation of 5-BDBD at Human P2X4 Receptors. In (Vol. 101, pp. 33-44): *Molecular Pharmacology*.
- Blackburn, M. R., Vance, C. O., Morschl, E., Wilson, C. N. (2009). Adenosine Receptors and Inflammation. In (pp. 215-269): *Adenosine receptors in health and disease*.
- Bleasdale, J. E., Fisher, S. K. (1993). Use of U-73122 as an Inhibitor of Phospholipase C-Dependent Processes. In (Vol. 3(2), 125-133) : *Neuroprotocols*.
- Bles, N., Horckmans, M., Lefort, A., Libert, Macours, P., El Housni, H., Marteau, Boeynaems, J. M., Communi, D. (2007). Gene Expression Profiling Defines ATP as a Key Regulator of Human Dendritic Cell Functions. In (Vol. 179, pp. 3550-3558): *The Journal of Immunology*.
- Bo, X., Jiang, L.-H., Wilson, H. L., Kim, M., Burnstock, G., Surprenant, A., North, R. A. (2003). Pharmacological and Biophysical Properties of the Human P2X 5 Receptor. In (Vol. 63, pp. 1407-1416): *Molecular Pharmacology*.
- Bo, X., Kim, M., Nori, S. L., Schoepfer, R., Burnstock, G., North, R. A. (2003). Tissue distribution of P2X4 receptors studied with an ectodomain antibody. In (Vol. 313, pp. 159-165): *Cell and Tissue Research*.
- Bodin, P., Bailey, D., Burnstock, G.(1991). Increased flow-induced ATP release from isolated vascular endothelial cells but not smooth muscle cells. In (Vol. 103, pp. 1203-1205): *British Journal of Pharmacology*.
- Bodnar, R. J., Yates, C. C., Wells, A. (2006). IP-10 blocks vascular endothelial growth factor-induced endothelial cell motility and tube formation via inhibition of calpain. In (Vol. 98, pp. 617-625): *Circulation Research*.
- Bootman, M. D., Bultynck, G. (2020). Fundamentals of cellular calcium signaling: A primer. In (Vol. 12): *Cold Spring Harbor Perspectives in Biology*.
- Bootman, M. D., Collins, T. J., Peppiatt, C. M., Prothero, L. S., MacKenzie, L., De Smet, P., Travers, M., Tovey, S. C., Seo, J. T., Berridge, M. J., Ciccolini, F., Lipp, P. (2001). Calcium signalling - An overview. In (Vol. 12, pp. 3-10): *Seminars in Cell and Developmental Biology*.
- Botello-Smith, W. M., Jiang, W., Zhang, H., Ozkan, A. D., Lin, Y. C., Pham, C. N., Lacroix, J. J., Luo, Y. (2019). A mechanism for the activation of the mechanosensitive Piezo1 channel by the small molecule Yoda1. In (Vol. 10): *Nature Communications*.
- Bouđè, D., Hospers, G. A. P., Meijer, C., Molema, G., Mulder, N. H. (2001). Endothelium in vitro: A review of human vascular endothelial cell lines for blood vessel-related research. In (vol. 4, pp. 91-102): *Angiogenesis*.
- Bowman, C. L., Gottlieb, P. A., Suchyna, T. M., Murphy, Y. K., Sachs, F. (2007). Mechanosensitive Ion Channels and the Peptide Inhibitor GsMTx-4: History, Properties, Mechanisms and Pharmacology. In (Vol. 49(2), pp. 249-270): *Toxicon*.
- Bradford, M. M. (1976). A Rapid and Sensitive Method for the Quantitation of Microgram Quantities of Protein Utilizing the Principle of Protein-Dye Binding. In (Vol. 72, pp. 248-254): *Analytical biochemistry*.
- Bredt, D. S., Snyder, S. H. (1994). Nitric oxide: A Physiologic Messenger Molecule. In (Vol. 63(1), pp. 175-195): *Annual review of biochemistry*.
- Brini, M., Carafoli, E. (2011). The Plasma Membrane Ca²⁺ ATPase and the Plasma Membrane Sodium Calcium Exchanger Cooperate in the Regulation of Cell Calcium. In (Vol. 3, pp. a004168-a004168): *Cold Spring Harbor Perspectives in Biology*.

- Brown, D. C., Larson, R. S. (2001). Improvements to parallel plate flow chambers to reduce reagent and cellular requirements. In (Vol. 2, pp. 1-7): BMC immunology.
- Burnstock, G. (1977). The purinergic nerve hypothesis. In (pp. 295-314): Purine and Pyrimidine Metabolism.
- Burnstock, G. (2006). Purinergic signalling. In (Vol. 147(S1), pp. S172-S181): British journal of pharmacology.
- Burnstock, G. (2007). Purine and pyrimidine receptors. In (Vol. 64, pp. 1471-1483): Cellular and molecular life sciences.
- Burnstock, G. (2014). Purinergic signalling: From discovery to current developments. In (Vol. 99, pp. 16-34): Experimental physiology.
- Burnstock, G., Kennedy, C. (2011). P2X Receptors in Health and Disease. In (pp. 333-372): Advances in pharmacology.
- Burnstock, G., Ralevic, V. (2014). Purinergic signaling and blood vessels in health and disease. In (Vol. 66, pp. 102-192): Pharmacological Reviews.
- Butler, C. T., Reynolds, A. L., Tosetto, M., Dillon, E. T., Guiry, P. J., Cagney, G., O'Sullivan, J., Kennedy, B. N. (2017). A quininib analogue and cysteinyl leukotriene receptor antagonist inhibits vascular endothelial growth factor (VEGF)-independent angiogenesis and exerts an additive antiangiogenic response with bevacizumab. In (Vol. 292, pp. 3552-3567): Journal of Biological Chemistry.
- Byzova, T. V., Goldman, C. K., Pampori, N., Thomas, K. A., Bett, A., Shattil, S. J., Plow, E. F. (2000). A Mechanism for Modulation of Cellular Responses to VEGF. In (Vol. 6, pp. 851-860): Molecular Cell.
- Cabou, C., & Martinez, L. O. (2022). Purinergic P2Y receptors in endothelium: from vascular physiology to pathology, a review based on recent advances. In Preprints.
- Cao, J., Cetrulo, C. L., Theoharides, T. C. (2006). Corticotropin-releasing hormone induces vascular endothelial growth factor release from human mast cells via the cAMP/protein kinase A/p38 mitogen-activated protein kinase pathway. In (Vol. 69, pp. 998-1006): Molecular Pharmacology.
- Caolo, V., Debant, M., Endesh, N., Futers, T. S., Lichtenstein, L., Bartoli, F., Parsonage, G., Jones, E. A., Beech, D. J. (2020). Shear stress activates ADAM10 sheddase to regulate Notch1 via the Piezo1 force sensor in endothelial cells. In (Vol. 9): ELife.
- Cárdenas, A., Toledo, C., Oyarzún, C., Sepúlveda, A., Quezada, C., Guillén-Gómez, E., Díaz-Encarnación, M. M., Pastor-Anglada, M., San Martín, R. (2013). Adenosine A2B receptor-mediated VEGF induction promotes diabetic glomerulopathy. In (Vol. 93, pp. 135-144): Laboratory Investigation.
- Carrillo-Garcia, J., Herrera-Fernández, V., Serra, S. A., Rubio-Moscardo, F., Vogel-Gonzalez, M., Doñate-Macian, P., Hevia, C. F., Pujades, C., Valverde, M. A. (2021). The mechanosensitive Piezo1 channel controls endosome trafficking for an efficient cytokinetic abscission. In (Vol. 7, pp. 7785-7814): Sci. Adv.
- Cerezo, A., Hornedo-Ortega, R., Álvarez-Fernández, M., Troncoso, A., García-Parrilla, M., (2017). Inhibition of VEGF-Induced VEGFR-2 Activation and HUVEC Migration by Melatonin and Other Bioactive Indolic Compounds. In (Vol. 9, pp. 249): Nutrients.
- Chadet, S., Ivanes, F., Benoist, L., Salmon-Gandonnière, C., Guibon, R., Velge-Roussel, F., Babuty, D., Baron, C., Roger, S., Angoulvant, D. (2015). Hypoxia/Reoxygenation Inhibits P2Y11 Receptor Expression and Its Immunosuppressive Activity in Human Dendritic Cells. In (Vol. 195, pp. 651-660): The Journal of Immunology.

- Charlton, S. J., Brown, C. A., Weisman, G. A., Turner, J. T., Erb, L., Boarder, M. R. (1996a). Cloned and transfected P2Y4 receptors: Characterization of a suramin and PPADS-insensitive response to UTP. In (Vol. 119, pp. 1301-1303): British Journal of Pharmacology.
- Charlton, S. J., Brown, C. A., Weisman, G. A., Turner, J. T., Erb, L., Boarder, M. R. (1996b). PPADS and suramin as antagonists at cloned P2Y- and P2U-purinoceptors. In (Vol. 118, pp. 704-710): British Journal of Pharmacology.
- Chen, H., Cong, Q., Du, Z., Liao, W., Zhang, L., Yao, Y., Ding, K. (2016). Sulfated fucoidan FP08S2 inhibits lung cancer cell growth in vivo by disrupting angiogenesis via targeting VEGFR2/VEGF and blocking VEGFR2/Erk/VEGF signaling. In (Vol. 382, pp. 44-52): Cancer Letters.
- Cheng, C. P., Herfkens, R. J., Taylor, C. A. (2003). Comparison of abdominal aortic hemodynamics between men and women at rest and during lower limb exercise. In (Vol. 37, pp. 118-123): Journal of Vascular Surgery.
- Chessell, I. P., Michel, A. D., Humphrey, P. P. A. (1998). Effects of antagonists at the human recombinant P2X7 receptor. In (Vol. 124, pp. 1314-1320): British Journal of Pharmacology.
- Chhatriwala, M., Ravi, R. G., Patel, R. I., Boyer, J. L., Jacobson, K. A., Harden, T. K. (2004). Induction of novel agonist selectivity for the ADP-activated P2Y 1 receptor versus the ADP-activated P2Y12 and P2Y 13 receptors by conformational constraint of an ADP analog. In (Vol. 311, pp. 1038-1043): Journal of Pharmacology and Experimental Therapeutics.
- Chistiakov, D. A., Orekhov, A. N., Bobryshev, Y. V. (2017). Effects of shear stress on endothelial cells: go with the flow. In (Vol. 219, pp. 382-408): Acta Physiologica.
- Chiu, J.-J., Chien, S. (2011). Effects of Disturbed Flow on Vascular Endothelium: Pathophysiological Basis and Clinical Perspectives. In (Vol. 91, pp. 327-387): Physiological Reviews.
- Choi, E. J., Xia, Z., Storm, D. R. (1992). Stimulation of the type III olfactory adenylyl cyclase by calcium and calmodulin. In (Vol. 31(28), pp. 6492-6498): Biochemistry.
- Chomczynski, P., Sacchi, N. (1987). Single-Step Method of RNA Isolation by Acid Guanidinium Thiocyanate-Phenol-Chloroform Extraction. In (Vol. 162, pp. 156-159): Analytical biochemistry.
- Coddou, C., Yan, Z., Obsil, T., Pablo Huidobro-Toro, J., Stojilkovic, S. S. (2011). Activation and regulation of purinergic P2X receptor channels. In (Vol. 63, pp. 641-683): Pharmacological Reviews.
- Cohen, M. V., Yang, X., Downey, J. M. (2010). A2b adenosine receptors can change their spots. In (Vol. 159, pp. 1595-1597): British Journal of Pharmacology.
- Communi, D., Govaerts, C., Parmentier, M., Boeynaems, J. M. (1997). Cloning of a human purinergic P2Y receptor coupled to phospholipase C and adenylyl cyclase. In (Vol. 272, pp. 31969-31973): Journal of Biological Chemistry.
- Communi, D., Robaye, B., Boeynaems, J. M. (1999). Pharmacological characterization of the human P2Y11 receptor. In (Vol. 128, pp. 1199-1206): British Journal of Pharmacology.
- Communi, D., Motte, S., Boeynaems, J.-M., Pirotton, S. (1996). Pharmacological characterization of the human P2Y4 receptor. In (Vol. 317, pp. 383-389): European Journal of Pharmacology.
- Communi, D., Parmentier, M., Boeynaems, J.-M. (1996). Cloning, Functional Expression and Tissue Distribution of the Human P2Y6 Receptor 1. In (Vol. 222, pp. 303-308): Biochemical and biophysical research communications.

- Cook, S. P., McCleskey, E. W. (2002). Cell damage excites nociceptors through release of cytosolic ATP. In (Vol. 95, pp. 41-47): Pain.
- Cooper, D. M. F. (2015). Cell Calcium Store-operated Ca²⁺-entry and adenylyl cyclase. In (Vol. 58, pp. 368-375): Cell Calcium.
- Cooper, D. M. F., Tabbasum, V. G., & (2014). Adenylate cyclase-centred microdomains. In (Vol. 462, pp. 199-213): Biochemical Journal.
- Cortés, M. P., Becerra, J. P., Vinet, R., Álvarez, R., Quintana, I. (2013). Inhibition of ATP-induced calcium influx by homocysteine in human umbilical vein endothelial cells. In (Vol. 37, pp. 600-607): Cell Biology International.
- Coste, B., Mathur, J., Schmidt, M., Earley, T. J., Ranade, S., Petrus, M. J., Dubin, A. E., Patapoutian, A. (2010). Piezo1 and Piezo2 Are Essential Components of Distinct Mechanically Activated Cation Channels. In (Vol. 330 (6000), pp. 55-60): Science.
- Cudmore, M. J., Hewett, P. W., Ahmad, S., Wang, K. Q., Cai, M., Al-Ani, B., Fujisawa, T., Ma, B., Sissaoui, S., Ramma, W. (2012). The role of heterodimerization between VEGFR-1 and VEGFR-2 in the regulation of endothelial cell homeostasis. In (Vol. 3): Nature Communications.
- Cyr, A. R., Huckaby, L. V., Shiva, S. S., Zuckerbraun, B. S. (2020). Nitric Oxide and Endothelial Dysfunction. In (Vol. 36, pp. 307-321): Critical Care Clinics.
- da Silva, C. G. a., Specht, A., Wegiel, B., Ferran, C., Kaczmarek, E. (2009). Mechanism of Purinergic Activation of Endothelial Nitric Oxide Synthase in Endothelial Cells. In (Vol. 119, pp. 871-879): Circulation.
- Dal Ben, D., Buccioni, M., Lambertucci, C., Marucci, G., Thomas, A., Volpini, R. (2015). Purinergic P2X receptors: Structural models and analysis of ligand-target interaction. In (Vol. 89, pp. 561-580): European Journal of Medicinal Chemistry.
- Dalal, P. J., Muller, W. A., Sullivan, D. P. (2020). Endothelial Cell Calcium Signaling during Barrier Function and Inflammation. In (Vol. 190, pp. 535-542): American Journal of Pathology.
- Daniel, H., Rancillac, A., Crepel, F. (2004). Mechanisms underlying cannabinoid inhibition of presynaptic Ca²⁺ influx at parallel fibre synapses of the rat cerebellum. In (Vol. 557, pp. 159-174): Journal of Physiology.
- Dănilă, M.-D., Piollet, M., Aburel, O.-M., Angoulvant, D., Lefort, C., Chadet, S., Roger, S., Muntean, M.-D., Ivanes, F. (2020). Modulation of P2Y₁₁-related purinergic signaling in inflammation and cardio-metabolic diseases. In (Vol. 876, pp. 173060): European Journal of Pharmacology.
- Davies, J. E., Lopresto, D., Apta, B. H. R., Lin, Z., Ma, W., Harper, M. T. (2019). Using Yoda-1 to mimic laminar flow in vitro: A tool to simplify drug testing. In (Vol. 168, pp. 473-480): Biochemical Pharmacology.
- Davies, P. F. (2009). Hemodynamic shear stress and the endothelium in cardiovascular pathophysiology. In (Vol. 6, pp. 16-26): Nature Clinical Practice Cardiovascular Medicine.
- Dawson, V. L., Dawson, T. M. (1996). Nitric oxide actions in neurochemistry. In (Vol. 29, pp. 97-110): Neurochemistry international.
- de Vries, C., Escobedo, J. A., Ueno, H., Houck, K., Ferrara, N., Williams, L. T. (1992). The fms-Like Tyrosine Kinase, a Receptor for Vascular Endothelial Growth Factor. In (Vol. 255, pp. 989-991): Science.
- Dedkova, E. N., Sigova, A. A., Zinchenko, V. P. (2000). Mechanism of action of calcium ionophores on intact cells: Ionophore-resistant cells. In (Vol. 13(3), pp. 357-368): Membr cell biol.

- Deguchi, H., Takeya, H., Urano, H., Gabazza, E. C., Zhou, H., Suzuki, K. (1998). Adenosine Regulates Tissue Factor Expression on Endothelial Cells. In (Vol. 91, pp. 57-64): *Thrombosis Research*.
- Deivasikamani, V., Dhayalan, S., Abudushalamu, Y., Mughal, R., Visnagri, A., Cuthbertson, K., Scragg, J. L., Munsey, T. S., Viswambharan, H., Muraki, K. (2019). Piezo1 channel activation mimics high glucose as a stimulator of insulin release. In (Vol. 9, pp. 16876): *Scientific Reports*.
- del Carmen Gonzalez-Montelongo, M., Meades, J. L., Fortuny-Gomez, A., Fountain, S. J. (2023). Neuropeptide Y: Direct vasoconstrictor and facilitatory effects on P2X1 receptor-dependent vasoconstriction in human small abdominal arteries. In (Vol. 151, pp. 107192): *Vascular Pharmacology*.
- Del Carratore, R., Carpi, A., Befy, P., Lubrano, V., Giorgetti, L., Maserti, B. E., Carluccio, M. A., Simili, M., Iervasi, G., Balzan, S. (2012). Itraconazole inhibits HMEC-1 angiogenesis. In (Vol. 66, pp. 312-317): *Biomedicine and Pharmacotherapy*.
- Delaune, K., Alsayouri, K. (2023). Physiology, Noncompetitive Inhibitor. In Europe PMC.
- Deng, Y., Zhang, X., Simons, M. (2015). Molecular controls of lymphatic VEGFR3 signaling. In (Vol. 35, pp. 421-429): *Arteriosclerosis, Thrombosis, and Vascular Biology*.
- Denhollander, N., Befus, D. (1989). Loss of antigens from immunoblotting membranes. In (Vol. 122, pp. 129-135): *Journal of Immunological Methods*.
- Desplat, A., Penalba, V., Gros, E., Parpaite, T., Coste, B., Delmas, P., Parpaite, T., Coste, B., Delmas, P. (2021). Piezo1-Pannexin1 complex couples force detection to ATP secretion in cholangiocytes. In (Vol. 153): *Journal of General Physiology*.
- Ding, Y., Gao, Z. G., Jacobson, K. A., Suffredini, A. F. (2010). Dexamethasone enhances ATP-induced inflammatory responses in endothelial cells. In (Vol. 335, pp. 693-702): *Journal of Pharmacology and Experimental Therapeutics*.
- Doktor, F., Prager, P., Wiedemann, P., Kohen, L., Bringmann, A., Hollborn, M. (2018). Hypoxic expression of NLRP3 and VEGF in cultured retinal pigment epithelial cells: contribution of P2Y 2 receptor signaling. In (Vol. 14, pp. 471-484): *Purinergic Signalling*.
- Dombroski, J. A., Hope, J. M., Sarna, N. S., King, M. R. (2021). Channeling the force: Piezo1 mechanotransduction in cancer metastasis. In (Vol. 10): MDPI.
- Drury, A. N., Szent-Györgyi, A. (1929). The physiological activity of adenine compounds with especial reference to their action upon the mammalian heart¹. In (Vol. 68, pp. 213-237): *The Journal of Physiology*.
- Du, X., Ou, X., Song, T., Zhang, W., Cong, F., Zhang, S., Xiong, Y. (2015). Adenosine A2B receptor stimulates angiogenesis by inducing VEGF and eNOS in human microvascular endothelial cells. In (Vol. 240, pp. 1472-1479): *Experimental Biology and Medicine*.
- Dubrow, A., Zuniga, B., Topo, E., Cho, J. H. (2022). Suppressing Nonspecific Binding in Biolayer Interferometry Experiments for Weak Ligand-Analyte Interactions. In (Vol. 7, pp. 9206-9211): *ACS omega*.
- Dulak, J., Józkwicz, A. (2003). Regulation of Vascular Endothelial Growth Factor Synthesis by Nitric Oxide: Facts and Controversies. In (Vol. 5, pp. 123-132): *Antioxidants & Redox Signaling*.
- Effendi, W. I., Nagano, T., Kobayashi, K., Nishimura, Y. (2020). Focusing on Adenosine Receptors as a Potential Targeted Therapy in Human Diseases. In (Vol. 9): *NLM (Medline)*.
- Emery, A. C., Eiden, M. V., Eiden, L. E. (2013). A new site and mechanism of action for the widely used adenylate cyclase inhibitor SQ22,536. In (Vol. 83, pp. 95-105): *Molecular Pharmacology*.

- Emmelin, N., FELDBERG, W. (1948). Systemic effects of adenosine triphosphate. In (Vol. 3, pp. 273-284): British Journal of Pharmacology and Chemotherapy.
- Erb, L., Liao, Z., Seye, C. I., Weisman, G. A. (2006). P2 receptors: Intracellular signaling. In (Vol. 452, pp. 552-562): Pflugers Archiv European Journal of Physiology.
- Erb, L., Weisman, G. A. (2012). Coupling of P2Y receptors to G proteins and other signaling pathways. In (Vol. 1, pp. 789-803): Wiley Interdisciplinary Reviews: Membrane Transport and Signaling.
- Evans, E. L., Cuthbertson, K., Endesh, N., Rode, B., Blythe, N. M., Hyman, A. J., Hall, S. J., Gaunt, H. J., Ludlow, M. J., Foster, R. (2018). Yoda1 analogue (Dooku1) which antagonizes Yoda1-evoked activation of Piezo1 and aortic relaxation. In (Vol. 175, pp. 1744-1759): British Journal of Pharmacology.
- Faucherre, A., Kissa, K., Nargeot, J., Mangoni, M. E., Jopling, C. (2014). Piezo1 plays a role in erythrocyte volume homeostasis. In (Vol. 99, pp. 70-75): Haematologica.
- Favot, L., Keravis, T., Holl, V., Bec, A. L., Lugnier, C. (2003). VEGF-induced HUVEC migration and proliferation are decreased by PDE2 and PDE4 inhibitors. In (Vol. 90, pp. 334-343): thrombosis and Haemostasis.
- Féléto, M. (2011). The endothelium, Part I: Multiple functions of the endothelial cells--focus on endothelium-derived vasoactive mediators. In Google Books.
- Feoktistov, I., Goldstein, A. E., Ryzhov, S., Zeng, D., Belardinelli, L., Voyno-Yasenetskaya, T., Biaggioni, I. (2002). Differential expression of adenosine receptors in human endothelial cells: Role of A2B receptors in angiogenic factor regulation. In (Vol. 90, pp. 531-538): Circulation Research.
- Feoktistov, I., Ryzhov, S., Zhong, H., Goldstein, A. E., Matafonov, A., Zeng, D., Biaggioni, I. (2004). Hypoxia modulates adenosine receptors in human endothelial and smooth muscle cells toward an A2B angiogenic phenotype. In (Vol. 44, pp. 649-654): Hypertension.
- Fernandez, P., Jara, C., Aguilera, V., Caviedes, L., Diaz, F., Radojkovic, C., Veas, C., Lamperti, L., Escudero, C., Aguayo, C. (2012). Adenosine A2A and A3 Receptors Are Involved in the Human Endothelial Progenitor Cells Migration. In (Vol. 59(5), pp. 397-404): Journal of cardiovascular pharmacology.
- Filippini, A., D'Amore, A., D'Alessio, A. (2019). Calcium mobilization in endothelial cell functions. In (Vol. 20): International Journal of Molecular Sciences.
- Folkman, J. (1989). What Is the Evidence That Tumors Are Angiogenesis Dependent? In (Vol. 82(1), p. 4-7): Journal of the National Cancer Institute.
- Foufelle, F., Fromenty, B. (2016). Role of endoplasmic reticulum stress in drug-induced toxicity. In (Vol. 4): Pharmacology Research and Perspectives.
- Franklin, K. M., Asatryan, L., Jakowec, M. W., Trudell, J. R., Bell, R. L., Davies, D. L. (2014). P2X4 receptors (P2X4Rs) represent a novel target for the development of drugs to prevent and/or treat alcohol use disorders. In (Vol. 8): Frontiers in Neuroscience.
- Fruscione, F., Scarfi, S., Ferraris, C., Bruzzone, S., Benvenuto, F., Guida, L., Uccelli, A., Salis, A., Usai, C., Jacchetti, E. (2011). Regulation of human mesenchymal stem cell functions by an autocrine loop involving NAD⁺ release and P2Y11-mediated signaling. In (Vol. 20, pp. 1183-1198): Stem Cells and Development.
- Fu, L., Kim, H. N., Sterling, J. D., Baker, S. M., Lord, M. S. (2022). The role of the cell surface glycocalyx in drug delivery to and through the endothelium. In (Vol. 184): Advanced Drug Delivery Reviews.

- Gallagher, S. R. (2012). One-dimensional SDS gel electrophoresis of proteins. In (Vol. 75(1), pp. 8.4. 1-8.4. 37): Current protocols in immunology.
- Gao, C., Yu, Q., Xu, H., Zhang, L., Liu, J., Jie, Y., Ma, W., Samways, D. S. K., Li, Z. (2015). Roles of the lateral fenestration residues of the P2X4 receptor that contribute to the channel function and the deactivation effect of ivermectin. In (Vol. 11, pp. 229-238): Purinergic Signalling.
- Gao, Z. G., Inoue, A., Jacobson, K. A. (2018). On the G protein-coupling selectivity of the native A2B adenosine receptor. In (Vol. 151, pp. 201-213): Biochemical Pharmacology.
- Ge, J., Li, W., Zhao, Q., Li, N., Chen, M., Zhi, P., Li, R., Gao, N., Xiao, B., Yang, M. (2015). Architecture of the mammalian mechanosensitive Piezo1 channel. In (Vol. 527, pp. 64-69): Nature.
- Gendron, F.-P. Neary, J. T., Theiss, P. M., Sun, G. Y., Gonzalez, F. A., Weisman, G. A. (2003). Mechanisms of P2X7 receptor-mediated ERK1/2 phosphorylation in human astrocytoma cells. In (Vol. 284, no 2, pp. C571-C581): American Journal of Physiology-Cell Physiology.
- Genova, T., Gaglioti, D., Munaron, L. (2020). Regulation of Vessel Permeability by TRP Channels. In (Vol. 11): Frontiers in Physiology.
- George, B., Swartz, K. J., Li, M. (2019). Hearing loss mutations alter the functional properties of human P2X2 receptor channels through distinct mechanisms. In (Vol. 116, pp. 22862-22871): Proceedings of the National Academy of Sciences of the United States of America.
- Gerhold, K. A., Schwartz, M. A. (2016). Ion channels in endothelial responses to fluid shear stress. In (Vol. 31, pp. 359-369): Physiology.
- Gerrie, H. (2018). Characterization of the mechanosensitive cation channel piezo1 in microglia. In Doctoral dissertation, University of British Columbia.
- Gidlöf, O., Sathanoori, R., Magistri, M., Faghihi, M. A., Wahlestedt, C., Olde, B., Erlinge, D. (2015). Extracellular Uridine Triphosphate and Adenosine Triphosphate Attenuate Endothelial Inflammation through miR-22-Mediated ICAM-1 Inhibition. In (Vol. 52, pp. 71-80): Journal of Vascular Research.
- Glass, R., Loesch, A., Bodin, P., Burnstock, G. (2002). P2X4 and P2X6 receptors associate with VE-cadherin in human endothelial cells. In (Vol. 59, pp. 870-881): Cellular and Molecular Life Sciences.
- GmbH, Ibidi (2022). Application Note 11: Shear Stress and Shear Rates for ibidi μ -Slides Based on Numerical Calculations. In Ibidi.
- Goedicke-Fritz, S., Kaistha, A., Kacik, M., Markert, S., Hofmeister, A., Busch, C., Bänfer, S., Jacob, R., Grgic, I., Hoyer, J. (2015). Evidence for functional and dynamic microcompartmentation of Cav-1/TRPV4/KCa in caveolae of endothelial cells. In (Vol. 94, pp. 391-400): European Journal of Cell Biology.
- Green, L. C., Wagner, D. A., Glogowski, J., Skipper, P. L., Wishnok, J. S., Tannenbaum, S. R. (1982). Analysis of nitrate, nitrite, and [15N]nitrate in biological fluids. In (Vol. 126, pp. 131-138): Analytical Biochemistry.
- Gruenbacher, G., Gander, H., Rahm, A., Dobler, G., Drasche, A., Troppmair, J., Nussbaumer, W., Thurnher, M. (2019). The human G protein-coupled ATP receptor P2Y11 is associated with IL-10 driven macrophage differentiation. In (Vol. 10): Frontiers in Immunology.
- Grynkiewicz, G., Poenie, M., Tsien, R. Y. (1985). A new generation of Ca²⁺ indicators with greatly improved fluorescence properties. In (Vol. 260, pp. 3440-3450): Journal of Biological Chemistry.

- Habermacher, C., Dunning, K., Chataigneau, T., Grutter, T. (2016). Molecular structure and function of P2X receptors. In (Vol. 104, pp. 18-30): Neuropharmacology.
- Hajnóczky, G., Davies, E., Madesh, M. (2003). Calcium signaling and apoptosis. In (Vol. 304, pp. 445-454): Biochemical and Biophysical Research Communications.
- Halls, M. L., Cooper, D. M. F. (2011). Regulation by Ca²⁺-signaling pathways of adenylyl cyclases. In (Vol. 3, pp. 1-22): Cold Spring Harbor Perspectives in Biology.
- Hamdollah Zadeh, M. A., Glass, C., Magnussen, A., Hancox, J., Bates, D. (2008). VEGF-Mediated elevated intracellular calcium and angiogenesis in human microvascular endothelial cells In vitro are inhibited by dominant negative TRPC6. In (Vol. 15, pp. 605-614): Microcirculation.
- Han, X. (2022). Inhibiting P2Y12 receptor relieves LPS-induced inflammation and endothelial dysfunction. In (Vol. 10): Immunity, Inflammation and Disease.
- Harris, D. N., , Asaad, M. M., , Phillips, M. B., , Goldenberg, H. J., , Antonaccio, M. J., & (1979). Inhibition of adenylyl cyclase in human blood platelets by 9-substituted adenine derivatives. In (Vol. 5, pp. 125-134): Journal of Cyclic Nucleotide Research.
- Hatem, A., Poussereau, G., Gachenot, M., Pérès, L., Bouyer, G., Egée, S. (2023). Dual action of Dooku1 on PIEZO1 channel in human red blood cells. In (Vol. 14): Frontiers in Physiology.
- He, J., Zhou, Y., Arredondo Carrera, H. M., Sprules, A., Neagu, R., Zarkesh, S. A., Eaton, C. , Luo, J., Gartland, A., Wang, N. (2020). Inhibiting the P2X4 Receptor Suppresses Prostate Cancer Growth In Vitro and In Vivo, Suggesting a Potential Clinical Target. In (Vol. 9): Cells.
- Heinolainen, K., Karaman, S., D'Amico, G., Tammela, T., Sormunen, R., Eklund, L. , Alitalo, K., Zarkada, G. (2017). VEGFR3 Modulates Vascular Permeability by Controlling VEGF/VEGFR2 Signaling. In (Vol. 120, pp. 1414-1425): Circulation Research.
- Hemmerich, K., Suschek, C. V., Lorzynski, G., Kolb-Bachofen, V., (2003). iNOS activity is essential for endothelial stress gene expression protecting against oxidative damage. In (Vol. 95, pp. 1937-1946): Journal of Applied Physiology.
- Henke, W., Herdel, K., Jung, K., Schnorr, D., Loening, S. A. (1997). Betaine improves the PCR amplification of GC-rich DNA sequences. In (Vol. 25, pp. 3957-3958): Nucleic Acids Research.
- Hernandez-Olmos, V., Abdelrahman, A., El-Tayeb, A., Freudendahl, D., Weinhausen, S., Müller, C. E. 2012). N-substituted phenoxazine and acridone derivatives: Structure-activity relationships of potent P2X4 receptor antagonists. In (Vol. 55, pp. 9576-9588): Journal of Medicinal Chemistry.
- Herndon, J. M., Tome, M. E., Davis, T. P. (2017). Development and Maintenance of the Blood–Brain Barrier. In (pp. 51-56): Primer on Cerebrovascular Diseases.
- Hille, B., Catterall, W. A. (2012). Electrical Excitability and Ion Channels. In (pp. 63-80): Basic Neurochemistry.
- Hofer, A. M. (2012). Send Orders of Reprints at reprints@benthamscience.org Interactions Between Calcium and cAMP Signaling. In (Vol. 19, pp. 5768-5773): Current Medicinal Chemistry.
- Hofer, A. M. (2021). The Love Story between Orai Calcium Entry Channels and Adenylyl Cyclases Gets even more Complicated. In (Vol. 2, pp. 10-11): Function.
- Holton, P (1959). The liberation of adenosine triphosphate on antidromic stimulation of sensory nerves. In (Vol. 145, pp. 494-504): The Journal of Physiology.

- Hood, J. D., Meininger, C. J., Ziche, M., Granger, H. J. (1998). VEGF upregulates ecNOS message, protein, and NO production in human endothelial cells. In (Vol. 274, no 3, pp. H1054-H1058): *American Journal of Physiology-Heart and Circulatory Physiology*.
- Horowitz, L. F., Hirdes, W., Suh, B. C., Hilgemann, D. W., Mackie, K., Hille, B. (2005). Phospholipase C in living cells: Activation, inhibition, Ca²⁺ requirement, and regulation of M current. In (Vol. 126, pp. 243-262): *Journal of General Physiology*.
- Hourani, S. M. O., Chown, J. A. (1988). The effects of some possible inhibitors of ectonucleotidases on the breakdown and pharmacological effects of ATP in the guinea-pig urinary bladder. In (Vol. 20(4), 413-416): *General Pharmacology: The Vascular System*.
- Hsu, M. C., Pan, M. R., Hung, W. C. (2019). Two birds, one stone: Double hits on tumor growth and lymphangiogenesis by targeting vascular endothelial growth factor receptor 3. In (Vol. 8): *MDPI*.
- Hubbi, M. E., Hyun Ahn, E., Downey, J., Afzal, J., Kim, D.-H., Rey, S., Chang, C., Kundu, A., Semenza, G. L., Abraham, R. M. (2012). Matrix Rigidity Controls Endothelial Differentiation and Morphogenesis of Cardiac Precursors. In (Vol. 5, no 227, p. ra41): *Science signaling*.
- Ibidi. (2019). *Application Guide Cell Culture Under Flow*. In Ibidi.
- Illes, P., Müller, C. E., Jacobson, K. A., Grutter, T., Nicke, A., Fountain, S. J., Kennedy, C., Schmalzing, G., Jarvis, M. F., Stojilkovic, S. S. (2021). Update of P2X receptor properties and their pharmacology: IUPHAR Review 30. In (Vol. 178, pp. 489-514): *British Journal of Pharmacology*.
- Jackson ImmunoResearch Laboratories, I. (2017). *Western blotting guide: Part 6, Secondary Antibodies*. In.
- Jackson, M. L., Bond, A. R., George, S. J. (2023). Mechanobiology of the endothelium in vascular health and disease: in vitro shear stress models. In (Vol. 37, pp. 997-1010): *Cardiovascular Drugs and Therapy*.
- Jackson, R. J., Hellen, C. U. T., Pestova, T. V. (2010). The mechanism of eukaryotic translation initiation and principles of its regulation. In (Vol. 11, pp. 113-127): *Nature Reviews Molecular Cell Biology*.
- Jho, D., Mehta, D., Ahmed, G., Gao, X. P., Tirupathi, C., Broman, M., Malik, A. B. (2005). Angiopoietin-1 opposes VEGF-induced increase in endothelial permeability by inhibiting TRPC1-dependent Ca²⁺ influx. In (Vol. 96, pp. 1282-1290): *Circulation Research*.
- Ji, X.D., Kim, Y.C., Ahern, D.G., Linden, J., Jacobson, K. A. (2001). [3H]MRS 1754, a selective antagonist radioligand for A_{2B} adenosine receptors HHS Public Access. In (Vol. 61, pp. 657-663): *Biochem Pharmacol*.
- Jiang, P., Xing, F., Guo, B., Yang, J., Li, Z., Wei, W., Hu, F., Lee, I., Zhang, X., Pan, L. (2017). Nucleotide transmitters ATP and ADP mediate intercellular calcium wave communication via P2Y_{12/13} receptors among BV-2 microglia. In (Vol. 12): *British Journal of Pharmacology*.
- John, K., Barakat, A. I. (2001). Modulation of ATP/ADP Concentration at the Endothelial Surface by Shear Stress: Effect of Flow-Induced ATP Release. In (Vol. 29, pp. 740-751): *Annals of Biomedical Engineering*.
- Johnsen, B., Klaus Eric Kaschubowski, Soroush Nader, E. S., Jan-Andrei Nicola, Ralf Fliegert, Insa M. A. Wolf, Andreas H. Guse, Viacheslav O. Nikolaev, Friedrich Koch-Nolte, Friedrich

- Haag. (2019). P2X7-mediated ATP secretion is accompanied by depletion of cytosolic ATP. In (Vol.15, pp. 155-166): Purinergic Signalling.
- Jones, C. A., Chessell, I. P., Simon, J., Barnard, E. A., Miller, K. J., Michel, A. D., Humphrey, P. P. A. (2000). Functional characterization of the P2X4 receptor orthologues. In (Vol. 129, pp. 388-394): British Journal of Pharmacology.
- Joshi, M. S., Ferguson, T. B., Johnson, F. K., Johnson, R. A., Parthasarathy, S., Lancaster, J. R. (2007). Receptor-mediated activation of nitric oxide synthesis by arginine in endothelial cells. In (Vol. 104, no 24, p. 9982-9987): Proceedings of the National Academy of Sciences.
- Kamouchi, M., Mamin, A., Droogmans, G., Nilius, B. (1999). Nonselective Cation Channels in Endothelial Cells Derived from Human Umbilical Vein. In (Vol. 169, pp. 29-38): The Journal of membrane biology.
- Kanellopoulos, J. M., Almeida-da-Silva, C. L. C., Rützel Boudinot, S., Ojcius, D. M. (2021). Structural and Functional Features of the P2X4 Receptor: An Immunological Perspective. In (Vol. 12): Frontiers in Immunology.
- Karamysheva, A. F. (2008). Mechanisms of angiogenesis. In (Vol. 73, pp. 751-762): Biochemistry.
- Kaur, H., Carriveau, R., Mutus, B. (2012). A Simple Parallel Plate Flow Chamber to Study Effects of Shear Stress on Endothelial Cells. In (pp. 70-78): American Journal of Biomedical Sciences.
- Kellogg, D. L., Zhao, J. L., Coey, U., Green, J. V., Green Kellogg, J. V. (2005). Acetylcholine-induced vasodilation is mediated by nitric oxide and prostaglandins in human skin. In (Vol. 98, pp. 629-632): J Appl Physiol.
- Kemp, P. A., Sugar, R. A., Jackson, A. D. (2004). Nucleotide-mediated mucin secretion from differentiated human bronchial epithelial cells. In (Vol. 31, pp. 446-455): American Journal of Respiratory Cell and Molecular Biology.
- Kennedy, C. (2017). P2Y11 Receptors: Properties, Distribution and Functions. In (pp. 107-122): Protein Reviews.
- Kennedy, C. (2021). The P2Y/P2X divide: How it began. In (Vol. 187, pp. 114408): Biochemical Pharmacology.
- Kettlun, A. M., Espinosa, V., García, L., Valenzuela, M. A. (2005). Potato tuber isoapyrases: Substrate specificity, affinity labeling, and proteolytic susceptibility. In (Vol. 66, pp. 975-982): Phytochemistry.
- Kettlun, A. M., Uribe, L., Calvo, V., Silva, S., Rivera, J., Mancilla, M., Valenzuela, M. A., Traverso-Cori, A. d. (1982). Properties of two apyrases from tuberosum. In (Vol. 21, pp. 551-558): Phytochemistry.
- Khakh, B. S., Proctor, W. R., Dunwiddie, T. V., Labarca, C., Lester, H. A. (1999). Allosteric Control of Gating and Kinetics at P2X 4 Receptor Channels. In (Vol. 19, no 17, pp. 7289-7299): Journal of Neuroscience.
- Khan, Z. S., Vanapalli, S. A. (2013). Probing the mechanical properties of brain cancer cells using a microfluidic cell squeezer device. In (Vol. 7): Biomechanics.
- Kijimag, Y., Ogunbunmi, E., Fleischer, S. (1991). Drug Action of Thapsigargin on the Ca²⁺ Pump Protein of Sarcoplasmic Reticulum. In (Vol. 266, pp. 22912-22918): The journal of biological chemistry.
- Kim, S. H., Cho, Y. R., Kim, H. J., Oh, J. S., Ahn, E. K., Ko, H. J., Hwang, B. J., Lee, S. J., Cho, Y., Kim, Y. K. (2012). Antagonism of VEGF-A-induced increase in vascular permeability by an

- integrin $\alpha 3\beta 1$ -Shp-1-cAMP/PKA pathway. In (Vol. 120, pp. 4892-4902): American Society of Hematology.
- Kimura, H., Esumi, H. (2003). Reciprocal regulation between nitric oxide and vascular endothelial growth factor in angiogenesis. In (Vol. 50, no 1, pp. 49-59): Acta Biochimica Polonica.
- King, B. F. (2023). Rehabilitation of the P2X5 receptor: a re-evaluation of structure and function. In (Vol. 19, pp. 421-439): Purinergic Signalling.
- Klaver, D., Gander, H., Dobler, G., Rahm, A., Thurnher, M. (2022). The P2Y11 receptor of human M2 macrophages activates canonical and IL-1 receptor signaling to translate the extracellular danger signal ATP into anti-inflammatory and pro-angiogenic responses. In (Vol. 79, pp. 1-17): Cellular and Molecular Life Sciences.
- Klotz, K. N., Kachler, S. (2016). Inhibitors of membranous adenylyl cyclases with affinity for adenosine receptors. In (Vol. 389, pp. 349-352): Naunyn-Schmiedeberg's Archives of Pharmacology.
- Korenaga, R., Yamamoto, K., Ohura, N., Sokabe, T., Kamiya, A., Ando, J. (2001). Sp1-mediated downregulation of P2X4 receptor gene transcription in endothelial cells exposed to shear stress. In (Vol. 280, pp. H2214-H2221): American Journal of Physiology-Heart and Circulatory Physiology.
- Koser, D. E., Thompson, A. J., Foster, S. K., Dwivedy, A., Pillai, E. K., Sheridan, G. K., Svoboda, H., Viana, M., Costa, L. d. F., Guck, J. (2016). Mechanosensing is critical for axon growth in the developing brain. In (Vol. 19, pp. 1592-1598): Nature Neuroscience.
- Kotnis, S., Bingham, B., Vasilyev, D. V., Miller, S. W., Bai, Y., Yeola, S., Chanda, P. K., Bowlby, M. R., Kaftan, E. J., Samad, T. A. (2010). Genetic and Functional Analysis of Human P2X5 Reveals a Distinct Pattern of Exon 10 Polymorphism with Predominant Expression of the Nonfunctional Receptor Isoform. In (Vol. 77, pp. 953-960): Molecular Pharmacology.
- Kozak, M. (1989). Circumstances and Mechanisms of Inhibition of Translation by Secondary Structure in Eucaryotic mRNAs. In (Vol. 9, pp. 5134-5142): Molecular and Cellular Biology.
- Kraiss, L. W., Alto, N. M., Dixon, D. A., McIntyre, T. M., Weyrich, A. S., Zimmerman, G. A. (2003). Fluid flow regulates e-selectin protein levels in human endothelial cells by inhibiting translation. In (Vol. 37, pp. 161-168): Journal of Vascular Surgery.
- Kraiss, L. W., Weyrich, A. S., Alto, N. M., Dixon, D. A., Ennis, T. M., Modur, V., McIntyre, T. M., Prescott, S. M., Zimmerman, G. A. (2000). Fluid flow activates a regulator of translation, p70/p85 S6 kinase, in human endothelial cells. In (Vol. 278, pp. H1537-H1544): American Journal of Physiology-Heart and Circulatory Physiology.
- Kroll, J., Waltenberger, J. (1999). A Novel Function of VEGF Receptor-2 (KDR): Rapid Release of Nitric Oxide in Response to VEGF-A Stimulation in Endothelial Cells. In (Vol. 265, pp. 636-639): Biochemical and Biophysical Research Communications.
- Krüger-Genge, A., Blocki, A., Franke, R. P., Jung, F. (2019). Vascular endothelial cell biology: An update. In (Vol. 20): International Journal of Molecular Sciences.
- Kuang, Y., Liu, H., Guo, S., Wang, Y., Zhang, H., Qiao, Y. (2019). The antagonist of P2Y11 receptor NF157 ameliorates oxidized LDL-induced vascular endothelial inflammation. In (Vol. 47, pp. 1839-1845): Artificial Cells, Nanomedicine, and Biotechnology.
- Kukulski, F., Yebdri, F. B., Bahrami, F., Fausther, M., Tremblay, A., Sévigny, J. (2010). Endothelial P2Y2 receptor regulates LPS-induced neutrophil transendothelial migration in vitro. In (Vol. 47, pp. 991-999): Molecular Immunology.

- Lambrecht, G. (2000). Agonists and antagonists acting at P2X receptors: Selectivity profiles and functional implications. In (Vol. 362, pp. 340-350): Naunyn-Schmiedeberg's Archives of Pharmacology.
- Lang, M. B., Leung, K. Y., Greene, N. D. E., Malone, K. M., Saginc, G., Randi, A. M., Kiprianos, A., Maughan, R. T., Pericleous, C., Mason, J. C. (2023). The actions of methotrexate on endothelial cells are dependent on the shear stress-induced regulation of one carbon metabolism. In (Vol. 14): Frontiers in Immunology.
- Lange, C., Storkebaum, E., Ruiz de Almodóvar, C., Dewerchin, M., Carmeliet, P. (2016). Vascular endothelial growth factor: a neurovascular target in neurological diseases. In (Vol.12, pp. 439-454): Nature Reviews Neurology.
- Lau, S., Gossen, M., Lendlein, A., Jung, F. (2021). Venous and arterial endothelial cells from human umbilical cords: Potential cell sources for cardiovascular research. In (Vol. 22, pp. 1-14): International Journal of Molecular Sciences.
- Layhadi, J. A., Fountain, S. J.(2017). P2X4 receptor-dependent Ca²⁺ influx in model human monocytes and macrophages. In (Vol. 18): International Journal of Molecular Sciences.
- Layhadi, J. A., Turner, J., Crossman, D., Fountain, S. J. (2018). ATP Evokes Ca²⁺ Responses and CXCL5 Secretion via P2X4 Receptor Activation in Human Monocyte-Derived Macrophages. In (Vol. 200, pp. 1159-1168): The Journal of Immunology.
- Lazarowski, T. R., Watt, C., Stutts, T. J., Boucher, C., Harden, T. K. (1995). Pharmacological selectivity of the cloned human P₂-purinoceptor: potent activation by diadenosine tetraphosphate. In (Vol. 116(1), pp. 1619): British journal of pharmacology.
- Lee, P. C., Kibbe, M. R., Schuchert, M. J., Stolz, D. B., Watkins, S. C., Griffith, B. P., Billiar, T. R., Shears, L. L. (2000). Nitric Oxide Induces Angiogenesis and Upregulates $\alpha\beta 3$ Integrin Expression on Endothelial Cells. In (Vol. 60, pp. 269-280): Microvascular Research.
- Lee, W., Leddy, H. A., Chen, Y., Lee, S. H., Zelenski, N. A., McNulty, A. L., Wu, J., Beicker, K. N., Coles, J., Zauscher, S. (2014). Synergy between Piezo1 and Piezo2 channels confers high-strain mechanosensitivity to articular cartilage. In (Vol. 111): Proceedings of the National Academy of Sciences.
- Lefkimmatis, K., Srikanthan, M., Maiellaro, I., Moyer, M. P., Curci, S., Hofer, A. M. (2009). Store-operated cyclic AMP signalling mediated by STIM1. In (Vol. 11, pp. 433-442): Nature Cell Biology.
- Lenasi, H., Štrucl, M. (2008). The effect of nitric oxide synthase and cyclooxygenase inhibition on cutaneous microvascular reactivity. In (Vol. 103, pp. 719-726): European journal of applied physiology.
- Ley, K., Lundgren, E., Berger, E., Arfors, K. (1989). Shear-dependent inhibition of granulocyte adhesion to cultured endothelium by dextran sulfate. In (Vol. 73, pp. 1324-1330): Blood.
- Li, H., Li, Y., Cai, L., Bai, B., Wang, Y. (2015). Original Article Effects of CASP5 gene overexpression on angiogenesis of HMEC-1 cells. In (Vol. 8, pp. 15794-15800): Int J Clin Exp Pathol.
- Li, H., Zhou, W. Y., Xia, Y. Y., Zhang, J. X. (2022). Endothelial Mechanosensors for Atheroprone and Atheroprotective Shear Stress Signals. In (Vol. 15, pp. 1771-1783): Journal of Inflammation Research.
- Li, J., Bruns, A. F., Hou, B., Rode, B., Webster, P. J., Bailey, M. A., Appleby, H. L., Moss, N. K., Ritchie, J. E., Yuldasheva, N. Y. (2015). Orai3 surface accumulation and calcium entry evoked by vascular endothelial growth factor. In (Vol. 35, pp. 1987-1994): Arteriosclerosis, Thrombosis, and Vascular Biology.

- Li, J., Cubbon, R. M., Wilson, L. A., Amer, M. S., McKeown, L., Hou, B., Majeed, Y., Tumova, S., Seymour, V. A. L., Taylor, H. (2011). Orai1 and CRAC channel dependence of VEGF-activated Ca²⁺ entry and endothelial tube formation. In (Vol. 108, pp. 1190-1198): *Circulation Research*.
- Li, J., Hou, B., Tumova, S., Muraki, K., Bruns, A., Ludlow, M. J., Sedo, A., Hyman, A. J., McKeown, L., Young, R. S. (2014). Piezo1 integration of vascular architecture with physiological force. In (Vol. 515, pp. 279-282): *Nature*.
- Li, J., LoBue, A., Heuser, S. K., Leo, F., Cortese-Krott, M. M. (2021). Using diaminofluoresceins (DAFs) in nitric oxide research. In (Vol. 115, pp. 44-54): *Nitric Oxide*.
- Li, N., Sul, J.Y., Haydon, P. G. (2003). A Calcium-Induced Calcium Influx Factor, Nitric Oxide, Modulates the Refilling of Calcium Stores in Astrocytes. In (Vol. 23, pp. 10302-10310): *The Journal of Neuroscience*.
- Li, X., Han, L., Nookaew, I., Mannen, E., Silva, M. J., Almeida, M., Xiong, J. (2019). Stimulation of piezo1 by mechanical signals promotes bone anabolism. In (Vol. 8, pp. 1-22): *elife*.
- Liao, Z., Cao, C., Wang, J., Huxley, V. H., Baker, O., Weisman, G. A., Erb, L. (2014). The P2Y2 Receptor Interacts with VE-Cadherin and VEGF Receptor-2 to Regulate Rac1 Activity in Endothelial Cells. In (Vol. 07, pp. 1105-1121): *Journal of Biomedical Science and Engineering*.
- Licor. (2008). Application Guide Good Westerns Gone Bad Tips to Make Your Fluorescent Western Great.
- Lin, C.F., Lei, H.Y., Shiau, A.L., Liu, H.S., Yeh, T.M., Chen, S.H., Liu, C.C., Chiu, S.C., Lin, Y.S., (2002). Endothelial Cell Apoptosis Induced by Antibodies Against Dengue Virus Nonstructural Protein 1 Via Production of Nitric Oxide. In (Vol. 169, pp. 657-664): *The Journal of Immunology*.
- Lisec, B., Bozic, T., Santek, I., Markelc, B., Vrecl, M., Robert Frangez, L. (2023). Characterization of two distinct immortalized endothelial cell lines, EA.hy926 and HMEC-1, for in vitro studies: exploring the impact of calcium electroporation, Ca²⁺ signaling and transcriptomic profiles. In (Vol. 22(1), p. 118): *Cell Communication and Signaling*.
- Liu, K., Southall, N., Titus, S. A., Inglese, J., Eskay, R. L., Shinn, P., Austin, C. P., Heilig, M. A., Zheng, W. (2010). A multiplex calcium assay for identification of GPCR agonists and antagonists. In (Vol. 8, pp. 362-374): *Assay and Drug Development Technologies*.
- Lohman, A. W., Billaud, M., Isakson, B. E. (2012). Mechanisms of ATP release and signalling in the blood vessel wall. In (Vol. 95, pp. 269-280): *Cardiovascular Research*.
- Lockwood, S. Y., Erkal, J. L., & Spence, D. M. (2014). Endothelium-derived nitric oxide production is increased by ATP released from red blood cells incubated with hydroxyurea. In (Vol. 38(1), pp. 1-7): *Nitric Oxide - Biology and Chemistry*.
- Lv, Q., Xue, Y., Li, G., Zou, L., Zhang, X., Ying, M., Wang, S., Guo, L., Gao, Y., Li, G. (2015). Beneficial effects of evodiamine on P2X4-mediated inflammatory injury of human umbilical vein endothelial cells due to high glucose. In (Vol. 28, pp. 1044-1049): *International Immunopharmacology*.
- Lyttonsg, J., Westlins, M., Hanleyll, M. R. (1991). Thapsigargin Inhibits the Sarcoplasmic or Endoplasmic Reticulum Ca-ATPase Family of Calcium Pumps. In (Vol. 266, pp. 17067-17071): *The journal of biological chemistry*.
- Madry, C., Arancibia-Cárcamo, I. L., Kyrargyri, V., Chan, V. T. T., Hamilton, N. B., Attwell, D. (2018). Effects of the ecto-ATPase apyrase on microglial ramification and surveillance reflect cell depolarization, not ATP depletion. In (Vol. 115, pp. E1608-E1617): *Proceedings of the National Academy of Sciences of the United States of America*.

- Maiellaro, I., Lefkimmiatis, K., Moyer, M. P., Curci, S., Hofer, A. M. (2012). Termination and activation of store-operated cyclic AMP production. In (Vol. 16, pp. 2715-2725): *Journal of Cellular and Molecular Medicine*.
- Malko, P., Jia, X., Wood, I., Jiang, L. H. (2023). Piezo1 channel-mediated Ca²⁺ signaling inhibits lipopolysaccharide-induced activation of the NF- κ B inflammatory signaling pathway and generation of TNF- α and IL-6 in microglial cells. In (Vol. 71, pp. 848-865): *Glia*.
- Mancini, J. E., Ortiz, G., Potilinstki, C., Salica, J. P., Lopez, E. S., Croxatto, J. O., Gallo, J. E. (2018). Possible neuroprotective role of P2X2 in the retina of diabetic rats. In (Vol. 10, pp. 1-12): *Diabetology and Metabolic Syndrome*.
- Marteau, F., Le Poul, E., Communi, D., Communi, D., Labouret, C., Savi, P., Boeynaems, J.M., Gonzalez, N. S. (1995). Pharmacological Characterization of the Human P2Y 13 Receptor. In (Vol. 64, pp. 104-112): *Molecular Pharmacology*.
- Marteau, F., Le Poul, E., Communi, D., , Communi, D., Labouret, C., Savi, P., Boeynaems, J. M., Gonzalez, N. S. (2003). Pharmacological characterization of the human P2Y13 receptor. In (Vol. 64, pp. 104-112): *Molecular Pharmacology*.
- Martin-Almedina, S., Mansour, S., Ostergaard, P. (2018). Human phenotypes caused by PIEZO1 mutations; one gene, two overlapping phenotypes? In (Vol. 596, pp. 985-992): *The Journal of Physiology*.
- Martinez, N. A., Ayala, A. M., Martinez, M., Martinez-Rivera, F. J., Miranda, J. D., Silva, W. I. (2016). Caveolin-1 regulates the P2Y2 receptor signaling in human 1321N1 astrocytoma cells. In (Vol. 291, pp. 12208-12222): *Journal of Biological Chemistry*.
- Masłowska, K., Halik, P. K., Tymecka, D., Misicka, A., Gniazdowska, E. (2021). The role of vegf receptors as molecular target in nuclear medicine for cancer diagnosis and combination therapy. In (Vol. 13, pp. 1-46): *Cancers*.
- Matsunaga, M., Kimura, M., Ouchi, T., Nakamura, T., Ohyama, S., Ando, M., Nomura, S., Azuma, T., Ichinohe, T., Shibukawa, Y. (2021). Mechanical Stimulation-Induced Calcium Signaling by Piezo1 Channel Activation in Human Odontoblast Reduces Dentin Mineralization. In (Vol. 12): *Frontiers in Physiology*.
- McHugh, B. J., Buttery, R., Lad, Y., Banks, S., Haslett, C., ,ethi, T. (2010). Integrin activation by Fam38A uses a novel mechanism of R-Ras targeting to the endoplasmic reticulum. In (Vol. 123, pp. 51-61): *Journal of Cell Science*.
- Meis, S., Hamacher, A., Hongwiset, D., Marzian, C., Wiese, M., Eckstein, N., Royer, H. D., Communi, D., Boeynaems, J. M., Hausmann, R. (2010). NF546 [4,4'-(carbonylbis(imino-3,1-phenylene-carbonylimino-3,1-(4-methyl-phenylene)-carbonylimino))-bis(1,3-xylene- α,α' - diphosphonic acid) tetrasodium salt] is a non-nucleotide P2Y11 agonist and stimulates release of interleukin-8 from human monocyte-derived dendritic cells. In (Vol. 332, pp. 238-247): *Journal of Pharmacology and Experimental Therapeutics*.
- Michel, A. D., Chambers, L. J., , Walter, D. S. (2008). Negative and positive allosteric modulators of the P2X 7 receptor. In (Vol. 153, pp. 737-750): *British Journal of Pharmacology*.
- Michel, A. D., Clay, W. C., Ng, S. W., Roman, S., Thompson, K., Condreay, J. P., Hall, M., Holbrook, J., Livermore, D., Senger, S. 2008). Identification of regions of the P2X 7 receptor that contribute to human and rat species differences in antagonist effects. In (Vol. 155, pp. 738-751): *British Journal of Pharmacology*.
- Miras-Portugal, M. T., Ortega, F., Gualix, J., Perez-Sen, R., Delicado, E. G., Gomez-Villafuertes, R. (2020). Intracellular Calcium Recording After Purinoceptor Activation Using a Video-Microscopy Equipment. In (pp. 311-321): *Purinergic Signaling: Methods and Protocols*.

- Miyashita, T., Takeishi, Y., Takahashi, H., Miyamoto, T., Fujii, S., Yoshimura, T., Tomoike, H., Kato, S., Kubota, I. (2002). Comparison of Nitric Oxide Production in Response to Carbachol Between Macrovascular and Microvascular Cardiac Endothelial Cells. In (Vol. 66, pp. 511-515): *Circulation Journal*.
- Moccia, F., Negri, S., Shekha, M., Faris, P., Guerra, G. (2019). Endothelial Ca²⁺ signaling, angiogenesis and vasculogenesis: Just what it takes to make a blood vessel. In (Vol. 20, pp. 1-39): *International Journal of Molecular Sciences*.
- Moccia, F., Brunetti, V., Perna, A., Guerra, G., Soda, T., Berra-Romani, R. (2023). The Molecular Heterogeneity of Store-Operated Ca²⁺ Entry in Vascular Endothelial Cells: The Different roles of Orai1 and TRPC1/TRPC4 Channels in the Transition from Ca²⁺-Selective to Non-Selective Cation Currents. In (Vol. 24): *Multidisciplinary Digital Publishing Institute (MDPI)*.
- Mohammadi, L., Han, D. D., Xu, F., Huang, A., Derakhshandeh, R., Rao, P., Whitlatch, A., Cheng, J., Keith, R. J., Hamburg, N. M. (2022). Chronic E-Cigarette Use Impairs Endothelial Function on the Physiological and Cellular Levels. In (Vol. 42, pp. 1333-1350): *Arteriosclerosis, Thrombosis, and Vascular Biology*.
- Moran, M. M., Xu, H., Clapham, D. E. (2004). TRP ion channels in the nervous system. In (Vol. 14, pp. 362-369): *Current Opinion in Neurobiology*.
- Morrone, F. B., Oliveira, D. L., Gamermann, P., Stella, J., Wofchuk, S., Wink, M. R., Meurer, L., Edelweiss, M. I. A., Lenz, G., Battastini, A. M. O. (2006). In vivo glioblastoma growth is reduced by apyrase activity in a rat glioma model. In (Vol. 6, pp. 1-10): *BMC Cancer*.
- Mortazavi, A., Williams, B. A., McCue, K., Schaeffer, L., Wold, B. (2008). Mapping and quantifying mammalian transcriptomes by RNA-Seq. In (Vol. 5, pp. 621-628): *Nature Methods*.
- Mousawi, F., Peng, H., Li, J., Ponnambalam, S., Roger, S., Zhao, H., Yang, X., Jiang, L. H. (2020). Chemical activation of the Piezo1 channel drives mesenchymal stem cell migration via inducing ATP release and activation of P2 receptor purinergic signaling. In (Vol. 38, pp. 410-421): *Stem Cells*.
- Mühleder, S., Fuchs, C., Basílio, J., Szwarc, D., Pill, K., Labuda, K., Slezak, P., Siehs, C., Pröll, J., Priglinger, E. (2020). Purinergic P2Y2 receptors modulate endothelial sprouting. In (Vol. 77, pp. 885-901): *Cellular and Molecular Life Sciences*.
- Müller, C. E., Baqi, Y., Namasivayam, V. (2020). Agonists and Antagonists for Purinergic Receptors. In (pp. 45-64): *Methods Mol Biol*.
- Muñoz-Vega, M., Massó, F., Páez, A., Carreón-Torres, E., Cabrera-Fuentes, H. A., Fragoso, J. M., Pérez-Hernández, N., Martínez, L. O., Najib, S., Vargas-Alarcón, G. (2018). Characterization of immortalized human dermal microvascular endothelial cells (HMEC-1) for the study of HDL functionality. In (Vol. 17): *Lipids in Health and Disease*.
- Muoboghare, M. O., Drummond, R. M., Kennedy, C. (2019). Characterisation of P2Y2 receptors in human vascular endothelial cells using AR-C118925XX, a competitive and selective P2Y2 antagonist. In (Vol. 176, pp. 2894-2904): *British Journal of Pharmacology*.
- Nasoni, M. G., Benedetti, S., Crinelli, R., Palma, F., Canonico, B., Monittola, F., Zerbinati, C., Iuliano, L., Luchetti, F. (2022). 3 β -Hydroxy-5 β -hydroxy-B-norcholestane-6 β -carboxaldehyde (SEC-B) Induces Proinflammatory Activation of Human Endothelial Cells Associated with Nitric Oxide Production and Endothelial Nitric Oxide Synthase/Caveolin-1 Dysregulation. In (Vol. 11, pp. 1148): *Antioxidants*.
- Newman, E. A. (2005). Calcium increases in retinal glial cells evoked by light-induced neuronal activity. In (Vol. 25, pp. 5502-5510): *Journal of Neuroscience*.

- Ng, P. Y., McIntosh, K. A., Hargrave, G., Ho, K. H., Paul, A., Plevin, R. (2018). Inhibition of cytokine-mediated JNK signalling by purinergic P2Y11 receptors, a novel protective mechanism in endothelial cells. In (Vol. 51, pp. 59-71): Cellular Signalling.
- Nguyen, K. T., Eskin, S. G., Patterson, C., Runge, M. S., McIntire, L. V. (2001). Shear stress reduces protease activated receptor-1 expression in human endothelial cells. In (Vol. 29, pp. 145-152): Annals of Biomedical Engineering.
- Nicholas, R. A., Watt, W. C., Lazarowski, E. R., Li, Q., Kendall Harden, T. (1996). Uridine Nucleotide Selectivity of Three Phospholipase C-Activating P2 Receptors: Identification of a UDP-Selective, a UTP-Selective, and an ATP-and UTP-Specific Receptor. In (Vol. 50, pp. 224-229): Molecular pharmacology.
- Nieto Pescador, M. G., Raquel, G. A., Raquel, Valdez Morales, E., Espinosa Luna, R., Jiménez Vargas, N., Liñan Rico, A., Ramos Lomas, T. L., Verónica, D. H., Luis M., M., Carlos, B. L. (2013). P2X4 subunits are part of P2X native channels in murine myenteric neurons. In (Vol. 709, pp. 93-102): European journal of pharmacology.
- Nishimura, A., Sunggip, C., Oda, S., Numaga-Tomita, T., Tsuda, M., Nishida, M. (2017). Purinergic P2Y receptors: Molecular diversity and implications for treatment of cardiovascular diseases. In (Vol. 180, pp. 113-128): Pharmacology & Therapeutics.
- North, R. A. (2002). Molecular Physiology of P2X Receptors. In (Vol. 82, pp. 1013-1067): Physiological Reviews.
- North, R. A., Surprenant, A. (2000). Pharmacology of cloned P2X receptors. In (Vol. 40, pp. 563-580): Annual review of pharmacology and toxicology.
- Novus Biologicals, H. (2017). Secondary Antibody Handbook.
- O'Grady, S. M., Elmquist, E., Filtz, T. M., Nicholas, R. A., Harden, T. K. (1996). A guanine nucleotide-independent inwardly rectifying cation permeability is associated with P2Y1 receptor expression in *Xenopus* oocytes. In (Vol. 271, pp. 29080-29087): Journal of Biological Chemistry.
- Oken, A. C., Krishnamurthy, I., Savage, J. C., Lisi, N. E., Godsey, M. H., Mansoor, S. E. (2022). Molecular Pharmacology of P2X Receptors: Exploring Druggable Domains Revealed by Structural Biology. In (Vol. 13): Frontiers in Pharmacology.
- Olanrewaju, H. A., Qin, W., Feoktistov, I., Scemama, J.L., Mustafa, S. J. (2000). Adenosine A2A and A2B receptors in cultured human and porcine coronary artery endothelial cells. In (Vol. 279, pp. H650-H656): American Journal of Physiology-Heart and Circulatory Physiology.
- Ollivier, H., Pichavant-Rafini, K., Puill-Stephan, E., Calvès, P., Nonnotte, L., Nonnotte, G. (2006). Effects of hypo-osmotic stress on ATP release in isolated turbot (*Scophthalmus maximus*) hepatocytes. In (Vol. 98, pp. 427-437): Biology of the Cell.
- Olofsson, B., Korpelainen, E., Pepper, M. S., Mandriota, S. J., Aase, K., Kumar, V., Gunji, Y., Jeltsch, M. M., Shibuya, M., Alitalo, K. (1998). Vascular endothelial growth factor B (VEGF-B) binds to VEGF receptor-1 and regulates plasminogen activator activity in endothelial cells. In (Vol. 95, pp. 11709-11714): Cell Biology.
- Orriss, I. R., Davies, B. K., Bourne, L. E., Arnett, T. R. (2023). Modulation of osteoblast differentiation and function by the P2X4 receptor. In (Vol. 19, pp. 367-378): Purinergic Signalling.
- Ostrom, K. F., Lavigne, J. E., Brust, T. F., Seifert, R., Dessauer, C. W., Watts, V. J., Ostrom, R. S. (2022). Physiological Roles of Mammalian Transmembrane Adenylyl Cyclase Isoforms. In (Vol. 102, pp. 815-857): Physiological Reviews.

- Otrock, Z., Mahfouz, R., Makarem, J., Shamseddine, A. (2007). Understanding the biology of angiogenesis: Review of the most important molecular mechanisms. In (Vol. 39, pp. 212-220): *Blood Cells, Molecules, and Diseases*.
- Ottolini, M., Sonkusare, S. K. (2021). The Calcium Signaling Mechanisms in Arterial Smooth Muscle and Endothelial Cells. In (Vol. 11, pp. 1831-1869): *Comprehensive Physiology*.
- Pardo-Pastor, C., Rosenblatt, J. (2023). Piezo1 activates noncanonical EGFR endocytosis and signaling. In (Vol. 9(39), pp. eadi1328): *Science Advances*.
- Paredes, R. M., Etzler, J. C., Watts, L. T., Zheng, W., Lechleiter, J. D. (2008). Chemical calcium indicators. In (Vol. 46, pp. 143-151): *Methods*.
- Parekh, A. B., Putney, J. W. (2005). Store-operated calcium channels. In (Vol. 85, pp. 757-810): *Physiological Reviews*.
- Parr, C. E., Sullivant, D. M., Paradiso, A. M., Lazarowski, E. R., Burch, L. H., Olsen, J. C., Erb, L., Weismant, G. A., Boucher, R. C., Turnert, J. T. (1994). Cloning and expression of a human P2U nucleotide receptor, a target for cystic fibrosis pharmacotherapy. In (Vol. 91, pp. 3275-3279): *Medical Sciences*.
- Pascual, S. A. S., Manuel Fernández-Fernández, J., Valverde, M. Á. (2011). CACNA1A mutations with clinical relevance in migraine affect Ca V 2.1 channel regulation by G proteins and SNAREs. In *Universitat Pompeu Fabra, doctoral thesis*.
- Patel, L., Thaker, A. (2014). The effects of adenosine A2B receptor inhibition on VEGF and nitric oxide axis-mediated renal function in diabetic nephropathy. In (Vol. 36, pp. 916-924): *Renal Failure*.
- Paton, W. D. M., Vane, J. R. (1963). An analysis of the responses of the isolated stomach to electrical stimulation and to drugs. In (Vol. 165, pp. 10-46): *The Journal of Physiology*.
- Patton, J. T. (1996). Dynamic Flow Assay in a Parallel Plate Flow Chamber. In *GlycoTech Corporation*.
- Paz Prada, M., Syed, A. U., Buonarati, O. R., Reddy, G. R., Nystoriak, M. A., Ghosh, D., Simó, S., Sato, D., Sasse, K. C., Ward, S. M. (2019). A G s-coupled purinergic receptor boosts Ca²⁺ influx and vascular contractility during diabetic hyperglycemia. In (vol. 8, pp. e42214): *Elife*.
- Paz, S., Nagy, D., Karatsiompani, S., Kefauver, J., Pak, R., Sauter, D. (2023). Automated high throughput patch clamp studies of Piezo1 channel. In *Society of Neurosciences (SfN) (Sophion Bioscience)*.
- Peach, C. J., Mignone, V. W., Arruda, M. A., Alcobia, D. C., Hill, S. J., Kilpatrick, L. E., Woolard, J. (2018). Molecular pharmacology of VEGF-A isoforms: Binding and signalling at VEGFR2. In (Vol. 19): *International Journal of Molecular Sciences*.
- Pearce, M. J., McIntyre, T. M., Prescott, S. M., Zimmerman, G. A., Whatley, R. E. (1996). Shear Stress Activates Cytosolic Phospholipase A2(cPLA2) and MAP Kinase in Human Endothelial Cells. In (Vol. 218, pp. 500-504): *Biochemical and Biophysical Research Communications*.
- Periasamy, M., Kalyanasundaram, A. (2007). SERCA pump isoforms: Their role in calcium transport and disease. In (Vol. 35, pp. 430-442): *Muscle & Nerve*.
- Pillai-Kastoori, L., Heaton, S., Shiflett, S. D., Roberts, A. C., Solache, A., Schutz-Geschwender, A. R. (2020). Antibody validation for Western blot: By the user, for the user. In (Vol. 295, pp. 926-939): *Journal of Biological Chemistry*.
- Pimenta, P. H. C., Silva, C. L. M., Noel, F. (2010). Ivermectin is a nonselective inhibitor of mammalian P-type ATPases. In (Vol. 381, pp. 147-152): *Naunyn-Schmiedeberg's Archives of Pharmacology*.

- Piollet, M., Sturza, A., Chadet, S., Gabillard-Lefort, C., Benoist, L., Muntean, D.-M., Aburel, O.-M., Angoulvant, D., Ivanov, F. (2021). P2Y₁₁ Agonism Prevents Hypoxia/Reoxygenation- and Angiotensin II-Induced Vascular Dysfunction and Intimal Hyperplasia Development. In (Vol. 22, pp. 855): International Journal of Molecular Sciences.
- Polk, T., Schmitt, S., Aldrich, J. L., Long, D. S., & (2022). Human dermal microvascular endothelial cell morphological response to fluid shear stress. In (Vol. 143): Microvascular Research.
- Ponten, J., Macintyre, E. H. (1968). Long term culture of normal and neoplastic human glia. In (Vol. 74, pp. 465-486): Acta Pathologica Microbiologica Scandinavica.
- Popot, J.I., Changeux, J.P. (1984). Nicotinic Receptor of Acetylcholine: Structure of an Oligomeric Integral Membrane Protein. In (Vol. 64): Physiological reviews.
- Prakriya, M. (2013). Store-Operated Orai Channels: Structure and Function. In (Vol. 71, pp. 1-32): Current Topics in Membranes.
- Prakriya, M., Lewis, R. S. (2015). Store-operated calcium channels. In (Vol. 95, pp. 1383-1436): Physiol Rev.
- Priel, A., Silberberg, S. D. (2004). Mechanism of Ivermectin Facilitation of Human P2X₄ Receptor Channels. In (Vol. 123, pp. 281-293): Journal of General Physiology.
- Prindle, A., Liu, J., Asally, M., Ly, S., Garcia-Ojalvo, J., Süel, G. M. (2015). Ion channels enable electrical communication in bacterial communities. In (Vol. 527, pp. 59-63): Nature.
- Qi, A. D., Kennedy, C., Harden, T. K., Nicholas, R. A. (2001). Differential coupling of the human P2Y₁₁ receptor to phospholipase C and adenylyl cyclase. In (Vol. 132, pp. 318-326): British Journal of Pharmacology.
- Rafehi, M., Burbiel, J. C., Attah, I. Y., Abdelrahman, A., Müller, C. E. (2017). Synthesis, characterization, and in vitro evaluation of the selective P2Y₂ receptor antagonist AR-C118925. In (Vol. 13, pp. 89-103): Purinergic Signalling.
- Rafehi, M., Müller, C. E. (2018). Tools and drugs for uracil nucleotide-activated P2Y receptors. In (Vol. 190, pp. 24-80): Pharmacology and Therapeutics.
- Rahimi, N. (2006). VEGFR-1 and VEGFR-2: two non-identical twins with a unique physiognomy. In (Vol.11, pp. 818): Frontiers in bioscience: a journal and a virtual library.
- Ralevic, V. (2012). P2X receptors in the cardiovascular system. In (Vol. 1, pp. 663-674): Wiley Interdisciplinary Reviews: Membrane Transport and Signaling.
- Ralevic, V., Burnstock, G. (1996). Discrimination by PPADS between endothelial P2y- and P2U-purinoceptors in the rat isolated mesenteric arterial bed. In (Vol. 118, pp. 428-434): British Journal of Pharmacology.
- Ralevic, V., Burnstock, G. (1998). Receptors for purines and pyrimidines. In (Vol. 50, pp. 413-492): Pharmacological Reviews.
- Ranade, S. S., Qiu, Z., Woo, S. H., Hur, S. S., Murthy, S. E., Cahalan, S. M., Xu, J., Mathur, J., Bandell, M., Coste, B. (2014). Piezo1, a mechanically activated ion channel, is required for vascular development in mice. In (Vol. 111, pp. 10347-10352): Proceedings of the National Academy of Sciences of the United States of America.
- Raqeeb, A., Sheng, J., Ao, N., Braun, A. P. (2011). Purinergic P2Y₂ receptors mediate rapid Ca²⁺ mobilization, membrane hyperpolarization and nitric oxide production in human vascular endothelial cells. In (Vol. 49, pp. 240-248): Cell Calcium.
- Reinhart-King, C. A., Fujiwara, K., Berk, B. C. (2008). Chapter 2 Physiologic Stress-Mediated Signaling in the Endothelium. In (Vol. 443, pp. 25-44): Methods in Enzymology.
- Retailleau, K., Arhatte, M., Demolombe, S., Peyronnet, R., Baudrie, V., Jodar, M., Bourreau, J., Henrion, D., Offermanns, S., Nakamura, F. (2016). Arterial Myogenic Activation through Smooth Muscle Filamin A. In (Vol. 14, pp. 2050-2058): Cell Reports.

- Riegel, A.-K., Faigle, M., Zug, S., Rosenberger, P., Robaye, B., Boeynaems, J.M., Idzko, M., Eltzschig, H. K. (2011). Selective induction of endothelial P2Y6 nucleotide receptor promotes vascular inflammation. In (Vol. 117, pp. 2548-2555): Blood.
- Risau, W., Flamme, I. (1995). Vasculogenesis. In (Vol. 11, pp. 73-91): Annual Review of Cell and Developmental Biology.
- Robaye, B., Boeynaems, J.M., Communi, D. (1997). Slow desensitization of the human P2Y 6 receptor. In (Vol. 329, pp. 236): European Journal of Pharmacology.
- Robinson, C. J., Stringer, S. E. (2001). The splice variants of vascular endothelial growth factor (VEGF) and their receptors. In (Vol. 114, pp. 853-865): Journal of Cell Science.
- Rode, B., Shi, J., Endesh, N., Drinkhill, M. J., Webster, P. J., Lotteau, S. J., Bailey, M. A., Yuldasheva, N. Y., Ludlow, M. J., Cubbon, R. M. (2017). Piezo1 channels sense whole body physical activity to reset cardiovascular homeostasis and enhance performance. In (Vol. 8, pp. 350): Nature Communications.
- Roux, E., Bougaran, P., Dufourcq, P., Couffignal, T. (2020). Fluid Shear Stress Sensing by the Endothelial Layer. In (Vol. 11): Frontiers in Physiology.
- Ryzhov, S., McCaleb, J. L., Goldstein, A. E., Biaggioni, I., Feoktistov, I. (2007). Role of adenosine receptors in the regulation of angiogenic factors and neovascularization in hypoxia. In (Vol. 320, pp. 565-572): Journal of Pharmacology and Experimental Therapeutics.
- Samways, D. S. K., Li, Z., Egan, T. M. (2014). Principles and properties of ion flow in P2X receptors. In (Vol. 8): Frontiers in Cellular Neuroscience.
- Sanabria, P., Ross, E., Ramirez, E., Colon, K., Hernandez, M., Maldonado, H. M., Silva, W. I., Jimenez-Rivera, C. A., Gonzalez, F. A. (2008). P2Y2 receptor desensitization on single endothelial cells. In (Vol. 15, pp. 43-51): Endothelium: Journal of Endothelial Cell Research.
- Sanchez-collado, J., Lopez, J. J., Jardin, I., Salido, G. M., Rosado, J. A. (2020). Cross-Talk Between the Adenylyl Cyclase / cAMP Pathway and Ca²⁺ Homeostasis. In (pp.73-116): Reviews of physiology, biochemistry and pharmacology.
- Sandoo, A., Veldhuijzen van Zanten, J. J. C. S., Metsios, G. S., Carroll, D., Kitas, G. D. (2010). The Endothelium and Its Role in Regulating Vascular Tone. In (Vol. 4, pp. 302-312): The Open Cardiovascular Medicine Journal.
- Sathanoori, R., Bryl-Gorecka, P., Müller, C. E., Erb, L., Weisman, G. A., Olde, B., Erlinge, D. (2017). P2Y2 receptor modulates shear stress-induced cell alignment and actin stress fibers in human umbilical vein endothelial cells. In (Vol. 74, pp. 731-746): Cell Mol Life Sci.
- Sathanoori, R., Rosi, K., Gu, F., Wiley, Müller, Olde, Erlinge (2015). Shear stress modulates endothelial KLF2 through activation of P2X4. In (Vol. 11, pp. 139-153): Purinergic Signalling.
- Sathanoori, R., Swärd, K., Olde, B., Erlinge, D. (2015). The ATP Receptors P2X7 and P2X4 Modulate High Glucose and Palmitate-Induced Inflammatory Responses in Endothelial Cells. In (Vol. 10, pp. e0125111): Plos One.
- Scarr, E., Gibbons, A. S., Neo, J., Udawela, M., Dean, B. (2013). Cholinergic connectivity: it's implications for psychiatric disorders. In (Vol. 7, p. 55): Frontiers in cellular neuroscience.
- Schmid, R., Evans, R. J. (2019). ATP-Gated P2X Receptor Channels: Molecular Insights into Functional Roles. In (Vol. 81, pp. 43-62): Annual Review of Physiology.
- Schwachtgen, J. L., Houston, P., Campbell, C., Sukhatme, V., Braddock, M. (1998). Fluid shear stress activation of egr-1 transcription in cultured human endothelial and epithelial

cells is mediated via the extracellular signal- related kinase 1/2 mitogen-activated protein kinase pathway. In (Vol. 101, pp. 2540-2549): *Journal of Clinical Investigation*.

Sedlak, J., Clyne, A. (2023). Application of Shear Stress to Endothelial Cells Using a Parallel Plate Flow Chamber. In (Vol. 2600, pp. 81-90): *Mechanobiology: Methods and Protocols*.

Seiffert, K., Ding, W., Wagner, J. A., Granstein, R. D. (2006). ATP γ S enhances the production of inflammatory mediators by a human dermal endothelial cell line via purinergic receptor signaling. In (Vol. 126, pp. 1017-1027): *Journal of Investigative Dermatology*.

Seye, C. I., Yu, N., González, F. A., Erb, L., Weisman, G. A. (2004). The P2Y2 nucleotide receptor mediates vascular cell adhesion molecule-1 expression through interaction with VEGF receptor-2 (KDR/Flk-1). In (Vol. 279, pp. 35679-35686): *Journal of Biological Chemistry*.

Shanker, G., Kontos, J. L., Eckman, D. M., Wesley-Farrington, D., Sane, D. C. (2006). Nicotine upregulates the expression of P2Y12 on vascular cells and megakaryoblasts. In (Vol. 22, pp. 213-220): *Journal of Thrombosis and Thrombolysis*.

Shen, B., Kwan, H.Y., Ma, X., Wong, C.O., Du, J., Huang, Y., Yao, X. (2011). cAMP Activates TRPC6 Channels via the Phosphatidylinositol 3-Kinase (PI3K)-Protein Kinase B (PKB)-Mitogen-activated Protein Kinase Kinase (MEK)-ERK1/2 Signaling Pathway. In (Vol. 286, pp. 19439-19445): *FEBS Letters*.

Sheng, Q., Vickers, K., Zhao, S., Wang, J., Samuels, D. C., Koues, O., Shyr, Y., Guo, Y. (2017). Multi-perspective quality control of Illumina RNA sequencing data analysis. In (Vol. 16, pp. 194-204): *Briefings in Functional Genomics*.

Shibuya, M. (2011). Vascular Endothelial Growth Factor (VEGF) and Its Receptor (VEGFR) Signaling in Angiogenesis: A Crucial Target for Anti- and Pro-Angiogenic Therapies. In (Vol. 2, pp. 1097-1105): *Genes and Cancer*.

Simons, M., Gordon, E., Claesson-Welsh, L. (2016). Mechanisms and regulation of endothelial VEGF receptor signalling. In (Vol. 17, pp. 611-625): *Nature Reviews Molecular Cell Biology*.

Skeberdis, V. A., Chevalyere, V., Lau, C. G., Goldberg, J. H., Pettit, D. L., Suadicani, S. O., Lin, Y., Bennett, M. V. L., Yuste, R., Castillo, P. E. (2006). Protein kinase A regulates calcium permeability of NMDA receptors. In (Vol. 9, pp. 501-510): *Nature Neuroscience*.

Smith, P. K., Krohn, R. I., Hermanson, G. T., Mallia, A. K., Gartner, F. H., Frovenzano, M. D., Fujimoto, E. K., Goeke, N. M., Olson, B. J., Klenk, D. C. (1985). Measurement of Protein Using Bicinchoninic Acid'. In (Vol. 150 (1), pp. 76-85): *Analytical biochemistry*.

Sonenberg, N., Hinnebusch, A. G. (2009). Regulation of Translation Initiation in Eukaryotes: Mechanisms and Biological Targets. In (Vol. 136, pp. 731-745): *Cell*.

Song, J., Liu, L., Lv, L., Hu, S., Tariq, A., Wang, W., Dang, X. (2020). Fluid shear stress induces Runx-2 expression via upregulation of PIEZO1 in MC3T3-E1 cells. In (Vol. 44, pp. 1491-1502): *Cell Biology International*.

Soto, F., Garcia-Guzman, M., Stühmer, W. (1997). Cloned ligand-gated channels activated by extracellular ATP (P2X receptors). In (Vol. 160, pp. 91-100): *Journal of Membrane Biology*.

Sprague, S. M., Popovtzer, M. M., Dranitzki-elhalel, M., Wald, H., Dranitzki-Elhalel, M., Wald Parathyroid, H. (1996). Parathyroid hormone-induced calcium efflux from cultured bone is mediated by protein kinase C translocation. In (Vol. 271, no 6, p. F1139-F1146): *American Journal of Physiology-Renal Physiology*.

Stokes, L., Bidula, S., Bibič, L., Allum, E. (2020). To Inhibit or Enhance? Is There a Benefit to Positive Allosteric Modulation of P2X Receptors? In (Vol. 11): *Frontiers in Pharmacology*.

- Stokes, L., Jiang, L. H., Alcaraz, L., Bent, J., Bowers, K., Fagura, M., Furber, M., Mortimore, M., Lawson, M., Theaker, J., Laurent, C., Braddock, M., Surprenant, A. (2006). Characterization of a selective and potent antagonist of human P2X 7 receptors, AZ11645373. In (Vol. 149, pp. 880-887): British Journal of Pharmacology.
- Stokes, L., Layhadi, J. A., Bibic, L., Dhuna, K., Fountain, S. J. (2017). P2X4 receptor function in the nervous system and current breakthroughs in pharmacology. In (Vol. 8, pp. 1-15): Frontiers in Pharmacology.
- Strassheim, D., Verin, A., Batori, R., Nijmeh, H., Burns, N., Kovacs-Kasa, A., Umapathy, N. S., Kotamarthi, J., Gokhale, Y. S., Karoor, V. (2020). P2Y Purinergic Receptors, Endothelial Dysfunction, and Cardiovascular Diseases. In (Vol. 21, pp. 6855): International Journal of Molecular Sciences.
- Suchyna, T. M., Johnson, J. H., Hamer, K., Leykam, J. F., Gage, D. A., Clemo, H. F., Baumgarten, C. M., Sachs, F. (2000). Identification of a Peptide Toxin from *Grammostola spatulata* Spider Venom that Blocks Cation-selective Stretch-activated Channels. In (Vol. 115, pp. 583-598): J. Gen. Physiol.
- Sugimoto, A., Miyazaki, A., Kawarabayashi, K., Shono, M., Akazawa, Y., Hasegawa, T., Ueda-Yamaguchi, K., Kitamura, T., Yoshizaki, K., Fukumoto, S. (2017). Piezo type mechanosensitive ion channel component 1 functions as a regulator of the cell fate determination of mesenchymal stem cells. In (Vol. 7, pp. 17696): Scientific Reports.
- Sulpice, E., Ding, S., Muscatelli-Groux, B., Bergé, M., Han, Z. C., Plouet, J., Tobelem, G., Merkulova-Rainon, T. (2009). Cross-talk between the VEGF-A and HGF signalling pathways in endothelial cells. In (Vol. 101, pp. 525-539): Biology of the Cell.
- Swain, S. M., Liddle, R. A. (2021). Piezo1 acts upstream of TRPV4 to induce pathological changes in endothelial cells due to shear stress. In (Vol. 296): Journal of Biological Chemistry.
- Syeda, R., Xu, J., Dubin, A. E., Coste, B., Mathur, J., Huynh, T., Matzen, J., Lao, J., Tully, D. C., Engels, I. H. (2015). Chemical activation of the mechanotransduction channel Piezo1. In (Vol. 4, p. e07369): eLife.
- Szabó, L., Balogh, N., Tóth, A., Angyal, Á., Gönczi, M., Csiki, D. M., Tóth, C., Balatoni, I., Jeney, V., Csernoch, L. (2022). The mechanosensitive Piezo1 channels contribute to the arterial medial calcification. In (Vol. 13): Frontiers in Physiology.
- Tabrizchi, R., Bedi, S. Pharmacology of adenosine receptors in the vasculature. In (Vol. 91(2), p. 133-147): Pharmacology & therapeutics.
- Taite, L. J., Rowland, M. L., Ruffino, K. A., Smith, B. R. E., Lawrence, M. B., West, J. L. (2006). Bioactive Hydrogel Substrates: Probing Leukocyte Receptor–Ligand Interactions in Parallel Plate Flow Chamber Studies. In (Vol. 34, pp. 1705-1711): Annals of Biomedical Engineering.
- Tamargo, I. A., Baek, K. I., Kim, Y., Park, C., Jo, H. (2023). Flow-induced reprogramming of endothelial cells in atherosclerosis. In (Vol. 20, pp. 738-753): Nature Reviews Cardiology.
- Tanaka, N., Kawasaki, K., Nejime, N., Kubota, Y., Nakamura, K., Kunitomo, M., Takahashi, K., Hashimoto, M., Shinozuka, K. (2004). P2Y Receptor-Mediated Ca²⁺ Signaling Increases Human Vascular Endothelial Cell Permeability. In (Vol. 95, pp. 174-180): Journal of Pharmacological Sciences J Pharmacol Sci.
- Tang, H., Zeng, R., He, E., Zhang, I., Ding, C., Zhang, A. (2022). Piezo-Type Mechanosensitive Ion Channel Component 1 (Piezo1): A Promising Therapeutic Target and Its Modulators. In (Vol. 65, pp. 6441-6453): Journal of Medicinal Chemistry.

- Tang, Y., Matsuoka, I., Ono, T., Inoue, K., Kimura, J. (2008). Selective up-regulation of P2X4-receptor gene expression by interferon- γ in vascular endothelial cells. In (Vol. 107, pp. 419-427): *Journal of Pharmacological Sciences*.
- Taruno, A. (2018). ATP Release Channels. In (Vol. 19, pp. 808): *International Journal of Molecular Sciences*.
- Thakore, P., Earley, S. (2019). Transient receptor potential channels and endothelial cell calcium signaling. In (Vol. 9, pp. 1249-1277): *Comprehensive Physiology*.
- Thuringer, D. (2004). The vascular endothelial growth factor-induced disruption of gap junctions is relayed by an autocrine communication via ATP release in coronary capillary endothelium. In (Vol. 1030, pp. 14-27): *Annals of the New York Academy of Sciences*.
- Toma, I., Bansal, E., Meer, E. J., Julie Kang, J., Vargas, S. L., Peti-Peterdi, J. (2008). renal glomerular endothelial cells. In (Vol. 294, pp. 1769-1776): *American Journal of Physiology-Regulatory, Integrative and Comparative Physiology*.
- Tsai, F. C., Kuo, G. H., Chang, S. W., Tsai, P. J. (2015). Ca²⁺ signaling in cytoskeletal reorganization, cell migration, and cancer metastasis. In (Vol. 2015): *BioMed Research International*.
- Tsikas, D. (2007). Analysis of nitrite and nitrate in biological fluids by assays based on the Griess reaction: Appraisal of the Griess reaction in the l-arginine/nitric oxide area of research. In (Vol. 851, pp. 51-70): *Journal of Chromatography*.
- Tzima, E., Irani-Tehrani, M., Kiosses, W. B., Dejana, E., Schultz, D. A., Engelhardt, B., Cao, G., DeLisser, H., Schwartz, M. A. (2005). A mechanosensory complex that mediates the endothelial cell response to fluid shear stress. In (Vol. 437, pp. 426-431): *Nature*.
- Ullmann, H., Meis, S., Hongwiset, D., Marzian, C., Wiese, M., Nickel, P., Communi, D., Boeynaems, J. M., Wolf, C., Hausmann, R., R., Schmalzing, G., Kassack, M. U. (2005). Synthesis and structure-activity relationships of suramin-derived P2Y₁₁ receptor antagonists with nanomolar potency. In (Vol. 48, pp. 7040-7048): *Journal of Medicinal Chemistry*.
- Vassalle, C., Domenici, C., Lubrano, V., L'Abbate, A. (2003). Interaction between Nitric Oxide and Cyclooxygenase Pathways in Endothelial Cells. In (Vol. 40, pp. 491-499): *Journal of Vascular Research*.
- Venturini, V., Pezzano, F., Castro, F. C., Häkkinen, H. M., Jiménez-Delgado, S., Colomer-Rosell, M., Marro, M., Tolosa-Ramon, Q., Paz-López, S., Valverde, M. A., Weghuber, J., Loza-Alvarez, P., Krieg, M., Wieser, S., & Ruprecht, V. (2020). The nucleus measures shape changes for cellular proprioception to control dynamic cell behavior. In (Vol. 370): *Science*.
- Viana, F., De Smedt, H., Droogmans, G., Nilius, B. (1998). Calcium signalling through nucleotide receptor P2Y₂ in cultured human vascular endothelium. In (Vol. 24, pp. 117-127): *Cell Calcium*.
- Victorino, G. P., Chong, T. J., Curran, B. (2004). Endothelin-1 decreases postcapillary fluid efflux via prostacyclin release. In (Vol. 136(2), 473-477): *Surgery*.
- Von Kügelgen, I., Hoffmann, K. (2016). Pharmacology and structure of P2Y receptors. In (Vol. 104, pp. 50-61): *Neuropharmacology*.
- Vriens, J., Nilius, B., Voets, T. (2014). Peripheral thermosensation in mammals. In (Vol. 15, pp. 573-589): *Nature Reviews Neuroscience*.

- Wadud, R., Hannemann, A., Rees, D. C., Brewin, J. N., Gibson, J. S. (2020). Yoda1 and phosphatidylserine exposure in red cells from patients with sickle cell anaemia. In (Vol. 10): Scientific Reports.
- Walshe, T. E., dela Paz, N. G., D'Amore, P. A. (2013). The Role of Shear-Induced Transforming Growth Factor- β Signaling in the Endothelium. In (Vol. 33, pp. 2608-2617): Arteriosclerosis, Thrombosis, and Vascular Biology.
- Wang, L., Karlsson, L., Moses, S., Hultgårdh-Nilsson, A., Andersson, M., Borna, C., Gudbjartsson, T., Jern, S., Erlinge, D. (2002). P2 Receptor Expression Profiles in Human Vascular Smooth Muscle and Endothelial Cells. In (Vol. 40, pp. 841-853): Journal of Cardiovascular Pharmacology.
- Wang, S., Zhang, Y., Wier, W. G., Yu, X., Zhao, M., Hu, H., Sun, L., He, X., Wang, Y., Wang, B., Zang, W. (2009). Role of store-operated Ca²⁺ entry in adenosine-induced vasodilatation of rat small mesenteric artery. In (Vol. 297): American Journal of Physiology - Heart and Circulatory Physiology.
- Wang, S. P., Chennupati, R., Kaur, H., Iring, A., Wettschureck, N., Offermanns, S. (2016). Endothelial cation channel PIEZO1 controls blood pressure by mediating flow-induced ATP release. In (Vol. 126, pp. 4527-4536): Journal of Clinical Investigation.
- Wang, S. P., Iring, A., Strilic, B., Juárez, J. A., Kaur, H., Troidl, K., Tonack, S., Burbiel, J. C., Müller, C. E., Fleming, I., Lundberg, J. O., Wettschureck, N., Offermanns, S. (2015). P2Y₂ and Gq/G11 control blood pressure by mediating endothelial mechanotransduction. In (Vol. 125, pp. 3077-3086): Journal of Clinical Investigation.
- Warboys, C. M., Ghim, M., Weinberg, P. D. (2019). Understanding mechanobiology in cultured endothelium: A review of the orbital shaker method. In (Vol. 285, pp. 170-177): Atherosclerosis.
- Webb, D. J., Haynes, W. G. (1993). Venoconstriction to endothelin-1 in humans is attenuated by local generation of prostacyclin but not nitric oxide. In (Vol. 22, pp. S317-S320): Journal of cardiovascular pharmacology.
- Wei, L., Mousawi, F., Li, D., Roger, S., Li, J., Yang, X., Jiang, L.H. (2019). Adenosine triphosphate release and P2 receptor signaling in Piezo1 channel-dependent mechanoregulation. In (Vol. 10, pp. 1-10): Frontiers in Pharmacology.
- Weinhausen, S., Nagel, J., Namasivayam, V., Spanier, C., Abdelrahman, A., Hanck, T., Hausmann, R., Müller, C. E. (2022). Extracellular binding sites of positive and negative allosteric P2X₄ receptor modulators. In (Vol. 311, pp. 121143): Life Sciences.
- Wenker, I. C. (2005). The role of nucleotide signaling in the regulation of ICL, swell in human 1321n1 astrocytoma cells. In Wright State University.
- Werner, S., Mesch, S., Hillig, R. C., Ter Laak, A., Klint, J., Neagoe, I., Laux-Biehlmann, A., Dahllöf, H., Bräuer, N., Puetter, V., Nubbemeyer, R., Schulz, S., Bairlein, M., Zollner, T. M., Steinmeyer, A. (2019). Discovery and Characterization of the Potent and Selective P2X₄ Inhibitor N-[4-(3-Chlorophenoxy)-3-sulfamoylphenyl]-2-phenylacetamide (BAY-1797) and Structure-Guided Amelioration of Its CYP3A4 Induction Profile. In (Vol. 62, pp. 11194-11217): Journal of Medicinal Chemistry.
- Wiechelmann, K. J., Braun, R. D., Fitzpatrick, J. D., Smith, P. K., Krohn, R. I., Hermanson, G. T., Mallia, A. K., Gartner, F. H., Provenzano, M. D., Fujimoto, E. K., E. K., Goeke, N. M., Olson, B. J., Klenk, D. C. (1988). Investigation of the Bicinchoninic Acid Protein Assay: Identification of the Groups Responsible for Color Formation. In (Vol. 175(1), pp. 231-237): Analytical biochemistry.

- Willoughby, D., Everett, K. L., Halls, M. L., Pacheco, J., Skroblin, P., Vaca, L., Klussmann, E., Cooper, D. M. F. (2012). Direct binding between Orai1 and AC8 mediates dynamic interplay between Ca²⁺ and cAMP signaling. In (Vol. 5, pp. 1-11): *Science Signaling*.
- Willoughby, D., Cooper, D. M. F. (2007). Organization and Ca²⁺ Regulation of Adenylyl Cyclases in cAMP Microdomains. In (Vol. 87 (3), pp. 965-1010): *Physiological reviews*.
- Wilson, H. L., Varcoe, R. W., Stokes, L., Holland, K. L., Francis, S. E., Dower, S. K., Surprenant, A., Crossman, D. C. (2007). P2X receptor characterization and IL-1/IL-1Ra release from human endothelial cells. In (Vol. 151, pp. 96-108): *British Journal of Pharmacology*.
- Woods, L. T., Forti, K. M., Shanbhag, V. C., Camden, J. M., Weisman, G. A. (2021). P2Y receptors for extracellular nucleotides: Contributions to cancer progression and therapeutic implications. In (Vol. 187): *Biochemical Pharmacology*.
- Wu, J., Lewis, A. H., Grandl, J. (2017). Touch, Tension, and Transduction – The Function and Regulation of Piezo Ion Channels. In (Vol. 42, pp. 57-71): *Trends in Biochemical Sciences*.
- Wu, X. M., Zhang, N., Li, J. S., Yang, Z. H., Huang, X. L., Yang, X. F. (2023). Purinergic receptors mediate endothelial dysfunction and participate in atherosclerosis. In (Vol. 19, pp. 265-272): *Purinergic Signalling*.
- Xia, P. U., Gamble, J. R., Rye, K.-A., Wang, L., Hii, C. S. T., Cockerill, P., Khew-Goodall, Y., Bert, A. G., Barter, P. J., Vadas, M. A. (1998). Tumor necrosis factor- α induces adhesion molecule expression through the sphingosine kinase pathway. In (Vol. 95, pp. 14196-14201): *Proceedings of the National Academy of Sciences*.
- Xiang, Z., Jiang, X., Ji, R., Yuan, H. (2021). Enhanced expression of P2X4 purinoceptors in pyramidal neurons of the rat hippocampal CA1 region may be involved ischemia-reperfusion injury. In (Vol. 17, pp. 425-438): *Purinergic Signalling*.
- Xiao, Z., Yang, M., Lv, Q., Wang, W., Deng, M., Liu, X., He, Q., Chen, X., Chen, M., Fang, L., Xie, X., Hu, J. (2011). P2Y11 impairs cell proliferation by induction of cell cycle arrest and sensitizes endothelial cells to cisplatin-induced cell death. In (Vol. 112, pp. 2257-2265): *Journal of Cellular Biochemistry*.
- Xu, Y., Kruckoff, T. L. (2007). Adrenomedullin Stimulates Nitric Oxide Production from Primary Rat Hypothalamic Neurons: Roles of Calcium and Phosphatases. In (Vol. 72, pp. 112-120): *Molecular Pharmacology*.
- Yamamoto, K., Furuya, K., Nakamura, M., Kobatake, E., Sokabe, M., Ando, J. (2011). Visualization of flow-induced ATP release and triggering of Ca²⁺ waves at caveolae in vascular endothelial cells. In (Vol. 124, pp. 3477-3483): *Journal of Cell Science*.
- Yamamoto, K., Imamura, H., Ando, J. (2018). Shear stress augments mitochondrial ATP generation that triggers ATP release and Ca²⁺ signaling in vascular endothelial cells. In (Vol. 315, pp. H1477-H1485): *American Journal of Physiology-Heart and Circulatory Physiology*.
- Yamamoto, K., Sokabe, T., Matsumoto, T., Yoshimura, K., Shibata, M., Ohura, N., Fukuda, T., Sato, T., Sekine, K., Kato, S., Isshiki, M., Fujita, T., Kobayashi, M., Kawamura, K., Masuda, H., Kamiya, A., Ando, J. (2006). Impaired flow-dependent control of vascular tone and remodeling in P2X4-deficient mice. In (Vol. 12, pp. 133-137): *Nature Medicine*.
- Yamamoto, K., Sokabe, T., Ohura, N., Nakatsuka, H., Kamiya, A., Ando, J. (2003). Endogenously released ATP mediates shear stress-induced Ca²⁺ influx into pulmonary artery endothelial cells. In (Vol. 285, pp. 793-803): *Am J Physiol Heart Circ Physiol*.

- Yamamoto, K., Korenaga, R., Kamiya, A., Ando, J. (2000). Fluid shear stress activates Ca²⁺ influx into human endothelial cells via P2X₄ purinoceptors. In (Vol. 87, pp. 385-391): *Circulation Research*.
- Yamamoto, K., Korenaga, R., Kamiya, A., Qi, Z., Sokabe, M., Ando, J., & (2000). P2X₄ receptors mediate ATP-induced calcium influx in human vascular endothelial cells. In (Vol. 279, (1), p. H285-H292): *American Journal of Physiology-Heart and Circulatory Physiology*.
- Yang, B., Cai, B., Deng, P., Wu, X., Guan, Y., Zhang, B., Cai, W., Schaper, J., Schaper, W. (2015). Nitric Oxide Increases Arterial Endothelial Permeability through Mediating VE-Cadherin Expression during Arteriogenesis. In (Vol. 10, pp. e0127931): *PLOS ONE*.
- Yang, Z., Yang, Y., Xiong, K., Li, X., Qi, P., Tu, Q., Jing, F., Weng, Y., Wang, J., Huang, N. (2015). Nitric oxide producing coating mimicking endothelium function for multifunctional vascular stents. In (Vol. 63, pp. 80-92): *Biomaterials*.
- Yazdani, Y., Mohammadi, S., Yousefi, M., Shokri, F (2015). Preliminary Assessment of Various Additives on the Specific Reactivity of Anti-rHBsAg Monoclonal Antibodies. In (Vol. 7, p. 145): *Avicenna Journal of Medical Biotechnology*.
- Yegutkin, G. G. (2014). Enzymes involved in metabolism of extracellular nucleotides and nucleosides: Functional implications and measurement of activities. In (Vol. 49, pp. 473-497): *Critical Reviews in Biochemistry and Molecular Biology*.
- Yoshikawa, N., Ariyoshi, H., Ikeda, M., Sakon, M., Kawasaki, T., Monden, M. (1997). Shear-stress causes polarized change in cytoplasmic calcium concentration in human umbilical vein endothelial cells (HUVECs). In (Vol. 22(3), 189-194): *Cell Calcium*.
- Yucel, A., Gulen, S., Dincer, S., Yucel, A., Yetkin, G. (2012). Comparison of two different applications of the Griess method for nitric oxide measurement. In (Vol. 2, pp. 167): *Journal of Experimental and Integrative Medicine*.
- Zhang, C., Han, X., Xu, J., Zhou, Y. (2022). Matrix Stiffness-Induced Transcriptome Alterations and Regulatory Mechanisms Revealed by RNA-Seq in Endothelial Cells. In (Vol. 13, pp. 61-79): *Journal of Biomaterials and Nanobiotechnology*.
- Zhang, T., Chi, S., Jiang, F., Zhao, Q., Xiao, B. (2017). A protein interaction mechanism for suppressing the mechanosensitive Piezo channels. In (Vol. 8, pp. 1797): *Nature Communications*.
- Zhang, Y., Lau, P., Pansky, A., Kassack, M., Hemmersbach, R., Tobiasch, E. (2014). The Influence of Simulated Microgravity on Purinergic Signaling is Different between Individual Culture and Endothelial and Smooth Muscle Cell Coculture. In (Vol. 2014): *BioMed Research International*.
- Zhang, Y., Zhu, W., Yu, H., Yu, J., Zhang, M., Pan, X., Gao, X., Wang, Q., Sun, H. (2019). P2Y₄/TSP-1/TGF- β 1/pSmad2/3 pathway contributes to acute generalized seizures induced by kainic acid. In (Vol. 149, pp. 106-119): *Brain Research Bulletin*.
- Zhao, Y., Vanhoutte, P. M., Leung, S. W. S. (2015). Vascular nitric oxide: Beyond eNOS. In (Vol. 129, pp. 83-94): *Journal of Pharmacological Sciences*.